Knotting Statistics After a Local Strand Passage in Unknotted Self-Avoiding Polygons in $\mathbb{Z}^3$

A Thesis Submitted to the
College of Graduate Studies and Research
in Partial Fulfillment of the Requirements
for the Degree of
Doctor of Philosophy
in the
Department of Mathematics and Statistics
University of Saskatchewan
Saskatoon, Saskatchewan

By

Michael Lorne Szafron

April 2009

Permission to Use

In presenting this thesis in partial fulfilment of the requirements for a Postgraduate degree from the University of Saskatchewan, I agree that the Libraries of this University may make it freely available for inspection. I further agree that permission for copying of this thesis in any manner, in whole or in part, for scholarly purposes may be granted by the professor or professors who supervised my thesis work or, in their absence, by the Head of the Department or the Dean of the College in which my thesis work was done. It is understood that any copying or publication or use of this thesis or parts thereof for financial gain shall not be allowed without my written permission. It is also understood that due recognition shall be given to me and to the University of Saskatchewan in any scholarly use which may be made of any material in my thesis.

Requests for permission to copy or to make other use of material in this thesis in whole or part should be addressed to:

Head of the Department of Mathematics and Statistics
University of Saskatchewan
Saskatoon, Saskatchewan
Canada
S7N 5E6

Abstract

We study here a model for a strand passage in a ring polymer about a randomly chosen location at which two strands of the polymer have been brought "close" together. The model is based on Θ-SAPs, which are unknotted self-avoiding polygons in $\mathbb{Z}^3$ that contain a fixed structure Θ that forces two segments of the polygon close together. To study this model, the Composite Markov Chain Monte Carlo (CMCMC) algorithm, referred to as the CMC Θ-BFACF algorithm, that I developed and proved to be ergodic for unknotted Θ-SAPs in my M. Sc. Thesis [150], is used. Ten simulations (each consisting of 9.6×10^{10} time steps) are performed and the results from a statistical analysis of the simulated data are presented. To this end, a new maximum likelihood method, based on previous work of Berretti and Sokal [7], is developed for obtaining maximum likelihood estimates for the growth constants and critical exponents associated with the numbers of unknotted $(2n)$-edge Θ-SAPs, $p_n^{\Theta}(\phi)$; unknotted $(2n)$-edge successful-strand-passage Θ-SAPs, $p_n^{\Theta}(\phi, s)$; unknotted $(2n)$-edge failed-strand-passage Θ-SAPs, $p_n^{\Theta}(\phi, f)$; and after-strand-passage knot-type-K unknotted successful-strand-passage Θ-SAPs, $p_n^{\Theta}(K|\phi, s)$. The maximum likelihood estimates are consistent with the result (proved here) that these growth constants are all equal, and provide evidence that the critical exponents are all equal.

We then investigate the question, "Given that a successful local strand passage occurs at a random location in a $(2n)$-edge, knot-type K Θ-SAP, with what probability will the Θ-SAP have knot-type K' after the strand passage?". To this end, the CMCMC data is used to obtain estimates for $1 - p_n^{\Theta}(\phi|\phi, s)/(p_n^{\Theta}(\phi, s)$, the probability of knotting given a $(2n)$-edge successful-strand-passage Θ-SAP, and $p_n^{\Theta}(K|\phi, s)/p_n^{\Theta}(\phi, s)$, the probability of an after-strand-passage knot-type K polygon given a $(2n)$-edge unknotted successful-strand-passage Θ-SAP. The computed estimates numerically support the unproven conjecture that these probabilities, in the $n \to \infty$ limit, go to a value lying strictly between 0 and 1. We further prove here that the rate of approach to each of these limits (should the limits exist) is less than exponential.

We conclude with a study of whether or not there is a difference in the "size" of an unknotted successful-strand-passage Θ-SAP whose after-strand-passage knot-type is K when compared to the "size" of an unknotted Θ-SAP whose knot-type does not change after a strand passage. The two measures of "size" used are the expected lengths of, and the expected mean-square radius of gyration of, subsets of Θ-SAPs. How these two measures of "size" behave as a function of a polygon's length and after-strand-passage knot-type is investigated.

Acknowledgements

I would first like to thank my supervisor, Dr. C. E. Soteros, who has, throughout my Ph.D. program, provided me with guidance and advice and has been a sounding-board for some of my "brilliant" ideas. I also wish to thank her for the financial support provided through her NSERC grant. My thanks are extended to the members of my advisory committee for the suggested improvements to the thesis and to Dr. R. Srinivasan, Dr. S. G. Whittington, Dr. M. Bickis, Dr. W. Laverty, Dr. D. W. Sumners, Dr. E. J. Janse van Rensburg, Dr. E. Orlandini, and Dr. I. Darcy for their advice and useful discussions on topics relevant to this thesis. I would also like to thank Dr. S. G. Whittington for providing his computer code for calculating $\tau_{int,A}$, Dr. E. J. Janse van Rensburg for providing his computer code which became the backbone of the program I developed to evaluate the Alexander Polynomial of a self-avoiding polygon, and Dr. R. Sharein for allowing me to use *KnotPlot* to create the knot diagrams included in this thesis. I would like to thank NSERC for the financial support provided via a two year PGS B Scholarship. As well, I wish to extend my thanks to the College of Graduate Studies and Research, the Department of Mathematics and Statistics, and St. Peter's College for the financial support provided throughout my Ph.D. program. I finally would like to thank my family for their support and encouragement throughout my Ph.D. program. Without their continued support and at times, kicks in the "proverbial pants", my completion would not have become a reality.

Table of Contents

List of Tables

List of Figures

List of Symbols

3_1^+ the notation used to denote the knot-type referred to as the right-handed trefoil Page 14

4_1 the notation used to denote the knot-type referred to as the figure 8 ..... Page 14

α the entropic critical exponent for all SAPs in $\mathbb{Z}^3$ ..... Page 33

α_ϕ the entropic critical exponent for unknotted SAPs in $\mathbb{Z}^3$ ..... Page 33

α_K the entropic critical exponent for SAPs in $\mathbb{Z}^3$ with knot-type K ..... Page 33

$\hat{\boldsymbol{\omega}}^{(r)}$ the sequence of 14-tuples of Θ-SAPs sampled every 1200 time steps from $\boldsymbol{\omega}^{(r)}$ Page 150

$\hat{\boldsymbol{\omega}}_R^{(u)}$ the sequence of samples from Replication u used in Chapter 7 ..... Page 282

$\boldsymbol{\omega}^{(r)}$ the sequence of 14-tuples of Θ-SAPs realized in the r'th replication ..... Page 150

$\breve{\pi}_{2n}(z)$ the probability of randomly selecting a $(2n)$-edge unknotted Θ-SAP ..... Page 70

$\breve{\pi}_\omega(q,z)$ the probability of randomly selecting the unknotted Θ-SAP ω ..... Page 70

$\breve{Q}(q,z)$ the partition function $\breve{Q}(z,14)$ ..... Page 70

$\breve{Q}(q,z,M)$ the partition function for the LSP Model ..... Page 69

$\mathcal{I}_{\boldsymbol{X}}(\boldsymbol{\theta})$ the Fisher Information Matrix based on $\boldsymbol{X}$ ..... Page 208

$\mathcal{X}_k^{(r)}$ the r'th replication of the Markov chain $\mathcal{X}$ of length k ..... Page 122

$\mathcal{E}(G)$ the edge set of the graph G ..... Page 23

$\mathcal{M}(G)$ the midpoints of the edges in $\mathcal{E}(G)$ ..... Page 57

$\mathcal{R}_n(a,b,c,d,r)$ the function $\mathcal{R}_n(a,b,c,d,r) = an^{2b}(1+cn^{-d}+r(n))$ with $r(n) = O(n^{-1})$ Page 39

$\mathcal{V}(G)$ the vertex set of the graph G ..... Page 23

Δ the confluent exponent for all SAPs in $\mathbb{Z}^3$ ..... Page 33

Δ the confluent exponent in the scaling form for the radius of gyration of the set of n-edge SAPs in $\mathbb{Z}^3$ ..... Page 39

Δ_ϕ the confluent exponent for unknotted SAPs in $\mathbb{Z}^3$ ..... Page 33

Δ_K the confluent exponent for SAPs in $\mathbb{Z}^3$ with knot-type K ..... Page 33

$\Delta_R(K)$ the confluent exponent in the scaling form for the radius of gyration of the set of n-edge knot-type K SAPs in $\mathbb{Z}^3$ ..... Page 40

$\gamma_f(h)$ the autocovariance function for the stationary stochastic process $f(\mathcal{X})$ with respect to the distribution π ..... Page 117

$\hat{\delta}^{(r)}(*)$ the minimum (taken over n) of $\hat{\delta}_{2n}^{(r)}$ ..... Page 149

$\hat{\delta}_{2n}^{(r)}(*)$ the estimated relative standard error for a function g using property-$*$ Θ-SAPs from Replication r ..... Page 149

$\hat{N}_{\max}^{(r)}(*)$ the estimated polygon length for which the Replication r sample of property-$*$ Θ-SAPs becomes unreliable ..... Page 149

$\hat{N}_{\max}(*)$ the estimated polygon length for which the sample of property-$*$ Θ-SAPs becomes unreliable ..... Page 150

$\hat{N}_{\min}(*)$ an estimate for $N_{\min}^{*}$ ..... Page 229

$\hat{N}_l$ the smallest unknotted polygon length observed across all the replicationsPage 193

$\hat{N}_l^{(r)}$ the smallest unknotted polygon length observed in Replication r ..... Page 192

$\hat{N}_u$ the largest unknotted polygon length observed across all the replications Page 193

$\hat{N}_u^{(r)}$ the largest unknotted polygon length observed in Replication r ..... Page 192

κ the connective constant for self-avoiding walks and self-avoiding polygons in $\mathbb{Z}^3$ defined by Equation (1.10) ..... Page 27

$\kappa_{(\phi,f)}^{\Theta}$ the connective constant for the set of unknotted unsuccessful-strand-passage polygons in $\mathbb{Z}^3$ ..... Page 65

$\kappa_{(\phi,s)}^{\Theta}$ the connective constant for the set of unknotted successful-strand-passage polygons in $\mathbb{Z}^3$ ..... Page 65

$\kappa_{(K,f)}^{\Theta}$ the limit supremum defined by Equation (2.44) ..... Page 67

$\kappa_{(K,s)}^{\Theta}$ the limit supremum defined by Equation (2.43) ..... Page 67

$\kappa_{(K\prime|K,s)}^{\Theta}$ the limit supremum defined by Equation (2.45) ..... Page 67

κ_K^{Θ} the limit supremum defined by Equation (2.42) ..... Page 67

κ_ϕ the connective constant for unknotted SAPs in $\mathbb{Z}^3$ defined by Equation (1.21)Page 31

κ_K the limit supremum defined by Equation (1.22) ..... Page 32

$\langle f \rangle_n$ an estimator for the sample mean of the observable f based on a sample of size n Page 120

$\langle L_{2n}(\mathscr{E}^c(*)) \rangle$ an estimator for $\mathrm{E}\left[L_{2n}(\mathscr{E}^c(*))\right]$ ..... Page 285

$\langle l_{2n}(\mathscr{E}^c(*)) \rangle$ the point estimate computed using the estimator $\langle L_{2n}(\mathscr{E}^c(*)) \rangle$ ..... Page 286

$\mathscr{C}_n^d(\boldsymbol{x},\boldsymbol{y})$ the set of n-step SAWs in $\mathbb{Z}^d$ that start at $\boldsymbol{x}\in\mathbb{Z}^d$ and end at $\boldsymbol{y}\in\mathbb{Z}^d$ ... Page 25

$\mathscr{E}$ the set of all equal-sided SAPs in $\mathscr{P}^{\Theta}(\phi)$ ... Page 84

$\mathscr{E}^{ec}$ the set of all unequal-sided SAPs in $\mathscr{P}^{\Theta}(\phi)$ ... Page 84

$\mathscr{E}_{2n}^{ec}$ the set of $(2n)$-edge unequal-sided SAPs in $\mathscr{P}^{\Theta}(\phi)$ ... Page 83

$\mathscr{E}_{2n}^{ec}(*)$ the set of $(2n)$-edge property-$*$ unequal-sided SAPs in $\mathscr{P}^{\Theta}(\phi)$ ... Page 85

$\mathscr{E}_{2n}$ the set of $(2n)$-edge equal-sided SAPs in $\mathscr{P}^{\Theta}(\phi)$ ... Page 83

$\mathscr{E}_{2n}(*)$ the set of $(2n)$-edge property-$*$ equal-sided SAPs in $\mathscr{P}^{\Theta}(\phi)$ ... Page 85

$\mathscr{F}_8(n,k)$ the set of n-edge Figure-of-Eights that consist of one loop with k-edges, the other loop has $(n-k)$-edges, and $k\geq n-k$ ... Page 79

$\mathscr{I}_A(x)$ for the set A, an indicator function returning 1 if $x\in A$ and 0 otherwise Page 129

$\mathscr{K}^{\Theta}(K)$ the set of all knot-types that can be obtained when a strand passage about Θ is implemented in a successful-strand-passage SAP whose knot-type is K ... Page 55

$\mathscr{K}^{\dagger}(K)$ the set of after-strand-passage properties based on a successful strand passage in a knot-type K Θ-SAP ... Page 56

$\mathscr{M}_n(t)$ an indicator function returning 1 if $t=0(\mod n)$ and 0 otherwise ... Page 129

$\mathscr{P}$ the set of all SAPs in $\mathbb{Z}^3$ ... Page 28

$\mathscr{P}(K)$ the set of all SAPs in $\mathbb{Z}^3$ with knot-type K ... Page 28

$\mathscr{P}^{\Theta}(K'|K,s)$ the set of SAPs in $\mathscr{P}^{\Theta}(K,s)$ that have knot-type K' after a successful strand passage ... Page 56

$\mathscr{P}^{\Theta}(K)$ the set of SAPs $\mathscr{P}^{\Theta}(K:CD,AH)$ where $A=(1,0,0)$; $C=(-1,0,0)$; $D=(0,-1,-2)$; and $H=(0,1,-2)$ ... Page 55

$\mathscr{P}^{\Theta}(K,f)$ the set of SAPs in $\mathscr{P}^{\Theta}(K)$ for which strand passage is not viable ... Page 56

$\mathscr{P}^{\Theta}(K,s)$ the set of SAPs in $\mathscr{P}^{\Theta}(K)$ for which strand passage is viable ... Page 56

$\mathscr{P}^{\Theta}(K:CD,AH)$ the set of SAPs in $\mathbb{Z}^3$ whose knot-type is K that result from connecting Vertex C and Vertex D of the structure Θ with a uSAW and Vertex A and Vertex H of Θ with a uSAW ... Page 53

$\mathscr{P}^{\Theta}(K:CH,AD)$ the set of SAPs in $\mathbb{Z}^3$ whose knot-type is K that result from connecting Vertex C and Vertex H of the structure Θ with a uSAW and Vertex A and Vertex D of Θ with a uSAW ... Page 53

$\mathscr{P}_n^{\Theta}(K:CD,AH)$ the set of n-edge SAPs in $\mathbb{Z}^3$ whose knot-type is K that result from connecting Vertex C and Vertex D of the structure Θ with a uSAW and Vertex A and Vertex H of Θ with a uSAW ... Page 53

$\mathscr{P}_n^{\Theta}(K:CH,AD)$ the set of n-edge SAPs in $\mathbb{Z}^3$ whose knot-type is K that result from connecting Vertex C and Vertex H of the structure Θ with a uSAW and Vertex A and Vertex D of Θ with a uSAW ... Page 54

Ω_2 the symbol used to denote a Reidemeister II move ..... Page 14

Ω_3 the symbol used to denote a Reidemeister III move ..... Page 14

$\mathrm{col}(i,\text{“}a\text{”})$ the proportion of time colour a spends in Chain i ..... Page 129

$\mathrm{E}\left[L_{2n}(\mathscr{E}^c(*))\right]$ the expected length of the large uSAW in a randomly-selected, $(2n)$-edge, property-$*$ Θ-SAP ..... Page 88

$\mathrm{E}\left[S_{2n}(\mathscr{E}^c(*))\right]$ the expected length of the small uSAW in a randomly-selected, $(2n)$-edge, property-$*$ Θ-SAP ..... Page 88

$\mathrm{E}_\pi(f)$ the mean of the stationary stochastic process $f(\mathcal{X})$ with respect to the distribution π ..... Page 117

$\Pr^{\Theta}_{n_1,n_2}(*)$ the probability of observing a property-$*$ Θ-SAP given that the Θ-SAP has length in $[n_1, n_2]$ ..... Page 261

$\mathrm{var}_{\boldsymbol{\pi}}\left(\langle f\rangle_n\right)$ an estimator for the sample variance of $\langle f\rangle_n$ ..... Page 120

$\mathrm{var}_\pi(f)$ the variance of the stationary stochastic process $f(\mathcal{X})$ with respect to the distribution π ..... Page 117

Φ the set of properties $\{\phi, (\phi, s), (\phi, f)\} \cup \mathscr{K}^\dagger(\phi)$ ..... Page 56

ϕ the notation used to denote the knot-type referred to as the unknot ..... Page 11

$\Phi(K)$ the set of properties $\{K, (K, s), (K, f)\} \cup \mathscr{K}^\dagger(K)$ ..... Page 56

$\Pr^{\Theta}(K'|K, s)$ the limiting $(K \to K')$-transition knotting probability for the LSP Model Page 71

$\Pr^{\Theta}(K, f)$ the limiting failed strand passage probability for knot-type K Θ-SAPs Page 71

$\Pr^{\Theta}(K, s)$ the limiting successful strand passage probability for knot-type K Θ-SAPs Page 71

$\Pr^{\Theta}_{2n}(K'|K, s)$ the probability of a knot-type K' SAP given a $(2n)$-edge, knot-type K, successful-strand-passage Θ-SAP ..... Page 70

$\Pr^{\Theta}_{2n}(K, f)$ the probability of a failed strand passage in a $(2n)$-edge, knot-type K, Θ-SAP Page 70

$\Pr^{\Theta}_{2n}(K, s)$ the probability of a successful strand passage in a $(2n)$-edge, knot-type K, Θ-SAP ..... Page 70

$\Pr_n(K)$ the probability that an n-edge SAP in $\mathbb{Z}^3$ has knot-type K ..... Page 41

$\rho_f(h)$ the autocorrelation function for the stationary stochastic process $f(\mathcal{X})$ with respect to the distribution π ..... Page 117

$\sigma^2_{s_0^{(r)},j}(h)$ the conditional variance of $h(X_j^{(r)})$ starting in state $s_0^{(r)}$ ..... Page 123

$\sqrt{\hat{R}_j}$ the estimated potential scale reduction ..... Page 128

$\widehat{\tau}_{\text{int},S}$ the estimated integrated autocorrelation using a series/windowing analysis defined by Equation 4.75 . . . . . Page 138

$\widehat{\tau}_{\text{int},W}$ the estimated integrated autocorrelation using a warm-up analysis defined by Equation 4.72 . . . . . Page 138

$\widehat{\tau}^{(r)}_{\text{int},W}$ the estimated integrated autocorrelation from Replication r using a warm-up analysis . . . . . Page 138

$\widehat{\tau}_{\text{int}}$ the estimated integrated autocorrelation defined by Equation 4.77 . . . . . Page 139

$\widetilde{\text{pr}}^{\Theta}_{2n}(*)$ the point estimate for $\text{Pr}^{\Theta}_{2n}(*)$ based on the CMC Θ-BFACF data from all n_0 replications . . . . . Page 258

$\xi_{\mathscr{V}}(\omega)$ the indicator function which returns one if $\omega \in \mathscr{V}$ and zero otherwise . . . Page 179

$\mathbb{Z}^d$ the d-dimensional hyper-cubic lattice . . . . . Page 23

A the amplitude in the scaling form for the number of n-edge SAPs in $\mathbb{Z}^3$ . . . Page 33

A_ϕ the amplitude in the scaling form for the number of n-edge unknotted SAPs in $\mathbb{Z}^3$ Page 33

A_K the amplitude in the scaling form for the number of n-edge knot-type K SAPs in $\mathbb{Z}^3$ . . . . . Page 33

A_R the amplitude in the scaling form for the radius of gyration of the set of n-edge SAPs in $\mathbb{Z}^3$ . . . . . Page 39

$A_R(K)$ the amplitude in the scaling form for the radius of gyration of the set of n-edge knot-type K SAPs in $\mathbb{Z}^3$ . . . . . Page 40

$A^{\Theta}_{\mathscr{E}}(*)$ the amplitude in the $n \to \infty$ asymptotic form for $r^2\left(\mathscr{E}_{2n}(*)\right)$ . . . . . Page 92

$A^{\Theta}_{\mathscr{E}^c}(*)$ the amplitude in the $n \to \infty$ asymptotic form for $r^2\left(\mathscr{E}^c_{2n}(*)\right)$ . . . . . Page 92

$A^{\Theta}_{\mathscr{P}}(*)$ the amplitude in the $n \to \infty$ asymptotic form for $r^2\left(\mathscr{P}^{\Theta}_{2n}(*)\right)$ . . . . . Page 92

$A^{\Theta}_{\mathfrak{w}_e(\mathscr{E})}(*)$ the amplitude in the $n \to \infty$ asymptotic form for $r^2\left(\mathfrak{w}_e(\mathscr{E}_{2n}(*))\right)$ . . . . . Page 92

$A^{\Theta}_{\mathfrak{w}_l(\mathscr{E}^c)}(*)$ the amplitude in the $n \to \infty$ asymptotic form for $r^2\left(\mathfrak{w}_l(\mathscr{E}^c_{2n}(*))\right)$ . . . . . Page 93

$A^{\Theta}_{\mathfrak{w}_s(\mathscr{E}^c)}(*)$ the amplitude in the $n \to \infty$ asymptotic form for $r^2\left(\mathfrak{w}_s(\mathscr{E}^c_{2n}(*))\right)$ . . . . . Page 93

B_{n_0,t_0} the between-the-replication variance . . . . . Page 126

c_n the number of distinct n-step SAWs in $\mathbb{Z}^3$ starting at the origin . . . . . Page 25

c^d_n the number of distinct n-step SAWs in $\mathbb{Z}^d$ starting at the origin . . . . . Page 25

$c^d_n[k,(P,Q)]$ the number of elements in $\mathscr{C}^d_n$ for which (P,Q) occurs at no more than k different steps . . . . . Page 30

$c^d_n[k,P]$ the number of elements in $\mathscr{C}^d_n$ for which the pattern P occurs at no more than k different steps . . . . . Page 30

$p_n^{\Theta}(K)$ the number of n-edge self-avoiding polygons in $\mathscr{P}^{\Theta}(K)$ . . . . . Page 56

$p_n^{\Theta}(K,f)$ the number of n-edge self-avoiding polygons in $\mathscr{P}^{\Theta}(K)$ for which strand passage is not viable about Θ . . . . . Page 56

$p_n^{\Theta}(K,s)$ the number of n-edge self-avoiding polygons in $\mathscr{P}^{\Theta}(K)$ for which strand passage is viable about Θ . . . . . Page 56

$q_n(K)$ the number of n-step SAPs in $\mathbb{Z}^3$ that are rooted at the origin and have knot-type K . . . . . Page 28

q_n^d the number of n-step SAPs in $\mathbb{Z}^d$ that are rooted at the origin . . . . . Page 25

$q_n^d[k,(P,Q)]$ the number of elements in $\mathscr{Q}_n^d$ for which (P,Q) occurs at no more than k different steps . . . . . Page 30

$q_n^d[k,P]$ the number of elements in $\mathscr{Q}_n^d$ for which the pattern P occurs at no more than k different steps . . . . . Page 30

$r^2(\mathscr{U}_n)$ the mean-square radius of gyration of the polygons in the set of n-edge polygons denoted $\mathscr{U}_n$ . . . . . Page 38

$r^2(\omega)$ the square radius of gyration of the polygon ω in $\mathbb{Z}^3$ . . . . . Page 38

$r^2_{\boldsymbol{\pi}}(\mathscr{U})$ the mean-square (with respect to the p.m.f. $\boldsymbol{\pi}$) radius of gyration of the varying length polygons in the set denoted $\mathscr{U}$ . . . . . Page 39

$r^2(f(\mathscr{U}_{2n}))$ the f-transformed mean-square radius of gyration for the set $\mathscr{U}_{2n}$ . . . Page 91

$r^2\left(\mathfrak{w}_e(\mathscr{E}_{2n}(*))\right)$ the expected mean-square radius of gyration for the equal-sided uSAWs in a randomly chosen element from $\mathscr{E}_{2n}(*)$ . . . . . Page 92

$r^2\left(\mathfrak{w}_l(\mathscr{E}^c_{2n}(*))\right)$ the expected mean-square radius of gyration for the large uSAWs in a randomly chosen element from $\mathscr{E}^c_{2n}(*)$ . . . . . Page 93

$r^2\left(\mathfrak{w}_s(\mathscr{E}^c_{2n}(*))\right)$ the expected mean-square radius of gyration for the small uSAWs in a randomly chosen element from $\mathscr{E}^c_{2n}(*)$ . . . . . Page 93

$r^2\left(\mathscr{E}_{2n}(*)\right)$ the expected mean-square radius of gyration for a randomly chosen element from $\mathscr{E}_{2n}(*)$ . . . . . Page 92

$r^2\left(\mathscr{E}^c_{2n}(*)\right)$ the expected mean-square radius of gyration for a randomly chosen element from $\mathscr{E}^c_{2n}(*)$ . . . . . Page 92

$r^2\left(\mathscr{P}^{\Theta}_{2n}(*)\right)$ the expected mean-square radius of gyration for a randomly chosen element from $\mathscr{P}^{\Theta}_{2n}(*)$ . . . . . Page 92

$r^2_{\boldsymbol{\pi}(M)}(f(\mathscr{U}))$ the f-transformed mean-square (with respect to the p.m.f. $\boldsymbol{\pi}(M)$) radius of gyration for the set $\mathscr{U}$ . . . . . Page 91

$s_0^{(r)}$ the initial starting state of $\mathcal{X}_k^{(r)}$ . . . . . Page 122

$s_{|\omega|}(\omega)$ the length of the small uSAW in an unequal-sided Θ-SAP ω . . . . . Page 88

$w_B^*(2n)$ the number of SAPs in $\mathscr{B}_{2n}(*)$ . . . . . Page 85

$w_E^*(2n)$ the number of SAPs in $\mathscr{E}_{2n}(*)$ ..... Page 85

$w_S^*(2n)$ the number of SAPs in $\mathscr{S}_{2n}(*)$ ..... Page 85

$w_+(\omega)$ the uSAW in $\omega \in \mathscr{P}_n^{\Theta}(\phi)$ connecting the vertices $(1,0,0)$ and $(0,1,-2)$ ... Page 82

$w_-(\omega)$ the uSAW in $\omega \in \mathscr{P}_n^{\Theta}(\phi)$ connecting the vertices $(-1,0,0)$ and $(0,-1,-2)$ Page 82

$w_B(2n)$ the number of SAPs in $\mathscr{B}_{2n}$ ..... Page 85

$w_E(2n)$ the number of SAPs in $\mathscr{E}_{2n}$ ..... Page 85

$w_S(2n)$ the number of SAPs in $\mathscr{S}_{2n}$ ..... Page 85

W_{n_0,t_0} the within-the-n_0-replication variance ..... Page 126

z_ϕ the critical point (radius of convergence) of the ordinary generating function for $(p_{2n}(\phi))_{n=0}^{\infty}$ ..... Page 35

$z_p(d)$ the critical point (radius of convergence) of the ordinary generating function for $(p_{2n}^d)_{n=0}^{\infty}$ ..... Page 35

z_Θ the critical value for $\breve{Q}(z,M)$ ..... Page 69

colour(X) the colour assigned to state X ..... Page 129

SAP the acronym for self-avoiding polygon ..... Page 23

SAW the acronym for self-avoiding walk ..... Page 23

uSAW the acronym for undirected self-avoiding walk ..... Page 53

Chapter 1

Introduction

The work presented in this thesis is inspired by two open questions. The first question was proposed by D. W. Sumners at the 1998 Program in Mathematics and Molecular Biology Short Course held in Berkeley, California from June 22 to July 3:

Problem 1.1 *If a local strand passage occurs at a random location within a ring polymer with knot-type K, with what probability will the ring polymer be transformed into a ring polymer with knot-type K'?.*

The second question is motivated by Problem 1.1, that is

Problem 1.2 *Is there any difference in the "size" of a ring polymer whose knot-type changes after a local strand passage at a random location when compared to those ring polymers whose knot-type does not change after the strand passage?*

Problem 1.1 is motivated (cf. Section 1.1) by trying to better understand a particular enzyme's action on DNA. The first step in addressing Problems 1.1 and 1.2 is to model the entanglement complexity of a ring polymer, that is to model a local strand passage occurring at a random location within a ring polymer with a fixed knot-type. The model used in this work to study Problems 1.1 and 1.2 was developed by the author in his M.Sc. thesis [150]. This model, defined precisely in Section 2.1, is from here-on-in referred to as the *Local Strand Passage Model for Ring Polymers with fixed knot-type K* or simply the *Local Strand Passage (LSP) Model*. Because self-avoiding polygons (defined in Section 1.3) on the simple cubic lattice have been used since the 1960's to model ring polymers [53], the LSP Model is a self-avoiding polygon model. For $K = \phi$, the unknot, to address Problem 1.1 using the LSP Model, the proportion of $(2n)$-edge unknotted self-avoiding polygons associated with the LSP Model (Θ-SAPs) which have knot-type K' after a successful strand passage must be determined. This proportion is denoted $\frac{p^{\Theta}_{2n}(K'|\phi,s)}{p^{\Theta}_{2n}(\phi,s)}$.

Properties of $p_{2n}^{\Theta}(K'|\phi, s)$ and $p_{2n}^{\Theta}(\phi, s)$ are explored in Chapter 2. In Chapters 2 through 7 a new technique, that is based on the LSP Model and is designed to address Problems 1.1 and 1.2, is presented. This new approach can be viewed as a new general technique for investigating similar models.

Being consistent with the view that this work provides a new general technique for investigating similar models, the document will be structured as follows. Chapter 1 first provides an overview of the thesis. Then the remainder of the chapter is dedicated to outlining the motivation for the work and providing the basic terminology and theory that are required to formulate and study the thesis problems. Chapters 2 through 7 include a demonstration of how this new technique can be used to address Problems 1.1 and 1.2 for the case where the initial ring polymer is unknotted.

In Chapter 2, the reader is introduced to the Local Strand Passage Model that the author developed in [150]. The chapter then presents proofs of new theoretical results regarding the growth rates for $p_{2n}^{\Theta}(*)$, the number of $(2n)$-edge Θ-SAPs having a certain property $*$, and presents conjectures regarding the possible relationships amongst the growth rates of $p_{2n}^{\Theta}(*)$ for different properties $*$. An example of such a property is the property that an after-strand-passage unknotted Θ-SAP has knot-type K' and, for this property, $p_{2n}^{\Theta}(*) = p_{2n}^{\Theta}(K'|\phi, s)$. Then assuming $p_{2n}^{\Theta}(*)$ has a particular asymptotic $(n \to \infty)$ form which is defined in terms of a critical exponent α_*^{Θ}, the chapter includes conjectures regarding the relationships amongst the exponents α_*^{Θ}, for different properties $*$. Next several different probabilities that can be defined using $p_{2n}^{\Theta}(*)$ (for example $\frac{p_{2n}^{\Theta}(K'|\phi,s)}{p_{2n}^{\Theta}(\phi,s)}$) are introduced and possible asymptotic $(n \to \infty)$ forms for these probabilities are conjectured. These probabilities are of the type that allow Problem 1.1 to be addressed. To address Problem 1.2 for $K = \phi$, the unknot, the chapter concludes by introducing two measures for the "size of a knot" in a Θ-SAP and by posing several conjectures and questions (regarding how these measures behave as polygon length increases) that will be explored numerically throughout the remainder of this thesis.

Because numerically investigating the conjectures and questions posed in Chapter 2 requires computer simulation, Chapter 3 focuses on simulating the LSP Model. The background material necessary to develop a Composite Markov Chain Monte Carlo (CMCMC) algorithm to study the LSP Model is first provided. Then the Θ-BFACF algorithm and its CMCMC implementation (to be referred to as the CMC Θ-BFACF algorithm) that

were developed in [150] to study the LSP Model are reviewed. The chapter ends with the details of a simulation consisting of ten replications of the CMC Θ-BFACF algorithm.

Chapter 4 discusses several techniques that can be used to determine whether the data generated from a Markov Chain Monte Carlo (MCMC) algorithm is sampled from the desired equilibrium distribution. To this end, three methods for estimating the amount of time a simulation takes to reach its equilibrium distribution are presented. Because of the correlation that exists between the states of a Markov chain, methods for determining the number of time steps that must pass between two states before the two states can be considered essentially independent are also provided. The chapter then provides an algorithm for determining which data generated can be considered "reliable" and discusses how certain functions of the data might be expected to behave. The techniques and algorithms presented throughout the chapter are then applied to the data generated using the CMC Θ-BFACF algorithm. The results of these applications are analyzed, discussed, and used to verify the consistency of the data generated and the programs written to analyze the data.

Having verified the consistency of the CMC Θ-BFACF data, the focus of the fifth chapter is the design and implementation of a new maximum likelihood estimation method, based on the method introduced by Berretti and Sokal [7], that uses the CMC Θ-BFACF data to estimate unknown parameters in the CMC's equilibrium distribution. This method is referred to as Composite Markov Chain Maximum Likelihood Estimation (CMC MLE). To this end, the notation, definitions, and theorems required throughout the chapter are first reviewed. A procedure for estimating the required length of a CMCMC simulation to achieve a given confidence interval width is then discussed. The remainder of the chapter then focuses on the new CMC MLE technique. First a CMC MLE technique is developed, including how to estimate the corresponding $(1-\alpha)\cdot 100\%$ margin of error and the systematic error associated with each of the parameters estimated. The chapter concludes by applying the CMC MLE technique to the CMC Θ-BFACF data and uses the estimates generated to numerically verify some of the facts and conjectures posed in Chapter 2 regarding the growth rates of $p_{2n}^{\Theta}(*)$ and the exponents α_{*}^{Θ}, respectively.

Chapter 6 focuses on using the CMC Θ-BFACF data to study the fixed-n and limiting transition probabilities (that are introduced in Chapter 2). One method for estimating the fixed-n transition probabilities is presented and two methods for estimating the limiting

transition probabilities are discussed and compared. The method for estimating the fixed-n transition probabilities and the better of the two methods for estimating the limiting transition probabilities are then applied to the CMC Θ-BFACF data. The chapter ends by presenting the estimated limiting transition probabilities.

The seventh chapter is a preliminary discussion of the two measures of the "size of a knot" in a self-avoiding polygon that are used to study Problem 1.2 and are introduced in Chapter 2. The CMC Θ-BFACF data is first used to explore the validity of the conjectures posed and to answer the questions asked in Chapter 2 regarding the first measure of the "size of a knot", that is the length of the undirected self-avoiding walks (as introduced in Section 2.2.3) comprising a Θ-SAP. The CMC Θ-BFACF data is then used to test the validity of the conjectures posed and to answer the questions asked in Chapter 2 regarding the second measure of the "size of a knot", that is the mean-squared radii of gyration of the undirected self-avoiding walks comprising a Θ-SAP. A method for estimating the parameters in the asymptotic form of the expected mean-squared radius of gyration of the undirected self-avoiding walks is then outlined and used to estimate these parameters. These estimates are then used to explore the conjectures and questions posed in Chapter 2 regarding the parameters in these asymptotic forms. The final discussion in the chapter begins by presenting a second method for estimating the parameters in the asymptotic form of the expected mean-squared radius of gyration of the undirected self-avoiding walks and ends with a comparison of the two methods.

Chapter 8 begins with a summary of the thesis. It then provides directions that remain to be explored. Appendix A provides additional information that is either referred to or used repeatedly throughout the thesis. Appendix B includes some of the sequences of data that are used in Chapters 6 and 7.

Before the work laid out in the above outline is presented, a question that comes to mind is "Why is Problem 1.1 of interest?". This question is answered in the next section.

1.1 Motivation

The definitions in this and the subsequent paragraph are based on the discussion of polymers in [103]. A *polymer* is a molecule formed by combining small molecular units, called *monomers*, into long chains via chemical bonds. The number of chemical bonds available

to a monomer is called the *functionality of the monomer*. A polymer that is made of a string of bonded monomers, each of which has functionality two, is either terminated at each of its ends by a monomer with functionality one or its ends bond to each other. These polymers are respectively called linear and ring polymers. A molecule that is formed by combining different kinds of monomers (called *comonomers*) is called a *copolymer*. A *linear copolymer* is a copolymer that is comprised of a string of bonded comonomers with functionality two that is terminated on both ends by a comonomer with functionality one.

A polymer is said to be in *dilute solution with a good solvent* if it is more favourable for the (co)monomers of the (co)polymer to be surrounded by solvent molecules rather than other (co)monomers (either from the same or from another (co)polymer). For (co)polymers in dilute solution, the *excluded volume* is the region surrounding each (co)monomer in which the probability of finding another (co)monomer is zero.

A single strand of a DNA (deoxyribonucleic acid) molecule [6] is an example of a linear copolymer because the strand is comprised of four distinct, functionality-two, monomers, which are referred to as *nucleotides*. The four types of nucleotides each have three components: a sugar; a phosphate; and one of the bases adenine, guanine, thymine, and cytosine. A single strand of DNA is formed when the sugar molecule in one nucleotide binds to the phosphate molecule in the subsequent nucleotide. To form double-stranded DNA, two single strands of DNA are bound together via hydrogen bonding, a different kind of bonding than to what the functionality refers.

In the early 1960's, there was much interest in studying the DNA of viruses, in particular polynoma, a DNA tumor virus [31, 159, 168]. In [31], Dulbecco and Vogt showed that polynoma's DNA must be a closed circular ring polymer. In fact, the circular nature of polynoma's DNA is not a rare occurrence in nature; it is now commonly accepted that the DNA of most bacteria and viruses is circular [160] and the DNA of most animals and plants is linear. In 1976, Liu *et al.* [94] first observed knots in single-stranded circular DNA. Figure 1.1 provides two examples of circular DNA that is knotted. Both examples are in fact trefoils and were originally published in [86]. Although the DNA of plants and animals is linear, it is susceptible to topological constraints similar to those that affect circular DNA because linear DNA is attached at several points to a protein scaffold and is highly self-entangled and compacted within the nucleus of a cell [6].

Whether the topological constraints are the result of the DNA being circular or being

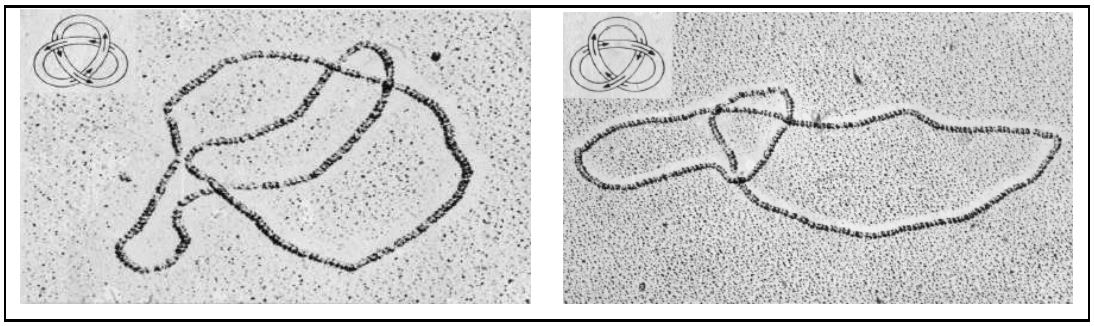

Figure 1.1: Examples of circular DNA that are right and left-handed trefoils. Reproduced from [86] with permission from the author.

linear and attached to a protein scaffold, the constraints can interfere with metabolic processes, such as DNA replication and transcription [18]. In order for the DNA illustrated in Figure 1.1 to be replicated, the DNA first must be unknotted and unwound and then, near the end of the replication process, the mother and daughter strands of DNA, which are linked together, must be unlinked. The replication process requires a solution to these entanglement and linking problems. It just so happens that the solutions to both these problems are an enzyme. Experimental evidence indicates that the enzyme needed to unknot and unwind the DNA strand is the same enzyme which unlinks the two replicated strands of DNA [137, 165]. This enzyme belongs to the group of enzymes referred to as topoisomerases [6].

Topoisomerases are enzymes that act locally (via a strand passage) on either single or double stranded DNA. The topoisomerase enzyme initiates the passage of one segment of DNA through another strand of DNA by first binding to the DNA strand, breaking the DNA strand, passing a second strand of DNA through the opening, and then sealing the break [6]. It is this action of the topoisomerase which unwinds and unlinks the DNA during the replication process. In essence, the topoisomerase enzymes are responsible for unknotting, unlinking, and maintaining the proper supercoiling of DNA during the replication process. These enzymes have the ability to, through local actions on the DNA molecule, alter the global properties of the molecule. In fact, the result of this very local strand passage is a possible change in the topology of the DNA molecule. This prompted researchers to look for ways, *in vitro* and *in silico*, to study these changes in topology within DNA molecules.

Much *in vitro* experimental work has been conducted to study DNA topology and the

relationship between the topoisomerase enzymes and DNA topology, cf. [130, 133, 138, 140, 164] for a few examples. Mann [106] experimentally showed that human topoisomerase IIα enzymes very efficiently unknot DNA molecules whose knot-type is either a 5-crossing or 7-crossing twist knot. (A twist knot and its clasp region are defined in Definition 1.12 of Section 1.2.) Her experimental work suggested that the enzyme preferred to act on the clasp region of the twist knot; the consequence of such an interaction was that the DNA was unknotted.

To further explore the results of Mann's experimental work, Liu *et al.* [96] created a lattice model to study how the local geometry of the strand passage site impacts the after-strand-passage knot-type. Whether the enzyme acts at random locations on the DNA is still an open question in molecular biology but Mann's experimental work [106] and Liu *et al.*'s [96] simulation of their lattice model suggest that the topoisomerase enzymes are not acting at locations completely chosen at random. Understanding exactly how the topoisomerase enzymes perform the unknotting task with a seemingly high rate of success is still an open problem in molecular biology. The work embodied in this thesis approaches the problem from a direction that differs from that presented in [96]. Instead of modelling the unknotting of a knotted ring polymer via strand passages (as in [96]), this work models the knotting of unknotted ring polymers via a strand passage about a fixed location in an unknotted polygon and studies some statistics (and their dependence on polygon length as the length tends to infinity) associated with this model.

The interest in knotting in long ring polymers is not just a recent consequence of trying to better understand the DNA replication process. The interest first appeared about a decade after Watson and Crick [167] proposed their model for the structure of DNA. Knotting in long ring polymers was first discussed by Frisch and Wasserman in 1961 [39] and by Delbruck in 1962 [24]. In both of these papers, the authors conjectured that the knotting probability was one for infinitely long ring polymers, that is:

Conjecture 1.1.1 ([39, 24]) *For a randomly closed chain of length n, the knot probability tends to unity as n tends to infinity.*

The above conjecture, now referred to as the *Frisch-Wasserman-Delbruck Conjecture*, was proved in 1988 by Sumners and Whittington [149] and independently in 1989 by Pippenger [129] using self-avoiding polygons (SAPs) (defined in Definition 1.3.2 of Section 1.3)

in $\mathbb{Z}^3$ by showing that exponentially few sufficiently long self-avoiding polygons embedded in $\mathbb{Z}^3$ are unknotted. (For the precise result proved by Sumners and Whittington in [149], cf. Theorem 1.3.5 in Section 1.3.) Soteros, Sumners, and Whittington [145] extended the results of [149] in several directions. In particular, they showed that all but exponentially few sufficiently long self-avoiding polygons in $\mathbb{Z}^3$ are highly composite knots, with any knot-type appearing numerous times in the prime knot factorization (cf. Section 1.2 for the definitions of prime and composite knots).

In addition to the above theoretical results, much numerical work has been completed in order to estimate the rate of increase of the knotting probability with polymer length. The first detailed *in silico* work studying models of knotted ring polymers was conducted in 1974 by Vologodskii *et al.* [163] using an off-lattice model. The first detailed *in silico* studies using lattice models of ring polymers did not follow for more than a decade later because the algorithms commonly used at the time to simulate self-avoiding polygons were generally either computationally inefficient or were known to not sample from the entire sample space. In 1969, Lal [89] proposed an algorithm (referred to here as the "Pivot Algorithm") for simulating fixed length lattice polygons, but at the time, the algorithm's efficiency was unknown. Although estimates for the knotting probability with respect to lattice polygon length were computed by Michels and Wiegel in 1982 [112] and 1986 [113], further estimates were not computed until the 1990's (Janse van Rensburg and Whittington in 1990 [67], Deguchi and Tsurusaki in 1994 [20], E. Orlandini, M. C. Tesi, E. J. Janse van Rensburg, and S. G. Whittington in 1998 [125], and Janse van Rensburg in 2002 [65], as just a few examples) because it was not until 1988 and 1990 respectively that Dubins *et al.* [30] and Madras *et al.* [102] proved that the Pivot Algorithm was a very efficient algorithm for simulating lattice polygons.

Then, in [148], Sumners bridged the topological and molecular biological worlds by showing that the mathematical construct of a knot can be used to characterize, and hence study, the actions of the topoisomerase enzyme via the *unknotting number of a knot*, that is the minimum number of crossing changes that must be implemented to convert a knot into the unknot. In 1996, Darcy [18] defined a strand-passage metric on knot-types to be the minimal number of strand passages necessary to convert knot K_1 into K_2. The importance of this metric for studying the actions of topoisomerases with DNA is that, in addition to providing the minimum number of times topoisomerase enzymes must implement a strand

passage to change one knot into another knot, the metric provides a tool for determining every possible sequence of steps necessary to transform one knot-type into another knot-type.

Because DNA-topoisomerase interactions can produce a variety of knots by performing strand-passages in DNA, the results of Sumners and Darcy can be combined to identify the possible knot-types that can result from the DNA-topoisomerase interactions. In other words, the combined results of Sumners and Darcy can be used to identify the possible knot-types that can result after a single strand passage occurs at a location within a ring polymer (relevant to Problem 1.1).

The first step in addressing Problem 1.1 is to model a local strand passage occurring at a random location within a ring polymer with a fixed knot-type. This model is the LSP Model mentioned in the Introduction. To define the LSP Model, some definitions and terminology are needed and hence are presented throughout the remainder of this chapter.

1.2 What is a Knot?

Unless otherwise referenced, the discussion in this section is based on [136]. To precisely define a knot, let

$$\mathbb{S}^1 := \{(x_1, x_2) \in \mathbb{R}^2 : \sqrt{x_1^2 + x_2^2} = 1\} \tag{1.1}$$

be the unit circle and, for two sets A and B and the map $g : A \to B$, let the notation $g(A)$ represent the set

$$g(A) := \bigcup_{x \in A} \{g(x)\} \subseteq B. \tag{1.2}$$

Then any map k from $\mathbb{S}^1$ to $\mathbb{R}^3$, $k : \mathbb{S}^1 \to \mathbb{R}^3$, is said to be an *embedding of the unit circle into Euclidean 3-space*. A subset $K \subset \mathbb{R}^3$ is said to be a *knot* if K is homeomorphic to $\mathbb{S}^1$, that is if there exists an embedding k of the unit circle into Euclidean 3-space such that k is a homeomorphism satisfying $k(\mathbb{S}^1)=K$. Denote such an embedding of $\mathbb{S}^1$ into $\mathbb{R}^3$ by $(k; \mathbb{S}^1, \mathbb{R}^3)$, or briefly by k, and denote the resulting knot by K. If a direction was initially associated with $\mathbb{S}^1$ then the resulting knot is said to be an *oriented knot*. Refer to Figure 1.2 for an illustration of the definition of the knot K.

Two knots F and G (with respective associated homeomorphisms f and g) are said to be *equivalent* if there is a homotopy $h : \mathbb{R}^3 \times [0, 1] \to \mathbb{R}^3$ such that $h(f(\mathbb{S}^1), 0) = f(\mathbb{S}^1) = F$, $h(f(\mathbb{S}^1), 1) = g(\mathbb{S}^1) = G$, and $h(\mathbb{R}^3, t)$ is a homeomorphism for every $t \in [0, 1]$. This

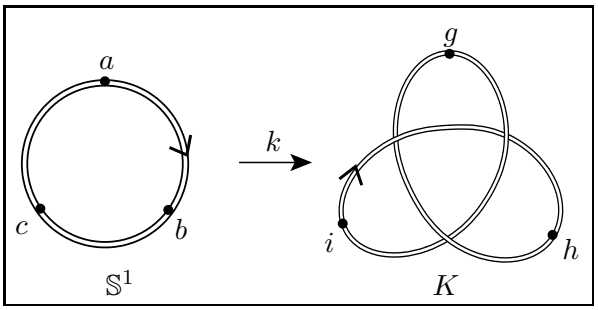

Figure 1.2: $\mathbb{S}^1$ is the unit circle in $\mathbb{R}^2$ centered at $(0,0)$ and K is the knot resulting from applying the map $k : \mathbb{S}^1 \to \mathbb{R}^3$ such that, for example, $k(a) = g, k(b) = i$, and $k(c) = h$.

equivalence relation partitions the set of all knots in $\mathbb{R}^3$. The resulting equivalence classes of knots are referred to as *knot-types*. Two knots F and G are said to be distinct if F and G are not equivalent, that is F and G do not have the same knot-type.

A *polygonal knot* in $\mathbb{R}^3$ is a knot embedded in $\mathbb{R}^3$ that is the union of a finite number of closed linear segments called *edges*. The endpoints of these linear segments are referred to as *vertices*. A knot in $\mathbb{R}^3$ that is not a polygonal knot is simply referred to as a *non-polygonal knots*.

In order to work with knots more effectively, it is useful to convert a three dimensional knot into a two dimensional representation. To create a two dimensional rendering of a knot K, some terminology and theorems are required. The following definitions and theorems have been adapted from [128]. Suppose K is the knot in $\mathbb{R}^3$ defined by the embedding $(k; \mathbb{S}^1, \mathbb{R}^3)$ and φ is the projection $\varphi : \mathbb{R}^3 \to \mathbb{R}^2$ defined by $\varphi((x, y, z)) = (x, y)$ for $(x, y, z) \in \mathbb{R}^3$. A point $\boldsymbol{a} \in \varphi(K)$ is called a *multiple point* if $\varphi^{-1}(\boldsymbol{a}) \cap K$ consists of more than one point. The *order* of $\boldsymbol{a} \in \varphi(K)$ is the cardinality of $\varphi^{-1}(\boldsymbol{a}) \cap K$. A *double point* in $\varphi(K)$ is a point with order 2. The projection φ of a knot K is said to be *regular* if there are only a finite number of multiple points in $\varphi(K)$, each of which is a double point. If K is a polygonal knot, the projection φ of K is said to be *regular* if there are only a finite number of multiple points in $\varphi(K)$, each of which is a double point, and if no double point in $\varphi(K)$ is the image of a vertex of K.

A knot K is considered to be in *regular position* if there exists a regular projection of K onto the xy-plane. The next theorem states that it is always possible to transform a polygonal knot into a polygonal knot in regular position.

Theorem 1.2.1 ([128]) *If K is a polygonal knot, then there is an arbitrarily small rota-*

tion of $\mathbb{R}^3$ *onto* $\mathbb{R}^3$ *that maps* K *into a polygonal knot in regular position.*

Theorem 1.2.1 leads to the following corollary.

Corollary 1.2.1 ([128]) *Every polygonal knot is equivalent to a polygonal knot in regular position.*

Suppose K is a knot in regular position. Then each double point in the regular projection of K is the image of two points in the original embedding. The locations of the double points in the regular projection are called *crossings*. For a particular crossing in the regular projection, there are two associated points in the original embedding. The point in the original embedding whose z-coordinate is larger is said to be an *overcrossing* and the other point is said to be an *undercrossing*. The segment of the projection going through an overcrossing (undercrossing) is called an *overcrossing (undercrossing) segment*.

A *knot projection* [8] is a regular projection of a knot K such that, at every crossing, the overcrossing segments and the orientation of the knot are marked. The image resulting from the knot projection of the knot K is called the *knot diagram* of K. Then the *crossing number of a knot* is the minimum number of crossings that appears in any knot diagram of the knot. Figure 1.3 contains illustrations of the knot diagrams of three distinct knots. If the number of crossings appearing in a knot diagram of a knot K is equal to the crossing number of K, then the knot diagram is referred to as a *minimal knot diagram*.

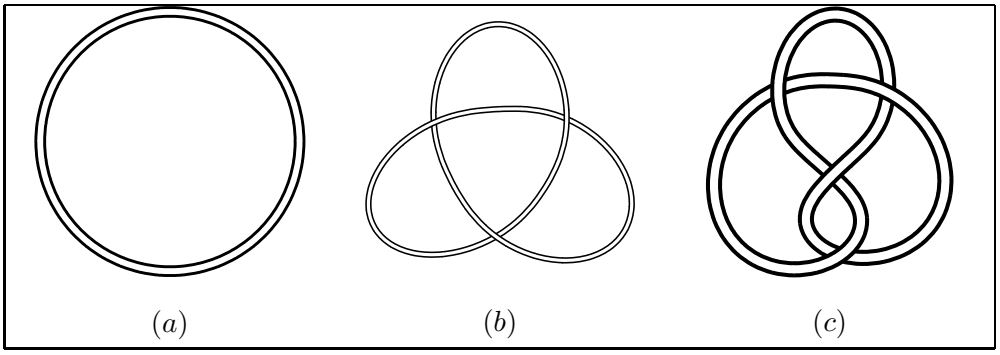

Figure 1.3: Examples of some common knots. The knot-type of a knot whose knot diagram is illustrated in (a) is referred to as the unknot. The knot-type of a knot whose knot diagram is illustrated in (b) is referred to as the right-handed trefoil. The knot-type of a knot whose knot diagram is illustrated in (c) is referred to as the figure 8.

The knot-type of a knot whose knot diagram is illustrated in Figure 1.3 (a) is referred to as the *unknot* and is denoted ϕ. The knot-type ϕ is referred to as the *trivial knot-type*.

Any other knot-type is referred to as a *non-trivial knot-type*. Similarly a knot whose knot-type is ϕ is referred to as a *trivial knot*, and a knot whose knot-type is non-trivial is referred to as a *non-trivial knot*. From this point forward, any reference to a knot in a figure will refer to a knot whose knot diagram is illustrated in the figure.

Suppose F and G are two oriented knots. The *connect sum of F and G*, denoted $F\#G$, is the knot resulting from placing F and G side by side and joining them as illustrated in Figure 1.4 in such a manner that the orientation is preserved in the sum. The reader is referred to [136] for a precise mathematical definition of $F\#G$.

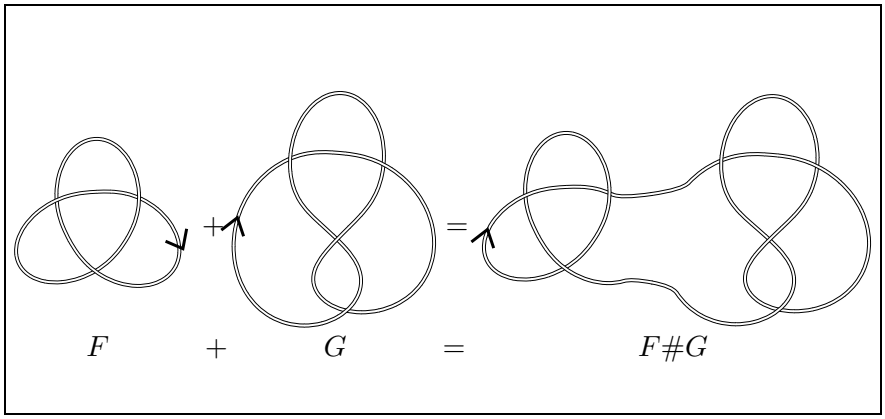

Figure 1.4: The connect sum of two knots F and G.

A knot is said to be *composite* if it can be represented as the connect sum of two non-trivial knots [17]. A knot that cannot be expressed as the connect sum of two non-trivial knots is referred to as *prime* [17]. In Figure 1.4, the knots labelled F and G are prime knots and the knot labelled $F\#G$ is composite.

For a given knot projection, suppose that, for a given crossing i in the knot projection, crossing i is relabelled so that its undercrossing segment becomes an overcrossing segment and its overcrossing segment becomes an undercrossing segment. This switching of an undercrossing segment with its overcrossing segment (and vice versa) at a crossing in a knot projection is referred to as a *strand passage*.

Consider a knot K in regular position whose knot diagram has n crossings. A knot K^* corresponding to the knot diagram formed by implementing a strand passage at each of the n crossings in the knot diagram of K is said to be a *mirror image* of K. If K and K^* are equivalent, then the knot K is said to be *achiral*. If no homotopy exists such that K and K^* are equivalent, then K is said to be *chiral*. For the knots whose knot diagrams

are presented in Figure 1.3, the trefoil (cf. Figure 1.3 (b)) is chiral and the figure 8 (cf. Figure 1.3 (c)) is achiral. Suppose K is a chiral knot. Then the knot-type of K is referred to as a *chiral knot-type*. If K is an achiral knot, then the knot-type of K is referred to as an *achiral knot-type*.

Suppose K is an oriented knot in regular position and D is a knot diagram of K. When traversing D in the direction imposed by the orientation of K, if a crossing has the form as illustrated in Figure 1.5, then the crossing is referred to as a *positive (or right-handed) crossing*. Otherwise, the crossing is said to be a *negative (or left-handed) crossing*.

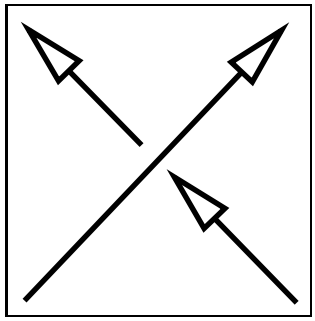

Figure 1.5: A right-handed (or positive) crossing.

Suppose K is a knot in regular position with chiral knot-type. Then the knot-type of the sets of knots that are homotopic to K and K^* are denoted c_i^+ and c_i^-, where c is the crossing number of K, i represents the i'th distinct knot-type (as defined in Rolfsen's Knot Table [136]) having crossing number c, and in this work the $+$ or $-$ in this work is assigned as follows. If a minimal knot diagram of K only contains positive crossings then its knot-type is c_i^+ and K^* has knot-type c_i^- [117]; if a minimal knot diagram of K only contains negative crossings then its knot-type is c_i^- and K^* has knot-type c_i^+ [117]; and otherwise the reader is referred to Liang and Mislow's algorithm [92] for the $+/-$ classification of the knots K and K^*. In this work, if K has knot-type c_i^+ then K is referred to as a *positive (or right-handed)* knot. If K has knot-type c_i^- then K is referred to as a *negative (or left-handed)* knot. For the purposes of this work, only chiral knots will be said to exhibit "handedness". For example, any knot that is equivalent to a knot whose knot diagram is illustrated in Figure 1.3 (b) has knot-type 3_1^+.

The notation 3_1^+ (also referred to as a *right-handed trefoil*) indicates that the minimum number of crossings in a knot projection of a right-handed trefoil is three and the tre-

foil (either right-handed or left-handed) was arbitrarily denoted to be the first knot-type whose minimal projection has three crossings. Further to this, Figure 1.3 (b) provides an illustration of a knot diagram corresponding to a knot whose knot-type is a right-handed trefoil. When a knot-type is achiral or chirality is not important, the superscripts + and − are dropped and the knot-type is simply denoted c_i. For example, the knot-type of a knot, whose knot diagram is illustrated in Figure 1.3 (c), is referred to as the *figure 8* and is denoted 4_1. The knot-types of the knots (ignoring chirality) whose knot projections minimally consist of five crossings are referred to as 5_1 and 5_2. Refer to Figure 1.6 for the knot diagrams of knots with knot-type 5_1 and 5_2. Note that although the subscripts assigned to each knot-type were initially assigned arbitrarily, they have since been adopted as convention [2].

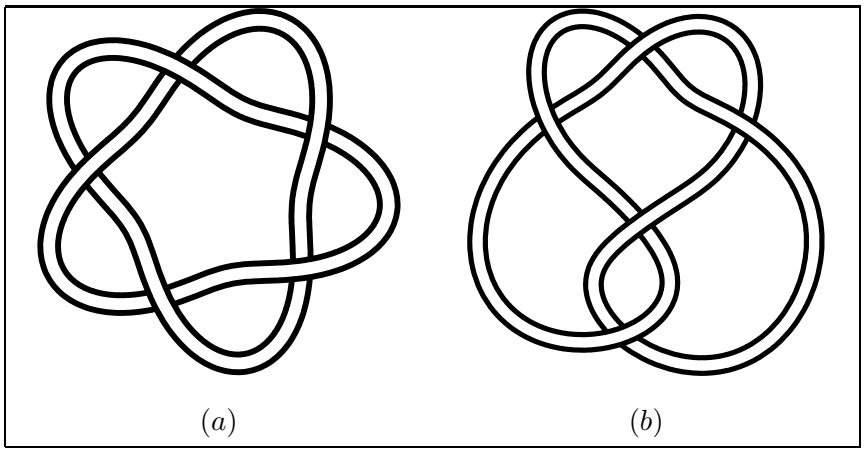

Figure 1.6: The knot-type of a knot whose knot diagram is illustrated in (a) is referred to as 5_1. The knot-type of a knot whose knot diagram is illustrated in (b) is referred to as 5_2.

Let φ_1 and φ_2 be two knot projections. φ_1 and φ_2 are said to be *equivalent projections* (as opposed to equivalent knots) if there exists a finite sequence of moves, referred to as the *Reidemeister moves* [135], which transforms φ_1 into φ_2 and vice versa. A *Reidemeister move* is one of three moves that can be used to change the positioning of the crossings in a knot projection. The first Reidemeister move, denoted Ω_1, allows a twist to be added to or removed from a knot, as illustrated in Figure 1.7. The second Reidemeister move, denoted Ω_2, allows two crossings to be added to or removed from a knot, cf. Figure 1.8. The final Reidemeister move, denoted Ω_3, allows a strand of a knot on one side of a crossing to slide to the opposite side of the crossing, cf. Figure 1.9.

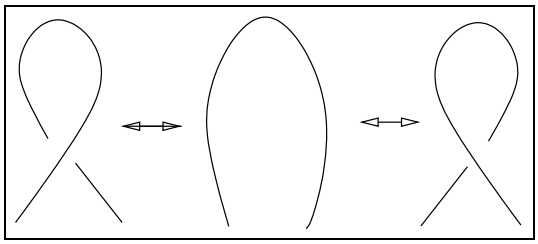

Figure 1.7: Reidemeister I Move (Ω_1).

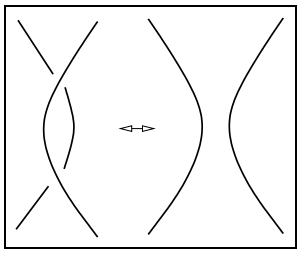

Figure 1.8: Reidemeister II Move (Ω_2).

It can be shown that two knots K_1 and K_2 have the same knot-type if and only if a knot projection of K_1 is equivalent to a knot projection of K_2 [136], that is, if and only if there is a finite sequence of Reidemeister moves that transforms the knot projection of K_1 into the knot projection of K_2. Because determining such a sequence of Reidemeister moves (if one exists) is not particularly easy, an efficient knot-type identification algorithm (that is, an algorithm more efficient than trying to find a sequence of Reidemeister moves) is desired. Such an algorithm, regardless of the initial presentation of the knot, should correctly identify the knot-type of the knot. Perhaps an easier route (rather than trying to determine a sequence of Reidemeister moves) for identifying the knot-type of a knot is

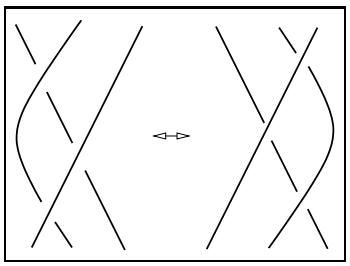

Figure 1.9: Reidemeister III Move (Ω_3).

to look for quantities ρ_i, such that $\rho_i(K_1) = \rho_i(K_2)$ for all equivalent knots K_1 and K_2. Any such quantity ρ_i is referred to as a *knot invariant*.

Although knot invariants do not necessarily uniquely identify the knot-types of knots, they can help reduce the problem of knot identification. One of the simplest knot invariants is the Alexander Polynomial [2]. Other knot invariants include the Jones Polynomial [77], the Kauffman Bracket Polynomial [81], and the HOMFLY Polynomial [38]. Because the Alexander Polynomial is to be used in this work, the algorithm for generating the Alexander Polynomial of a given knot will be discussed next.

1.2.1 Alexander Polynomials

Using the following procedure [163], the Alexander Polynomial of an arbitrary knot K can be determined.

1. Construct a knot projection $\varphi(K)$ of K.

2. Arbitrarily mark "0" on $\varphi(K)$ at a location which is not a multiple point. From this "0" assign a direction in which to traverse the contour of $\varphi(K)$.

3. Starting at "0", move along the contour of $\varphi(K)$ in the preassigned direction until reaching the first undercrossing. Label this undercrossing "1". Continue along the contour of $\varphi(K)$ in the preassigned direction labelling each consecutive undercrossing "2", "3", ... , "n", where n is the total number of distinct undercrossings, until one returns to the starting point "0". Denote undercrossing "i" by u_i.

4. The part of the contour lying between u_{k-1} and u_k, for $k = 2, \ldots, n$, is said to be the k^{th}-*overcrossing generator* and is denoted x_k, and the part of the contour lying between u_n and $u_{n+1} = u_1$ is said to be the 1^{st}-*overcrossing generator* and is denoted x_1.

   Define $x_{n+1} = x_1$, that is the $(n+1)^{th}$-overcrossing generator is the 1^{st}-overcrossing generator.

5. Classify the n undercrossings into the two categories: Type I and Type II, based on the direction of the overcrossing generator above each undercrossing, cf. Figure 1.10 (a) and (b).

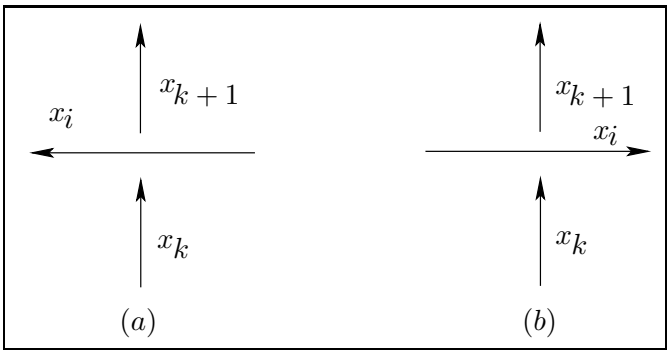

Figure 1.10: (a) is a Type I (negative) undercrossing and (b) is a Type II (positive) undercrossing.

6. Let j_g, for $j = 1$ to n, be the subscript of the overcrossing generator at the j'th undercrossing. For example, for the Type II undercrossing in Figure 1.10 (b), $k_g = i$. Every knot projection can be expressed as a sequence of undercrossings, each of whose type (I or II) and overcrossing generator label is known. This qualitative description of a knot projection can be converted into an $(n \times n)$-matrix referred to as the *Alexander Matrix*, denoted $M(\Delta(t))$, by letting the j^{th} row of $M(\Delta(t))$ represent the j^{th} undercrossing.

7. To construct $M(\Delta(t))$, let a_{ij} represent the (i, j)'th element of $M(\Delta(t))$.

   (a) Set $M(\Delta(t)) = \mathbf{0}$, where $\mathbf{0}$, that is an $n \times n$-matrix consisting entirely of zeroes.

   (b) If, for all $i, j \in \{1, \ldots, n\}$,

      i. $i_g = j$ or $i_g = j + 1$, regardless of the undercrossing type, then, in $M(\Delta(t))$, set

      $$a_{j,j} = -1, a_{j,j+1} = 1.$$

      ii. If u_j is a Type I, cf. Figure 1.10 (a), undercrossing, and $i_g \neq j$ and $i_g \neq j + 1$, then, in $M(\Delta(t))$, set

      $$a_{j,j} = 1, a_{j,j+1} = -t, a_{j,i_g} = t - 1.$$

      iii. If u_j is a Type II, cf. Figure 1.10 (b), undercrossing, and $i_g \neq j$ and $i_g \neq j + 1$, then, in $M(\Delta(t))$, set

      $$a_{j,j} = -t, a_{j,j+1} = 1, a_{j,i_g} = t - 1.$$

8. To construct the Alexander Polynomial $\Delta(t)$ from $M(\Delta(t))$,

(a) calculate the determinant of any $[(n-1)\times(n-1)]$ minor of $M(\Delta(t))$,

(b) multiply the determinant by $\pm t^{-m}$, where m is the smallest integer such that the resulting product is a polynomial in t, and the sign of t^{-m} is chosen in such a manner that the coefficient of the leading term of the resultant product is positive.

The Alexander Polynomials for knots with the same knot-type have been proven to be the same [2, 116], but two knots having the same Alexander Polynomial do NOT necessarily have the same knot-type. For instance, in the above construction of the Alexander Polynomial, note that the assignment of undercrossings (and therefore the type of each undercrossing) was dependent only on the direction chosen to traverse the contour of the knot. Since this direction was chosen arbitrarily, the relationship between the rows of the corresponding Alexander matrix and the type of each undercrossing is also arbitrary. Therefore, as long as the chosen direction remains fixed for the computation of the matrix for the entire knot, interchanging the type of undercrossing for all undercrossings in the knot does not change $\Delta(t)$. Hence $\Delta(t)$ cannot distinguish between a knot and its mirror image. In fact, it is known that the Alexander Polynomial fails to distinguish the difference:

1. between a knot and its mirror image (for example, the Alexander Polynomials of a trefoil and its mirror image are identical);

2. between some complex knots and the unknot (for instance the pretzel knot denoted (-3 5 7), as seen in Figure 1.11, and the unknot) [1]; and

3. between some particular complex knots. For instance 8_{11} has the same Alexander Polynomial as the composite knot-type $3_1^+ \# 6_1$ [126].

Note that the only knot-types that are of concern to this work have unknotting number one, that is those knots which can be transformed into the unknot via ONE strand passage, and that every unknotting number one knot is a prime knot. Also, for this work, note that because only right-handed knots are generated by the CMC Θ-BFACF Algorithm (as defined in Section 3.4 of Chapter 3), a knot does not need to be distinguished from its mirror image. Finally, note that because in this work no Θ-SAP is observed to have a length greater than 7000 and because in [173], Yao *et al.* estimate $\mathcal{N}(\phi)$ to be $(2.5 \pm 0.3) \times 10^5$ (where $\mathcal{N}(\phi)$ is the polygon length for which the unknot dominates the sets of SAPs with

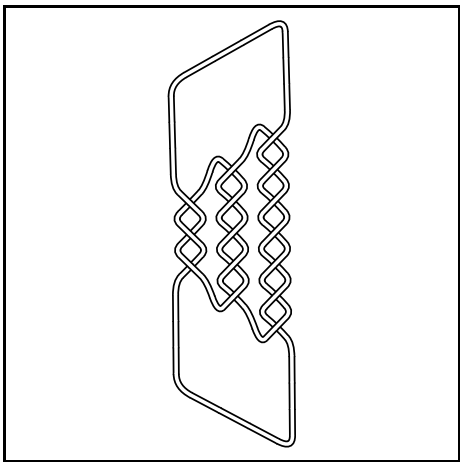

Figure 1.11: The Pretzel Knot (-3 5 7).

lengths less than $\mathcal{N}(\phi)$), very few complex knots are expected. Hence, for this work, the Alexander Polynomial is a suitable knot-type identifier and from this point forth, the superscripts + and − will be dropped from the notation for the different knot-types unless the chirality dependence is explicitly needed.

1.2.2 Unknotting Number One Knots

Examples of unknotting number one knots include the unknot, the trefoil, and the figure 8. The complete list of unknotting number one knots (up to and including 8 crossings) and their associated Alexander Polynomial is given in Table 1.1.

A special class of unknotting number one knots are the *twist knots*.

Definition 1.2.1 ([136]) *Given any $n \in \mathbb{Z}$, a twist knot is a knot which is formed by a twist region with $|2n|$ crossings all of the same sign as $(-1)n$ and a clasp consisting of two positive crossings, cf. Figures 1.12(a) and 1.12(b).*

In Figures 1.12(a) and 1.12(b), the two crossings aligned vertically near the top of the knot projection form the *clasp* of the twist knot. The $|2n|$ crossings aligned horizontally near the bottom of the knot projection form what is referred to as the *twist region* of the twist knot.

The trefoil and the figure 8 are the two simplest non-trivial twist knots consisting of a twist region containing two crossings. If the crossings in this twist region are positive, then the twist knot is a trefoil, cf. Figure 1.13. Otherwise if the crossings in the twist

Table 1.1: The Alexander Polynomial and its corresponding evaluations at $t = -1$ and $t = -2$ for the unknotting number one knots with up to and including eight crossings.

Knot	$\Delta(t)$	Δ(-1)	Δ(-2)	Knot	$\Delta(t)$	Δ(-1)	Δ(-2)
3_1	t^2-t+1	3	7	8_9	$t^6-3t^5+5t^4-7t^3$ $+5t^2-3t+1$	25	323
4_1	t^2-3t+1	5	11	8_{10}	$t^6-3t^5+6t^4-7t^3$ $+6t^2-3t+1$	27	343
5_2	$2t^2-3t+2$	7	16	8_{11}	$2t^4-7t^3+9t^2$ $-7t+2$	27	140
6_1	$2t^2-5t+2$	9	20	8_{13}	$2t^4-7t^3+11t^2$ $-7t+2$	29	148
6_2	$t^4-3t^3+3t^2$ $-3t+1$	11	59	8_{14}	$2t^4-8t^3+11t^2$ $-8t+2$	31	158
6_3	$t^4-3t^3+5t^2$ $-3t+1$	13	67	8_{16}^+	$t^6-4t^5+8t^4-9t^3$ $+8t^2-4t+1$	35	433
7_2	$3t^2-5t+3$	11	25	8_{17}	$t^6-4t^5+8t^4-11t^3$ $+8t^2-4t+1$	37	449
7_6	$t^4-5t^3+7t^2$ $-5t+1$	19	95	8_{18}^+	$t^6-5t^5+10t^4-13t^3$ $+10t^2-5t+1$	45	539
7_7	$t^4-5t^3+9t^2$ $-5t+1$	21	103	8_{20}	$t^4-2t^3+3t^2-2t+1$	9	49
8_1	$3t^2-7t+3$	13	29	8_{21}	$t^4-4t^3+5t^2-4t+1$	15	77
8_7	$t^6-3t^5+5t^4-5t^3$ $+5t^2-3t+1$	23	307				

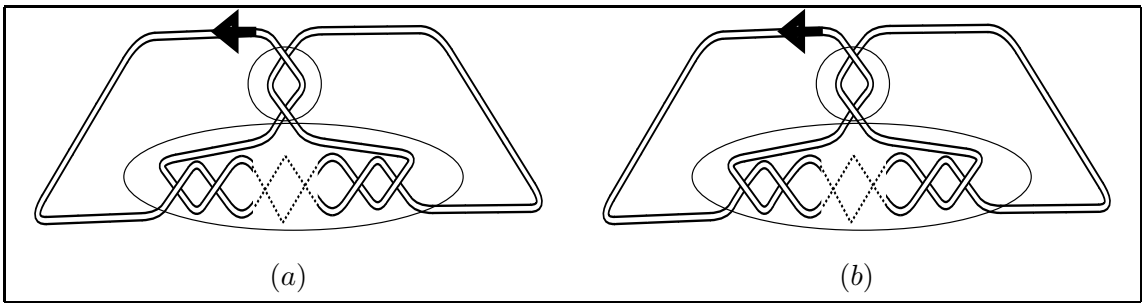

Figure 1.12: (a) is a twist knot formed from a twisted region with $|2n|$ positive crossings. (b) is a twist knot formed from a twisted region with $|2n|$ negative crossings. In Figures (a) and (b) the portion of the knot contained in the circle is referred to as the *clasp* and the portion of the knot contained within the ellipse is referred to as the *twist region*.

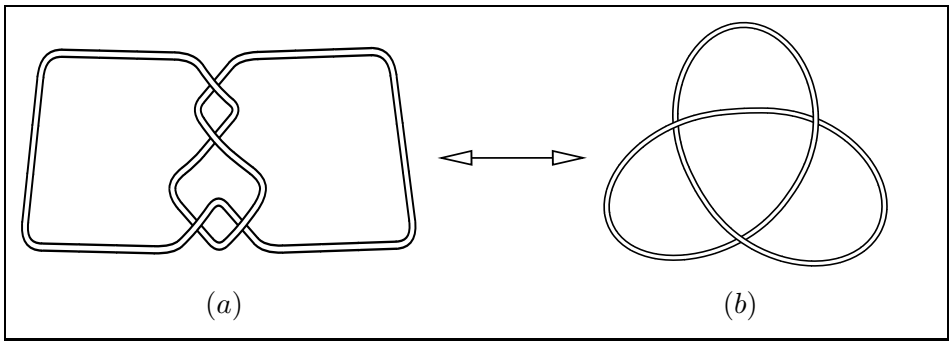

Figure 1.13: (a) is a knot diagram of a trefoil drawn in the form of the definition of a twist knot with 2 positive crossings in the twist region. (b) is a knot diagram that is commonly used to represent a trefoil.

region are negative, then the twist knot is the figure 8, cf. Figure 1.14.

It can be seen from Figure 1.12 that if a strand passage is implemented at one of the crossings in the twist region, the knot-type of the resulting knot is a twist knot with 2 fewer crossings in the twist region. Further, it can be seen from Figure 1.12 that if a strand passage occurs in the clasp region of a twist knot, the knot-type of the resulting after-strand-passage knot is always the unknot. In the case of the trefoil and the figure 8, it can be seen from Figures 1.13 and 1.14 respectively that a strand passage in the twist region leads to, after the strand passage, a knot whose knot-type is the unknot.

Because a strand passage in the clasp region unknots a twist knot in only one strand passage, it is believed that the twist knots play a particularly important role in molecular biology [106]. When the topology of a DNA molecule is a twist knot, the twist region corresponds to the supercoils of the DNA molecule and the clasp region results from a

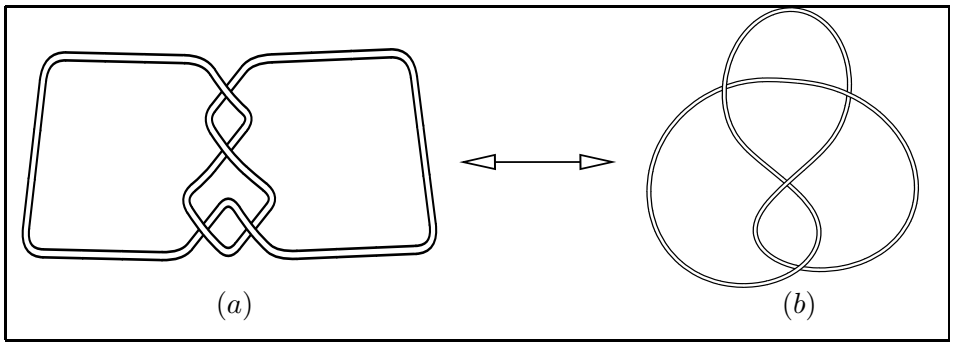

Figure 1.14: (a) is a knot diagram of a figure 8 drawn in the form of the definition of a twist knot with 2 negative crossings in the twist region. (b) is a knot diagram that is commonly used to represent a figure 8.

strand passage of two segments of the DNA molecule. In [106], Mann's experimental work suggested that human topoisomerase IIα enzymes preferred to act on the clasp region of the twist knot; the consequence of such an interaction was that the DNA was unknotted.

In order to better understand the human topoisomerase IIα enzyme-twist knot DNA interaction, Liu *et al.* [96] created a lattice model to study how the local geometry of the strand passage site impacts the after-strand-passage knot-type. As the work presented in this thesis is also based on a model of a ring polymer on the simple cubic lattice (to be defined formally in the next section), the next section provides an overview of modelling polymers on the simple cubic lattice.

1.3 Lattice Models of Polymers

To define any lattice model of a polymer, the following definitions from [46] are required. Let $\boldsymbol{x} := (x(1), x(2), ..., x(d)) \in \mathbb{R}^d$, the d-dimensional Euclidean space and define, for $\boldsymbol{x}, \boldsymbol{y} \in \mathbb{R}^d$,

$$\boldsymbol{x} \cdot \boldsymbol{y} := \sum_{i=1}^{d} x(i)y(i) \tag{1.3}$$

(the Euclidean dot product) and

$$||\boldsymbol{x}||_r := \sqrt[r]{\sum_{i=1}^{d} [x(i)]^r}. \tag{1.4}$$

If $r = 2$ in Equation (1.4), then Equation (1.4) represents the Euclidean norm.

As defined in [172], define a graph (directed graph) G to be the pair $G := (\mathcal{V}(G), \mathcal{E}(G))$, where $\mathcal{V}(G)$ is a set and $\mathcal{E}(G)$ is a set of unordered (ordered) pairs of elements from $\mathcal{V}(G)$.

$\mathcal{V}(G)$ and $\mathcal{E}(G)$ are respectively the vertex set and edge (arc) set of G. The elements of $\mathcal{V}(G)$ are called the vertices or sites of G and the elements of $\mathcal{E}(G)$ are called the edges (arcs) or bonds of G. The d-dimensional hyper-cubic lattice, or equivalently the d-dimensional integer lattice, is the infinite graph embedded in $\mathbb{R}^3$, whose vertex set, denoted $\mathcal{V}(\mathbb{Z}^d)$, is $\mathbb{Z}^d$ and whose edge set $\mathcal{E}(\mathbb{Z}^d)$, is given by $\mathcal{E}(\mathbb{Z}^d) = \{\{\boldsymbol{x}, \boldsymbol{y}\} | \boldsymbol{x}, \boldsymbol{y} \in \mathcal{V}(\mathbb{Z}^d), ||\boldsymbol{x} - \boldsymbol{y}||_1 = 1\}$. For convenience, from this point on, $\mathbb{Z}^d$ will be used to denote the d-dimensional hypercubic lattice. $\mathbb{Z}^2$ is called the *square lattice* and $\mathbb{Z}^3$ is called the *simple cubic lattice*.

Many interesting graphs and graph embeddings can be defined in $\mathbb{Z}^d$. The work embodied in this thesis focuses on two specific types of embeddings. The first type is the set of all self-avoiding walks in $\mathbb{Z}^d$ beginning at site $\boldsymbol{x}$ and ending at the site $\boldsymbol{y}$.

Definition 1.3.1 ([103]) *An n-step self-avoiding walk (SAW) u in $\mathbb{Z}^d$ beginning at site $\boldsymbol{x}$ and ending at the site $\boldsymbol{y}$ is defined to be a directed graph embedding $u = (\mathcal{V}(u), \mathcal{E}(u))$ in $\mathbb{Z}^d$ consisting of a sequence of n distinct arcs in $\mathbb{Z}^d$, $\mathcal{E}(u) = ((\boldsymbol{u}_0, \boldsymbol{u}_1), (\boldsymbol{u}_1, \boldsymbol{u}_2), \ldots, (\boldsymbol{u}_{n-2}, \boldsymbol{u}_{n-1}), (\boldsymbol{u}_{n-1}, \boldsymbol{u}_n))$, and a corresponding sequence of $n+1$ distinct vertices in $\mathbb{Z}^d$, $\mathcal{V}(u) = (\boldsymbol{u}_0, \boldsymbol{u}_1, \boldsymbol{u}_2, \ldots, \boldsymbol{u}_{n-1}, \boldsymbol{u}_n)$, such that the vertices $\boldsymbol{u}_i \in \mathbb{Z}^d$ for $i = 0, ..., n$, $\boldsymbol{u}_0 = \boldsymbol{x}$, $\boldsymbol{u}_n = \boldsymbol{y}$, and for each $i = 0, ..., n-1$ the arc $(\boldsymbol{u}_i, \boldsymbol{u}_{i+1})$ joins two nearest neighbour vertices in $\mathbb{Z}^d$ (i.e. $||\boldsymbol{u}_{i+1} - \boldsymbol{u}_i||_1 = 1$). The length of the self-avoiding walk u is denoted $|u|$ and is defined to be the number of arcs in $\mathcal{E}(u)$.*

The second type of graph embedding relevant to this work is the set of all self-avoiding polygons in $\mathbb{Z}^d$. A self-avoiding polygon (SAP) in $\mathbb{Z}^d$ can be viewed as a simple closed curve embedded in $\mathbb{Z}^d$ that never intersects itself and has neither a starting point nor an orientation specified. More precisely:

Definition 1.3.2 *A $(2n)$-edge self-avoiding polygon (SAP) ω, for $n \geq 2$, is defined to be a graph embedding $\omega = (\mathcal{V}(\omega), \mathcal{E}(\omega))$ in $\mathbb{Z}^d$ consisting of a set of $2n$ distinct edges in $\mathbb{Z}^d$, $\mathcal{E}(\omega) = \{\{\boldsymbol{\omega}_0, \boldsymbol{\omega}_1\}, \{\boldsymbol{\omega}_1, \boldsymbol{\omega}_2\}, \ldots, \{\boldsymbol{\omega}_{2n-2}, \boldsymbol{\omega}_{2n-1}\}, \{\boldsymbol{\omega}_{2n-1}, \boldsymbol{\omega}_0\}\}$, and a corresponding set of $2n$ distinct vertices in $\mathbb{Z}^d$, $\mathcal{V}(\omega) = \{\boldsymbol{\omega}_0, \boldsymbol{\omega}_1, \boldsymbol{\omega}_2, \ldots, \boldsymbol{\omega}_{2n-2}, \boldsymbol{\omega}_{2n-1}\}$, such that for all $i = 0, 1, ..., 2n-2$, $||\boldsymbol{\omega}_i - \boldsymbol{\omega}_{i+1}||_1 = 1$ and $||\boldsymbol{\omega}_{2n-1} - \boldsymbol{\omega}_0||_1 = 1$. It should be noted that the length of the SAP ω is denoted $|\omega|$ and is defined to be the number of edges in $\mathcal{E}(\omega)$.*

Definition 1.3.3 *For a SAP ω in $\mathbb{Z}^d$, ω is referred to as a* rooted polygon *if one of its vertices is designated as the root of ω. If no vertex of ω is specified as the root, then ω is referred to as an* unrooted polygon.

Rooted SAPs are of particular interest to this work because Θ-SAPs are rooted SAPs.

Since the late 1940's [114, 127], self-avoiding walks have been used to model linear polymers in dilute solution and since the early 1960's [53], self-avoiding polygons have been used as lattice models for ring polymers in dilute solution. The standard underlying assumptions required to model a linear/ring polymer in dilute solution with a good solvent using a self-avoiding walk (SAW)/self-avoiding polygon (SAP) are [154]:

1. the vertices of the SAW/SAP represent the monomers of the linear/ring polymer;
2. the edges of the SAW/SAP represent the chemical bonds between the monomers;
3. the self-avoidance property of the SAW/SAP represents the effect of the excluded volume;
4. the excluded volume property is assumed to dominate all other interactions so that interactions between a polymer and itself and a polymer and the solvent can be ignored;
5. all polymer configurations with the same number of monomers are considered equally likely; and
6. the polymer is considered to be isolated from other polymers in the solution and is therefore unaffected by the other polymers in the solution.

For the Local Strand Passage Model of this thesis, two further assumptions are made. One assumption is that the location of the strand passage in the polymer has already been chosen and the other assumption is that the two strands of the polymer have already been brought close together. The specific details of the LSP model are presented in Chapter 2.

In order to study the LSP Model, some definitions and properties related to self-avoiding walks and self-avoiding polygons are needed. One of the reasons self-avoiding walks are included in this discussion, even though it has already been stated that a self-avoiding polygon model is going to be used, is that many of the asymptotic properties of self-avoiding polygons can be derived from those for self-avoiding walks. Therefore sufficient terminology and information about the properties of self-avoiding walks must be presented so that the properties of self-avoiding polygons can be better understood.

Define $\mathscr{C}_n^d(\boldsymbol{x},\boldsymbol{y})$ to be the set of n-step SAWs in $\mathbb{Z}^d$ beginning at site $\boldsymbol{x}\in\mathbb{Z}^d$ and ending at site $\boldsymbol{y}\in\mathbb{Z}^d$. Denote the n-step SAWs whose end is not specified but still begin at site $\boldsymbol{x}\in\mathbb{Z}^d$ by

$$\mathscr{C}_n^d(\boldsymbol{x}) := \bigcup_{\boldsymbol{y}\in\mathbb{Z}^d} \mathscr{C}_n^d(\boldsymbol{x},\boldsymbol{y}) \tag{1.5}$$

and define $\mathscr{C}_n^d := \mathscr{C}_n^d(\mathbf{0})$. Note that $\mathscr{C}_n^d$ is nothing but the set of all n-step self-avoiding walks in $\mathbb{Z}^d$ that start at the origin. Now define the set of all SAWs in $\mathbb{Z}^3$ that start at the origin by

$$\mathscr{C} := \bigcup_{n\geq 0} \mathscr{C}_n^3. \tag{1.6}$$

Let $\mathscr{P}_n^d$ denote the set of all n-step self-avoiding polygons in $\mathbb{Z}^d$. Unless otherwise specified, from this point forward the term walk will be used synonymously with SAW and the term polygon will be used synonymously with SAP. If an orientation of a polygon in $\mathbb{Z}^d$ is specified, the SAP is said to be *directed*. Let $\mathscr{Q}_n^d$ be the set of all n-step directed self-avoiding polygons in $\mathbb{Z}^d$ that are rooted at the origin.

An interesting question regarding the set of all SAWs (SAPs) is "How many distinct SAWs (SAPs) of length n can exist in $\mathbb{Z}^d$?", where two SAWs (SAPs) are considered *distinct* if one SAW (SAP) cannot be obtained from the other by some translation. In order to discuss this question in detail, the following notation is needed. Define $c_n^d(\boldsymbol{x},\boldsymbol{y})$, c_n^d and p_n^d respectively to be the number of n-step SAWs starting at site $\boldsymbol{x}\in\mathbb{Z}^d$ and ending at site $\boldsymbol{y}\in\mathbb{Z}^d$; the number of n-step SAWs in $\mathbb{Z}^d$ starting at the origin and whose end site is not specified; and the number of distinct n-edge SAPs in $\mathbb{Z}^d$. Now define $c_n := c_n^3$, $p_n := p_n^3$, and $p_n(K)$ to be the number of distinct n-edge SAPs in $\mathbb{Z}^3$ that have knot-type K. Let q_n^d be the number of n-edge SAPs in $\mathbb{Z}^d$ that are rooted at the origin. Because SAPs can only consist of an even number of edges,

$$p_n^d = \begin{cases} 0, & \text{if } n \text{ is odd} \\ p_n^d, & \text{if } n \text{ is even} \end{cases} \tag{1.7}$$

and

$$q_n^d = \begin{cases} 0, & \text{if } n \text{ is odd} \\ q_n^d, & \text{if } n \text{ is even.} \end{cases} \tag{1.8}$$

To determine q_{2n}^d, note that, for each unrooted $(2n)$-edge SAP in $\mathbb{Z}^d$, there are $2n$ possible ways of rooting, and then translating, the SAP so that the root is the origin.

Therefore the number of rooted $(2n)$-edge SAPs in $\mathbb{Z}^d$, [103], is

$$q_{2n}^d = 2np_{2n}^d. \tag{1.9}$$

One method for determining c_n^d and p_{2n}^d for a fixed dimension d is to simply count the number of distinct SAWs, c_n^d, and SAPs, p_{2n}^d, for each value of n. Tables 1.2 and 1.3 respectively present the number of distinct n-step SAWs starting at the origin (for $d \in \{2,3,4,5,6\}$ and $n \in \{0,1,2,3,4,5,6\}$) and $(2n)$-edge unrooted SAPs (for $d \in \{2,3,4,5,6\}$ and $n \in \{2,3,4,5\}$). The values in Table 1.2 for $d = 2$ are taken from [110]; for $d = 3$ are

Table 1.2: The number c_n^d of distinct n-step SAWs starting at the origin.

n	$d=2$ [110]	$d=3$ [51]	$d=4$ [33]	$d=5$ [33]	$d=6$ [33]
0	1	1	1	1	1
1	4	6	8	10	12
2	12	30	56	90	132
3	36	150	392	810	1452
4	100	726	2696	7210	15852
5	284	3534	18584	64250	173172
6	780	16926	127160	570330	1887492

taken from [51]; and for $d \in \{4,5,6\}$ are taken from [33]. The values in Table 1.3 for $d = 2$

Table 1.3: The number p_{2n}^d of distinct unrooted $(2n)$-edge SAPs.

$2n$	$d=2$ [50]	$d=3$ [33]	$d=4$ [33]	$d=5$ [33]	$d=6$ [33]
4	1	3	6	10	15
6	2	22	76	180	350
8	7	207	1434	5170	13545
10	28	2412	32616	186856	679716

are taken from [50]; and for $d \in \{3,4,5,6\}$ are taken from [33].

Using exact enumeration to determine the values for c_n^d and p_{2n}^d is a very CPU intensive problem. Because current enumeration algorithms rely on the available computational power to implement the algorithm, for fixed dimension d, enumerating c_n^d and p_{2n}^d, even for moderately small values of n, would currently take years. For instance, p_{2n}^2 has now been enumerated up to $n = 55$, that is p_{110}^2 =97,148,177,367,657,853,074,723,038,687,712,338,567,772 [73], and p_{2n} has been enumerated only up to $n = 16$, that is $p_{32} = 53{,}424{,}552{,}150{,}523{,}386$ [13]. Hence using current enumeration techniques to completely characterize the behaviour of c_n^d and p_{2n}^d as $n \to \infty$, is not feasible. But, back in 1954, Hammersley and Morton determined part of the asymptotic form (as $n \to \infty$) of c_n^d, that is they proved the following result.

Theorem 1.3.1 (Hammersley and Morton [54]) *For every natural number $d \geq 2$, the following limit exists:*

$$\kappa(d) := \lim_{n\to\infty} n^{-1} \log c_n^d, \tag{1.10}$$

where $\kappa(d)$ is referred to as the connective constant for self-avoiding walks in $\mathbb{Z}^d$.

The existence of $\kappa(d)$ for every natural number $d \geq 2$, implies that c_n^d increases exponentially in n. The quantity

$$\mu(d) := e^{\kappa(d)} \tag{1.11}$$

is referred to as the *growth constant for self-avoiding walks in $\mathbb{Z}^d$*.

In 1961, Hammersley also determined part of the asymptotic form (as $n \to \infty$) of p_{2n}^d. He proved that the connective constant for self-avoiding polygons in $\mathbb{Z}^d$ is equal to the connective constant for self-avoiding walks in $\mathbb{Z}^d$, that is he proved the following result.

Theorem 1.3.2 (Hammersley [53]) *For every natural number $d \geq 2$,*

$$\lim_{n\to\infty} (2n)^{-1} \log p_{2n}^d = \kappa(d). \tag{1.12}$$

The upshot of Theorem 1.3.2 is two-fold. For fixed dimension d, p_{2n}^d increases exponentially in $2n$, and c_n^d and p_{2n}^d both grow at the same exponential rate. In $\mathbb{Z}^3$, the growth and connective constants, $\mu(3)$ and $\kappa(3)$, from this point forward, will simply be denoted μ and κ, respectively.

Because this work focuses on knotting probabilities and because the concept of a knot only makes sense in $\mathbb{R}^3$, the discussion will be restricted to the set of SAPs in $\mathbb{Z}^3$. Let $\mathscr{P}_n$

be the set of all n-edge SAPs in $\mathbb{Z}^3$ and define the set of all SAPs in $\mathbb{Z}^3$ to be

$$\mathscr{P} := \bigcup_{4 \leq n \in \mathbb{N}} \mathscr{P}_n. \tag{1.13}$$

Now let $\mathscr{P}_n(K)$ be the set of n-edge SAPs in $\mathbb{Z}^3$ that have knot-type K and define the set of all SAPs in $\mathbb{Z}^3$ that have knot-type K to be

$$\mathscr{P}(K) := \bigcup_{4 \leq n \in \mathbb{N}} \mathscr{P}_n(K). \tag{1.14}$$

For the set of SAPs that have knot-type K, define $p_n(K)$ to be the number of distinct n-edge SAPs in $\mathbb{Z}^3$ that have knot-type K. Now define $q_n(K)$ to be the number of n-edge SAPs in $\mathbb{Z}^3$ that are rooted at the origin and have knot-type K. Combining Equation (1.8) with the result of an argument similar to that which was used to obtain Equation (1.9) yields

$$q_n(K) = \begin{cases} 0, & \text{if } n \text{ is odd} \\ np_n(K), & \text{if } n \text{ is even.} \end{cases} \tag{1.15}$$

Equation (1.15) yields that studies of $p_{2n}(K)$ can be used directly to study $q_{2n}(K)$. Because Θ-SAPs are rooted SAPs, subsets of the polygons counted by $p_{2n}(K)$ can be used to study the number of $(2n)$-edge knot-type K Θ-SAPs. Hence the discussion turns to studies of $p_{2n}(K)$.

In [26], Diao proved that the smallest non-trivial knot that can be embedded in $\mathbb{Z}^3$ has 24 edges and that the knot-type of every 24-edge non-trivial knotted SAP is the trefoil. In fact, Diao determined enumeratively that $p_{24}(3_1) = 3496$ [27]. Diao also proved that in order to embed any other non-trivial knot (other than the trefoil) in $\mathbb{Z}^3$, the resulting SAP would have to have at least 26 edges. In [83], Kim *et al.* proved that the smallest figure eight that can be embedded in $\mathbb{Z}^3$ has 30 edges. Refer to Figures 1.15 and 1.16 respectively for an example of a 24-edge trefoil and a 30-edge figure 8 embedded in $\mathbb{Z}^3$.

In order to investigate the exponential growth of $p_{2n}(K)$, one useful tool is Kesten's Pattern Theorem. In order to state Kesten's Pattern Theorem for SAWs in $\mathbb{Z}^3$, some definitions based on [82] are required. The first definitions required are that of a *cube* and a *pattern* as defined in $\mathbb{Z}^d$.

Definition 1.3.4 (Kesten [82]) *A d-dimensional cube D is a set of lattice points of the form*

$$D = \left\{ \boldsymbol{x} \in \mathbb{Z}^d : b_i \leq x(i) \leq b_i + b, \ \textit{for } i = 1, .., d \right\}, \tag{1.16}$$

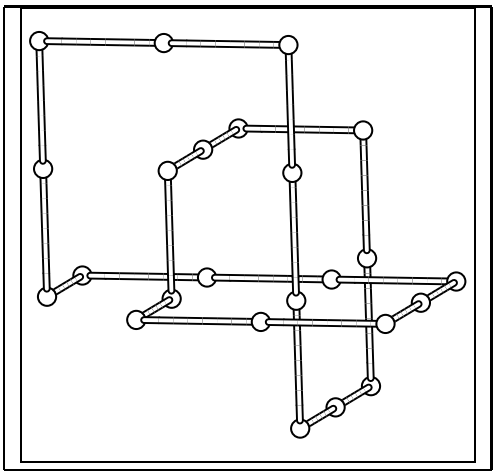

Figure 1.15: A 24-edge SAP whose knot-type is 3_1.

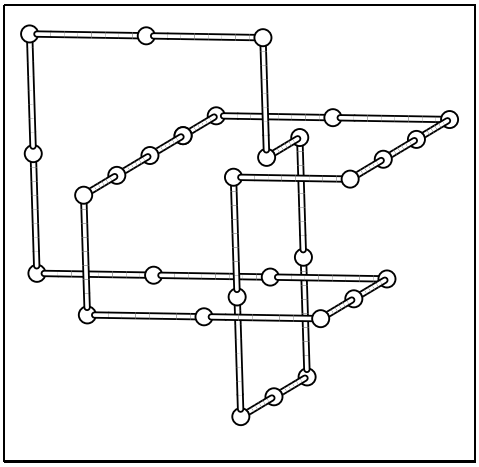

Figure 1.16: A 30-edge SAP whose knot-type is 4_1.

where $b_1, b_2, ..., b_d$ are integer values and b is a positive integer.

Definition 1.3.5 (Kesten [82]) *A pattern $P = (\mathcal{V}(P), \mathcal{E}(P))$ is a directed graph embedding in $\mathbb{Z}^d$ consisting of a sequence of n distinct arcs in $\mathbb{Z}^d$, where $\mathcal{E}(P) = ((\boldsymbol{P}_0, \boldsymbol{P}_1), (\boldsymbol{P}_1, \boldsymbol{P}_2), \ldots, (\boldsymbol{P}_{n-2}, \boldsymbol{P}_{n-1}), (\boldsymbol{P}_{n-1}, \boldsymbol{P}_n))$ and a corresponding sequence of n distinct vertices in $\mathbb{Z}^d$, $\mathcal{V}(P) = (\boldsymbol{P}_0, \boldsymbol{P}_1, \boldsymbol{P}_2, \ldots, \boldsymbol{P}_{n-1}, \boldsymbol{P}_n)$.*

Definition 1.3.6 (Kesten [82]) *A pattern P is said to occur at the j'th step of a self-avoiding walk w if there exists a vector $\boldsymbol{v} \in \mathbb{Z}^d$ such that $\boldsymbol{w}_{j+k} = \boldsymbol{P}_k + \boldsymbol{v}$ for every $k = 0, ..., n$.*

Now that a pattern has been defined, two very special types of patterns can be defined. To this end, recall that $\mathscr{C}_n^d$ is the set of all n-step self-avoiding walks $w \in \mathbb{Z}^d$ such that

$\boldsymbol{w}_0 = \mathbf{0}$ and that $\mathscr{Q}_n^d$ is the set of all n-step directed self-avoiding polygons in $\mathbb{Z}^d$ that are rooted at the origin.

Definition 1.3.7 *For fixed $n \in \mathbb{N}\backslash\{1\}$ and given $\omega \in \mathscr{Q}_{2n}^d$, consider the walk u (self-avoiding except for the last vertex) that is formed by starting at the origin and following along the arcs as specified by their orientation. A pattern P is said to occur at the j'th step of ω if it occurs at the j'th step of u.*

Definition 1.3.8 (Kesten [82]) *Given $k \geq 0$ and a pattern P, let $c_n^d[k,P]$ ($q_{2n}^d[k,P]$) denote the number of elements in $\mathscr{C}_n^d$ ($\mathscr{Q}_{2n}^d$) for which P occurs at no more than k different steps. Let $\mathscr{C}_n^d(P) \subseteq \mathscr{C}_n^d$ ($\mathscr{Q}_{2n}^d(P) \subseteq \mathscr{Q}_{2n}^d$) for which P occurs at the 0'th step. P is said to be a proper front pattern if $\mathscr{C}_n^d(P) \neq \{\}$ ($\mathscr{Q}_{2n}^d(P) \neq \{\}$) for all sufficiently large n. P is said to be a proper internal pattern if for every k there exists an element in $\mathscr{C}_n^d$ ($\mathscr{Q}_{2n}^d$) such that P occurs at k or more different steps.*

Definition 1.3.9 (Kesten [82]) *Suppose Q is a cube in $\mathbb{Z}^d$ and P is an m-step pattern in $\mathbb{Z}^d$ such that $\boldsymbol{P}_0$ and $\boldsymbol{P}_m$ are corners of Q and $\boldsymbol{P}_i \in Q$ for all $i = 0, 1, ..., m$. (P,Q) occurs at the j'th step of a self-avoiding walk (directed rooted SAP) w if there exists a vector $\boldsymbol{v} \in \mathbb{Z}^d$ such that $\boldsymbol{w}_{j+k} = \boldsymbol{P}_k + \boldsymbol{v}$ for every $k = 0, ..., m$ and $\boldsymbol{w}_i$ is not in $Q + \boldsymbol{v}$ for every $i < j$ and every $i > j + m$. For $k \geq 0$, let $c_n^d[k,(P,Q)]$ ($q_{2n}^d[k,(P,Q)]$) denote the number of elements in $\mathscr{C}_n^d$ ($\mathscr{Q}_{2n}^d$) for which (P,Q) occurs at no more than k different steps.*

Definitions 1.3.4 through 1.3.9 allow the theorem, that is now referred to as the *Kesten Pattern Theorem for SAWs*, to be stated precisely.

Theorem 1.3.3 (Kesten Pattern Theorem for SAWs [82]) *(a) Let Q be a cube in $\mathbb{Z}^d$ and P be a pattern in $\mathbb{Z}^d$ as in Definition 1.3.9. Then there exists an $a > 0$ such that*

$$\limsup_{n\to\infty} \left(c_n^d[an,(P,Q)]\right)^{1/n} < \mu(d). \tag{1.17}$$

(b) For any proper internal pattern P as in Definition 1.3.8, there exists an $a > 0$ such that

$$\limsup_{n\to\infty} \left(c_n^d[an,P]\right)^{1/n} < \mu(d). \tag{1.18}$$

Basically Kesten's Pattern Theorem states that if a given pattern can possibly occur three times in a SAW, then it must occur at least an times in all but an exponentially small fraction of sufficiently large n-step SAWs, for some $a > 0$, cf. [82]. In [149], Sumners and Whittington adapted Theorem 1.3.3 to the set of all self-avoiding polygons. Their resulting theorem, referred to from-here-on-in as the *Pattern Theorem for all Polygons*, is stated below.

Theorem 1.3.4 (Pattern Theorem for all Polygons [149]) *(a) Let Q be a cube in $\mathbb{Z}^3$ and P be a pattern in $\mathbb{Z}^3$ as in Definition 1.3.9. Then there exists an $a > 0$ such that*

$$\limsup_{n\to\infty} \left(q^3_{2n}\left[2an, (P, Q)\right]\right)^{1/2n} < \mu. \tag{1.19}$$

(b) For any proper internal pattern P in $\mathbb{Z}^3$ as in Definition 1.3.8 and for $0 \leq k \in \mathbb{Z}$, let $q^3_{2n}[k, P])$ denote the number of elements in $\mathcal{Q}^3_{2n}$ for which P occurs at no more than k different steps. Then there exists an $a > 0$ such that

$$\limsup_{n\to\infty} \left(q^3_{2n}\left[2an, P\right]\right)^{1/2n} < \mu. \tag{1.20}$$

The pattern illustrated in Figure 1.17 is referred to as a *tight trefoil pattern* and has been redrawn from [149]. It can be seen from Figure 1.17 that if this tight trefoil pattern is transformed into a SAP with the fewest number of edges, the resulting SAP is a trefoil. In fact, using this tight trefoil pattern and the Pattern Theorem for all Polygons, Sumners and Whittington proved the following result.

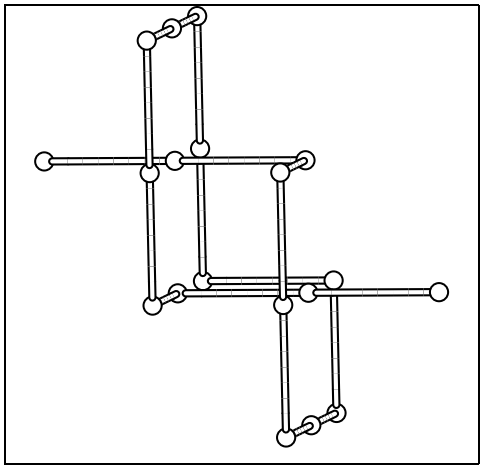

Figure 1.17: A tight trefoil pattern.

Theorem 1.3.5 (Sumners and Whittington [149])

$$\lim_{n\to\infty} (2n)^{-1} \log p_{2n}(\phi) := \kappa_\phi < \kappa \tag{1.21}$$

and hence the probability that an $(2n)$*-edge self-avoiding polygon is knotted, that is* $1-\frac{p_{2n}(\phi)}{p_{2n}}$ *goes to unity as* $1 - e^{-2\alpha n+o(n)}$ *when* $n \to \infty$ *and* $\alpha = \kappa - \kappa_\phi > 0$.

The proof of the strict inequality in Equation (1.21) of Theorem 1.3.5 relies on the Pattern Theorem for all Polygons. Theorem 1.3.5 itself implies that the unknot is asymptotically, exponentially rare in the set of all self-avoiding polygons in $\mathbb{Z}^3$, that is, as the length of a self-avoiding polygon in $\mathbb{Z}^3$ tends to infinity, the probability of the polygon being unknotted tends to zero. This implies that the knotting probability goes to one, confirming the Frisch-Wasserman-Delbruck Conjecture (cf. Conjecture 1.1.1) for $\mathbb{Z}^3$.

Soteros, Sumners, and Whittington [145] extended the results of Sumners and Whittington [149] in a number of directions. They proved a weaker result for polygons with non-trivial knot-type K, that is

$$k_K := \liminf_{n\to\infty} \frac{\log p_{2n}(K)}{2n} \leq \limsup_{n\to\infty} \frac{\log p_{2n}(K)}{2n} =: \kappa_K < \kappa = \log \mu. \tag{1.22}$$

Note that it is not known whether $k_K = \kappa_K$ for any non-trivial knot-type K. They also proved that all but exponentially few sufficiently long polygons in $\mathbb{Z}^3$ are highly composite knots, with any knot-type appearing numerous times in the prime knot factorization. For polygons with knot-type K, the following result can be proved [145]:

$$\kappa_\phi \leq \kappa_K. \tag{1.23}$$

Although it is believed that [125]

$$\kappa_\phi = \kappa_K, \tag{1.24}$$

proving the inequality

$$\kappa_\phi \geq \kappa_K \tag{1.25}$$

remains an open question.

A consequence of Theorem 1.3.2 is that p_{2n} grows exponentially in n, where $n \in \mathbb{N}\backslash\{1\}$. In fact, for the set of all SAPs in $\mathbb{Z}^3$, it is believed that there exist constants A, α, μ, B, and Δ, and a function g_p (with $g_p(2n) = O(n^{-1})$ such that p_{2n} (as $n \to \infty$) has the scaling form [125]

$$A\,(2n)^{\alpha-3}\,\mu^{2n}\left(1 + \frac{B}{(2n)^{\Delta}} + g_p(2n)\right), \tag{1.26}$$

where A is the *amplitude*, $\mu = e^{\kappa}$ is the previously discussed growth constant, α is referred to as the *entropic critical exponent*, and Δ is the exponent for the dominant correction due to scaling term referred to as a *confluent exponent*. Sumners and Whittington's result in Theorem 1.3.5 shows that $p_{2n}(\phi)$ (for $n \in \mathbb{N}\backslash\{1\}$) grows at an exponential rate that is less than the growth rate for p_{2n} and hence, by the extension of Equation (1.26), Orlandini *et al.* [125] proposed that there exist constants $A_\phi, \alpha_\phi, \mu_\phi, B_\phi$, and Δ_ϕ, and a function g_ϕ (with $g_\phi(2n) = O(n^{-1})$) such that $p_{2n}(\phi)$ (as $n \to \infty$) scales like

$$A_\phi (2n)^{\alpha_\phi - 3} \mu_\phi^{2n} \left(1 + \frac{B_\phi}{(2n)^{\Delta_\phi}} + g_\phi(2n)\right), \tag{1.27}$$

where A_ϕ is the amplitude, $\mu_\phi = e^{\kappa_\phi}$, α_ϕ is the corresponding entropic critical exponent, and Δ_ϕ is the exponent for the dominate correction due to scaling term.

Now assuming that $k_K = \kappa_K$ in Equation (1.22), Orlandini *et al.* [125] extended the scaling form given by Equation (1.26) to the number of $(2n)$-edge SAPs with knot-type K. They proposed that there exist constants $A_K, \alpha_K, \mu_K, B_K$, and Δ_K, and a function g_K (with $g_K(2n) = O(n^{-1})$) such that $p_{2n}(K)$ (as $n \to \infty$) scales like

$$A_K (2n)^{\alpha_K - 3} \mu_K^{2n} \left(1 + \frac{B_K}{(2n)^{\Delta_K}} + g_K(2n)\right), \tag{1.28}$$

where A_K is the amplitude, $\mu_K = e^{\kappa_K}$, α_K is the corresponding entropic critical exponent, and Δ_K is the exponent for the dominate correction due to scaling term.

The relationship between α_ϕ and α_K is also unknown, but α_K is believed to be a function of α_ϕ and the knot-type K [125] , that is, it is conjectured that

$$\alpha_K = \alpha_\phi + n_K, \tag{1.29}$$

where n_K is a constant which depends only on the knot-type K and is thought to be the number of prime factors in the prime factor decomposition of the knot-type K [125]. There is no rigorous proof of this relationship, only estimates that do not contradict the form given by Equation (1.29) [125].

There has been much numerical work completed, which, based on the above scaling form assumptions, has lead to estimates for α, μ, μ_K, α_K, and Δ_K for $K \in \{\phi, 3_1, 4_1\}$. For instance, Clisby *et al.* [13] used exact enumeration and series analysis to estimate μ and θ to be

$$\begin{aligned} \mu &= \ \ 4.6840431 \pm 0.00001 \\ \theta &= -0.76798 \pm 0.00016, \end{aligned} \tag{1.30}$$

where

$$\theta = \alpha - 1. \tag{1.31}$$

Because Diao [26] showed that the smallest knotted SAP is a trefoil with 24 edges, all values of $p_{2n} = p_{2n}(\phi)$ for all the enumerated values up to and including $n = 11$. Since p_{2n} has only been enumerated up to SAPs of length 32 (that is up to $n = 16$), there is not enough enumeration data available to estimate κ_K for $K = 3_1$, let alone for knots with more than three crossings. Hence exact enumeration techniques have not lead to useful estimates for κ_K, for any non-trivial knot-type K. In order to estimate κ_K, some other approach, such as a Monte Carlo approach, must be used.

Orlandini *et al.* [125] presented Monte Carlo estimates for the growth constants of the more common knot-types. They reported

$$\mu_K = \begin{cases} 4.6852 & \text{, if } K = \emptyset, \text{ (the unknot)}, \\ 4.6832 & \text{, if } K = 3_1, \text{ (the trefoil)}, \\ 4.6833 & \text{, if } K = 4_1, \text{ (the figure eight)}, \end{cases} \tag{1.32}$$

which are considered accurate to the second decimal place. Based on these estimates, the μ_K's are equal to the second decimal place and are possibly independent of the knot-type K.

In [125], Orlandini *et al.* also estimated α_ϕ using Monte Carlo data. They estimated

$$\alpha_\phi = 0.27 \pm 0.02 \tag{1.33}$$

and, for every $K, K' \in \{3_1, 4_1, 6_2\}$, their numerics support

$$\alpha_K = a_{K'} \neq \alpha_\phi \tag{1.34}$$

and

$$\alpha_K = \alpha_\phi + 1, \tag{1.35}$$

which is consistent with Equation (1.29) since $n_K = 1$ for the three prime knot-types $3_1, 4_1$, and 6_2.

1.4 Generating Functions and Probability Distributions

Define the *ordinary generating function* for a sequence $(a_n)_{n=0}^{\infty}$ by

$$\chi(z) := \sum_{n=0}^{\infty} a_n z^n \tag{1.36}$$

and define the *critical point* for $\chi(z)$ to be its radius of convergence. Let $\mathscr{S}(*)$ denote the set of SAPs that have some desired property $*$ and suppose $s_{2n}(*)$ is the number of $(2n)$-edge SAPs that have some desired property $*$. Then, $Q_*(z)$, the ordinary generating function for $(s_{2n}(*))_{n=0}^{\infty}$, is defined to be

$$Q_*(z) := \sum_{n=0}^{\infty} s_{2n}(*) z^{2n}. \tag{1.37}$$

Assuming $\mu_* := \lim_{n\to\infty} \sqrt[2n]{s_{2n}(*)}$ exists and $0 < \mu_* < \infty$, then the *critical point for* $Q_*(z)$ is the radius of convergence of $Q_*(z)$ and is given by

$$z_* := \frac{1}{\lim_{n\to\infty} \sqrt[2n]{s_{2n}(*)}} = \frac{1}{\mu_*}. \tag{1.38}$$

For example, the ordinary generating function for $(p_{2n}^d)_{n=0}^{\infty}$ is defined as

$$Q_d(z) := \sum_{n=0}^{\infty} p_{2n}^d z^{2n} = \sum_{\omega\in\mathscr{P}} z^{|\omega|}, \tag{1.39}$$

where the critical point for $Q_d(z)$ is [25]

$$z_p(d) := \frac{1}{\lim_{n\to\infty} \sqrt[2n]{p_{2n}^d}} = \frac{1}{\mu(d)}. \tag{1.40}$$

In [49], using exact enumeration data, Guttmann determined the following estimates for $z_p(d)$:

$$z_p(d) \approx \begin{cases} 0.2135, & d = 3, \\ 0.1477, & d = 4, \\ \leq 1/d, & \text{for all } d. \end{cases} \tag{1.41}$$

For a second example, the ordinary generating function for $(p_{2n}(\phi))_{n=0}^{\infty}$ is defined as

$$Q_\phi(z) := \sum_{n=0}^{\infty} p_{2n}(\phi) z^{2n} = \sum_{\omega\in\mathscr{P}(\phi)} z^{|\omega|}, \tag{1.42}$$

where the critical point for $Q_\phi(z)$ is given by

$$z_\phi := \frac{1}{\lim_{n\to\infty} \sqrt[2n]{p_{2n}(\phi)}} = \frac{1}{\mu_\phi}. \tag{1.43}$$

Now if the standard assumptions required to model a ring polymer in dilute solution with a good solvent using a self-avoiding polygon (as discussed in [154] and outlined in Section 1.3) are made, then for a *canonical ensemble* in which the number of monomers

$2n$ is fixed, at equilibrium, the polymer's configuration W is given by a specific property-$*$ $(2n)$-edge SAP $\omega \in \mathscr{S}(*)$ with probability

$$\Pr(W = \omega : |W| = 2n) := \frac{1}{s_{2n}(*)}, \tag{1.44}$$

where $|W|$ denotes the number of edges in W.

If it is further assumed that the size of the polygon is allowed to vary, that is for a *grand canonical ensemble* [103], then the probability that a polymer has conformation $\omega \in \mathscr{S}(*)$ is given by the equation

$$\Pr(W = \omega) := \frac{z^{|\omega|}}{\sum_{j=0}^{\infty} s_{2j}(*) z^{2j}} \tag{1.45}$$

where z is referred to as the *fugacity of the system.* The denominator of Equation (1.45) is the *normalization factor* (also referred to as the *partition function*) [103]. Any probability distribution that can be expressed in the form given by Equation (1.45) is referred to as a *Boltzmann distribution.*

If the properties of large polymers are of interest, then the distribution given by Equation (1.45) can be reweighted so that larger probabilities are associated with larger polygons, that is $\pi_\omega(z)$, the probability that (at equilibrium) a polymer's configuration W is given by a specific property-$*$ SAP $\omega \in \mathscr{S}(*)$, is given by

$$\pi_\omega(z) := \frac{f(|\omega|) z^{|\omega|}}{Q(z)}, \tag{1.46}$$

where z such that $0 < z < z_*$ is fixed, $Q(z) := \sum_{j=0}^{\infty} f(2j) s_{2j}(*) z^{2j}$, and $f(n)$ is a polynomial in n. Any probability distribution that can be expressed in the form given by Equation (1.46) is referred to as a *modified Boltzmann distribution.* Furthermore, $\pi_{2n}(z)$, the probability that the polymer's conformation, W, is given by a $(2n)$-edge property-$*$ SAP $\omega \in \mathscr{S}(*)$, is given by

$$\pi_{2n}(z) := \frac{f(2n) s_{2n}(*) z^{2n}}{Q(z)}. \tag{1.47}$$

Now, if N is a random variable representing the length of a SAP W chosen randomly according to the probability mass function $\{\pi_{2n}(z) : \text{for every integer } n \geq 0\}$, then it can be easily verified that, for $\beta := \log(z)$, the expected value of N is given by

$$\mathrm{E}[N] = \frac{\partial}{\partial \beta} \log Q(e^\beta) \tag{1.48}$$

and the variance of N is given by

$$\mathrm{var}(N) = \frac{\partial^2}{\partial \beta^2} \log Q(e^\beta). \tag{1.49}$$

Consequently, the fugacity $z = e^{\beta}$ controls the expected length of the polygon where the expectation is with respect to the probability mass function $\{\pi_{2n}(z) : \text{for every integer } n \geq 0\}$.

1.5 The Size of a Knot in $\mathbb{Z}^3$

Precisely defining what is meant by the phrase "the size of a knot in a SAP" is not an easy problem. Much work has been done in this area in an attempt to define the phrase [48, 80, 107, 108, 111, 125, 141]. Of these studies, those with results that directly apply to the work in this thesis are summarized next.

In [125], Orlandini *et al.* define the size of the knot in a knotted polygon by intersecting the knotted polygon with spheres that divide it into two arcs in such a manner that one arc will be knotted (when the arc is closed by an arc on the sphere) and will have the same knot-type as the original SAP. The "length of the knot" in a particular polygon is then characterized by the length of such a knotted arc in the smallest such sphere. Now, for n even and $\omega \in \mathscr{P}_n(K)$, define $m_{K,n}(\omega)$ to be the length of the knot as just defined. Then, for W chosen at random from $\mathscr{P}_{2n}(K)$, the expected value of $m_{K,2n}(W)$ is

$$\mathrm{E}\left[m_{K,2n}(W)\right] := \frac{1}{p_{2n}(K)} \sum_{\omega' \in \mathscr{P}_{2n}(K)} m_{K,2n}(\omega'). \tag{1.50}$$

The average length of the knot in a polygon in $\mathscr{P}_{2n}(K)$ is said to *grow at the same rate as the length of the polygon* if there exists $\zeta > 0$ such that, as $n \to \infty$,

$$\frac{\mathrm{E}\left[m_{K,2n}(W)\right]}{2n} \to \zeta. \tag{1.51}$$

Furthermore, the average length of the knot in a polygon in $\mathscr{P}_{2n}(K)$ is said to *grow at a rate less than the length of the polygon*, if, as $n \to \infty$,

$$\frac{\mathrm{E}\left[m_{K,2n}(W)\right]}{2n} \to 0. \tag{1.52}$$

Another definition of the size of a knot in a SAP was presented in [107]. In [107], Marcone *et al.* define the "length of a knot" in a knotted $(2n)$-edge SAP ω by dividing ω into two walks at various locations and closing the ends of the walks with an off-lattice path that is chosen to minimize the risk of modifying/disentangling the knotted portion. If $m'_{K,2n}(\omega)$, the "length of the knot" in a $(2n)$-edge polygon, is the length of the smallest

walk in a $(2n)$-edge SAP ω such that the off-lattice closure results in a knot with the same knot-type as ω, then $\mathrm{E}\left[m'_{K,2n}(W)\right]$, the expected length of a knot in a randomly chosen polygon W from $\mathscr{P}_{2n}(K)$, is given by

$$\mathrm{E}\left[m'_{K,2n}(W)\right] := \frac{1}{p_{2n}(K)} \sum_{\omega' \in \mathscr{P}_{2n}(K)} m'_{K,2n}(\omega'). \tag{1.53}$$

In [107], Marcone *et al.* hypothesize that in the good solvent regime, as $n \to \infty$,

$$\mathrm{E}\left[m'_{K,2n}(W)\right] \sim (2n)^t, \tag{1.54}$$

where $t \simeq 0.75$ and that $\mathrm{E}\left[m'_{K,2n}(W)\right]$ is independent of the knot-type K. Their numerics support this hypothesis for the knot-types $\{3_1, 4_1, 5_1\}$.

In addition to using the average length to characterize the length of a knot, another measure for determining the size of a knot is to determine how much volume in space a knotted SAP occupies. One measure of this is the *radius of gyration of a SAW (SAP)*.

The *square radius of gyration* of a SAW (SAP) ω in $\mathbb{Z}^3$, denoted $r^2(\omega)$, is defined to be

$$r^2(\omega) := \frac{1}{|\omega|} \sum_{i=0}^{|\omega|-1} \left([X(\boldsymbol{\omega}_i) - X_M(\omega)]^2 + [Y(\boldsymbol{\omega}_i) - Y_M(\omega)]^2 + [Z(\boldsymbol{\omega}_i) - Z_M(\omega)]^2 \right), \tag{1.55}$$

where $X(\boldsymbol{x})$, $Y(\boldsymbol{x})$, and $Z(\boldsymbol{x})$ are respectively the first, second, and third coordinates of the vertex $\boldsymbol{x}$ and $X_M(\omega)$, $Y_M(\omega)$, and $Z_M(\omega)$ are respectively the first, second, and third coordinates of the vertex corresponding to the center of mass of ω. Note that

$$X_M(\omega) := \frac{1}{|\omega|} \sum_{i=0}^{|\omega|-1} X(\boldsymbol{\omega}_i) \tag{1.56}$$

and that $Y_M(\omega)$ and $Z_M(\omega)$ are determined similarly. Given a fixed positive integer n and a set $\mathscr{S}_n \subseteq \mathscr{C}_n^3$(or $\mathscr{P}_n$) such that $0 < |\mathscr{S}_n| < \infty$, the *mean-square radius of gyration of the elements in* $\mathscr{S}_n$ is defined to be

$$r^2(\mathscr{S}_n) := \frac{1}{|\mathscr{S}_n|} \sum_{\omega \in \mathscr{S}_n} r^2(\omega). \tag{1.57}$$

Given a fixed even positive integer m, let $\boldsymbol{\pi}(m) := \{ \pi_{n|m} : n \geq m \}$ denote the probability mass function for the length of a randomly selected element from $\mathscr{S}$, given that the length is greater than or equal to m. When either $\mathscr{S} \subseteq \mathscr{C}$ or $\mathscr{S} \subseteq \mathscr{P}$, the

mean-square radius of gyration of the elements in $\mathscr{S}$, $r^2_{\boldsymbol{\pi}(m)}(\mathscr{S})$, is defined as

$$r^2_{\boldsymbol{\pi}(m)}(\mathscr{S}) := \sum_{n=m/2}^{\infty} r^2(\mathscr{S}_{2n})\pi_{2n|m}. \tag{1.58}$$

Recall from Section 1.3 that $\mathscr{P}$ is the set of all self-avoiding polygons in $\mathbb{Z}^3$ and that p_n is the number of distinct n-edged SAPs in $\mathscr{P}$. Then $r^2(\mathscr{P}_{2n})$, the mean-square radius of gyration of the polygons in $\mathscr{P}_{2n}$, is defined to be

$$r^2(\mathscr{P}_{2n}) = \frac{1}{p_{2n}} \sum_{\omega\in\mathscr{S}:|\omega|=2n} r^2\left(\omega\right). \tag{1.59}$$

Now, given any real values a, b, c, and d and a function $r(n) = O(n^{-1})$, define

$$\mathcal{R}_n(a, b, c, d, r) := an^{2b}\left(1 + cn^{-d} + r(n)\right). \tag{1.60}$$

It is expected that there exist real-valued constants A_R, ν, B_R, and Δ and a function r_R with $r_R(n) = O(n^{-1})$ such that $r^2(\mathscr{P}_{2n})$ has the asymptotic form [125], as $n \to \infty$,

$$r^2(\mathscr{P}_{2n}) \sim \mathcal{R}_{2n}(A_R, \nu, B_R, \Delta, r_R), \tag{1.61}$$

where A_R is referred to as an *amplitude*; ν is referred to as a *metric exponent*; and Δ is referred to as the *confluent exponent*. The scaling forms for p_n and $r^2(\mathscr{P}_n)$ are not rigorously proved but there are field theoretic ([47], [90], and [105]) and numerical evidence ([97]) supporting the validity of their asymptotic form.

In 1949, Flory [37] proposed a method for predicting ν in three dimensions. In 1969, Fisher [32] observed that Flory's method could be extended to predict ν in other dimensions. The values of ν as predicted using Flory's method are

$$\nu_{Flory} = \begin{cases} 1 & \text{if } d = 1 \\ 3/4 & \text{if } d = 2 \\ 3/5 & \text{if } d = 3 \\ 1/2 & \text{if } d \geq 4 \end{cases} \tag{1.62}$$

where d is the dimension. The values of ν_{Flory} for $d = 1$ and $d \geq 5$ are known to be correct; the values for $d = 2$ and $d = 4$ are believed to be correct; but the value of ν_{Flory} for $d = 3$ is believed to be too large. Field theoretic computations [47] and Monte Carlo simulations [97] for $d = 3$ estimate ν to be 0.5882 ± 0.0010 and 0.5877 ± 0.0006 respectively and Δ to be 0.478 ± 0.010 and 0.56 ± 0.53 respectively.

In [125] it was assumed, in analogy with Equation (1.61), that, for each knot-type K there exist real-valued constants $A_R(K)$, $\nu(K)$, $B_R(K)$, and $\Delta_R(K)$ and a function $r_R(K)$ with $r_R(K)(n) = O(n^{-1})$ such that, for polygons in $\mathscr{P}_{2n}(K)$, $r^2(\mathscr{P}_{2n}(K))$, the mean-square radius of gyration, has the asymptotic form, as $n \to \infty$,

$$r^2(\mathscr{P}_{2n}(K)) \sim \mathcal{R}_{2n}(A_R(K), \nu(K), B_R(K), \Delta_R(K), r_R(K)). \tag{1.63}$$

Also in [125], the following Monte Carlo estimates for the metric exponents $\nu(K)$ and amplitudes $A_R(K)$ were given:

$$\nu(K) = \begin{cases} 0.588 \pm 0.008 & \text{if } K = \phi \\ 0.599 \pm 0.008 & \text{if } K = 3_1 \\ 0.603 \pm 0.010 & \text{if } K = 4_1 \\ 0.586 \pm 0.010 & \text{if } K = 6_2 \\ 0.604 \pm 0.020 & \text{if } K = 3_1 \# 3_1 \\ 0.596 \pm 0.012 & \text{if } K = 3_1 \# 4_1 \end{cases} \tag{1.64}$$

and

$$A_R(K) = \begin{cases} 0.103 \pm 0.028 & \text{if } K = \phi \\ 0.1032 \pm 0.0016 & \text{if } K = 3_1 \\ 0.0967 \pm 0.0022 & \text{if } K = 4_1 \\ 0.0842 \pm 0.0012 & \text{if } K = 6_2 \\ 0.0889 \pm 0.0042 & \text{if } K = 3_1 \# 3_1 \\ 0.089 \pm 0.012 & \text{if } K = 3_1 \# 4_1. \end{cases} \tag{1.65}$$

The estimates in Equation (1.64) are consistent with the best estimate for $\nu = 0.5882 \pm 0.0010$ for SAPs and SAWs based on field theoretic computations [47]. They consequently support the hypothesis that the metric exponent ν is independent of knot-type. In [125], the authors argue that the estimates in Equation (1.65) support the hypothesis that the amplitudes are independent of knot-type.

1.6 The Probability of Knotting

Much attention has been given to determining the probability of knotting in a ring polymer. Various studies, based on both lattice [21, 22, 23, 65, 61, 67, 124, 125, 149, 150, 151, 153] and off-lattice [36, 93, 163] models, have been implemented to investigate these probabilities.

Table 1.4: Monte Carlo estimates for $1 - \Pr_{2n}(\phi)$ for $2n \in \{200, 400, 800, 1200, 1600\}$, as presented in [67].

$2n$	$1 - \Pr_{2n}(\phi)$
200	$(3.80 \pm 1.60) \times 10^{-4}$
400	$(2.42 \pm 0.44) \times 10^{-3}$
800	$(4.26 \pm 0.69) \times 10^{-3}$
1200	$(9.40 \pm 2.60) \times 10^{-3}$
1600	$(1.20 \pm 0.27) \times 10^{-2}$

Define the probability that an $(2n)$-edge SAP has knot-type K to be $\Pr_{2n}(K)$. Then

$$\Pr_{2n}(K) = \frac{p_{2n}(K)}{p_{2n}}. \tag{1.66}$$

One of the first numerical studies estimating $\Pr_{2n}(\phi)$ as a function of polygon length $2n$ was published in 1990 [67]. In [67], Janse van Rensburg and Whittington use a Monte Carlo algorithm based on the pivot algorithm to estimate $1 - \Pr_{2n}(\phi)$, the probability of an $(2n)$-edge polygon being knotted (according to Equation (1.66)). A summary of their estimates is provided in Table 1.4. The estimates in Table 1.4 are increasing as a function of n. Janse van Rensburg and Whittington [67] show that the estimates in Table 1.4 support the conclusion of Theorem 1.3.5, that is, that all but exponentially few sufficiently large SAPs in $\mathbb{Z}^3$ are knotted. Hence this supports the Frisch-Wasserman-Delbruck Conjecture (cf. Conjecture 1.1.1) for $\mathbb{Z}^3$.

Now recall from Section 1.3 that the proposed scaling forms (as $n \to \infty$) for p_{2n} and $p_{2n}(K)$ are respectively

$$A\,(2n)^{\alpha-3}\,\mu^{2n}\left(1 + \frac{B}{(2n)^{\Delta}} + g_p(2n)\right) \tag{1.67}$$

and

$$A_K\,(2n)^{\alpha_K-3}\,\mu_K^{2n}\left(1 + \frac{B_K}{(2n)^{\Delta_K}} + g_K(2n)\right). \tag{1.68}$$

Then $\Pr_{2n}(K)$, the probability that a $(2n)$-edge SAP has knot-type K, scales like

$$\begin{aligned}
&\frac{A_K\,(2n)^{\alpha_K-3}\,\mu_K^{2n}\left(1 + \frac{B_K}{(2n)^{\Delta_K}} + g_K(2n)\right)}{A\,(2n)^{\alpha-3}\,\mu^{2n}\left(1 + \frac{B}{(2n)^{\Delta}} + g_p(2n)\right)} \\
&\simeq \frac{A_K}{A}\,(2n)^{\alpha_K-\alpha}\left(\frac{\mu_K}{\mu}\right)^{2n}, \text{ for } n \text{ sufficiently large.}
\end{aligned} \tag{1.69}$$

Table 1.5: The estimates for $\Pr_{2n}(K)$ as computed in [173]. Error bars are one standard deviation.

$2n$	$\Pr_{2n}(\phi)$	$\Pr_{2n}(3_1)$	$\Pr_{2n}(4_1)$
500	0.99849(0.00025)	0.00147(0.00024)	0.00003(0.00003)
1000	0.99640(0.00038)	0.00344(0.00037)	0.00009(0.00006)
1500	0.99430(0.00048)	0.00541(0.00046)	0.00024(0.00010)
2000	0.99208(0.00056)	0.00752(0.00055)	0.00027(0.00010)
2500	0.98965(0.00064)	0.00985(0.00062)	0.00038(0.00012)
3000	0.98787(0.00069)	0.01157(0.00068)	0.00040(0.00012)

In fact, Deguchi and Tsurusaki [21, 22, 23] show (based on numerical results) that

$$C(K)\,(2n)^{M(K)}\exp\left(-\frac{2n}{\mathcal{N}(K)}\right) \tag{1.70}$$

is a suitable scaling form for $\Pr_{2n}(K)$ using off-lattice Gaussian and rod-bead models. In [173], Yao *et al.* numerically show that, for sufficiently large n, Equation (1.70) is also a suitable scaling form for the knotting probability of polygons modelled on the simple cubic lattice, where $C(K)$ is the amplitude ratio $\frac{A_K}{A}$ in Equation (1.69), $M(K) = \alpha_K - \alpha$, and $\frac{\mu_K}{\mu} = \exp\left(-\frac{1}{\mathcal{N}(K)}\right)$. The quantity $\mathcal{N}(K)$ is referred to as the *characteristic length of knot-type* K. For example, $\mathcal{N}(\phi)$ is the characteristic length of the unknot and $\mathcal{N}(\phi)$ is the polygon length for which unknots dominate the set of all SAPs for polygon lengths less than $\mathcal{N}(\phi)$. In [173], Yao *et al.*, estimate $\mathcal{N}(\phi)$ to be $(2.5 \pm 0.3) \times 10^5$ and estimate $\Pr_{2n}(K)$ as presented in Table 1.5

From the estimates for $\Pr_{2n}(\phi)$ in Table 1.5, $\Pr_{2n}(\phi)$ is decreasing as n increases and, from Theorem 1.3.5, $\Pr_{2n}(\phi) \to 0$ exponentially as $n \to \infty$, but at what exponential rate does $\Pr_{2n}(\phi) \to 0$ as $n \to \infty$? In other words, what is the value of $\kappa - \kappa_\phi$? In [65], Janse van Rensburg estimated $\kappa - \kappa_\phi \approx (4.15 \pm 0.32) \times 10^{-6}$ using Monte Carlo simulated polygons in $\mathbb{Z}^3$ with lengths up to 4000 edges. Janse van Rensburg's estimate for the difference $\kappa - \kappa_\phi$ suggests that κ and κ_ϕ differ in the sixth decimal place. Hence, estimating κ_ϕ and being able to distinguish it from an estimate for κ is extremely difficult to do numerically.

From the estimates for $\Pr_{2n}(\phi)$ in Table 1.5, the probability of knotting (as a function of polygon length) can be estimated. These estimates for the probability of knotting (based on the numerics presented in Table 1.5) are presented in Table 1.6. The estimates

Table 1.6: Monte Carlo estimates for $1 - \Pr_{2n}(\phi)$ for $2n \in \{500, 1000, 1500, 2000, 2500, 3000\}$ from [173].

$2n$	$1 - \Pr_{2n}(\phi)$
500	$(1.51 \pm 2.50) \times 10^{-3}$
1000	$(3.60 \pm 0.38) \times 10^{-3}$
1500	$(5.70 \pm 0.48) \times 10^{-3}$
2000	$(7.92 \pm 0.56) \times 10^{-3}$
2500	$(1.035 \pm 0.064) \times 10^{-2}$
3000	$(1.213 \pm 0.069) \times 10^{-2}$

for the probability of knotting presented in Table 1.6 are increasing as a function of n.

It was not until relatively recently [36, 61, 93, 96] that people began numerically studying the probability of knotting after a local strand passage has been performed and the corresponding transition knotting probabilities (the probability that an after-strand-passage polygon has knot-type K' given that one starts with a knot-type K polygon). Let $\Pr_{2n}(K'|K, s)$ denote the transition knotting probability characterized by starting with an $(2n)$-edge knot-type K polygon and ending, after a successful strand-passage, with a knot-type K' polygon, and define, if the limit exists,

$$\Pr(K'|K, s) := \lim_{n\to\infty} \Pr_{2n}(K'|K, s). \tag{1.71}$$

Note that $\Pr(K'|K, s)$, provided it exists, is referred to herein as the *limiting transition knotting probability from K to K'*.

In [36], an off-lattice simulation of a freely jointed isolateral 33-edge polygon was performed in which two non-consecutive vertices of the polygon were randomly selected such that the second vertex chosen could be located no more than eight consecutive edges along the polygon from the first vertex. Then, the segment between these two chosen vertices was rotated through a uniformly random selected angle from $-180°$ to $180°$. 20,000 of these moves were performed and the outcome of each move was only accepted if no strand passage occurred as a result of the rotation. Then after the $20,000$ moves, another move was performed and accepted if a single strand passage occurred. This procedure was repeated for a total of $20,000$ times for each of the knot-types with up to and including six crossings. (Note that the after-strand-passage knot-type of each generated polygon

Table 1.7: The transition knotting probabilities estimated using the off-lattice strand passage model from [36].

Transition	Probability
$\phi \to \phi$	0.9457
$\phi \to 3_1$	0.0454
$\phi \to 4_1$	0.0073
$\phi \to 5_2$	0.0012

need not be an unknotting number one knot-type.) The relative frequencies (referred to as *transition knotting probabilities*) were estimated for the transitions from knot-type K_i to knot-type K_j after a strand passage. Table 8.3 presents the transition knotting probabilities from K to K' (denoted $K \to K'$) estimated using the model of Flammini *et al.* [36].

In 2006, Liu *et al.* [96] further explored the concept of transition knotting probabilities. They investigated the transition knotting probabilities as a function of the before-strand-passage local geometry of a juxtaposition of two segments of a polygon in $\mathbb{Z}^3$ via virtual strand passages. (Virtual strand passages are implemented by replacing the before-strand-passage structures with graphs of after-strand-passage structures that can be embedded in $\mathbb{R}^3$ but not in $\mathbb{Z}^3$.) Figures 1.18 (a) and (b) provide illustrations of the graph embeddings that Liu *et al.* [96] define as a *hooked juxtaposition* and a *semi-hooked juxtaposition* respectively. Figure 1.19 provides illustrations of the three graph embeddings that Liu *et al.* [96] refer to as the *free juxtapositions*.

For 500-edge SAPs, the authors estimated the probability of knotting when a strand passage occurred about the hooked juxtaposition (cf. Figure 1.18 (a)) to be 0.0139. They found that strand passages about a hooked juxtaposition (when compared to strand passages about the semi-hooked and free juxtapositions) tended to decrease the after-strand-passage knot-probability thus increasing the transition knotting probability from being knotted to unknotted. They also found that strand passages about a free juxtaposition tended to increase the after-strand-passage knot-probability thus decreasing the transition knotting probability from being knotted to being unknotted. In [93], Liu and Chan developed an off-lattice model which they used to study, among other questions, the impact of the strand passage site juxtaposition on the probability of knotting. They concluded

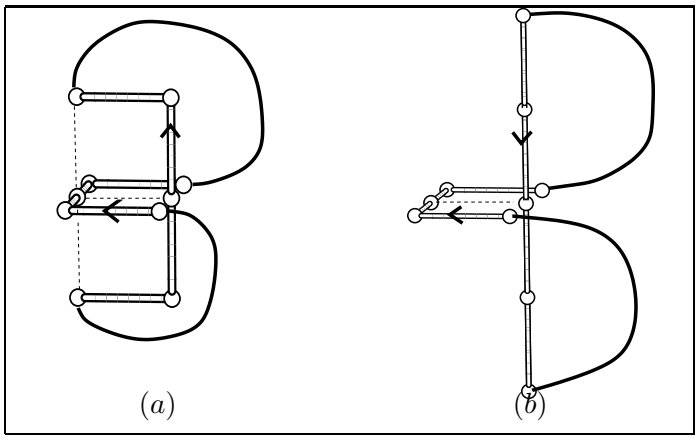

Figure 1.18: (a): The hooked juxtaposition structure and (b): the semi-hooked juxtaposition from [96].

that certain characteristics of their model is approximated by the Liu *et al.* [96] model.

The LSP Model (presented in Section 2.1 of this thesis) specifies another juxtaposition about which a strand passage in a SAP can be implemented. At the crossing where a strand passage is implemented, a strand passage changes the crossing type and hence can actually change the knot-type of the original polygon. The LSP Model is used to investigate the probability of the formation of distinct knot-types after a strand passage is implemented. This allows the probability of knotting and the transition knotting probabilities to be estimated for the LSP Model. It should be pointed out however that in addition to a different juxtaposition being used, another key difference between the structure used in the LSP Model and those studied in [96] is that the LSP Model structure was designed so that a strand passage can be modelled in $\mathbb{Z}^3$ as opposed to the virtual strand passages used in [96]. Obtaining a better understanding of the differences between the LSP Model and the model presented in [96] is future work (cf. Section 8.2).

In [61], Hua *et al.* present another lattice model for studying transition knotting probabilities. They developed a new strand-passage algorithm that generates a Markov chain whose state space is the set of knot-types with 8 or fewer crossings. For a fixed average polygon length L and fixed non-negative integer e, the one-step transition probability matrix (denoted $P_{L\pm e}$) for this Markov chain was estimated using the relative frequencies for the transitions from knot-type K_i to knot-type K_j after a single strand passage at randomly chosen crossings in the knot projections of BFACF-generated (cf. Section 3.1) polygons in $\mathbb{Z}^3$ with lengths in $[L-e, L+e]$ having knot-type K_i. The knot diagram corresponding

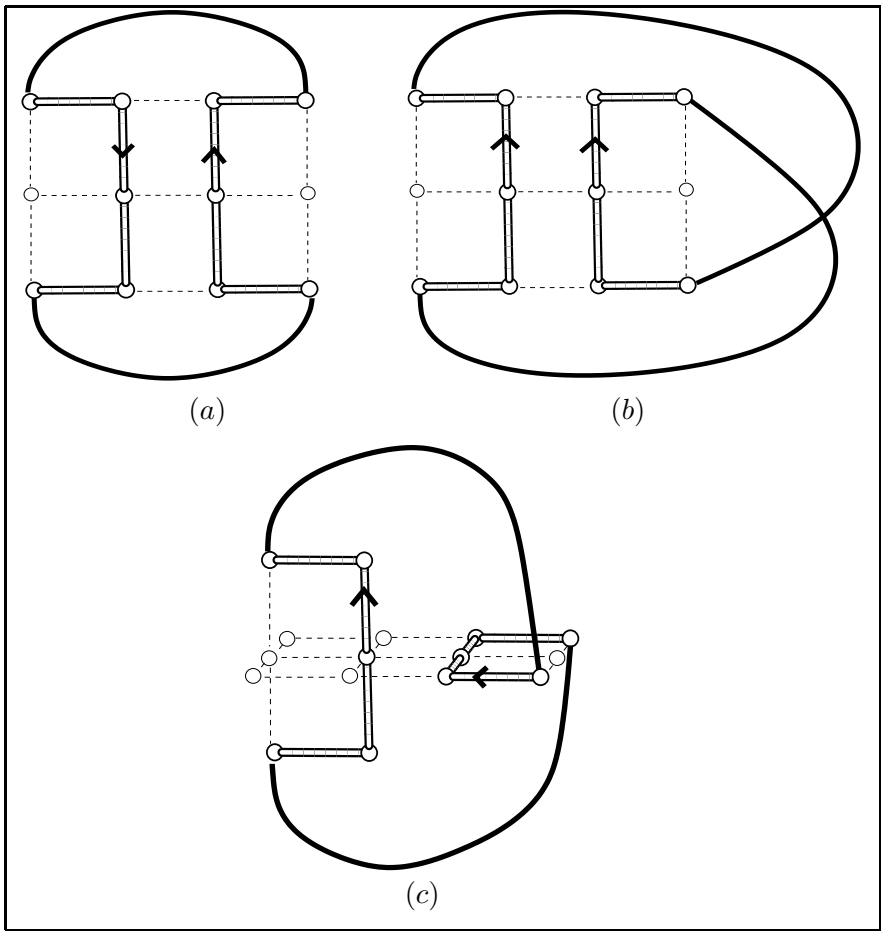

Figure 1.19: The three free juxtapositions from [96].

to the knot projection is represented using Dowker-Thistlethwaite (DT) code (cf. [29] for a detailed discussion regarding the DT code representation of a knot diagram). These transition knotting probabilities were then used to study the evolution of the knot-type resulting after repeated strand passages. For example, using their algorithm for $L = 100$ and $e = 4$, for a randomly chosen unknotted polygon whose expected length is 100, Hua *et al.* estimate that the probability of knotting given one successful strand passage is 0.148 and that the corresponding transition knotting probabilities are as stated in Table 1.8. Whether or not the transition knotting probabilities presented in Table 1.8 can be compared to the corresponding probabilities estimated in Chapter 6 of this work is left as future work (cf. Section 8.2).

Though each of the works [36, 61, 93, 96] study knotting probabilities and/or transition knotting probabilities, the work presented throughout the remainder of this document differs significantly from the work presented in each if [36, 61, 93, 96] in several key aspects.

Table 1.8: The one-step transition knotting probabilities estimated using the lattice strand passage model from [61].

Transition	Probability
$\phi \to \phi$	0.852
$\phi \to 3_1$	0.061
$\phi \to 4_1$	0.022
$\phi \to 5_2$	0.002

Firstly, strand passages implemented in the LSP Model are implemented in $\mathbb{Z}^3$. The strand passages in each of [36, 61, 93, 96] could not be implemented in $\mathbb{Z}^3$. Secondly, this work investigates the limiting probability of knotting and the limiting transition knotting probabilities associated with the LSP Model. None of the works [36, 61, 93, 96] investigated limiting probabilities. Thirdly, this work investigates two different measures of the "size" of Θ-SAPs and presents new conjectures (supported by simulation data) related to each of these measures of the "size". Consequently the LSP model is a model which has many properties that are of interest. In the next chapter, the LSP Model and some of these interesting properties are discussed.

Chapter 2

Modelling a Local Strand Passage in a Ring Polymer

To investigate the effects of a local strand passage at a random location in a ring polymer with fixed knot-type K, it is assumed that two of the strands of the polymer have been brought "close" together at a random location. These polymers will be from here-on-in referred to as *pinched* ring polymers. A SAP in $\mathbb{Z}^3$, that has fixed knot-type K and that contains a fixed structure representing two "strands" of the polygon being "close" together, is then used to represent the conformations of these pinched polymers. From this point forward, any reference to a self-avoiding polygon will be to a self-avoiding polygon in $\mathbb{Z}^3$ and any illustration of a self-avoiding polygon will be drawn according to the axis system defined by Figure 2.1.

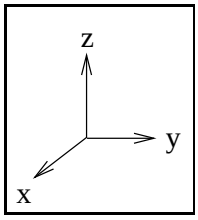

Figure 2.1: The axis system used to illustrate graph embeddings in $\mathbb{Z}^3$.

This chapter first reviews the SAP model of pinched polymers that was developed in [150]. Then, in Section 2.2, some new theoretical results regarding the growth constants associated with subsets of Θ-SAPs are proved. The section also provides heuristic arguments supporting several new conjectures regarding the critical exponents α_*^{Θ} (as defined in Equation (2.84)), regarding the scaling forms for the fixed-n strand passage probabilities, and regarding the possible values for the limiting strand passage probabilities. The section concludes by presenting several conjectures and questions regarding the "size" of

the Θ-SAPs used in the Local Strand Passage Model.

2.1 A Simplified Model of Strand Passage

To model the "pinched" portion of the ring polymer, the SAPs used will be required to contain a specific pattern $\Theta(a,b,c)$ fixed at $(a,b,c) \in \mathbb{Z}^3$, or Θ for short, where Θ is defined by the graph embedding $\Theta := (\mathcal{V}(\Theta), \mathcal{E}(\Theta))$ in $\mathbb{Z}^3$ with vertex set

$$\begin{aligned} \mathcal{V}(\Theta) = \quad & \{(a+1,b,c),(a,b,c),(a-1,b,c),(a,b-1,c-2),(a,b-1,c-3), \\ & (a,b,c-3),(a,b+1,c-3),(a,b+1,c-2)\} \end{aligned} \tag{2.1}$$

and edge set

$$\begin{aligned} \mathcal{E}(\Theta) = \quad & \{\{(a+1,b,c),(a,b,c)\},\{(a,b,c),(a-1,b,c)\}, \\ & \{(a,b-1,c-2),(a,b-1,c-3)\},\{(a,b-1,c-3),(a,b,c-3)\}, \\ & \{(a,b,c-3),(a,b+1,c-3)\},\{(a,b+1,c-3),(a,b+1,c-2)\}\}, \end{aligned} \tag{2.2}$$

as illustrated in Figure 2.2.

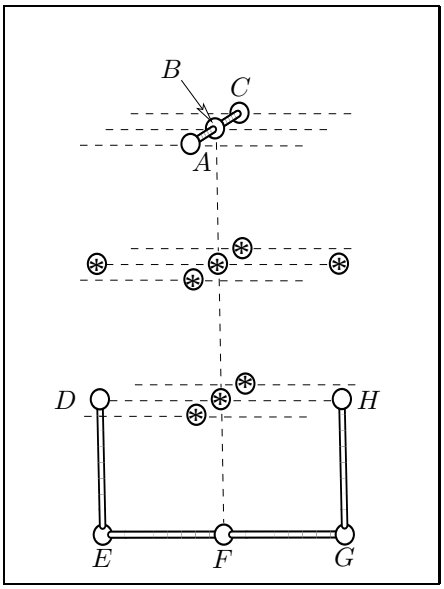

Figure 2.2: The fixed strand passage structure Θ in which open and empty circles represent the vertices of Θ and open bonds represent the edges of Θ. Dashed lines and circles containing asterisks represent, respectively, lattice edges and vertices that Θ does not occupy. The circles containing asterisks represent the vertices in the set $\mathcal{V}_s(\Theta)$. Vertex $A = (a+1,b,c)$; Vertex $B = (a,b,c)$; Vertex $C = (a-1,b,c)$; Vertex $D = (a,b-1,c-2)$; Vertex $E = (a,b-1,c-3)$; Vertex $F = (a,b,c-3)$; Vertex $G = (a,b+1,c-3)$; and Vertex $H = (a,b+1,c-2)$.

Because Θ represents the location in a SAP where a strand passage is to be attempted, from this point forward, a SAP with knot-type K which contains the fixed pattern Θ will be referred to as a *before-strand-passage polygon* and Θ will be referred to as the *before-strand-passage structure*. Note that Θ-SAPs (to which have already been referred) are nothing but before-strand-passage polygons that contain $\Theta(0,0,0)$.

To model a strand passage at a chosen location in a ring polymer with knot-type K, define the *after-strand-passage structure* $\Theta_s(a,b,c)$ fixed at $(a,b,c) \in \mathbb{Z}^3$, or Θ_s for short, by the graph embedding $\Theta_s := (\mathcal{V}(\Theta_s), \mathcal{E}(\Theta_s))$ in $\mathbb{Z}^3$ with vertex set

$$\begin{aligned}\mathcal{V}(\Theta_s) := \quad & \{(a+1,b,c),(a+1,b,c-1),(a+1,b,c-2),(a,b,c-2),\\ & (a-1,b,c-2),(a-1,b,c-1),(a-1,b,c),(a,b-1,c-2),\\ & (a,b-1,c-1),(a,b,c-1),(a,b+1,c-1),(a,b+1,c-2)\}\end{aligned} \tag{2.3}$$

and edge set

$$\begin{aligned}\mathcal{E}(\Theta_s) := \quad & \{\{(a+1,b,c),(a+1,b,c-1)\},\{(a+1,b,c-1),(a+1,b,c-2)\},\\ & \{(a+1,b,c-2),(a,b,c-2)\},\{(a,b,c-2),(a-1,b,c-2)\},\\ & \{(a-1,b,c-2),(a-1,b,c-1)\},\{(a-1,b,c-1),(a-1,b,c)\}\\ & \{(a,b-1,c-2),(a,b-1,c-1)\},\{(a,b-1,c-1),(a,b,c-1)\},\\ & \{(a,b,c-1),(a,b+1,c-1)\},\{(a,b+1,c-1),(a,b+1,c-2)\}\},\end{aligned} \tag{2.4}$$

as illustrated in Figure 2.3.

Now consider a before-strand-passage polygon ω. Because of how the strand passage is to be performed in ω, it will be "successful" if and only if the vertices (cf. the vertices in Figure 2.2 that are represented by circles containing asterisks) in the set

$$\begin{aligned}\mathcal{V}_s(\Theta) := \quad & \{(a+1,b,c-1),(a+1,b,c-2),(a,b,c-1),(a,b,c-2),\\ & (a-1,b,c-1),(a-1,b,c-2),(a,b-1,c-1),(a,b+1,c-1)\},\end{aligned} \tag{2.5}$$

are not end points of any edge in $\mathcal{E}(\omega)$. A strand passage is said to be *viable in* ω if no vertex in $\mathcal{V}_s(\Theta)$ is an end point of an edge in $\mathcal{E}(\omega)$. If a vertex in $\mathcal{V}_s(\Theta)$ is an end point of an edge in $\mathcal{E}(\omega)$, then the strand passage in ω is not viable and the attempted strand passage is said to be an *unsuccessful strand passage*. If a strand passage in ω is viable, then the before-strand-passage structure Θ can be removed from ω and can be replaced by the after-strand-passage structure Θ_s to yield a new polygon ω_s. When a strand passage in a polygon is viable, the original polygon ω will be referred to as a *successful-strand-passage*

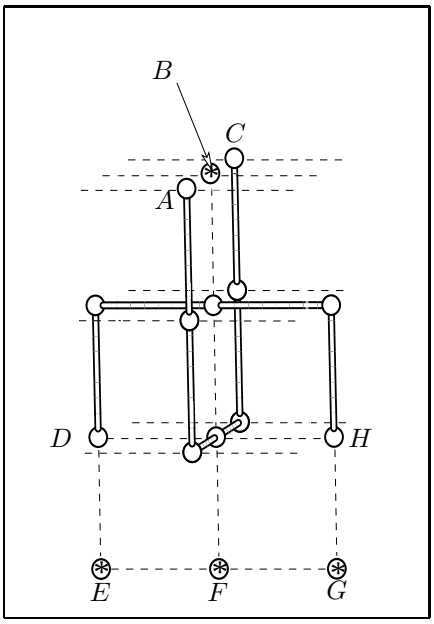

Figure 2.3: The after-strand-passage structure Θ_s in which open and empty circles represent the vertices of Θ_s and open bonds represent the edges of Θ_s. The circles containing asterisks are vertices in Θ not occupied by Θ_s. Dashed lines represent lattice edges not occupied by Θ_s. Vertex $A = (a+1, b, c)$; Vertex $B = (a, b, c)$; Vertex $C = (a-1, b, c)$; Vertex $D = (a, b-1, c-2)$; Vertex $E = (a, b-1, c-3)$; Vertex $F = (a, b, c-3)$; Vertex $G = (a, b+1, c-3)$; and Vertex $H = (a, b+1, c-2)$.

polygon and the transformed polygon ω_s will be referred to as the resulting *after-strand-passage polygon*. When a strand passage in ω is not viable, ω will be referred to as an *unsuccessful-strand-passage polygon* or a *failed-strand-passage polygon*. Figure 2.4 (a) is an illustration of a 14-edge polygon containing the structure Θ in which a strand passage is viable. Figure 2.4 (b) is an illustration of the polygon resulting from replacing the structure Θ in Figure 2.4 (a) with the after-strand-passage structure Θ_s.

Note that the strand passage structure was constructed so that there is enough space for a strand of the polygon to occupy one or more of the vertices in the set $\{B+(0,0,-1), B+(0,0,-2)\}$ (the set of vertices that lie between the upper and lower part of the structure). Allowing space for such a strand to pass through the structure Θ is required to ensure the irreducibility of the Monte Carlo algorithm used to study the Local Strand Passage Model of this thesis (cf. Section 3.3 and [150] for a discussion of this algorithm). Note however that, if indeed either of the vertices in the set $\{B+(0,0,-1), B+(0,0,-2)\}$ is occupied by the before-strand-passage polygon, then a strand passage about Θ is not viable.

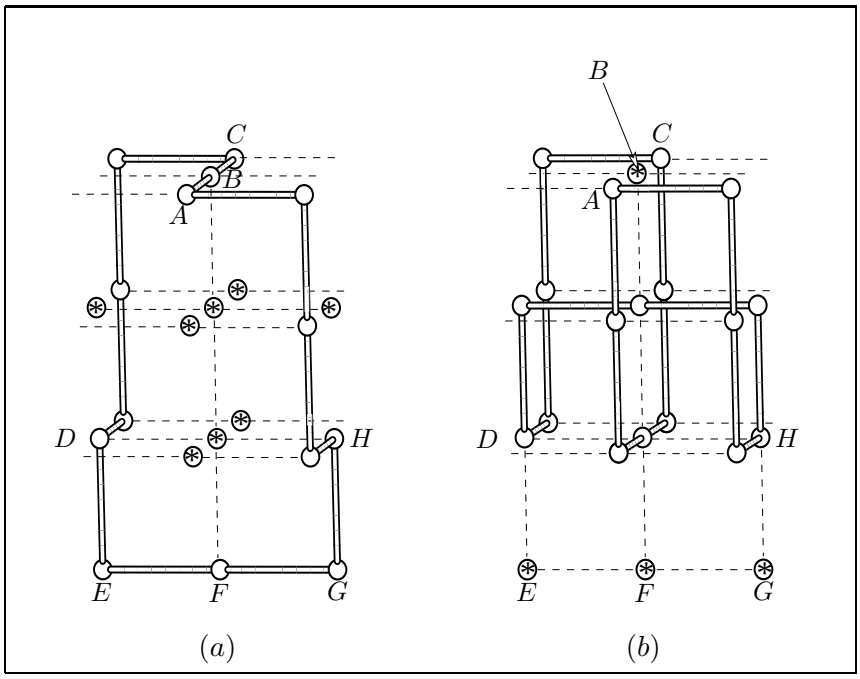

Figure 2.4: (a) Example of a 14-edge unknotted SAP in $\mathbb{Z}^3$ that contains the structure Θ and a strand passage is possible about Θ. The circles containing asterisks are vertices occupied by $\mathcal{V}_s(\Theta)$. Dashed lines represent lattice edges not occupied by the SAP or Θ_s. (b) The 18-edge unknotted SAP in $\mathbb{Z}^3$ that results when a strand passage is implemented in the SAP in (a) . The circles containing asterisks are vertices that were occupied by the 14-edge before-strand-passage polygon that are not occupied by 18-edge after-strand-passage polygon. Dashed lines represent lattice edges not occupied by the SAP . In both (a) and (b), open and empty circles represent the vertices of the SAPs and open bonds represent the edges of the SAPs. Vertex $A = (a+1, b, c)$; Vertex $B = (a, b, c)$; Vertex $C = (a-1, b, c)$; Vertex $D = (a, b-1, c-2)$; Vertex $E = (a, b-1, c-3)$; Vertex $F = (a, b, c-3)$; Vertex $G = (a, b+1, c-3)$; and Vertex $H = (a, b+1, c-2)$.

The next section provides the conjectures and questions that are explored numerically in Chapters 5, 6, and 7. More specifically, the next section provides new results regarding the growth constants associated with subsets of Θ-SAPs. The section also provides conjectures for the critical exponents α_*^{Θ} (as defined in Equation (2.84)), for the scaling forms for the fixed-n strand passage probabilities, for the possible values for the limiting strand passage probabilities, and regarding the "size" of the Θ-SAPs used in the LSP Model.

2.2 Theoretical Results Corresponding to the LSP Model

Two classes of before-strand-passage polygons can be defined based on Θ. These two classes are relevant to the Monte Carlo algorithm used to study the LSP Model (cf. Section 3.3 and [150]). To define these two classes, the definition of an undirected self-avoiding walk (uSAW) in $\mathbb{Z}^d$ is required.

Definition 2.2.1 *For any $n \geq 0$, a graph embedding $\upsilon = (\mathcal{V}(\upsilon), \mathcal{E}(\upsilon))$ in $\mathbb{Z}^d$ consisting of n distinct edges in $\mathbb{Z}^d$, $\mathcal{E}(\upsilon) = \{\{\boldsymbol{u}_0, \boldsymbol{u}_1\}, \{\boldsymbol{u}_1, \boldsymbol{u}_2\}, \ldots, \{\boldsymbol{u}_{n-2}, \boldsymbol{u}_{n-1}\}, \{\boldsymbol{u}_{n-1}, \boldsymbol{u}_n\}\}$, and $n+1$ distinct vertices in $\mathbb{Z}^d$, $\mathcal{V}(\upsilon) = \{\boldsymbol{u}_0 = \boldsymbol{x}, \boldsymbol{u}_1, \boldsymbol{u}_2, \ldots, \boldsymbol{u}_{n-1}, \boldsymbol{u}_n = \boldsymbol{y}\}$, where $||\boldsymbol{u}_{i+1} - \boldsymbol{u}_i||_1 = 1$, is referred to as an* undirected self-avoiding walk *υ. The vertices $\boldsymbol{x}$ and $\boldsymbol{y}$ are referred to as the* terminal ends (vertices) *of υ.*

Definition 2.2.2 *Let $\mathscr{W}(\boldsymbol{x}, \boldsymbol{y})$ be the set of all uSAWs in $\mathbb{Z}^3$ with terminal ends $\boldsymbol{x}$ and $\boldsymbol{y}$.*

Referring to Figure 2.5, for any before-strand-passage polygon ω consider the uSAW ϖ contained in ω that does not contain B and has terminal vertices A and C. If ϖ contains an uSAW that does not contain F and has terminal vertices C and D, then ω is defined to be in the first class (cf. Figure 2.5 (a)). Otherwise ω is defined to be in the second class. Figure 2.5 (a) below provides an illustration of a SAP in the first class and Figure 2.5 (b) provides an illustration of a SAP in the second class.

Based on these two classes, the set of before-strand-passage polygons can be partitioned into the following two distinct sets.

Definition 2.2.3 *Given $(a, b, c) \in \mathbb{Z}^3$, define $\mathscr{P}^{\Theta}(K : CD, AH)$ to be the set of self-avoiding polygons in $\mathscr{P}(K)$ that can be decomposed into the fixed structure Θ, as illustrated in Figure 2.2, and two uSAWs w_- and w_+, where w_- and w_+ are mutually avoiding, $w_- \in \mathscr{W}(C,D)$, $w_+ \in \mathscr{W}(A, H)$, $\mathcal{V}(w_-) \cap \mathcal{V}(\Theta) = \{C, D\}$, and $\mathcal{V}(w_+) \cap \mathcal{V}(\Theta) = \{A, H\}$. Note that $A = (a+1, b, c)$, $C = (a-1, b, c)$, $D = (a, b-1, c-2)$, and $H = (a, b+1, c-2)$. Then let $\mathscr{P}_n^{\Theta}(K : CD, AH)$ be the set of n-edge SAPs in $\mathscr{P}^{\Theta}(K : CD, AH)$.*

Definition 2.2.4 *Given $(a, b, c) \in \mathbb{Z}^3$, define $\mathscr{P}^{\Theta}(K : CH, AD)$ to be the set of self-avoiding polygons in $\mathscr{P}^{\Theta}(K)$ that can be decomposed into the fixed structure Θ, as illustrated in Figure 2.2, and the two uSAWs w_- and w_+, where w_- and w_+ are mutually avoiding, $w_- \in \mathscr{W}(C,H)$, $w_+ \in \mathscr{W}(A, D)$, $\mathcal{V}(w_-) \cap \mathcal{V}(\Theta) = \{C, H\}$, and $\mathcal{V}(w_+) \cap \mathcal{V}(\Theta) = \{A, D\}$.*

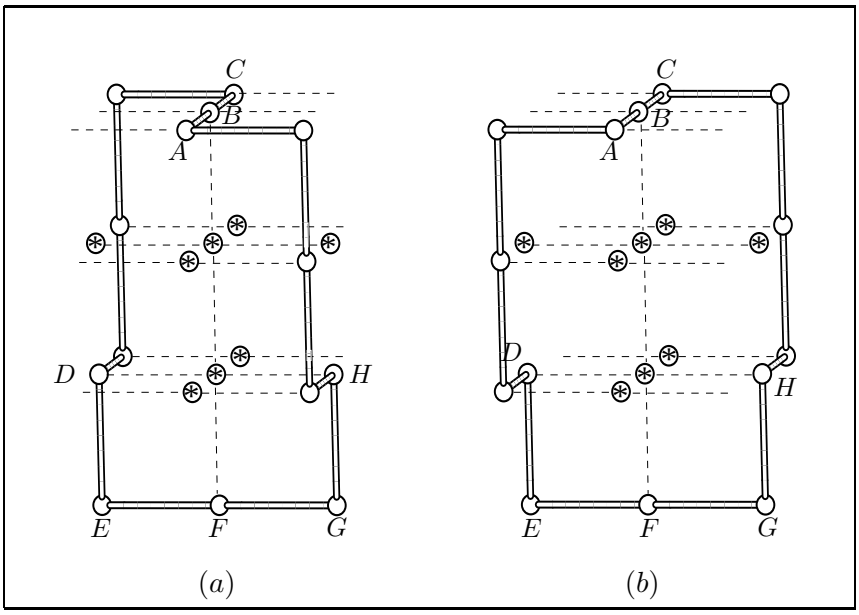

Figure 2.5: (a) is an example of a SAP in the first class of SAPs containing Θ. (b) is an example of a SAP in the second class of SAPs containing Θ. Open and empty circles represent the vertices of the SAP and open bonds represent the edges of the SAP. The circles containing asterisks are vertices in $\mathcal{V}_s(\Theta)$. Dashed lines represent lattice edges not occupied by the SAP. Vertex $A = (a+1, b, c)$; Vertex $B = (a, b, c)$; Vertex $C = (a-1, b, c)$; Vertex $D = (a, b-1, c-2)$; Vertex $E = (a, b-1, c-3)$; Vertex $F = (a, b, c-3)$; Vertex $G = (a, b+1, c-3)$; and Vertex $H = (a, b+1, c-2)$.

Note that $A = (a+1, b, c)$, $C = (a-1, b, c)$, $D = (a, b-1, c-2)$, *and* $H = (a, b+1, c-2)$. *Then let* $\mathscr{P}_n^{\Theta}(K : CH, AD)$ *be the set of* n*-edge SAPs in* $\mathscr{P}^{\Theta}(K : CH, AD)$.

Because the length of any SAP must be even,

$$\mathscr{P}^{\Theta}(K : CH, AD) = \bigcup_{n \in \mathbb{N}} \mathscr{P}_{2n}^{\Theta}(K : CH, AD) \tag{2.6}$$

and

$$\mathscr{P}^{\Theta}(K : CD, AH) = \bigcup_{n \in \mathbb{N}} \mathscr{P}_{2n}^{\Theta}(K : CD, AH). \tag{2.7}$$

In [150], Szafron proved the following result regarding $\mathscr{P}^{\Theta}(\phi : CD, AH)$ and $\mathscr{P}^{\Theta}(\phi : CH, AD)$ using the mapping $f : \mathbb{Z}^3 \to \mathbb{Z}^3$ defined by

$$f(x, y, z) := (2a - x, y, z), \tag{2.8}$$

where a is the x-coordinate of the point at which the structure $\Theta(a, b, c)$ is fixed.

Theorem 2.2.1 (Szafron [150]) *Given $(a,b,c) \in \mathbb{Z}^3$, let $7 \leq n$ be any natural number. Then for every $\omega' \in \mathscr{P}^{\Theta}_{2n}(\phi : CD, AH)$ there exists a unique $\omega \in \mathscr{P}^{\Theta}_{2n}(\phi : CH, AD)$ and for every $\omega \in \mathscr{P}^{\Theta}_{2n}(\phi : CH, AD)$ there exists a unique $\omega' \in \mathscr{P}^{\Theta}_{2n}(\phi : CD, AH)$, that is*

$$\left|\mathscr{P}^{\Theta}_{2n}(\phi : CD, AH)\right| = \left|\mathscr{P}^{\Theta}_{2n}(\phi : CH, AD)\right|. \tag{2.9}$$

Note that throughout this work, the empty-set will be denoted by $\{\}$ rather than by $\varnothing$ in order to minimize any confusion that might arise between using the symbol $\varnothing$ for the empty-set and using the symbol ϕ for the unknot.

Combining Theorem 2.2.1 with the facts that, for any natural number $n \geq 14$,

$$\mathscr{P}^{\Theta}_{n}(\phi : CH, AD) \cap \mathscr{P}^{\Theta}_{n}(\phi : CD, AH) = \{\} \tag{2.10}$$

and

$$\mathscr{P}^{\Theta}(\phi : CH, AD) \cap \mathscr{P}^{\Theta}(\phi : CD, AH) = \{\}, \tag{2.11}$$

results in the following two corollaries.

Corollary 2.2.1 *For any natural number $n \geq 14$,*

$$\left|\mathscr{P}^{\Theta}_{n}(\phi : CH, AD) \cup \mathscr{P}^{\Theta}_{n}(\phi : CD, AH)\right| = 2\left|\mathscr{P}^{\Theta}_{n}(\phi : CH, AD)\right| = 2\left|\mathscr{P}^{\Theta}_{n}(\phi : CD, AH)\right|. \tag{2.12}$$

Corollary 2.2.2

$$\left|\mathscr{P}^{\Theta}(\phi : CH, AD) \cup \mathscr{P}^{\Theta}(\phi : CD, AH)\right| = 2\left|\mathscr{P}^{\Theta}(\phi : CH, AD)\right| = 2\left|\mathscr{P}^{\Theta}(\phi : CD, AH)\right|. \tag{2.13}$$

Note that Theorem 2.2.1 and Corollaries 2.2.1 and 2.2.2 and their respective proofs can be generalized to any knot-type K by changing any reference to ϕ in them to knot-type K. Also, without loss of generality, in the remainder of this thesis the discussion will be restricted to the choice of $(a,b,c) = (0,0,0)$ in Definition 2.2.5; any reference to Θ will imply $\Theta(0,0,0)$; and any reference to Θ_s will imply $\Theta_s(0,0,0)$.

Definition 2.2.5 *For each knot-type K, define $\mathscr{P}^{\Theta}(K) := \mathscr{P}^{\Theta}(K : CD, AH)$ where $A = (1,0,0)$; $C = (-1,0,0)$; $D = (0,-1,-2)$; and $H = (0,1,-2)$.*

Definition 2.2.6 *Define $\mathscr{K}^{\Theta}(K)$ to be the set of all knot-types K' that can result when a successful strand passage about Θ is implemented on the elements of $\mathscr{P}^{\Theta}(K)$.*

Definition 2.2.7 *For each knot-type K, let $\mathscr{P}^{\Theta}(K,s)$ be the set of all SAPs in $\mathscr{P}^{\Theta}(K)$ for which strand passage is viable. Then define*

$$\mathscr{P}^{\Theta}(K,f) := \mathscr{P}^{\Theta}(K) \backslash \mathscr{P}^{\Theta}(K,s); \tag{2.14}$$

and, for each knot-type $K' \in \mathscr{K}^{\Theta}(K)$, define $\mathscr{P}^{\Theta}(K'|K,s)$ to be the set of all SAPs in $\mathscr{P}^{\Theta}(K,s)$ that have knot-type K' after Θ is replaced with Θ_s.

Given any knot-type K, note that $\mathscr{P}^{\Theta}(K,f)$ is the set of all SAPs in $\mathscr{P}^{\Theta}(K)$ for which strand passage is not viable, that is has failed. The following definition specifies the notation that will be used to refer to respectively the set of, and the number of, n-edge Θ-SAPs in $\mathscr{P}^{\Theta}(K)$, $\mathscr{P}^{\Theta}(K,s)$, $\mathscr{P}^{\Theta}(K,f)$, and, for each knot-type $K' \in \mathscr{K}^{\Theta}(K)$, $\mathscr{P}^{\Theta}(K'|K,s)$.

Definition 2.2.8 *For each knot-type K, let $\mathscr{P}_n^{\Theta}(K)$ be the set of n-edge polygons in $\mathscr{P}^{\Theta}(K)$; $\mathscr{P}_n^{\Theta}(K,s)$ be the set of n-edge polygons in $\mathscr{P}^{\Theta}(K,s)$; $\mathscr{P}_n^{\Theta}(K,f)$ be the set of n-edge polygons in $\mathscr{P}^{\Theta}(K,f)$; and $\mathscr{P}_n^{\Theta}(K'|K,s)$, for each knot-type $K' \in \mathscr{K}^{\Theta}(K)$, be the set of n-edge polygons in $\mathscr{P}^{\Theta}(K'|K,s)$. Now define $p_n^{\Theta}(K)$ to be the number of polygons in $\mathscr{P}_n^{\Theta}(K)$; $p_n^{\Theta}(K,s)$ to be the number of polygons in $\mathscr{P}_n^{\Theta}(K,s)$; $p_n^{\Theta}(K,f)$ to be the number of polygons in $\mathscr{P}_n^{\Theta}(K,f)$; and $p_n^{\Theta}(K'|K,s)$ to be the number of polygons in $\mathscr{P}_n^{\Theta}(K'|K,s)$.*

Given any knot-type K, a question that arises regarding the sets $\mathscr{P}_{2n}^{\Theta}(K)$, $\mathscr{P}_{2n}^{\Theta}(K,s)$, $\mathscr{P}_{2n}^{\Theta}(K,f)$, and, for each knot-type $K' \in \mathscr{K}^{\Theta}(K)$, $\mathscr{P}_{2n}^{\Theta}(K'|K,s)$, is "For each $* \in \Phi(K)$, does there exist a positive integer n_*^{Θ} such that $\mathscr{P}_{2n}^{\Theta}(*) \neq \{\}$ for all $n \geq n_*^{\Theta}$?", where $\Phi(K) := \{K, (K,s), (K,f)\} \cup \mathscr{K}^{\dagger}(K)$ and $\mathscr{K}^{\dagger}(K)$ is defined by

$$\mathscr{K}^{\dagger}(K) := \bigcup_{K' \in \mathscr{K}^{\Theta}(K)} \left\{(K'|K,s)\right\}. \tag{2.15}$$

Note that when $K = \phi$, $\Phi(K)$ is simply denoted Φ. In order to answer this question, the following definitions and algorithm for concatenating two polygons are required.

To define the top (last) and bottom (first) vertices of a polygon in $\mathbb{Z}^3$, the concept of *lexicographic ordering for vertices* in $\mathbb{Z}^3$ needs to be defined. For the vertices $\boldsymbol{a} = (a(1), a(2), a(3))$ and $\boldsymbol{b} = (b(1), b(2), b(3)) \in \mathbb{Z}^3$, define $\boldsymbol{a} \prec \boldsymbol{b}$ (that is $\boldsymbol{a}$ precedes $\boldsymbol{b}$ lexicographically) if for some j, $1 \leq j \leq 3$, $a(j) < b(j)$ and, for all $i = 1, \ldots, j-1$, $a(i) = b(i)$. Then the *top (last) vertex* in a set $S \subseteq \mathbb{Z}^3$ is defined to be the vertex $\boldsymbol{b} \in S$

such that for all $\boldsymbol{a} \in S \backslash \{\boldsymbol{b}\}$, $\boldsymbol{a} \prec \boldsymbol{b}$ and the *bottom (first) vertex* in a set $S \subseteq \mathbb{Z}^d$ is defined to be the vertex $\boldsymbol{a} \in S$ such that for all $\boldsymbol{b} \in S \backslash \{\boldsymbol{a}\}$, $\boldsymbol{a} \prec \boldsymbol{b}$. If $\boldsymbol{a} \prec \boldsymbol{b}$, $\boldsymbol{a}$ is said to be smaller than $\boldsymbol{b}$ lexicographically.

Now suppose $G = (\mathcal{V}(G), \mathcal{E}(G))$ is a graph embedding in $\mathbb{Z}^3$ and let $\boldsymbol{b}_G$ be the bottom vertex in $\mathcal{V}(G)$ and $\boldsymbol{t}_G$ be the top vertex in $\mathcal{V}(G)$. Define the new set of vertices $\mathcal{M}(G)$ to be

$$\mathcal{M}(G) = \left\{ \left(\frac{g(1)+h(1)}{2}, \frac{g(2)+h(2)}{2}, \frac{g(3)+h(3)}{2} \right) \middle| \text{ for all } \{\boldsymbol{g}, \boldsymbol{h}\} \in \mathcal{E}(G) \right\}. \tag{2.16}$$

Note that $\mathcal{M}(G)$ consists of the vertices which are the midpoints of the edges in $\mathcal{E}(G)$. Let $\boldsymbol{m}_b$ be the bottom vertex in $\mathcal{M}(G)$ and let $\boldsymbol{m}_t$ be the top vertex in $\mathcal{M}(G)$. Then define the *top (last) edge* in $\mathcal{E}(G)$ to be the edge incident on $\boldsymbol{t}_G$ whose midpoint is $\boldsymbol{m}_t$ and the *bottom (first) edge* in $\mathcal{E}(G)$ to be the edge incident on $\boldsymbol{b}_G$ whose midpoint is $\boldsymbol{m}_b$.

With the above definitions, two polygons ω and ω' in $\mathbb{Z}^3$ can be concatenated to form a new polygon $\omega \circ \omega'$, where $\omega \circ \omega'$ is formed as follows. The following concatenation algorithm is from [103] and will be referred to as the *concatenation algorithm for two SAPs*.

Algorithm 2.2.1 (Concatenation Algorithm for two SAPs [103]) *Let ω be a polygon in $\mathbb{Z}^3$ with top vertex $\boldsymbol{t}_\omega$ and let ω' be a polygon in $\mathbb{Z}^3$ with bottom vertex $\boldsymbol{b}_{\omega'}$. Let the top edge in ω be denoted $\{\boldsymbol{t}_1, \boldsymbol{t}_2\}$ and the bottom edge in ω' be denoted $\{\boldsymbol{b}_1, \boldsymbol{b}_2\}$. Rotate ω' appropriately (a $0°$-rotation is allowed) so that after the rotation the edge $\{\boldsymbol{b}_1, \boldsymbol{b}_2\}$ is parallel to the edge $\{\boldsymbol{t}_1, \boldsymbol{t}_2\}$. Denote the after-rotation polygon as ω'' and the edge $\{\boldsymbol{b}_1, \boldsymbol{b}_2\}$ after the rotation as $\{\boldsymbol{b}_1', \boldsymbol{b}_2'\}$. Now apply the appropriate translation to ω'' so that the edge $\{\boldsymbol{b}_1', \boldsymbol{b}_2'\}$ gets translated to the edge $\{(t_1(1)+1, t_1(2), t_1(3)), (t_2(1)+1, t_2(2), t_2(3))\}$. Delete the edges $\{\boldsymbol{t}_1, \boldsymbol{t}_2\}$ and $\{\boldsymbol{b}_1', \boldsymbol{b}_2'\}$ from ω and ω'', respectively, and add the new edges $\{\boldsymbol{t}_1, (t_1(1)+1, t_1(2), t_1(3))\}$ and $\{\boldsymbol{t}_2, (t_2(1)+1, t_2(2), t_2(3))\}$ to obtain an $(|\omega| + |\omega'|)$-edge polygon denoted by $\omega \circ \omega'$. We say that ω' is concatenated to ω, and that ω and ω' are* concatenated *at the edges $\{\boldsymbol{t}_1, \boldsymbol{t}_2\}$ and $\{\boldsymbol{b}_1, \boldsymbol{b}_2\}$ to form the polygon $\omega \circ \omega'$. If the knot-type of ω is K and the knot-type of ω' is K', then the knot-type of $\omega \circ \omega'$ is $K \# K'$.*

The next theorem yields that concatenation in a Θ-SAP never occurs at an edge in Θ.

Theorem 2.2.2 *The bottom (top) edge of the structure $\Theta(0,0,0)$ is never the bottom (top) edge of a Θ-SAP.*

Proof. Note that the bottom edge of Θ is the edge $\boldsymbol{b}_\Theta := \{(-1,0,0),(0,0,0)\}$ and the top edge of Θ is the edge $\boldsymbol{t}_\Theta := \{(0,0,0),(1,0,0)\}$. Suppose that ω is a Θ-SAP. Then ω must contain one of the edges in $e_\omega(\boldsymbol{b}_\Theta) := \{\{(-2,0,0),(-1,0,0)\}, \{(-1,-1,0),(-1,0,0)\}, \{(-1,1,0),(-1,0,0)\}, \{(-1,0,0),(-1,0,-1)\}, \{(-1,0,0),(-1,0,1)\}\}$. Since every edge $\boldsymbol{e} \in e_\omega(\boldsymbol{b}_\Theta)$, contains a vertex that is lexicographically less than or equal to $(-1,0,0)$ (the bottom vertex of Θ), the edge $\boldsymbol{b}_\Theta$ cannot be the bottom edge of ω. Since ω was chosen arbitrarily, the bottom edge of the structure $\Theta(0,0,0)$ is never the bottom edge of a Θ-SAP. A similar argument can be used to show that the top edge of the structure $\Theta(0,0,0)$ is never the top edge of a Θ-SAP. ∎

Suppose that a Θ-SAP is to be concatenated with a SAP. One consequence of Theorem 2.2.2 is that the only way that the Concatenation Algorithm for two SAPs can possibly alter the structure Θ is if the Θ-SAP needs to be rotated or translated during the concatenation process, that is if the Θ-SAP is the polygon denoted ω' in the Concatenation Algorithm for two SAPs. The following corollary results when a Θ-SAP is not the polygon ω' in the concatenation algorithm.

Corollary 2.2.3 (Θ-preserving concatenation) *For even positive integers $m \geq 4$ and $n \geq 4$, for each $\omega \in \mathscr{P}_n^\Theta(K)$ and $\omega' \in \mathscr{P}_m(K')$,*

$$\omega \circ \omega' \in \mathscr{P}_{m+n}^\Theta(K\#K'). \tag{2.17}$$

The specific concatenation in Corollary 2.2.3 from here-on-in will be referred to as Θ-*preserving concatenation*. Figure 2.6 illustrates a Θ-preserving concatenation that involves concatenating a 10-edge SAP to a 14-edge Θ-SAP to form a 24-edge Θ-SAP.

Now, for a fixed knot-type K, to answer the question "For each $* \in \Phi(K)$, does there exist a positive integer n_*^Θ such that $\mathscr{P}_{2n}^\Theta(*) \neq \{\}$ for all $n \geq n_*^\Theta$?", if a single $(2N)$-edge property-$*$ Θ-SAP can be found for each $* \in \Phi(K)$, then Θ-preserving concatenation can be used to create a $(2N+2k)$-edge property-$*$ Θ-SAP for each integer $k \geq 2$ simply by concatenating a SAP from $\mathscr{P}_{2k}(\phi)$ to this property-$*$ Θ-SAP. Consequently showing that $\mathscr{P}_{2n}^\Theta(*) \neq \{\}$ for all sufficiently large integers n requires finding a single $(2N)$-edge property-$*$ Θ-SAP for some positive integer N.

Theorem 2.2.3 *For a fixed knot-type K, $\mathscr{P}^\Theta(K) \neq \{\}$, $\mathscr{P}^\Theta(K,s) \neq \{\}$, $\mathscr{P}^\Theta(K,f) \neq \{\}$, and, for each knot-type $K' \in \mathscr{K}^\Theta(K)$, $\mathscr{P}^\Theta(K'|K,s) \neq \{\}$.*

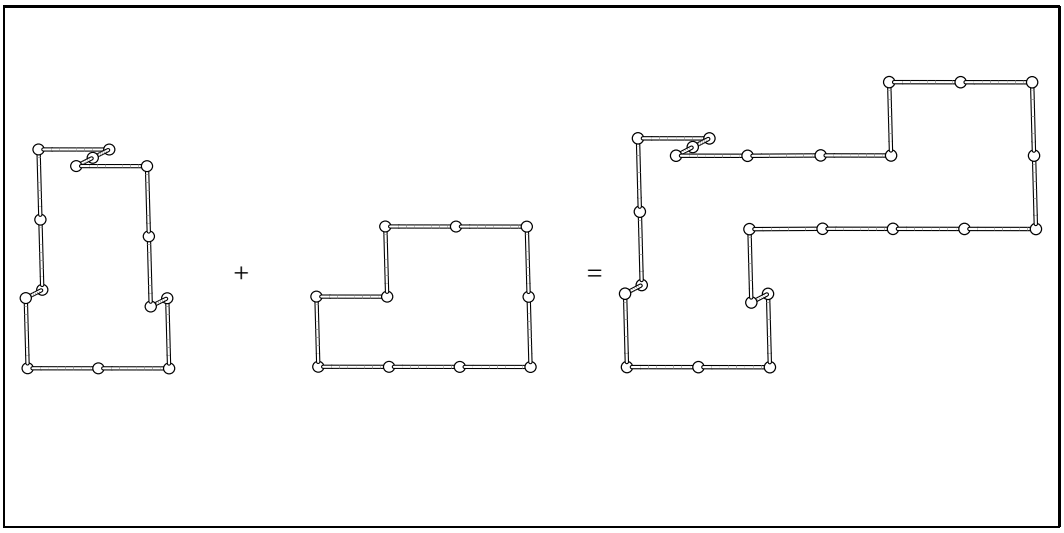

Figure 2.6: A 10-edge SAP and a 14-edge Θ-SAP are concatenated using a Θ-preserving concatenation to form a 24-edge Θ-SAP.

Proof. For this entire proof, suppose that the knot-type K has been fixed and define n_K to be the smallest length of a SAP in $\mathscr{P}(K)$. Then to show that $\mathscr{P}^{\Theta}(K) \neq \{\}$ and $\mathscr{P}^{\Theta}(K,s) \neq \{\}$, choose any (n_K)-edge SAP in $\mathscr{P}(K)$. Call this SAP ω. Use Θ-preserving concatenation to concatenate ω to the Θ-SAP in Figure 2.4 (a) to obtain a (n_K+14)-edge Θ-SAP in $\mathscr{P}^{\Theta}_{n_K+14}(K,s) \subseteq \mathscr{P}^{\Theta}_{n_K+14}(K)$. Similarly to show that $\mathscr{P}^{\Theta}_{n_K+14}(K,f) \neq \{\}$, use Θ-preserving concatenation to concatenate ω to the Θ-SAP in Figure 2.7 to create a (n_K+14)-edge Θ-SAP in $\mathscr{P}^{\Theta}_{n_K+14}(K,f)$. Hence $\mathscr{P}^{\Theta}(K) \neq \{\}$, $\mathscr{P}^{\Theta}(K,s) \neq \{\}$, and $\mathscr{P}^{\Theta}(K,f) \neq \{\}$.

For a fixed knot-type $K' \in \mathscr{K}^{\Theta}(K)$, an outline of the proof that $\mathscr{P}^{\Theta}(K'|K,s) \neq \{\}$ is as follows. Fix a knot-type $K' \in \mathscr{K}^{\Theta}(K)$. In [18], it is shown that there exists a knot-type K knot in $\mathbb{R}^3$ that has a regular projection and has the property that, after a single strand passage about a crossing c_Ω in this regular projection, the resulting knot has knot-type K'. Let Ω be such a knot in $\mathbb{R}^3$. Now embed Ω in $\mathbb{Z}^3$ using the algorithm of Diao *et al.* discussed in [28]. Call this embedding ω and denote the crossing in ω that corresponds to c_Ω by c_ω. Note that $\omega \in \mathscr{P}(K)$. Using the constructions found in Section 5.4.1 of [150] , the configuration of ω around c_ω can be altered in such a way that c_ω can be converted into Θ and a strand passage is possible about Θ. The polygon resulting from this conversion is a polygon in $\mathscr{P}^{\Theta}(K'|K,s)$. Hence $\mathscr{P}^{\Theta}(K'|K,s) \neq \{\}$. ∎

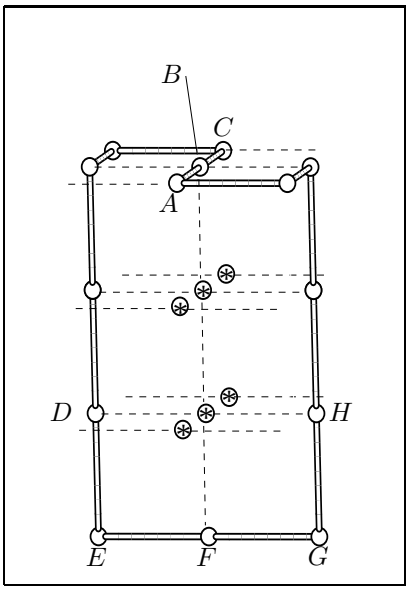

Figure 2.7: A 14-edge SAP that contains the structure Θ for which strand passage is not viable. Open and empty circles represent the vertices of the SAP and open bonds represent the edges of the SAP. The circles containing asterisks are vertices not occupied by the SAP. Dashed lines represent lattice edges not occupied by the SAP. Vertex $A = (a+1, b, c)$; Vertex $B = (a, b, c)$; Vertex $C = (a-1, b, c)$; Vertex $D = (a, b-1, c-2)$; Vertex $E = (a, b-1, c-3)$; Vertex $F = (a, b, c-3)$; Vertex $G = (a, b+1, c-3)$; and Vertex $H = (a, b+1, c-2)$.

Then the following is a corollary to Theorem 2.2.3.

Corollary 2.2.4 *For each knot-type K and every $* \in \Phi(K)$, there exists a positive integer n_*^{Θ} such that $\mathscr{P}_{2n}^{\Theta}(*) \neq \{\}$ for all $n \geq n_*^{\Theta}/2$.*

Definition 2.2.9 *For each knot-type K, n_K^{Θ}, $n_{(K,f)}^{\Theta}$, $n_{(K,s)}^{\Theta}$, and, for each knot-type $K' \in \mathscr{K}^{\Theta}(K)$, $n_{(K'|K,s)}^{\Theta}$ are respectively the smallest lengths of a Θ-SAP in $\mathscr{P}^{\Theta}(K)$, $\mathscr{P}^{\Theta}(K,f)$, $\mathscr{P}^{\Theta}(K,s)$, and, for each $K' \in \mathscr{K}^{\Theta}(K)$, $\mathscr{P}^{\Theta}(K'|K,s)$.*

Note that, for each $* \in \{\phi, (\phi,s), (\phi,f), (\phi|\phi,s)\}$,

$$n_*^{\Theta} = 14. \tag{2.18}$$

Recall from Section 1.3 that in [26], Diao proved that the smallest non-trivial knotted SAP in $\mathbb{Z}^3$ has 24 edges. Since the trefoil is one of the knot-types in $\mathscr{K}^{\Theta}(\phi)$ and since an after-strand-passage polygon is four edges larger than its corresponding before-strand-passage polygon, for each non-trivial knot-type $K' \in \mathscr{K}^{\Theta}(\phi)$,

$$n_{(K'|\phi,s)}^{\Theta} \geq 20. \tag{2.19}$$

An interesting question resulting from Corollary 2.2.4 is "For each knot-type K and every $* \in \Phi(K)$, how does $p_{2n}^{\Theta}(*)$ grow as $n \to \infty$?". To explore this question, first note that for each knot-type K, Definitions 2.2.8 and 2.2.9 give the following three inequalities:

$$\text{for } n \geq n_{(K,s)}^{\Theta},\ p_n^{\Theta}(K,s) \leq p_n^{\Theta}(K), \tag{2.20}$$

$$\text{for } n \geq n_{(K,f)}^{\Theta},\ p_n^{\Theta}(K,f) \leq p_n^{\Theta}(K), \tag{2.21}$$

and, for each knot-type $K' \in \mathscr{K}^{\Theta}(K)$ and for $n \geq n_{(K'|K,s)}^{\Theta}$,

$$p_n^{\Theta}\left(K'|K,s\right) \leq p_n^{\Theta}(K,s). \tag{2.22}$$

The purpose of the following discussion is to establish upper and lower bounds for the number of SAPs in the specific subsets of $\mathscr{P}^{\Theta}(K)$ described in Definition 2.2.8 in terms of the number of SAPs in $\mathscr{P}_n(K)$. To this end, using the quantities defined in Definitions 2.2.8 and 2.2.9, the following lemma shows that, for all $n \geq n_K^{\Theta}$, $p_n^{\Theta}(K)$ is bounded above by a function of $p_n(K)$ and hence both $p_n^{\Theta}(K,s)$ and $p_n^{\Theta}(K,f)$ are bounded above by the same function of $p_n(K)$.

Lemma 2.2.1 *For any fixed knot-type K and for all $n \geq n_K^{\Theta}$,*

$$p_n^{\Theta}(K) \leq n p_n(K). \tag{2.23}$$

Proof. Let K be any fixed knot-type. For $n \geq n_K^{\Theta}$, when n is odd, $p_n^{\Theta}(K) = p_n(K) = 0$ and Inequality (2.23) is trivially true. Now, if n is even, by definition, $\mathscr{P}_n^{\Theta}(K) \subseteq \{\omega \in \mathscr{P}_n(K) | \omega \text{ contains the origin } (0,0,0)\}$, and the number of SAPs in $\mathscr{P}_n(K)$ that contain the origin is exactly the number of n-edge SAPs with knot-type K that are rooted at the origin (which is $np_n(K)$). Hence

$$p_n^{\Theta}(K) \leq n p_n(K) \text{ for all } n \geq n_K^{\Theta}. \tag{2.24}$$

■

The next goal is to establish that, for $n \geq \max\{n_K^{\Theta}, n_K + 14\}$, $p_n^{\Theta}(K)$ is bounded below by a scalar multiple of the number of $(n-14)$-edge SAPs with knot-type K. The next lemma uses Θ-preserving concatenation to show that, for $n \geq \max\{n_K^{\Theta}, n_K + 14\}$, a specific scalar multiple of $p_{n-14}(K)$ provides a lower bound for $p_n^{\Theta}(K)$, that is:

Lemma 2.2.2 *For any fixed knot-type K and for all $n \geq \max\{n_K^{\Theta}, n_K + 14\}$,*

$$\frac{1}{2} p_{n-14}(K) \leq p_n^{\Theta}(K). \tag{2.25}$$

Proof. Given any fixed knot-type K and $n \geq \max\{n_K^{\Theta}, n_K + 14\}$, if n is odd, then $p_{n-14}(K) = p_n^{\Theta}(K) = 0$ and hence Inequality (2.25) holds. Now suppose n is even. Let $\omega' \in \mathscr{P}_{n-14}(K)$. Let $\omega \in \mathscr{P}_{14}^{\Theta}(\phi)$. Then, by Corollary 2.2.3, $\omega \circ \omega' \in \mathscr{P}_n^{\Theta}(K)$. Because a non-zero rotation might have been used in the concatenation process, it is possible that two different SAPs counted in $p_{n-14}(K)$ (when concatenated with $\omega \in \mathscr{P}_{14}^{\Theta}(\phi)$) yield the same SAP in $\mathscr{P}_n^{\Theta}(K)$. Also note that there exist polygons in $\mathscr{P}_n^{\Theta}(K)$ that cannot be formed by such a concatenation. Combining these two facts gives

$$p_{n-14}(K) \leq 2p_n^{\Theta}(K), \tag{2.26}$$

which implies Inequality 2.25 holds for all $n \geq \max\{n_K^{\Theta}, n_K + 14\}$. ∎

It can also be shown that, for $n \geq \max\{n_{(K,s)}^{\Theta}, n_K + 14\}$, a specific scalar multiple of $p_{n-14}(K)$ provides a lower bound for $p_n^{\Theta}(K, s)$, that is:

Corollary 2.2.5 *For any fixed knot-type K and $n \geq \max\{n_{(K,s)}^{\Theta}, n_K + 14\}$,*

$$\frac{1}{2} p_{n-14}(K) \leq p_n^{\Theta}(K, s). \tag{2.27}$$

Proof. Given any fixed knot-type K and $n \geq \max\{n_{(K,s)}^{\Theta}, n_K + 14\}$, if n is odd then $p_{n-14}(K) = p_n^{\Theta}(K, s) = 0$ and hence Inequality (2.27) holds. Now suppose n is even. Let ω' be an $(n-14)$-edge polygon with knot-type K. Let ω be a 14-edge unknotted Θ-SAP in which a strand passage is possible about Θ. Now using these definitions for ω and ω' and following the proof of Lemma 2.2.2, the corollary follows. ∎

Figure 2.8 illustrates the 28-edge after-strand-passage polygon that results when Θ-preserving concatenation is used to concatenate a 10-edge SAP to a 14-edge successful-strand-passage Θ-SAP.

The following corollary provides a lower bound for $p_n^{\Theta}(K, f)$.

Corollary 2.2.6 *For any fixed knot-type K and for all $n \geq \max\{n_{(K,f)}^{\Theta}, n_K + 14\}$,*

$$\frac{1}{2} p_{n-14}(K) \leq p_n^{\Theta}(K, f). \tag{2.28}$$

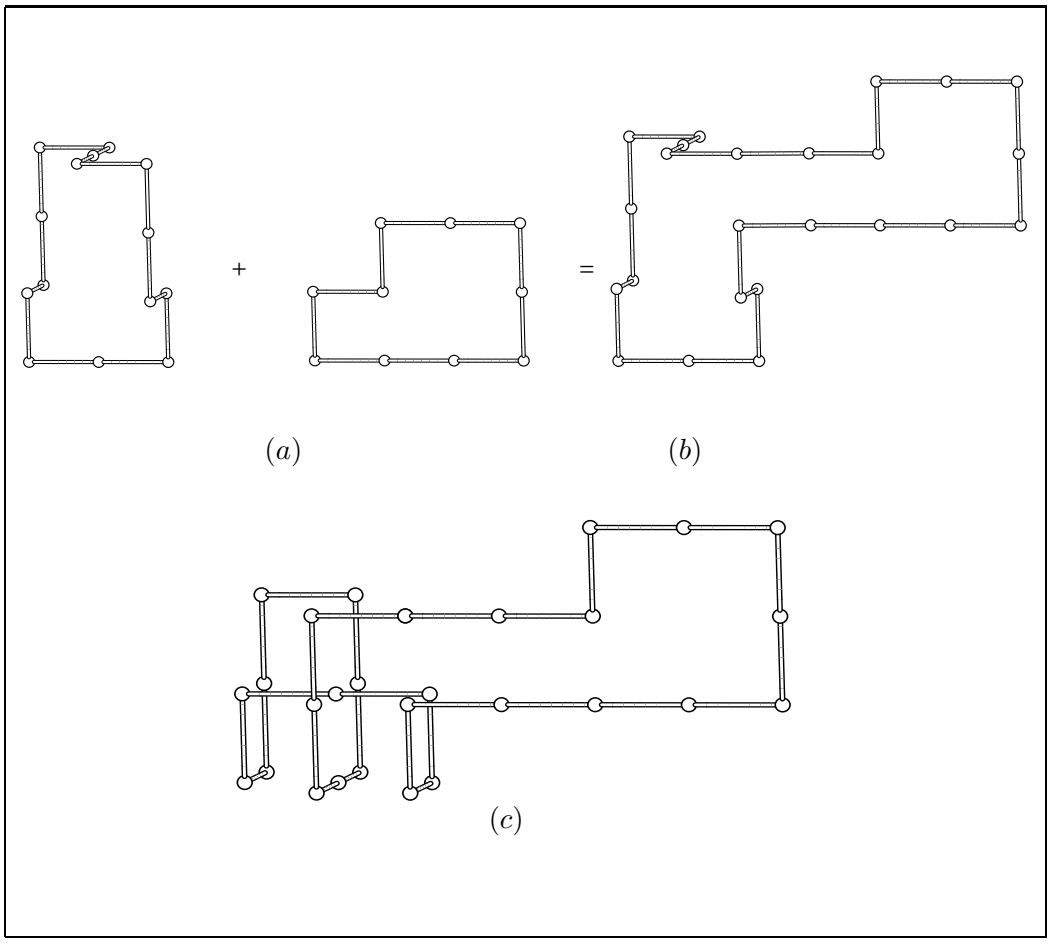

Figure 2.8: (a) two SAPs F and G, respectively, where F is the 10-edge SAP and G is the 14-edge SAP that contains Θ in which a strand passage is viable. (b) F and G are concatenated using Θ-preserving concatenation to form a 24-edge SAP that contains the structure Θ in which a strand passage is viable. (c) The 28-edge SAP that results from implementing a strand passage in the SAP illustrated in (b).

Proof. Given any fixed knot-type K and $n \geq \max\{n^{\Theta}_{(K,f)}, n_K + 14\}$, if n is odd, then $p_{n-14}(K) = p^{\Theta}_n(K, f) = 0$ and hence Inequality (2.28) holds. If n is even, let ω be a 14-edge unknotted Θ-SAP in which a strand passage is not viable (such as the Θ-SAP illustrated in Figure 2.7). Let ω' be an $(n-14)$-edge polygon with knot-type K. Then using these definitions of ω and ω' and following the proof of Lemma 2.2.2 the corollary follows. ∎

It can also be shown that, for each $K' \in \mathscr{K}^{\Theta}(K)$ and $n \geq n^{\Theta}_{(K'|K,s)} + 4$, a specific scalar multiple of $p_{n-n^{\Theta}_{(K'|K,s)}}(\phi)$ provides a lower bound for $p^{\Theta}_n(K'|K, s)$, that is:

Lemma 2.2.3 *For any fixed knot-type K, for each $K' \in \mathscr{K}^{\Theta}(K)$ and $n \geq n^{\Theta}_{(K'|K,s)} + 4$,*

$$\frac{1}{2} p_{n-n^{\Theta}_{(K'|K,s)}}(\phi) \leq p^{\Theta}_{n}\left(K'|K,s\right). \tag{2.29}$$

Proof. Given any fixed knot-type K, fix $K' \in \mathscr{K}^{\Theta}(K)$. For $n \geq n^{\Theta}_{(K'|K,s)} + 4$, if n is odd, then $p_{n-n^{\Theta}_{(K'|K,s)}}(\phi) = p^{\Theta}_{n}(K'|K,s) = 0$ thus supporting Inequality (2.29). If n is even, let ω be an $\left(n^{\Theta}_{(K'|K,s)}\right)$-edge polygon in $\mathscr{P}^{\Theta}(K'|K,s)$. Let ω' be any $\left(n - n^{\Theta}_{(K'|K,s)}\right)$-edge unknotted polygon. Then using these definitions of ω and ω', the argument used in the proof of Lemma 2.2.2 proves the lemma. The basic idea of this proof (for the case where $K = \phi$ and $K' = 10_1$) is illustrated in Figure 2.9. ∎

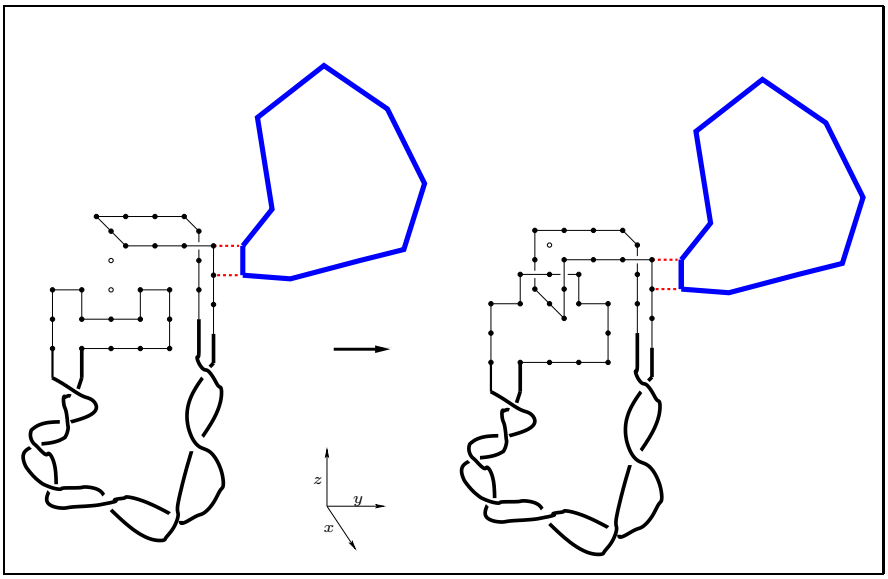

Figure 2.9: The concatenation of a successful-strand-passage unknotted Θ-SAP with an unknotted SAP and the post-concatenation after-strand-passage polygon whose knot-type is 10_1.

Lemmas 2.2.1, 2.2.2, and 2.2.3 and Corollaries 2.2.5 and 2.2.6 provide relationships between the number of SAPs in specific subsets of $\mathscr{P}(K)$ and $\mathscr{P}^{\Theta}(K)$, but how do the numbers of $(2n)$-edge Θ-SAPs in subsets of $\mathscr{P}^{\Theta}(K)$ (that is $p^{\Theta}_{2n}(K)$, $p^{\Theta}_{2n}(K,f)$, $p^{\Theta}_{2n}(K,s)$, and $p^{\Theta}_{2n}(K'|K,s)$) behave asymptotically as $n \to \infty$? This question is explored in the following section.

2.2.1 Connective Constants

Because $\mathscr{P}^{\Theta}(\phi) \subset \mathscr{P}(\phi)$, an interesting question is "What, if any, are the relationships between the "growth rates" of $p_{2n}(\phi)$, $p^{\Theta}_{2n}(\phi)$, $p^{\Theta}_{2n}(\phi,f)$, and $p^{\Theta}_{2n}(\phi,s)$ (as defined in Def-

inition 2.2.8 with $K = \phi$)?". A second interesting question is "How do $p_{2n}^{\Theta}(\phi)$, $p_{2n}^{\Theta}(\phi, f)$, and $p_{2n}^{\Theta}(\phi, s)$ individually grow as $n \to \infty$?". These two questions and the concept of "growth rate" are addressed next in Theorem 2.2.4. Before stating the theorem, recall from Section 1.3 that

$$\lim_{n\to\infty} (2n)^{-1} \log p_{2n}(\phi) = \kappa_{\phi}. \tag{2.30}$$

Then:

Theorem 2.2.4 *For the set of unknotted Θ-SAPs,*
I. the growth rate for $p_{2n}^{\Theta}(\phi)$ is given by $\lim_{n\to\infty} (2n)^{-1} \log p_{2n}^{\Theta}(\phi) = \kappa_{\phi}$;
II. the growth rate for $p_{2n}^{\Theta}(\phi, s)$, given by $\kappa_{(\phi,s)}^{\Theta} := \lim_{n\to\infty} (2n)^{-1} \log p_{2n}^{\Theta}(\phi, s)$, exists;
III. the growth rate for $p_{2n}^{\Theta}(\phi, f)$, given by $\kappa_{(\phi,f)}^{\Theta} := \lim_{n\to\infty} (2n)^{-1} \log p_{2n}^{\Theta}(\phi, f)$, exists; and
IV. $\kappa_{(\phi,s)}^{\Theta} = \kappa_{(\phi,f)}^{\Theta} = \kappa_{\phi}$.

Proof. Part I: Combining Lemmas 2.2.1 and 2.2.2 yields, for all $n \geq 9$, the double inequality:

$$\frac{1}{2} p_{2n-14}(\phi) \leq p_{2n}^{\Theta}(\phi) \leq (2n)\, p_{2n}(\phi). \tag{2.31}$$

Now taking logarithms of Inequality (2.31), dividing by $2n$, and taking the limit as $n \to \infty$ yields

$$\lim_{n\to\infty} (2n)^{-1} \log p_{2n-14}(\phi) \leq \lim_{n\to\infty} (2n)^{-1} \log p_{2n}^{\Theta}(\phi) \leq \lim_{n\to\infty} (2n)^{-1} \log p_{2n}(\phi), \tag{2.32}$$

which, using Equation (1.21), can be rewritten as

$$\kappa_{\phi} \leq \lim_{n\to\infty} (2n)^{-1} \log p_{2n}^{\Theta}(\phi) \leq \kappa_{\phi}, \tag{2.33}$$

thus proving Part I of the theorem.

Part II: Combining Lemma 2.2.1, Inequality (2.20), and Corollary 2.2.5 and following the proof of Part I of this theorem yields that $\kappa_{(\phi,s)}^{\Theta}$ exists and satisfies

$$\kappa_{(\phi,s)}^{\Theta} = \kappa_{\phi}, \tag{2.34}$$

thus proving Parts II and part of Part IV of the theorem.

Part III: Combining Lemma 2.2.1, Inequality (2.21), and Corollary 2.2.6 and following the proof of Part I of this theorem yields that $\kappa^{\Theta}_{(\phi,f)}$ exists and satisfies

$$\kappa^{\Theta}_{(\phi,f)} = \kappa_{\phi}, \tag{2.35}$$

thus proving Part III and the remainder of Part IV of the theorem. ∎

With the $n \to \infty$ behaviour of $p^{\Theta}_{2n}(\phi)$, $p^{\Theta}_{2n}(\phi, s)$, and $p^{\Theta}_{2n}(\phi, f)$ established, the discussion turns to the question "For each $K \in \mathscr{K}^{\Theta}(\phi)$, how does $p^{\Theta}_{2n}(K|\phi, s)$ (defined in Definition 2.2.8) behave as $n \to \infty$?". This question is addressed in the next theorem.

Theorem 2.2.5 *For each $K \in \mathscr{K}^{\Theta}(\phi)$, the "growth rate" for $p^{\Theta}_{2n}(K|\phi, s)$, given by*

$$\kappa^{\Theta}_{(K|\phi,s)} := \lim_{n\to\infty} (2n)^{-1} \log p^{\Theta}_{2n}(K|\phi, s), \text{ exists.} \tag{2.36}$$

Moreover

$$\kappa^{\Theta}_{(K|\phi,s)} = \kappa_{\phi}. \tag{2.37}$$

Proof. For fixed $K \in \mathscr{K}^{\Theta}(\phi)$ and each $n \geq (n^{\Theta}_{(K|\phi,s)} + 4)/2$, combining Inequality (2.22) and Lemma 2.2.3 yields the double inequality

$$\frac{1}{2} p_{2n-n^{\Theta}_{(K|\phi,s)}}(\phi) \leq p^{\Theta}_{2n}(K|\phi, s) \leq p^{\Theta}_{2n}(\phi, s). \tag{2.38}$$

After first taking logarithms, then dividing by $2n$, and finally taking the limit as $n \to \infty$, the above double inequality yields

$$\lim_{n\to\infty} \frac{\log p_{2n-n^{\Theta}_{(K|\phi,s)}}(\phi)}{2n} \leq \lim_{n\to\infty} \frac{\log p^{\Theta}_{2n}(K|\phi, s)}{2n} \leq \lim_{n\to\infty} \frac{\log p^{\Theta}_{2n}(\phi, s)}{2n}, \tag{2.39}$$

which is equivalent to

$$\kappa_{\phi} \leq \lim_{n\to\infty} \frac{\log p^{\Theta}_{2n}(K|\phi, s)}{2n} \leq \kappa^{\Theta}_{(\phi,s)} = \kappa_{\phi}, \tag{2.40}$$

where the last inequality follows from Theorem 2.2.4. Equation (2.40) thus yields the existence of $\kappa^{\Theta}_{(K|\phi,s)}$ and that

$$\kappa^{\Theta}_{(K|\phi,s)} = \kappa_{\phi}. \tag{2.41}$$

∎

A consequence of Theorem 2.2.5 is the fact that, for each $K \in \mathscr{K}^{\Theta}(\phi)$, $p^{\Theta}_{2n}(K|\phi, s)$ grows at the same exponential rate as $p_{2n}(\phi)$ and this rate does not depend on K, the knot-type of the after-strand-passage polygons.

Because the existence of the connective constant κ_K for any non-trivial knot-type K is still an open question, the best results regarding the exponential growth rates of $p^{\Theta}_{2n}(K)$, $p^{\Theta}_{2n}(K,s)$, and $p^{\Theta}_{2n}(K,f)$ are the inequalities stated below in Theorem 2.2.6. In order to succinctly write the inequalities in Theorem 2.2.6, the following definitions are required. For each non-trivial knot-type K, define

$$\kappa^{\Theta}_{K} := \limsup_{n\to\infty} (2n)^{-1} \log p^{\Theta}_{2n}(K), \tag{2.42}$$

$$\kappa^{\Theta}_{(K,s)} := \limsup_{n\to\infty} (2n)^{-1} \log p^{\Theta}_{2n}(K,s), \tag{2.43}$$

$$\kappa^{\Theta}_{(K,f)} := \limsup_{n\to\infty} (2n)^{-1} \log p^{\Theta}_{2n}(K,f), \tag{2.44}$$

$$\kappa^{\Theta}_{(K'|K,s)} := \limsup_{n\to\infty} (2n)^{-1} \log p^{\Theta}_{2n}\left(K'|K,s\right), \tag{2.45}$$

$$k^{\Theta}_{K} := \liminf_{n\to\infty} (2n)^{-1} \log p^{\Theta}_{2n}(K), \tag{2.46}$$

$$k^{\Theta}_{(K,s)} := \liminf_{n\to\infty} (2n)^{-1} \log p^{\Theta}_{2n}(K,s), \tag{2.47}$$

$$k^{\Theta}_{(K,f)} := \liminf_{n\to\infty} (2n)^{-1} \log p^{\Theta}_{2n}(K,f). \tag{2.48}$$

and, for each $K' \in \mathscr{K}^{\Theta}(K)$,

$$k^{\Theta}_{(K'|K,s)} := \liminf_{n\to\infty} (2n)^{-1} \log p^{\Theta}_{2n}\left(K'|K,s\right), \tag{2.49}$$

Theorem 2.2.6 *For each non-trivial knot-type K with κ^{Θ}_{K}, $\kappa^{\Theta}_{(K,s)}$, ($\kappa^{\Theta}_{(K'|K,s)}$, $K' \in \mathscr{K}^{\Theta}(K)$), $\kappa^{\Theta}_{(K,f)}$, k^{Θ}_{K}, $k^{\Theta}_{(K,s)}$, $\left(k^{\Theta}_{(K'|K,s)}, K' \in \mathscr{K}^{\Theta}(K)\right)$, and $k^{\Theta}_{(K,f)}$ as defined, respectively, by Equations (2.42)-(2.48), and k_K and κ_K defined by Inequality (1.22), the following inequalities hold:*

$$k_K \leq k^{\Theta}_{K} \leq \kappa^{\Theta}_{K} \leq \kappa_K, \tag{2.50}$$

$$k_K \leq k^{\Theta}_{(K,s)} \leq \kappa^{\Theta}_{(K,s)} \leq \kappa_K, \tag{2.51}$$

$$k_K \leq k^{\Theta}_{(K,f)} \leq \kappa^{\Theta}_{(K,f)} \leq \kappa_K, \tag{2.52}$$

and, for each $K' \in \mathscr{K}^{\Theta}(K)$,

$$\kappa_{\phi} \leq k^{\Theta}_{(K'|K,s)} \leq \kappa^{\Theta}_{(K'|K,s)} \leq \kappa^{\Theta}_{K}. \tag{2.53}$$

Proof. Inequality (2.50) follows from combining the inequalities specified in Lemmas 2.2.1 and 2.2.2 with the result of Soteros *et al* [145] stated in Inequality (1.22).
Inequality (2.51) follows from combining the inequalities specified in Corollary 2.2.5, Inequality (2.20), and Lemma 2.2.1 with the result of Soteros *et al* [145] given by Inequality

(1.22). Inequality (2.52) follows from combining the inequalities specified in Corollary 2.2.6, Inequality (2.21) and Lemma 2.2.1 with the result of Soteros *et al* [145] stated in Inequality (1.22). Inequality (2.53) follows directly from Inequalities (2.20) and (2.22) and Lemma 2.2.3. ∎

It is conjectured [125, 145] that:

Conjecture 2.2.1 ([125, 145]) *For each non-trivial knot-type K,*

$$k_K = \kappa_K. \tag{2.54}$$

Then if Equation (2.54) is assumed to be true, then the following are direct consequences.

Consequence 2.2.1 *Assuming Conjecture 2.2.1 is true, for each non-trivial knot-type K with κ_K^Θ, $\kappa_{(K,s)}^\Theta$, $\kappa_{(K,f)}^\Theta$, k_K^Θ, $k_{(K,s)}^\Theta$, and $k_{(K,f)}^\Theta$ as defined, respectively, by Equations (2.42)-(2.44) and Equations (2.46)-(2.48), and k_K and κ_K defined by Inequality (1.22), the following statement is true.*

$$k_K^\Theta = \kappa_K^\Theta = k_{(K,s)}^\Theta = \kappa_{(K,s)}^\Theta = k_{(K,f)}^\Theta = \kappa_{(K,f)}^\Theta. \tag{2.55}$$

Conjecture 2.2.2 *For each non-trivial knot-type K with κ_K^Θ, $\kappa_{(K'|K,s)}^\Theta$, k_K^Θ, and $k_{(K'|K,s)}^\Theta$ as defined, respectively, by Equations (2.42), (2.45), (2.46), and (2.47), and k_K and κ_K defined by Inequality (1.22), the following statements are true. For each $K' \in \mathscr{K}^\Theta(K)$,*

$$k_K^\Theta = k_{(K'|K,s)}^\Theta = \kappa_{(K'|K,s)}^\Theta = \kappa_K^\Theta. \tag{2.56}$$

Proving Conjectures 2.2.1 and Consequences 2.2.1 and 2.2.2 remain open questions. Though the validity of Consequences 2.2.1 and 2.2.2 are not going to be explored in this thesis, the algorithms developed in this thesis can be used to numerically compare the growth rates stated in the consequences.

In addition to being interested in how $p_{2n}^\Theta(K)$, $p_{2n}^\Theta(K,s)$, $p_{2n}^\Theta(K,f)$, and $p_{2n}^\Theta(K'|K,s)$ grow as a function of n, other interesting quantities can be defined in terms of $p_{2n}^\Theta(K)$, $p_{2n}^\Theta(K,s)$, $p_{2n}^\Theta(K,f)$, and $p_{2n}^\Theta(K'|K,s)$. Some of these quantities will be discussed in the next section.

2.2.2 Probabilities Associated with the Local Strand Passage Model

In this section two different kinds of probabilities associated with the Local Strand Passage Model are presented. First the conditional probability mass function for the length of a random unknotted Θ-SAP is presented. Then the conditional probabilities associated with strand passage are discussed.

The Conditional Probability Mass Function for the Length of an Unknotted Θ-SAP

The *partition function for the LSP Model* (to be denoted $\breve{Q}(q, z, M)$) is defined as follows. Given a fixed positive even integer M, a positive integer q, and a real value z,

$$\breve{Q}(q, z, M) := \sum_{n=M}^{\infty} (n-6) n^{q-1} p_{2n}^{\Theta}(\phi) z^{2n} \tag{2.57}$$

$$= \sum_{\omega \in \mathscr{P}^{\Theta}: |\omega| \geq M} (|\omega| - 6) \, |\omega|^{q-1} \, z^{|\omega|}. \tag{2.58}$$

A corollary of Theorem 2.2.4 is:

Corollary 2.2.7 *For each fixed positive even integer M and fixed positive integer q, the radius of convergence of $\breve{Q}(q, z, M)$, denoted z_{Θ}, is $z_{\Theta} = 1/\mu_{\phi}$, where $\mu_{\phi} = e^{\kappa_{\phi}}$ and κ_{ϕ} is defined by Equation (1.21).*

Given a fixed positive even integer M, a fixed positive integer q, and a positive real-valued $z < z_{\Theta}$, then using $\breve{Q}(q, z, M)$, the conditional probability mass function for a random $W \in \mathscr{P}^{\Theta}(\phi)$ such that $|W| \geq M$ can be defined as follows. For each $\omega \in \mathscr{P}^{\Theta}(\phi)$ such that $|\omega| \geq M$,

$$\breve{\pi}_{\omega}(q, z, M) := \Pr(W = \omega | q, z, M) \tag{2.59}$$

$$:= \frac{(|\omega| - 6) \, |\omega|^{q-1} \, z^{|\omega|}}{\breve{Q}(q, z, M)}. \tag{2.60}$$

Hence the conditional probability mass function for the length of a random $W \in \mathscr{P}^{\Theta}(\phi)$ being $2n$ edges given that $|W| \geq M$ is

$$\breve{\pi}_{2n|M}(q, z) := \Pr(|W| = 2n | q, z, M) \tag{2.61}$$

$$:= \frac{(2n-6) \, (2n)^{q-1} \, z^{2n} p_{2n}^{\Theta}(\phi)}{\breve{Q}(q, z, M)}, \tag{2.62}$$

and the conditional probability mass function for the length of a randomly chosen $(2n)$-edge SAP in $\mathscr{P}^{\Theta}(\phi)$ given that $2n \geq M$ is given by the set

$$\breve{\boldsymbol{\pi}}_z(q, M) := \{\breve{\pi}_{2n|M}(q, z) : \text{ for every integer } n \geq M/2\}. \tag{2.63}$$

Suppose that $f : \mathscr{P}^{\Theta}(\phi) \to \mathbb{R}$ is a function which assigns the same value to polygons in $\mathscr{P}^{\Theta}(\phi)$ that have the same length. Then the expected value of f with respect to $\breve{\boldsymbol{\pi}}_z(q, M)$ is

$$\mathrm{E}_{\breve{\boldsymbol{\pi}}_z(q,M)}\left(f(\omega)\right) := \sum_{n \geq M/2} f_{2n} \breve{\pi}_{2n|M}(q, z), \tag{2.64}$$

where $f_{2n} := f(\omega)$ when $|\omega| = 2n$. Note that if $M = 14$, then the following notation will be used:

$$\breve{Q}(q, z) := \breve{Q}(q, z, 14); \tag{2.65}$$

$$\breve{\pi}_{\omega}(q, z) := \Pr(W = \omega | q, z, M = 14); \tag{2.66}$$

and

$$\breve{\pi}_{2n}(q, z) := \Pr(|W| = 2n | q, z, M = 14). \tag{2.67}$$

Probabilities Associated with a Strand Passage

In this section, a fixed length ensemble is considered. Given a fixed length $2n$, for each knot-type K, the quantities $p^{\Theta}_{2n}(K)$, $p^{\Theta}_{2n}(K, s)$, $p^{\Theta}_{2n}(K, f)$, and $p^{\Theta}_{2n}(K'|K, s)$, for each $K' \in \mathscr{K}^{\Theta}(K)$, can be used to define the quantities that are to be referred to as the *strand passage probabilities*. More specifically, given any knot-type K, for all $n \in \mathbb{N}$ such that $n \geq n^{\Theta}_{(K,s)}/2$, define

$$\Pr^{\Theta}_{2n}(K, s) := \frac{p^{\Theta}_{2n}(K, s)}{p^{\Theta}_{2n}(K)} \tag{2.68}$$

to be the *probability of a successful strand passage in a* $(2n)$*-edge, knot-type* K, Θ*-SAP*; for all $n \in \mathbb{N}$ such that $n \geq n^{\Theta}_{(K,f)}/2$, define

$$\Pr^{\Theta}_{2n}(K, f) := \frac{p^{\Theta}_{2n}(K, f)}{p^{\Theta}_{2n}(K)} \tag{2.69}$$

to be the *probability of a failed strand passage in a* $(2n)$*-edge, knot-type* K, Θ*-SAP*; and for each $K' \in \mathscr{K}^{\Theta}(K)$ and all $n \in \mathbb{N}$ such that $n \geq n^{\Theta}_{(K'|K,s)}/2$, define

$$\Pr^{\Theta}_{2n}(K'|K, s) := \frac{p^{\Theta}_{2n}(K'|K, s)}{p^{\Theta}_{2n}(K, s)} \tag{2.70}$$

to be the *probability of a knot-type K', after-strand-passage SAP given a* $(2n)$-edge*, knot-type* K*, successful-strand-passage* Θ-SAP. For each property $* \in \Phi(K)$, the probabilities $\Pr_{2n}^{\Theta}(*)$, for all $n \in \mathbb{N}$ such that $n \geq n_*^{\Theta}/2$, are to be referred to as the fixed-n *probabilities for property* $*$.

The following limits, if they exist, are referred to as the *limiting strand passage probabilities:*

$$\Pr^{\Theta}(K, s) := \lim_{n\to\infty} \Pr_{2n}^{\Theta}(K, s), \tag{2.71}$$

$$\Pr^{\Theta}(K, f) := 1 - \lim_{n\to\infty} \Pr_{2n}^{\Theta}(K, f), \tag{2.72}$$

and, for each $K' \in \mathscr{K}^{\Theta}(K)$,

$$\Pr^{\Theta}(K'|K, s) := \lim_{n\to\infty} \Pr_{2n}^{\Theta}(K'|K, s). \tag{2.73}$$

More specifically, $\Pr^{\Theta}(K, s)$ is the *limiting probability of a successful strand passage in a knot-type* K Θ*-SAP* ; $\Pr^{\Theta}(K, f)$ is the *limiting probability of a failed strand passage in a knot-type* K Θ*-SAP*; and $\Pr^{\Theta}(K'|K, s)$ is the *limiting probability of a knot-type* K' *after-strand-passage SAP given a knot-type* K *successful-strand-passage* Θ*-SAP*. From this point forward $\Pr^{\Theta}(K, s)$ will be referred to as the *limiting successful strand passage probability for knot-type* K; $\Pr^{\Theta}(K, f)$ will be referred to as the *limiting failed (unsuccessful) strand passage probability for knot-type* K; and $\Pr^{\Theta}(K'|K, s)$ will be referred to as the *limiting* $(K \to K')$*-transition knotting probability.* Furthermore, the notation $\Pr^{\Theta}(*)$ will denote the limiting probability associated with property $*$.

Several questions regarding the limiting probabilities arise. First, "Do the limits defining them exist?". Second, "If the limiting probabilities exist, what are their values?". Finally, "If the limiting probabilities exist, how quickly do the fixed-n probabilities approach their limit?". These three questions will now be explored in the case where $K = \phi$.

With $K = \phi$ in Equations (2.68-2.70), the following is a consequence of Theorems 2.2.4 and 2.2.5.

Corollary 2.2.8 *For each* $K' \in \mathscr{K}^{\Theta}(\phi)$,

$$\lim_{n\to\infty} \frac{\log \Pr_{2n}^{\Theta}(\phi, s)}{2n} = \lim_{n\to\infty} \frac{\log \Pr_{2n}^{\Theta}(\phi, f)}{2n} = \lim_{n\to\infty} \frac{\log \Pr_{2n}^{\Theta}(K'|\phi, s)}{2n} = 0. \tag{2.74}$$

Proof. For each $n \geq n_{(\phi,s)}^{\Theta}/2$, after taking logarithms and dividing both sides by $2n$, the definition of the probability $\Pr_{2n}^{\Theta}(\phi, s)$ (given by Equation (2.68) with $K = \phi$) becomes

$$\frac{\log\left(\Pr_{2n}^{\Theta}(\phi, s)\right)}{2n} = \frac{\log p_{2n}^{\Theta}(\phi, s)}{2n} - \frac{\log p_{2n}^{\Theta}(\phi)}{2n}. \tag{2.75}$$

Now taking the $(n \to \infty)$-limit of Equation (2.75) yields

$$\lim_{n\to\infty} \frac{\log\left(\Pr^{\Theta}_{2n}(\phi, s)\right)}{2n} = \lim_{n\to\infty} \frac{\log p^{\Theta}_{2n}(\phi, s)}{2n} - \lim_{n\to\infty} \frac{\log p^{\Theta}_{2n}(\phi)}{2n}, \tag{2.76}$$

which by Theorem 2.2.4 is equivalent to

$$\lim_{n\to\infty} \frac{\log\left(\Pr^{\Theta}_{2n}(\phi, s)\right)}{2n} = \kappa_\phi - \kappa_\phi = 0. \tag{2.77}$$

Thus $\Pr^{\Theta}_{2n}(\phi, s)$ and consequently $\Pr^{\Theta}_{2n}(\phi, f)$ (by its definition) do not grow exponentially. Using a similar argument with Theorem 2.2.5 instead of Theorem 2.2.4 yields, for any $K' \in \mathscr{K}^{\Theta}(\phi)$,

$$\lim_{n\to\infty} \frac{\log\left(\Pr^{\Theta}_{2n}(K'|\phi, s)\right)}{2n} = \kappa_\phi - \kappa_\phi = 0, \tag{2.78}$$

which implies that $\Pr^{\Theta}_{2n}(K'|\phi, s)$ does not grow exponentially. ∎

From Equations (2.71)-(2.73), the limiting probabilities for $K = \phi$, assuming the limits exist, are

$$\Pr^{\Theta}(\phi, s) := \lim_{n\to\infty} \Pr^{\Theta}_{2n}(\phi, s), \tag{2.79}$$

$$\Pr^{\Theta}(\phi, f) := \lim_{n\to\infty} \Pr^{\Theta}_{2n}(\phi, f) = 1 - \lim_{n\to\infty} \Pr^{\Theta}_{2n}(\phi, s), \tag{2.80}$$

and, for each $K' \in \mathscr{K}^{\Theta}(\phi)$,

$$\Pr^{\Theta}(K'|\phi, s) := \lim_{n\to\infty} \Pr^{\Theta}_{2n}(K'|\phi, s). \tag{2.81}$$

In reality, the existence of these limiting probabilities is an open question. The best that can be done is to explore numerically the issue of their existence. Assuming that the limiting probabilities do exist, Corollary 2.2.8 implies that the rates at which these limiting probabilities are approached are less than exponential. Further to this, because the smallest trefoils in $\mathbb{Z}^3$ have 24-edges [26], the smallest figure 8's in $\mathbb{Z}^3$ have 30-edges [83], and the lengths of the smallest SAPs with prime knot-type K seemingly are increasing in the crossing number of a knot with knot-type K, it is suspected that $\Pr^{\Theta}_{2n}(\phi|\phi, s)$ decreases to $\Pr^{\Theta}(\phi|\phi, s)$ and, for each non-trivial $K' \in \mathscr{K}^{\Theta}(\phi)$, $\Pr^{\Theta}_{2n}(K'|\phi, s)$ increases to $\Pr^{\Theta}(K'|\phi, s)$. To this end, the following is conjectured.

Conjecture 2.2.3 $\Pr^{\Theta}(\phi, s)$, $\Pr^{\Theta}(\phi, f)$, *and* $\Pr^{\Theta}(K'|\phi, s)$, *for each* $K' \in \mathscr{K}^{\Theta}(\phi)$, *exist. Furthermore,*

I. the fixed-n probabilities $\Pr^{\Theta}_{2n}(\phi, s)$ *and, for each non-trivial* $K' \in \mathscr{K}^{\Theta}(\phi)$, $\Pr^{\Theta}_{2n}(K'|\phi, s)$

increase to their respective limits $\Pr^{\Theta}(\phi, s)$ *and* $\Pr^{\Theta}(K'|\phi, s)$ *at a rate that is less than exponential.*

II. the fixed-n probabilities $\Pr^{\Theta}_{2n}(\phi, f)$ *and* $\Pr^{\Theta}_{2n}(\phi|\phi, s)$ *decrease to their respective limits* $\Pr^{\Theta}(\phi, f)$ *and* $\Pr^{\Theta}(\phi|\phi, s)$ *at a rate that is less than exponential.*

Note that the validity of Conjecture 2.2.3 is explored numerically in Chapter 6.

In order to discuss the question "If the limiting probabilities exist, what are their values?", assume, for the rest of this section, that the limiting probabilities $\Pr^{\Theta}(\phi, s)$, $\Pr^{\Theta}(\phi, f)$, and, for each $K' \in \mathscr{K}^{\Theta}(\phi)$, $\Pr^{\Theta}(K'|\phi, s)$ exist, and define the following notation.

Given $a, b, c, d, h,$ and a function g (with $g(n) = O(n^{-1})$), define

$$\mathcal{F}_n(a, b, c, d, h, g) := an^b e^{cn} \left(1 + dn^h + g(n)\right). \tag{2.82}$$

It is conjectured (cf. Equation (1.26)) that there exist real-valued constants $A, \alpha, \mu, B, \Delta$, and a function $g_p(n) = O(n^{-1})$, such that, for sufficiently large integer values of n, the number of $(2n)$-edge SAPs is given by

$$p_{2n} = \mathcal{F}_{2n}(A, \alpha - 3, \log \mu, B, -\Delta, g_p). \tag{2.83}$$

For each property $* \in \Phi$ (recall that $\Phi := \{\phi, (\phi, s), (\phi, f)\} \cup \mathscr{K}^{\dagger}(\phi)$), assume that $p^{\Theta}_{2n}(*)$ has a similar scaling form to that of p_{2n}. This leads to the conjecture that, for each property $* \in \Phi$, there exist real-valued constants $A^{\Theta}_*, \alpha^{\Theta}_*, \kappa^{\Theta}_*, B^{\Theta}_*, -\Delta^{\Theta}_*$ and a function g^{Θ}_* (with $g^{\Theta}_*(n) = O(n^{-1})$) such that, for sufficiently large integer values of n, the number of $(2n)$-edge property-$*$ Θ-SAPs is given by

$$p^{\Theta}_{2n}(*) = \mathcal{F}_{2n}(A^{\Theta}_*, \alpha^{\Theta}_*, \kappa^{\Theta}_*, B^{\Theta}_*, -\Delta^{\Theta}_*, g^{\Theta}_*). \tag{2.84}$$

Since Theorems 2.2.4 and 2.2.5 yield, for each $K' \in \mathscr{K}^{\Theta}(\phi)$,

$$\kappa_{\phi} = \kappa^{\Theta}_{(\phi,s)} = \kappa^{\Theta}_{(\phi,f)} = \kappa^{\Theta}_{(K'|\phi,s)}, \tag{2.85}$$

the scaling form for $p^{\Theta}_{2n}(*)$, for sufficiently large integer values of n, is conjectured to be:

Conjecture 2.2.4 *For every* $* \in \Phi$, *there exist real valued constants* A^{Θ}_*, α^{Θ}_*, κ_{ϕ}, B^{Θ}_*, *and* $-\Delta^{\Theta}_*$ *and a function* g^{Θ}_* *(with* $g^{\Theta}_*(n) = O(n^{-1})$*) such that for sufficiently large integer values of* n,

$$p^{\Theta}_{2n}(*) = \mathcal{F}_{2n}(A^{\Theta}_*, \alpha^{\Theta}_*, \kappa_{\phi}, B^{\Theta}_*, -\Delta^{\Theta}_*, g^{\Theta}_*). \tag{2.86}$$

Assuming Conjecture 2.2.4 is true has the following consequence for the fixed-n probabilities given by Equations (2.68)-(2.70) with $K = \phi$.

Consequence 2.2.2 *Suppose that Conjecture 2.2.4 is true. Then, for* $* \in \{(\phi, s), (\phi, f)\}$,

$$\begin{aligned}\Pr_{2n}^{\Theta}(*) &= \frac{\mathcal{F}_{2n}(A_*^{\Theta}, \alpha_*^{\Theta}, \kappa_\phi, B_*^{\Theta}, -\Delta_*^{\Theta}, g_*^{\Theta})}{\mathcal{F}_{2n}(A_\phi^{\Theta}, \alpha_\phi^{\Theta}, \kappa_\phi, B_\phi^{\Theta}, -\Delta_\phi^{\Theta}, g_\phi^{\Theta})} \\ &= \frac{A_*^{\Theta}}{A_\phi^{\Theta}} \left((2n)^{\alpha_*^{\Theta} - \alpha_\phi^{\Theta}} \right) \left(\frac{1 + B_*^{\Theta} (2n)^{-\Delta_*^{\Theta}} + g_*^{\Theta}(2n)}{1 + B_\phi^{\Theta} (2n)^{-\Delta_\phi^{\Theta}} + g_\phi^{\Theta}(2n)} \right), \end{aligned} \tag{2.87}$$

and, for $* \in \mathscr{K}^{\dagger}(\phi)$,

$$\begin{aligned}\Pr_{2n}^{\Theta}(*) &= \frac{\mathcal{F}_{2n}(A_*^{\Theta}, \alpha_*^{\Theta}, \kappa_\phi, B_*^{\Theta}, -\Delta_*^{\Theta}, g_*^{\Theta})}{\mathcal{F}_{2n}(A_{(\phi,s)}^{\Theta}, \alpha_{(\phi,s)}^{\Theta}, \kappa_\phi, B_{(\phi,s)}^{\Theta}, -\Delta_{(\phi,s)}^{\Theta}, g_{(\phi,s)}^{\Theta})} \\ &= \frac{A_*^{\Theta}}{A_{(\phi,s)}^{\Theta}} \left((2n)^{\alpha_*^{\Theta} - \alpha_{(\phi,s)}^{\Theta}} \right) \left(\frac{1 + B_*^{\Theta} (2n)^{-\Delta_*^{\Theta}} + g_*^{\Theta}(2n)}{1 + B_{(\phi,s)}^{\Theta} (2n)^{-\Delta_{(\phi,s)}^{\Theta}} + g_{(\phi,s)}^{\Theta}(2n)} \right), \end{aligned} \tag{2.88}$$

where the quantities $\frac{A_*^{\Theta}}{A_\phi^{\Theta}}$, *for* $* \in \{(\phi, s), (\phi, f)\}$, *and* $\frac{A_*^{\Theta}}{A_{(\phi,s)}^{\Theta}}$, *for* $* \in \mathscr{K}^{\dagger}(\phi)$, *are referred to as amplitude ratios.*

Assuming that $\Pr_{2n}^{\Theta}(*)$ has the form given by Equations (2.87) and (2.88), substituting Equations (2.87) and (2.88) into Equations (2.79)-(2.81) has the following consequence for the limiting strand passage probabilities.

Consequence 2.2.3 *Suppose that Conjecture 2.2.4 is true. Then, for* $* \in \{(\phi, s), (\phi, f)\}$,

$$\Pr^{\Theta}(*) = \frac{A_*^{\Theta}}{A_\phi^{\Theta}} \lim_{n \to \infty} \left(n^{\alpha_*^{\Theta} - \alpha_\phi^{\Theta}} \right), \tag{2.89}$$

and

$$\Pr^{\Theta}(*) = \frac{A_*^{\Theta}}{A_{(\phi,s)}^{\Theta}} \lim_{n \to \infty} \left(n^{\alpha_*^{\Theta} - \alpha_{(\phi,s)}^{\Theta}} \right), \text{ for } * \in \mathscr{K}^{\dagger}(\phi). \tag{2.90}$$

If Conjecture 2.2.4 holds, $\Pr^{\Theta}(*)$, for $* \in \Phi$, is finite when $\lim_{n \to \infty} \left(n^{\alpha_*^{\Theta} - \alpha_\phi^{\Theta}} \right)$ and $\lim_{n \to \infty} \left(n^{\alpha_*^{\Theta} - \alpha_{(\phi,s)}^{\Theta}} \right)$ are finite, which requires knowing that $\alpha_*^{\Theta} - \alpha_\phi^{\Theta} \leq 0$, for $* \in \{(\phi, s), (\phi, f)\}$, and knowing that $\alpha_*^{\Theta} - \alpha_{(\phi,s)}^{\Theta} \leq 0$, for $* \in \mathscr{K}^{\dagger}(\phi)$. Combining the facts stated in Inequalities (2.20)-(2.22) with the assumption that Conjecture 2.2.4 holds has the following consequence.

Consequence 2.2.4 *Suppose Conjecture 2.2.4 is true. Then,*

I. $\alpha_\phi^{\Theta} \geq \alpha_{(\phi,s)}^{\Theta}$;

II. $\alpha_\phi^{\Theta} \geq \alpha_{(\phi,f)}^{\Theta}$; *and*

III. for each $* \in \mathscr{K}^{\dagger}(\phi)$, $\alpha_{(\phi,s)}^{\Theta} \geq \alpha_*^{\Theta}$.

Now assuming that both Consequences 2.2.3 and 2.2.4 are true results in $\Pr^{\Theta}(*)$ being one of two values (cf. Consequence 2.2.5).

Consequence 2.2.5 *Suppose that Consequences 2.2.3 and 2.2.4 hold. Then, for* $* \in \{(\phi, s), (\phi, f)\}$,

$$\Pr^{\Theta}(*) = \begin{cases} 0, & \text{if } \alpha_*^{\Theta} < \alpha_{\phi}^{\Theta} \\ \dfrac{A_*^{\Theta}}{A_{\phi}^{\Theta}}, & \text{if } \alpha_*^{\Theta} = \alpha_{\phi}^{\Theta}, \end{cases} \tag{2.91}$$

and, for $* \in \mathscr{K}^{\dagger}(\phi)$,

$$\Pr^{\Theta}(*) = \begin{cases} 0, & \text{if } \alpha_*^{\Theta} < \alpha_{(\phi,s)}^{\Theta} \\ \dfrac{A_*^{\Theta}}{A_{(\phi,s)}^{\Theta}}, & \text{if } \alpha_*^{\Theta} = \alpha_{(\phi,s)}^{\Theta}. \end{cases} \tag{2.92}$$

To determine which of these two values is $\Pr^{\Theta}(*)$ (under the assumption that Consequences 2.2.3 and 2.2.4 hold), one further result is required.

Given any $\epsilon > 0$ and any proper pattern P (cf. Definition 1.3.8 in Section 1.3) that can occur in an unknotted SAP, let $p_{2n}(\leq \lfloor 2\epsilon n \rfloor, P|\phi)$ be the number of $(2n)$-edge unknotted SAPs in $\mathbb{Z}^3$ that contain at most $\lfloor 2\epsilon n \rfloor$ occurrences of the pattern P. Then the required result, which will be referred to in this work as the *Pattern Theorem for Unknotted SAPs*, is stated in the following conjecture.

Conjecture 2.2.5 (Pattern Theorem for Unknotted SAPs) *For any proper pattern* P, *there exists* $\epsilon > 0$ *such that*

$$\limsup_{n\to\infty} \frac{\log p_{2n}(\leq \lfloor 2\epsilon n \rfloor, P|\phi)}{2n} < \kappa_{\phi}. \tag{2.93}$$

In other words, if the Pattern Theorem for Unknotted SAPs holds, then the number of $(2n)$-edge unknotted SAPs in $\mathbb{Z}^3$ that contain more than $\lfloor 2\epsilon n \rfloor$ occurrences of the proper pattern P, that is $p_{2n}(\phi) - p_{2n}(\leq \lfloor 2\epsilon n \rfloor, P|\phi)$, grows at the same exponential rate as $p_{2n}(\phi)$. Although proving the Pattern Theorem for Unknotted SAPs is still an open question, it is believed to be true [64, 125]. Therefore, for the purposes of this discussion, the Pattern Theorem for Unknotted SAPs is assumed to be true.

Figures 2.10 (a) and (b) are illustrations of two proper patterns that can occur in an unknotted SAP. If the pattern in Figure 2.10 (a) occurs in an unknotted SAP in $\mathbb{Z}^3$, the unknotted SAP becomes (after an appropriate translation) an element of $\mathscr{P}^{\Theta}(\phi, f) \subseteq \mathscr{P}^{\Theta}(\phi)$. Similarly, if the pattern in Figure 2.10 (b) occurs in an unknotted SAP in $\mathbb{Z}^3$,

the unknotted SAP becomes (after an appropriate translation) an element of $\mathscr{P}^{\Theta}(\phi, s) \subseteq \mathscr{P}^{\Theta}(\phi)$. Because either of these patterns can occur in an unknotted SAP an arbitrary number of times, both patterns are proper patterns for unknotted SAPs. Note that, for any polygon which contains one of these two patterns several times, the polygon can be translated so that the vertex labelled B in any one of these pattern occurrences becomes the origin. Hence assuming Conjecture 2.2.5 is true has the following consequence.

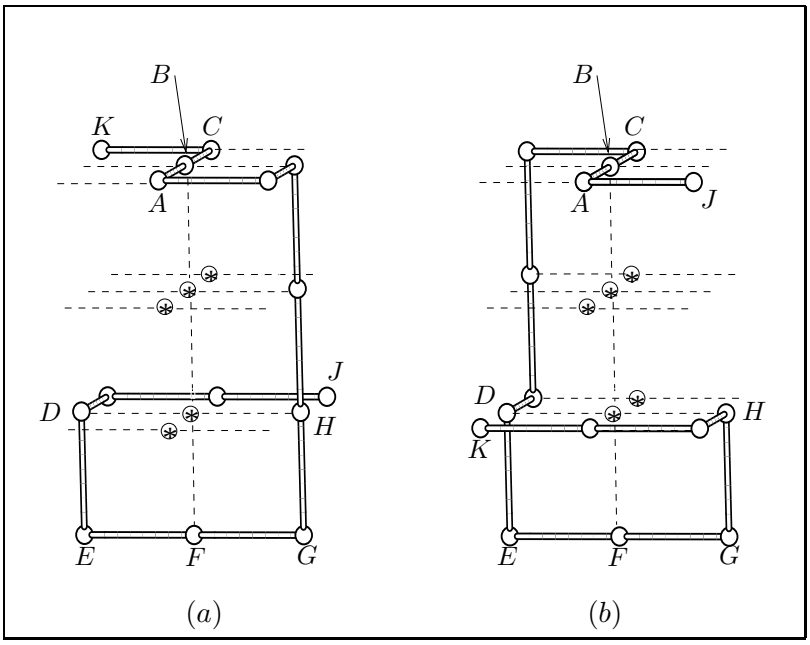

Figure 2.10: Two 14-edge proper patterns that contain the structure Θ. A strand passage is not viable in the pattern illustrated in Figure (a) and is viable in the pattern illustrated in Figure (b). Open circles and open bonds represent the vertices and edges of the pattern. The circles containing asterisks are vertices not occupied by the pattern. Dashed lines represent lattice edges not occupied by the pattern. The vertices labelled A, B, C, D, E, F, G, and H are vertices in Θ.

Consequence 2.2.6 *Assuming Conjecture 2.2.5 is true, there exist positive constants* $\varepsilon_{(\phi,s)}$, $\varepsilon_{(\phi,f)}$, $N_{(\phi,s)}$, *and* $N_{(\phi,f)}$, *such that, for every integer* $n \geq N_{(\phi,s)}$,

$$\varepsilon_{(\phi,s)} n p_{2n}(\phi) \leq p^{\Theta}_{2n}(\phi, s) \tag{2.94}$$

and, for every integer $n \geq N_{(\phi,f)}$,

$$\varepsilon_{(\phi,f)} n p_{2n}(\phi) \leq p^{\Theta}_{2n}(\phi, f), \tag{2.95}$$

where Inequalities (2.94) and (2.95) result from arguments similar to those presented in [63].

Given an unknotted $(2n)$-edge Θ-SAP that contains the pattern P (the pattern displayed in Figure 2.10 (b)), by replacing Θ with Θ_s in P, the resulting after-strand-passage SAP is unknotted and is an element counted in $p^{\Theta}_{2n}(\phi|\phi, s)$. Hence there exist positive constants $\varepsilon_{(\phi|\phi,s)}$ and $N_{(\phi|\phi,s)}$, such that, for every integer $n \geq N_{(\phi|\phi,s)}$,

$$\varepsilon_{(\phi|\phi,s)} n p_{2n}(\phi) \leq p^{\Theta}_{2n}(\phi|\phi, s), \tag{2.96}$$

where Inequality (2.96) results from arguments similar to those presented in [63]. Similarly, for each $K' \in \mathscr{K}^{\Theta}(\phi)$, creating a suitable pattern for which a strand passage about the structure in the pattern yields an after-strand-passage polygon whose knot-type is K', has the following consequence.

Consequence 2.2.7 *Assuming Conjecture 2.2.5 is true, then, for each $K' \in \mathscr{K}^{\Theta}(\phi)$ there exist positive constants $\varepsilon_{(K'|\phi,s)}$ and $N_{(K'|\phi,s)}$, such that, for every integer $n \geq N_{(K'|\phi,s)}$,*

$$\varepsilon_{(K'|\phi,s)} n p_{2n}(\phi) \leq p^{\Theta}_{2n}(K'|\phi, s), \tag{2.97}$$

where Inequality (2.97) results from arguments presented in [63].

Inequalities (2.20)-(2.22) and Lemma 2.2.1, combined with Inequalities (2.94)-(2.97), yield, for every integer $n \geq \max\{N_{(\phi,f)}, N_{(\phi,s)}, \max_{K' \in \mathscr{K}^{\Theta}(\phi)}\{N_{(K'|\phi,s)}\}\}$, the inequalities

$$\varepsilon_{(\phi,s)} n p_{2n}(\phi) \leq p^{\Theta}_{2n}(\phi, s) \leq p^{\Theta}_{2n}(\phi) \leq 2n p_{2n}(\phi), \tag{2.98}$$

$$\varepsilon_{(\phi,f)} n p_{2n}(\phi) \leq p^{\Theta}_{2n}(\phi, f) \leq p^{\Theta}_{2n}(\phi) \leq 2n p_{2n}(\phi), \tag{2.99}$$

$$\varepsilon_{(\phi|\phi,s)} n p_{2n}(\phi) \leq p^{\Theta}_{2n}(\phi|\phi, s) \leq p^{\Theta}_{2n}(\phi) \leq 2n p_{2n}(\phi), \tag{2.100}$$

and

$$\varepsilon_{(K'|\phi,s)} n p_{2n}(\phi) \leq p^{\Theta}_{2n}(K'|\phi, s) \leq p^{\Theta}_{2n}(\phi) \leq 2n p_{2n}(\phi). \tag{2.101}$$

Further assuming that, for sufficiently large integer values of n, the forms of $p^{\Theta}_{2n}(\phi)$, $p^{\Theta}_{2n}(\phi, s)$, $p^{\Theta}_{2n}(\phi, f)$, and $p^{\Theta}_{2n}(K'|\phi, s)$, for each $K' \in \mathscr{K}^{\Theta}(\phi)$, are given by Equation (2.86), yields the following two consequences.

Consequence 2.2.8 *Assuming that α_{ϕ}, as defined in Equation (1.27), exists, that Conjecture 2.2.5 (the Pattern Theorem for Unknotted SAPs) holds, and that Conjecture 2.2.4 is true, then*

$$\alpha^{\Theta}_{\phi} = \alpha_{\phi} - 2. \tag{2.102}$$

Consequence 2.2.9 *Assuming that Conjecture 2.2.5 (the Pattern Theorem for Unknotted SAPs) holds and that Conjecture 2.2.4 is true, then for each* $K' \in \mathscr{K}^{\Theta}(\phi)$,

$$\alpha_{\phi}^{\Theta} = \alpha_{(\phi,s)}^{\Theta} = \alpha_{(\phi,f)}^{\Theta} = \alpha_{(K'|\phi,s)}^{\Theta}. \tag{2.103}$$

Note that the amplitudes A_{ϕ}^{Θ}, $A_{(\phi,s)}^{\Theta}$, $A_{(\phi,f)}^{\Theta}$, and $A_{(K'|\phi,s)}^{\Theta}$, for each $K' \in \mathscr{K}^{\Theta}(\phi)$, are all positive constants, that

$$\sum_{K' \in \mathscr{K}^{\Theta}(\phi)} \Pr^{\Theta}(K'|\phi, s) = 1, \tag{2.104}$$

and that

$$\Pr^{\Theta}(\phi, s) + \Pr^{\Theta}(\phi, f) = 1. \tag{2.105}$$

Hence the limiting probabilities $\Pr^{\Theta}(\phi, s)$, $\Pr^{\Theta}(\phi, f)$, and $\Pr^{\Theta}(K'|\phi, s)$, for each $K' \in \mathscr{K}^{\Theta}(\phi)$, must all be greater than zero and strictly less than one. Furthermore, assuming that Conjecture 2.2.3 and Consequences 2.2.3 and 2.2.9 are true has the following consequence for the limiting strand passage probabilities given by Equations (2.89) and (2.90).

Consequence 2.2.10 *Assuming that Conjecture 2.2.3 and Consequences 2.2.3 and 2.2.9 are true, then the limiting strand passage probabilities are given by the following amplitude ratios:*

$$\Pr^{\Theta}(\phi, s) = \frac{A_{(\phi,s)}^{\Theta}}{A_{\phi}^{\Theta}}, \tag{2.106}$$

$$\Pr^{\Theta}(\phi, f) = \frac{A_{(\phi,f)}^{\Theta}}{A_{\phi}^{\Theta}}, \tag{2.107}$$

and, for each $K' \in \mathscr{K}^{\Theta}(\phi)$,

$$\Pr^{\Theta}(K'|\phi, s) = \frac{A_{(K'|\phi,s)}^{\Theta}}{A_{(\phi,s)}^{\Theta}}. \tag{2.108}$$

Furthermore, the limiting strand passage probabilities all lie in the interval $(0, 1)$.

The final question that was posed in this section but has not been addressed yet, is "What is the scaling form for $\Pr_{2n}^{\Theta}(*)$, for $* \in \Phi \backslash \{\phi\}$?". A consequence of assuming that both $p_{2n}^{\Theta}(*)$ and $p_{2n}^{\Theta}(\phi)$ have a scaling form as given by Equation (2.86), and of assuming that Consequence 2.2.9 is true is that the scaling form for $\Pr_{2n}^{\Theta}(*)$ for $* \in \Phi \backslash \{\phi\}$ is given as follows.

Consequence 2.2.11 *Assuming that Conjecture 2.2.4 and Consequence 2.2.9 are true, for sufficiently large positive integers n, a suitable scaling form (as $n \to \infty$) for $\Pr^{\Theta}_{2n}(*)$ is, for $* \in \{(\phi, s), (\phi, f)\}$,*

$$\frac{A^{\Theta}_{*}}{A^{\Theta}_{\phi}} + \left(B'^{\Theta}_{*}\right)(2n)^{-\Delta'^{\Theta}_{*}} + g^{*}_{1}(2n), \tag{2.109}$$

where

$$g^{*}_{1}(2n) = O(\min\left\{(2n)^{-1}, \max\left\{(2n)^{-\Delta^{\Theta}_{\phi}}, (2n)^{-\Delta^{\Theta}_{*}}\right\}\right\}), \tag{2.110}$$

and, for $* \in \mathscr{K}^{\dagger}(\phi)$, is

$$\frac{A^{\Theta}_{*}}{A^{\Theta}_{(\phi,s)}} + \left(B'^{\Theta}_{*}\right)(2n)^{-\Delta'^{\Theta}_{*}} + g^{*}_{2}(2n), \tag{2.111}$$

where

$$g^{*}_{2}(2n) = O(\min\left\{(2n)^{-1}, \max\left\{(2n)^{-\Delta^{\Theta}_{(\phi,s)}}, (2n)^{-\Delta^{\Theta}_{*}}\right\}\right\}). \tag{2.112}$$

The conjectures and consequences involving the critical exponents presented throughout this section are explored numerically in Chapters 4 and 5. The conjectures and consequences regarding the fixed-n and the limiting strand passage probabilities are explored numerically in Chapter 6.

2.2.3 The Size of a Θ-SAP

Another open question regarding the Θ-SAPs in $\mathscr{P}^{\Theta}_{2n}(\phi)$ is "For $\omega \in \mathscr{P}^{\Theta}_{2n}(\phi)$, how do the lengths of the uSAWs w_+ and w_- (as defined in Definition 2.2.3) compare (on average) to each other?". A possible answer to this question is formally stated later in Conjecture 2.2.7. Before introducing Conjecture 2.2.7, some definitions and results are first required.

Definition 2.2.10 *Suppose ω, $\omega' \in \mathscr{P}$ are two SAPs such that $|\mathcal{V}(\omega) \cap \mathcal{V}(\omega')| = 1$ and $\mathcal{E}(\omega) \cap \mathcal{E}(\omega') = \{\}$. Then the graph embedding $(\mathcal{V}(\omega) \cup \mathcal{V}(\omega'), \mathcal{E}(\omega) \cup \mathcal{E}(\omega'))$ in $\mathbb{Z}^3$ is called a Figure-of-Eight graph, or Figure-of-Eight for short and the vertex in $\mathcal{V}(\omega) \cap \mathcal{V}(\omega')$ is called the contact point of the Figure-of-Eight. The two SAPs that are connected via the contact point of a Figure-of-Eight are referred to as the loops of the Figure-of-Eight. Let $\mathscr{F}_8(n, k)$ be the set of n-edge Figure-of-Eights that consist of one loop with k-edges and the other loop with $(n-k)$-edges, for $k \geq n-k$, and define $f_8(n, k)$ to be the number of Figure-of-Eights in $\mathscr{F}_8(n, k)$ (up to translation).*

Figure 2.11 depicts an element of $\mathscr{F}_8(10, 6)$, that is a 10-edge Figure-of-Eight with contact point C that has one loop of length six and the other loop of length four. In

general, if ϱ_8 is a $(2n)$-edge Figure-of-Eight having one of its loops larger than the other loop, then the length of the larger loop must be bounded strictly below by n and above by $2n$. Hence the length of the larger loop is $O(n)$. But why is the discussion focussing on Figure-of-Eights? The following lemma relates certain polygons in $\mathscr{P}^{\Theta}(\phi)$ to Figure-of-Eights.

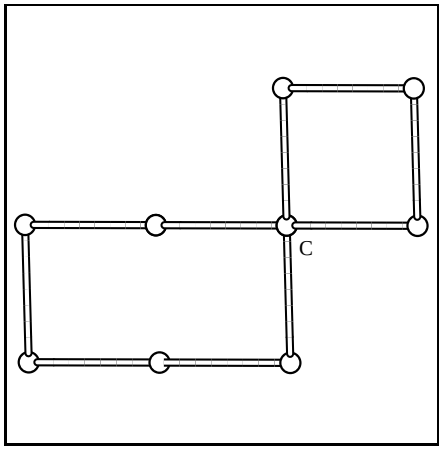

Figure 2.11: A Figure-of-Eight with contact point C and one loop of length six and one loop of length four.

Lemma 2.2.4 *Every polygon in $\mathscr{P}^{\Theta}(\phi, s)$ can be converted into a Figure-of-Eight.*

Proof. For fixed $(0,0,0) \in \mathbb{Z}^3$, define the graph embedding $\Theta_8{:=}(\mathcal{V}(\Theta_8), \mathcal{E}(\Theta_8))$ in $\mathbb{Z}^3$ to be the graph embedding with vertex set

$$\begin{aligned}\mathcal{V}(\Theta_8) = \; & \{(0,0,0),(1,0,0),(1,0,-1),(-1,0,-1),\\ & (0,0,-2),(-1,0,0),(0,-1,-2),(0,-1,-1),(0,0,-1),\\ & (0,1,-1),(0,1,-2),(0,-1,-3),(0,0,-3),\\ & (1,0,-2),(-1,0,-2),(0,1,-3)\},\end{aligned} \tag{2.113}$$

and edge set

$$\begin{aligned}\mathcal{E}(\Theta_8) = \; & \{\{(1,0,0),(1,0,-1)\},\{(1,0,-1),(0,0,-1)\},\\ & \{(0,0,-1),(-1,0,-1)\},\{(-1,0,-1),(-1,0,0)\},\\ & \{(0,-1,-2),(0,-1,-1)\},\{(0,-1,-1),(0,0,-1)\},\\ & \{(0,0,-1),(0,1,-1)\},\{(0,1,-1),(0,1,-2)\}\}.\end{aligned} \tag{2.114}$$

Θ_8 is illustrated in Figure 2.12.

Now, since strand passage is viable for every $\omega \in \mathscr{P}^{\Theta}(\phi, s)$, the pattern Θ in every

$\omega \in \mathscr{P}^{\Theta}(\phi, s)$ can be replaced with the pattern Θ_8. Let ϖ be the graph embedding obtained from a polygon $\omega \in \mathscr{P}^{\Theta}(\phi, s)$ by replacing Θ with the pattern Θ_8. The vertex $(0, 0, -1) \in \mathcal{V}(\Theta_8)$ becomes the contact point for ϖ. Starting at the contact point of ϖ and travelling in the direction induced by moving to the vertex $(-1, 0, 0)$, the walk connecting the vertex $(-1, 0, 0)$ to the vertex $(0, -1, -2)$ can be traversed. Continuing in this direction, the vertex $(0, -1, -1)$ will eventually be visited, followed immediately by a return to the contact point. Hence the undirected version of the path just described defines a self-avoiding polygon. Let this SAP be ϖ_+. Similarly, if the path starting at the contact point of ϖ is traversed in the direction induced by moving to the vertex $(0, 1, -1)$, the contact point will also eventually be revisited. At this point, the undirected version of the path traversed defines a self-avoiding polygon. Call this SAP ϖ_-. Since ϖ_+ and ϖ_- are two self-avoiding polygons in which $\mathcal{V}(\varpi_+) \cap \mathcal{V}(\varpi_-) = \{(0, 0, -1)\}$, ϖ is a Figure-of-Eight. Because ω was chosen arbitrarily, the lemma is proved. ∎

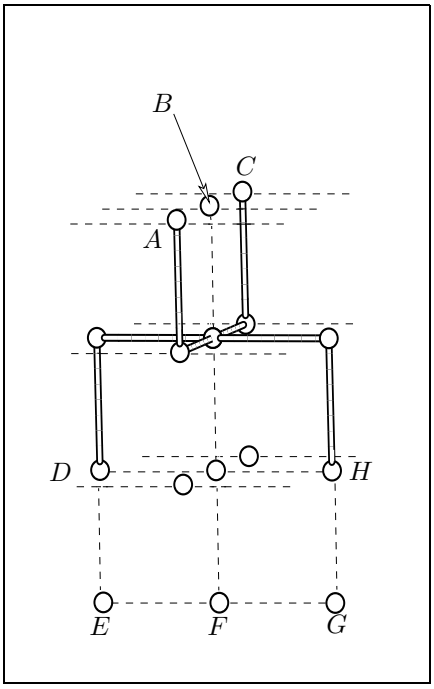

Figure 2.12: The Figure-of-Eight pattern Θ_8 that converts an unknotted successful-strand-passage polygon into a Figure-of-Eight. Open and empty circles represent the vertices of Θ_8 and open bonds represent the edges of Θ_8. Dashed lines represent lattice edges not occupied by Θ_8.

In [125], Orlandini *et al.* provide a heuristic argument supporting the following conjecture.

Conjecture 2.2.6 ([125]) *For sufficiently large even n, the set of all Figure-of-Eights in $\mathbb{Z}^3$ is dominated by Figure-of-Eights with one large loop (length is $O(n)$) and one small loop.*

Now recall that the set $\mathscr{P}^{\Theta}(\phi, s)$ is the set of self-avoiding polygons that can be decomposed into the fixed structure Θ and the uSAWs w_- and w_+, where w_- and w_+ are mutually self-avoiding, $w_- \in \mathscr{W}(C,D)$, $w_+ \in \mathscr{W}(A,H)$, $\mathcal{V}(w_-) \cap \mathcal{V}(\Theta) = \{C, D\}$, and $\mathcal{V}(w_+) \cap \mathcal{V}(\Theta) = \{A, H\}$, where vertices A, C, D, and H are those vertices illustrated in Figure 2.12. For each $\omega \in \mathscr{P}^{\Theta}(\phi)$, define $w_+(\omega) := w_+$ and $w_-(\omega) := w_-$ where w_+ and w_- are defined in Definition 2.2.3. $w_+(\omega)$ is loosely referred to as the *uSAW on the right of* ω and $w_-(\omega)$ is loosely referred to as the *uSAW on the left of* ω.

Suppose the two uSAWs $w_+(\omega)$and $w_-(\omega)$in $\omega \in \mathscr{P}^{\Theta}_{2n}(\phi)$satisfy $|w_+(\omega)| \neq |w_-(\omega)|$. If $w(\omega)$is the larger of the two uSAWs $w_+(\omega)$and $w_-(\omega)$, then

$$n - 3 < |w(\omega)| \leq 2n - 6, \tag{2.115}$$

and hence its length is $O(n)$. Also note that combining Lemma 2.2.4 with the arguments that lead to Conjecture 2.2.6 suggests the following regarding SAPs in $\mathscr{P}^{\Theta}(\phi, s)$.

Conjecture 2.2.7 *Assuming Conjecture 2.2.6 is true, then $\mathscr{P}^{\Theta}(\phi, s)$ is dominated by polygons ω in which one of $|w_-(\omega)|$ and $|w_+(\omega)|$ is large (whose length is $O(n)$) and the other is small (whose length is $O(1)$).*

Because of the design of the structure Θ, all Θ-SAPs, not just those in $\mathscr{P}^{\Theta}(\phi, s)$, are figure-of-eight-like. Thus the following conjecture can be posed regarding SAPs in $\mathscr{P}^{\Theta}(\phi)$.

Conjecture 2.2.8 *$\mathscr{P}^{\Theta}(\phi)$ is dominated by polygons ω in which one of $|w_-(\omega)|$ and $|w_+(\omega)|$ is large (length $O(n)$) and the other is small (whose length is $O(1)$).*

If Conjectures 2.2.7 and 2.2.8 are true, then $\mathscr{P}^{\Theta}(\phi, s)$ and $\mathscr{P}^{\Theta}(\phi)$ are dominated by polygons comprised of one large and one small uSAW. From this point forward, any reference to a "large" loop in an $(2n)$-edge Figure-of-Eight or a "large" uSAW in an $(2n)$-edge Θ-SAP will refer to a loop or uSAW whose length is $O(n)$, but, what is meant by the term "small"?

In [111], Metzler *et al.* provide one particular quantification for the large and small loops in Conjecture 2.2.6. They argue that, based on their model for $d = 3$, for a randomly

chosen n-edge Figure-of-Eight, the expected length of the large loop and the expected length of the small loop scale according to the power-law relations given in the following conjecture.

Conjecture 2.2.9 ([111]) *In $d = 3$, a randomly chosen n-edge Figure-of-Eight consists of one large and one small loop such that the expected length of the large loop scales according to the power-law relation n^1 and the small loop is strongly localized, that is the expected length of the small loop is $O(1)$.*

The average lengths of uSAWs $w_+(\omega)$ and $w_-(\omega)$ in a Θ-SAP ω generated by the CMC Θ-BFACF simulation are explored in Chapter 7.

The discussion now turns to addressing the question "What other characteristics do the uSAWs comprising polygons in $\mathscr{P}^{\Theta}(\phi)$ have?". In order to introduce and discuss some of these characteristics, the following definitions are required.

Define the "*big right-side* $(2n)$*-edge* Θ*-SAPs*" to be

$$\mathscr{B}^{+}_{2n} := \left\{\omega \in \mathscr{P}^{\Theta}_{2n}(\phi) : |w_+(\omega)| > n-3\right\}; \tag{2.116}$$

the "*big left-side* $(2n)$*-edge* Θ*-SAPs*" to be

$$\mathscr{B}^{-}_{2n} := \left\{\omega \in \mathscr{P}^{\Theta}_{2n}(\phi) : |w_-(\omega)| > n-3\right\}; \tag{2.117}$$

the "*small right-side* $(2n)$*-edge* Θ*-SAPs*" to be

$$\mathscr{S}^{+}_{2n} := \left\{\omega \in \mathscr{P}^{\Theta}_{2n}(\phi) : |w_+(\omega)| < n-3\right\}; \tag{2.118}$$

the "*small left-side* $(2n)$*-edge* Θ*-SAPs*" to be

$$\mathscr{S}^{-}_{2n} := \left\{\omega \in \mathscr{P}^{\Theta}_{2n}(\phi) : |w_-(\omega)| < n-3\right\}; \tag{2.119}$$

the "*equal-sided* $(2n)$*-edge* Θ*-SAPs*" to be

$$\begin{aligned}\mathscr{E}^{+}_{2n} &:= \left\{\omega \in \mathscr{P}^{\Theta}_{2n}(\phi) : |w_+(\omega)| = n-3\right\} \\ &= \left\{\omega \in \mathscr{P}^{\Theta}_{2n}(\phi) : |w_-(\omega)| = n-3\right\} \\ &:= \mathscr{E}^{-}_{2n} := \mathscr{E}_{2n};\end{aligned} \tag{2.120}$$

and the "*unequal-sided* $(2n)$*-edge* Θ*-SAPs*" to be

$$\mathscr{E}^{c}_{2n} := \mathscr{P}^{\Theta}_{2n}(\phi) \backslash \mathscr{E}_{2n}.$$

Note that, for every even integer $n \geq 8$, $\mathscr{E}_{2n} = \{\}$ and that, for every odd integer $n \geq 7$, $\mathscr{E}_{2n} \neq \{\}$. Further note that for an arbitrary $(2n)$-edge SAP $\omega \in \mathscr{P}^{\Theta}(\phi)$, if

1. $|w_+(\omega)| < |w_-(\omega)|$ then $|w_+(\omega)| < n-3 < |w_-(\omega)|$, $\omega \in \mathscr{S}^+_{2n}$ and $\omega \in \mathscr{B}^-_{2n}$, and hence $\mathscr{S}^+_{2n} = \mathscr{B}^-_{2n}$; and
2. $|w_+(\omega)| > |w_-(\omega)|$ then $|w_-(\omega)| < n-3 < |w_+(\omega)|$, $\omega \in \mathscr{B}^+_{2n}$ and $\omega \in \mathscr{S}^-_{2n}$, and hence $\mathscr{B}^+_{2n} = \mathscr{S}^-_{2n}$.

Using these facts and a suitable mapping (as defined in the proof of the following theorem), the following result holds.

Theorem 2.2.7 *For every positive $n \geq 7$,*

1. $\left|\mathscr{B}^+_{2n}\right| = \left|\mathscr{B}^-_{2n}\right|$.
2. $\left|\mathscr{S}^+_{2n}\right| = \left|\mathscr{S}^-_{2n}\right|$.

Proof. Consider the mapping $f : \mathbb{Z}^3 \to \mathbb{Z}^3$ defined by

$$f(x,y,z) := (-x,-y,z) \tag{2.121}$$

and consider any $(2n)$-edge SAP $\omega \in \mathscr{B}^+_{2n}$. Then $f(\omega)$, where $f(\omega)$ is the SAP that results when f is applied to the vertices and edges in ω, will be an $(2n)$-edge SAP in $\mathscr{B}^-_{2n}$. Similarly, for every $(2n)$-edge SAP $\omega \in \mathscr{B}^-_{2n}$, $f(\omega)$ will be an $(2n)$-edge SAP in $\mathscr{B}^+_{2n}$. Thus Part (1) of this theorem holds, that is $\left|\mathscr{B}^+_{2n}\right| = \left|\mathscr{B}^-_{2n}\right|$. Part (2) of this theorem follows analogously by the proof of Part (1). ∎

Combining these two properties with Theorem 2.2.7 implies that the sets $\mathscr{B}^+_{2n}$ and $\mathscr{S}^+_{2n}$ can be used without loss of generality to study the properties of the uSAWs comprising polygons in $\mathscr{P}^{\Theta}_{2n}(\phi)$. Hence for the remainder of this chapter, for every positive even integer n, define $\mathscr{B}_n := \mathscr{B}^+_n$ and $\mathscr{S}_n := \mathscr{S}^+_n$. Also define

$$\mathscr{B} := \bigcup_n \mathscr{B}_{2n}, \tag{2.122}$$

$$\mathscr{S} := \bigcup_n \mathscr{S}_{2n}, \tag{2.123}$$

$$\mathscr{E} := \bigcup_n \mathscr{E}_{2n}, \tag{2.124}$$

and

$$\mathscr{E}^c := \mathscr{P}^{\Theta}(\phi) \backslash \mathscr{E}. \tag{2.125}$$

Now, for every positive integer $n \geq 7$ and for each property $* \in \Phi \backslash \{\phi\}$, define $\mathscr{E}_{2n}(*)$ to be the set of Θ-SAPs in $\mathscr{E}_{2n}$ that have property $*$, $\mathscr{B}_{2n}(*)$ to be the set of Θ-SAPS in $\mathscr{B}_{2n}$ that have property $*$, $\mathscr{S}_{2n}(*)$ to be the set of Θ-SAPs in $\mathscr{S}_{2n}$ that have property $*$, and $\mathscr{E}^c_{2n}(*)$ to be the set of Θ-SAPs in $\mathscr{E}^c_{2n}$ that have property $*$. Then

$$\mathscr{B}(*) := \bigcup_n \mathscr{B}_{2n}(*), \tag{2.126}$$

$$\mathscr{S}(*) := \bigcup_n \mathscr{S}_{2n}(*), \tag{2.127}$$

$$\mathscr{E}(*) := \bigcup_n \mathscr{E}_{2n}(*), \tag{2.128}$$

and

$$\mathscr{E}^c(*) := \mathscr{P}^{\Theta}(*) \backslash \mathscr{E}(*). \tag{2.129}$$

Finally, for every integer $n \geq 7$ and $* \in \Phi$, define

$$w_E(2n) := |\mathscr{E}_{2n}|, \tag{2.130}$$

$$w_S(2n) := |\mathscr{S}_{2n}|, \tag{2.131}$$

$$w_B(2n) := |\mathscr{B}_{2n}|, \tag{2.132}$$

$$w^*_E(2n) := |\mathscr{E}_{2n}(*)|, \tag{2.133}$$

$$w^*_S(2n) := |\mathscr{S}_{2n}(*)|, \tag{2.134}$$

and

$$w^*_B(2n) := |\mathscr{B}_{2n}(*)|. \tag{2.135}$$

With these definitions, properties regarding the number of Θ-SAPs, and the average lengths and the average radii of gyration of the uSAWs in the Θ-SAPs in $\mathscr{B}_{2n}$, $\mathscr{S}_{2n}$, and $\mathscr{E}_{2n}$ can be explored.

The Number of Θ-SAPs in $\mathscr{B}_{2n}$, $\mathscr{S}_{2n}$, and $\mathscr{E}_{2n}$

The following three theorems determine the rate at which $w_B(2n)$, $w_S(2n)$, and $w_E(2n)$, respectively, increase with even n.

Theorem 2.2.8 *For the number of Θ-SAPs in $\mathscr{B}_{2n}$ where $n \geq 7$, the growth rate is given by*

$$\lim_{n\to\infty} \frac{\log w_B(2n)}{2n} = \kappa_\phi. \tag{2.136}$$

Proof. For integers $n \geq 7$, because $\mathscr{B}_{2n} \subseteq \mathscr{P}^{\Theta}_{2n}(\phi)$,

$$w_B(2n) \leq p^{\Theta}_{2n}(\phi). \tag{2.137}$$

For integers $n \geq 9$, using Θ-preserving concatenation to concatenate a $(2n-14)$-edge SAP in $\mathscr{P}_{2n-14}(\phi)$ to a 14-edge Θ-SAP in $\mathscr{P}^{\Theta}_{14}(\phi)$, such as the SAP illustrated in Figure 2.4 (a), yields a $(2n)$-edge SAP in $\mathscr{P}^{\Theta}_{2n}(\phi)$ that is in $\mathscr{B}^{-}_{2n}$. Therefore, for integers $n \geq 9$,

$$p_{2n-14}(\phi)\, p^{\Theta}_{14}(\phi) \leq 2|\mathscr{B}^{-}_{2n}|. \tag{2.138}$$

Because Theorem 2.2.7 gives that, for integers $n \geq 7$, $|\mathscr{B}^{-}_{2n}| = |\mathscr{B}^{+}_{2n}| = w_B(2n)$, then, for integers $n \geq 9$,

$$p_{2n-14}(\phi)\, p^{\Theta}_{14}(\phi) \leq 2w_B(2n). \tag{2.139}$$

Combining Inequalities (2.137) and (2.139) yields the following double inequality for integers $n \geq 9$:

$$p_{2n-14}(\phi)\, p^{\Theta}_{14}(\phi) \leq 2w_B(2n) \leq 2p^{\Theta}_{2n}(\phi). \tag{2.140}$$

Now, for the above double inequality, taking logarithms, dividing by $2n$, and taking the limit as $n \to \infty$, and using the definition of κ_ϕ given by Equation (1.21) and Theorem 2.2.4, yields the required result. ∎

Theorem 2.2.9 *For the number of Θ-SAPs in $\mathscr{S}_{2n}$ where $n \geq 7$, the growth rate is given by*

$$\lim_{n\to\infty} \frac{\log w_S(2n)}{2n} = \kappa_\phi. \tag{2.141}$$

Proof. For integers $n \geq 7$, because $\mathscr{S}_{2n} \subseteq \mathscr{P}^{\Theta}_{2n}(\phi)$,

$$w_S(2n) \leq p^{\Theta}_{2n}(\phi). \tag{2.142}$$

For integers $n \geq 9$, using Θ-preserving concatenation to concatenate a $(2n-14)$-edge SAP in $\mathscr{P}(\phi)$ to a 14-edge SAP in $\mathscr{P}^{\Theta}_{14}(\phi)$, such as the SAP illustrated in Figure 2.4 (a), yields a $(2n)$-edge SAP in $\mathscr{P}^{\Theta}_{2n}(\phi)$ which is in $\mathscr{S}^{+}_{2n}$. Therefore, for integers $n \geq 9$,

$$p_{2n-14}(\phi)\, p^{\Theta}_{14}(\phi) \leq 2w_S(2n). \tag{2.143}$$

Combining Inequalities (2.142) and (2.143) yields the following double inequality for integers $n \geq 9$:

$$p_{2n-14}(\phi)\, p^{\Theta}_{14}(\phi) \leq 2w_S(2n) \leq 2p^{\Theta}_{2n}(\phi). \tag{2.144}$$

Now, for the above double inequality, taking logarithms, dividing by $2n$, and taking the limit as $n \to \infty$, and using the definition of κ_ϕ given by Equation (1.21) and Theorem 2.2.4, yields the required result. ∎

Theorem 2.2.10 *For the number of Θ-SAPs in $\mathscr{E}_{2n}$ where $n \geq 7$ and n is odd, the growth rate is given by*

$$\lim_{n\to\infty} \frac{\log w_E(2n)}{2n} = \kappa_\phi, \tag{2.145}$$

where the limit is taken through odd integer values of n.

Proof. For integers $n \geq 7$, because $\mathscr{E}_{2n} \subseteq \mathscr{P}^{\Theta}_{2n}(\phi)$,

$$w_E(2n) \leq p^{\Theta}_{2n}(\phi). \tag{2.146}$$

Now, for odd integers $n \geq 11$, choose any $\omega_1, \omega_2 \in \mathscr{P}_{\frac{2n-14}{2}}(\phi)$ and any $\omega \in \mathscr{P}^{\Theta}_{14}(\phi)$. Then form (via Θ-preserving concatenation) the SAP $\omega \circ \omega_1$. Note that $\omega \circ \omega_1$ is a Θ-SAP. Now using the Concatenation Algorithm for SAPs, form the polygon $\omega_2 \circ (\omega \circ \omega_1)$ and then apply the appropriate rotation (a 0° rotation is allowed) and translation to $\omega_2 \circ (\omega \circ \omega_1)$ to obtain a SAP $\omega' \in \mathscr{E}_{2n}$ that contains Θ. Hence, for odd integers $n \geq 11$,

$$p_{\frac{2n-14}{2}}(\phi) \leq p_{\frac{2n-14}{2}}(\phi) p^{\Theta}_{14}(\phi) p_{\frac{2n-14}{2}}(\phi) \leq 8 w_E(2n). \tag{2.147}$$

Combining Inequalities (2.146) and (2.147), yields, for odd integers $n \geq 11$, the double inequality

$$p_{\frac{2n-14}{2}}(\phi) \leq 8 w_E(2n) \leq 8 p^{\Theta}_{2n}(\phi). \tag{2.148}$$

Now, for the above double inequality, taking logarithms, dividing by $2n$, taking the limit as $n \to \infty$ (where the limit is taken through the odd integer values), and using the definition of κ_ϕ given by Equation (1.21) and Theorem 2.2.4, yields the required result. ∎

Theorems 2.2.8 to 2.2.10 yield that the numbers $w_B(2n)$, $w_S(2n)$, and $w_E(2n)$ grow exponentially (at a rate of κ_ϕ) with n. Hence the number of Θ-SAPs in $\mathscr{B}_{2n}$, the number of Θ-SAPs in $\mathscr{S}_{2n}$, and the number of Θ-SAPs in $\mathscr{E}_{2n}$, each grow at an exponential rate. Since these growth rates do not say anything about the average lengths or the average radii of gyration for the uSAWs in these sets of Θ-SAPs, these two properties will be discussed, respectively, in the following two sections.

The Average Lengths of the uSAWs in a Θ-SAP

For $\omega \in \mathscr{P}^{\Theta}(\phi)$, recall that $w_+(\omega)$ denotes the uSAW on the right side of ω and that $w_-(\omega)$ denotes the uSAW on the left side of ω. Note that, for odd integers $n \geq 7$, if $\omega \in \mathscr{E}_{2n}(*)$, then

$$|w_+(\omega)| = |w_-(\omega)| = n - 3. \tag{2.149}$$

Otherwise, if $\omega \in \mathscr{E}^c(*)$, define the length of the small uSAW to be

$$s_{|\omega|}(\omega) := \begin{cases} |w_+(\omega)|, & \text{if } |w_+(\omega)| < |w_-(\omega)| \\ |w_-(\omega)|, & \text{otherwise,} \end{cases} \tag{2.150}$$

and define the length of the large uSAW to be

$$l_{|\omega|}(\omega) := \begin{cases} |w_+(\omega)|, & \text{if } |w_+(\omega)| > |w_-(\omega)| \\ |w_-(\omega)|, & \text{otherwise.} \end{cases} \tag{2.151}$$

Furthermore, if $s_{|\omega|}(\omega) = |w_+(\omega)|$, then $w_+(\omega)$ is referred to as the small uSAW on the right of ω and $w_-(\omega)$ is referred to as the large uSAW on the left side of ω, while if $s_{|\omega|}(\omega) = |w_-(\omega)|$, then $w_+(\omega)$ is referred to as the large uSAW on the right of ω and $w_-(\omega)$ is referred to as the small uSAW on the left side of ω. Note that given $* \in \Phi$, for every integer $n \geq 8$ and for every $\omega \in \mathscr{E}^c_{2n}(*)$,

$$s_{2n}(\omega) < n - 3 < l_{2n}(\omega). \tag{2.152}$$

Now, for every natural number $n \geq 8$ and a randomly chosen Θ-SAP $W \in \mathscr{E}^c_{2n}(*)$, let $\mathrm{E}[S_{2n}(\mathscr{E}^c(*))]$ denote the expected length of the small uSAW in W and let $\mathrm{E}[L_{2n}(\mathscr{E}^c(*))]$ denote the expected length of the large uSAW in W. Then

$$\mathrm{E}[S_{2n}(\mathscr{E}^c(*))] := \frac{1}{2w^*_S(2n)} \sum_{\omega \in \mathscr{E}^c_{2n}(*)} s_{2n}(\omega) \tag{2.153}$$

and

$$\mathrm{E}[L_{2n}(\mathscr{E}^c(*))] := \frac{1}{2w^*_B(2n)} \sum_{\omega \in \mathscr{E}^c_{2n}(*)} l_{2n}(\omega). \tag{2.154}$$

Now combining Inequality (2.152) with Equations (2.153) and (2.154) yields that, for every natural number $n \geq 8$ and a randomly chosen Θ-SAP $W \in \mathscr{E}^c_{2n}(*)$,

$$\mathrm{E}[S_{2n}(\mathscr{E}^c(*))] < n - 3 < \mathrm{E}[L_{2n}(\mathscr{E}^c(*))]. \tag{2.155}$$

Because, for every natural number $n \geq 8$, the lengths of the large uSAWs in Θ-SAPs in $\mathscr{E}^c_{2n}(*)$ are $O(n)$, for a randomly chosen Θ-SAP $W \in \mathscr{E}^c_{2n}(*)$, $\mathrm{E}\left[L_{2n}(\mathscr{E}^c(*))\right]$ is bounded linearly in $2n$, that is there exist constants c_1, c_2 such that $c_1 < c_2$ and

$$2c_1 n \leq \mathrm{E}\left[L_{2n}(\mathscr{E}^c(*))\right] \leq 2c_2 n. \tag{2.156}$$

Hence $\mathrm{E}\left[L_{2n}(\mathscr{E}^c(*))\right] = O(n)$. Two interesting open questions regarding $\mathrm{E}\left[L_{2n}(\mathscr{E}^c(*))\right]$ are stated below.

Question 2.2.1 *For each $* \in \Phi$, given the set $\mathscr{E}^c(*)$, as $n \to \infty$,*
(1) does the limit $\lim_{n\to\infty} \dfrac{\mathrm{E}\left[L_{2n}(\mathscr{E}^c(*))\right]}{2n}$ exist and
(2) if the limit exists, does

$$\lim_{n\to\infty} \frac{\mathrm{E}\left[L_{2n}(\mathscr{E}^c(*))\right]}{2n} = 1? \tag{2.157}$$

In other words, as $n \to \infty$, is

$$\mathrm{E}\left[L_{2n}(\mathscr{E}^c(*))\right] \sim 2n? \tag{2.158}$$

The above question will be explored numerically in Section 7.1 of Chapter 7. The remainder of the discussion in this subsection turns to what can be said regarding $\mathrm{E}\left[S_{2n}(\mathscr{E}^c(*))\right]$ as $n \to \infty$.

First note that the smallest unknotted Θ-SAPs in $\mathscr{E}^c(\phi, f)$ and $\mathscr{E}^c(\phi|\phi, s)$ have sixteen edges and these smallest SAPs each have a small uSAW with four edges. For each $* \in \mathscr{K}^\dagger(\phi)\backslash\{(\phi|\phi, s)\}$, note that the smallest Θ-SAPs in $\mathscr{E}^c(*)$ must have at least twenty edges (cf. Section 2.2) and consequently the small uSAW in each Θ-SAP in $\mathscr{E}^c(*)$ must have more than four edges. This suggests that in order for the after-strand-passage SAP to have a non-trivial knot-type:

Conjecture 2.2.10 *For each $* \in \mathscr{K}^\dagger(\phi)\backslash\{(\phi|\phi, s)\}$ and each natural number $n \geq n^\Theta_*/2$,*

$$\mathrm{E}\left[S_{2n}(\mathscr{E}^c(*))\right] > \mathrm{E}\left[S_{2n}(\mathscr{E}^c(\phi, f))\right], \tag{2.159}$$

$$\mathrm{E}\left[S_{2n}(\mathscr{E}^c(*))\right] > \mathrm{E}\left[S_{2n}(\mathscr{E}^c(\phi|\phi, s))\right], \tag{2.160}$$

$$\mathrm{E}\left[L_{2n}(\mathscr{E}^c(*))\right] < \mathrm{E}\left[L_{2n}(\mathscr{E}^c(\phi, f))\right], \tag{2.161}$$

and

$$\mathrm{E}\left[L_{2n}(\mathscr{E}^c(*))\right] < \mathrm{E}\left[L_{2n}(\mathscr{E}^c(\phi|\phi, s))\right]. \tag{2.162}$$

In fact, it is expected that in some way these average lengths capture the fact that the after-strand-passage SAP is a non-trivial knot.

Now recall from the discussion in Section 1.5 that in [107], Marcone *et al.* conjecture that, for their measure of the length of a knot, the knot is weakly localized, that is the average length of a knot in an n-edge SAP scales according to a power-law relation n^t, where $0 < t < 1$. This conjecture and Conjecture 2.2.9 suggest the possibility that, on average, for a randomly chosen Θ-SAP $W \in \mathscr{E}^c_{2n}(*)$, $\mathrm{E}\left[S_{2n}(\mathscr{E}^c(*))\right]$ grows sub-linearly in $2n$. This is summarized in the following conjecture.

Conjecture 2.2.11 *For each $* \in \Phi$, the expected length of the small uSAW in a randomly chosen Θ-SAP $W \in \mathscr{E}^c_{2n}(*)$, as $n \to \infty$, has the asymptotic form*

$$\mathrm{E}\left[S_{2n}(\mathscr{E}^c(*))\right] \sim (2n)^{\zeta_s(*)}, \tag{2.163}$$

where $0 \leq \zeta_s(*) < 1$.

If Conjecture 2.2.11 is true, then two interesting questions are:

Question 2.2.2 *How do the exponents $\zeta_s(*)$ depend on $* \in \Phi$?*

Question 2.2.3 *How do the exponents $\zeta_s(*)$ compare to zero, that is for what properties, if any, are the small uSAWs strongly localized (length $O(1)$)?*

The validity of Conjectures 2.2.7, 2.2.8, 2.2.10, and 2.2.11 will be explored numerically in Chapter 7. Questions 2.2.1-2.2.3 will also be investigated numerically in Chapter 7.

In addition to exploring the rate at which the number of elements in different subsets of $\mathscr{P}^{\Theta}_{2n}(\phi)$ increase as a function of n and how the average lengths of uSAWs in the Θ-SAPs in different subsets of $\mathscr{P}^{\Theta}_{2n}(\phi)$ behave as a function of n, two other interesting questions regarding the elements in $\mathscr{P}^{\Theta}_{2n}(\phi)$ are: "How much space, on average, do the large, small, and equal-length uSAWs comprising Θ-SAPs occupy?" and "How does this amount of space change as a function of n?". The measure, used here, of the amount of space that Θ-SAPs occupy is the radius of gyration (as defined in Section 1.5 of Chapter 1).

The Average Radius of Gyration of the uSAWs in a Θ-SAP

Recall from Section 1.5 that, for a fixed positive even integer n, the mean-square radius of gyration of the elements in a finite, non-empty set $\mathscr{U}_{2n}$ of $(2n)$-edge SAPs, is given by

$$r^2(\mathscr{U}_{2n}) := \frac{1}{|\mathscr{U}_{2n}|} \sum_{\omega \in \mathscr{U}_{2n}} r^2(\omega). \tag{2.164}$$

Also recall from Section 1.5 that, given a fixed even positive integer M and a conditional probability mass function $\boldsymbol{\pi}_z(q, M) := \{\pi_{2n|M}(q, z) : n \geq M/2\}$ for the length of a randomly selected element from $\mathscr{U} := \bigcup_{n \geq M/2} \mathscr{U}_{2n}$, the mean-square radius of gyration over $\mathscr{U}$ is given by

$$r^2_{\boldsymbol{\pi}_z(q,M)}(\mathscr{U}) := \sum_{n=M/2}^{\infty} r^2(\mathscr{U}_{2n}) \pi_{2n|M}(q, z). \tag{2.165}$$

Now consider the function $f : \mathbb{Z}^3 \to \mathbb{Z}^3$. Then the f-transformed mean-square radii of gyration are respectively defined to be: for each fixed positive integer $n \geq 2$,

$$r^2(f(\mathscr{U}_{2n})) := \frac{1}{|\mathscr{U}_{2n}|} \sum_{\omega \in \mathscr{U}_{2n}} r^2(f(\omega)) \tag{2.166}$$

and

$$r^2_{\boldsymbol{\pi}_z(q,M)}(f(\mathscr{U})) := \sum_{n=M/2}^{\infty} r^2(f(\mathscr{U}_{2n})) \pi_{2n|M}(q, z). \tag{2.167}$$

Further define, for each $\omega \in \mathscr{E}^c$, $\mathfrak{w}_s$, the small uSAW function, and $\mathfrak{w}_l$, the large uSAW function, respectively by

$$\mathfrak{w}_s(\omega) := \begin{cases} w_+(\omega), & \text{if } |w_+(\omega)| < |w_-(\omega)| \\ w_-(\omega), & \text{otherwise} \end{cases} \tag{2.168}$$

and

$$\mathfrak{w}_l(\omega) := \begin{cases} w_+(\omega), & \text{if } |w_+(\omega)| > |w_-(\omega)| \\ w_-(\omega), & \text{otherwise,} \end{cases} \tag{2.169}$$

and, for each $\omega \in \mathscr{E}$, the equal-length uSAW function $\mathfrak{w}_e$, by

$$\mathfrak{w}_e(\omega) := (w_+(\omega), w_-(\omega)). \tag{2.170}$$

Given $* \in \Phi$, let $r^2(\mathfrak{w}_s(\mathscr{E}^c_{2n}(*)))$ be the mean-square radius of gyration of the small uSAW in a randomly chosen element of $\mathscr{E}^c_{2n}(*)$ and $r^2(\mathfrak{w}_l(\mathscr{E}^c_{2n}(*)))$ be the mean-square radius of gyration of the large uSAW in a randomly chosen element of $\mathscr{E}^c_{2n}(*)$. Also define

$$r^2(\mathfrak{w}_e(\mathscr{E}_{2n}(*))) := \frac{1}{2\,|\mathscr{E}_{2n}(*)|} \sum_{\omega \in \mathscr{E}_{2n}(*)} \left[r^2(w_+(\omega)) + r^2(w_-(\omega))\right]. \tag{2.171}$$

Then $r^2(\mathfrak{w}_e(\mathscr{E}_{2n}(*)))$ is the mean-square radius of gyration of the equal-sided uSAWs for a randomly chosen element of $\mathscr{E}_{2n}(*)$.

Recall from Section 1.5 that, for real-valued constants a, b, c, and d and a function r with $r(n) = O(n^{-1})$, $\mathcal{R}_n(a, b, c, d, r)$ is defined by Equation (1.60) to be

$$\mathcal{R}_n(a, b, c, d, r) = an^{2b}\left(1 + cn^{-d} + r(n))\right). \tag{2.172}$$

Then in analogy with Equation (1.63), for sufficiently large $n \in \mathbb{N}$ and for each $* \in \Phi$, $r^2\left(\mathscr{P}^{\Theta}_{2n}(*)\right)$, $r^2\left(\mathscr{E}_{2n}(*)\right)$, and $r^2\left(\mathscr{E}^{c}_{2n}(*)\right)$, the expected mean-square radii of gyration for a randomly chosen element from $\mathscr{P}^{\Theta}_{2n}(*)$, $\mathscr{E}_{2n}(*)$, and $\mathscr{E}^{c}_{2n}(*)$, respectively, are conjectured to satisfy:

Conjecture 2.2.12 *For each $* \in \Phi$ with:*
(1) $\mathscr{P}^{\Theta}(*) \subseteq \mathscr{P}^{\Theta}(\phi)$, there exist constants $A^{\Theta}_{\mathscr{P}}(*)$, $\nu^{\Theta}_{\mathscr{P}}(*)$, $B^{\Theta}_{\mathscr{P}}(*)$, and $\Delta^{\Theta}_{\mathscr{P}}(*)$ and a function $h^{*}_{\mathscr{P}}(n) = O(n^{-1})$ such that, for sufficiently large $n \in \mathbb{N}$,

$$r^2\left(\mathscr{P}^{\Theta}_{2n}(*)\right) = \mathcal{R}_{2n}\left(A^{\Theta}_{\mathscr{P}}(*), \nu^{\Theta}_{\mathscr{P}}(*), B^{\Theta}_{\mathscr{P}}(*), \Delta^{\Theta}_{\mathscr{P}}(*), h^{*}_{\mathscr{P}}\right); \tag{2.173}$$

(2) $\mathscr{E}(*) \subseteq \mathscr{P}^{\Theta}(\phi)$, there exist constants $A^{\Theta}_{\mathscr{E}}(*)$, $\nu^{\Theta}_{\mathscr{E}}(*)$, $B^{\Theta}_{\mathscr{E}}(*)$, and $\Delta^{\Theta}_{\mathscr{E}}(*)$ and a function $h^{*}_{\mathscr{E}}(n) = O(n^{-1})$ such that, for sufficiently large $n \in \mathbb{N}$,

$$r^2\left(\mathscr{E}_{2n}(*)\right) = \mathcal{R}_{2n}\left(A^{\Theta}_{\mathscr{E}}(*), \nu^{\Theta}_{\mathscr{E}}(*), B^{\Theta}_{\mathscr{E}}(*), \Delta^{\Theta}_{\mathscr{E}}(*), h^{*}_{\mathscr{E}}\right); \text{ and} \tag{2.174}$$

(3) $\mathscr{E}^{c}(*) \subseteq \mathscr{P}^{\Theta}(\phi)$, there exist constants $A^{\Theta}_{\mathscr{E}^c}(*)$, $\nu^{\Theta}_{\mathscr{E}^c}(*)$, $B^{\Theta}_{\mathscr{E}^c}(*)$, and $\Delta^{\Theta}_{\mathscr{E}^c}(*)$ and a function $h^{*}_{\mathscr{E}^c}(n) = O(n^{-1})$ such that, for sufficiently large $n \in \mathbb{N}$,

$$r^2\left(\mathscr{E}^{c}_{2n}(*)\right) = \mathcal{R}_{2n}\left(A^{\Theta}_{\mathscr{E}^c}(*), \nu^{\Theta}_{\mathscr{E}^c}(*), B^{\Theta}_{\mathscr{E}^c}(*), \Delta^{\Theta}_{\mathscr{E}^c}(*), h^{*}_{\mathscr{E}^c}\right). \tag{2.175}$$

Further to this, in analogy with Equation (1.63), it is also conjectured that:

Conjecture 2.2.13 *For each $* \in \Phi$,*
(1) there exist constants $A^{\Theta}_{\mathfrak{w}_e(\mathscr{E})}(*)$, $\nu^{\Theta}_{\mathfrak{w}_e(\mathscr{E})}(*)$, $B^{\Theta}_{\mathfrak{w}_e(\mathscr{E})}(*)$, $\Delta^{\Theta}_{\mathfrak{w}_e(\mathscr{E})}(*)$, and a function $h^{*}_{\mathfrak{w}_e(\mathscr{E})}(n) = O(n^{-1})$ such that, for sufficiently large $n \in \mathbb{N}$, the expected mean-square radius of gyration for the equal-sided uSAWs in a randomly chosen element from $\mathscr{E}_{2n}(*)$ is given by

$$r^2\left(\mathfrak{w}_e(\mathscr{E}_{2n}(*))\right) = \mathcal{R}_{2n}\left(A^{\Theta}_{\mathfrak{w}_e(\mathscr{E})}(*), \nu^{\Theta}_{\mathfrak{w}_e(\mathscr{E})}(*), B^{\Theta}_{\mathfrak{w}_e(\mathscr{E})}(*), \Delta^{\Theta}_{\mathfrak{w}_e(\mathscr{E})}(*), h^{*}_{\mathfrak{w}_e(\mathscr{E})}\right); \tag{2.176}$$

(2) there exist constants $A^{\Theta}_{\mathfrak{w}_l(\mathscr{E}^c)}(*)$, $\nu^{\Theta}_{\mathfrak{w}_l(\mathscr{E}^c)}(*)$, $B^{\Theta}_{\mathfrak{w}_l(\mathscr{E}^c)}(*)$, $\Delta^{\Theta}_{\mathfrak{w}_l(\mathscr{E}^c)}(*)$, *and a function* $h^*_{\mathfrak{w}_l(\mathscr{E}^c)}(n) = O(n^{-1})$ *such that, for sufficiently large* $n \in \mathbb{N}$, *the expected mean-square radius of gyration for the large uSAW in a randomly chosen element from* $\mathscr{E}^c_{2n}(*)$ *is given by*

$$r^2\left(\mathfrak{w}_l\left(\mathscr{E}^c_{2n}(*)\right)\right) = \mathcal{R}_{2n}\left(A^{\Theta}_{\mathfrak{w}_l(\mathscr{E}^c)}(*), \nu^{\Theta}_{\mathfrak{w}_l(\mathscr{E}^c)}(*), B^{\Theta}_{\mathfrak{w}_l(\mathscr{E}^c)}(*), \Delta^{\Theta}_{\mathfrak{w}_l(\mathscr{E}^c)}(*), h^*_{\mathfrak{w}_l(\mathscr{E}^c)}\right); \text{ and} \tag{2.177}$$

(3) there exist constants $A^{\Theta}_{\mathfrak{w}_s(\mathscr{E}^c)}(*)$, $\nu^{\Theta}_{\mathfrak{w}_s(\mathscr{E}^c)}(*)$, $B^{\Theta}_{\mathfrak{w}_s(\mathscr{E}^c)}(*)$, $\Delta^{\Theta}_{\mathfrak{w}_s(\mathscr{E}^c)}(*)$, *and a function* $h^*_{\mathfrak{w}_s(\mathscr{E}^c)}(n) = O(n^{-1})$ *such that, for sufficiently large* $n \in \mathbb{N}$, *the expected mean-square radius of gyration for the small uSAW in a randomly chosen element from* $\mathscr{E}^c_{2n}(*)$ *is given by*

$$r^2\left(\mathfrak{w}_s\left(\mathscr{E}^c_{2n}(*)\right)\right) = \mathcal{R}_{2n}\left(A^{\Theta}_{\mathfrak{w}_s(\mathscr{E}^c)}(*), \nu^{\Theta}_{\mathfrak{w}_s(\mathscr{E}^c)}(*), B^{\Theta}_{\mathfrak{w}_s(\mathscr{E}^c)}(*), \Delta^{\Theta}_{\mathfrak{w}_s(\mathscr{E}^c)}(*), h^*_{\mathfrak{w}_s(\mathscr{E}^c)}\right). \tag{2.178}$$

How do each of $r^2\left(\mathscr{P}^{\Theta}_{2n}(*)\right)$, $r^2\left(\mathscr{E}_{2n}(*)\right)$, $r^2\left(\mathscr{E}^c_{2n}(*)\right)$, $r^2\left(\mathfrak{w}_e(\mathscr{E}_{2n}(*))\right)$, $r^2\left(\mathfrak{w}_l\left(\mathscr{E}^c_{2n}(*)\right)\right)$, and $r^2\left(\mathfrak{w}_s\left(\mathscr{E}^c_{2n}(*)\right)\right)$ depend on $* \in \Phi$ and what, if any, relationship exists between each of these expected mean-square radii of gyration? These two questions are rather broad in nature, and, as a consequence, are difficult to address. Some questions that naturally arise regarding these expected mean-square radii of gyration are presented next.

Recall from Definition 2.2.9 that n^{Θ}_* is the length of a smallest Θ-SAP with property $* \in \Phi$ and note that for the even integers $n \geq n^{\Theta}_*/2$, $\mathscr{E}_{2n}(*) = \{\}$, which implies $\mathscr{E}^c_{2n}(*) = \mathscr{P}^{\Theta}_{2n}(*)$. Then for the odd integers $n \geq n^{\Theta}_*/2$, the first question arises from the facts that $r^2\left(\mathscr{P}^{\Theta}_{2n}(*)\right)$, $r^2\left(\mathscr{E}_{2n}(*)\right)$, $r^2\left(\mathscr{E}^c_{2n}(*)\right)$, $r^2\left(\mathfrak{w}_e(\mathscr{E}_{2n}(*))\right)$, $r^2\left(\mathfrak{w}_l\left(\mathscr{E}^c_{2n}(*)\right)\right)$, and $r^2\left(\mathfrak{w}_s\left(\mathscr{E}^c_{2n}(*)\right)\right)$ are functions of the property $* \in \Phi$ and that $\mathscr{E}_{2n}(*) \subset \mathscr{P}^{\Theta}_{2n}(*)$ and $\mathscr{E}^c_{2n}(*) \subset \mathscr{P}^{\Theta}_{2n}(*)$. Roughly speaking, do the equal-sided property-$*$ Θ-SAPs have asymptotically the same expected mean-square radius of gyration as the unequal-sided property-$*$ Θ-SAPs? More specifically:

Question 2.2.4 *For each* $* \in \Phi$ *and for sufficiently large odd* $n \geq n^{\Theta}_*/2$, *does*

$$r^2\left(\mathscr{E}_{2n}(*)\right) \sim r^2\left(\mathscr{P}^{\Theta}_{2n}(*)\right) \tag{2.179}$$

and

$$r^2\left(\mathscr{E}^c_{2n}(*)\right) \sim r^2\left(\mathscr{P}^{\Theta}_{2n}(*)\right)? \tag{2.180}$$

The next question involving the expected mean-square radii of gyration arises from the facts that, for each $* \in \Phi$, for every integer $n \geq n_*^{\Theta}/2$ and for every $\omega \in \mathscr{E}_{2n}^{c}(*)$,

$$s_{2n}(\omega) < n - 3 < l_{2n}(\omega), \tag{2.181}$$

and that, for every $\omega \in \mathscr{E}_{2n}(*)$,

$$|w_{+}(\omega)| = n - 3 = |w_{-}(\omega)|. \tag{2.182}$$

Do these same types of inequalities hold true for the expected mean-square radius of gyration? Specifically:

Question 2.2.5 *For each $* \in \Phi$ and for every odd integer $n \geq n_*^{\Theta}/2$, is*

$$r^2(\mathfrak{w}_s(\mathscr{E}_{2n}^{c}(*))) < r^2(\mathfrak{w}_e(\mathscr{E}_{2n}(*))) < r^2(\mathfrak{w}_l(\mathscr{E}_{2n}^{c}(*))), \tag{2.183}$$

and, for every even integer $n \geq n_*^{\Theta}/2$, is

$$r^2\left(\mathfrak{w}_s\left(\mathscr{P}_{2n}^{\Theta}(*)\right)\right) < r^2\left(\mathfrak{w}_l\left(\mathscr{P}_{2n}^{\Theta}(*)\right)\right)? \tag{2.184}$$

Note that in the above question, for the even integers $n \geq n_*^{\Theta}/2$, $\mathscr{E}_{2n}^{c}(*) = \mathscr{P}_{2n}^{\Theta}(*)$.

The next question regarding the expected mean-square radii of gyration for the small and large uSAWs is a question that arises from Conjecture 2.2.10.

Question 2.2.6 *For each $* \in \mathscr{K}^{\dagger}(\phi) \setminus \{(\phi|\phi, s)\}$ and each natural number $n \geq n_*^{\Theta}/2$, is*

$$r^2(\mathfrak{w}_s(\mathscr{E}_{2n}^{c}(*))) > r^2(\mathfrak{w}_s(\mathscr{E}_{2n}^{c}(\phi, f))), \tag{2.185}$$

$$r^2(\mathfrak{w}_s(\mathscr{E}_{2n}^{c}(*))) > r^2(\mathfrak{w}_s(\mathscr{E}_{2n}^{c}(\phi|\phi, s))), \tag{2.186}$$

$$r^2(\mathfrak{w}_l(\mathscr{E}_{2n}^{c}(*))) < r^2(\mathfrak{w}_l(\mathscr{E}_{2n}^{c}(\phi, f))), \tag{2.187}$$

and

$$r^2(\mathfrak{w}_l(\mathscr{E}_{2n}^{c}(*))) < r^2(\mathfrak{w}_l(\mathscr{E}_{2n}^{c}(\phi|\phi, s)))? \tag{2.188}$$

The final question regarding the expected mean-square radii of gyration for the small, equal-length, and large uSAWs compares them respectively to the expected mean-square radius of gyration of a randomly selected Θ-SAP from $\mathscr{P}_{2n}^{\Theta}(\phi)$ in the $n \to \infty$ limit.

Question 2.2.7 *For each* $* \in \Phi\backslash\{\phi,(\phi,s)\}$, *do the following limits exist and, if they exist, what are their values:*

$$\lim_{n\to\infty}\frac{r^2\left(\mathfrak{w}_s\left(\mathscr{E}_{2n}^{\mathscr{E}^c}(*)\right)\right)}{r^2\left(\mathscr{P}_{2n}^{\Theta}(\phi)\right)},\ \lim_{n\to\infty}\frac{r^2\left(\mathfrak{w}_e\left(\mathscr{E}_{2n}(*)\right)\right)}{r^2\left(\mathscr{P}_{2n}^{\Theta}(\phi)\right)},\ \textit{and}\ \lim_{n\to\infty}\frac{r^2\left(\mathfrak{w}_l\left(\mathscr{E}_{2n}^{\mathscr{E}^c}(*)\right)\right)}{r^2\left(\mathscr{P}_{2n}^{\Theta}(\phi)\right)}? \tag{2.189}$$

Now, if Conjectures 2.2.12 and 2.2.13 are true, then, what, if any, is the relationship between the metric exponents $\nu_{\mathscr{P}}^{\Theta}(*)$, $\nu_{\mathscr{E}}^{\Theta}(*)$, $\nu_{\mathscr{E}^c}^{\Theta}(*)$, $\nu_{\mathfrak{w}_e(\mathscr{E})}^{\Theta}(*)$, $\nu_{\mathfrak{w}_s(\mathscr{E}^c)}^{\Theta}(*)$, $\nu_{\mathfrak{w}_l(\mathscr{E}^c)}^{\Theta}(*)$, $\nu(K)$, and ν?

Recall from Section 2.2.1 that, for each $* \in \Phi$ and for each $n \in \mathbb{N}$, $p_{2n}^{\Theta}(*)$ grows at the same exponential rate as $p_{2n}(\phi)$. Also recall from Section 1.5 that it is hypothesized in [125] that, for each knot-type K, the metric exponent $\nu(K)$ is independent of knot-type and that $\nu(K)=\nu$. Based on these two recollections, for each property $* \in \Phi$, a possible relationship between $\nu_{\mathscr{E}}^{\Theta}(*)$, $\nu_{\mathscr{E}^c}^{\Theta}(*)$, and $\nu_{\mathscr{P}}^{\Theta}(*)$ and a possible relationship between $\nu_{\mathscr{P}}^{\Theta}(*)$ and ν are stated, respectively, in the following two questions.

Question 2.2.8 *Does* $\nu_{\mathscr{E}}^{\Theta}(*)=\nu_{\mathscr{E}^c}^{\Theta}(*)=\nu_{\mathscr{P}}^{\Theta}(\phi)$, *for each property* $* \in \Phi$*?*

Question 2.2.9 *Does* $\nu_{\mathscr{P}}^{\Theta}(\phi)=\nu$*?*

If the answer to both Questions 2.2.8 and 2.2.9 is "yes", then the metric exponents $\nu_{\mathscr{E}}^{\Theta}(*)$, $\nu_{\mathscr{E}^c}^{\Theta}(*)$ are independent of the property $* \in \Phi$, and $\nu_{\mathscr{P}}^{\Theta}(\phi)$ is independent of knot-type.

The questions posed thus far in this section have been regarding the metric exponents associated with polygons in various subsets of $\mathscr{P}_{2n}^{\Theta}(\phi)$, but, for each property $* \in \Phi$, none of these questions involved the metric exponents for the equal-length, large, or small uSAWs in the polygons and none of the conjectures in this section involve the amplitudes $A_{\mathscr{P}}^{\Theta}(*)$, $A_{\mathscr{E}}^{\Theta}(*)$, $A_{\mathscr{E}^c}^{\Theta}(*)$, $A_{\mathfrak{w}_e(\mathscr{E})}^{\Theta}(*)$, $A_{\mathfrak{w}_s(\mathscr{E}^c)}^{\Theta}(*)$, and $A_{\mathfrak{w}_l(\mathscr{E}^c)}^{\Theta}(*)$. What can be said about these metric exponents and these amplitudes?

The argument leading up to Question 2.2.1 also suggests the following question involving the exponents $\nu_{\mathscr{E}^c}^{\Theta}(*)$ and $\nu_{\mathfrak{w}_l(\mathscr{E}^c)}^{\Theta}(*)$.

Question 2.2.10 *Does* $\nu_{\mathfrak{w}_l(\mathscr{E}^c)}^{\Theta}(*)=\nu_{\mathscr{E}^c}^{\Theta}(*)$, *for each property* $* \in \Phi$*?*

Because, for each property $* \in \Phi$ and for every $n \in \mathbb{N}$, the lengths of the equal-length uSAWs in the polygons from $\mathscr{E}_{2n}(*)$ grow linearly in $2n$ (cf. Equation (2.149)), the following question is posed.

Question 2.2.11 *Does* $\nu^{\Theta}_{\mathfrak{w}_e(\mathscr{E})}(*) = \nu^{\Theta}_{\mathscr{E}}(*)$, *for each property* $* \in \Phi$*?*

If Conjecture 2.2.11 is true, (that is, for each property $* \in \Phi$ and for every $n \in \mathbb{N}$, the expected length for the small uSAW in a randomly chosen element of $\mathscr{S}_{2n}(*)$ grows at a rate less than $o(n)$), then, for each property $* \in \Phi$, the relationship between $\nu^{\Theta}_{\mathfrak{w}_s(\mathscr{E}^c)}(*)$ and $\nu^{\Theta}_{\mathscr{E}^c}(*)$, as posed in the following question, is suggested.

Question 2.2.12 *Is* $\nu^{\Theta}_{\mathfrak{w}_s(\mathscr{E}^c)}(*) < \nu^{\Theta}_{\mathscr{E}^c}(*)$, *for each property* $* \in \Phi$*?*

Questions 2.2.10, 2.2.11, and 2.2.12 present, for each property $* \in \Phi$, possible relationships amongst the metric exponents $\nu^{\Theta}_{\mathfrak{w}_l(\mathscr{E}^c)}(*)$, $\nu^{\Theta}_{\mathfrak{w}_e(\mathscr{E})}(*)$, and $\nu^{\Theta}_{\mathfrak{w}_s(\mathscr{E}^c)}(*)$ and $\nu^{\Theta}_{\mathscr{E}^c}(*)$, $\nu^{\Theta}_{\mathscr{E}}(*)$, and $\nu^{\Theta}_{\mathscr{E}^c}(*)$, respectively, but what, if any, are the relationships between the amplitudes $A^{\Theta}_{\mathscr{P}}(*)$, $A^{\Theta}_{\mathscr{E}}(*)$, $A^{\Theta}_{\mathscr{E}^c}(*)$, $A^{\Theta}_{\mathfrak{w}_e(\mathscr{E})}(*)$, $A^{\Theta}_{\mathfrak{w}_s(\mathscr{E}^c)}(*)$, and $A^{\Theta}_{\mathfrak{w}_l(\mathscr{E}^c)}(*)$? The numerical evidence in [68, 125, 134] supports the hypothesis that, for each knot-type K, the amplitudes $A_R(K)$ given by Equation (1.63) are independent of knot-type. Although unrelated to the amplitudes $A_R(K)$, a natural question regarding the amplitudes in Equations (2.173)-(2.178) is the following.

Question 2.2.13 *For each property* $* \in \Phi$, *are* $A^{\Theta}_{\mathscr{P}}(\phi)$, $A^{\Theta}_{\mathscr{E}}(*)$, $A^{\Theta}_{\mathscr{E}^c}(*)$, $A^{\Theta}_{\mathfrak{w}_e(\mathscr{E})}(*)$, $A^{\Theta}_{\mathfrak{w}_s(\mathscr{E}^c)}(*)$, *and* $A^{\Theta}_{\mathfrak{w}_l(\mathscr{E}^c)}(*)$ *independent of the property* $*$*?*

Questions 2.2.4-2.2.13 will be investigated numerically in Section 7.2 of Chapter 7.

2.3 In Summary

The chapter begins by reviewing the simplified SAP model for strand passage in a "pinched" ring polymer as introduced in [150]. In Section 2.2.1, the new result that for every $* \in \Phi$, $p^{\Theta}_n(*)$ grows at the same exponential rate as $p_n(\phi)$, is proved. Further to this, in Section 2.2.3 the new result that $w_B(n)$, $w_S(n)$, and $w_E(n)$ (as defined in Equations (2.130)-(2.132)) grow exponentially at the same rate as $p_n(\phi)$ was also proved.

The chapter presents heuristic arguments supporting the validity of several new conjectures regarding the critical exponents α^{Θ}_* (as defined in Equation (2.84)), that is, for each $* \in \Phi$,

$$\alpha_\phi - 2 = \alpha^{\Theta}_\phi = \alpha^{\Theta}_*. \tag{2.190}$$

Note that these conjectures regarding the critical exponents are tested numerically in Chapters 4 and 5.

The chapter also includes conjectures regarding scaling forms for the fixed-n strand passage probabilities and regarding the possible values for the limiting strand passage probabilities (Conjectures 2.2.3, 2.2.10, 2.2.10, and 2.2.11). The validity of these conjectures is tested numerically in Chapter 6.

The chapter concludes by presenting several conjectures and questions regarding the size of the SAPs used in the Local Strand Passage Model. Conjecture 2.2.8 hypothesizes that $\mathscr{P}_{2n}(\phi)$, for sufficiently large n, consists primarily of Θ-SAPs that are formed by one large uSAW (length $O(n)$) and one small uSAW (length $O(1)$). Conjectures 2.2.10 and 2.2.11 propose how, on average, the lengths of the large and small uSAWs for randomly chosen elements from subsets of $\mathscr{P}_n^{\Theta}(\phi)$ are expected to behave. The final questions in the chapter are related to a second measure of the amount of space that elements of subsets of $\mathscr{P}^{\Theta}(\phi)$ occupy. In particular, these final questions involve possible relationships amongst the mean-square radius of gyration for subsets of $\mathscr{P}^{\Theta}(\phi)$ and possible relationships amongst the metric exponents and amplitudes in the scaling forms of the mean-square radius of gyration for subsets of $\mathscr{P}^{\Theta}(\phi)$. These questions are explored numerically in Section 7.2 of Chapter 7.

Because the conjectures and questions posed in this chapter are to be studied numerically, the elements in $\mathscr{P}^{\Theta}(\phi)$ need to be generated. The next chapter discusses simulating the Local Strand Passage Model, that is generating elements in $\mathscr{P}^{\Theta}(\phi)$.

Chapter 3

Simulating the Local Strand Passage Model

In order to study the Local Strand Passage Model, an algorithm which generates a sample from $\mathscr{P}^{\Theta}(\phi)$ for a given β and positive integer q according to the distribution given by

$$\breve{\pi}_{\omega}(q, e^{\beta}) = \frac{|\omega|^{q-1}\,(|\omega|-6)p^{\Theta}_{|\omega|}(\phi)e^{\beta|\omega|}}{\breve{Q}(q, e^{\beta})},$$

where

$$\breve{Q}(q, e^{\beta}) := \sum_{n\geq 7}(2n)^{q-1}(2n-6)p^{\Theta}_{2n}(\phi)e^{2\beta n}, \tag{3.1}$$

is used. In order to explain the generation of this sample further, Monte Carlo methods are reviewed next.

A *Monte Carlo method* is a numerical method for generating states of a random variable according to a specific probability distribution. Monte Carlo methods can be used to obtain estimates for some quantity or quantities of interest in a system that has been rigorously defined but not solved theoretically. Provided a large enough sample of random states is observed, statistical inference can be used to determine confidence intervals for the quantity or quantities of interest. Monte Carlo methods have been used extensively to study polymer models, cf. [103, 122, 150] for just a few examples.

There are two main types of Monte Carlo methods: static and dynamic [105]. A *static Monte Carlo method* generates a sequence of statistically independent samples directly from a specific probability distribution. A *dynamic Monte Carlo method* generates a stochastic process on a desired state space where the probability distribution of interest is the unique stationary distribution of the stochastic process.

Each Monte Carlo method has its advantages and disadvantages. For instance, the sample generated from a static Monte Carlo method is a statistically independent sample drawn from the probability distribution of interest. However, if the state space is too large and/or complicated, it may not be feasible to implement a static method. Dynamic

methods can be used to generate a sample from large and/or really complicated sample spaces by generating the current state of the stochastic process $\{X_t, t \in T\}$ from the previous states. As a result, for all $i, j \in T$, states X_i and X_j will be correlated, and, for all $i, j \in T$ and for any real-valued function f defined on $\{X_t, t \in T\}$, $f(X_i)$ and $f(X_j)$ will also be correlated. The further j is from i, the smaller the correlation between X_j and X_i and hence the smaller the correlation between $f(X_j)$ and $f(X_i)$. In fact, for some j sufficiently large, $f(X_j)$ is considered to be "essentially independent" of $f(X_i)$. The concept of "essentially independent" will be formally defined and discussed in Section 4.1.2 of Chapter 4. Another issue arising from using a dynamic method is that the initial distribution of the stochastic process may be a distribution other than the desired stationary distribution and hence there is an initial period (for each distinct observable) in which the data generated does not reflect the desired stationary distribution. Determining the amount of time required for a process to converge to a stationary distribution is discussed in Section 4.1.1 of Chapter 4. Since the focus in this thesis is on dynamic Monte Carlo, the issue of the existence of a stationary distribution will be discussed next.

Any stochastic process that can be constructed such that the current state of the process only depends on the previous state, and not the entire history of the stochastic process, is said to have the Markov property and such a process is referred to as a Markov process. If the state space upon which a Markov process is defined is countable, then the process is referred to as a Markov chain. Because the current state only depends on the previous state, a Markov process is desirable since it is easier to generate than a stochastic process that does not have the Markov property. Since a discrete state space is the focus of this work, from here-on-in the discussion, unless otherwise stated, will be restricted to Markov chains. The notation, definitions, and results in the remainder of this section, unless otherwise stated, have been taken from [78]. The next definition formally defines a Markov process and a Markov chain.

Definition 3.0.1 *A Markov process $\{X_t, t \in T\}$ is a stochastic process that has the property that, given the state of X_t, the states of X_s, for all $s > t$, do not depend on the states of X_u, for all $u < t$. Formally, a stochastic process is said to be Markov if*

$$\Pr(a < X_s \leq b | X_u = x_u, \ \forall u \leq t) = \Pr(a < X_s \leq b | X_t = x_t).$$

A Markov process that has a finite or countable state space is called a Markov chain. A

discrete time Markov chain $\{X_t, t \in T\}$ *is a Markov chain with the index parameter set* $T = \{0, 1, 2, \ldots\}$.

Let $\{X_t, t \in T\}$ be a discrete time Markov chain with state space $\mathscr{S}$. Define the *one-step transition probability* to go from the Markov chain's state at time t to its state at time $t+1$ to be the probability that at time $t+1$ the Markov chain is in state y given that at time t the chain was in state x, that is

$$P_{xy}^{t,t+1} := \Pr(X_{t+1} = y | X_t = x). \tag{3.2}$$

If $P_{xy}^{t,t+1}$ is independent of the time t, then the Markov chain is said to be *time homogeneous* and $P_{xy}^{t,t+1}$ is denoted P_{xy}. For all $x, y \in \mathscr{S}$, P_{xy} are represented by the *one-step transition probability matrix* $\mathbb{P} = (P_{xy})_{x,y\in\mathscr{S}}$. A set $\pi = \{\pi_x\}_{x\in\mathscr{S}}$ is a stationary distribution of $\{X_t, t \in T\}$ if π satisfies the following definition.

Definition 3.0.2 *The set* $\pi = \{\pi_x\}_{x\in\mathscr{S}}$ *is said to be a stationary distribution for the discrete time, time homogeneous, Markov chain* $\{X_t, t \in T\}$ *with state space* $\mathscr{S}$ *and transition probability matrix* $\mathbb{P} = (P_{xy})_{x,y\in\mathscr{S}}$, *if, for all* $x \in \mathscr{S}$,

$$\pi_x \geq 0, \sum_{x\in\mathscr{S}} \pi_x = 1, \text{ and } \sum_{x\in\mathscr{S}} \pi_x P_{xy} = \pi_y, \text{ for all } y \in \mathscr{S}. \tag{3.3}$$

From hence forth, the term "Markov chain" will refer to a discrete time, time homogeneous Markov chain. For any $x, y \in \mathscr{S}$, the probability that after n-steps the process has moved from state x to state y is $P_{xy}^{(n)}$, the *n-step transition probability*, that is

$$P_{xy}^{(n)} := \Pr(X_{t+n} = y | X_t = x). \tag{3.4}$$

$(P_{xy}^{(n)})_{x,y\in\mathscr{S}}$ is the *n-step transition probability matrix* and it has been established that $(P_{xy}^{(n)})_{x,y\in\mathscr{S}} = \mathbb{P}^n$ [78].

A Markov chain is *irreducible* if, for each pair of $x, y \in \mathscr{S}$, there exists an $n \geq 0$ such that $P_{xy}^{(n)} > 0$. A Markov chain is *aperiodic* if $d := \gcd_{x\in\mathscr{S}} \delta(x) = 1$, where d is the *period* of the Markov chain and $\delta(x)$ is the *period* of state x, and this is defined to be the greatest common divisor of the numbers $n > 0$ such that $P_{xx}^{(n)} > 0$. If $f_{xy}^{(i)}$ denotes the probability that the first passage from state x to state y occurs at the i'th transition, then for arbitrary but fixed states x and y, and, for every $i \geq 1$,

$$f_{xy}^{(i)} = \Pr(X_i = y, X_t \neq y, t = 1, 2, \ldots, i-1 | X_0 = x). \tag{3.5}$$

With $f_{xx}^{(1)} = P_{xx}$ and $f_{xx}^{(0)} = 0$, for all states x, a state x is said to be *recurrent* if and only if

$$\sum_{i=1}^{\infty} f_{xx}^{(i)} = 1. \tag{3.6}$$

Since the sum given in Equation (3.6) is not easily computed, Chung [12] established that the concept of the recurrence of a state can be stated in terms of the transition probability matrix as follows:

Theorem 3.0.1 ([12]) *For a Markov chain $\{X_t, t \in T\}$ defined on $\mathscr{S}$ with one-step transition probability matrix $\mathbb{P}$, a state $x \in \mathscr{S}$ is recurrent if and only if*

$$\sum_{i=1}^{\infty} P_{xx}^{(i)} = \infty. \tag{3.7}$$

A Markov chain $\{X_t, t \in T\}$ is said to be *recurrent* if, for each $x \in \mathscr{S}$, x is a recurrent state. $\{X_t, t \in T\}$ is said to be *positive recurrent* if it is recurrent and, for some $x \in \mathscr{S}$, the $\lim_{n\to\infty} P_{xx}^{(n)} > 0$. The following result states one possible method for determining whether or not a Markov chain is positive recurrent.

Theorem 3.0.2 ([78]) *If a Markov chain $\{X_t, t \in T\}$ defined on $\mathscr{S}$ is irreducible and one state in $\mathscr{S}$ is positive recurrent, then all states in $\mathscr{S}$ are positive recurrent.*

If an irreducible, positive-recurrent Markov chain $\{X_t, t \in T\}$ defined on $\mathscr{S}$ with one-step transition probability matrix $\mathbb{P}$ has the property that, for all $x, y \in \mathscr{S}$, there exists probabilities π_x and π_y such that

$$\pi_x P_{xy} = \pi_y P_{yx}, \tag{3.8}$$

then $\{X_t, t \in T\}$ is said to be *reversible* [35]. The condition that Equation (3.8) holds for all $x, y \in \mathscr{S}$ is referred to as *detailed balance* [35].

If a Markov chain is irreducible, positive recurrent, and aperiodic, then the Markov chain is called *ergodic* in $\mathscr{S}$. Suppose $\mathscr{S}_i$ is the largest subset of $\mathscr{S}$ for which the Markov chain $\{X_t, t \in T\}$ is irreducible in $\mathscr{S}_i$ but not in $\mathscr{S}$. Then $\mathscr{S}_i$ is called an *irreducible class* of $\mathscr{S}$. Furthermore, if $\mathscr{S}_i$ is the largest subset of $\mathscr{S}$ for which the Markov chain $\{X_t, t \in T\}$ is ergodic in $\mathscr{S}_i$ but not in $\mathscr{S}$, then $\mathscr{S}_i$ is called an *ergodic class* of $\mathscr{S}$.

In order for a Markov chain $\{X_t, t \in T\}$ with transition probability matrix $\mathbb{P}$ to have a unique stationary distribution π such that $\pi_x > 0$ for all $x \in \mathscr{S}$, the necessary and sufficient conditions are that $\{X_t, t \in T\}$ must be an irreducible, positive-recurrent Markov chain, that is:

Theorem 3.0.3 ([12]) *Let $\mathbb{P}$ be the transition probability matrix of an irreducible, positive-recurrent Markov chain $\{X_t, t \in T\}$, then a unique stationary distribution π exists and $\pi_x > 0$ for all x. Moreover, for d, the period of $\{X_t, t \in T\}$,*

$$\lim_{n\to\infty} P_{xy}^{(nd+r)} = \begin{cases} d \cdot \pi_y & \text{if } x \in \mathscr{S}_i,\ y \in \mathscr{S}_j,\ \text{with } j - i = r \mod d \\ 0 & \text{if } x \in \mathscr{S}_i,\ y \in \mathscr{S}_j,\ \text{with } j - i \neq r \mod d \end{cases},$$

for all $x, y \in \mathscr{S}$. In particular, if $\mathbb{P}$ is aperiodic, then $\lim_{n\to\infty} P_{xy}^{(n)} = \pi_y$.

The above theorem also states that if $\{X_t, t \in T\}$ is an irreducible, positive-recurrent, aperiodic Markov chain, as $n \to \infty$, then $\{X_t, t \in T\}$ will eventually converge to a unique *equilibrium distribution* π, independent of the initial starting state. The irreducibility of a Markov chain can usually be proved directly but showing that a Markov chain is positive-recurrent (and hence ergodic) directly can be quite difficult. The next theorem is quite powerful as it expresses the reversibility and positive-recurrence of a Markov chain in terms of several easily determined conditions for a Markov chain.

Theorem 3.0.4 ([46]) *For an irreducible Markov chain, if there exists a set $\pi = \{\pi_x\}_{x\in\mathscr{S}}$ such that $0 \leq \pi_x \leq 1$, $\pi_x P_{xy} = \pi_y P_{yx}$, for all $x, y \in \mathscr{S}$, and $\sum_{x\in\mathscr{S}} \pi_x = 1$, then the chain is reversible and positive-recurrent with stationary distribution π.*

Note that in future sections, in order to show a Markov chain on a state space $\mathscr{S}$ is ergodic, the chain will be shown to be irreducible, aperiodic, and a set $\pi = \{\pi_x\}_{x\in\mathscr{S}}$ that satisfies Theorem 3.0.4 will be obtained.

In a dynamic Monte Carlo simulation, if a Monte Carlo method generates a stochastic process which happens to be a Markov chain, we call the Monte Carlo method a *Markov Chain Monte Carlo Method*. An example of a Markov Chain Monte Carlo algorithm used to study some polymer models is the Θ-BFACF algorithm, the algorithm created to study Problem 1.1 in [150] and discussed in Section 3.3. Because the Θ-BFACF algorithm is based on the BFACF algorithm [9, 14, 15], it will be reviewed next.

3.1 The BFACF Algorithm

The *BFACF algorithm* [9, 14, 15], was initially designed to simulate walks of variable length with fixed end points in $\mathbb{Z}^d$. The algorithm generates a Markov process on the set of all possible walks of variable length with fixed end points in the d-dimensional hypercubic lattice. It has been shown that the algorithm generates a collection of paths which have a Boltzmann distribution [9], cf. Section 1.4.

In the mid-1980's Madras proved that the BFACF algorithm is ergodic on the set of all possible SAPs in $\mathbb{Z}^2$ and hence could be applied to polygons in the square lattice. The proof of Madras's result was not published until the early 1990's, cf. [103]. In general, the BFACF algorithm, when applied to a polygon in $\mathbb{Z}^d$, generates another polygon (not necessarily distinct) in $\mathbb{Z}^d$. Janse van Rensburg and Whittington [69] proved that when the BFACF algorithm is applied to polygons in $\mathbb{Z}^3$, the algorithm generates polygons having the same knot-type as the initial state, that is, when the BFACF algorithm is applied to polygons in $\mathbb{Z}^3$, the ergodic classes of the algorithm are exactly the sets of polygons partitioned according to knot-type. Because polygons with a specific knot-type in the simple cubic lattice are required for this work, the BFACF algorithm is a useful starting point.

Unless otherwise specified, for the remainder of this section, the BFACF algorithm will be assumed to generate a Markov chain $\{X_t, t \in T\}$ on $\mathscr{P}(K)$, the set of all SAPs in $\mathbb{Z}^3$ with fixed knot-type K, where the elementary transformations, as illustrated in Figure 3.1, are applied in a probabilistic manner to move from state X_t to state X_{t+1}. Before the BFACF algorithm can be stated, some notation is required.

Let ω and ω' be two SAPs in $\mathbb{Z}^3$ and $|\omega|$ and $|\omega'|$ be their respective lengths. We define $\Delta(\omega, \omega') = |\omega'| - |\omega|$, that is the difference in lengths of the two polygons ω and ω'. For $\mathbb{Z}^3$, define $\overrightarrow{\boldsymbol{k}} := \langle 0, 0, 1\rangle$ to be the positive unit vector in the z direction, $\overrightarrow{\boldsymbol{j}} := \langle 0, 1, 0\rangle$ to be the positive unit vector in the y direction, and $\overrightarrow{\boldsymbol{i}} := \langle 1, 0, 0\rangle$ to be the positive unit vector in the x direction. $\pm\overrightarrow{\boldsymbol{i}}, \pm\overrightarrow{\boldsymbol{j}}$, and $\pm\overrightarrow{\boldsymbol{k}}$ will be referred to as the *unit lattice directions*. The *right-hand rule* states that the positive unit vectors are assigned in the order $\overrightarrow{\boldsymbol{i}}$ to $\overrightarrow{\boldsymbol{j}}$ to $\overrightarrow{\boldsymbol{k}}$ and back to $\overrightarrow{\boldsymbol{i}}$. Now define $e_1(\boldsymbol{r}), e_2(\boldsymbol{r}), e_3(\boldsymbol{r})$, and $e_4(\boldsymbol{r})$ to be the four distinct directions perpendicular to direction $\boldsymbol{r}$ (or equally $-\boldsymbol{r}$), where $\boldsymbol{r} \in \left\{\overrightarrow{\boldsymbol{i}}, \overrightarrow{\boldsymbol{j}}, \overrightarrow{\boldsymbol{k}}\right\}$, that is $e_j(\boldsymbol{r}) \neq \boldsymbol{r}$ and $e_j(\boldsymbol{r}) \neq -\boldsymbol{r}$, for $j = 1, \ldots, 4$. To further specify the definition of $e_j(\boldsymbol{r})$: if starting at $\boldsymbol{r}$,

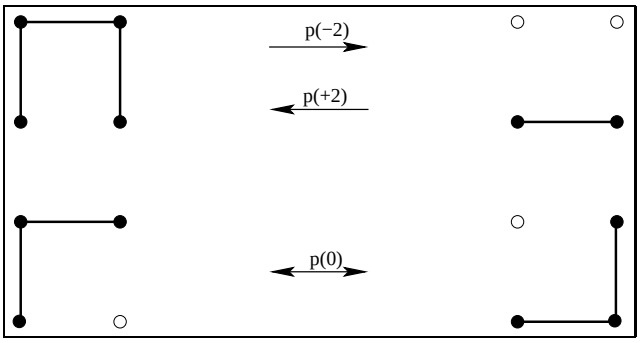

Figure 3.1: The elementary BFACF moves as applied to SAPs in $\mathbb{Z}^3$.

$e_1(\boldsymbol{r})$ is the next positive unit vector assigned by the right-hand rule; $e_3(\boldsymbol{r})$ is the second positive unit vector assigned by the right-hand rule; $e_2(\boldsymbol{r}) = -e_1(\boldsymbol{r})$; and $e_4(\boldsymbol{r}) = -e_3(\boldsymbol{r})$. Then the precise definition for the BFACF algorithm for the set of all SAPs in $\mathbb{Z}^3$ with fixed knot-type K is as follows.

3.1.1 Precise Definition of the BFACF Algorithm in $\mathbb{Z}^3$

The BFACF algorithm generates a Markov chain $\{X_t, t \in T\}$ on $\mathscr{P}(K)$.

1. Select a fugacity z such that $0 < z < z_\phi$, where z_ϕ is as defined by Equation (1.43); select an integer $q > 0$; and choose $\omega^{[0]}$ to be any polygon in $\mathscr{P}(K)$. Set $t = 0$, $X_0 = \omega^{[0]}$, and select one of the vertices of $\omega^{[0]}$, to be denoted $\boldsymbol{\omega}_0^{[0]}$. Now select one of the two vertices of $\omega^{[0]}$ adjacent to $\boldsymbol{\omega}_0^{[0]}$ and denote this vertex $\boldsymbol{\omega}_1^{[0]}$. $\boldsymbol{\omega}_0^{[0]}$ will be referred to as the first vertex of $\omega^{[0]}$. $\boldsymbol{\omega}_1^{[0]}$ will be referred to as the second vertex of $\omega^{[0]}$. The edge connecting $\boldsymbol{\omega}_0^{[0]}$ to $\boldsymbol{\omega}_1^{[0]}$ will be referred to as the 0'th edge of $\omega^{[0]}$. This imposes an orientation on $\omega^{[0]}$ which induces a numbering of the edges. Choose a set of one-step transition probabilities $P_{\omega\omega'}$ such that the one-step transition probabilities satisfy detailed balance, cf. Equation (3.8), and such that $\lim_{n\to\infty} P_{\omega\omega'}^{(n)} = \pi_{\omega'}(q;z)$, where $\pi_{\omega'}(q;z)$ is given by

$$\pi_{\omega'}(q;z) = \frac{|\omega'|^q z^{|\omega'|}}{\sum_{i=0}^{\infty} i^q p_i(K) z^i}. \tag{3.9}$$

2. At the $(t+1)$'st step, select an integer I uniformly at random from $\{0, 1, 2, \ldots, |\omega_t| - 1\}$.

3. Define $\boldsymbol{r} := \begin{cases} \boldsymbol{\omega}_{I+1}^{[t]} - \boldsymbol{\omega}_I^{[t]}, & \text{if } I < |\omega_t| - 1 \\ \boldsymbol{\omega}_0^{[t]} - \boldsymbol{\omega}_I^{[t]}, & \text{if } I = |\omega_t| - 1, \end{cases}$ where $\boldsymbol{\omega}_j^{[t]}$ is the j'th vertex in $\omega^{[t]}$. Consider the 4 graph embeddings W_1, W_2, W_3, and W_4 in $\mathbb{Z}^3$ that can be formed by moving the I'th edge one lattice unit respectively in the $e_1(\boldsymbol{r}), e_2(\boldsymbol{r}), e_3(\boldsymbol{r})$, or $e_4(\boldsymbol{r})$ direction, and then adding the necessary edges to join the newly shifted edge to the polygon, and removing any double edges which may result. Define

$$\xi = \sum_{l=1}^{4} p(\Delta(\omega^{[t]}, W_l)) \tag{3.10}$$

where, for $\omega \in \mathscr{P}(K)$ and any graph embedding ϖ in $\mathbb{Z}^3$,

$$\Delta(\omega, \varpi) = |\varpi| - |\omega| \tag{3.11}$$

and

$$p(\Delta(\omega, \varpi)) = \begin{cases} \dfrac{|\varpi|^{q-1} Z^2}{|\omega|^{q-1} + 3\,|\varpi|^{q-1} z^2}, & \text{if } \Delta(\omega, \varpi) = +2 \\ \dfrac{|\omega|^{q-1}}{|\omega|^{q-1} + 3\,|\varpi|^{q-1} z^2}, & \text{if } \Delta(\omega, \varpi) = -2 \\ \dfrac{1 + z^2}{2\,[1 + 3z^2]}, & \text{if } \Delta(\omega, \varpi) = 0 \text{ and } \omega \neq \varpi \\ 0, & \text{otherwise.} \end{cases} \tag{3.12}$$

Choose one of the five embeddings W_1, W_2, W_3, W_4, ω_t with respective probabilities $p(\Delta(\omega^{[t]}, W_l))$, $l = 1, \ldots, 4$, $\max\{0, 1 - \xi\}$, and denote the chosen embedding (which need not be a SAP) as W.

4. If W is not a SAP, set $X_{t+1} = \omega^{[t]}$, otherwise set $X_t = W$. Increase t by 1 and return to Step 2.

5. Repeat until $t = T$.

□

One appropriate choice for the one-step transition probabilities $P_{\omega\omega'}$ is given by

$$P_{\omega\omega'} := \frac{1}{|\omega|} p(\Delta(\omega, \omega')). \tag{3.13}$$

A detailed discussion for why the choice of the one-step transition probabilities as defined by Equation (3.13) is a valid choice can be found in [150].

Because the design of the BFACF algorithm (and hence the Θ-BFACF algorithm) guarantees sampling from $\mathscr{P}(K)$ if the algorithm is started in $\mathscr{P}(K)$, a major advantage of the algorithm is that one never has to check the knot-type of the SAPs generated. A major disadvantage of the BFACF algorithm (and hence the Θ-BFACF algorithm) is that, as $z \to z_\phi$, the exponential autocorrelation time for the algorithm (the time it takes the algorithm to attain equilibrium from its initial configuration) approaches infinity (Sokal and Thomas, [143]). Consequently the algorithm has very long exponential autocorrelation times for fugacities that are very close to z_ϕ. If the behaviour of some observable as polygon length increases is of interest, then, because the average length of the polygons generated by the BFACF increases as $z \to z_\phi$, fugacities closer and closer to z_ϕ need to be chosen.

Note that the exponential autocorrelation time of an algorithm and the correlation that exists among the data generated by a MCMC algorithm will be explored in more detail in the next chapter, but, at this point, suffice it to say, as the exponential autocorrelation time for a MCMC algorithm increases, the data generated by the algorithm become more positively correlated. As $z \to z_\phi$, the resulting simulation will take longer and longer to reach the equilibrium distribution and will generate fewer and fewer independent data points. Although these disadvantages seem to exclude using the BFACF algorithm when studying the asymptotic properties of the Local Strand Passage Model, techniques have been developed to decrease the integrated autocorrelation times associated with the BFACF algorithm [43, 95, 100, 122, 152]. One such technique is the so-called Multiple Markov chain sampling [43] and is discussed next.

3.2 Multiple Markov Chain Monte Carlo Methods

In 1991, Geyer [43] introduced a concept which he referred to as *Metropolis-coupled Markov chain Monte Carlo.* The concept has since been called Multiple Markov Chain (MMC) Sampling [152], Parallel Tempering [58] and Exchange Monte Carlo [62]. In 1996, the technique was adapted to study interacting self-avoiding walks with fixed length [152] and to study self-avoiding polygons [122]. The remainder of the discussion of MMC sampling will be based on the terminology, notation, and concepts as discussed by Orlandini *et al.* in [122].

MMC sampling is a method that samples along a set of M Markov chains which are run in parallel. Fix M and let $\pi(i)$ be the equilibrium distribution of Markov chain i, where consecutive natural numbers from one to M have been assigned to Markov chains 1 through M, respectively. Denote the probability of Chain i being in a particular state x by $\pi_x(i)$. Suppose that, for some $i \in \{1, 2, ..., M\}$, convergence of Chain i to its equilibrium distribution $\pi(i)$ is slow and that for some $j \in \{1, 2, ..., M\}$ convergence of Chain j to its equilibrium distribution $\pi(j)$ is known to be quite fast. Then, ideally to implement the MMC method, for some integer $M \geq 2$, M Markov chains (such that there is "considerable overlap" between the distributions of $\pi(i)$ and $\pi(i+1)$ for $1 \leq i < M$) are desired. Note that the state space $\mathscr{S}$ for each chain is the same.

After the M Markov chains have been run in parallel for a fixed number of steps ρ, Chains i and j are chosen with probability $\tilde{p}_{ij}$ from the total possible pairings of i and j, where the $\tilde{p}_{ij}$ are chosen such that they satisfy $\tilde{p}_{ij} = \tilde{p}_{ji}$ and

$$\sum_{i,j \leq M} \tilde{p}_{ij} = 1.$$

Suppose at time t, for $x, y \in \mathscr{S}$, Chain i is in state x and Chain j is in state y. Then with probability $r(i,j)$, where

$$r(i,j) = \min\left(1, \frac{\pi_y(i)\pi_x(j)}{\pi_x(i)\pi_y(j)}\right) \tag{3.14}$$

(referred to as the *swapping probability between Chains i and j*), the current configurations in Chains i and j are exchanged. This exchange between Chains i and j is referred to as a *chain swap* or *swap* for short. This swapping process induces dependence between the chains. As a result, each chain on its own is not Markov, but, on the other hand, the whole process has the Markov property and is referred to as a *composite Markov chain* (CMC) [123].

A single time-step in the CMC consists of either one non-chain-swap move attempted on each of the M components of the CMC (to be referred to as a *move in parallel*) or one single attempted swap. Define the *period for attempted swapping*, denoted $\rho \geq 0$, to be the number of moves in parallel implemented before each attempted swap, that is a swap is attempted after every ρ moves in parallel. For $\rho = 0$, no moves in parallel are allowed between attempted swaps; the M components of the CMC are just permuted. Consequently setting $\rho = 0$ is not permitted.

A precise definition of a CMC is now provided.

Definition 3.2.1 *Given $M > 0$ and state space $\mathscr{S}$, for each $i = 1, \ldots, M$, let $\{X_t(i), t \in T\}$ be an ergodic Markov chain on $\mathscr{S}$ with one-step transition probability matrix $\{P_{xy}(i)\}_{x,y\in\mathscr{S}}$, where*

$$P_{xy}(i) = \Pr[X_{t+1}(i) = y | X_t(i) = x],$$

and $P_{xx}(X_t(i)) > 0$ for all $x \in \mathscr{S}$, and with equilibrium distribution given by $\pi(i) = \{\pi_x(i)\}_{x\in\mathscr{S}}$. Suppose ρ is some given positive integer and the $\tilde{p}_{ij}$'s are chosen to satisfy $\tilde{p}_{ij} = \tilde{p}_{ji}$ and $\sum_{i,j\leq M} \tilde{p}_{ij} = 1$. Then, define the composite chain $\{\boldsymbol{Y}_t, t \in T\}$ with $\boldsymbol{Y}_t = (Y_t(1), Y_t(2), \ldots, Y_t(M)) \in \mathscr{S}^M$ to be the stochastic process on the state space $\mathscr{S}^M$ with one-step transition probabilities specified by

$$P_{\boldsymbol{xy}} = \begin{cases} \prod_{i=1}^{M} P_{x_i y_i}(i), & \text{if } t \mod (\rho+1) \neq 0, \\ \tilde{p}_{ij} r(i,j), & \text{if } t \mod (\rho+1) = 0,\ \boldsymbol{y} = \boldsymbol{x}^{(i,j)}, \\ 1 - \sum_{i,j} \tilde{p}_{ij} r(i,j), & \text{if } t \mod (\rho+1) = 0,\ \boldsymbol{y} = \boldsymbol{x}, \\ 0, & \text{otherwise,} \end{cases} \tag{3.15}$$

where for $\boldsymbol{x} = (x(1), x(2), \ldots, x(i), \ldots, x(j), \ldots, x(M)) \in \mathscr{S}^M$,

$$\boldsymbol{x}^{(i,j)} = (x(1), x(2), \ldots, x(i-1), x(j), x(i+1), \ldots, x(j-1), x(i), x(j+1), \ldots, x(M)) \in \mathscr{S}^M, \tag{3.16}$$

and

$$r(i,j) = \min\left(1, \frac{\pi_y(i)\pi_x(j)}{\pi_x(i)\pi_y(j)}\right). \tag{3.17}$$

$\{\boldsymbol{Y}_t, t \in T\}$, referred to as a Composite Markov Chain, is a stochastic process on state space $\mathscr{S}^M$

Note that $Y_t(i)$ is the *i'th component of* $\boldsymbol{Y}_t$. The sequence $(Y_t(i), t \in T)$ formed from the sequence of states that appear in the i'th component of $\boldsymbol{Y}_t$ is referred to as *sub-chain* i or *Chain* i; and $\{X_t(i), t \in T\}$ is referred to as *Uncoupled Chain* i.

If $\tilde{p}_{ij} > 0$, for all $i \neq j$, a swap can occur between any pair of the M chains (this is referred to as *global swapping* or *global coupling*). The acceptance of a swap between non-adjacent chains should noticeably change the configurations for the chains swapped and therefore should decrease the time it takes the whole process to reach its stationary distribution. In practice, such a swap rarely occurs because the overlap of the distributions of two distinct non-adjacent chains is usually minimal. As most non-adjacent swaps are rejected, any possible CPU time savings from allowing such swaps is overshadowed by the

cost of determining the viability of the swap. Therefore *local swapping* or equivalently *local coupling*, that is swapping only between adjacent chains, will be used in this work. From now on, it is assumed that the term swapping (coupling) refers to local swapping (local coupling).

Since swapping induces a dependence among the components of the Composite chain, each component of the Composite Chain is no longer Markov. Hence the usage of the term Multiple Markov Chain is a bit of a misnomer. The next lemma establishes that the entire Composite chain however is a Markov chain. The following four lemmas are due to Geyer [43].

Lemma 3.2.1 (Geyer [43]) *The stochastic process* $\{\boldsymbol{Y}_t, t \in T\}$ *as defined in Definition 3.2.1 has the Markov property and hence is a Markov chain.* $\{\boldsymbol{Y}_t, t \in T\}$ *is referred to as a Composite Markov Chain.*

Lemma 3.2.2 (Geyer [43]) *The CMC* $\{\boldsymbol{Y}_t, t \in T\}$ *as defined in Definition 3.2.1 is irreducible.*

Lemma 3.2.3 (Geyer [43]) *The CMC* $\{\boldsymbol{Y}_t, t \in T\}$ *as defined in Definition 3.2.1 is aperiodic.*

For $\boldsymbol{x} \in \mathscr{S}^M$, define the set $\pi_{\boldsymbol{Y}} := \{\pi_{\boldsymbol{x}}\}_{\boldsymbol{x} \in \mathscr{S}^M}$ where

$$\pi_{\boldsymbol{x}} = \prod_{i=1}^{M} \pi_{x_i}(i). \tag{3.18}$$

Lemma 3.2.4 (Geyer [43]) *Equations 3.15 and the set* $\pi_{\boldsymbol{Y}}$ *satisfy*

1. $0 \leq \pi_{\boldsymbol{x}} \leq 1$ *for all* $\boldsymbol{x} \in \mathscr{S}^M$,
2. $\sum_{\boldsymbol{x} \in \mathscr{S}^M} \pi_{\boldsymbol{x}} = 1$, *and*
3. $\pi_{\boldsymbol{x}} P_{\boldsymbol{xy}}(\boldsymbol{Y}_t) = \pi_{\boldsymbol{y}} P_{\boldsymbol{yx}}(\boldsymbol{Y}_t)$, *for all* $\boldsymbol{x}, \boldsymbol{y} \in \mathscr{S}^M$.

Lemmas 3.2.2, 3.2.3, and 3.2.4 as stated above and Theorem 3.0.4 establish the ergodicity of a Composite Markov chain. Also, Theorem 3.0.4 establishes that $\pi_{\boldsymbol{Y}}$ is the unique stationary distribution for $\{\boldsymbol{Y}_t, t \in T\}$. The ergodicity of a CMC was first discussed by Geyer [43]. Detailed proofs of Lemmas 3.2.1, 3.2.2, 3.2.3, and 3.2.4 for a composite Markov chain $\{\boldsymbol{Y}_t, t \in T\}$ generated by the Θ-BFACF algorithm, can be found in [150].

By carefully selecting the swapping probabilities between two adjacent chains, each individual chain might reach its marginal stationary distribution much faster than any of the individual chains when uncoupled (that is with no swapping). The possible faster convergence is because when a swap is accepted, it introduces a large change in the configurations for the chains involved and this tends to reduce the exponential autocorrelation time. As one can collect information for all M subchains, another "perk" of the MMC method is that there is very little difference in CPU time between MMC sampling and sampling along the M chains uncoupled for the same number of times steps. Hence faster convergence is obtained at no significant additional cost in CPU time.

Since M chains are being run simultaneously and quantities from each chain need to be stored, a disadvantage of MMC sampling is that MMC simulations require a significant increase in computer memory as compared to the uncoupled simulations. Any constraint imposed by computer memory will depend on the number of chains being run in parallel. Therefore, the number of chains needs to be determined in order to minimize the number of time steps it takes to converge to the equilibrium distribution, to minimize the amount of CPU time required to implement the simulation to collect a sufficiently large sample, and, at the same time, to not exceed the memory resources available. A procedure for determining the number of chains and the distribution of the z values over an interval $[z', z'']$ for a CMC generated by the BFACF algorithm whose underlying distribution is given by Equation (3.9) can be found in [122].

3.3 The Θ-BFACF Algorithm

Because the ergodic classes of the BFACF algorithm, when applied to SAPs in $\mathbb{Z}^3$, are the different types of knots in $\mathbb{Z}^3$, therefore the BFACF algorithm (when applied to polygons in $\mathbb{Z}^3$) is a very useful tool for studying properties that are dependent on knot-type. For this reason, to study the Local Strand Passage Model, a Markov Chain Monte Carlo technique in which the BFACF algorithm was adapted to study $\mathscr{P}^{\Theta}(\phi)$ was designed (Szafron, M.Sc. thesis, [150]) and was called the Θ-*BFACF algorithm*.

The Θ-BFACF algorithm generates a Markov Chain $\{X_t, t = 0, .., T\}$ such that at each time t, X_t is a polygon from the state space $\mathscr{P}^{\Theta}(\phi)$. At each time step t, one of five possible graph embeddings is chosen according to an appropriate probability distribution so as to

move the chain from state X_{t-1} to the state X_t. These five possible graph embeddings are the same as those generated at each time step of the BFACF algorithm (that is, four of the embeddings are created using the moves shown in Figure 3.1 and the fifth embedding is the polygon in state X_{t-1}). However, the probability distribution according to which these five embeddings are chosen must be modified (from the distribution used by the BFACF algorithm) to accommodate for the reduced state space $\mathscr{P}^{\Theta}(\phi)$.

The following is the precise Θ-BFACF algorithm as defined in [150]. Given $q > 0$, z such that $0 < z < z_{\phi}$, $t > 0$,and $\omega_{t-1} \in \mathscr{P}^{\Theta}(\phi)$ such that $|\omega_{t-1}| = n$, define, for any graph embedding ω_t in $\mathbb{Z}^3$,

$$p(\omega_t|\omega_{t-1}) := \begin{cases} \dfrac{(n+2)^{q-1}z^2}{n^{q-1}+3(n+2)^{q-1}z^2}, & \text{if } |\omega_t| = n+2 \text{ and } \omega_t \text{ can be} \\ & \text{obtained from } \omega_{t-1} \text{ using one BFACF move;} \\ \dfrac{n^{q-1}}{n^{q-1}+3(n-2)^{q-1}z^2}, & \text{if } |\omega_t| = n-2 \text{ and } \omega_t \text{ can be} \\ & \text{obtained from } \omega_{t-1} \text{ using one BFACF move;} \\ \dfrac{1+z^2}{2[1+3z^2]}, & \text{if } |\omega_t| = n \text{ and } \omega_t \neq \omega_{t-1} \text{ can be} \\ & \text{obtained from } \omega_{t-1} \text{ using one BFACF move;} \\ 0 & \text{otherwise.} \end{cases} \tag{3.19}$$

Then, the Θ-BFACF algorithm proceeds as follows:

1. At the $i = 0$'th step, set X_0 to be any SAP in $\mathscr{P}^{\Theta}(\phi)$.

2. (a) Label the 0'th edge as the edge which is incident on vertices $(0,0,0)$ and $(-1,0,0)$. Continue labelling all X_0's edges consecutively (skipping any edges which are in Θ) in the order induced by directing the 0'th edge to go from the origin to $(-1,0,0)$;

   (b) At the $(i+1)$'st step, select an integer I uniformly at random from $\{0,1,2,\ldots,|X_i|-7\}$;

   (c) Consider the four graph embeddings W_1, W_2, W_3, W_4 (not necessarily polygons) that can be formed by moving the I'th edge one lattice unit in one of the four directions perpendicular to the I'th edge, adding the necessary edges to join the newly shifted edge to the polygon, and then removing any double edges which may result.

(d) Select randomly one of the five embeddings W_1, W_2, W_3, W_4, X_i with respective probabilities $p(W_l|X_i)$, for $l \in \{1,2,3,4\}$, $\max\{0, 1-\xi\}$, where

$$\xi = \sum_{l=1}^{4} p(W_l|X_i), \tag{3.20}$$

and denote it ω.

(e) If ω is a SAP, set $X_{i+1} = \omega$; otherwise set $X_{i+1} = X_i$.

(f) $i := i + 1$; return to Step 2. (a).

3. Repeat until $i = T$.

In [150], Szafron showed that one acceptable choice for the one-step transition probabilities $P_{\omega\omega'}$ of the Θ-BFACF algorithm is given by

$$P_{\omega\omega'} := \frac{1}{|\omega|} p(\omega'|\omega). \tag{3.21}$$

[150] also contains a proof of the following result regarding the Θ-BFACF algorithm and the state space $\mathscr{P}^{\Theta}(\phi)$ (recall $\mathscr{P}^{\Theta}(\phi)$ is the set defined by Definition 2.2.3 with $K = \phi$).

Theorem 3.3.1 *The Θ-BFACF algorithm is ergodic (that is, the algorithm is irreducible, aperiodic, and positive recurrent) for the state space $\mathscr{P}^{\Theta}(\phi)$.*

The proof of Theorem 3.3.1 was based on the proof of Janse van Rensburg and Whittington [69] that the ergodicity classes for the BFACF algorithm are the different knot-types. Szafron's proof of the irreducibility of the Θ-BFACF algorithm on the set $\mathscr{P}^{\Theta}(\phi)$ relied on the fact that the structure Θ contains sufficient empty lattice space to allow a strand of a before-strand-passage polygon to pass through the structure. This empty space is a necessity for the proof as it guarantees that Reidemeister III moves are permitted about the structure.

The ergodicity of the Θ-BFACF algorithm ensures that the entire space $\mathscr{P}^{\Theta}(\phi)$ will be sampled according to the distribution function $\breve{\pi}_{\omega}(q, z_i, M)$, given by Equation (2.63), but, because the Θ-BFACF algorithm is based on the BFACF algorithm, the Θ-BFACF algorithm also suffers from the same major disadvantage of the BFACF algorithm, that is, as $z \to z_{\phi}$, the exponential autocorrelation time for the algorithm approaches infinity. To address this limitation, the next section defines the composite Markov chain implementation of the Θ-BFACF algorithm.

3.4 The CMC Implementation of the Θ-BFACF Algorithm

For some specified integer $M > 1$, let $\{X_t(i), t \in T\}$ be a Markov chain generated by the Θ-BFACF algorithm on $\mathscr{P}^{\Theta}(\phi)$ with stationary distribution having the form

$$\breve{\pi}_{\omega}(q, z_i, 2) = \frac{(|\omega| - 6)\,|\omega|^{q-1} z_i^{|\omega|}}{\sum_{n=1}^{\infty} (2n-6)\,(2n)^{q-1}\, p_{2n}^{\Theta}(\phi) z_i^{2n}}, \tag{3.22}$$

and with one-step transition probabilities, for all $\omega, \omega' \in \mathscr{P}^{\Theta}(\phi)$, given by $P_{\omega\omega'}(i)$, where $P_{\omega\omega'}(i)$ is given by Equation (3.21) with $z = z_i$. Define $\breve{\pi}_{\boldsymbol{\omega}}(q, \boldsymbol{z}, M) := \left(\breve{\pi}_{\omega(i)}(q, z_i), i = 1, ..., M\right)$.

Now, given any fixed positive integer ρ, define one Θ-*BFACF move in parallel* to be one Θ-BFACF move implemented on each of the individual components of $\boldsymbol{Y}_t$, where $\{\boldsymbol{Y}_t, t \in T\}$ is a Markov chain with state space $\mathscr{S}^M := \left[\mathscr{P}^{\Theta}(\phi)\right]^M$ and one-step transition probabilities given by

$$P_{\boldsymbol{\omega}\boldsymbol{\omega}'} = \begin{cases} \prod_{i=1}^{M} P_{\omega(i)\omega'(i)}(i), & \text{if } t \bmod (\rho+1) \neq 0, \\ 13^{-1} r(i, i+1), & \text{if } t \bmod (\rho+1) = 0,\ \boldsymbol{\omega}' = \boldsymbol{\omega}^{(i,i+1)}, \\ 1 - 13^{-1} \sum_{i=1}^{13} r(i, i+1), & \text{if } t \bmod (\rho+1) = 0,\ \boldsymbol{\omega}' = \boldsymbol{\omega}, \\ 0, & \text{otherwise,} \end{cases} \tag{3.23}$$

where

$$\boldsymbol{Y}_t = (Y_t(1), Y_t(2), \ldots, Y_t(M)), \tag{3.24}$$

$$\boldsymbol{\omega} = (\omega(1), \omega(2), \ldots, \omega(M)) \in \mathscr{S}^M, \tag{3.25}$$

for $1 \leq i < j \leq M$,

$$\boldsymbol{\omega}^{(i,j)} = (\omega(1), \ldots, \omega(i-1), \omega(j), \omega(i+1), \ldots, \omega(j-1), \omega(i), \omega(j+1), \ldots, \omega(M)) \in \mathscr{S}^M, \tag{3.26}$$

and, for some i such that $1 \leq i < M$,

$$r(i, i+1) = \min\left(1, \left(\frac{z_{i+1}}{z_i}\right)^{|\omega(i)| - |\omega(i+1)|}\right). \tag{3.27}$$

Note that $P_{\boldsymbol{\omega}\boldsymbol{\omega}'}$ describes the two types of moves for a local swapping CMC algorithm.

Since in [150] Szafron proved Lemmas 3.2.2, 3.2.3, and 3.2.4 hold using the above definition of $P_{\boldsymbol{\omega}\boldsymbol{\omega}'}$ and the set $\pi_{\boldsymbol{Y}} = \{\breve{\pi}_{\boldsymbol{\omega}}(q, M)\}_{\boldsymbol{\omega} \in \mathscr{S}^M}$, the CMC implementation of the Θ-BFACF algorithm (to be referred to as the CMC Θ-BFACF algorithm) is ergodic on $\mathscr{S}^M$ and has the desired stationary distribution $\pi_{\boldsymbol{Y}}$.

3.4.1 The Simulation of the CMC Θ-BFACF algorithm

The simulation of the MMC Θ-BFACF algorithm implemented consisted of ten independent replications. Each replication was run for a total of 9.6×10^{10} time steps (8.0×10^{10} Θ-BFACF moves in parallel and 1.6×10^{10} attempted swaps) where every five Θ-BFACF moves in parallel were followed by an attempted swap. The polygon lengths for the initial starting states of each chain and each replication are given in Table 3.1.

Table 3.1: The length of the polygon in the starting state of the i'th component during the r'th replication.

	Replication r									
Chain i	**1**	**2**	**3**	**4**	**5**	**6**	**7**	**8**	**9**	**10**
1	38	16	52	20	26	44	36	52	42	14
2	50	22	36	52	26	64	54	74	18	14
3	30	14	136	16	24	30	58	46	54	14
4	72	126	44	60	168	94	34	66	32	14
5	78	246	56	198	150	60	36	90	162	14
6	82	172	48	58	64	44	68	58	86	14
7	72	88	94	66	62	42	308	194	180	14
8	134	246	28	218	96	64	200	188	212	14
9	204	160	52	850	176	170	18	18	110	14
10	316	528	222	292	124	802	112	266	130	14
11	178	1074	198	304	76	48	184	592	358	14
12	154	66	312	914	244	838	1582	1740	34	14
13	1304	344	992	372	120	554	180	1570	516	14
14	888	2436	156	1626	142	796	1276	216	200	14

In the CMC Θ-BFACF simulation, for the probabilities given by Equation (3.19), q is set to 2. For each of the individual replications, the number of chains and the distribution of the fugacities over the interval $[0.2030, 0.2132]$ to be used were taken from [124], that is $M = 14$, and the following distribution of z-values from the interval $[0.2030, 0.2132]$ was used: $z_1 = 0.2030$, $z_2 = 0.2050$, $z_3 = 0.2070$, $z_4 = 0.2090$, $z_5 = 0.2100$, $z_6 = 0.2105$, $z_7 = 0.2110$, $z_8 = 0.2115$, $z_9 = 0.2120$, $z_{10} = 0.2124$, $z_{11} = 0.2128$, $z_{12} = 0.2130$, $z_{13} = 0.2131$,

and $z_{14} = 0.2132$. These values of z are valid for the Θ-BFACF algorithm because for $i = 1, \ldots, 14$,

$$z_i < z_\Theta = z_\phi < 0.2135,$$

where the equality is a consequence of Corollary 2.2.7 and the inequality $z_\phi < 0.2135$ is a consequence of $z_\phi < z_p(3) \approx 0.2135$ [49]. Hence the transition probabilities presented in Equation (3.19) are valid for the CMC Θ-BFACF algorithm. The motivation for using this distribution of z-values and choice of M is to compare, for a fixed z value, the average length of a SAP in $\mathscr{P}(\phi)$ (as estimated in [121]) with an estimate of the average length of an unknotted SAP in $\mathscr{P}^\Theta(\phi)$. This comparison is presented in Section 4.7.3.

The pseudo-random number generator used in the Monte Carlo simulation is a variant of the add-with-carry generator developed by Marsaglia and Zaman [109]. The computer program used to implement this pseudo-random number generator was provided by [66]. The period of this pseudo-random number generator is over 2^{931} which is much greater than the estimated 2^{50} numbers generated throughout the course of the simulation. Hence any error introduced because of the "non-randomness" of the pseudo-random numbers generated has been assumed to be negligible.

Whether a Composite Markov chain sampling experiment or some other experiment is chosen to study a model, the data generated from the experiment needs to be analyzed. In the next chapter, some issues surrounding the analysis of simulation data are discussed.

Chapter 4

Convergence to the Equilibrium Distribution

Markov Chain Monte Carlo simulation is a powerful tool that allows many different kinds of problems to be studied. In general, the implementation of these simulations is straight-forward but there are several challenges that arise when analyzing the results of a MCMC simulation.

Given a MCMC algorithm for simulating an ergodic Markov chain with a given target distribution as its equilibrium distribution, two challenges must be overcome before statistical inferences about parameters of interest can be made using simulation data. The first issue results from the fact that in any simulation of a Markov chain, the Markov chain is usually started in some distribution other than the Markov chain's equilibrium distribution. Hence there is an initial period (for each distinct observable) in which the data generated does not reflect the equilibrium distribution. Consequently the amount of time that must pass before the equilibrium distribution is reached must be determined.

The second issue that needs to be addressed is related to the fundamental property of a Markov chain $\{X_t, t \in \mathbb{N} \cup \{0\}\}$ that random variables X_i and X_j, for all $i < j$, are correlated. The further j is from i, the smaller the correlation is expected to be between X_j and X_i. In fact, for some j large enough, X_j is expected to be "essentially independent" from X_i.

These two issues, the amount of time required for an arbitrary stationary process to reach its equilibrium distribution and the concept of two random variables of the process being "essentially independent", will be discussed in the next section.

4.1 For a Stationary Process

The following definitions and notation will be used throughout this chapter. Define $T = \mathbb{N} \cup \{0\}$. Then suppose that $\mathcal{X} := \{X_t, t \in T\}$ is a stationary stochastic process defined on

some countable state space $\mathscr{S}$ and that, for every $t \in T$, X_t is distributed according to a distribution given by the probability mass function $\boldsymbol{\pi} = \{\pi_x\}_{x \in \mathscr{S}}$. Let $\mathscr{H}$ be the set of all real-valued functions defined on $\mathcal{X}$ and note that for each of the elements $f \in \mathscr{H}$, the process $f(\mathcal{X})$ will be referred to as an *observable of the process* $\mathcal{X}$. Then, for every $f \in \mathscr{H}$, define $f(\mathcal{X}) := \{f(X_t), t \in T\}$ and also denote $f(\mathcal{X})$ by $\{f_{X_t}, t \in T\}$. It should be noted that $f(\mathcal{X})$ is a stationary stochastic process [78] and that whenever the notation $f(\mathcal{X})$ is used to denote a stochastic process, the notation implies that the process $f(\mathcal{X})$ was formed by applying the real-valued function f to the stochastic process $\{X_t, t \in T\}$.

Using the above notation and definitions, four key functions associated with the stationary stochastic process $f(\mathcal{X})$ are defined next.

Definition 4.1.1 ([35]) *For a stationary stochastic process $f(\mathcal{X})$ whose underlying stationary stochastic process $\mathcal{X}$ is distributed according to $\boldsymbol{\pi} = \{\pi_x\}_{x \in \mathscr{S}}$,*

1. *the* mean with respect to π, *denoted* $\mathrm{E}_{\boldsymbol{\pi}}(f)$, *is defined by*

$$\mathrm{E}_{\boldsymbol{\pi}}(f) := \sum_{x \in \mathscr{S}} f(x)\pi_x; \tag{4.1}$$

2. *the* variance with respect to π, *denoted* $\mathrm{var}_{\boldsymbol{\pi}}(f)$, *is defined by*

$$\mathrm{var}_{\boldsymbol{\pi}}(f) := \sum_{x \in \mathscr{S}} \left[f\left(x\right) - \mathrm{E}_{\boldsymbol{\pi}}(f)\right]^2 \pi_x; \tag{4.2}$$

3. *the* autocovariance function with respect to π, *denoted* $\gamma_f(h)$, *is defined by*

$$\begin{aligned} \gamma_f(h) &= \mathrm{E}_{\boldsymbol{\pi}}(f_{X_t} f_{X_{t+|h|}}) - \left(\mathrm{E}_{\boldsymbol{\pi}}(f)\right)^2. \\ &= \sum_{x,y \in \mathscr{S}} f(x) \left[\pi_x p_{x,y}^{(|h|)} - \pi_x \pi_y\right] f(y), \end{aligned} \tag{4.3}$$

where $p_{x,y}^{(k)} = \Pr\left(X_{t+k} = y | X_t = x\right)$; *and*

4. *the* autocorrelation function with respect to π, *denoted* $\rho_f(h)$, *is defined by*

$$\rho_f(h) = \frac{\gamma_f(h)}{\gamma_f(0)}. \tag{4.4}$$

With the above notation and concepts defined for a stationary stochastic process, all further discussion is restricted to the scenario where the stochastic process $\mathcal{X}$ is actually an ergodic Markov chain (because an ergodic Markov chain is used later in this thesis). Now that sufficient machinery has been provided, the discussion turns to the time it takes an ergodic Markov chain $\mathcal{X}$ to reach its stationary distribution.

4.1.1 Are We There Yet?

Suppose $\mathcal{X}$ is started in its equilibrium distribution. Then $\gamma_f(h)$ is a measure of the covariance that exists between the random variables of $f(\mathcal{X})$ that are $|h|$ time steps apart and $\rho_f(h)$ is the correlation that exists between the random variables of $f(\mathcal{X})$ that are $|h|$ time steps apart. Generally, for $|h|$ sufficiently large, $\rho_f(h)$ decays exponentially [142], that is for $|h|$ sufficiently large, $\rho_f(h)$ decays like $e^{\frac{-|h|}{\tau_{\exp}(f)}}$ for some constant $\tau_{\exp}(f)$. The constant $\tau_{\exp}(f)$ is called the *exponential autocorrelation time of the observable* f . The precise definitions of $\tau_{\exp}(f)$ and $\tau_{\exp}$ that follow have been taken from [142].

Definition 4.1.2 ([142]) *For a stationary stochastic process $f(\mathcal{X})$ started in its stationary distribution $\boldsymbol{\pi} = \{\pi_x\}_{x\in\mathscr{S}}$, the exponential autocorrelation time of the observable f, denoted $\tau_{\exp}(f)$, is defined as*

$$\tau_{\exp}(f) = \limsup_{h\to\infty} \frac{h}{-\log|\rho_f(h)|}. \tag{4.5}$$

Since, for every observable $f \in \mathscr{H}$, there is a corresponding value $\tau_{\exp}(f)$, it makes sense to define an exponential autocorrelation time for the entire system. This systemic exponential autocorrelation time, denoted $\tau_{\exp}$, is formally defined as:

Definition 4.1.3 *The exponential autocorrelation time for the ergodic Markov chain $\mathcal{X}$ with stationary distribution $\boldsymbol{\pi} = \{\pi_x\}_{x\in\mathscr{S}}$, is defined as*

$$\tau_{\exp} = \sup_{f\in\mathscr{H}} \tau_{\exp}(f). \tag{4.6}$$

Now suppose that $\mathcal{X}$ is started in some distribution other than its equilibrium distribution. Sokal [142] shows that the rate of convergence from some initial, non-equilibrium distribution to the equilibrium distribution is bounded above by $\tau_{\exp}$. Therefore $\tau_{\exp}$ can be used as a measure for the amount of time that it takes the observable with the largest exponential autocorrelation time to reach the stationary distribution and $\tau_{\exp}$ can be interpreted as the amount of time required for the entire process to equilibrate.

Because $\tau_{\exp}$ represents the slowest convergence time, $\tau_{\exp}$ can be used as a measure for the amount of time that it will take every function $f \in \mathscr{H}$ to reach the stationary distribution [142]. Thus, in practice, to determine $\tau_{\exp}$, $\tau_{\exp}(f)$, for the observable $f \in \mathscr{H}$ with the slowest convergence time to the stationary distribution, needs to be determined.

In theory, theoretical analysis can be used to determine whether or not the stationary distribution has been reached, but in practice, many problems are too complex for such an analysis [101]. In these situations, a numerical approach is used to estimate $\tau_{\exp}(f)$ and hence $\tau_{\exp}$. Some numerical methods for estimating $\tau_{\exp}$ and $\tau_{\exp}(f)$ (for the observable $f(\mathcal{X})$) will be discussed in Section 4.2.

Once the amount of time for the process to equilibrate has been determined, the correlation between the random variables of the process $\{f_{X_t}, t \in T\}$ that are $|h|$ time steps apart needs to be calculated. A discussion of how to determine this correlation is presented in the next section.

4.1.2 Are We Related?

Suppose $\mathcal{X}$ is started in its equilibrium distribution. $\rho_f(h)$, as given by Definition 4.1.1, is a measure of the normalized covariance between the random variables of $\{f_{X_t}, t \in T\}$ that are $|h|$ time steps apart, that is, it is a measure of the normalized covariance between f_{X_t} and $f_{X_{t+|h|}}$. Generally, the greater the amount of time that passes between observations f_{X_i} and f_{X_j}, the smaller the value of $\rho_f(j-i)$ is expected to be. As the value of $\rho_f(j-i)$ decreases, the random variables f_{X_i} and f_{X_j} that are $|j-i|$ time units apart are expected to be less correlated and consequently less likely to depend on each other. Note that an infinitesimally small (and for all practical purposes zero) correlation between f_{X_t} and $f_{X_{t+|h|}}$ does not imply independence according to the usual definition of independence of two random variables. Instead, for a stochastic process $\{f_{X_t}, t \in T\}$, if the correlation between f_{X_i} and f_{X_j} is infinitesimally small then f_{X_i} and f_{X_j} are said to be "essentially independent".

Mathematically the concept of "essentially independent" can be characterized by the integrated autocorrelation time of the observable $f(\mathcal{X})$, denoted $\tau_{\text{int}}(f)$. The functional definition of $\tau_{\text{int}}(f)$, as presented below, has been taken from [142].

Definition 4.1.4 ([142]) *For a stationary stochastic process $f(\mathcal{X})$ with stationary distribution $\boldsymbol{\pi} = \{\pi_x\}_{x \in \mathscr{S}}$, the integrated autocorrelation time of the observable f, denoted $\tau_{\text{int}}(f)$, is defined as*

$$\tau_{\text{int}}(f) = \frac{1}{2} \sum_{h=-\infty}^{\infty} \rho_f(h). \tag{4.7}$$

Since $\tau_{\text{int}}(f)$ is an even function, $\tau_{\text{int}}(f)$ can alternatively be expressed as

$$\tau_{\text{int}}(f) = \frac{1}{2} + \sum_{h=1}^{\infty} \rho_f(h). \tag{4.8}$$

The reason $\tau_{\text{int}}(f)$ is associated with the concept of "essentially independent" is as follows. Consider the estimator for the sample mean

$$\langle f \rangle_n := \frac{1}{n} \sum_{i=1}^{n} f_{X_i} \tag{4.9}$$

based on the observable $f(\mathcal{X})$. Then

$$\begin{aligned}
\text{var}_{\boldsymbol{\pi}} \left(\langle f \rangle_n \right) &= \text{E}_{\boldsymbol{\pi}} \left[\frac{1}{n^2} \sum_{r=1}^{n} \sum_{s=1}^{n} f_{X_r} f_{X_{r+s-r}} - \left(\text{E}_{\boldsymbol{\pi}}[f] \right)^2 \right] \\
&= \frac{\gamma_f(0)}{n^2} \sum_{r=1}^{n} \sum_{s=1}^{n} \rho_f(s-r) \\
&= \frac{\gamma_f(0)}{n^2} \sum_{h \leq |n-1|} (n - |h|) \, \rho_f(|h|) \\
&= \frac{\gamma_f(0)}{n} \sum_{h \leq |n-1|} \left(1 - \frac{|h|}{n} \right) \rho_f(|h|) \\
&= \frac{2\gamma_f(0)}{n} \sum_{1 \leq h \leq n-1} \left(\rho_f(|h|) - \frac{h \rho_f(|h|)}{n} + \frac{1}{2(n-1)} \right) \\
&\approx \frac{2\gamma_f(0)}{n} \tau_{\text{int}}(f), \text{ if } n \gg \tau_{\text{int}}(f),
\end{aligned} \tag{4.10}$$

where it is assumed that for $n \gg \tau_{\text{int}}(f)$, $\tau_{\text{int}}(f)$ can be approximated by [142]

$$\tau_{\text{int}}(f) \approx \frac{1}{2} + \sum_{1 \leq h \leq n-1} \rho_f(h). \tag{4.11}$$

Note that the validity of this assumption is explored later in this section.

The approximation

$$\text{var}_{\boldsymbol{\pi}} \left(\langle f \rangle_n \right) \approx \frac{2\gamma_f(0)}{n} \tau_{\text{int}}(f), \text{ if } n \gg \tau_{\text{int}}(f), \tag{4.12}$$

implies that the variance of the sample mean $\langle f \rangle_n$ is approximately a factor of $2\tau_{\text{int}}(f)$ larger than $\frac{\gamma_f(0)}{n}$ which is the variance of the sample mean computed using independent data. The upshot is that if n values of the observable $f(\mathcal{X})$ are correlated, then there are really $\frac{n}{2\tau_{\text{int}}(f)}$ essentially independent observations. More formally, for the rest of this work, the concept of "essentially independent" will be defined as follows:

Definition 4.1.5 *For a stationary stochastic process $f(\mathcal{X})$ with stationary distribution $\boldsymbol{\pi} = \{\pi_x\}_{x\in\mathscr{S}}$, two random variables, say f_{X_i} and f_{X_j}, are said to be* essentially independent *if*

$$|j - i| \geq 2\tau_{\text{int}}(f). \tag{4.13}$$

Since the observable $f(\mathcal{X})$, for each $f \in \mathscr{H}$, has an associated integrated autocorrelation time, how much time must pass between random variables X_i and X_j in the original process before X_i and X_j are considered essentially independent? This amount of time is referred to as the *integrated autocorrelation time for the system.* The functional definition of τ_{int}, as presented below, has been modified from the corresponding definition of τ_{int} in [142] to the specific case where a stationary stochastic process $f(\mathcal{X})$ has a stationary distribution $\boldsymbol{\pi} = \{\pi_x\}_{x\in\mathscr{S}}$.

Definition 4.1.6 *The integrated autocorrelation time for the ergodic Markov chain $\mathcal{X}$ with stationary distribution given by $\boldsymbol{\pi} = \{\pi_x\}_{x\in\mathscr{S}}$, is defined as*

$$\tau_{\text{int}} := \sup_{f\in\mathscr{H}} \tau_{\text{int}}(f). \tag{4.14}$$

Because, in practice, many problems are too complex to be able to calculate τ_{int} [101], practical methods for estimating τ_{int} and $\tau_{\text{int}}(f)$ (for the observable $f(\mathcal{X})$) are needed. Such methods will be discussed in Section 4.3. Before these methods for estimating τ_{int} and $\tau_{\text{int}}(f)$ are discussed, practical methods for estimating τ_{exp} will be discussed.

4.2 Estimating the Time to Equilibrate, τ_{exp}

Several techniques exist to determine τ_{exp}, the number of time steps required for the influence of the initial non-stationary starting state to diminish to the point of having a negligible effect on inferences. Three techniques will be used in this work to estimate τ_{exp}. In order to facilitate the discussion of these three methods, some definitions and notation are required. The following discussion, including the notation and the definitions, is based on Fishman [35].

Suppose that $\mathcal{X}$ is an ergodic Markov chain defined on the state space $\mathscr{S}$ with stationary distribution $\boldsymbol{\pi} = \{\pi_x\}_{x\in\mathscr{S}}$ that was started in some non-equilibrium distribution $\boldsymbol{\pi}_0$. Because all three methods for estimating τ_{exp} that are to be presented are based on

n_0 preliminary simulations of $\mathcal{X}$, each of length t_0+1, some definitions and notation are required.

Define $\mathcal{X}_{t_0}^{(r)} := \{X_t^{(r)}, t \in \{0,1,...,t_0\}\}$, for $1 \leq r \leq n_0$, where $\mathcal{X}_{t_0}^{(r)}$ is the r'th replication of $\mathcal{X}$ of length t_0+1 starting in state $s_0^{(r)} \in \mathscr{S}$. Now, for each $h \in \mathscr{H}$, define $h\left(\mathcal{X}_{t_0}^{(r)}\right) := \left\{h\left(X_t^{(r)}\right), t \in \{0,1,...,t_0\}\right\}$,

$$\langle h(X_t)\rangle := \frac{1}{n_0}\sum_{r=1}^{n_0} h\left(X_t^{(r)}\right), \tag{4.15}$$

and, for $m \geq k$,

$$\left\langle h\left(X_{k,m}^{(r)}\right)\right\rangle := \frac{1}{m-k+1}\sum_{t=k}^{m} h\left(X_t^{(r)}\right), \tag{4.16}$$

and

$$\langle h(X_{k,m,n_0})\rangle := \frac{1}{n_0}\sum_{r=1}^{n_0}\left\langle h\left(X_{k,m}^{(r)}\right)\right\rangle. \tag{4.17}$$

The quantity $\langle h(X_t)\rangle$, for $1 \leq t \leq t_0$, is referred to as the t'th column average of $h(\mathcal{X})$; the quantity $\langle h(X_{1,j,n_0})\rangle$, for $1 \leq j \leq t_0$, is referred to as the average of the first j column averages of $h(\mathcal{X})$; and the quantity $\langle h(X_{k,t_0,n_0})\rangle$, for $1 \leq k \leq t_0$, is referred to as the average of the last k column averages of $h(\mathcal{X})$. It is these three averages for various choices of j and k which can be used to determine an estimate for $\tau_{\exp}$ for the stationary process $\mathcal{X}$.

Recall from Parts (1) and (2) of Definition 4.1.1 that

$$\mathrm{E}_{\boldsymbol{\pi}}(h) = \sum_{x\in\mathscr{S}} h(x)\,\pi_x \tag{4.18}$$

and

$$\mathrm{var}_{\boldsymbol{\pi}}(h) = \sum_{x\in\mathscr{S}} [h(x) - \mathrm{E}_{\boldsymbol{\pi}}(h)]^2\,\pi_x. \tag{4.19}$$

Now, for replication r, define $\mu_{s_0^{(r)},j}(h)$, the *conditional expectation of* $h\left(X_j^{(r)}\right)$ *resulting from starting in state* $s_0^{(r)}$, by

$$\mu_{s_0^{(r)},j}(h) := \mathrm{E}_{\boldsymbol{\pi}}\left[h\left(X_j^{(r)}\right)|X_0^{(r)} = s_0^{(r)}\right] \tag{4.20}$$

$$= \sum_{x\in\mathscr{S}} h(x)\,p_{s_0^{(r)},x}^{(j)} \tag{4.21}$$

and $\sigma^2_{s_0^{(r)},j}(h)$, the *conditional variance of* $h\left(X_j^{(r)}\right)$ *resulting from starting in state* $s_0^{(r)}$, by

$$\sigma^2_{s_0^{(r)},j}(h) := \mathrm{var}_{\boldsymbol{\pi}}\left[h\left(X_j^{(r)}\right)|X_0^{(r)} = s_0^{(r)}\right] \tag{4.22}$$

$$= \sum_{x\in\mathscr{S}} h\left(x\right)\left[h(x) - \mu_{s_0^{(r)},j}(h)\right] p^{(j)}_{s_0^{(r)},x}, \tag{4.23}$$

where $p^{(j)}_{s_0^{(r)},x}$ is the probability of moving from state $s_0^{(r)}$ to x in j time steps. The corresponding *conditional expectation of* $\left\langle h\left(X_{k,m}^{(r)}\right)\right\rangle$ is denoted $\mu_{s_0^{(r)},k,m}(h)$ and is given by

$$\mu_{s_0^{(r)},k,m}(h) := \mathrm{E}\left[\left\langle h\left(X_{k,m}^{(r)}\right)\right\rangle |X_0^{(r)} = s_0^{(r)}\right] \tag{4.24}$$

$$= \frac{1}{m-k+1}\sum_{j=k}^{m}\mu_{s_0^{(r)},j}(h). \tag{4.25}$$

The corresponding *conditional variance of* $\left\langle h\left(X_{k,m}^{(r)}\right)\right\rangle$ is denoted $\sigma^2_{s_0^{(r)},k,m}(h)$ and is given by

$$\begin{aligned}\sigma^2_{s_0^{(r)},k,m}(h) &:= \mathrm{var}\left[\left\langle h\left(X_{k,m}^{(r)}\right)\right\rangle |X_0^{(r)} = s_0^{(r)}\right] \\ &= \frac{1}{(m-k+1)^2}\sum_{j=k}^{m}\sigma^2_{s_0^{(r)},j}(h) \\ &+ \frac{2}{(m-k+1)^2}\sum_{j=k}^{m-1}\sum_{l=j+k}^{m}\mathrm{cov}\left[h\left(X_j^{(r)}\right), h\left(X_l^{(r)}\right)|X_0^{(r)} = s_0^{(r)}\right],\end{aligned} \tag{4.26}$$

where, for $j \geq 1$ and $l \geq 1$,

$$\begin{aligned}\mathrm{cov}\left[h\left(X_j^{(r)}\right), h\left(X_l^{(r)}\right)|X_0^{(r)} = s_0^{(r)}\right] &:= -\mu_{s_0^{(r)},j}(h)\mu_{s_0^{(r)},l}(h) \\ &+ \sum_{x,y\in\mathscr{S}} h\left(x\right)h(y)p^{\min(j,l)}_{s_0^{(r)},x}p^{(|l-j|)}_{x,y}.\end{aligned} \tag{4.27}$$

Initially the thought of estimating τ_{exp} seems to be a daunting task since it requires estimating $\tau_{\mathrm{exp}}(h)$ for every $h \in \mathscr{H}$. However, Fishman [35, p. 506] showed that if $\{X_t, t \in T\}$ is a reversible Markov chain, then $\tau_{\mathrm{exp}}(h')$, where h' is a function in $\mathscr{H}$ such that

$$\sigma(h') := \max_{h\in\mathscr{H}}\sqrt{\mathrm{var}_{\boldsymbol{\pi}}\left(h\right)}, \tag{4.28}$$

only needs to be estimated.

Unfortunately, determining h' is no less daunting a task. Fishman [35, p. 506] states that to determine an estimate for τ_{exp}, in practice the set of functions $\mathscr{H}$ used to determine

the function h' can be replaced with the set of functions $\mathscr{H}'$ where $\mathscr{H}'$ is the set consisting of only those functions that are of interest in the study. Then, for the function $h' \in \mathscr{H}'$ such that

$$\sigma(h') := \max_{h \in \mathscr{H}'} \sqrt{\mathrm{var}_{\boldsymbol{\pi}}(h)}, \tag{4.29}$$

$$\tau_{\exp} = \tau_{\exp}(h') \tag{4.30}$$

for the study. Because the first two of the three methods ("Warm-up Analysis" method and the "Estimated Potential Scale Reduction") for estimating $\tau_{\exp}$ require the function $h' \in \mathscr{H}'$, the following discussions of the "Warm-up Analysis" method and the "Estimated Potential Scale Reduction" assume that h' has already been found. Note that both of these methods can be used to estimate $\tau_{\exp}(h)$ for any function $h \in \mathscr{H}$.

4.2.1 Warm-up Analysis

The goal of a warm-up analysis is to estimate a finite length interval $[0, k]$, the *warm-up interval for the Markov chain* $\mathcal{X}$, such that $\tau_{\exp} \in [0, k]$. The right end point of a warm-up interval estimates an upper bound for the number of time steps required for the underlying ergodic Markov chain $\{X_t, t \in T\}$ to reach its stationary distribution $\boldsymbol{\pi}$. The following discussion for implementing a warm-up analysis is based on "Section 6.3: Warm-up Analysis" presented in [35].

To estimate the interval $[0, k]$, n_0 independent replications of the Markov chain $\mathcal{X}$ are generated, where each of the n_0 realizations (each of length $t_0 + 1$ time steps) is started in the same initial state $s_0 \in \mathscr{S}$, that is, for $1 \leq r \leq n_0$, set $X_0^{(r)} = s_0$. Note that t_0 should be chosen so that $k \ll t_0$. Suppose the interval $[0, \hat{k}]$ represents an estimate for $[0, k]$. Then $\hat{k}$ provides an estimate for an upper bound on the time steps required for the underlying ergodic Markov chain $\{X_t, t \in T\}$ to reach its stationary distribution $\boldsymbol{\pi}$. The quantities $\langle h'(X_t) \rangle$, for $0 \leq t \leq t_0$, $\langle h'(X_{0,j,n_0}) \rangle$, for $0 \leq j \leq t_0$, and $\langle h'(X_{l,t_0,n_0}) \rangle$, for $0 \leq l \leq t_0$, can be used as follows to determine $\hat{k}$.

Because $\langle h'(X_{0,j,n_0}) \rangle$ contains all the data from the n_0 replications up to step j, the tendency for the sequence of the first j column averages $(\langle h'(X_{0,j,n_0}) \rangle, j \in \{0, 1, ..., t_0\})$ to follow the trend of the sequence $(\langle h'(X_t) \rangle, t \in \{0, 1, ..., t_0\})$ starts to dissipate for all values of j greater than some $k^* \leq t_0$. This implies that $\hat{k} \leq k^*$. Since $\langle h'(X_{j,t_0,n_0}) \rangle$ contains all the data from the n_0 replications from time step j to t_0, the tendency for the

last j column averages $(\langle h'(X_{j,t_0,n_0})\rangle, j \in \{0,1,...,t_0\})$ to follow the trend of the sequence $(\langle h'(X_t)\rangle, t \in \{0,1,...,t_0\})$ starts to dissipate for all values of j greater than some $k_* \leq t_0$. This implies that $\hat{k} \leq k_*$. Therefore, to err on the side of conservatism, set $\hat{k} = \max\{k^*, k_*\}$.

The actual amount of time it takes for the process to lose the effect of the initial starting state is expected to be somewhere in the interval $[0, \hat{k}]$, which is referred to as the *warm-up interval for the sampling experiment*. Let $\widehat{\tau}_{\exp,W}$ denote the estimate for $\tau_{\exp}$ determined using a warm-up analysis, then, erring on the side of conservatism, set $\widehat{\tau}_{\exp,W} = \hat{k}$, the upper limit of the warm-up interval. This estimate is a very rough upper bound for $\tau_{\exp}(h')$.

Though this method for determining the warm-up interval estimates the time it takes for the effects of the initial states to dissipate, the warm-up interval as determined using this technique does not ensure that the simulation has reached the desired global equilibrium distribution. If convergence to the global equilibrium distribution is slow, the finite process may have converged to a "local equilibrium". Fishman [35, p. 513] states that "this local stagnation of a process can occur when its equilibrium distribution is multimodal and its transition matrix makes one-step transitions only in a small neighborhood around the current state in the process." This local stagnation is a possibility for the work presented here as the changes to SAPs resulting from the CMC Θ-BFACF algorithm are primarily made on a very local scale (with the exception of swapping). With the Θ-BFACF algorithm, there is very little change in the SAP from time step i to $i+1$. Another possible limitation of this technique is the fact that some starting states may result in an extremely long time before the effect of the starting state has dissipated from the process. The technique "Estimated Potential Scale Reduction" for estimating $\tau_{\exp}$ addresses these two limitations.

4.2.2 Estimated Potential Scale Reduction

Suppose that n_0 initial states are chosen at random from $\boldsymbol{\pi}_0$, some non-degenerate distribution, and that these initial states are denoted $s_0^{(r)}$, for $1 \leq r \leq n_0$. Then each of the n_0 simulations (each of length t_0 time steps) is started in the initial state $s_0^{(r)} \in \mathscr{S}$, that is, for $1 \leq r \leq n_0$, set $X_0^{(r)} = s_0^{(r)}$. Each of the replications is started in the same distribution but not the same state as was the case for a warm-up analysis.

A warm-up interval can be determined using data from these n_0 simulations using a technique outlined by Fishman in Section 6.3 of [35]. Fishman states that a suitable warm-up interval can be determined if there exists "a positive integer $k < t_0$ such that all n_0 truncated sample paths $\left(\left\langle h'\left(X_{0,j}^{(1)}\right)\right\rangle, j \in \{k, k+1, ..., t_0\}\right)$, $\left(\left\langle h'\left(X_{0,j}^{(2)}\right)\right\rangle, j \in \{k, k+1, ..., t_0\}\right), ..., \left(\left\langle h'\left(X_{0,j}^{(n_0)}\right)\right\rangle, j \in \{k, k+1, ..., t_0\}\right)$ have converged to a common region and repeatedly intersect each other" [35, p. 513]. The rest of this section presents a numerical method, developed by Gelman and Rubin [42], that is used in this work to quantify Fishman's statement "have converged to a common region and repeatedly intersect each other" [35, p. 513].

Gelman and Rubin's method requires that the initial states are chosen from $\boldsymbol{\pi}_0$ such that $\boldsymbol{\pi}_0$ is an overdispersed distribution, that is

$$\text{var}\left[h'\left(X_0^{(r)}\right) | X_0^{(r)} \sim \boldsymbol{\pi}_0\right] \geq \text{var}_{\boldsymbol{\pi}}\left(h'\right) = \sum_{x \in \mathscr{S}} \left[h'(x) - \text{E}_{\boldsymbol{\pi}}\left(h'\right)\right]^2 \pi_x,$$

where $X_0^{(r)} \sim \boldsymbol{\pi}_0$ means the state of $X_0^{(r)}$ is generated from the distribution $\boldsymbol{\pi}_0$. Choosing overdispersed starting states is an important part of this method because choosing overdispersed starting states ensures that:

1. the starting states are "relatively far apart" which provides a better chance for detecting any lack of convergence to the desired equilibrium distribution and for detecting any dependence of subsequent states on the starting state of the replication, and

2. in terms of inference, the sample will be drawn from all regions of the state space according to the equilibrium distribution.

Now for the function $h' \in \mathscr{H}$, define the quantities

$$B_{n_0,t_0} = \frac{t_0 + 1}{n_0 - 1} \sum_{i=1}^{n_0} \left(\left\langle h'\left(X_{0,t_0}^{(r)}\right)\right\rangle - \left\langle h'\left(X_{0,t_0,n_0}\right)\right\rangle\right)^2 \tag{4.31}$$

and

$$W_{n_0,t_0} = \frac{1}{n_0 t_0} \sum_{i=1}^{n_0} \sum_{j=0}^{t_0} \left(h'\left(X_j^{(r)}\right) - \left\langle h'\left(X_{0,t_0}^{(r)}\right)\right\rangle\right)^2. \tag{4.32}$$

Note that B_{n_0,t_0} is the "*between the replication variance*" and W_{n_0,t_0} is the "*within the replication variance*". From these two variances, two estimates for the variance of $h'(X_{t_0})$ can be formed.

The first estimate for the variance of $h'(X_{t_0})$ is

$$\widehat{\text{var}}\left(h'(X_{t_0})\right) = \frac{t_0}{t_0+1}W_{n_0,t_0} + \frac{1}{t_0+1}B_{n_0,t_0} \tag{4.33}$$

which is an unbiased estimate for the variance of $h'(X_{t_0})$ under the assumption of stationarity but is an over-estimate for the variance of $h'(X_{t_0})$ under the assumption that the starting states are drawn from an overdispersed distribution [41].

The second estimate for the variance of $h'(X_{t_0})$ is W_{n_0,t_0}. While the realized states remain concentrated around the starting state, W_{n_0,t_0} under-estimates the variance of $h'(X_{t_0})$. The reason for this under-estimation is that the individual sequences may not have been run long enough to sample from the entire equilibrium distribution and, as a result, be less variable [41]. Gelman and Rubin [42] show that, as $t_0 \to \infty$,

$$W_{n_0,t_0} \to \text{var}_{\boldsymbol{\pi}}\left(h'\right) \tag{4.34}$$

and

$$\widehat{\text{var}}\left(h'(X_{t_0})\right) \to \text{var}_{\boldsymbol{\pi}}\left(h'\right). \tag{4.35}$$

Assuming that the initial starting state is drawn from an overdispersed distribution, Gelman [41] shows that the convergence of the Markov chain to its equilibrium distribution can be detected by monitoring the convergence of the sequence $\left(\sqrt{\widehat{R_j}}, j \in \{1,2,...,t_0\}\right)$, where

$$\sqrt{\widehat{R_j}} := \sqrt{\frac{\widehat{\text{var}}\left(h'(X_j)\right)}{W_{n_0,j}}}. \tag{4.36}$$

Gelman and Rubin [42] refer to the elements of the sequence $\left(\sqrt{\widehat{R_j}}, j \in \{1,2,...,t_0\}\right)$ as the *estimated potential scale reduction.*

For fixed positive integer values t_0, n_0, and $j \leq t_0$, $\sqrt{\widehat{R_j}}$ reduces to

$$\sqrt{\widehat{R_j}} = \sqrt{\frac{j}{j+1} + \frac{1}{j+1}\frac{B_{n_0,j}}{W_{n_0,j}}}. \tag{4.37}$$

Hence, as $t_0 \to \infty$ (that is, as the n_0 simulations begin converging to the equilibrium distribution), $\sqrt{\widehat{R_{t_0}}}$ will converge to 1. As $\sqrt{\widehat{R_{t_0}}}$ converges to 1, the replications of the Markov chain start overlapping and one replication is no longer statistically different from any other replication. Gelman [41] states that if there exists some $k < t_0$ such that the estimates $\sqrt{\widehat{R_j}}$, for all $k \leq j \leq t_0$, are less than 1.1 or 1.2, then the simulation can be

thought to have converged for the function h'. This value of k can be thought to be the upper limit of a warm-up interval for all n_0 replications. Hence, the estimate for τ_{exp} based on the estimated potential scale reduction is given by

$$\widehat{\tau}_{\text{exp},E} := k. \tag{4.38}$$

The estimated potential scale reduction $\sqrt{\widehat{R_j}}$ is a measure of how large the estimate $\widehat{\text{var}}\,(h'(X_j))$ is relative to the estimate $W_{n_0,j}$. Hence $\sqrt{\widehat{R_j}}$ is a measure of how large the "between the replication" variance is relative to the "within the replication" variance. Gelman's [41] convergence condition, that is requiring that $\sqrt{\widehat{R_j}} \leq 1.1$, for all $k \leq j \leq t_0$, can be interpreted as requiring that the estimated "between the replication" standard deviation is less than 10% larger than the estimated "within the replication" standard deviation.

The methods discussed thus far for estimating τ_{exp} can be used to determine whether a Markov Chain, and hence a composite Markov chain, has reached its stationary distribution. The final method for monitoring the convergence to the stationary distribution is presented next and is designed specifically to monitor the convergence of a CMC to its stationary distribution.

4.2.3 The Mixing of the Chains in a Composite Markov Chain

Warm-up analysis and estimated potential scale reduction can be used to estimate the time it takes the Markov chain $\mathcal{X}$, and hence a composite Markov chain based on $\mathcal{X}$, to reach its stationary distribution. In the case where $\mathcal{X}$ is an ergodic Markov chain, the following technique, based on [122], can be used to estimate the time it takes the corresponding CMC to converge to its equilibrium distribution. The technique is implemented as follows.

At time $t = 0$, attach a different colour to each of the M chains in a CMC. This colouring stays with the configuration until a swap between Chains i and j $(j \neq i)$ is accepted. When a swap between Chains i and j $(j \neq i)$ is accepted, the colours associated with Chains i and j $(j \neq i)$ are also swapped.

Suppose Chain 1 is coloured red. At some point, the red colour will be swapped into chain M, and then, at some later time, it will return to Chain 1. During the time it takes the colour red to travel from Chain 1 to Chain M and back, the state of Chain 1 will most likely be considerably different from its configuration than the previous time it was

coloured red. The ergodicity of the composite Markov chain implies that, for a run that is sufficiently long, each colour will spend an equal amount of time in each chain. More formally, if col(i,"a") is the proportion of the time chain i is labelled colour "a", then, for a fixed colour "a" and for all i such that $1 \leq i \leq M$, it is expected that $\text{col}(i,\text{“}a\text{”}) = \dfrac{1}{M}$.

From the data generated in Replication r, define

$$\widehat{\text{col}}_{\Bbbk}^{(r)}(i, \text{“}a\text{”}) := \frac{1}{t_0 - \Bbbk + 1} \sum_{t=0}^{t_0} \delta_{\text{“}a\text{”}} \left(\text{colour} \left(X_t^{(r)}(i) \right) \right) \left[1 - \mathscr{I}_{(0,\Bbbk]}(t) \right] \left[\mathscr{M}_n(t) \right], \tag{4.39}$$

where colour (X) is the colour of X, $\Bbbk$ is the number of data points to be excluded from the analysis,

$$\delta_{\text{“}a\text{”}}(\text{colour}(X)) := \begin{cases} 1, & \text{if colour}(X) = \text{“}a\text{”} \\ 0, & \text{otherwise} \end{cases}, \tag{4.40}$$

for any $A \subseteq \mathbb{R}$,

$$\mathscr{I}_A(x) := \begin{cases} 1, & \text{if } x \in A \\ 0, & \text{otherwise} \end{cases}, \tag{4.41}$$

and

$$\mathscr{M}_n(t) := \begin{cases} 1, & \text{if } t = 0 \,(\text{mod}\, n) \\ 0, & \text{otherwise} \end{cases}. \tag{4.42}$$

Then $\widehat{\text{col}}_{\Bbbk}^{(r)}(i,\text{“}a\text{”})$ can be used to estimate col(i,"a").

To determine whether the colourings appear uniformly amongst the M chains, a test based on the χ^2-Test for Goodness of Fit can be used. First, to implement a χ^2-Test for Goodness of Fit, a sample consisting of independent data points is required.

Assuming that an independent sample is available, to determine whether a fixed colour "a" appears uniformly in Chains 1 through M, a *χ^2-Test for Goodness of Fit* [147] can be used to test the null hypothesis $H_0 : \text{col}(1,\text{“}a\text{”}) = \text{col}(2,\text{“}a\text{”}) = ... = \text{col}(M,\text{“}a\text{”}) = \dfrac{1}{M}$ against the alternative that colour "a" does not appear uniformly in each of the M chains. If, at the significance level α, the null hypothesis is rejected, then colour "a" is not uniformly distributed amongst the M chains.

The above test is repeated for each of the M colours. Define the function p-value("a_i") to be the p-value associated with the χ^2-Test for Goodness of Fit for colour "a" in Chain i. Then the sample used for the M χ^2-Tests for Goodness of Fit is said to be *well-mixed* if

$$\sum_{i=1}^{M} \mathscr{I}_{(\alpha,1]}(p\text{-value}(\text{“}a_i\text{”})) \geq (1-\alpha)M. \tag{4.43}$$

In other words, a sample is said to be well-mixed if approximately $(1-\alpha)\cdot 100\%$ of the χ^2-Tests for Goodness of Fit for the distinct colours fail to reject the null hypothesis, that is there is not enough evidence to conclude that approximately (or more than) $(\alpha)\cdot 100\%$ of the colours are not uniformly distributed across the M chains. If it is concluded that the sample is well-mixed, then this is considered to support the facts that the equilibrium distribution has been reached and that the equilibrium distribution has been sampled for a sufficient length of time.

The sample is said to be *not well-mixed* if considerably greater than $\alpha\cdot 100\%$ of the χ^2-Tests for Goodness of Fit for the distinct colours reject the null hypothesis. A conclusion that the sample is not well-mixed supports the hypothesis that either the equilibrium distribution has not been reached or that the equilibrium distribution has been reached but there has not been sufficient sampling from it to make the burn-period statistically insignificant. To determine which of these two scenarios is affecting the sample, the above test can be repeated for different values of $\Bbbk$ to determine whether there is a value of $\Bbbk$ for which the sample drawn, after ignoring the first $\Bbbk$ data points, is well-mixed.

The determination of the number of data points $\Bbbk$ to burn may lead to a sample so small that the required condition for the χ^2-Test for Goodness of Fit (that is the expected cell frequencies must be at least five) is violated [85]. Koehler and Larntz [85] show that, for contingency tables with expected cell frequencies less than 5, if the total number of observations is at least ten, the number of categories (c) is at least three, and the square of the total number of observations is at least ten times the number of categories, then, under the null-hypothesis, the distribution of the test statistic is approximately chi-square with $c-1$ degrees of freedom. For the determination of being well-mixed, Koehler and Larntz's condition implies that the sample size must be greater than $\sqrt{10M}$, where M is the number of subchains in the composite Markov chain. If the value of $\Bbbk$ must be chosen so large that the number of independent data points resulting from ignoring the first $\Bbbk$ data points is smaller than $\sqrt{10M}$, then either the equilibrium distribution has not been sampled from a long enough period or perhaps the equilibrium distribution has not even been reached.

In Section 4.7.1 of this thesis τ_{exp} will be estimated using these three techniques (warm-up analysis, estimated potential scale reduction, and the mixing of the chains of a composite Markov chain). The purpose for estimating τ_{exp} via these three techniques is to be able

to compare the three estimates and check their consistency with each other. Note that the estimate for τ_{exp} from Replication r, based on:

1. a warm-up analysis will be denoted $\widehat{\tau}^{(r)}_{\text{exp},W}$;
2. an estimated potential scale reduction will be denoted $\widehat{\tau}^{(r)}_{\text{exp},E}$; and
3. the mixing of the chains of a CMC will be denoted $\widehat{\tau}^{(r)}_{\text{exp},C}$.

Then the estimate for τ_{exp} based on the sample data from all the replications and:

1. a warm-up analysis will be denoted $\widehat{\tau}_{\text{exp},W}$, where

$$\widehat{\tau}_{\text{exp},W} := \max_{r} \left\{ \widehat{\tau}^{(r)}_{\text{exp},W} \right\}; \tag{4.44}$$

2. an estimated potential scale reduction will be denoted $\widehat{\tau}_{\text{exp},E}$, where

$$\widehat{\tau}_{\text{exp},E} := \max_{r} \left\{ \widehat{\tau}^{(r)}_{\text{exp},E} \right\}; \tag{4.45}$$

and

3. the mixing of the chains of a CMC will be denoted $\widehat{\tau}_{\text{exp},C}$, where

$$\widehat{\tau}_{\text{exp},C} := \max_{r} \left\{ \widehat{\tau}^{(r)}_{\text{exp},C} \right\}. \tag{4.46}$$

Then the estimate for τ_{exp} that will be used for this work will be denoted $\widehat{\tau}_{\text{exp}}$ where

$$\widehat{\tau}_{\text{exp}} := \max \left\{ \widehat{\tau}_{\text{exp},W}, \widehat{\tau}_{\text{exp},E}, \widehat{\tau}_{\text{exp},C} \right\}. \tag{4.47}$$

The reason that the maximum of the estimates $\widehat{\tau}^{(r)}_{\text{exp},W}$, $\widehat{\tau}^{(r)}_{\text{exp},E}$, and $\widehat{\tau}^{(r)}_{\text{exp},C}$ over the ten replications is used for $\widehat{\tau}_{\text{exp}}$ is so that, for each replication, all the data generated in each of the replications after $\widehat{\tau}_{\text{exp}}$ Θ-BFACF moves in parallel can be assumed to be from the equilibrium distribution. Because the distributions of $\widehat{\tau}^{(r)}_{\text{exp},W}, \widehat{\tau}^{(r)}_{\text{exp},E}$, and $\widehat{\tau}^{(r)}_{\text{exp},C}$ are unknown, the distribution of $\widehat{\tau}_{\text{exp}}$ is also unknown. Therefore a $(1-\alpha)\cdot 100\%$ confidence interval for τ_{exp} cannot be computed based on the point estimates $\widehat{\tau}_{\text{exp},W}$, $\widehat{\tau}_{\text{exp},E}$, $\widehat{\tau}_{\text{exp},C}$, or $\widehat{\tau}_{\text{exp}}$.

In order to gain some insight into how $\widehat{\tau}_{\text{exp},W}$ and $\widehat{\tau}_{\text{exp},C}$ vary across the replications,

$$\bar{\tau}_{\text{exp},W} := \frac{1}{10}\sum_{r=1}^{10} \widehat{\tau}^{(r)}_{\text{exp},W} \tag{4.48}$$

and

$$\bar{\tau}_{\text{exp},C} := \frac{1}{10}\sum_{r=1}^{10} \widehat{\tau}^{(r)}_{\text{exp},C}, \tag{4.49}$$

and the standard errors of the samples used to compute $\bar{\tau}_{\text{exp},W}$ and $\bar{\tau}_{\text{exp},C}$ will be calculated. Note that because the estimated potential scale reduction technique uses all the replications, $\bar{\tau}^{(r)}_{\text{exp},E}$ is the same value for each replication, that is $\bar{\tau}_{\text{exp},E} = \widehat{\tau}^{(r)}_{\text{exp},E}$, for each $r \in \{1, 2, ..., n_0\}$. Therefore no further information is gained by calculating the average of the values $\widehat{\tau}^{(r)}_{\text{exp},E}$ across the ten replications. Also note that because the distributions of $\widehat{\tau}^{(r)}_{\text{exp},W}$ and $\widehat{\tau}^{(r)}_{\text{exp},C}$ are unknown, the distributions of $\bar{\tau}_{\text{exp},W}$, $\bar{\tau}_{\text{exp},E}$, and $\bar{\tau}_{\text{exp},C}$ are also unknown. Because the distributions of $\bar{\tau}_{\text{exp},W}$, $\bar{\tau}_{\text{exp},E}$, and $\bar{\tau}_{\text{exp},C}$ are unknown and because $\bar{\tau}_{\text{exp},\bullet}$ is based on fewer than 30 observations, it is not known whether the Central Limit Theorem applies, $(1-\alpha)\cdot 100\%$ confidence intervals for τ_{exp} cannot be computed based on $\bar{\tau}_{\text{exp},W}$, $\bar{\tau}_{\text{exp},E}$, and $\bar{\tau}_{\text{exp},C}$. At least the sample standard error will provide some information about how $\widehat{\tau}^{(r)}_{\text{exp},W}$ and $\widehat{\tau}^{(r)}_{\text{exp},C}$ are dispersed. For example, if it is assumed that the Central Limit Theorem holds for Equations (4.48) and (4.49), then a $(1-\alpha)\cdot 100\%$ confidence interval for $\tau_{\text{exp},W}$ and $\tau_{\text{exp},C}$ can be obtained from the estimated standard errors reported.

Because $\tau_{\text{int}}(f)$ and τ_{int} are quantities defined on the stationary distribution, once an estimate for the amount of time it takes the process to equilibrate has been established, $\tau_{\text{int}}(f)$ and τ_{int} can be estimated. The different techniques used in this work for estimating $\tau_{\text{int}}(f)$ and τ_{int} are discussed next.

4.3 Estimating $\tau_{\text{int}}(f)$ and τ_{int}

There are several techniques for estimating $\tau_{\text{int}}(f)$, each having different degrees of computational complexity. The three techniques used in this work will be presented in the order of least computationally intensive to the most computationally intensive. All three techniques will be used to estimate $\tau_{\text{int}}(f)$ and τ_{int} in order to compare the resulting estimates. This comparison is provided at the end of Section 4.7.2.

Because estimating $\tau_{\text{int}}(f)$ and τ_{int} requires data drawn from the equilibrium distribution, first assume that k is an estimate for τ_{exp}. Now define the new Markov chain $\mathcal{X}' := \left\{X'_j, j \in T'\right\}$, where $X'_j := X_{j+k}$ and $T' := \{0, 1, ..., t_0 - k\}$. Then all three techniques for estimating $\tau_{\text{int}}(f)$ use a realization of $\mathcal{X}'$.

The first technique, that is the technique that is presented next, uses an estimate for τ_{exp} to estimate $\tau_{\text{int}}(f)$ [142]. The second technique, that is the technique based on blocking the data [35], is presented in Section 4.3.2. The final technique, that is the technique based on a time series analysis [142], is presented in Section 4.3.3.

4.3.1 Via the Time to Reach π

The first technique that can be used to estimate $\tau_{\text{int}}(f)$ relies solely on an estimated for τ_{exp}. Hence the technique adds no additional CPU overhead to the data analysis because, by the time $\tau_{\text{int}}(f)$ is to be estimated, an estimate for τ_{exp} is already available. In [142] it is discussed that the estimated upper limit of the interval $[0, \hat{k}]$, which is an estimate for $\tau_{\text{exp}}(h')$, is approximately $20\tau_{\text{int}}(h')$, but this is very approximate. Quite often $\tau_{\text{int}}(h')$ has the same order of magnitude as $\tau_{\text{exp}}(h')$; by setting $\tau_{\text{exp}}(h') = 20\tau_{\text{int}}(h')$, more of the initial data (than possibly necessary) would be discarded, a big problem if the generation of the data is very costly in computer time. The estimated value of τ_{exp} can be used as a basis for estimating $\tau_{\text{int}}(f)$ (the autocorrelation time for the observable function f) of the experiment, because it is believed that [142]

$$20\tau_{\text{int}}(f) \approx \tau_{\text{exp}}(f). \tag{4.50}$$

Because $\tau_{\text{exp}} = \max_{f \in \mathscr{H}} \tau_{\text{exp}}(f)$, using

$$\tau_{\text{int}}(f) \approx \tau_{\text{exp}}/20 := k/20 \tag{4.51}$$

provides an estimate for $\tau_{\text{int}}(f)$. Estimates based on Relation (4.51) provide estimates for $\tau_{\text{int}}(f)$ that are generally larger than the actual value of $\tau_{\text{int}}(f)$ [142] and hence lead to the conclusion that there is less essentially independent data than there actually is. This under-estimate for the amount of essentially independent data results in the associated $(1-\alpha)\cdot 100\%$ confidence interval of any estimate based on a realization of $\mathcal{X}'$ being wider than the $(1-\alpha)\cdot 100\%$ confidence interval computed using the actual value of the integrated autocorrelation time. To overcome the possible conservative nature of this estimate for

$\tau_{\text{int}}(f)$, the next technique presented involves an actual analysis of $\mathcal{X}'$ via "batch means" [35].

4.3.2 Via a Batch Means Analysis

The discussion now turns to the "batch means technique", cf. [35]. Suppose $F_i = f(X'_i)$ for all $i = 0, 1, ..., t_0 - k$. For fixed natural numbers b and l such that $bl \leq t_0 - k$, consider a partition of the data from a single sample path of length $t_0 - k$ into l non-overlapping, consecutive sequences for which each sequence's length is b (referred to as the *batch size*); that is batch 1 consists of the data points $F_1, \ldots, F_b$; batch 2 consists of the data points $F_{b+1}, \ldots, F_{2b}$; ...; and batch l consists of data points $F_{(l-1)b+1}, \ldots, F_{lb}$. Now define

$$Y_{j,b} := b^{-1} \sum_{i=1}^{b} F_{(j-1)b+i}, \qquad 1 \leq j \leq l, \tag{4.52}$$

$$\langle F \rangle_{l,b} := l^{-1} \sum_{j=1}^{l} Y_{j,b} \tag{4.53}$$

and

$$s^2(\langle F \rangle_{l,b}) := (l-1)^{-1} \sum_{j=1}^{l} (Y_{j,b} - \langle F \rangle_{l,b})^2. \tag{4.54}$$

Now if there exist natural numbers b and l such that $lb \leq t_0 - k$, and such that the $Y_{j,b}$, for all $j = 1, \ldots, l$, are statistically independent according to an appropriate test for independence, then b is referred to as an *independent batch size.* The *Test for Independence* [35] (used in this work) is as follows:

Algorithm 4.3.1 (Test for Independence, p. 562, [35]) *Define the null hypothesis to be* $H_0 : \Psi_{l,b} = 0$, *where*

$$\Psi_{l,b} := 1 - \frac{\sum_{i=1}^{l-1} (Y_{i,b} - Y_{(i+1),b})^2}{\sum_{i=1}^{l} \left(Y_{i,b} - \langle F \rangle_t\right)^2}, \tag{4.55}$$

for $Y_{j,b}$ *as defined by Equation (4.52) and* $\langle F \rangle_t$ *as defined by Equation (4.9). Then* H_0 *is not rejected when*

$$\Psi_{l,b} \leq \left[\Phi^{-1}(1-\alpha)\right] \sqrt{\frac{l-2}{l^2-1}}, \tag{4.56}$$

where $\Phi^{-1}(1-\alpha)$ *is the* $(1-\alpha)$ *critical value of the standard normal distribution as determined from*

$$\sqrt{2\pi} \int_{-\infty}^{\Phi^{-1}(1-\alpha)} e^{-z^2/2} dz = 1 - \alpha. \tag{4.57}$$

If the null hypothesis H_0 *is not rejected, then the batches are considered to be independent.*

Assuming equality in Relation (4.12), that is,

$$\mathrm{var}_{\boldsymbol{\pi}}\left(\langle f\rangle_n\right) = \frac{2\gamma_f\left(0\right)}{n}\tau_{\mathrm{int}}(f), \tag{4.58}$$

then an estimate for $\tau_{\mathrm{int}}(f)$ is given by

$$\widehat{\tau}_{\mathrm{int}}(f) = \frac{b}{2}\frac{\hat{\gamma}_f\left(0\right)}{s^2(\langle F\rangle_{l,b})}. \tag{4.59}$$

In other words, $\tau_{\mathrm{int}}(f)$ can be estimated as a function of the batch size b. In fact, if the sample drawn from the equilibrium distribution is sufficiently large, then $\hat{\gamma}_f\left(0\right) \approx s^2(\langle F\rangle_{l,b})$ as both $\hat{\gamma}_f\left(0\right)$ and $s^2(\langle F\rangle_{l,b})$ are both estimates for $\mathrm{var}_{\boldsymbol{\pi}}\left(f\right)$. Hence

$$\widehat{\tau}_{\mathrm{int}}(f) \approx \frac{b}{2}. \tag{4.60}$$

Therefore, if sampling from the equilibrium distribution, $\tau_{\mathrm{int}}(f)$ can be estimated as half the batch size b.

Fishman [35] presents algorithms for determining b and l. However, if the data is batched according to the batch size calculated from Equation (4.60) using the estimate for $\tau_{\mathrm{int}}(f)$ determined by the technique in Section 4.3.1, and if this batched data passes the Test for Independence, then, up to the significance level α used in the Test for Independence, the data sampled every b time steps apart will be essentially independent.

If, in addition to needing to determine the amount of essentially independent data that has been generated, the correlation structure is of interest, then the approach presented next is the technique that should be used to estimate $\tau_{\mathrm{int}}(f)$.

4.3.3 Via a Series/Windowing Approach

The third, and most computationally intensive, method for estimating $\tau_{\mathrm{int}}(f)$ is based on computing the estimate directly using Equation (4.8) and the sample data. Two problems quickly arise. The first problem is that often $\mathrm{E}_{\boldsymbol{\pi}}(f)$ is unknown. The second problem results from the fact that $\tau_{\mathrm{int}}(f)$, as given by Equation (4.8), requires a sample of infinite length.

The first problem can be solved by using the sample mean $\langle f\rangle_n$, as defined by Equation (4.9), as an estimator of $\mathrm{E}_{\boldsymbol{\pi}}(f)$. From the definition of $\tau_{\mathrm{int}}(f)$, the logical choices for estimators of $\gamma_f(t)$, $\rho_f(t)$, and $\tau_{\mathrm{int}}(f)$, when $\mathrm{E}_{\boldsymbol{\pi}}(f)$ is unknown, are respectively

$$\widehat{\gamma}_f(t) := \frac{1}{n-|t|}\sum_{i=1}^{n-|t|}(F_i - \langle f\rangle_n)(F_{i+|t|} - \langle f\rangle_n), \tag{4.61}$$

$$\widehat{\rho}_f(t) = \frac{\widehat{\gamma}_f(t)}{\widehat{\gamma}_f(0)}, \tag{4.62}$$

and

$$\widehat{\tau}_{\text{int}}(f) = \frac{1}{2} \sum_{t=-(n-1)}^{n-1} \widehat{\rho}_f(t). \tag{4.63}$$

In [4], it was shown that $\widehat{\gamma}_f(t)$ is a biased estimator of $\gamma_f(t)$ and the bias is of order $1/n$, that is

$$\begin{aligned}
\mathrm{E}_{\boldsymbol{\pi}}\left(\widehat{\gamma}_f(t)\right) = \frac{1}{n-|t|} \sum_{i=1}^{n-|t|} & \left(\mathrm{E}_{\boldsymbol{\pi}}\left(F_i F_{i+|t|}\right)\right. \\
& \left. -\frac{1}{n^2} \sum_{j,m=1}^{n} \left(\mathrm{E}_{\boldsymbol{\pi}}\left(F_i F_j\right) + \mathrm{E}_{\boldsymbol{\pi}}\left(F_j F_{i+|t|}\right) - \mathrm{E}_{\boldsymbol{\pi}}\left(F_j F_m\right)\right)\right) \\
= \gamma_f(t) & \\
- \frac{1}{n-|t|} & \left[\sum_{i=1}^{n-|t|} \left(\frac{1}{n^2} \sum_{j,m=1}^{n} \left(\mathrm{E}_{\boldsymbol{\pi}}\left(F_i F_j\right) + \mathrm{E}_{\boldsymbol{\pi}}\left(F_j F_{i+|t|}\right) - \mathrm{E}_{\boldsymbol{\pi}}\left(F_j F_m\right)\right)\right)\right. \\
& \left. - \left(\mathrm{E}_{\boldsymbol{\pi}}(f)\right)^2\right].
\end{aligned} \tag{4.64}$$

Because $\widehat{\rho}_f(t)$ is a function of $\widehat{\gamma}_f(t)$ and $\widehat{\gamma}_f(t)$ is a biased estimator of $\gamma_f(t)$, it follows that $\widehat{\rho}_f(t)$ and $\widehat{\tau}_{\text{int}}(f)$ will respectively be biased estimators of $\rho_f(t)$ and $\tau_{\text{int}}(f)$ of order $1/n$. Consequently, when trying to estimate $\tau_{\text{int}}(f)$ by using the sample mean $\langle f \rangle_n$ as an estimator of $\mathrm{E}_{\boldsymbol{\pi}}(f)$, the bias in the estimator $\widehat{\tau}_{\text{int}}(f)$ becomes less and less significant as the sample size n increases.

The second problem is more severe because it is not possible to generate an infinite length sample path. One solution, for some large sample size n, is to estimate $\tau_{\text{int}}(f)$ by

$$\widehat{\tau}_{\text{int}}(f) = \frac{1}{2} \sum_{t=-(n-1)}^{n-1} \widehat{\rho}_f(t). \tag{4.65}$$

However this is not a good estimator of $\tau_{\text{int}}(f)$ in the sense that the variance of the estimator defined by Equation (4.65) does not tend to zero as the sample size n tends to infinity [142].

One solution to this problem is to use a "windowing" approach, that is to truncate the sum in Equation (4.65) at a point which retains most of the "signal" and discards most of the "noise". In other words, to truncate the sum in Equation (4.65) at the values $\pm m$ such

that for all t where $m < t \leq n-1$, $\widehat{\rho}_f(t)$ is distributed as a $N(0, t^{-1/2})$ random variable. To do this, first rewrite Equation (4.65) as

$$\widehat{\tau}_{\text{int}}(f) = \frac{1}{2} \sum_{t=-(n-1)}^{n-1} \lambda(t)\widehat{\rho}_f(t), \tag{4.66}$$

where

$$\lambda(t) = \begin{cases} 1, & \text{if } |t| \leq \tau_{\text{int}}(f) \\ 0, & \text{otherwise,} \end{cases} \tag{4.67}$$

and $\lambda(t)$ is referred to as a *window*. Because this definition of $\lambda(t)$ relies on knowing $\tau_{\text{int}}(f)$, it is not a practical choice for a window.

A more practical solution for implementing the aforementioned "windowing" approach is to define $\lambda(t)$ by

$$\lambda(t) = \begin{cases} 1, & \text{if } |t| \leq W \\ 0, & \text{if } |t| > W, \end{cases} \tag{4.68}$$

where W is chosen in such a manner that

$$c\widehat{\tau}_{\text{int}}(f) \leq W \leq n, \tag{4.69}$$

for some constant $c > 0$.

With $\lambda(t)$ defined as in Equation (4.68), Equation (4.66) becomes

$$\widehat{\tau}_{\text{int}}(f) = \frac{1}{2} \sum_{t=-W}^{W} \widehat{\rho}_f(t). \tag{4.70}$$

An estimate for the variance of $\widehat{\tau}_{\text{int}}(f)$, valid for $\widehat{\tau}_{\text{int}}(f) \ll W \ll n$, where n is the run length, is [142]

$$\text{var}(\widehat{\tau}_{\text{int}}(f)) = \frac{2(2W+1)}{n} \tau^2_{\text{int}}(f). \tag{4.71}$$

The c in Inequality (4.69) is chosen to be 4 if $\rho_f(t)$ is approximately a pure exponential, since, in this case, the variance of $\rho_f(t)$, denoted $\text{var}(\rho_f(t))$, is of the order e^{-4} which is close to 2%. However, if $\rho_f(t)$ decays much more slowly than a pure exponential, in order to keep the magnitude of $\text{var}(\rho_f(t))$ around the 2% level, c must be increased. Since estimates for $\tau_{\text{int}}(f)$ are increasing as a function of c [142], as c tends to infinity, estimates for $\tau_{\text{int}}(f)$ may double or even triple. Hence, any estimate for $\tau_{\text{int}}(f)$ using this approach is an underestimate of the true value of $\tau_{\text{int}}(f)$.

Underestimates of c lead to the conclusion that there is more essentially independent data than there actually is. This leads to smaller confidence intervals which imply that

the estimates are better than they really are. Another drawback of the series/windowing approach is that a significant amount of physical storage space is required to store the data and calculations required to implement the method are very CPU intensive. Samples could be taken less frequently and "fast Fourier transform" techniques, cf. [131], could be used to shorten the total length of time necessary to compute an estimate for $\tau_{\text{int}}(f)$, but possibly at the cost of losing valuable information. Based on the experience gained via the composite Markov chain Monte Carlo analysis of this thesis, it is concluded that, unless estimates for the autocorrelations associated with different lag times are needed, in most circumstances the batch means technique for estimating $\tau_{\text{int}}(f)$ and τ_{int} suffices.

In Section 4.7.2 of this thesis, for the sake of comparison, all three methods for estimating τ_{int} will be used. The estimate for τ_{int} from Replication r, based on:

1. $\widehat{\tau}_{\text{exp}}^{(r)}$, will be denoted $\widehat{\tau}_{\text{int},W}^{(r)}$;
2. a batch means analysis with $\Bbbk$ burned data points, will be denoted $\widehat{\tau}_{\text{int},B(\Bbbk)}^{(r)}$; and
3. a windowing/series analysis with $\Bbbk$ burned data points, will be denoted $\widehat{\tau}_{\text{int},S(\Bbbk)}^{(r)}$.

Then the estimate for τ_{int} computed across the replications, based on:

1. $\widehat{\tau}_{\text{exp}}^{(r)}$, will be denoted $\widehat{\tau}_{\text{int},W}$, where

$$\widehat{\tau}_{\text{int},W} := \max_{r} \left\{ \widehat{\tau}_{\text{int},W}^{(r)} \right\}; \tag{4.72}$$

2. a batch means analysis with $\Bbbk$ burned data points, will be $\widehat{\tau}_{\text{int},B}$, where

$$\widehat{\tau}_{\text{int},B} := \max_{\Bbbk} \left\{ \widehat{\tau}_{\text{int},B(\Bbbk)} \right\} \tag{4.73}$$

and

$$\widehat{\tau}_{\text{int},B(\Bbbk)} := \max_{r} \left\{ \widehat{\tau}_{\text{int},B(\Bbbk)}^{(r)} \right\}; \tag{4.74}$$

and

3. a windowing/series analysis with k burned data points, will be denoted $\widehat{\tau}_{\text{int},S}$, where

$$\widehat{\tau}_{\text{int},S} := \max_{\Bbbk} \left\{ \widehat{\tau}_{\text{int},S(\Bbbk)} \right\} \tag{4.75}$$

and

$$\widehat{\tau}_{\text{int},S(\Bbbk)} := \max_{r} \left\{ \widehat{\tau}_{\text{int},S(\Bbbk)}^{(r)} \right\}. \tag{4.76}$$

Finally the estimate for τ_{int} that will be used for this work will be denoted $\widehat{\tau}_{\text{int}}$, where

$$\widehat{\tau}_{\text{int}} := \max\left\{\widehat{\tau}_{\text{int},W}, \widehat{\tau}_{\text{int},B}, \widehat{\tau}_{\text{int},S}\right\}. \tag{4.77}$$

The reason the estimator $\widehat{\tau}_{\text{int},W}$ is defined as the maximum over the estimates $\widehat{\tau}^{(r)}_{\text{int},W}$, for $r \in \{1, 2, .., 10\}$, is so that the assumption that data points every $2\widehat{\tau}_{\text{int},W}$ time steps apart will be essentially independent will hold for each of the ten replications. For the same reason, $\widehat{\tau}_{\text{int},B}$ and $\widehat{\tau}_{\text{int},S}$ are defined similarly in terms of a maximum over all replications. To err on the side of conservatism, $\widehat{\tau}_{\text{int}}$ is defined in terms of the maximum of $\widehat{\tau}_{\text{int},W}, \widehat{\tau}_{\text{int},B}$, and $\widehat{\tau}_{\text{int},S}$.

Because the distributions of $\widehat{\tau}^{(r)}_{\text{int},W}, \widehat{\tau}^{(r)}_{\text{int},B(\mathbb{k})}$, and $\widehat{\tau}^{(r)}_{\text{int},S(\mathbb{k})}$ are unknown, $(1-\alpha)\cdot 100\%$ confidence intervals for τ_{int} based on the point estimates $\widehat{\tau}_{\text{int},W}, \widehat{\tau}_{\text{int},B(\mathbb{k})}$, and $\widehat{\tau}_{\text{int},S(\mathbb{k})}$ cannot be computed. In order to gain some insight into how $\widehat{\tau}_{\text{int},W}, \widehat{\tau}_{\text{int},B(\mathbb{k})}$, and $\widehat{\tau}_{\text{int},S(\mathbb{k})}$ vary across the replications,

$$\bar{\tau}_{\text{int},W} := \frac{1}{10}\sum_{r=1}^{10} \widehat{\tau}^{(r)}_{\text{int},W}, \tag{4.78}$$

$$\bar{\tau}_{\text{int},B(\mathbb{k})} := \frac{1}{10}\sum_{r=1}^{10} \widehat{\tau}^{(r)}_{\text{int},B(\mathbb{k})}, \tag{4.79}$$

and

$$\bar{\tau}_{\text{int},S(\mathbb{k})} := \frac{1}{10}\sum_{r=1}^{10} \widehat{\tau}^{(r)}_{\text{int},S(\mathbb{k})}, \tag{4.80}$$

and the standard error of the samples used to compute $\bar{\tau}_{\text{int},W}$, $\bar{\tau}_{\text{int},B(\mathbb{k})}$, and $\bar{\tau}_{\text{int},S(\mathbb{k})}$ will be calculated. Also note that because the distributions of $\bar{\tau}_{\text{int},W}$, $\bar{\tau}_{\text{int},B(\mathbb{k})}$, and $\bar{\tau}_{\text{int},S(\mathbb{k})}$ are unknown, and $\bar{\tau}_{\text{int},\bullet}$ is based on fewer than 30 observations, whether the Central Limit Theorem can be applied is unknown. Therefore $(1-\alpha)\cdot 100\%$ confidence intervals for τ_{int} cannot be computed based on $\bar{\tau}_{\text{int},W}$, $\bar{\tau}_{\text{int},B(\mathbb{k})}$, and $\bar{\tau}_{\text{int},S(\mathbb{k})}$. Therefore the best information available for determining how $\widehat{\tau}_{\text{int},W}, \widehat{\tau}_{\text{int},B(\mathbb{k})}$, and $\widehat{\tau}_{\text{int},S(\mathbb{k})}$ vary across the replications is the standard error of $\bar{\tau}_{\text{int},W}$, $\bar{\tau}_{\text{int},B(\mathbb{k})}$, and $\bar{\tau}_{\text{int},S(\mathbb{k})}$ respectively.

Assuming that τ_{exp} and τ_{int} have been estimated, what should be done with the data that was generated in the interval $[0, \widehat{\tau}_{\text{exp}}]$? This question is addressed in the next section.

4.4 To Burn or not to Burn?

Warm-up analysis, estimated potential scale reduction, and the mixing of the chains in a CMC provide three methods for estimating $\tau_{\text{exp}} = k$, the number of time steps that

a simulation must be run to ensure that, for all i such that $k < i \leq t_0$, X_0 and X_i are essentially independent. (Note that t_0 is the total number of steps for which the simulation is to be run). Because the data that is generated during the warm-up interval $[0, k]$ is not from the desired equilibrium distribution, what should be done with this "contaminated" data?

In [142], Sokal defines the *burn-time of an observable* f to be the period in which the data generated does not reflect the stationary distribution. The error resulting from estimates based on data that includes data generated during the burn-time is defined to be the *bias of the simulation*. Consequently the burn-time of f can be thought to be the number of time-steps in the simulation from which the data collected (with respect to f) should be ignored (discarded). A data point collected during the burn-time is referred to as a *burned data point*.

Valuable information, such as estimates for $\tau_{\text{exp}}(f)$ and hence $\tau_{\text{int}}(f)$, can be obtained from the data which lies in the warm-up interval. If storage space and CPU time are not an issue, then the data from the warm-up period should be collected. The problem now becomes "what data should be used in estimating the parameters of interest?".

Sokal [142] argues that if τ_{exp} is a significant portion of the total run time, then the initialization bias introduced will lead to a significant error in one's results and, therefore, the data generated during the warm-up period should be discarded. If τ_{exp} represents an insignificant fraction of the total run time (Sokal recommends $< 5\%$), then the data generated in the warm-up period can be included in any estimates, as the statistical error of the estimate will be affected minimally. In [44], Geyer presents arguments that support the viewpoint discussed by Sokal. Both Geyer and Sokal recommend that the simulation should be run for a period of time long enough so that the warm-up interval introduces little statistical error. Therefore the issue of whether some or all of the data generated should be used to estimate a quantity is really problem specific.

Also, because sampling at every time step is not usually practical, the data available to estimate τ_{exp} is a subset of states observed throughout the simulation. Because the observed data points in this subset are used to estimate τ_{exp}, it is more practical to refer to the number of data points that need to be burned in the subset than it is to refer to the number of time steps in which the data generated is not from the equilibrium distribution.

Recall that $\mathbb{k}$ is the number of data points that must be discarded from the set of

sampled data. Then assuming the number of data points $\Bbbk$ has been determined, how can, at least preliminarily, the data generated be checked for consistency? How the data is expected to behave is discussed in the next section.

4.5 How Should We Behave?

Recall from Section 1.4 that several of the properties of the Local Strand Passage Model can be obtained from derivatives of the logarithm of the model's partition function. Now recall from Section 2.2.2 that for unknotted Θ-SAPs, the partition function for the Local Strand Passage Model is, for a fixed positive even integer M, a fixed positive integer q, and a fixed real value z, given by

$$\breve{Q}(q,z,M) = \sum_{n \geq M/2} (2n-6)\,(2n)^{q-1}\, p^{\Theta}_{2n}(\phi) z^{2n}. \tag{4.81}$$

Hence, in order to study and understand the behaviour of $\breve{Q}(q,z,M)$, it is important to investigate how it "behaves" as $M \to \infty$ and $\log(z) \to -\kappa_\phi$. This is one of the studies presented in this section.

The second function studied in this section is the expected value of the mean-square radius of gyration of a randomly chosen polygon in $\mathscr{P}^{\Theta}(\phi)$ selected according to the probability mass function $\breve{\boldsymbol{\pi}}_z(q,M)$ defined by Equation (2.63) with a fixed positive even integer M, a fixed positive integer q, and a fixed real value z:

$$r^2_{\breve{\boldsymbol{\pi}}_z(q,M)}\left(\mathscr{P}^{\Theta}\right) := \left[\breve{Q}(q,z,M)\right]^{-1} \sum_{m=M/2} r^2\left(\mathscr{P}^{\Theta}_{2m}\right) \breve{\pi}_{2n|M}(q,z), \tag{4.82}$$

where $r^2\left(\mathscr{P}^{\Theta}_{2m}\right)$ is defined by Equation (1.57) and is the expected mean-square radius of gyration of a random selected $(2m)$-edge polygon in $\mathscr{P}^{\Theta}(\phi)$.

In order to study $\breve{Q}(q,z,M)$ and $r^2_{\breve{\boldsymbol{\pi}}_z(q,M)}\left(\mathscr{P}^{\Theta}\right)$, it is important to know how both depend on M and z. More specifically, it is important to know how $\breve{Q}(q,z,M)$ and $r^2_{\breve{\boldsymbol{\pi}}_z(q,M)}\left(\mathscr{P}^{\Theta}\right)$ behave as $M \to \infty$ and $\log(z) \to -\kappa_\phi$. These limiting behaviours are investigated in the next two subsections, respectively.

4.5.1 How Does $\breve{Q}(q,z,M)$ Behave as $M \to \infty$ and $\log(z) \to -\kappa_\phi$?

If Conjecture 2.2.4 from Section 2.2.2 is true, then, for $M = N_{\min}$ sufficiently large, there exists $A^{\Theta}_{\phi}, \alpha^{\Theta}_{\phi}, q, \kappa_\phi, B^{\Theta}_{\phi}, -\Delta^{\Theta}_{\phi}$ and a function g_ϕ (with $g_\phi(n) = O(n^{-1})$, such that, for

$\beta := \log(z)$,

$$\breve{Q}(q, z, N_{\min}) = \sum_{n \geq N_{\min}/2} \mathcal{F}_{2n}(A_\phi^\Theta, \alpha_\phi^\Theta + q, \kappa_\phi + \beta, B_\phi^\Theta, -\Delta_\phi^\Theta, g_\phi). \tag{4.83}$$

Hence, in order to study and better understand the behaviour of $\breve{Q}(q, z, N_{\min})$ as $N_{\min} \to \infty$ and $\beta \to -\kappa_\phi$, the behaviour of the right hand side of Equation (4.83) needs to be explored as $N_{\min} \to \infty$ and $\beta \to -\kappa_\phi$. To this end, define

$$Q\left(\gamma_1, \gamma_2, \gamma_3, m, a, b, g\right) := a \sum_{\substack{n \geq m \\ n \text{ even}}} n^{\gamma_1} e^{n\gamma_2} \left(1 + bn^{\gamma_3} + g(n)\right), \tag{4.84}$$

where, as $n \to \infty$,

$$g(n) = O\left(n^{-1}\right). \tag{4.85}$$

Before continuing, the following result from Complex Analysis is needed.

Lemma 4.5.1 (Darboux [25]) *If $t \notin \{0, 1, 2, 3, ...\}$, then*

$$[z^n](1 - z)^t \sim \frac{n^{-t-1}}{\Gamma(-t)}, \tag{4.86}$$

where $[z^n](1-z)^t$ is the coefficient of the term z^n in the power series expansion of $(1-z)^t$.

For $z = e^{\gamma_2}$, the coefficient of z^n in $Q\left(\gamma_1, \gamma_2, \gamma_3, m, a, b, g\right)$ is asymptotic (as $n \to \infty$) to

$$[z^n]\, Q\left(\gamma_1, \gamma_2, \gamma_3, m, a, b, g\right) \sim an^{\gamma_1} + abn^{\gamma_1 + \gamma_3}. \tag{4.87}$$

By Equation (4.86) the coefficient of z^n in $Q\left(\gamma_1, \gamma_2, \gamma_3, m, a, b, g\right)$ for $z = e^{\gamma_2}$ is asymptotically (as $n \to \infty$) equal to:

$$[z^n]\, Q\left(\gamma_1, \gamma_2, \gamma_3, m, a, b, g\right) \tag{4.88}$$

$$\sim [z^n] \left[a\Gamma(\gamma_1 + 1)(1 - e^{\gamma_2})^{-\gamma_1 - 1}\right] + [z^n] \left[ab\Gamma(\gamma_1 + \gamma_3 + 1)(1 - e^{\gamma_2})^{-1-\gamma_1-\gamma_3}\right]. \tag{4.89}$$

Hence, for m even and sufficiently large, $Q\left(\gamma_1, \gamma_2, \gamma_3, m, a, b, g\right)$ (given by Equation (4.83)) can be approximated by

$$\begin{aligned} &Q\left(\gamma_1, \gamma_2, \gamma_3, m, a, b, g\right) \\ &\sim a\Gamma(\gamma_1 + 1)(1 - e^{\gamma_2})^{-1-\gamma_1} \\ &+ ab\Gamma(\gamma_1 + \gamma_3 + 1)(1 - e^{\gamma_2^*})^{-1-\gamma_1-\gamma_3} \qquad (4.90) \\ &= a'(1 - e^{\gamma_2})^{-1-\gamma_1} \left[1 + a''(1 - e^{\gamma_2})^{-\gamma_3}\right], \qquad (4.91) \end{aligned}$$

where $a' = a\Gamma(\gamma_1 + 1)$ and $a'' = \dfrac{b\Gamma(\gamma_1 + \gamma_3 + 1)}{\Gamma(\gamma_1 + 1)}$.

Now define

$$\mathrm{E}\left(\gamma_1, \gamma_2, \gamma_3, m, a, b, g\right) := \frac{\partial}{\partial \gamma_2}\left(\log Q\left(\gamma_1, \gamma_2, \gamma_3, m, a, b, g\right)\right). \tag{4.92}$$

Hence, for m even and sufficiently large, by applying logarithms to Equation (4.91) and differentiating the result with respect to γ_2 yields the following asymptotic form for $\mathrm{E}\left(\gamma_1, \gamma_2, \gamma_3, m, a, b, g\right)$:

$$\mathrm{E}\left(\gamma_1, \gamma_2, \gamma_3, m, a, b, g\right) \sim \frac{[\gamma_1 + 1]e^{\gamma_2}}{1 - e^{\gamma_2}}\left[1 + \frac{\gamma_3 a''(1 - e^{\gamma_2})^{-\gamma_3}}{[\gamma_1 + 1][1 + a''(1 - e^{\gamma_2})^{-\gamma_3}]}\right]. \tag{4.93}$$

For fixed m sufficiently large such that Approximation (4.93) is valid, note that, as $1 - e^{\gamma_2} \to 0$, that is, as $\gamma_2 \to 0$,

$$\frac{a''(1 - e^{\gamma_2})^{-\gamma_3}}{[1 + a''(1 - e^{\gamma_2})^{-\gamma_3}]} \to a''(1 - e^{\gamma_2})^{-\gamma_3}. \tag{4.94}$$

Hence, for values of γ_2 close to 0, Approximation (4.93) can be reduced to

$$\mathrm{E}\left(\gamma_1, \gamma_2, \gamma_3, m, a, b, g\right) \approx \frac{[\gamma_1 + 1]e^{\gamma_2}}{1 - e^{\gamma_2}}\left[1 + \frac{\gamma_3 a''(1 - e^{\gamma_2})^{-\gamma_3}}{[\gamma_1 + 1]}\right], \tag{4.95}$$

and this approximation improves as $\gamma_2 \to 0$. Moreover, for values of γ_2 close to 0, the ratio $[\mathrm{E}\left(\gamma_1, \gamma_2, \gamma_3, m, a, b, g\right)]^{-1}$, to first order, can be reduced to

$$\frac{1}{\mathrm{E}\left(\gamma_1, \gamma_2, \gamma_3, m, a, b\right)} \approx \frac{1}{[\gamma_1 + 1]e^{\gamma_2}} - \frac{1}{\gamma_1 + 1}, \tag{4.96}$$

Now assume that there exist $\gamma_1^{*1}, \gamma_2^{*1}, \gamma_3^{*1}, m_{*_1}, a_{*_1}, b_{*_1}, \gamma_1^{*2}, \gamma_2^{*2}, \gamma_3^{*2}, m_{*_2}, a_{*_2}, b_{*_2}$, and functions g_{*_1} and g_{*_2} (with $g_{*_1}(n) = O\left(n^{-1}\right)$ and $g_{*_2}(n) = O\left(n^{-1}\right)$) such that the functions $\mathrm{E}\left(\gamma_1^{*1}, \gamma_2, \gamma_3^{*1}, m_{*_1}, a_{*_1}, b_{*_1}, g_{*_1}\right)$ and $\mathrm{E}\left(\gamma_1^{*2}, \gamma_2, \gamma_3^{*2}, m_{*_2}, a_{*_2}, b_{*_2}, g_{*_2}\right)$ can be approximated by Approximation (4.93). Then the ratio $\dfrac{\mathrm{E}\left(\gamma_1^{*1}, \gamma_2, \gamma_3^{*1}, m_{*_1}, a_{*_1}, b_{*_1}, g_{*_1}\right)}{\mathrm{E}\left(\gamma_1^{*2}, \gamma_2, \gamma_3^{*2}, m_{*_2}, a_{*_2}, b_{*_2}, g_{*_2}\right)}$ can be reduced to

$$\frac{\mathrm{E}\left(\gamma_1^{*1}, \gamma_2, \gamma_3^{*1}, m_{*_1}, a_{*_1}, b_{*_1}, g_{*_1}\right)}{\mathrm{E}\left(\gamma_1^{*2}, \gamma_2, \gamma_3^{*2}, m_{*_2}, a_{*_2}, b_{*_2}, g_{*_2}\right)} \approx \frac{[\gamma_1^{*1} + 1]}{[\gamma_1^{*2} + 1]} \frac{\left[1 + \frac{\gamma_3^{*1} a''_{*_1}(1 - e^{\gamma_2})^{-\gamma_3^{*1}}}{[\gamma_1^{*1} + 1]}\right]}{\left[1 + \frac{\gamma_3^{*2} a''_{*_2}(K)(1 - e^{\gamma_2})^{-\gamma_3^{*2}}}{[\gamma_1^{*2} + 1]}\right]}. \tag{4.97}$$

Now if $\gamma_{*_1}^{*_2} := \min\left\{-\gamma_3^{*1}, -\gamma_3^{*2}\right\}$, then the first two terms in the expansion of Approximation (4.97) become

$$\frac{\mathrm{E}\left(\gamma_1^{*1}, \gamma_2, \gamma_3^{*1}, m_{*_1}, a_{*_1}, b_{*_1}, g_{*_1}\right)}{\mathrm{E}\left(\gamma_1^{*2}, \gamma_2, \gamma_3^{*2}, m_{*_2}, a_{*_2}, b_{*_2}, g_{*_2}\right)} \approx \frac{[\gamma_1^{*1} + 1]}{[\gamma_1^{*2} + 1]} + c_{*_1}^{*_2}(1 - e^{\gamma_2^*})^{\gamma_{*_1}^{*_2}}. \tag{4.98}$$

From Approximation (4.97), as $\gamma_2 \to 0$, the ratio $\dfrac{\mathrm{E}\left(\gamma_1^{*_1}, \gamma_2, \gamma_3^{*_1}, m_{*_1}, a_{*_1}, b_{*_1}, g_{*_1}\right)}{\mathrm{E}\left(\gamma_1^{*_2}, \gamma_2, \gamma_3^{*_2}, m_{*_2}, a_{*_2}, b_{*_2}, g_{*_2}\right)}$ is expected to become linear in $(1 - e^{\gamma_2^*})^{\gamma_{*_1}^{*_2}}$ and to converge to some constant, that is

$$\lim_{\gamma_2 \to 0} \frac{\mathrm{E}\left(\gamma_1^{*_1}, \gamma_2, \gamma_3^{*_1}, m_{*_1}, a_{*_1}, b_{*_1}, g_{*_1}\right)}{\mathrm{E}\left(\gamma_1^{*_2}, \gamma_2, \gamma_3^{*_2}, m_{*_2}, a_{*_2}, b_{*_2}, g_{*_2}\right)} = \frac{[\gamma_1^{*_1} + 1]}{[\gamma_1^{*_2} + 1]}. \tag{4.99}$$

If $\gamma_1^{*_1} = \gamma_1^{*2}$, then the following result is expected:

$$\lim_{\gamma_2 \to 0} \frac{\mathrm{E}\left(\gamma_1^{*_1}, \gamma_2, \gamma_3^{*_1}, m_{*_1}, a_{*_1}, b_{*_1}, g_{*_1}\right)}{\mathrm{E}\left(\gamma_1^{*_2}, \gamma_2, \gamma_3^{*_2}, m_{*_2}, a_{*_2}, b_{*_2}, g_{*_2}\right)} = 1. \tag{4.100}$$

Now relating back to the set of Θ-SAPs $\mathscr{P}^{\Theta}(\phi)$, if for $N_{\min}$ sufficiently large, there exists $A_*^{\Theta}, \alpha_*^{\Theta}, q, \kappa_*, B_*^{\Theta}, \Delta_*^{\Theta}$ and a function g_* (with $g_*(n) = O(n^{-1})$, such that for properties $*, *_1, *_2 \in \Phi$, Conjecture 2.2.4 holds, then, Approximation (4.96) can be rewritten as

$$\frac{1}{\mathrm{E}\left(\alpha_*^{\Theta} + q, \beta + \kappa_\phi, -\Delta_*^{\Theta}, N_{\min}^*, A_*^{\Theta}, B_*^{\Theta}\right)} \approx \frac{1}{[\alpha_\phi^{\Theta} + q + 1]e^{\beta + \kappa_\phi}} - \frac{1}{\alpha_\phi^{\Theta} + q + 1} \tag{4.101}$$

and Approximation (4.98) can be rewritten as

$$\frac{\mathrm{E}\left(\alpha_{*_1}^{\Theta} + q, \beta + \kappa_\phi, -\Delta_{*_1}^{\Theta}, N_{\min}^{*_1}, A_{*_1}^{\Theta}, B_{*_1}^{\Theta}\right)}{\mathrm{E}\left(\alpha_{*_2}^{\Theta} + q, \beta + \kappa_\phi, -\Delta_{*_2}^{\Theta}, N_{\min}^{*_2}, A_{*_2}^{\Theta}, B_{*_2}^{\Theta}\right)} \approx \frac{[\alpha_{*_1}^{\Theta} + q + 1]}{[\alpha_{*_2}^{\Theta} + q + 1]} + c_{*_1}^{*_2}(1 - e^{\beta + \kappa_\phi})^{\gamma_{*_1}^{*_2}}, \tag{4.102}$$

where $\gamma_{*_1}^{*_2} := \min\left\{\Delta_{*_1}^{\Theta}, \Delta_{*_2}^{\Theta}\right\}$.

For the set of all polygons in $\mathbb{Z}^3$, the exponent $\gamma_{*_1}^{*_2}$ is denoted Δ and is referred to as the confluent exponent and is believed to be universal for all lattices with the same dimension [103]. The value of Δ is believed to be very close to 0.5. In fact, in [47] Δ has been estimated to be 0.478 ± 0.010. In [125] Δ is assumed to be 0.5 regardless of the knot-type. Analogously, it will be assumed here that $\gamma_{*_1}^{*_2}$ is also 0.5.

The left hand side of Approximation (4.101) is the reciprocal of the expected length of a randomly selected polygon in $\mathscr{P}^{\Theta}(\phi)$ according to the distribution given by Equation (2.63) with $z = e^{\beta}$. The right hand side of Approximation (4.101) is an expression which is linear in $1/e^{\beta}$. The upshot of Approximation (4.101) is that as $\gamma_2 = \beta + \kappa_\phi \to 0$, $\left[\mathrm{E}\left(\alpha_\phi^{\Theta} + q, \beta + \kappa_\phi, -\Delta_\phi^{\Theta}, N_{\min}, A_\phi^{\Theta}, B_\phi^{\Theta}\right)\right]^{-1}$ is expected to be linear in $1/e^{\beta}$. This result will be used in Section (4.7.3) to check the consistency of the data generated from the CMC implementation of the Θ-BFACF algorithm.

The left hand side of Approximation (4.102) is the ratio of the expected lengths of randomly selected polygons with properties $*_1$ and $*_2$ in $\mathscr{P}^{\Theta}(\phi)$ (according to the distribution given by Equation (2.63) with $z = e^{\beta}$). The right hand side of Approximation (4.102) is an expression which is linear in $(1 - e^{\beta + \kappa_\phi})^{\gamma_{*_1}^{*_2}}$. The upshot of Approximation (4.102) is

that as $\gamma_2 = \beta + \kappa_\phi \to 0$, $\dfrac{\mathrm{E}\left(\alpha^{\Theta}_{*_1} + q, \beta + \kappa_\phi, -\Delta^{\Theta}_{*_1}, N^{*_1}_{\min}, A^{\Theta}_{*_1}, B^{\Theta}_{*_1}\right)}{\mathrm{E}\left(\alpha^{\Theta}_{*_2} + q, \beta + \kappa_\phi, -\Delta^{\Theta}_{*_2}, N^{*_2}_{\min}, A^{\Theta}_{*_2}, B^{\Theta}_{*_2}\right)} \to 1.0$, if $\alpha^{\Theta}_{*_1} = \alpha^{\Theta}_{*_2}$. This result will also be used in Section 4.7.3 to check the consistency of the data generated from the CMC implementation of the Θ-BFACF algorithm.

4.5.2 How Should $r^2_{\breve{\boldsymbol{\pi}}_z(q,M)}(\cdot)$ Behave as $M \to \infty$ and $\log(z) \to -\kappa_\phi$?

Recall from Section 2.2.3 that, for the property $* \in \Phi$, the function $f : \mathbb{Z}^3 \to \mathbb{Z}^3$, and $\mathscr{U}^{\Theta}(*) \subseteq \mathscr{P}^{\Theta}(\phi)$, the expected value $r^2_{\breve{\boldsymbol{\pi}}_z(q,M)}\left(f\left(\mathscr{U}^{\Theta}(*)\right)\right)$ (with respect to $\breve{\boldsymbol{\pi}}_z(q,M)$ given by Equation (2.63) for a fixed even integer M) is

$$r^2_{\breve{\boldsymbol{\pi}}_z(q,M)}\left(\mathscr{U}^{\Theta}(*)\right) = \sum_{m=M/2}^{\infty} r^2\left(f\left(\mathscr{U}^{\Theta}_{2m}(*)\right)\right)\pi_{2m|M}(q,z), \tag{4.103}$$

where $\mathscr{U}^{\Theta}_{2m}(*)$ is the set of $(2m)$-edge SAPs in $\mathscr{U}^{\Theta}(*)$. If Conjectures 2.2.4, 2.2.12, and 2.2.13 (from Sections 2.2.2 and 2.2.3 respectively) hold for the property $* \in \Phi$, the function $f : \mathbb{Z}^3 \to \mathbb{Z}^3$, and $\mathscr{U}^{\Theta}(*) \subseteq \mathscr{P}^{\Theta}(\phi)$, then, for even M sufficiently large, there exist $A^{(1)}_{f(\mathscr{U})}(*)$, $A^{(2)}_{f(\mathscr{U})}(*)$, $\alpha^{\Theta}_{f(\mathscr{U})}(*)$, q, κ_ϕ, $B^{(1)}_{f(\mathscr{U})}(*)$, $B^{(2)}_{f(\mathscr{U})}(*)$, $-\Delta^{(1)}_{f(\mathscr{U})}(*)$, and $-\Delta^{(2)}_{f(\mathscr{U})}(*)$ and functions $g^*_{f(\mathscr{U})}$ and $h^*_{f(\mathscr{U})}$ (with $g^*_{f(\mathscr{U})}(n) = O(n^{-1})$ and $h^*_{f(\mathscr{U})}(n) = O(n^{-1})$), such that

$$r^2_{\breve{\boldsymbol{\pi}}_z(q,M)}\left(\mathscr{U}^{\Theta}(*)\right) = [Q(*)]^{-1} \sum_{\substack{n \geq N_{\min} \\ n \text{ even}}} R_n(*)F_n(*), \tag{4.104}$$

where $\beta := \log(z)$,

$$F_n(\cdot) := \mathcal{F}_n\left(A^{(2)}_{f(\mathscr{U})}(*), \alpha^{\Theta}_{f(\mathscr{U})}(*) + q, \kappa_\phi + \beta, B^{(2)}_{f(\mathscr{U})}(*), -\Delta^{(2)}_{f(\mathscr{U})}(*), g^*_{f(\mathscr{U})}\right), \tag{4.105}$$

$$R_n(\cdot) := \mathcal{R}_n\left(A^{(1)}_{f(\mathscr{U})}(*), \nu^{\Theta}_{f(\mathscr{U})}(*), B^{(1)}_{f(\mathscr{U})}(*), \Delta^{(1)}_{f(\mathscr{U})}(*), h^*_{f(\mathscr{U})}\right), \tag{4.106}$$

and

$$Q(\cdot) := Q\left(\alpha^{\Theta}_{f(\mathscr{U})}(*) + q, \kappa_\phi + \beta, -\Delta^{(2)}_{f(\mathscr{U})}(*), M, A^{(2)}_{f(\mathscr{U})}(*), B^{(2)}_{f(\mathscr{U})}(*), g^*_{f(\mathscr{U})}\right). \tag{4.107}$$

Hence, in order to study and better understand the behaviour of $r^2_{\breve{\boldsymbol{\pi}}_z(q,M)}\left(\mathscr{U}^{\Theta}(*)\right)$ as $M \to \infty$ and $\beta \to -\kappa_\phi$, the behaviour of the right hand side of Equation (4.104) needs to be explored as $M \to \infty$ and $\beta \to -\kappa_\phi$. To this end, define the function $R_n(\cdot)$ by

$$\begin{aligned} &R_n(\gamma_{1,1}, \gamma_{1,2}, \gamma_2, \gamma_{3,1}, \gamma_{3,2}, a_1, a_2, b_1, b_2, h) \\ &:= e^{\gamma_2 n} a_1 a_2 n^{\gamma_{1,1}+\gamma_{1,2}}\left[1 + b_1 n^{-\gamma_{3,1}} + b_2 n^{-\gamma_{3,2}} + h(n)\right], \end{aligned} \tag{4.108}$$

where $h(n) = O(n^{-1})$, and define the function $R(\cdot)$ by

$$\begin{aligned} &R(\gamma_{1,1}, \gamma_{1,2}, \gamma_2, \gamma_{3,1}, \gamma_{3,2}, a_1, a_2, b_1, b_2, m, h) \\ &:= \sum_{\substack{n=m \\ n \text{ even}}} R_n(\gamma_{1,1}, \gamma_{1,2}, \gamma_2, \gamma_{3,1}, \gamma_{3,2}, a_1, a_2, b_1, b_2, h). \end{aligned} \tag{4.109}$$

Then, for $z = e^{\gamma_2}$, the coefficient of z^n in $R(\gamma_{1,1}, \gamma_{1,2}, \gamma_2, \gamma_{3,1}, \gamma_{3,2}, a_1, a_2, b_1, b_2, m, h)$ is, as $n \to \infty$, asymptotic to

$$\begin{aligned} &[z^n]R(\gamma_{1,1}, \gamma_{1,2}, \gamma_2, \gamma_{3,1}, \gamma_{3,2}, a_1, a_2, b_1, b_2, m, h) \\ &\sim a_1 a_2 n^{\gamma_{1,1}+\gamma_{1,2}} + a_1 a_2 b_1 n^{\gamma_{1,1}+\gamma_{1,2}-\gamma_{3,1}} + a_1 a_2 b_2 n^{\gamma_{1,1}+\gamma_{1,2}-\gamma_{3,2}}. \end{aligned} \tag{4.110}$$

By Equation (4.86), the coefficient of z^n in $R(\gamma_{1,1}, \gamma_{1,2}, \gamma_2, \gamma_{3,1}, \gamma_{3,2}, a_1, a_2, b_1, b_2, m, h)$ is, as $n \to \infty$, asymptotic to:

$$\begin{aligned} &[z^n]R(\gamma_{1,1}, \gamma_{1,2}, \gamma_2, \gamma_{3,1}, \gamma_{3,2}, a_1, a_2, b_1, b_2, m, h) \\ &\sim [z^n]\left[a_1 a_2 \Gamma\left(\gamma_{1,1} + \gamma_{1,2} + 1\right)\left(1 - e^{\gamma_2}\right)^{-\gamma_{1,1}-\gamma_{1,2}-1}\right] \\ &+ [z^n]\left[a_1 a_2 b_1 \Gamma\left(\gamma_{1,1} + \gamma_{1,2} - \gamma_{3,1} + 1\right)\left(1 - e^{\gamma_2}\right)^{\gamma_{3,1}-\gamma_{1,1}-\gamma_{1,2}-1}\right] \\ &+ [z^n]\left[a_1 a_2 b_2 \Gamma\left(\gamma_{1,1} + \gamma_{1,2} - \gamma_{3,2} + 1\right)\left(1 - e^{\gamma_2}\right)^{\gamma_{3,2}-\gamma_{1,1}-\gamma_{1,2}-1}\right]. \end{aligned} \tag{4.111}$$

Hence, for m even and sufficiently large, $R(\gamma_{1,1}, \gamma_{1,2}, \gamma_2, \gamma_{3,1}, \gamma_{3,2}, a_1, a_2, b_1, b_2, m, h)$ can be approximated by

$$\begin{aligned} &\mathrm{R}(\gamma_{1,1}, \gamma_{1,2}, \gamma_2, \gamma_{3,1}, \gamma_{3,2}, a_1, a_2, b_1, b_2, m, h) \\ &\approx a_1 a_2 \Gamma\left(\gamma_{1,1} + \gamma_{1,2} + 1\right)\left(1 - e^{\gamma_2}\right)^{-\gamma_{1,1}-\gamma_{1,2}-1} \\ &+ a_1 a_2 b_1 \Gamma\left(\gamma_{1,1} + \gamma_{1,2} - \gamma_{3,1} + 1\right)\left(1 - e^{\gamma_2}\right)^{\gamma_{3,1}-\gamma_{1,1}-\gamma_{1,2}-1} \\ &+ a_1 a_2 b_2 \Gamma\left(\gamma_{1,1} + \gamma_{1,2} - \gamma_{3,2} + 1\right)\left(1 - e^{\gamma_2}\right)^{\gamma_{3,2}-\gamma_{1,1}-\gamma_{1,2}-1} \end{aligned} \tag{4.112}$$

$$\begin{aligned} &= a_1 a_2 \left(1 - e^{\gamma_2}\right)^{-\gamma_{1,2}-1}\left[\Gamma\left(\gamma_{1,1} + \gamma_{1,2} + 1\right)\left(1 - e^{\gamma_2}\right)^{-\gamma_{1,1}}\right. \\ &+ b_1 \Gamma\left(\gamma_{1,1} + \gamma_{1,2} - \gamma_{3,1} + 1\right)\left(1 - e^{\gamma_2}\right)^{\gamma_{3,1}-\gamma_{1,1}} \\ &+ \left. b_2 \Gamma\left(\gamma_{1,1} + \gamma_{1,2} - \gamma_{3,2} + 1\right)\left(1 - e^{\gamma_2}\right)^{\gamma_{3,2}-\gamma_{1,1}}\right]. \end{aligned} \tag{4.113}$$

Now define the function $\mathrm{ER}(\cdot)$ by

$$\begin{aligned} &\mathrm{ER}(\gamma_{1,1}, \gamma_{1,2}, \gamma_2, \gamma_{3,1}, \gamma_{3,2}, a_1, a_2, b_1, b_2, m_1, m_2, h, g) \\ &:= \frac{R(\gamma_{1,1}, \gamma_{1,2}, \gamma_2, \gamma_{3,1}, \gamma_{3,2}, a_1, a_2, b_1, b_2, m_1, h)}{Q\left(\gamma_{1,2}, \gamma_2, \gamma_{3,2}, m_2, a_2, b_2, g\right)}, \end{aligned} \tag{4.114}$$

where $Q(\gamma_{1,2}, \gamma_2, \gamma_{3,2}, m_2, a_2, b_2, g)$ is defined by Equation (4.84). Then for m_1 and m_2, both even and sufficiently large, $\mathrm{ER}(\gamma_{1,1}, \gamma_{1,2}, \gamma_2, \gamma_{3,1}, \gamma_{3,2}, a_1, a_2, b_1, b_2, m_1, m_2, f, g)$ can be approximated by

$$\begin{aligned}
&\mathrm{ER}(\gamma_{1,1}, \gamma_{1,2}, \gamma_2, \gamma_{3,1}, \gamma_{3,2}, a_1, a_2, b_1, b_2, m_1, m_2, h, g) \\
&\sim \frac{a_1 \Gamma(\gamma_{1,1} + \gamma_{1,2} + 1)(1 - e^{\gamma_2})^{-\gamma_{1,1}}}{\Gamma(\gamma_{1,2} + 1)[1 + a_2'(1 - e^{\gamma_2})^{-\gamma_{3,2}}]}[1 && (4.115) \\
&+ b_1 \frac{\Gamma(\gamma_{1,1} + \gamma_{1,2} - \gamma_{3,1} + 1)}{\Gamma(\gamma_{1,1} + \gamma_{1,2} + 1)}(1 - e^{\gamma_2})^{\gamma_{3,1}} && (4.116) \\
&+ b_2 \frac{\Gamma(\gamma_{1,1} + \gamma_{1,2} - \gamma_{3,2} + 1)}{\Gamma(\gamma_{1,1} + \gamma_{1,2} + 1)}(1 - e^{\gamma_2})^{\gamma_{3,2}}\Big], && (4.117)
\end{aligned}$$

where $a_2' = \dfrac{b_2 \Gamma(\gamma_{1,2} + \gamma_{3,2} + 1)}{\Gamma(\gamma_{1,2} + 1)}$.

As $\gamma_2 \to 0$, $[1 + a_2'(1 - e^{\gamma_2})^{-\gamma_{3,2}}]^{-1} \to 1$. Hence, for γ_2 sufficiently close to zero, the above approximation for $\mathrm{ER}(\gamma_{1,1}, \gamma_{1,2}, \gamma_2, \gamma_{3,1}, \gamma_{3,2}, a_1, a_2, b_1, b_2, m_1, m_2, f, g)$ becomes

$$\begin{aligned}
&\mathrm{ER}(\gamma_{1,1}, \gamma_{1,2}, \gamma_2, \gamma_{3,1}, \gamma_{3,2}, a_1, a_2, b_1, b_2, m_1, m_2, f, g) \\
&\approx \frac{a_1 \Gamma(\gamma_{1,1} + \gamma_{1,2} + 1)(1 - e^{\gamma_2})^{-\gamma_{1,1}}}{\Gamma(\gamma_{1,2} + 1)}[1 \\
&+ b_1 \frac{\Gamma(\gamma_{1,1} + \gamma_{1,2} - \gamma_{3,1} + 1)}{\Gamma(\gamma_{1,1} + \gamma_{1,2} + 1)}(1 - e^{\gamma_2})^{\gamma_{3,1}} \\
&+ b_2 \frac{\Gamma(\gamma_{1,1} + \gamma_{1,2} - \gamma_{3,2} + 1)}{\Gamma(\gamma_{1,1} + \gamma_{1,2} + 1)}(1 - e^{\gamma_2})^{\gamma_{3,2}}\Big]. && (4.118)
\end{aligned}$$

Recall from Approximation (4.95) that, for values of γ_2 very close to zero,

$$\mathrm{E}(\gamma_1, \gamma_2, \gamma_3, m, a, b, g) \approx \frac{[\gamma_1 + 1]e^{\gamma_2}}{1 - e^{\gamma_2}}. \tag{4.119}$$

Solving the above approximation for $1 - e^{\gamma_2}$ yields the approximation

$$1 - e^{\gamma_2} \approx [\gamma_{1,2} + 1]e^{\gamma_2}(\mathrm{E}(\gamma_{1,2}, \gamma_2, \gamma_{3,2}, m_2, a_2, b_2, g))^{-1}. \tag{4.120}$$

Substituting Approximation (4.120) for $1 - e^{\gamma_2}$ into Approximation (4.118) yields

$$\begin{aligned}
&\mathrm{ER}(\gamma_{1,1}, \gamma_{1,2}, \gamma_2, \gamma_{3,1}, \gamma_{3,2}, a_1, a_2, b_1, b_2, m_1, m_2, h, g) \\
&\approx \frac{a_1 \Gamma(\gamma_{1,1} + \gamma_{1,2} + 1)[\gamma_{1,2} + 1]^{-\gamma_{1,1}} e^{-\gamma_2 \gamma_{1,1}} (\mathrm{E}(\gamma_{1,2}, \gamma_2, \gamma_{3,2}, m_2, a_2, b_2, g))^{\gamma_{1,1}}}{\Gamma(\gamma_{1,2} + 1)}[1 \\
&+ b_1 \frac{\Gamma(\gamma_{1,1} + \gamma_{1,2} - \gamma_{3,1} + 1)}{\Gamma(\gamma_{1,1} + \gamma_{1,2} + 1)}[\gamma_{1,2} + 1]^{\gamma_{3,1}} e^{\gamma_2 \gamma_{3,1}} (\mathrm{E}(\gamma_{1,2}, \gamma_2, \gamma_{3,2}, m_2, a_2, b_2, g))^{-\gamma_{3,1}} \\
&+ b_2 \frac{\Gamma(\gamma_{1,1} + \gamma_{1,2} - \gamma_{3,2} + 1)}{\Gamma(\gamma_{1,1} + \gamma_{1,2} + 1)}[\gamma_{1,2} + 1]^{\gamma_{3,2}} e^{\gamma_2 \gamma_{3,2}} (\mathrm{E}(\gamma_{1,2}, \gamma_2, \gamma_{3,2}, m_2, a_2, b_2, g))^{-\gamma_{3,2}}\Big].
\end{aligned} \tag{4.121}$$

Hence, for values of γ_2 sufficiently close to zero,
$\mathrm{ER}(\gamma_{1,1}, \gamma_{1,2}, \gamma_2, \gamma_{3,1}, \gamma_{3,2}, a_1, a_2, b_1, b_2, m_1, m_2, h, g)$ can be expressed in terms of
$\mathrm{E}\left(\gamma_{1,2}, \gamma_2, \gamma_{3,2}, m_2, a_2, b_2, g\right)$, that is

$$\begin{aligned}
&\mathrm{ER}(\gamma_{1,1}, \gamma_{1,2}, \gamma_2, \gamma_{3,1}, \gamma_{3,2}, a_1, a_2, b_1, b_2, m_1, m_2, h, g) \\
&\approx \left[A_1(a_1, \gamma_{1,1}, \gamma_{1,2}, \gamma_2)\right] \left(\mathrm{E}\left(\gamma_{1,2}, \gamma_2, \gamma_{3,2}, m_2, a_2, b_2, g\right)\right)^{\gamma_{1,1}} \\
&+ B_1(\gamma_{1,1}, \gamma_{1,2}, \gamma_2, \gamma_{3,1}, \gamma_{3,2}, a_1, a_2, b_1, b_2, m_1, m_2, g),
\end{aligned} \tag{4.122}$$

where $A_1(a_1, \gamma_{1,1}, \gamma_{1,2}, \gamma_2) = O(1)$ and $B_1(\gamma_{1,1}, \gamma_{1,2}, \gamma_2, \gamma_{3,1}, \gamma_{3,2}, a_1, a_2, b_1, b_2, m_1, m_2, g) = O(n^{-\gamma})$ with $\gamma = \min\{\gamma_{3,1}, \gamma_{3,2}\}$.

Now relating Approximation (4.122) back to subsets of $\mathscr{P}^{\Theta}(\phi)$, first

$$\mathrm{E}\left(\gamma_{1,2}, \gamma_2, \gamma_{3,2}, m_2, a_2, b_2, g\right) = \mathrm{E}_{\breve{\boldsymbol{\pi}}_z(q,M)}(|f(\omega)|), \tag{4.123}$$

and if, for $N_{\min}$ sufficiently large, there exist constants $A^{(1)}_{f(\mathscr{U})}(*)$, $A^{(2)}_{f(\mathscr{U})}(*)$, $\nu^{\Theta}_{f(\mathscr{U})}(*)$, $\alpha^{\Theta}_{f(\mathscr{U})}(*)$, q, κ_ϕ, $B^{(1)}_{f(\mathscr{U})}(*)$, $B^{(2)}_{f(\mathscr{U})}(*)$, $\Delta^{(1)}_{f(\mathscr{U})}(*)$, and $\Delta^{(2)}_{f(\mathscr{U})}(*)$ and functions $g^*_{f(\mathscr{U})}$ and $h^*_{f(\mathscr{U})}$ (with $g^*_{f(\mathscr{U})}(n) = O(n^{-1})$ and $h^*_{f(\mathscr{U})}(n) = O(n^{-1})$) such that Conjectures 2.2.4, 2.2.12, and 2.2.13 hold, then Approximation (4.122) becomes

$$\begin{aligned}
r^2_{\breve{\boldsymbol{\pi}}_z(q,M)}\left(f\left(\mathscr{U}^{\Theta}(*)\right)\right) &\approx \left[A_1(\cdot)\right]\left(\mathrm{E}_{\breve{\boldsymbol{\pi}}_z(q,M)}\left(|f(\omega)|\right)\right)^{2\nu^{\Theta}_{f(\mathscr{U})}(*)} \\
&+ B_1(\cdot).
\end{aligned} \tag{4.124}$$

Note that $\mathrm{E}_{\breve{\boldsymbol{\pi}}_z(q,M)}(|f(\omega)|)$ is the expected length of $f(\omega)$ where ω is a randomly selected polygon from $\mathscr{U}^{\Theta}(*)$ chosen according to $\breve{\boldsymbol{\pi}}_z(q, M)$ given by Equation (2.63). Hence for values of $\beta = \log(z)$ very close to $-\kappa_\phi$, $r^2_{\breve{\boldsymbol{\pi}}_z(q,M)}\left(f\left(\mathscr{U}^{\Theta}(*)\right)\right)$ should become linear in $\mathrm{E}_{\breve{\boldsymbol{\pi}}_z(q,M)}(|f(\omega)|)^{2\nu^{\Theta}_{f(\mathscr{U})}(*)}$.

The next section provides a technique for quantifying what is meant by the phrase "reliable data" in terms of an estimate for the parameter $N^*_{\max}$.

4.6 Can We Be Trusted?

In this section, a method for quantifying the expression "reliable data" will be provided. One of the purposes for determining which data is considered reliable is to take into account the finite nature of the simulation, that is, to take into account the fact that the observed proportions of large polygons may not accurately reflect the corresponding proportions determined using the true distribution.

Suppose a simulation consists of n_0 replications, where for Replication $r \in \{1, ..., n_0\}$, $\left(\left(\hat{\omega}_j^{(r)}(1), \hat{\omega}_j^{(r)}(2), ..., \hat{\omega}_j^{(r)}(14)\right), j = 0, ..., m\right)$ is a sequence of $(m+1)$ M-tuples sampled from $(\mathscr{P}^{\Theta})^M$. Then, for Replication r, define $\hat{g}^{(r)}(*, 2n)$ to be a function of interest that is defined on polygons whose lengths are $2n$, and let $\widehat{\mathrm{SE}}(\hat{g}^{(r)}(*, 2n))$ be the corresponding estimated standard error of $\hat{g}^{(r)}(*, 2n)$. Then the corresponding estimated relative standard error of $\hat{g}^{(r)}(*, 2n)$ is defined to be

$$\hat{\delta}_{2n}^{(r)}(*) := \begin{cases} \dfrac{\widehat{\mathrm{SE}}(\hat{g}^{(r)}(*, 2n))}{\hat{g}^{(r)}(*, 2n)}, & \text{if } \hat{g}^{(i)}(*, 2n) \neq 0 \\ \infty, & \text{otherwise.} \end{cases} \tag{4.125}$$

Now define

$$\hat{\delta}^{(r)}(*) := \min_n \hat{\delta}_{2n}^{(r)}(*) \tag{4.126}$$

and define $\hat{\eta}^{(r)}(*)$ to be the first value of $2n$ for which $\hat{\delta}_{2n}^{(r)}(*) = \hat{\delta}^{(r)}(*)$. Note that $\hat{\delta}^{(r)}(*)$ is the best (that is smallest) relative error in $\hat{g}^{(r)}(*, 2n)$ that can be achieved without generating more data. Therefore the estimates $\hat{g}^{(r)}(*, 2n)$ that have a standard error close to $\hat{\delta}^{(r)}(*)$ will be more reliable than estimates whose estimated standard error is much larger than $\hat{\delta}^{(r)}(*)$. Consequently, for a fixed amount of data, the most accurate data will be for values of n such that $\hat{\delta}_{2n}^{(r)}(*)$ is within some ε_* of $\hat{\delta}^{(r)}(*)$. How should ε_* be determined?

If $\varepsilon_* > 1.0$, then the estimated error of the point estimate $\hat{g}^{(r)}(*, 2n)$ would be greater than $\hat{g}^{(r)}(*, 2n)$ itself. Consequently, if the point estimate $\hat{g}^{(r)}(*, 2n)$ is used in some other calculation, any error in the point estimate $\hat{g}^{(r)}(*, 2n)$ would introduce error into the calculations based on $\hat{g}^{(r)}(*, 2n)$. Hence having $\varepsilon_* < 1.0$ is preferred. Therefore define

$$\varepsilon_* := \min_r(\hat{\delta}^{(r)}(*) + c), \tag{4.127}$$

where $c \cdot 100\%$ represents the maximum tolerated deviation from $\hat{\delta}^{(r)}(*)$ and c is chosen so that $0 < c < 1.0$ and $\varepsilon_* < 1.0$. Note that the choice of c in Equation (4.127) is somewhat arbitrary but c should be chosen in such a manner that using the point estimates $\hat{g}^{(r)}(*, 2n)$, whose estimated relative error is less than ε_*, minimizes the error introduced into subsequent calculations involving $\hat{g}^{(r)}(*, 2n)$.

Now assuming that $0 < c < 1$ has been chosen, then an estimate for $N_{\max}^*$ can be determined. Note for the sake of convenience, the value of $\hat{N}_{\max}^{(r)}(*)$ is chosen to be the value of $2n > \hat{\eta}^{(r)}(*)$ (rounded down to the nearest one hundred) for which $\hat{\delta}_{2n}^{(r)}(*)$ first

achieves a value greater than or equal to ε_*. In other words, $\hat{N}^{(r)}_{\max}(*)$ is the observed polygon for which the point estimates $\hat{g}^{(r)}(*, 2n)$ become unreliable. The estimate for $N^*_{\max}$ for the simulation (to be denoted $\hat{N}_{\max}(*)$) is

$$\hat{N}_{\max}(*) := \min_r \hat{N}^{(r)}_{\max}(*), \tag{4.128}$$

if $* \in \Phi \backslash \{\phi,\ (\phi, f),\ (\phi, s),\ (\phi|\phi, s)\}$, and

$$\hat{N}_{\max}(*') := \min_{*\in\{\phi,(\phi,f),(\phi,s),(\phi|\phi,s)\}} \min_r \hat{N}^{(r)}_{\max}(*), \tag{4.129}$$

if $*' \in \{\phi,\ (\phi, f),\ (\phi, s),\ (\phi|\phi, s)\}$.

The set of polygons from Replication r whose lengths are greater than $\hat{N}_{\max}(*)$ will be referred to as *unreliable data* and the set of polygons from Replication r whose lengths are less than or equal to $\hat{N}_{\max}(*)$ will be referred to as *reliable data* (cf. Section 4.7.4 for an implementation of this technique).

The discussion in this chapter thus far has been presented in the abstract. In the next section, the techniques outlined in this chapter will be applied to the CMC data generated by simulations of the CMC Θ-BFACF algorithm.

4.7 Preliminary Analysis of the CMC Θ-BFACF Simulation Data

For the rest of this document, let $t_0 = 9.6 \times 10^{10}$; for $r \in \{1, 2, ..., 10\}$, let

$$\boldsymbol{\omega}^{(r)} := \left(\left(\omega^{(r)}_t(1), \omega^{(r)}_t(2), ..., \omega^{(r)}_t(14) \right), t = 0, ..., t_0 \right) \tag{4.130}$$

be the sequence of $(t_0 + 1)$ 14-tuples of Θ-SAPs from $\left(\mathscr{P}^{\Theta}\right)^{14}$ realized in Replication r of the simulation of the CMC Θ-BFACF algorithm as described in Section 3.4.1; let

$$\hat{\boldsymbol{\omega}}^{(r)} := \left(\left(\hat{\omega}^{(r)}_j(1), \hat{\omega}^{(r)}_j(2), ..., \hat{\omega}^{(r)}_j(14) \right), j = 0, ..., l \right) \tag{4.131}$$

be the sequence of 14-tuples of SAPs sampled from Replication r, where $l := \lfloor t_0/1200 \rfloor = 80,000,000$, and, for $t := 1200j$, the j'th term (for $1 \leq j \leq l$) of $\hat{\boldsymbol{\omega}}^{(r)}$ is given by

$$\left(\hat{\omega}^{(r)}_j(1), \hat{\omega}^{(r)}_j(2), ..., \hat{\omega}^{(r)}_j(14) \right) := \left(\omega^{(r)}_t(1), \omega^{(r)}_t(2), ..., \omega^{(r)}_t(14) \right); \tag{4.132}$$

and note that the phrase "CMC Θ-BFACF data" refers to the data generated from all ten realizations of the CMC implementation of the Θ-BFACF algorithm. Further note

that, for each replication, a sample was taken immediately following the attempted swap after every 1000'th Θ-BFACF move in parallel. The resulting sample for each replication consisted of $80,000,001$ 14-tuples. Also let Φ_{ave} be the set of properties of the set $\mathscr{P}^{\Theta}(\phi)$ that are of interest where $\Phi_{\text{ave}} := \{\phi,\ (\phi,s),\ (\phi,f),\ (\phi|\phi,s),\ (3_1|\phi,s),\ (4_1|\phi,s),\ (5_2|\phi,s)\}$.

Given a polygon in $\mathscr{P}^{\Theta}(\phi)$, note that the property $* \in \Phi_{\text{ave}}$ abbreviated by the symbol:

- ϕ indicates that the polygon is in $\mathscr{P}^{\Theta}(\phi)$ (every polygon in $\mathscr{P}^{\Theta}(\phi)$ has this property);
- (ϕ,s) indicates that a strand passage about Θ in the polygon is possible;
- (ϕ,f) indicates that a strand passage about Θ is NOT possible in the polygon;
- $(\phi|\phi,s)$ indicates that a strand passage about Θ is possible in the polygon and that the after-strand-passage polygon is unknotted;
- $(3_1|\phi,s)$ indicates that a strand passage about Θ is possible in the polygon and that the after-strand-passage polygon has knot-type 3_1, i.e. is a trefoil;
- $(4_1|\phi,s)$ indicates that a strand passage about Θ is possible in the polygon and that the after-strand-passage polygon has knot-type 4_1, i.e. is a figure 8; and
- $(5_2|\phi,s)$ indicates that a strand passage about Θ is possible in the polygon and that the after-strand-passage polygon has knot-type 5_2.

In order to analyze and make any conclusions based on the sequence $\boldsymbol{\omega}^{(r)}$, whether or not the simulation was of sufficient length so that the CMC has reached its stationary distribution needs to be determined. Then, if the CMC has reached its stationary distribution, the amount of essentially independent data generated also needs to be determined.

In order to decrease the amount of computer time needed for the warm-up analysis and the estimated potential scale reduction, only every 40'th sample point was used in the analysis. Consequently the realized sample of polygon lengths from Replication r used for the warm-up analysis is the sequence $\left(\left(n_j^{(r)}(1), n_j^{(r)}(2), ..., n_j^{(r)}(14)\right), j = 0, ..., n\right)$, where $n := \lfloor t_0/48000 \rfloor$, that is $n := 2,000,000$; the first term of the realized sample is

$$\left(n_0^{(r)}(1), n_0^{(r)}(2), ..., n_0^{(r)}(14)\right) := \left(\left|\omega_0^{(r)}(1)\right|, \left|\omega_0^{(r)}(2)\right|, ..., \left|\omega_0^{(r)}(14)\right|\right); \tag{4.133}$$

and the j'th term (for $1 \le j \le n$) is given by

$$\left(n_j^{(r)}(1), n_j^{(r)}(2), ..., n_j^{(r)}(14)\right) := \left(\left|\omega_t^{(r)}(1)\right|, \left|\omega_t^{(r)}(2)\right|, ..., \left|\omega_t^{(r)}(14)\right|\right), \tag{4.134}$$

where $t := 48000j$.

Note that, of all the functions of the data that are required for making inferences in this thesis, the "across-the-chain averages" defined below in Equation (4.135) have the largest variance (as per the discussion in Section 4.2). Hence the quantities used to perform the warm-up analysis and the estimated potential scale reduction to obtain estimates for τ_{exp} and τ_{int} are actually based on the "across-the-chain averages" given by the sequences of data $\left(x_j^{(r)}, j = 0, ..., n\right)$, for $r \in \{1, 2, ..., 10\}$, where

$$x_j^{(r)} := \frac{1}{14} \sum_{i=1}^{14} n_j^{(r)}(i). \tag{4.135}$$

Consequently the estimates for τ_{exp} and τ_{int} (determined using the warm-up analysis and the estimated potential scale reduction) are based on the sequences of data $\left(x_j^{(r)}, j = 0, ..., n\right)$, for $r \in \{1, 2, ..., 10\}$. The resulting estimates for τ_{exp} and τ_{int} are presented respectively in the following two subsections.

4.7.1 Estimating τ_{exp}

In Section 4.2, three techniques were provided for estimating τ_{exp}: warm-up analysis, estimated potential scale reduction, and the mixing of the chains of a CMC. Recall from Section 4.2 that the estimates for τ_{exp} from Replication r for these three techniques are respectively $\widehat{\tau}_{\text{exp},W}^{(r)}$, $\widehat{\tau}_{\text{exp},E}^{(r)}$, and $\widehat{\tau}_{\text{exp},C}^{(r)}$, that the corresponding maximum values taken over all ten replications are $\widehat{\tau}_{\text{exp},W}$, $\widehat{\tau}_{\text{exp},E}$, and $\widehat{\tau}_{\text{exp},C}$, and that

$$\widehat{\tau}_{\text{exp}} = \max\left\{\widehat{\tau}_{\text{exp},W}, \widehat{\tau}_{\text{exp},E}, \widehat{\tau}_{\text{exp},C}\right\}. \tag{4.136}$$

Also recall from Section 4.2 that the averages taken over all ten replications of $\widehat{\tau}_{\text{exp},W}^{(r)}$, $\widehat{\tau}_{\text{exp},E}^{(r)}$, and $\widehat{\tau}_{\text{exp},C}^{(r)}$, for $r \in \{1, 2, ..., 10\}$, are respectively denoted $\bar{\tau}_{\text{exp},W}$, $\bar{\tau}_{\text{exp},E}$, and $\bar{\tau}_{\text{exp},C}$. Also recall from Section 4.2 that $\bar{\tau}_{\text{exp},E} = \widehat{\tau}_{\text{exp},E}$. The rest of this subsection presents the estimates for τ_{exp} computing using a warm-up analysis, an estimated potential scale reduction, and then finally the mixing of the chains in a composite Markov chain.

Using a Warmup Analysis

To estimate τ_{exp} using a warm-up analysis, the technique from Section 4.2.1 is employed using the sequences of data $\left(x_j^{(r)}, j = 0, ..., n\right)$, for $r \in \{1, 2, ..., 10\}$.

Figures 4.1 (a) and (b), 4.2 (a) and (b), ..., and 4.5 (a) and (b) are the graphical displays of, for Replications 1 through 10 respectively, the sequence $\left(x_j^{(r)}, j = 0, ..., n\right)$, the sequence of the associated first j column averages $\left(\left\langle x_{0,j}^{(r)} \right\rangle, j = 0, ..., n\right)$, and the sequence of the associated last $(n-j+1)$ column averages $\left(\left\langle x_{j,n}^{(r)} \right\rangle, j = 0, ..., n\right)$, where $r \in \{1, 2, 3, ..., 10\}$, and

$$\left\langle x_{k,m}^{(r)} \right\rangle = \frac{1}{m-k+1} \sum_{t=k}^{m} x_t^{(r)}. \tag{4.137}$$

Note that for each of Figures 4.1 (a) and (b), 4.2 (a) and (b), ..., and 4.5 (a) and (b), the horizontal axis is in terms of 1 Billion Θ-BFACF moves in parallel; the line labelled A represents the sequence of the transformed points $\left(\left(40,000j, x_j^{(r)}\right), j = 0, ..., n\right)$; the line labelled B represents the sequence of points associated with the first j column averages $\left(\left(40,000j, \left\langle x_{0,j}^{(r)} \right\rangle\right), j = 0, ..., n\right)$; and the line labelled C represents the sequence of points associated with the last $(n-j+1)$ column averages $\left(\left(40,000j, \left\langle x_{j,n}^{(r)} \right\rangle\right), j = 0, ..., n\right)$.

Referring to Figure 4.1 (a), as just mentioned, line B is the plot associated with the first j column averages computed from the data sampled during Replication 1. Starting at $j = 0$, which corresponds to time step $t = 0$, the plot of the first j column averages (line B) first follows the trend of the plot of the transformed points (line A), but as j increases, that is as the time step t increases, this tendency starts to dissipate. In fact, by the time approximately 10 billion Θ-BFACF moves in parallel have passed, the trend of the first j column averages has all but stopped mimicking the trend of line A. Hence an estimated upper bound for τ_{exp} obtained from this is 10 billion Θ-BFACF moves in parallel.

Still referring to Figure 4.1 (a), but now starting at $k = 80$ billion Θ-BFACF moves in parallel, as k decreases, that is as the time step t decreases, note that the plot of the last $(80,000,000,000-k+1)$ column averages (line C) follows the trend of the plot of the transformed points (line A), but after $k = 74$ billion Θ-BFACF moves in parallel, the trend of the last $(80,000,000,000-k+1)$ column averages has all but stopped following the trend of line A. Consequently an estimate for τ_{exp} would be $6 = 80-74$ billion Θ-BFACF moves in parallel. Hence it is concluded that τ_{exp} would lie somewhere between 6 and 10 billion Θ-BFACF moves in parallel yielding the estimate $\widehat{\tau}_{\text{exp},W}^{(1)} = 10$ billion Θ-BFACF moves in parallel.

Similarly an upper bound is estimated for the warm-up interval for each of the other nine replications from Figures 4.1 (b), 4.2 (a) and (b), ..., and 4.5 (a) and (b) and these

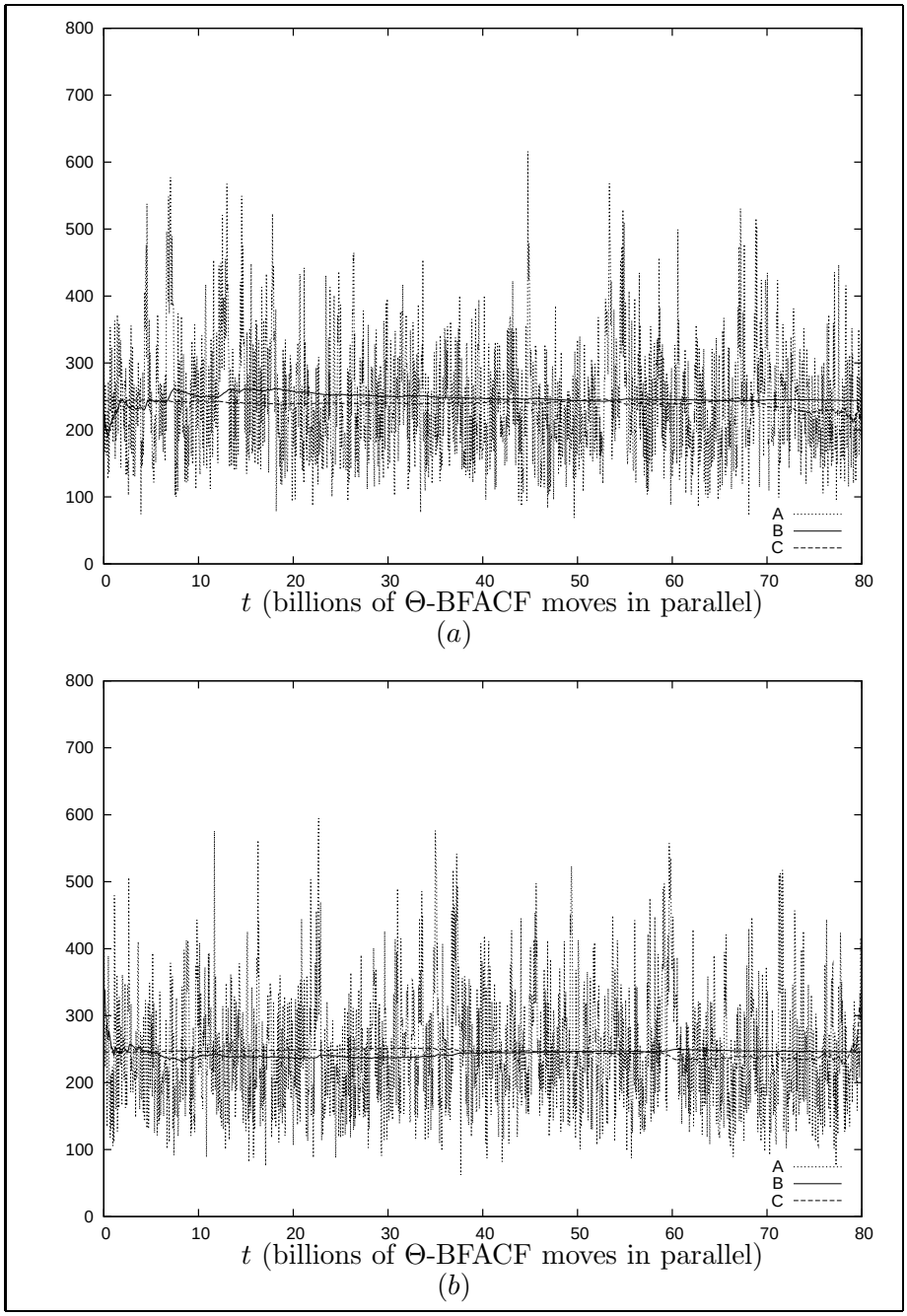

Figure 4.1: Figures (a) and (b) are the plots required to implement a warm-up analysis for Replications 1 and 2, respectively, where for $r \in \{1, 2\}$, the line labelled A represents the sequence of the transformed points $\left(\left(40,000j, x_j^{(r)}\right), j = 0, ..., n\right)$; the line labelled B represents the sequence of points associated with the first j column averages $\left(\left(40,000j, \left\langle x_{0,j}^{(r)} \right\rangle\right), j = 0, ..., n\right)$; and the line labelled C represents the sequence of points associated with the last $(n - j + 1)$ column averages $\left(\left(40,000j, \left\langle x_{j,n}^{(r)} \right\rangle\right), j = 0, ..., n\right)$.

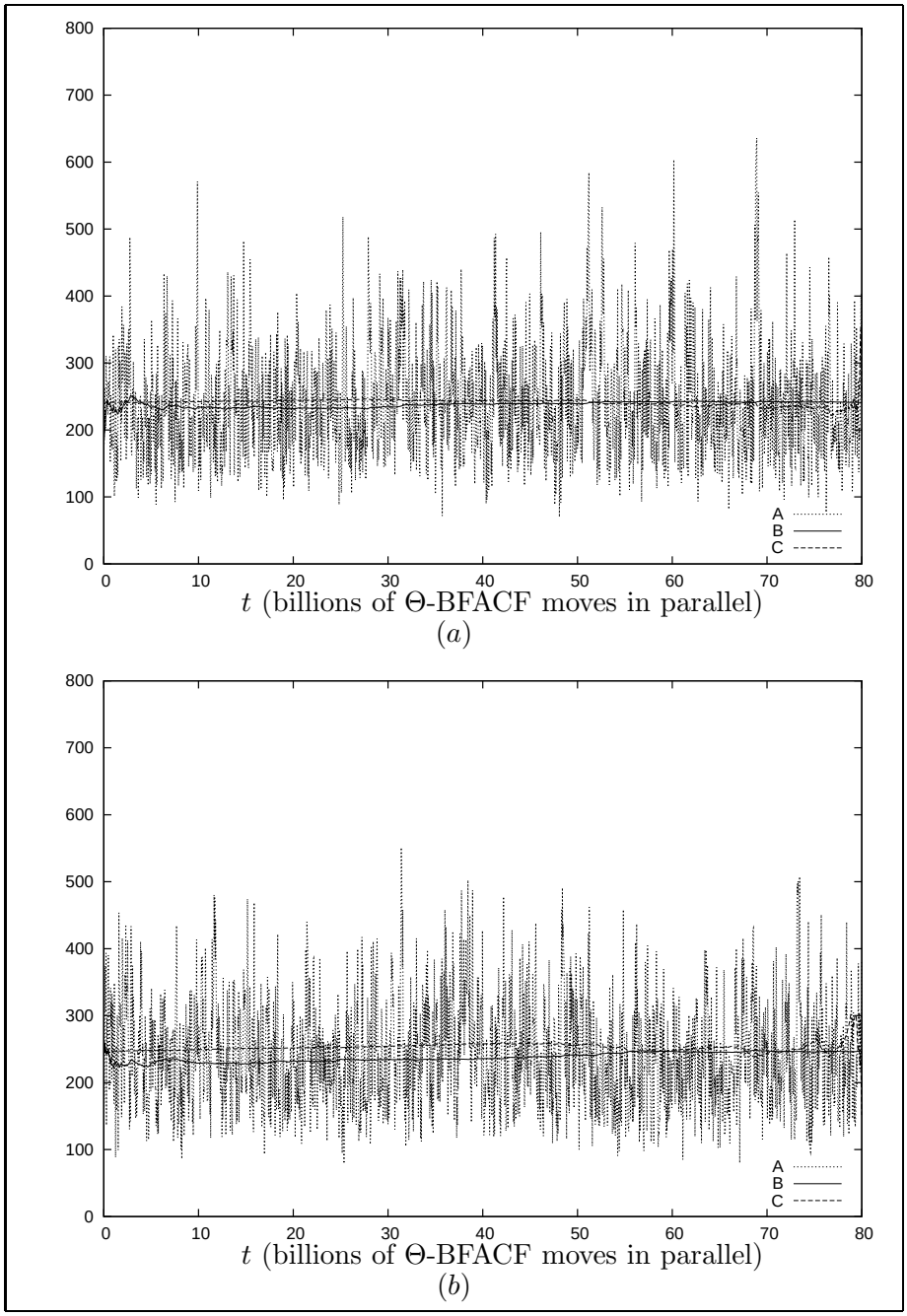

Figure 4.2: Figures (a) and (b) are the plots required to implement a warm-up analysis for Replications 3 and 4, respectively, where for $r \in \{3, 4\}$, the line labelled A represents the sequence of the transformed points $\left(\left(40,000j, x_j^{(r)}\right), j = 0, ..., n\right)$; the line labelled B represents the sequence of points associated with the first j column averages $\left(\left(40,000j, \left\langle x_{0,j}^{(r)} \right\rangle\right), j = 0, ..., n\right)$; and the line labelled C represents the sequence of points associated with the last $(n - j + 1)$ column averages $\left(\left(40,000j, \left\langle x_{j,n}^{(r)} \right\rangle\right), j = 0, ..., n\right)$.

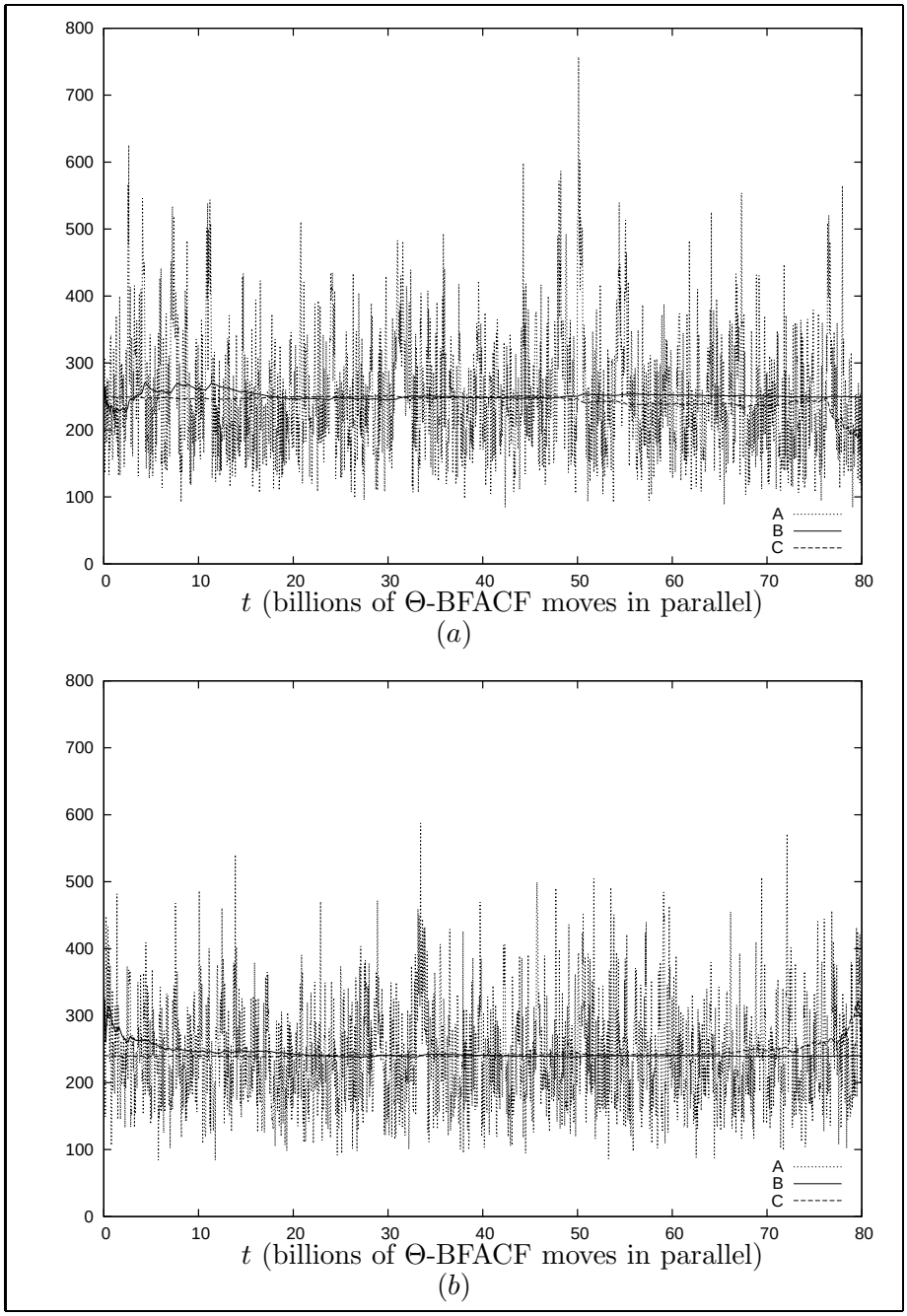

Figure 4.3: Figures (a) and (b) are the plots required to implement a warm-up analysis for Replications 5 and 6, respectively, where for $r \in \{5, 6\}$, the line labelled A represents the sequence of the transformed points $\left(\left(40,000j, x_j^{(r)}\right), j = 0, ..., n\right)$; the line labelled B represents the sequence of points associated with the first j column averages $\left(\left(40,000j, \left\langle x_{0,j}^{(r)} \right\rangle\right), j = 0, ..., n\right)$; and the line labelled C represents the sequence of points associated with the last $(n - j + 1)$ column averages $\left(\left(40,000j, \left\langle x_{j,n}^{(r)} \right\rangle\right), j = 0, ..., n\right)$.

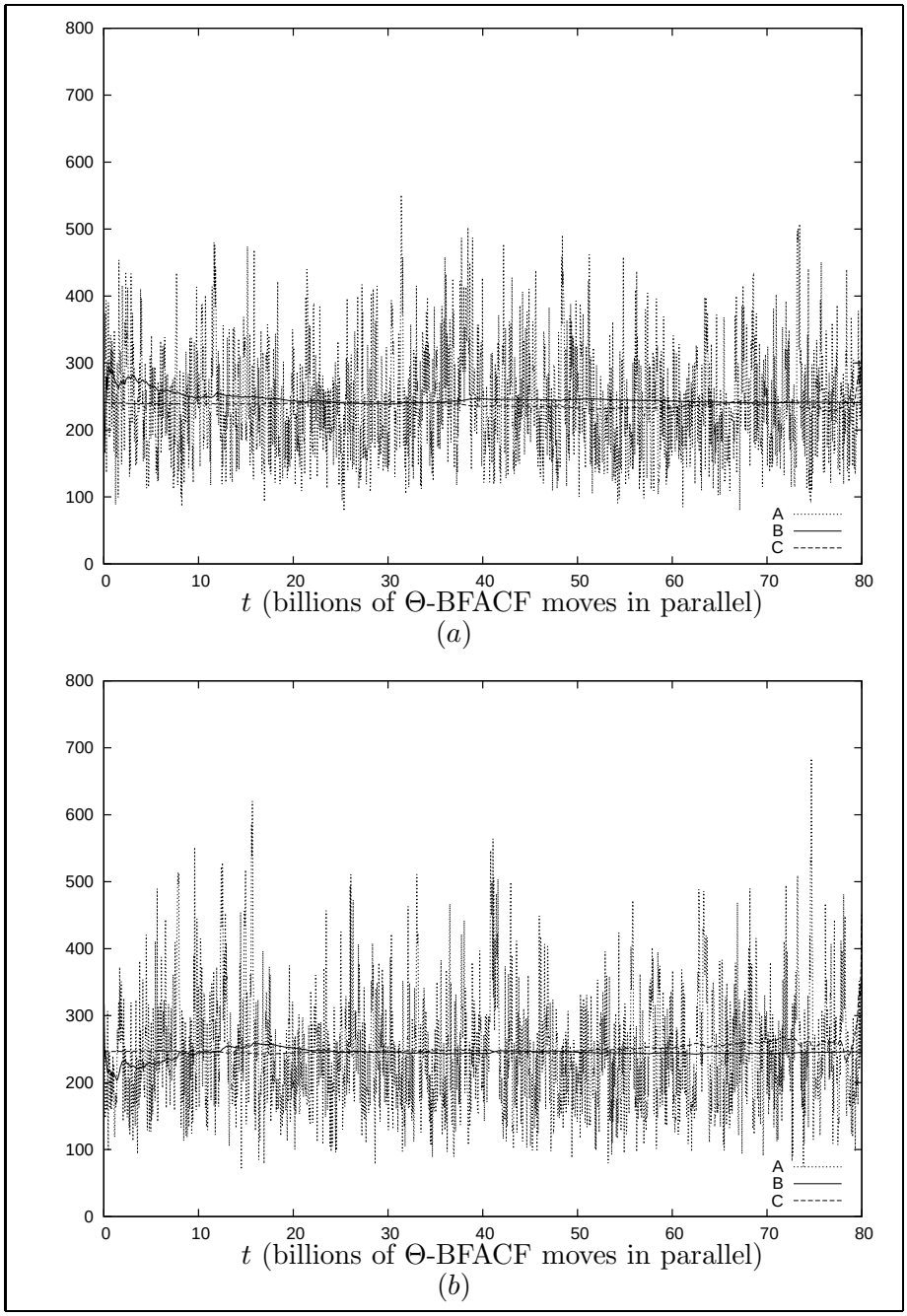

Figure 4.4: Figures (a) and (b) are the plots required to implement a warm-up analysis for Replications 7 and 8, respectively, where for $r \in \{7, 8\}$, the line labelled A represents the sequence of the transformed points $\left(\left(40,000j, x_j^{(r)}\right), j = 0, ..., n\right)$; the line labelled B represents the sequence of points associated with the first j column averages $\left(\left(40,000j, \left\langle x_{0,j}^{(r)} \right\rangle\right), j = 0, ..., n\right)$; and the line labelled C represents the sequence of points associated with the last $(n - j + 1)$ column averages $\left(\left(40,000j, \left\langle x_{j,n}^{(r)} \right\rangle\right), j = 0, ..., n\right)$.

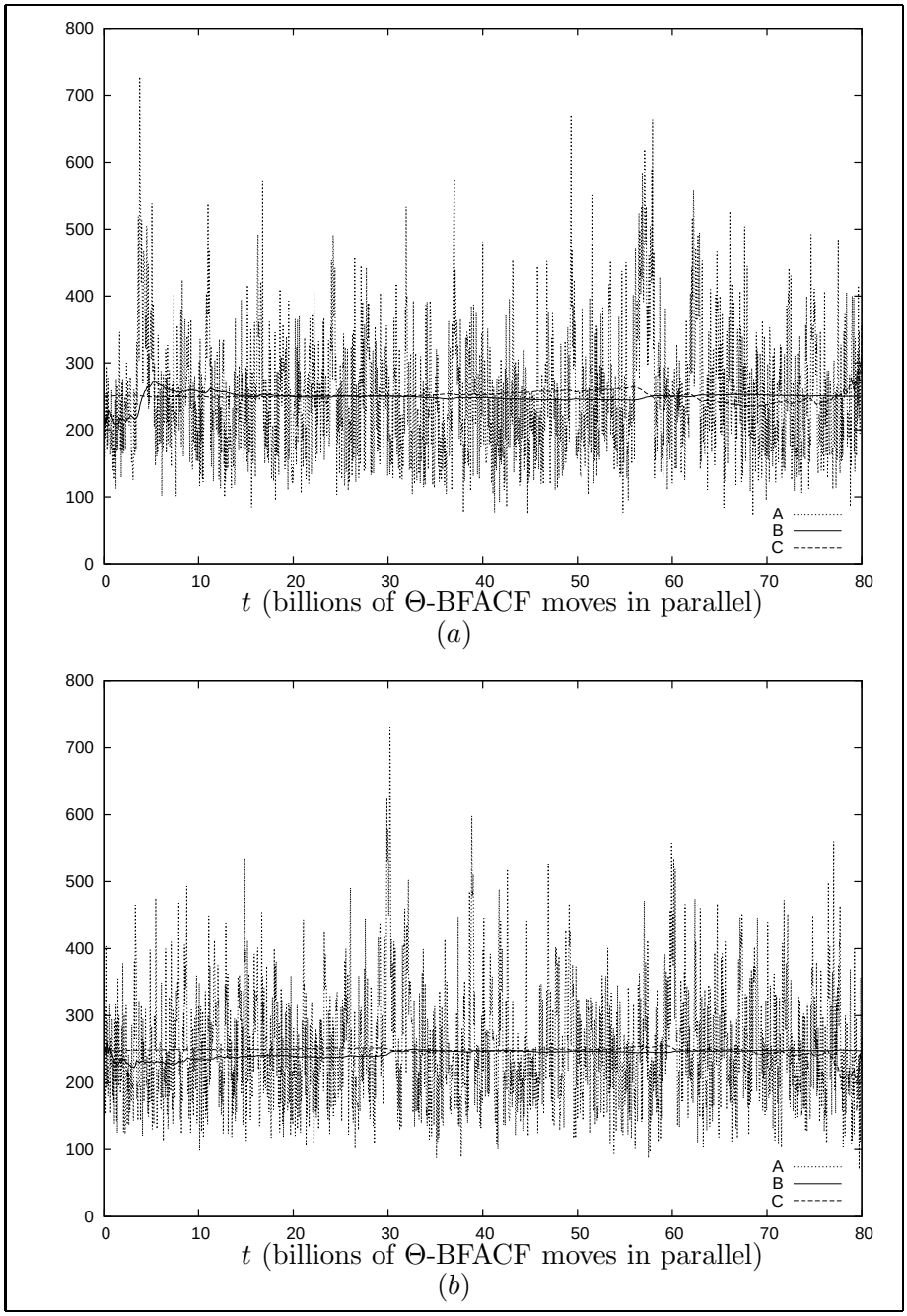

Figure 4.5: Figures (a) and (b) are the plots required to implement a warm-up analysis for Replications 9 and 10, respectively, where for $r \in \{9, 10\}$, the line labelled A represents the sequence of the transformed points $\left(\left(40,000j, x_j^{(r)}\right), j = 0, ..., n\right)$; the line labelled B represents the sequence of points associated with the first j column averages $\left(\left(40,000j, \left\langle x_{0,j}^{(r)} \right\rangle\right), j = 0, ..., n\right)$; and the line labelled C represents the sequence of points associated with the last $(n - j + 1)$ column averages $\left(\left(40,000j, \left\langle x_{j,n}^{(r)} \right\rangle\right), j = 0, ..., n\right)$.

Table 4.1: The estimates for τ_{exp} (in terms of 1 billion Θ-BFACF moves in parallel) based on a warm-up analysis of the data generated in Replication r.

Replication r	$\widehat{\tau}^{(r)}_{\text{exp},W}$	Replication r	$\widehat{\tau}^{(r)}_{\text{exp},W}$
1	10.0	6	8.0
2	9.0	7	10.0
3	8.0	8	10.0
4	6.0	9	9.0
5	12.0	10	4.0

estimated upper bounds are used to estimate the exponential autocorrelation time for Replication r. The resulting estimates $\widehat{\tau}^{(r)}_{\text{exp},W}$, for $r \in \{1, 2, .., 10\}$, are presented in Table 4.1.

Taking the maximum of the values presented in Table 4.1 (as defined by Equation (4.44)) yields $\widehat{\tau}_{\text{exp},W} = 12.0$ billion Θ-BFACF moves in parallel. To get a sense of how the estimates for $\widehat{\tau}^{(r)}_{\text{exp},W}$ vary across the ten replications, averaging the ten values in Table 4.1 and computing the corresponding standard error yields $\bar{\tau}_{\text{exp},W} = 8.6 \pm 0.7$ billion Θ-BFACF moves in parallel (where $\bar{\tau}_{\text{exp},W}$ is defined by Equation (4.48) and 0.7 is the sample standard error of the estimates in Table 4.1). Assuming the Central Limit Theorem can be applied, the corresponding 95% confidence would be $\tau_{\text{exp}} = 8.6 \pm 1.6$.

Depending on the starting state of a replication, the different replications may take different lengths of time to reach the stationary distribution. From the estimates for $\widehat{\tau}^{(r)}_{\text{exp},W}$, for $r \in \{1, 2, .., 10\}$, presented in Table 4.1, while some replications seemingly converge to the equilibrium distribution quickly, other replications take much longer (for example, Replication 5 is estimated to have taken three times as long as Replication 10 to converge to the equilibrium distribution). This illustrates the advantage of using more than one replication. For only a single replication, if the initial starting state leads to slow convergence to the equilibrium distribution, much time is wasted "converging" to the equilibrium distribution and less time is spent collecting data from the equilibrium distribution. To avoid this scenario, it is recommended that whenever possible, several replications, each starting in a different state, should be generated.

From Figures 4.1 (a) and (b), 4.2 (a) and (b), ..., and 4.5 (a) and (b), Replication r,

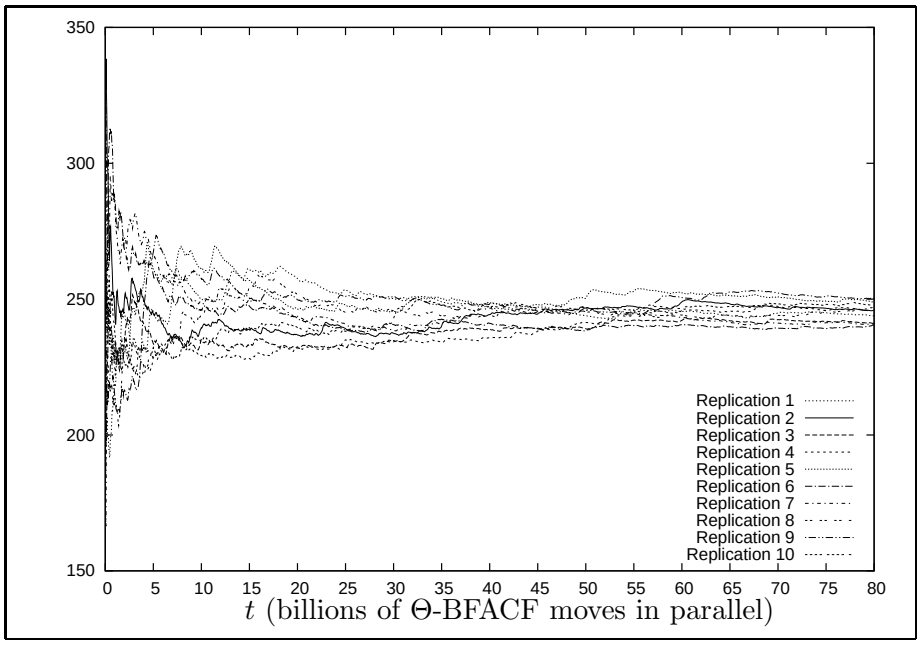

Figure 4.6: The first j column averages from Replications 1 through 10.

for $r \in \{1, 2, .., 10\}$, has apparently reached its equilibrium distribution after $\widehat{\tau}^{(r)}_{\exp,W}$ Θ-BFACF moves in parallel have passed, but, "Is the Markov chain really sampling from its equilibrium distribution or has the Markov chain reached a local equilibrium?". To answer this question, the estimated potential scale reduction method is implemented next.

Using an Estimated Potential Scale Reduction

To address whether or not the r'th replication has reached its equilibrium distribution, Fishman's suggestion [35] is followed and the sequence of points associated with the first j column averages $\left(\left(40,000j, \left\langle x^{(r)}_{0,j} \right\rangle\right), j = 0, ..., n\right)$, for each $r \in \{1, 2, .., 10\}$, are plotted on the same graph in order to determine whether the ten sequences have converged to the same region and repeatedly intersect one another. These ten sequences of points are displayed in Figure 4.6.

Referring to Figure 4.6, by inspection, the plots of the sequence of points associated with the first j column averages $\left(\left(40,000j, \left\langle x^{(r)}_{0,j} \right\rangle\right), j = 0, ..., n\right)$ seemingly are converging to the same region. The fact that the first j column averages plotted in Figure 4.6 do repeatedly intersect one and another is easier to see when the first j column averages for each replication are plotted using different colours. The conclusion that the first j column averages plotted in Figure 4.6 do repeatedly intersect one and another is based on this

colour plot. The colours are visible in the electronic version of this thesis. Hence, based on Figure 4.6, it is possible that the sample means are all converging to the same value but, to garner further support, the estimated potential scale reduction sequence as discussed in Section 4.2.2 is used.

Consider the sequence of points $\left(\left(40,000j, \sqrt{\widehat{R}_j}\right), j = 0, ..., n\right)$, where $\sqrt{\widehat{R}_j}$, as given by Equation (4.37), is

$$\sqrt{\widehat{R}_j} = \sqrt{\frac{j}{j+1} + \frac{1}{j+1}\frac{B_{10,j}}{W_{10,j}}}, \tag{4.138}$$

with

$$B_{10,j} = \frac{j+1}{9}\sum_{r=1}^{10}\left(\left\langle x_{0,j}^{(r)}\right\rangle - \langle x_{1,j,10}\rangle\right)^2 \tag{4.139}$$

and

$$W_{10,j} = \frac{1}{10j}\sum_{r=1}^{10}\sum_{k=0}^{j}\left(x_k^{(r)} - \left\langle x_{0,j}^{(r)}\right\rangle\right)^2. \tag{4.140}$$

Figure 4.7 (a) depicts the graph of the sequence $\left(\left(40,000j, \sqrt{\widehat{R}_j}\right), j = 0, ..., n\right)$ where the horizontal axis units are in terms of 1 billion Θ-BFACF moves in parallel. In order to get a better picture of what is happening near the beginning of each replication, Figure 4.7 (b) focusses on the region of Figure 4.7 (a) defined by the first 10 billion Θ-BFACF moves in parallel.

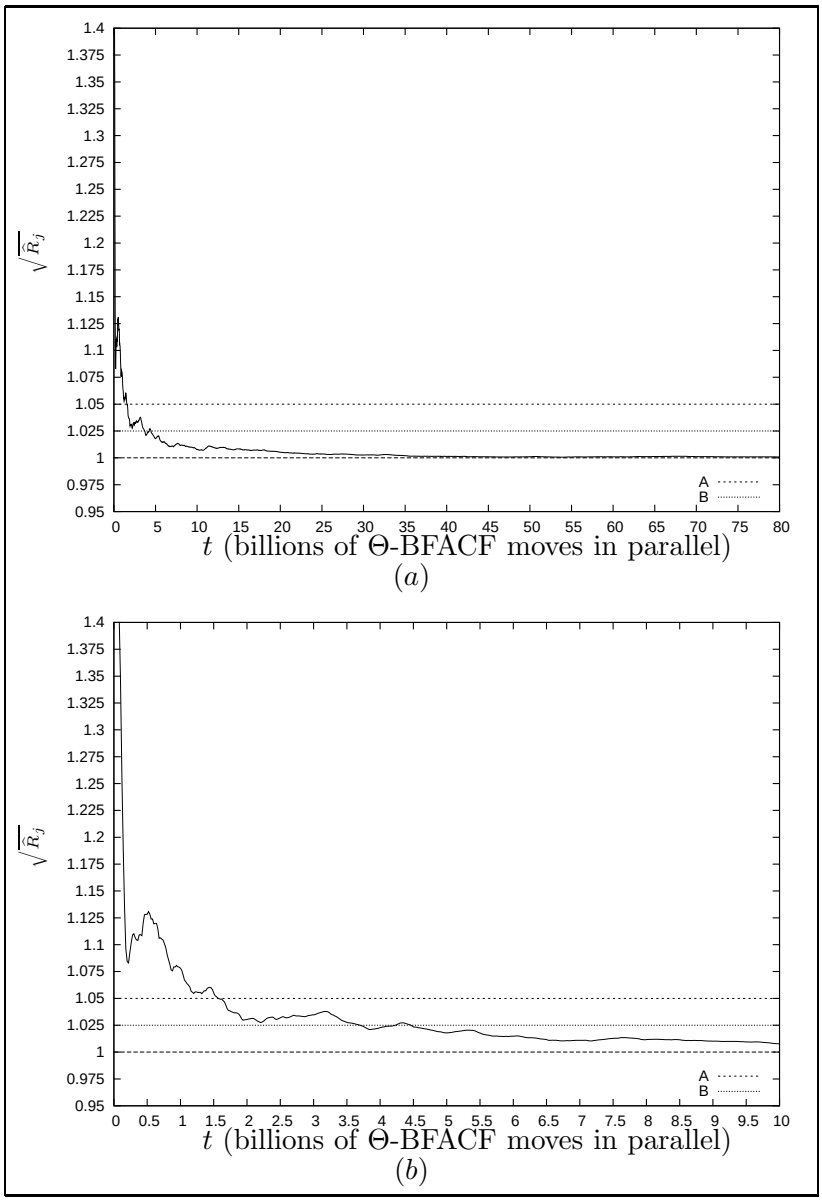

Figure 4.7: (a) The estimated potential scale reduction associated with $\left(\left(40,000j, \left\langle x_{0,j}^{(r)} \right\rangle\right), j = 0, ..., n\right)$. (b) The region in (a) defined by the first 10 billion Θ-BFACF moves in parallel. (In (a) and (b), the line A is the line $y = 1.05$ and the line B is the line $y = 1.025$.)

Using the value 1.1 (as suggested by Gelman [41]) as the cutoff value for $\sqrt{\widehat{R}_j}$, implies that after approximately 1.0 billion Θ-BFACF moves in parallel the "between the replication" standard deviation is always less than 10% higher than the "within the replication" standard deviation. To err on the side of conservatism and require that the "between the replication" standard deviation always be less than 2.5% higher than the "within the

replication" standard deviation, that is use 1.025 as the cutoff value for $\sqrt{\widehat{R}_j}$, then, from Figure 4.7 (b), the resulting estimate for $\tau_{\exp,E}$ is approximately 4.5 billion Θ-BFACF moves in parallel. Hence, for each replication, at the end of 5.0 billion Θ-BFACF moves in parallel (after rounding up to the nearest 1 billion Θ-BFACF moves in parallel), either a local equilibrium has been reached and the simulation is very slowly converging to the equilibrium distribution or the actual equilibrium distribution has been reached. Because the ten replications were started in distinct starting states, it is more likely that the replications have converged to the equilibrium distribution as opposed to all ten replications being trapped in the same local equilibrium. Therefore $\widehat{\tau}^{(r)}_{\exp,E} = 5.0$ billion Θ-BFACF moves in parallel, and, as a result, $\widehat{\tau}_{\exp,E}$ is also 5.0 billion Θ-BFACF moves in parallel.

Because the sub-sample formed by taking every $\left(1.2 \times 10^6\right)$'th data point passed the Test for Independence outlined in Algorithm 4.3.1, this sub-sample can be considered an essentially independent sample. This essentially independent sample is used in the next section

The Mixing of the Chains

Once in equilibrium, because the distribution of the colours throughout the CMC's chains is expected to be uniform, the time it takes to reach the CMC's equilibrium distribution can be estimated by determining the time step after which the colourings appear to be uniformly distributed amongst the CMC's chains. The χ^2 *Test for Goodness of Fit* is used to compare, for each replication, the proportion of the number of times a particular chain is labelled by a particular colour to the discrete uniform distribution in order to test the uniformity of: for fixed colour, uniformity across the chains; for fixed chain, uniformity across the colours; and uniformity across the entire CMC.

For each of the ten replications, the movement of the colourings throughout the CMC's sub-chains was monitored. To determine whether or not each sample from the ten replications is well-mixed, an essentially independent sub-sample is required from each of the ten replications. Because the sub-sample formed by taking every $\left(1.2 \times 10^6\right)$'th data point passed the Test for Independence outlined in Algorithm 4.3.1, this sub-sample is considered an essentially independent sample and is used to determine how well-mixed each of the replications is..

In order to have a sufficient number of observations to determine whether the sample

Table 4.2: The p-values calculated using df = 13 for each of the colors $a, b, c, ..., n$ for each of the ten replications after no data points were discarded.

	Replication									
Colour	1	2	3	4	5	6	7	8	9	10
a	0.222	0.451	0.712	0.519	0.318	0.878	0.427	0.718	0.212	0.609
b	0.047	0.075	0.159	0.816	0.102	0.071	0.164	0.555	0.755	0.837
c	0.147	0.228	0.827	0.236	0.493	0.284	0.750	0.019	0.540	0.581
d	0.851	0.667	0.883	0.262	0.018	0.946	0.047	0.600	0.944	0.209
e	0.929	0.726	0.309	0.747	0.255	0.889	0.647	0.008	0.210	0.059
f	0.115	0.830	0.825	0.002	0.768	0.297	0.220	0.060	0.089	0.283
g	0.162	0.814	0.187	0.595	0.751	0.119	0.142	0.052	0.493	0.900
h	0.887	0.081	0.935	0.425	0.713	0.004	0.013	0.014	0.469	0.526
i	0.875	0.718	0.664	0.965	0.050	0.049	0.150	0.671	0.513	0.418
j	0.495	0.139	0.090	0.919	0.230	0.850	0.375	0.178	0.931	0.447
k	0.465	0.258	0.008	0.531	0.172	0.625	0.250	0.487	0.604	0.215
l	0.713	0.546	0.429	0.372	0.217	0.642	0.354	0.212	0.025	0.446
m	0.436	0.197	0.398	0.031	0.299	0.220	0.647	0.276	0.652	0.634
n	0.960	0.150	0.610	0.325	0.111	0.338	0.286	0.270	0.573	0.832

is well-mixed (as defined in Section 4.2.3), at least $13(> \sqrt{10 \cdot 14})$ observations from each replication is required. As each replication consisted of 8.0×10^{10} Θ-BFACF moves in parallel, the resulting sub-sample consists of 66 essentially independent data points. Hence the essentially independent sample is of sufficient size. Recall from Section 4.2.3 that k is the first value in $[0, 66 - k]$ for which the sub-sample formed using the last $66 - k$ observations is considered well-mixed. Let d_r be the smallest number of data points that need to be burned (discarded) from the essentially independent sample created from Replication r so that the sample is considered well-mixed and let $\hat{d}_r$ be the estimate for d_r.

Assume that each replication is started in the equilibrium distribution. Then Table 4.2 contains the p-values calculated under this assumption using df = 13, for each of the colours $a, b, c, ..., n$, for each of the ten replications.

Table 4.3: The p-values calculated using df = 13 for each of the colors $a, b, c, ..., n$ for Replications 4, 5, and 7, after the first four 14-tuples were discarded from the essentially independent sample generated in Replications 4, 5, and 7.

	Replication				Replication		
Colour	4	5	7	Colour	4	5	7
a	0.402	0.214	0.245	h	0.549	0.533	0.038
b	0.951	0.278	0.192	i	0.928	0.084	0.360
c	0.187	0.617	0.785	j	0.980	0.143	0.423
d	0.168	0.069	0.065	k	0.359	0.237	0.211
e	0.733	0.283	0.748	l	0.489	0.320	0.279
f	0.001	0.663	0.125	m	0.165	0.314	0.677
g	0.487	0.876	0.448	n	0.351	0.078	0.164

For any colour whose associated p-value< 0.05 in Table 4.2, the proportion of time that colour (in the replication) appeared in each of the fourteen chains differs significantly from $\frac{1}{14}$, the hypothesized value. To be 95% confident that the realized CMC is well-mixed for a particular replication, at most one ($0.05 \cdot 14 \approx 1$) of the fourteen colours is expected to not be distributed uniformly across the chains. As long as none or one of the fourteen colours is not distributed uniformly across the chains, then the sample (and hence the underlying CMC) is considered well-mixed. Using this criterion for being well-mixed, from Table 4.2, Replications 1, 2, 3, 9, and 10 are well-mixed. Hence $\hat{d}_1 = \hat{d}_2 = \hat{d}_3 = \hat{d}_9 = \hat{d}_{10} = 0$.

In order for the sample from Replications 4, 5, and 7 to be considered well-mixed, the first four data points in the sample need to be discarded, that is $\hat{d}_4 = \hat{d}_5 = \hat{d}_7 = 4$. Table 4.3 displays the p-values for Replications 4, 5, and 7, calculated using df = 13, for each of the colours $a, b, c, ..., n$, after $\hat{d}_4 = \hat{d}_5 = \hat{d}_7 = 4$ data points are discarded.

In order for the sample from Replications 6 and 8, respectively, to be considered well-mixed, for Replication 6, the first thirty-seven data points need to be discarded, that is $\hat{d}_6 = 37$, and, for Replication 8, the first twenty-five data points need to be discarded, that is $\hat{d}_8 = 25$. Table 4.4 displays the p-values for Replications 6 and 8, calculated using df = 13, for each of the colours $a, b, c, ..., n$, after $\hat{d}_6 = 37$ and $\hat{d}_8 = 25$ data points, respectively, have been discarded. The values of $\hat{d}_r$ required for all ten replications to be considered well-mixed are summarized in Table 4.5.

Table 4.4: The p-values calculated using df $= 13$ for each of the colors $a, b, c, ..., n$ for Replications 6 and 8 calculated using df $= 13$ for each of the colors $a, b, c, ..., n$ after the first $\hat{d}_6 = 37$ and $\hat{d}_8 = 25$ 14-tuples were discarded from Replications 6 and 8, respectively.

	Replication			Replication	
Colour	6	8	Colour	6	8
a	0.752	0.182	h	0.135	0.198
b	0.143	0.181	i	0.467	0.260
c	0.084	0.042	j	0.169	0.138
d	0.523	0.665	k	0.705	0.666
e	0.394	0.282	l	0.547	0.261
f	0.195	0.262	m	0.201	0.427
g	0.263	0.204	n	0.565	0.430

Table 4.5: Column 2 displays the number of data points from Replication i's essentially independent sample that must be discarded in order to conclude that the sample is well-mixed. Column 3 displays the estimates for τ_{exp} from Replication r (in terms of billions of Θ-BFACF moves in parallel) based on the number of data points from an essentially independent sample that must be discarded so that the remaining sample is well-mixed.

Replication r	$\hat{d}_r$	$\widehat{\tau}^{(r)}_{\text{exp},C}$	Replication r	$\hat{d}_r$	$\widehat{\tau}^{(r)}_{\text{exp},C}$
1	0	0.0	6	37	45.0
2	0	0.0	7	4	5.0
3	0	0.0	8	25	30.0
4	4	5.0	9	0	0.0
5	4	5.0	10	0	0.0

Because each estimate $\hat{d}_r$, for $r \in \{1, 2, .., 10\}$, is the number of data points that should be discarded from Replication r's essentially independent sample so that the remaining sample can be considered well-mixed, the estimates $\hat{d}_r$, for $r \in \{1, 2, .., 10\}$, provide further estimates for τ_{exp}. Table 4.5 contains the values of $\widehat{\tau}^{(r)}_{\text{exp},C}$ (in terms of 1 billion Θ-BFACF moves in parallel) defined by

$$\widehat{\tau}^{(r)}_{\text{exp},C} := \left\lceil 2\hat{d}_r \widehat{\tau}_{\text{int}} \right\rceil, \tag{4.141}$$

where $\lceil x \rceil$ is the least integer greater than or equal to x. The estimates reported in Table 4.5 were calculated using Equation (4.141) and then rounded up to the nearest one billion Θ-BFACF moves in parallel.

Since the values of $\widehat{\tau}_{\text{exp},C}^{(r)}$, for $r \in \{1, 2, .., 10\}$, in Table 4.5 are all estimates for τ_{exp} for the Markov chain generated by the CMC Θ-BFACF algorithm, an estimate for τ_{exp} can be obtained by simply averaging the ten values in Table 4.5, that is

$$\bar{\tau}_{\text{exp},C} := \frac{1}{10} \sum_{r=1}^{10} \widehat{\tau}_{\text{exp},C}^{(r)}. \tag{4.142}$$

Recall that because the distribution of $\widehat{\tau}_{\text{exp},C}^{(r)}$ is unknown and because the Central Limit theorem may not hold (the estimate for $\bar{\tau}_{\text{exp},C}$ is based on only ten values), in order to explore the variability of the estimates $\widehat{\tau}_{\text{exp},C}^{(r)}$ as a function of the replication, the estimated standard error of $\bar{\tau}_{\text{exp},C}$ is reported. Using the data in Table 4.5 yields the estimate $\bar{\tau}_{\text{exp},C} = 9.0 \pm 5.0$ billion Θ-BFACF moves in parallel (where 5.0 is the estimated sample standard error of the estimate for $\bar{\tau}_{\text{exp},C}$). If the Central Limit Theorem can be applied, then a 95% confidence interval is $\tau_{\text{exp}} = 9.0 \pm 11.31$. Calculating an estimate for $\widehat{\tau}_{\text{exp},C}$, as defined by Equation (4.46), using the data in Table 4.5 yields $\widehat{\tau}_{\text{exp},C} = 37$.

Computing Equation (4.47) yields the estimate $\widehat{\tau}_{\text{exp}} = 37.0$ billion Θ-BFACF moves in parallel for τ_{exp}. Recall from Section 4.7.1 that an estimate for τ_{exp} from a warm-up analysis is $\bar{\tau}_{\text{exp},W} = 8.6 \pm 0.7$ billion Θ-BFACF moves in parallel and from an estimated potential scale reduction is $\bar{\tau}_{\text{exp},E} = 5.0$ billion Θ-BFACF moves in parallel. Because $\bar{\tau}_{\text{exp},E}$ has the same order of magnitude as $\bar{\tau}_{\text{exp},W}$ and $\bar{\tau}_{\text{exp},C}$ and because $\bar{\tau}_{\text{exp},W}$ and $\bar{\tau}_{\text{exp},E}$ lie within one estimated standard error of $\bar{\tau}_{\text{exp},C}$, these three estimates for τ_{exp} are consistent.

Erring on the side of conservatism, the estimate $\widehat{\tau}_{\text{exp}} = 37.0$ billion Θ-BFACF moves in parallel could be used as an estimate for τ_{exp} for the system. This would lead to the conclusion that, because $\widehat{\tau}_{\text{exp}}$ is greater than two percent of the total 80 billion Θ-BFACF moves in parallel implemented in each replication, all of the data generated by the first 37.0 billion Θ-BFACF moves in parallel must be excluded from all data analysis. In fact, $\widehat{\tau}_{\text{exp}} = 37.0$ billion Θ-BFACF moves in parallel of τ_{exp} suggests that almost half of the data generated in each replication should be discarded. But, is discarding the data generated by the first 37.0 billion Θ-BFACF moves in parallel too conservative?

For support that $\widehat{\tau}_{\text{exp}} = 37.0$ billion Θ-BFACF moves in parallel is too conservative an estimate for τ_{exp}, cf. Figure 4.8. Line A in Figure 4.8 is the sequence of points

$((40,000j, \langle x_j \rangle), j = 0, ..., n)$; Line B represents the sequence of points associated with the first j column averages $((40,000j, \langle x_{0,j} \rangle), j = 0, ..., n)$; and Line C represents the sequence of points associated with the last $(n-j+1)$ column averages $((40,000j, \langle x_{j,n} \rangle), j = 0, ..., n)$, where

$$\langle x_t \rangle = \frac{1}{10} \sum_{r=1}^{10} x_t^{(r)} \tag{4.143}$$

and

$$\langle x_{k,m} \rangle = \frac{1}{(m-k+1)} \sum_{t=k}^{m} \langle x_t \rangle . \tag{4.144}$$

The behaviour of Line B stops following the trend of Line A after the first 5.0 billion Θ-BFACF moves in parallel have been completed. The behaviour of Line C starts following the trend of Line A after 75.0 billion Θ-BFACF moves in parallel have been implemented (or equivalently, the behaviour of Line C follows the trend of Line A for the last 5.0 billion Θ-BFACF moves in parallel of the simulation). Figure 4.8 suggests that considering the data generated from all ten replications as one large data set, setting $\widehat{\tau}_{\text{exp}} = 5.0$ billion Θ-BFACF moves in parallel is sufficient and that setting $\widehat{\tau}_{\text{exp}} = 37.0$ billion Θ-BFACF moves in parallel would lead to discarding an extra forty percent of the data (data seemingly sampled from close to, if not from within, the equilibrium distribution).

For this reason, $\widehat{\tau}_{\text{exp}} = 5.0$ billion Θ-BFACF moves in parallel is the estimate that will be used for τ_{exp} in the data analysis in the following three chapters.

4.7.2 Estimating τ_{int}

In Section 4.3, three techniques were provided for estimating τ_{int}: using $\widehat{\tau}_{\text{exp},W}^{(r)}$, using a batch means analysis, and using a series/windowing analysis. Recall from Section 4.3 that the estimates for τ_{int} from Replication r for these three techniques are respectively $\widehat{\tau}_{\text{int},W}^{(r)}$, $\widehat{\tau}_{\text{int},B(\mathbb{k})}^{(r)}$, and $\widehat{\tau}_{\text{int},S(\mathbb{k})}^{(r)}$ and that the corresponding across all ten chain maximum estimates are respectively $\widehat{\tau}_{\text{int},W} = \max_r \left\{ \widehat{\tau}_{\text{int},W}^{(r)} \right\}$, $\widehat{\tau}_{\text{int},B(\mathbb{k})} = \max_r \left\{ \widehat{\tau}_{\text{int},B(\mathbb{k})}^{(r)} \right\}$, and $\widehat{\tau}_{\text{int},S(\mathbb{k})} = \max_r \left\{ \widehat{\tau}_{\text{int},S(\mathbb{k})}^{(r)} \right\}$, where $\mathbb{k}$ is the number of sample points burned in the analysis. Also recall from Section 4.3 that the desired estimate for τ_{int} is

$$\widehat{\tau}_{\text{int}} = \max \left\{ \widehat{\tau}_{\text{int},W}, \widehat{\tau}_{\text{int},B}, \widehat{\tau}_{\text{int},S} \right\}, \tag{4.145}$$

where $\widehat{\tau}_{\text{int},B} = \max_{\mathbb{k}} \left\{ \widehat{\tau}_{\text{int},B(\mathbb{k})} \right\}$ and $\widehat{\tau}_{\text{int},S} = \max_{\mathbb{k}} \left\{ \widehat{\tau}_{\text{int},S(\mathbb{k})} \right\}$, and that $\bar{\tau}_{\text{int},W}$, $\bar{\tau}_{\text{int},B(\mathbb{k})}$, and $\bar{\tau}_{\text{int},S(\mathbb{k})}$ are the corresponding across-the-replication averages.

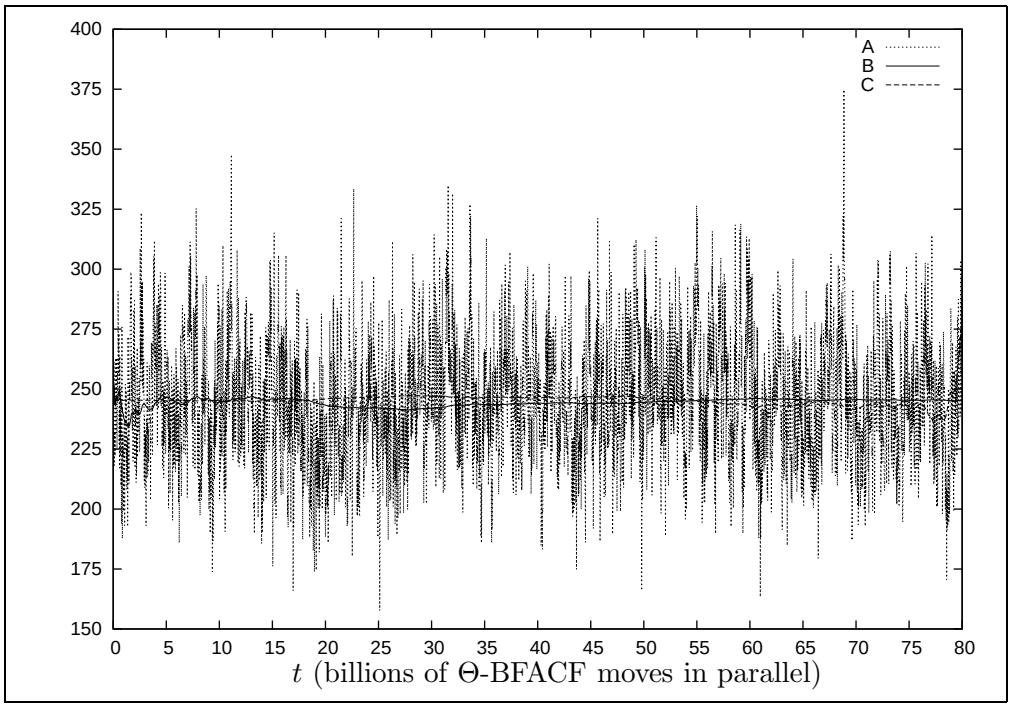

Figure 4.8: Line A is the sequence of points $((40,000j, \langle x_j \rangle), j = 0, ..., n)$; the line labelled B represents the sequence of points associated with the first j column averages $((40,000j, \langle x_{0,j} \rangle), j = 0, ..., n)$; and the line labelled C represents the sequence of points associated with the last $(n - j + 1)$ column averages $((40,000j, \langle x_{j,n} \rangle), j = 0, ..., n)$.

Table 4.6: The estimates for τ_{int} (in terms of 1 billion Θ-BFACF moves in parallel) based on a warm-up analysis of the data generated in Replication r.

Replication r	$\widehat{\tau}^{(r)}_{\text{int},W}$	Replication r	$\widehat{\tau}^{(r)}_{\text{int},W}$
1	0.50	6	0.40
2	0.45	7	0.50
3	0.40	8	0.50
4	0.30	9	0.45
5	0.60	10	0.20

Determining $\widehat{\tau}_{\text{int},W}$

Based on the relation $\tau_{\text{int}}(f) \approx \tau_{\text{exp}}/20$ (as discussed in Section 4.3.1), estimates for τ_{int} can be determined for each of the ten replications via the estimates $\widehat{\tau}^{(r)}_{\text{exp},W}$ as presented in Table 4.1. The estimates $\widehat{\tau}^{(r)}_{\text{int},W}$ corresponding to the estimates $\widehat{\tau}^{(r)}_{\text{exp},W}$ are presented in Table 4.6.

Calculating $\widehat{\tau}_{\text{int},W}$ using the data in Table 4.6 yields $\widehat{\tau}_{\text{int},W} = 0.60$ billion Θ-BFACF moves in parallel. To determine how $\widehat{\tau}^{(r)}_{\text{int},W}$ varies across the ten replications, averaging the ten estimates in Table 4.6 and computing the associated standard error yields $\bar{\tau}_{\text{int},W} = 0.43 \pm 0.04$ billion Θ-BFACF moves in parallel (where $\bar{\tau}_{\text{int},W}$ is computed using Equation (4.78) and 0.04 is the standard error computed using the estimates in Table 4.6). If the Central Limit does hold, then a 95% confidence interval for $\tau_{\text{int}} = 0.43 \pm 0.09$.

In the next two subsections, the estimates $\widehat{\tau}_{\text{int},B}$ and $\widehat{\tau}_{\text{int},S}$ are respectively determined. In both subsections, the dependence of the estimates $\widehat{\tau}_{\text{int},B}$ and $\widehat{\tau}_{\text{int},S}$ on the amount of data burned, for each replication, are explored. In each of the two following subsections, the first scenario (Case 1) assumes that sampling began from the equilibrium distribution and that no data is burned. This scenario is the $\mathbb{k} = 0$ case. The next scenario (Case 2) assumes that after $\widehat{\tau}_{\text{exp},E} = 5.0$ billion Θ-BFACF moves in parallel (the estimate for τ_{exp} based on an estimated potential scale reduction), the equilibrium distribution has been reached and that the first 5.0 million sample points have been discarded. This scenario is the $\mathbb{k} = 5.0 \times 10^6$ case. The third and final scenario (Case 3) assumes that, for Replication r, after $\widehat{\tau}^{(r)}_{\text{exp},W}$ billion Θ-BFACF moves in parallel (the estimate for τ_{exp} based on a warm-up analysis of Replication r), the equilibrium distribution has been reached and that the

first $\widehat{\tau}^{(r)}_{\text{exp},W}$ million sample points need to be discarded. This scenario is the $\mathbb{k} = \mathbb{k}_r \times 10^6$ case. Since both of the estimates $\widehat{\tau}_{\text{int},B}$ and $\widehat{\tau}_{\text{int},S}$ are functions of $\mathbb{k}$, the number of sample points discarded, the estimates $\widehat{\tau}_{\text{int},B(\mathbb{k})}$, $\widehat{\tau}_{\text{int},S(\mathbb{k})}$, $\bar{\tau}_{\text{int},B(\mathbb{k})}$, and $\bar{\tau}_{\text{int},S(\mathbb{k})}$ will be computed for each of the values of $\mathbb{k}$ described in the three different cases.

Determining $\widehat{\tau}_{\text{int},B}$

Given a particular value of $\mathbb{k}$, to determine $\widehat{\tau}_{\text{int},B(\mathbb{k})}$, for $r \in \{1, 2, .., 10\}$, the block sizes $b_r(\mathbb{k})$ are required such that the following sample averages pass the Test for Independence provided in Section 4.3.2: $\left\langle x^{(r)}_{1,b_r(\mathbb{k})} | \mathbb{k} \right\rangle$, $\left\langle x^{(r)}_{b_r(\mathbb{k})+1,2b_r(\mathbb{k})} | \mathbb{k} \right\rangle$, ..., $\left\langle x^{(r)}_{(l-1)b_r(\mathbb{k})+1,lb_r(\mathbb{k})} | \mathbb{k} \right\rangle$, where $lb_r(\mathbb{k}) \leq 8.0 \times 10^7$ (the size of the sample collected from each of the ten replications), and

$$\left\langle x^{(r)}_{l,m} | \mathbb{k} \right\rangle := \frac{1}{m - l + 1} \sum_{t=l+\mathbb{k}}^{m+\mathbb{k}} x^{(r)}_t. \tag{4.146}$$

Such estimates for $b_r(\mathbb{k})$, for $r \in \{1, 2, .., 10\}$, are denoted $\hat{b}_r(\mathbb{k})$. To explore how the estimate for τ_{int} based on a batch means analysis depends on $\mathbb{k}$, the three cases: $\mathbb{k} = 0$; $\mathbb{k} = 5.0 \times 10^6$; and $\mathbb{k} = \mathbb{k}_r \times 10^6$ are now considered.

Case 1: $\mathbb{k} = 0$. Each of the replications is started in the equilibrium distribution and no data is discarded in the analysis. The second column in Table 4.7 provides the required estimates $\hat{b}_r(0)$ (for each Replication r, where $r \in \{1, 2, .., 10\}$). The third column in Table 4.7 presents the associated estimate for τ_{int} computed using Equation (4.60). Note that the values of $\widehat{\tau}^{(r)}_{\text{int},B(0)}$, for $r \in \{1, 2, .., 10\}$, in Table 4.7 all have the same order of magnitude. In order to get a sense of how $\widehat{\tau}^{(r)}_{\text{int},B(0)}$ varies across the ten replications, calculating $\bar{\tau}_{\text{int},B(0)}$ (as given by Equation (4.79)) using the data in Table 4.7 yields the estimate $\bar{\tau}_{\text{int},B(0)} = 0.375 \pm 0.043$ billion Θ-BFACF moves in parallel (where 0.043 is the estimated standard error of $\bar{\tau}_{\text{int},B(0)}$). If the Central Limit does hold, then a 95% confidence interval for $\tau_{\text{int}} = 0.375 \pm 0.097$.

Case 2: $\mathbb{k} = 5.0 \times 10^6$. Each of the replications is started in some non-equilibrium distribution, but, after $\widehat{\tau}_{\text{exp},E}$ (5.0 billion Θ-BFACF moves in parallel), each replication has reached the equilibrium distribution. The fourth column in Table 4.7 provides the required estimates $\hat{b}_r(5.0 \times 10^6)$ (for Replication r, where $r \in \{1, 2, .., 10\}$). The fifth column in Table 4.7 presents the associated estimate for τ_{int} computed using Equation (4.60). Note that the estimates $\widehat{\tau}^{(r)}_{\text{int},B(5.0\times10^6)}$, for $r \in \{1, 2, .., 10\}$, in Table 4.7 all have the

Table 4.7: The estimates for the time between independent data points b_r and the integrated autocorrelation time τ_{int} (in terms of 1 billion Θ-BFACF moves in parallel) based on a batch means analysis of the data generated when 5.0×10^6 data points are burned from Replication r.

Replication r	$\hat{b}_r(0)$	$\widehat{\tau}^{(r)}_{\text{int},B(0)}$	$\hat{b}_r(5.0 \times 10^6)$	$\widehat{\tau}^{(r)}_{\text{int},B(5.0\times10^6)}$
1	0.60	0.30	0.60	0.30
2	0.60	0.30	0.60	0.30
3	0.30	0.15	0.40	0.20
4	1.00	0.50	0.90	0.45
5	0.90	0.45	0.60	0.30
6	0.50	0.25	0.50	0.25
7	1.00	0.50	1.00	0.50
8	0.70	0.35	0.70	0.35
9	1.20	0.60	1.00	0.50
10	0.70	0.35	0.90	0.45

same order of magnitude and all have the same order of magnitude as the estimates $\widehat{\tau}^{(r)}_{\text{int},B(0)}$, for $r \in \{1, 2, .., 10\}$, in the third column of Table 4.7. Calculating $\bar{\tau}_{\text{int},B(5.0\times10^6)}$ using Equation (4.79) yields $\bar{\tau}_{\text{int},B(5.0\times10^6)} = 0.360 \pm 0.034$ billion Θ-BFACF moves in parallel (where 0.034 is the estimated standard error of $\bar{\tau}_{\text{int},B(5.0\times10^6)}$). If the Central Limit can be applied, then a 95% confidence interval for $\tau_{\text{int}} = 0.360 \pm 0.077$. Note that the point estimate $\bar{\tau}_{\text{int},B(5.0\times10^6)}$ lies within one standard error of the point estimate $\bar{\tau}_{\text{int},B(0)}$ and the point estimate $\bar{\tau}_{\text{int},B(0)}$ lies within one standard error of $\bar{\tau}_{\text{int},B(5.0\times10^6)}$. Hence $\bar{\tau}_{\text{int},B(0)}$ and $\bar{\tau}_{\text{int},B(5.0\times10^6)}$ are consistent with each other.

Case 3: $\mathbb{k} = \mathbb{k}_r \times 10^6$. Each of the replications is started in some non-equilibrium distribution and after $\widehat{\tau}^{(r)}_{\text{exp},W}$, the single starting state warm-up period given in Table 4.1, each replication has reached the equilibrium distribution. The third column in Table 4.8 provides the estimates $\hat{b}_r(\mathbb{k}_r \times 10^6)$ (for Replication r, where $r \in \{1, 2, .., 10\}$). The fourth column in Table 4.8 presents the associated estimate for τ_{int} computed using Equation (4.60). Note that the estimates $\widehat{\tau}^{(r)}_{\text{int},B(\mathbb{k}_r\times10^6)}$, for $r \in \{1, 2, .., 10\}$, in Table 4.8 all have the same order of magnitude and all have the same order of magnitude as the estimates $\widehat{\tau}^{(r)}_{\text{int},B(0)}$ and $\widehat{\tau}^{(r)}_{\text{int},B(5.0\times10^6)}$ for $r \in \{1, 2, .., 10\}$ in the third and fifth columns of Table 4.7

Table 4.8: The estimates for the time between independent data points b_r and the integrated autocorrelation time τ_{int} (in terms of 1 billion Θ-BFACF moves in parallel) based on a batch means analysis of the data generated in Replication r when $\mathbb{k}_r \times 10^6$ data points are burned.

Replication r	$\mathbb{k}_r$	$\hat{b}_r(\mathbb{k}_r \times 10^6)$	$\widehat{\tau}^{(r)}_{\text{int},B(\mathbb{k}_r \times 10^6)}$
1	10.0	0.50	0.25
2	9.0	0.60	0.30
3	8.0	0.40	0.20
4	6.0	0.90	0.45
5	12.0	0.90	0.45
6	8.0	0.50	0.25
7	10.0	1.00	0.50
8	10.0	0.60	0.30
9	9.0	1.00	0.50
10	4.0	0.70	0.35

respectively. Calculating $\bar{\tau}_{\text{int},B(\mathbb{k}_r \times 10^6)}$ (as given by Equation (4.79)) yields $\bar{\tau}_{\text{int},B(\mathbb{k}_r \times 10^6)} = 0.355 \pm 0.036$ billion Θ-BFACF moves in parallel, (where 0.036 is the estimated standard error of $\bar{\tau}_{\text{int},B(\mathbb{k}_r \times 10^6)}$). If the Central Limit can be applied, then a 95% confidence interval for $\tau_{\text{int}} = 0.355 \pm 0.081$.

Calculating the estimator $\widehat{\tau}_{\text{int},B}$ using the data in columns three and five of Table 4.7 and the data in column 4 of Table 4.8 yields $\widehat{\tau}_{\text{int},B} = 0.60$ billion Θ-BFACF moves in parallel.

Because the point estimate for $\bar{\tau}_{\text{int},B(\mathbb{k}_r \times 10^6)}$ is within the estimated standard error of the point estimates for both $\bar{\tau}_{\text{int},B(0)}$ and $\bar{\tau}_{\text{int},B(5.0 \times 10^6)}$; the point estimate for $\bar{\tau}_{\text{int},B(5.0 \times 10^6)}$ is within the estimated standard error of the point estimates for both $\bar{\tau}_{\text{int},B(0)}$ and $\bar{\tau}_{\text{int},B(\mathbb{k}_r \times 10^6)}$; and the point estimate for $\bar{\tau}_{\text{int},B(0)}$ is within the estimated standard error of the point estimates for both $\bar{\tau}_{\text{int},B(5.0 \times 10^6)}$ and $\bar{\tau}_{\text{int},B(\mathbb{k}_r \times 10^6)}$, the estimates for $\bar{\tau}_{\text{int},B(0)}$, $\bar{\tau}_{\text{int},B(5.0 \times 10^6)}$, and $\bar{\tau}_{\text{int},B(\mathbb{k}_r \times 10^6)}$ are consistent. The fact that the estimates $\bar{\tau}_{\text{int},B(0)}$, $\bar{\tau}_{\text{int},B(5.0 \times 10^6)}$, and $\bar{\tau}_{\text{int},B(\mathbb{k}_r \times 10^6)}$ are consistent supports the hypothesis that the estimates $\bar{\tau}_{\text{int},B(\bullet)}$ are independent of the amount of data burned, which supports the hypothesis that the simulation has been run for a long enough time that any burn-time resulting from each replication starting in a non-equilibrium state is negligible in estimating τ_{int}. Hence, based on the

batch means analysis of the data generated by the simulation of the CMC Θ-BFACF algorithm, no data needs to be burned in the analysis presented in Chapters 5 to 7. In an attempt to support the conclusion that no data needs to be burned, the next section uses the series/windowing approach to determine whether or not $\widehat{\tau}_{\text{int},S}$ is independent of the amount of burned data.

Determining $\widehat{\tau}_{\text{int},S}$

Given that the amount of burned data is $\Bbbk$, recall from Equation (4.71) that an estimate for the variance of $\widehat{\tau}_{\text{int}}(f)$, valid for $\widehat{\tau}_{\text{int}}(f) \ll W \ll n$, where n is the run length, is

$$\text{var}(\widehat{\tau}_{\text{int}}(f)) = \frac{2(2W+1)}{n}\tau^2_{\text{int}}(f). \tag{4.147}$$

Define an estimate for the variance of $\widehat{\tau}^{(r)}_{\text{int},S(\Bbbk)}$ by

$$\text{var}\left(\widehat{\tau}^{(r)}_{\text{int},S(\Bbbk)}\right) := \frac{2(2\hat{W}_r(\Bbbk)+1)}{n}\left(\widehat{\tau}^{(r)}_{\text{int},S(\Bbbk)}\right)^2 \tag{4.148}$$

and an estimate for the associated standard error associated with $\widehat{\tau}^{(r)}_{\text{int},S}$ by

$$\text{SE}\left(\widehat{\tau}^{(r)}_{\text{int},S(\Bbbk)}\right) := \sqrt{\frac{2(2\hat{W}_r(\Bbbk)+1)}{n}}\widehat{\tau}^{(r)}_{\text{int},S(\Bbbk)}, \tag{4.149}$$

where $\hat{W}_r(\Bbbk)$ is the estimated window size based on the data in Replication r. Also define the average estimated window size when $\Bbbk$ data points are burned to be

$$\bar{W}(\Bbbk) := \frac{1}{10}\sum_{i=1}^{10}\hat{W}_r(\Bbbk). \tag{4.150}$$

Note that, for fixed $\Bbbk$, the distribution of the estimates $\hat{W}_r(\Bbbk)$ is unknown. Further, because there are only ten replications, the Central Limit theorem may not hold. Hence in an attempt to explore how the estimates for τ_{int} and W (based on the series/windowing approach) depend on $\Bbbk$, the three cases: $\Bbbk = 0$; $\Bbbk = 5.0 \times 10^6$; and $\Bbbk = \Bbbk_r \times 10^6$ will be considered.

Case 1: $\Bbbk = 0$. Each of the replications is started in the equilibrium distribution and no data is discarded in the analysis. Table 4.9 contains, for $r \in \{1, 2, .., 10\}$, the estimates $\widehat{\tau}^{(r)}_{\text{int},S(0)}$, the associated estimated standard error $\text{SE}\left(\widehat{\tau}^{(r)}_{\text{int},S(0)}\right)$, and the estimated window size $\hat{W}_r(0)$ required to compute $\widehat{\tau}^{(r)}_{\text{int},S(0)}$ and $\text{SE}\left(\widehat{\tau}^{(r)}_{\text{int},S(0)}\right)$.

Note that, if rounded to the first decimal place, the values of $\widehat{\tau}^{(r)}_{\text{int},S(0)}$, for $r \in \{1, 2, .., 10\}$, in Table 4.9 all have the same order of magnitude. In order to get some sense of how $\widehat{\tau}^{(r)}_{\text{int},S(0)}$

Table 4.9: The estimates for τ_{int} based on the series/windowing approach when no data are burned ($\mathbb{k} = 0$).

Replication r	$\widehat{\tau}^{(r)}_{\text{int},S(0)}$	SE $\left(\widehat{\tau}^{(r)}_{\text{int},S(0)}\right)$	$\hat{W}_r(0)$
1	0.100	0.003	0.619
2	0.078	0.002	0.503
3	0.071	0.002	0.403
4	0.128	0.005	1.109
5	0.121	0.004	0.808
6	0.061	0.002	0.541
7	0.066	0.002	0.454
8	0.094	0.003	0.727
9	0.190	0.008	1.272
10	0.100	0.003	0.648

varies across the ten replications, calculating $\bar{\tau}_{\text{int},S(0)}$ (as given by Equation (4.80)) using the data in Table 4.9 yields the estimate $\bar{\tau}_{\text{int},S(0)} = 0.101 \pm 0.004$ billion Θ-BFACF moves in parallel (where 0.004 is the estimated standard error of $\bar{\tau}_{\text{int},S(0)}$). If the Central Limit Theorem holds, then a 95% confidence interval for τ_{int} is $\tau_{\text{int}} = 0.101 \pm 0.009$. The average estimated window size (computed using the estimates in Table 4.9) $\bar{W}(0) = 0.708 \pm 0.090$ billion Θ-BFACF moves in parallel (where $\bar{W}(0)$ is computed using Equation (4.150) and 0.090 is the estimated standard error of $\bar{W}(0)$).

Case 2: $\mathbb{k} = 5.0 \times 10^6$. Each of the replications is started in some no-equilibrium distribution and after $\widehat{\tau}_{\text{exp},E}$ (5.0 billion Θ-BFACF moves in parallel), each replication has reached the equilibrium distribution. For $r \in \{1, 2, .., 10\}$,estimates for $\widehat{\tau}^{(r)}_{\text{int},S(5.0\times10^6)}$, SE $\left(\widehat{\tau}^{(r)}_{\text{int},S(5.0\times10^6)}\right)$, and the estimated window size $\hat{W}_r(5.0 \times 10^6)$ required to compute $\widehat{\tau}^{(r)}_{\text{int},S(5.0\times10^6)}$ and SE $\left(\widehat{\tau}^{(r)}_{\text{int},S(5.0\times10^6)}\right)$ are summarized in Table 4.10.

Note that, if rounded to the first decimal place, the values of $\widehat{\tau}^{(r)}_{\text{int},S(5.0\times10^6)}$, for $r \in \{1, 2, .., 10\}$, in Table 4.10 all have the same order of magnitude as each other and all have the same order of magnitude as the estimates for $\widehat{\tau}^{(r)}_{\text{int},S(0)}$ (rounded to the first decimal), for $r \in \{1, 2, .., 10\}$. Calculating $\bar{\tau}_{\text{int},S(5.0\times10^6)}$ (as given by Equation (4.80)) using the data in Table 4.10 yields $\bar{\tau}_{\text{int},S(5.0\times10^6)} = 0.100 \pm 0.004$ billion Θ-BFACF moves in parallel (where 0.004 is the estimated standard error of $\bar{\tau}_{\text{int},S(5.0\times10^6)}$). If the Central Limit Theorem holds,

Table 4.10: The estimates for τ_{int} based on the series/windowing approach when the data collected during the first five billion Θ-BFACF moves in parallel are discarded ($\mathbb{k} = 5.0 \times 10^6$).

Replication r	$\widehat{\tau}^{(r)}_{\text{int},S(5.0\times10^6)}$	SE $\left(\widehat{\tau}^{(r)}_{\text{int},S(5.0\times10^6)}\right)$	$\hat{W}_r(5.0 \times 10^6)$
1	0.103	0.003	0.618
2	0.083	0.003	0.565
3	0.072	0.002	0.402
4	0.129	0.005	1.106
5	0.123	0.004	0.789
6	0.061	0.002	0.546
7	0.064	0.002	0.454
8	0.095	0.003	0.731
9	0.169	0.007	1.248
10	0.102	0.004	0.660

then a 95% confidence interval for τ_{int} is $\tau_{\text{int}} = 0.100 \pm 0.009$. The average estimated window size (computed using the estimates from Table 4.10) is $\bar{W}(5.0\times10^6) = 0.710 \pm 0.086$ billion Θ-BFACF moves in parallel (where $\bar{W}(5.0 \times 10^6)$ is computed using Equation (4.150) and 0.086 is the estimated standard error of $\bar{W}(5.0 \times 10^6)$).

Note that the point estimate $\bar{\tau}_{\text{int},S(5.0\times10^6)}$ lies within one standard error of the point estimate $\bar{\tau}_{\text{int},S(0)}$ and the point estimate $\bar{\tau}_{\text{int},B(0)}$ lies within one estimated standard error of $\bar{\tau}_{\text{int},B(5.0\times10^6)}$. Similarly the point estimate for $\bar{W}(5.0 \times 10^6)$ lies within one estimated standard deviation of $\bar{W}(0)$. Hence $\bar{\tau}_{\text{int},S(0)}$ and $\bar{\tau}_{\text{int},S(5.0\times10^6)}$ are consistent with each other and $\bar{W}(0)$ and $\bar{W}(5.0 \times 10^6)$ are also consistent with each other.

Case 3: $\mathbb{k} = \mathbb{k}_r \times 10^6$. Each of the replications is started in some non-equilibrium distribution and after $\widehat{\tau}^{(r)}_{\text{exp},W}$, the single starting state warm-up period given in Table 4.1, each replication has reached the equilibrium distribution. The estimates for τ_{int} computed using the series/windowing approach based on $\mathbb{k}_r \times 10^6$ burned data points are summarized in Table 4.11.

Note that, if rounded to the first decimal place, the values of $\widehat{\tau}^{(r)}_{\text{int},S(\mathbb{k}_r\times10^6)}$, for $r \in \{1, 2, .., 10\}$, in Table 4.11 all have the same order of magnitude as each other and all have the same order of magnitude as the estimates for $\widehat{\tau}^{(r)}_{\text{int},S(0)}$ and $\widehat{\tau}^{(r)}_{\text{int},S(5.0\times10^6)}$ (rounded to the

Table 4.11: The estimates for $\widehat{\tau}_{\text{int}}$ based on the windowing/series approach when the data collected during the first $\widehat{\tau}^{(r)}_{\text{exp},W}$ billion Θ-BFACF moves in parallel are discarded ($k = 5.0 \times 106$).

Replication r	k_r	$\widehat{\tau}^{(r)}_{\text{int},S(k_r \times 10^6)}$	SE $\left(\widehat{\tau}^{(r)}_{\text{int},S(k_r \times 10^6)}\right)$	$\hat{W}_r(k_r \times 10^6)$
1	10.0	0.080	0.003	0.590
2	9.0	0.082	0.003	0.561
3	8.0	0.072	0.002	0.402
4	6.0	0.130	0.005	1.106
5	12.0	0.119	0.005	0.836
6	8.0	0.063	0.002	0.600
7	10.0	0.064	0.002	0.474
8	10.0	0.092	0.003	0.779
9	9.0	0.171	0.007	1.239
10	4.0	0.103	0.003	0.640

first decimal), for $r \in \{1, 2, .., 10\}$. Calculating $\bar{\tau}_{\text{int},S(\mathbb{k}_r \times 10^6)}$ (as given by Equation (4.80)) using the data in Table 4.11 yields $\bar{\tau}_{\text{int},S(\mathbb{k}_r \times 10^6)} = 0.098 \pm 0.004$ billion Θ-BFACF moves in parallel (where 0.004 is the estimated standard error of $\bar{\tau}_{\text{int},S(\mathbb{k}_r \times 10^6)}$). If the Central Limit Theorem holds, then a 95% confidence interval for τ_{int} is $\tau_{\text{int}} = 0.098 \pm 0.009$. The average estimated window size (computed using the estimates in Table 4.11) is $\bar{W}(\mathbb{k}_r \times 10^6) = 0.722 \pm 0.086$ billion Θ-BFACF moves in parallel (where 0.086 is the estimated standard error of $\bar{W}(\mathbb{k}_r \times 10^6)$).

Calculating $\widehat{\tau}_{\text{int},S}$ using the estimates for τ_{int} summarized in Tables 4.9, 4.10, and 4.11 yields $\widehat{\tau}_{\text{int},S} = 0.190$ billion Θ-BFACF moves in parallel. The window size used to determine $\widehat{\tau}_{\text{int},S}$ is 1.272 million data points. With estimates for $\widehat{\tau}_{\text{int},W}$, $\widehat{\tau}_{\text{int},B}$, and $\hat{\tau}_{\text{int},S}$ computed, the estimate $\widehat{\tau}_{\text{int}}$ can be determined using Equation (4.77), that is $\widehat{\tau}_{\text{int}} = 0.600$ billion Θ-BFACF moves in parallel. Note that doubling this yields estimates for the number of Θ-BFACF moves in parallel that must be implemented before two observations will be essentially independent. 1.2 billion Θ-BFACF moves in parallel is statistically consistent with the window size of 1.272 million data points that was required to estimate $\widehat{\tau}_{\text{int},S}$, because data was sampled every 1000 Θ-BFACF moves in parallel. Also, because data was sampled every 1000 billion Θ-BFACF moves in parallel, 1.200 million is the

predicted batch size required for independence.

Because the point estimate $\bar{\tau}_{\text{int},S(\mathbb{k}_r \times 10^6)}$ lies within one estimated standard error of the point estimates $\bar{\tau}_{\text{int},S(0)}$ and $\bar{\tau}_{\text{int},S(5.0\times 10^6)}$; the point estimate $\bar{\tau}_{\text{int},S(0)}$ lies within one estimated standard error of $\bar{\tau}_{\text{int},S(5.0\times 10^6)}$ and $\bar{\tau}_{\text{int},S(\mathbb{k}_r \times 10^6)}$; and the point estimate $\bar{\tau}_{\text{int},S(5.0\times 10^6)}$ lies within one estimated standard error of $\bar{\tau}_{\text{int},S(0)}$ and $\bar{\tau}_{\text{int},S(\mathbb{k}_r \times 10^6)}$, the estimates $\bar{\tau}_{\text{int},S(0)}$, $\bar{\tau}_{\text{int},S(5.0\times 10^6)}$, and $\bar{\tau}_{\text{int},S(\mathbb{k}_r \times 10^6)}$ are consistent. For the same reason, the point estimates for $\bar{W}(0)$, $\bar{W}(5.0 \times 10^6)$, and $\bar{W}(\mathbb{k}_r \times 10^6)$ are also consistent with each other. The consistency of the estimates $\bar{\tau}_{\text{int},S(\bullet)}$ and $\bar{W}(\bullet)$ implies that both estimators are independent of the amount of data burned. The fact that the estimates $\bar{\tau}_{\text{int},S(\bullet)}$ and $\bar{W}(\bullet)$ are independent of the amount of data burned supports the hypothesis that the simulation has been run for enough time so that any burn-time resulting from each replication starting in a non-equilibrium state is negligible in estimating τ_{int}. Hence the series/windowing analysis also supports the conclusion that in any subsequent data analysis, no data needs to be discarded.

The conclusion to be drawn from estimating τ_{int} is that all ten replications have been run for long enough so that the estimates $\bar{\tau}_{\text{int},B(\bullet)}$ and $\bar{\tau}_{\text{int},S(\bullet)}$ are independent of the amount of data burned in determining the estimates. This implies that no data needs to be discarded in any subsequent data analysis. Hence whether a warm-up analysis, batch means analysis, or a series/windowing approach is used to estimate τ_{int}, the estimates for τ_{int} are not affected by the amount of burned data. To err on the conservative side, for all further analysis in this thesis, $\widehat{\tau}_{\text{int}} = 0.6$ (where $\widehat{\tau}_{\text{int}}$ is defined by Equation (4.77)). Hence it will be assumed that data collected every 1.2×10^9 Θ-BFACF moves in parallel will be essentially independent and data blocked according to a block size of 1.2 million data points will be essentially independent.

4.7.3 Checking the Consistency of the CMC Θ-BFACF Data

In this section, the consistency and accuracy of the simulated data are checked. Before the methods for these checks can be specified, recall that $\Phi_{\text{ave}} = \{\phi, (\phi, f), (\phi, s), (\phi|\phi, s), (3_1|\phi, s), (4_1|\phi, s), (5_2|\phi, s)\}$. Note that throughout this thesis any $(1-\alpha)\cdot 100\%$ confidence interval for a parameter will be of the form

$$\text{point estimate} \ \pm \ (1-\alpha)\cdot 100\% \ \text{ME}\,, \tag{4.151}$$

where $(1-\alpha)\cdot 100\%$ ME will be referred to as the $(1-\alpha)\cdot 100\%$ margin of error resulting from using the point estimate to estimate the parameter of interest. If $\widehat{\mathrm{SE}}$ is the estimated standard error for the point estimator and $c(\alpha)$, referred to as the *critical value*, is the value for which the cumulative distribution function of the point estimator equals $1-\alpha$, then

$$(1-\alpha)\cdot 100\%\,\mathrm{ME} := c(\alpha)\widehat{\mathrm{SE}}. \tag{4.152}$$

Let $\boldsymbol{W} := \{(W_t(1), W_t(2), ..., W_t(14)), t = 0, ..., t_0\}$ be a Markov chain formed by the CMC Θ-BFACF algorithm and let $\boldsymbol{\omega}^{(u)}$, where

$$\boldsymbol{\omega}^{(u)} := \left(\left(\omega_t^{(u)}(1), \omega_t^{(u)}(2), ..., \omega_t^{(u)}(14)\right), t = 0, ..., t_0\right), \tag{4.153}$$

be the sequence of (t_0+1) 14-tuples of Θ-SAPs from $\left(\mathscr{P}^{\Theta}(\phi)\right)^{14}$ realized in Replication u of the simulation of the CMC Θ-BFACF algorithm as described in Section 3.4.1. Now, in order to estimate the expected length of W, a random property-$*$ Θ-SAP chosen according to $\boldsymbol{\pi}_{z_i}(2,14)$ (that is estimate $\mathrm{E}_{\boldsymbol{\pi}_{z_i}(2,14)}(\xi_{\mathscr{U}(*)}(W)\,|W|)$), for each $* \in \Phi$ and for $\mathscr{U}(*) \subseteq \mathscr{P}^{\Theta}(\phi)$, define the random variables X and Y (as defined in Section A.4 of Appendix A) by

$$X(L, W, \mathscr{U}(*)) := \mathscr{I}_{[L,\infty)}(|W|)\xi_{\mathscr{U}(*)}(W) \tag{4.154}$$

and

$$Y(L, W, \mathscr{U}(*)) := X(L, W, \mathscr{U}(*))\,|W|, \tag{4.155}$$

respectively, where, for $A \subseteq \mathbb{R}$, $\mathscr{I}_A(t)$is defined by Equation (7.6), and, for each $\omega \in \mathscr{P}^{\Theta}(\phi)$ and each subset of Θ-SAPs $\mathscr{V} \subseteq \mathscr{P}^{\Theta}(\phi)$,

$$\xi_{\mathscr{V}}(\omega) := \begin{cases} 1, & \text{if } \omega \in \mathscr{V} \\ 0, & \text{otherwise.} \end{cases} \tag{4.156}$$

Now define $X_{k,i}$ and $Y_{k,i}$ (as used in Section A.4 of Appendix A) by

$$\begin{aligned} X_{k,i} &:= X_{k,i}(N_{\min}, W, \mathscr{U}(*)) \\ &\quad \sum_{t=0}^{t_0} \mathscr{M}_T(t)\mathscr{I}_{B(k)}(t)\, X(N_{\min}, W_t(i), \mathscr{U}(*)). \end{aligned} \tag{4.157}$$

and

$$\begin{aligned} Y_{k,i} &:= Y_{k,i}(N_{\min}, W, \mathscr{U}(*)) \\ &:= \sum_{t=0}^{t_0} \mathscr{M}_T(t) \mathscr{I}_{B(k)}(t)\, Y(N_{\min}, W_t(i), \mathscr{U}(*)) \\ &:= N_{k,i}(\mathscr{U}(*)), \end{aligned} \tag{4.158}$$

where

$$B(k) := (2(k-1)\tau_{\text{int}} - 1, 2k\tau_{\text{int}} - 1], \tag{4.159}$$

$\mathscr{M}_T(t)$ is defined by Equation (4.42); and, for $A \subseteq \mathbb{R}$, $\mathscr{I}_A(t)$is defined by Equation (7.6). Then let $\left\langle N_{\boldsymbol{\pi}_{z_i}(q,N_{\min})}(\mathscr{U}(*)) \right\rangle$ be the ratio estimator (as defined by Equation (A.21) in Section A.3 of Appendix A) for $\mathrm{E}_{\boldsymbol{\pi}_{z_i}(q,N_{\min})}(\xi_{\mathscr{U}(*)}(W)\,|W|)$ formed using the sequence

$$((X_{k,i}, N_{k,i}(\mathscr{U}(*))), k = 1, .., l). \tag{4.160}$$

For each $* \in \Phi$ and for $t_0 = 9.6 \times 10^{10}$ time steps, $N_{\min} = 14$, $q = 2$, $\tau_{\text{int}} = 0.72 \times 10^9$ time steps, $T = 1200$ time steps, and $l := 66$, based on the u'th realization $\boldsymbol{\omega}^{(u)}$ of $\boldsymbol{W}$, $u \in \{1, 2, ..., 10\}$, let $n_{k,i}^{(u)}\left(\mathscr{P}^{\Theta}(*)\right)$ denote the u'th realization of $N_{k,i}\left(\mathscr{P}^{\Theta}(*)\right)$ and let $x_{k,i}^{(u)}$ denote the u'th realization of $X_{k,i}$. Then define $\left\langle n_{\boldsymbol{\pi}_{z_i}(2,14)}\left(\mathscr{P}^{\Theta}(*)\right)\right\rangle$ to be the point estimate for $\mathrm{E}_{\boldsymbol{\pi}_{z_i}(2,14)}(\xi_{\mathscr{U}(*)}(W)\,|W|)$ computed using the sequence

$$\left(\left(\left(x_{k,i}^{(u)}, n_{k,i}^{(u)}\left(\mathscr{P}^{\Theta}(*)\right)\right), k = 1, .., l\right), u = 1, ..., 10\right) \tag{4.161}$$

in Equation (A.21).

In this section, the point estimates $\left\langle n_{\boldsymbol{\pi}_{z_i}(2,14)}\left(\mathscr{P}^{\Theta}(\phi)\right)\right\rangle$, for $i = 1, ..., 14$, (the average lengths of the unknotted Θ-SAPs generated in each of the fourteen chains) are used to check the consistency and accuracy of the simulated data by first drawing a comparison to $\left\langle n_i^{\phi}\right\rangle$, the average lengths of the unknotted SAPs generated in chain i with z_i defined in [121]. Then, for $* \in \Phi_{\text{ave}}$, the sample averages $\left\langle n_{\boldsymbol{\pi}_{z_i}(2,14)}\left(\mathscr{P}^{\Theta}(*)\right)\right\rangle$ are used to determine whether or not, as $(\log(z) + \kappa_{\phi}) \to 0$, the data support that Equation (4.101) becomes linear in $1/z$ and Equation (4.102) goes to 1.0.

Verifying from an Outside Source [121]

Note that the average length of an unknotted Θ-SAP computed from a chain characterized by a smaller fugacity (lower chain number) will be influenced by the size of the structure Θ

more than the average length of an unknotted Θ-SAP computed from a chain with a larger fugacity (higher chain number). Also note that the relationship between the estimated average length of an unknotted polygon (denoted $\left\langle n_i^{\phi} \right\rangle$) which is not forced to contain Θ and the estimated average length of an unknotted Θ-SAP for $z_i < z_\phi$ is expected to be

$$\left\langle n_{\boldsymbol{\pi}_{z_i}(2,14)}\left(\mathscr{P}^{\Theta}(\phi)\right)\right\rangle > \left\langle n_i^{\phi}\right\rangle. \tag{4.162}$$

Also, because, as the fugacity $z_i \to z_\phi$, it is expected that the size of the structure Θ will impact the expected length of an unknotted polygon that contains the structure less and less, for z_i sufficiently close to z_ϕ,

$$\left\langle n_{\boldsymbol{\pi}_{z_i}(2,14)}\left(\mathscr{P}^{\Theta}(\phi)\right)\right\rangle \approx \left\langle n_i^{\phi}\right\rangle, \tag{4.163}$$

that is the lengths of SAPs with the structure, for large enough polygons, should not be influenced by the presence of the structure and essentially behave as unknotted SAPs.

Note that the values in Column 2 of Table 4.12 are estimates for $\left\langle n_i^{\phi} \right\rangle$ taken from [121] and the values in Columns 3 and 4 of Table 4.12, the values in Columns 2, 3, and 4 of Table 4.13, and the values in Columns 2 and 3 of Table 4.14 are the ratio estimates $\left\langle n_{\boldsymbol{\pi}_{z_i}(2,14)}\left(\mathscr{P}^{\Theta}(*)\right)\right\rangle$ computed as described at the beginning of this section. The estimates presented in Columns 2 and 3 of Table 4.12 are in excellent agreement with the two observations given by Equations (4.162) and (4.163).. Further note that, on average, in each of the chains as the property $*$ becomes more complex (that is changes from $(\phi|\phi,s)$ to $(3_1|\phi,s)$ to $(4_1|\phi,s)$ to $(5_2|\phi,s)$), the estimated average polygon length with property $*$ increases. This increase is also to be expected because the more complex the property $*$, the more complex the after-strand-passage knot-type and hence the larger the polygon required to form the property $*$ Θ-SAP.

Verifying by Fitting to Believed Forms

The estimates in Tables 4.12-4.14 can be used to estimate e^{κ_ϕ} by fitting to the form given by Approximation (4.101) using $\left\langle n_{\boldsymbol{\pi}_{z_i}(2,14)}\left(\mathscr{P}^{\Theta}(*)\right)\right\rangle$ as the estimate for
$\mathrm{E}\left(\alpha_*^{\Theta}+q, \log(z)+\kappa_\phi, -\Delta_*^{\Theta}, N_{\min}^*, A_*^{\Theta}, B_*^{\Theta}\right)$ and then extrapolating to the value of z for which the linear fit crosses the z-axis. In Figure 4.9, for $* \in \{(\phi,f),\ (\phi|\phi,s),\ (3_1|\phi,s),\ (4_1|\phi,s),\ (5_2|\phi,s)\}$, $\left\langle n_{\boldsymbol{\pi}_{z_i}(2,14)}\left(\mathscr{P}^{\Theta}(*)\right)\right\rangle^{-1}$ is plotted as a function of $1/z_i$, where the values $\left\langle n_{\boldsymbol{\pi}_{z_i}(2,14)}\left(\mathscr{P}^{\Theta}(*)\right)\right\rangle$ are from Tables 4.12-4.14. Note that in Figure 4.9: property-(ϕ,f)

Table 4.12: The values in Column 2 are estimates (taken from [121]) of the expected length of an unknotted polygon sampled from a modified Boltzmann distribution characterized by the fugacity z_i. The values in Columns 3 and 4 are the average lengths of Θ-SAPs in Chain i with property $*$ sampled from all 10 replications where $* \in \{\phi, (\phi, f)\}$. The values in parentheses are the estimated 95% margins of error. The 95% margins of error presented in Columns 3,and 4 were computed assuming $\widehat{\tau}_{\text{int}} = 0.6$ billion Θ-BFACF moves in parallel.

Chain i	$\left\langle n_i^{\phi} \right\rangle$	$\left\langle n_{\boldsymbol{\pi}_{z_i}(2,14)}\left(\mathscr{P}^{\Theta}(\phi)\right)\right\rangle$	$\left\langle n_{\boldsymbol{\pi}_{z_i}(2,14)}\left(\mathscr{P}^{\Theta}(\phi,f)\right)\right\rangle$
1	26.1(0.2)	34.9(1.6)	34.3 (1.6)
2	32.0(0.2)	40.0(2.0)	39.3 (2.0)
3	41.5(0.3)	48.5 (2.6)	47.6 (2.6)
4	59.6(0.5)	64.7 (3.8)	63.5 (3.8)
5	76.2(0.7)	80.0 (4.9)	78.7 (5.0)
6	88.9(0.8)	91.6 (5.8)	90.2 (5.9)
7	107.2(1.1)	108.0 (7.0)	106.5 (7.1)
8	132.7(1.8)	132.9 (8.8)	131.3 (8.9)
9	179.3(2.9)	174.9 (12.0)	173.2 (12.0)
10	243.6(5.4)	236.8 (16.5)	235.1 (16.5)
11	379(16)	371.6 (26.2)	369.9 (26.2)
12	522(30)	521.6 (36.9)	520.0 (37.0)
13	636(48)	653.7 (46.1)	652.1 (46.2)
14	830(70)	872.7 (60.7)	871.4 (60.8)

data is plotted using a $*$; property-$(\phi|\phi, s)$ data is plotted using a $\triangle$; property-$(3_1|\phi, s)$ data is plotted using a $\boxdot$; property-$(4_1|\phi, s)$ data is plotted using a $\blacksquare$; and property-$(5_2|\phi, s)$ data is plotted using a $\odot$. The error bars plotted in Figure 4.9 represent 95% confidence intervals for $[\mathrm{E}_{\boldsymbol{\pi}_{z_i}(2,14)}(\xi_{\mathscr{U}(*)}(W)\,|W|)]^{-1}$ for $* \in \{(\phi, f), (\phi|\phi, s), (3_1|\phi, s)\}$. Because the error bars for each $* \in \{(4_1|\phi, s), (5_2|\phi, s)\}$ that could be calculated are so large (at least five times the lengths of largest error bars displayed in the plot), they have not been plotted in Figure 4.9. Also note that the point estimates $\left\langle n_{\boldsymbol{\pi}_{z_i}(2,14)}\left(\mathscr{P}^{\Theta}(*)\right)\right\rangle^{-1}$ for $* \in \{(\phi, f), (\phi|\phi, s)\}$ are so close in value that they cannot be distinguished from each other in the figure.

Now recall from Section 4.5 that for values of β sufficiently close to $\beta_c := -\kappa_\phi$, the Approximation (4.101) is expected to hold. Therefore for values of β sufficiently close to β_c,

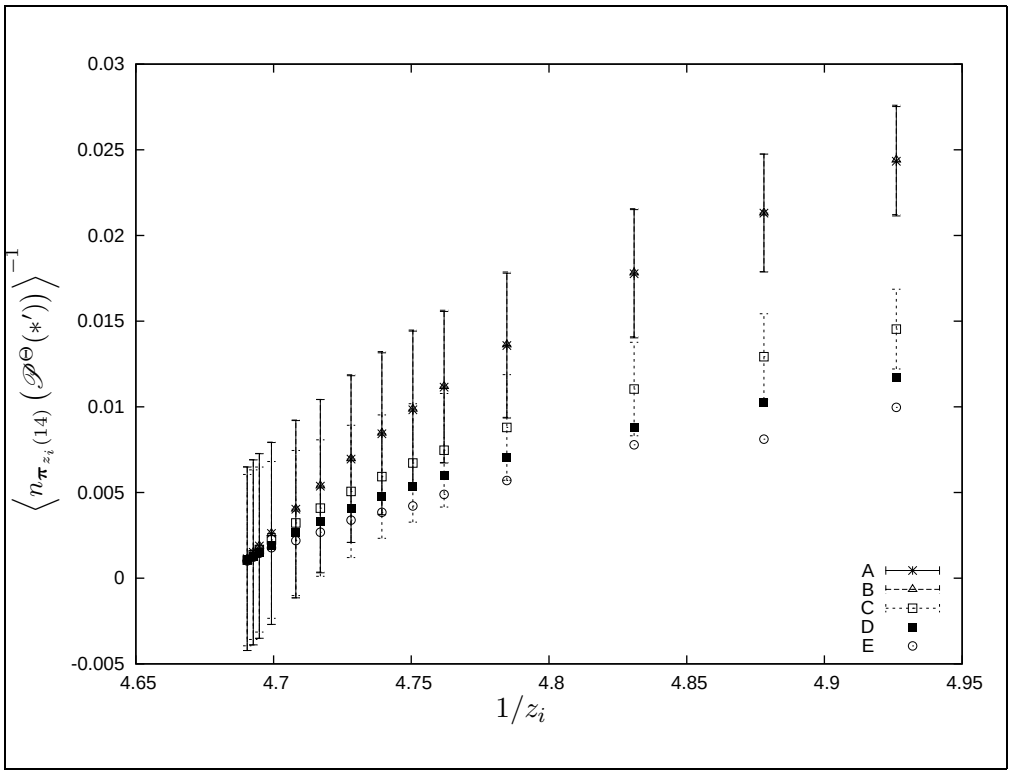

Figure 4.9: $\left\langle n_{\boldsymbol{\pi}_{z_i}(14)}\left(\mathscr{P}^{\Theta}(*')\right)\right\rangle^{-1}$ versus $1/z_i$ for $*' \in \{(\phi, f)\ [*],\ (\phi|\phi, s)\ [\triangle],\ (3_1|\phi, s)\ [\boxdot],\ (4_1|\phi, s)\ [\blacksquare],\ (5_2|\phi, s)\ [\odot]\}$. The error bars represent the corresponding estimated 95% margin of error.

Table 4.13: The average lengths of Θ-SAPs in Chain i with property $*$ sampled from all 10 replications where $* \in \{(\phi, s), (\phi|\phi, s), (3_1|\phi, s)\}$. The values in parentheses are the estimated 95% margins of error computed assuming $\widehat{\tau}_{\text{int}} = 0.6$ billion Θ-BFACF moves in parallel.

Chain	$\left\langle n_{\boldsymbol{\pi}_{z_i}(2,14)}\left(\mathscr{P}^{\Theta}(\phi, s)\right)\right\rangle$	$\left\langle n_{\boldsymbol{\pi}_{z_i}(2,14)}\left(\mathscr{P}^{\Theta}(\phi\|\phi, s)\right)\right\rangle$	$\left\langle n_{\boldsymbol{\pi}_{z_i}(2,14)}\left(\mathscr{P}^{\Theta}(3_1\|\phi, s)\right)\right\rangle$
1	41.1 (1.7)	41.0 (1.7)	68.8 (3.2)
2	46.9 (2.1)	46.9 (2.1)	77.4 (2.6)
3	56.3 (2.7)	56.1 (2.7)	90.6 (3.4)
4	73.7 (4.0)	73.4 (4.0)	113.7 (4.6)
5	89.7 (5.1)	89.3 (5.1)	134.0 (5.7)
6	101.8 (6.0)	101.3 (6.0)	148.7 (6.6)
7	118.6 (7.2)	118.0 (7.2)	168.6 (7.8)
8	143.9 (9.0)	143.2 (9.0)	197.6 (9.6)
9	186.3 (12.1)	185.5 (12.0)	244.5 (12.6)
10	248.5 (16.5)	247.4 (16.5)	310.6 (17.0)
11	382.9 (26.1)	381.7 (26.1)	447.8 (26.4)
12	532.1 (36.8)	530.8 (36.8)	598.2 (37.0)
13	663.4 (46.0)	662.0 (46.0)	730.1 (46.4)
14	881.2 (60.6)	879.8 (60.6)	947.9 (61.0)

(or equivalently for values of $1/z$ sufficiently close to μ_ϕ) the plots of $\left\langle n_{\boldsymbol{\pi}_{z_i}(2,14)}\left(\mathscr{P}^{\Theta}(*)\right)\right\rangle^{-1}$ versus $1/z_i$ should become linear as $1/z_i \to \mu_\phi$.

From Figure 4.9, for $* \in \{(\phi, f), (\phi|\phi, s)\}$, it appears as though the linear behaviour of $\left\langle n_{\boldsymbol{\pi}_{z_i}(2,14)}\left(\mathscr{P}^{\Theta}(*)\right)\right\rangle^{-1}$ with respect to $1/z_i$ begins after the ninth z value (which corresponds to the first five points plotted) Therefore the information in Figure 4.9 is replotted in Figure 4.10 where the values of $\left\langle n_{\boldsymbol{\pi}_{z_i}(2,14)}\left(\mathscr{P}^{\Theta}(*)\right)\right\rangle^{-1}$ for $* \in \{(\phi, f), (\phi|\phi, s)\}$ corresponding to the smallest nine z values are dropped, that is Figure 4.10 focuses on the area in Figure 4.9 near the critical value.

Referring to Figure 4.10, note that, for the values of $1/z_i$ plotted, for $* \in \{(\phi, f), (\phi|\phi, s)\}$, $\langle n_i(*)\rangle^{-1}$ appears to be linear in $1/z_i$. If the x-intercept of the regression line is determined from the set of points $\left\{\left(1/z_i, \left\langle n_{\boldsymbol{\pi}_{z_i}(2,14)}\left(\mathscr{P}^{\Theta}(*)\right)\right\rangle^{-1}\right)\right\}_{i=10}^{14}$, for $* \in \{(\phi, f), (\phi|\phi, s)\}$, the

Table 4.14: The average lengths of Θ-SAPs in Chain i with property $*$ sampled from all 10 replications where $* \in \{(4_1|\phi, s), (5_2|\phi, s)\}$. The values in parentheses are the estimated 95% margins of error computed assuming $\widehat{\tau}_{\text{int}} = 0.6$ billion Θ-BFACF moves in parallel. † indicates estimates are based on one essentially independent block of data.

Chain	$\left\langle n_{\boldsymbol{\pi}_{z_i}(2,14)}\left(\mathscr{P}^{\Theta}(4_1\|\phi,s)\right)\right\rangle$	$\left\langle n_{\boldsymbol{\pi}_{z_i}(2,14)}\left(\mathscr{P}^{\Theta}(5_2\|\phi,s)\right)\right\rangle$
1	85.3 (43.0)	$100.3(n/a)^{\dagger}$
2	97.8 (30.1)	$123.2(n/a)^{\dagger}$
3	113.3 (26.5)	$128.5(n/a)^{\dagger}$
4	141.8 (25.8)	$175.5(n/a)^{\dagger}$
5	166.8 (24.2)	$204.6(n/a)^{\dagger}$
6	186.0 (22.5)	$237.1(n/a)^{\dagger}$
7	210.3 (22.1)	$259.9(n/a)^{\dagger}$
8	245.6 (23.0)	294.9(166)
9	302.1 (25.4)	372.8(158)
10	378.6 (33.3)	456.7(152)
11	522.3 (48.2)	562.0(165)
12	659.6 (64.3)	686.4(212)
13	774.0 (78.2)	814.6(234)
14	930.0 (96.3)	995.1(271)

estimated x-intercept is $(4.6836 \pm 0.0012, 0)$ and the estimated y-intercept is $(0, -1.78 \pm 0.02)$. From these intercepts, the values of $\mu_\phi = 4.6836 \pm 0.0012$ and $\alpha_\phi^{\Theta} = -1.78 \pm 0.02$ are obtained. This point estimate for μ_ϕ (4.6836) computed based on the CMC data is exactly the value estimated for e^{κ_ϕ} by Orlandini *et al.* [125]. The point estimate for $\alpha_\phi^{\Theta}(-1.78)$ is completely consistent with Consequence 2.2.8 (that is $\alpha_\phi^{\Theta} = \alpha_\phi - 2$) because Orlandini *et al.* [125] estimated $\alpha_\phi \approx 0.23$. Hence, not only do the estimates $\left\langle n_{\boldsymbol{\pi}_{z_i}(2,14)}\left(\mathscr{P}^{\Theta}(*)\right)\right\rangle^{-1}$ support the fact that $\left[\mathrm{E}\left(\alpha_*^{\Theta} + q, \log(z) + \kappa_\phi, -\Delta_*^{\Theta}, N_{\min}^*, A_*^{\Theta}, B_*^{\Theta}\right)\right]^{-1}$ is expected to become linear as $1/z_i \to \mu_\phi$ but, from the linear fit to the form given by Approximation (4.101), the estimates obtained for μ_ϕ and α_ϕ^{Θ} are completely consistent with independently obtained estimates.

From Figure 4.10, it appears that data for z values larger than those used in the simulation are required in order to obtain data such that, when $\left\langle n_{\boldsymbol{\pi}_{z_i}(2,14)}\left(\mathscr{P}^{\Theta}(*)\right)\right\rangle^{-1}$ is plotted

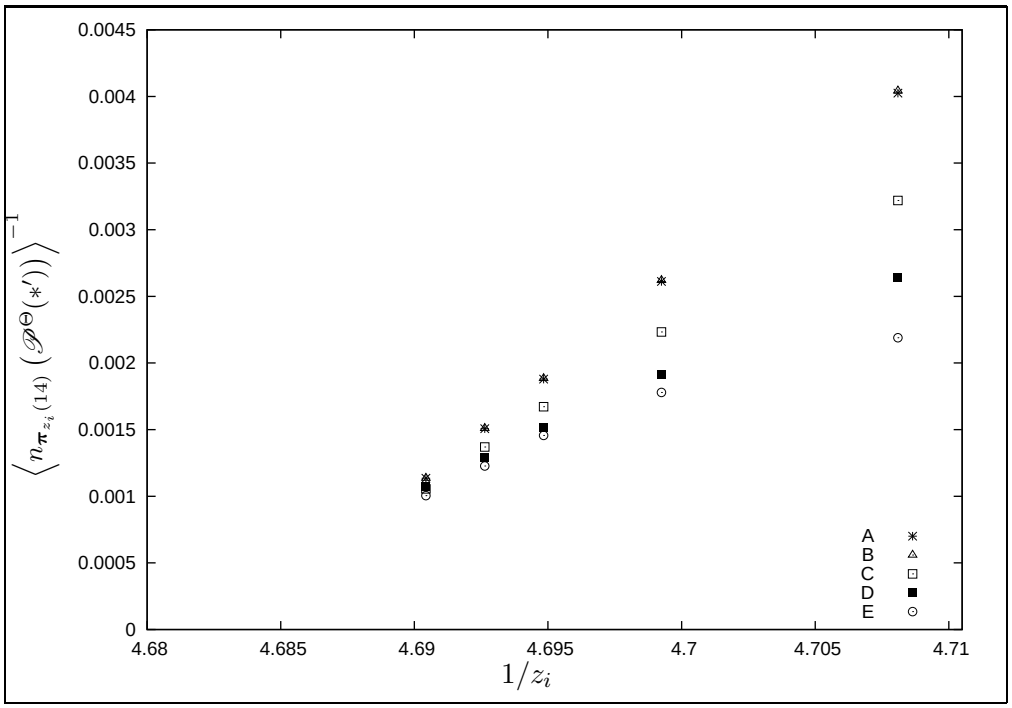

Figure 4.10: $\left\langle n_{\boldsymbol{\pi}_{z_i}(14)}\left(\mathscr{P}^{\Theta}(*')\right)\right\rangle^{-1}$ versus $1/z_i$ for $*' \in \{(\phi,f)\ [*],\ (\phi|\phi,s)\ [\triangle],\ (3_1|\phi,s)\ [\boxdot],\ (4_1|\phi,s)\ [\blacksquare],\ (5_2|\phi,s)\ [\odot]\}$ with focus on the $1/z_i$ values closest to μ_ϕ.

versus $1/z_i$, for $* \in \{(3_1|\phi,s),(4_1|\phi,s),(5_2|\phi,s)\}$, the estimates $\left\langle n_{\boldsymbol{\pi}_{z_i}(2,14)}\left(\mathscr{P}^{\Theta}(*)\right)\right\rangle^{-1}$ are not significantly influenced by the corrections to the linear form. One further important note (based on Figure 4.10) is that as $1/z_i \to \mu_\phi$, the estimates $\left\langle n_{\boldsymbol{\pi}_{z_i}(2,14)}\left(\mathscr{P}^{\Theta}(*)\right)\right\rangle^{-1}$ for each $* \in \{(\phi,f),\ (\phi|\phi,s),\ (3_1|\phi,s),\ (4_1|\phi,s),\ (5_2|\phi,s)\}$, are approaching each other. This numerically supports the conjecture $\mu_\phi = \mu_*^{\Theta}$. If, for each $* \in \{(\phi,f),\ (\phi|\phi,s),\ (3_1|\phi,s),\ (4_1|\phi,s),\ (5_2|\phi,s)\}$, the estimates $\left\langle n_{\boldsymbol{\pi}_{z_i}(2,14)}\left(\mathscr{P}^{\Theta}(*)\right)\right\rangle^{-1}$ are really approaching each other as $z_i^{-1} \to \mu_\phi$, then this would imply that, since $\mu_\phi = \mu_*^{\Theta}$, then $\alpha_\phi^{\Theta} = \alpha_*^{\Theta}$, which supports Consequence 2.2.9.

The discussion now turns to determining whether or not the point estimates $\left\langle n_{\boldsymbol{\pi}_{z_i}(2,14)}\left(\mathscr{P}^{\Theta}(*)\right)\right\rangle$ (for each $* \in \Phi_{\text{ave}}$) support Approximation (4.102). Recall from Section (4.5) that, for $\beta := \log(z)$ and $*_1, *_2 \in \Phi$, as $\beta + \kappa_\phi \to 0$,

$$\frac{\mathrm{E}\left(*_1\right)}{\mathrm{E}\left(*_2\right)} := \frac{\mathrm{E}\left(\alpha_{*_1}^{\Theta}+2, \beta+\kappa_\phi, -\Delta_{*_1}^{\Theta}, N_{\min}^{*_1}, A_{*_1}^{\Theta}, B_{*_1}^{\Theta}\right)}{\mathrm{E}\left(\alpha_{*_2}^{\Theta}+2, \beta+\kappa_\phi, -\Delta_{*_2}^{\Theta}, N_{\min}^{*_2}, A_{*_2}^{\Theta}, B_{*_2}^{\Theta}\right)} \to \frac{[\alpha_{*_1}^{\Theta}+3]}{[\alpha_{*_2}^{\Theta}+3]} \tag{4.164}$$

and that, if $\alpha_{*_1}^{\Theta} = \alpha_{*_2}^{\Theta}$, then, as $\beta + \kappa_\phi \to 0$, the ratios $\dfrac{\mathrm{E}\left(*_1\right)}{\mathrm{E}\left(*_2\right)} \to 1$. In order to explore

how $\dfrac{\mathrm{E}(*_1)}{\mathrm{E}(*_2)}$, behaves, for $*_1, *_2 \in \Phi_{\text{ave}}$, the estimates in Tables 4.12-4.14 can be used to approximate the ratios $\dfrac{\mathrm{E}(*_1)}{\mathrm{E}(*_2)}$ where $*_1, *_2 \in \Phi_{\text{ave}}$. Further to this, assuming that the confluent exponents for this work are all 0.5 and that $\hat{\kappa}_\phi = 1.544125$, then a plot of $\dfrac{\left\langle n_{\boldsymbol{\pi}_{z_i}(2,14)}\left(\mathscr{P}^{\Theta}(*)\right)\right\rangle}{\left\langle n_{\boldsymbol{\pi}_{z_i}(2,14)}\left(\mathscr{P}^{\Theta}(\phi)\right)\right\rangle}$ versus $\sqrt{1-e^{\beta_i+\hat{\kappa}_\phi}}$ should exhibit linear behaviour as $\beta_i + \kappa_\phi \to 0$. The reason $\left\langle n_{\boldsymbol{\pi}_{z_i}(2,14)}\left(\mathscr{P}^{\Theta}(\phi)\right)\right\rangle$ is used in the denominator is because the most reliable data available is for the property ϕ. Also note that the estimates in Tables 4.12-4.14 will be used to form the ratios $\dfrac{\left\langle n_{\boldsymbol{\pi}_{z_i}(2,14)}\left(\mathscr{P}^{\Theta}(*)\right)\right\rangle}{\left\langle n_{\boldsymbol{\pi}_{z_i}(2,14)}\left(\mathscr{P}^{\Theta}(\phi)\right)\right\rangle}$ to estimate the ratio $\dfrac{\mathrm{E}(*)}{\mathrm{E}(\phi)}$.

In the following two figures (Figures 4.11 and 4.12), note that property-(ϕ, f) data is plotted using a $*$; property-$(\phi|\phi, s)$ data is plotted using a $\triangle$; property-$(3_1|\phi, s)$ data is plotted using a $\boxdot$; property-$(4_1|\phi, s)$ data is plotted using a $\blacksquare$; and property-$(5_2|\phi, s)$ data is plotted using a $\odot$. Figure 4.11 contains the plots of $\dfrac{\left\langle n_{\boldsymbol{\pi}_{z_i}(2,14)}\left(\mathscr{P}^{\Theta}(*')\right)\right\rangle}{\left\langle n_{\boldsymbol{\pi}_{z_i}(2,14)}\left(\mathscr{P}^{\Theta}(\phi)\right)\right\rangle}$ versus $\sqrt{1-e^{\beta_i+\hat{\kappa}_\phi}}$ for Chains 1 through 14 and properties $*' \in \{(\phi, f),\ (\phi|\phi, s),\ (3_1|\phi, s),\ (4_1|\phi, s),\ (5_2|\phi, s)\}$, where the error bars represent the 95% confidence intervals computed using Section A.3 of Appendix A. In Figure 4.11, for each chain, the estimates $\dfrac{\left\langle n_{\boldsymbol{\pi}_{z_i}(2,14)}\left(\mathscr{P}^{\Theta}(\phi, f)\right)\right\rangle}{\left\langle n_{\boldsymbol{\pi}_{z_i}(2,14)}\left(\mathscr{P}^{\Theta}(\phi)\right)\right\rangle}$ and $\dfrac{\left\langle n_{\boldsymbol{\pi}_{z_i}(2,14)}\left(\mathscr{P}^{\Theta}(\phi|\phi, s)\right)\right\rangle}{\left\langle n_{\boldsymbol{\pi}_{z_i}(2,14)}\left(\mathscr{P}^{\Theta}(\phi)\right)\right\rangle}$ are so close in value that, when plotted versus $\sqrt{1-e^{\beta_i+\hat{\kappa}_\phi}}$, the estimates plotted respectively with a $(*)$ and a $(\triangle)$ in Figures 4.11 and 4.12 cannot be distinguished from each other. Figure 4.12 zooms in on the region $\beta_i \in (-1.554, -\kappa_\phi)$.

Note that in Figure 4.12 no error bars are plotted as they detracted from being able to determine whether the estimates for each of the properties appeared to be linear. The error bars (that is, the estimated 95% margins of error) are presented in Figure 4.11. From Figure 4.12, it is plausible that, for $* \in \{(\phi, f),\ (\phi|\phi, s),\ (3_1|\phi, s)\}$, the estimates $\dfrac{\left\langle n_{\boldsymbol{\pi}_{z_i}(2,14)}\left(\mathscr{P}^{\Theta}(*)\right)\right\rangle}{\left\langle n_{\boldsymbol{\pi}_{z_i}(2,14)}\left(\mathscr{P}^{\Theta}(\phi)\right)\right\rangle}$ are all approaching the same value as $\sqrt{1-e^{\beta_i+\hat{\kappa}_\phi}} \to 0$. Because, for β_i sufficiently close to $-\kappa_\phi$, Equation (4.98) is expected to be valid, the value the ratio $\dfrac{\mathrm{E}(*)}{\mathrm{E}(\phi)}$ is expected to approach is the y-intercept of the regression line estimated using the

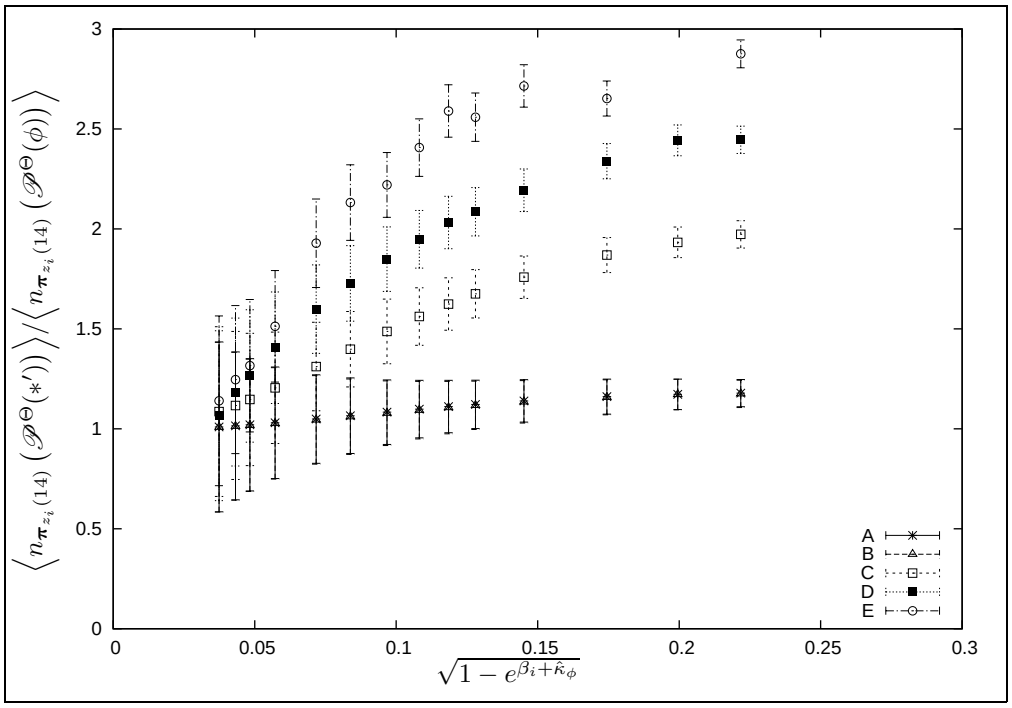

Figure 4.11: $\dfrac{\left\langle n_{\boldsymbol{\pi}_{z_i}(14)}\left(\mathscr{P}^{\Theta}(*')\right)\right\rangle}{\left\langle n_{\boldsymbol{\pi}_{z_i}(14)}\left(\mathscr{P}^{\Theta}(\phi)\right)\right\rangle}$ versus $\sqrt{1-e^{\beta_i+\hat{\kappa}_\phi}}$ for Chains 1 through 14 and $*' \in \{(\phi, f)\ [*],\ (\phi|\phi, s)\ [\triangle],\ (3_1|\phi, s)\ [\boxdot],\ (4_1|\phi, s)\ [\blacksquare],\ (5_2|\phi, s)\ [\odot]\}$, where the error bars are the estimated 95% margins of error.

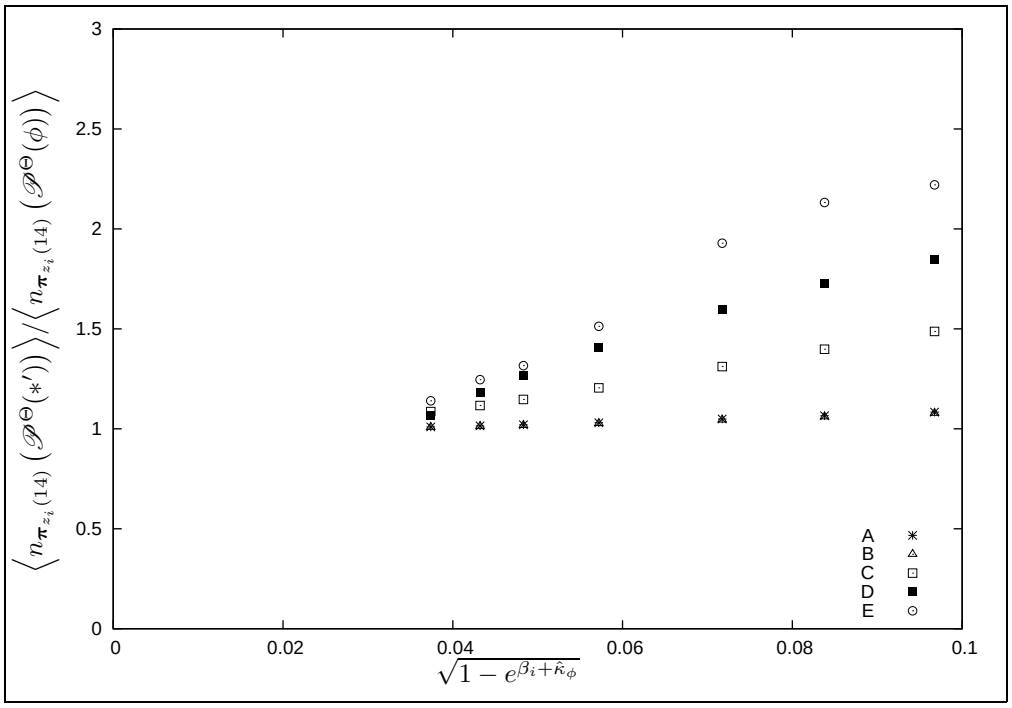

Figure 4.12: $\dfrac{\left\langle n_{\boldsymbol{\pi}_{z_i}(14)}\left(\mathscr{P}^{\Theta}(*')\right)\right\rangle}{\left\langle n_{\boldsymbol{\pi}_{z_i}(14)}\left(\mathscr{P}^{\Theta}(\phi)\right)\right\rangle}$ versus $\sqrt{1-e^{\beta_i+\hat{\kappa}_\phi}}$ for Chains 8 through 14 and $*' \in \{(\phi, f)\ [*],\ (\phi|\phi, s)\ [\triangle],\ (3_1|\phi, s)\ [\boxdot],\ (4_1|\phi, s)\ [\blacksquare],\ (5_2|\phi, s)\ [\odot]\}$.

data $\left\{\left(\sqrt{1-e^{\beta_i+\hat{\kappa}_\phi}}, \frac{\left\langle n_{\boldsymbol{\pi}_{z_i}(2,14)}\left(\mathscr{P}^\Theta(*)\right)\right\rangle}{\left\langle n_{\boldsymbol{\pi}_{z_i}(2,14)}\left(\mathscr{P}^\Theta(\phi)\right)\right\rangle}\right)\right\}_{i=l_*}^{14}$, where l_* is the value of i for which the plot of the points in $\left\{\left(\sqrt{1-e^{\beta_i+\hat{\kappa}_\phi}}, \frac{\left\langle n_{\boldsymbol{\pi}_{z_i}(2,14)}\left(\mathscr{P}^\Theta(*)\right)\right\rangle}{\left\langle n_{\boldsymbol{\pi}_{z_i}(2,14)}\left(\mathscr{P}^\Theta(\phi)\right)\right\rangle}\right)\right\}_{i=1}^{14}$ appears to start behaving linearly in $\sqrt{1-e^{\beta_i+\hat{\kappa}_\phi}}$.

For the rest of this section, any reference to y-intercept for property $*$ will refer to the y-intercept of the estimated regression line determined using the specified property-$*$ subsequence. The problem with trying to estimate the y-intercept of property $*$ for each of the five sequences in Figure 4.12 is that, the larger the value of β_i (or equivalently the smaller the value of $\sqrt{1-e^{\beta_i+\hat{\kappa}_\phi}}$), the more likely the corrections to the linear scaling form influence the estimate for the ratio $\frac{\mathrm{E}(*)}{\mathrm{E}(\phi)}$. Hence, in order to estimate the y-intercepts in Figure 4.12, the estimates for the ratios $\frac{\mathrm{E}(*)}{\mathrm{E}(\phi)}$ that are based on the β_i's which are as close as possible to $-\kappa_\phi$ should be used. The problem with using these estimates for the ratios $\frac{\mathrm{E}(*)}{\mathrm{E}(\phi)}$ is that, as $\beta_i+\kappa_\phi \to 0$, there is much more variability in the estimates for $\mathrm{E}\left(\alpha_*^\Theta+q, \beta_i+\kappa_\phi, -\Delta_*^\Theta, N_{\min}^*, A_*^\Theta, B_*^\Theta\right)$ and $\mathrm{E}\left(\alpha_\phi^\Theta+q, \beta_i+\kappa_\phi, -\Delta_\phi^\Theta, N_{\min}^\phi, A_\phi^\Theta, B_\phi^\Theta\right)$ and hence there is much more variability in the estimate for $\frac{\mathrm{E}(*)}{\mathrm{E}(\phi)}$.

The data $\left\{\left(\sqrt{1-e^{\beta_i+\hat{\kappa}_\phi}}, \frac{\left\langle n_{\boldsymbol{\pi}_{z_i}(2,14)}\left(\mathscr{P}^\Theta(\phi,f)\right)\right\rangle}{\left\langle n_{\boldsymbol{\pi}_{z_i}(2,14)}\left(\mathscr{P}^\Theta(\phi)\right)\right\rangle}\right)\right\}_{i=1}^{14}$ (plotted in Figure 4.11 using $*$) is used to estimate the y-intercept for property (ϕ,f). Fitting a straight line to the data $\left\{\left(\sqrt{1-e^{\beta_i+\hat{\kappa}_\phi}}, \frac{\left\langle n_{\boldsymbol{\pi}_{z_i}(2,14)}\left(\mathscr{P}^\Theta(\phi,f)\right)\right\rangle}{\left\langle n_{\boldsymbol{\pi}_{z_i}(2,14)}\left(\mathscr{P}^\Theta(\phi)\right)\right\rangle}\right)\right\}_{i=1}^{14}$ using Weighted Least-Squares Regression yields the following 95% confidence interval for the y-intercept for property (ϕ,f): 0.99 ± 0.02. Because 1.0 is in this confidence interval, it is plausible that the y-intercept for property (ϕ,f) is 1.0, which implies that, as $\beta_i+\kappa_\phi \to 0$, $\frac{\mathrm{E}(\phi,f)}{\mathrm{E}(\phi)} \to 1$ is possible. Hence, as $\beta_i+\kappa_\phi \to 0$, $\frac{\alpha_{(\phi,f)}^\Theta+3}{\alpha_\phi^\Theta+3} \to 1$ is also possible, that is $\alpha_\phi^\Theta = \alpha_{(\phi,f)}^\Theta$ is possible.

Referring to the plot of $\left\{\left(\sqrt{1-e^{\beta_i+\hat{\kappa}_\phi}}, \frac{\left\langle n_{\boldsymbol{\pi}_{z_i}(2,14)}\left(\mathscr{P}^\Theta(\phi|\phi,s)\right)\right\rangle}{\left\langle n_{\boldsymbol{\pi}_{z_i}(2,14)}\left(\mathscr{P}^\Theta(\phi)\right)\right\rangle}\right)\right\}_{i=1}^{14}$ in Figure 4.11, for the values $\beta_1, \beta_2, \beta_3$, and β_4, the plot does not seem to be linear. Hence, for these four β values, the estimates $\frac{\left\langle n_{\boldsymbol{\pi}_{z_i}(2,14)}\left(\mathscr{P}^\Theta(\phi|\phi,s)\right)\right\rangle}{\left\langle n_{\boldsymbol{\pi}_{z_i}(2,14)}\left(\mathscr{P}^\Theta(\phi)\right)\right\rangle}$ are being influenced by the

corrections to the linear scaling form. Therefore the points corresponding to these four β values should not be used to estimate the y-intercept for property $(\phi|\phi,s)$. Fitting a straight line to the restricted data set $\left\{\left(\sqrt{1-e^{\beta_i+\hat{\kappa}_\phi}}, \frac{\left\langle n_{\boldsymbol{\pi}_{z_i}(2,14)}\left(\mathscr{P}^\Theta(\phi|\phi,s)\right)\right\rangle}{\left\langle n_{\boldsymbol{\pi}_{z_i}(2,14)}\left(\mathscr{P}^\Theta(\phi)\right)\right\rangle}\right)\right\}_{i=5}^{14}$ via a Weighted Least-Squares Regression yields the following 95% confidence interval for the y-intercept for property $(\phi|\phi,s)$: 0.96 ± 0.05. Since one is in this confidence interval, it is plausible that the y-intercept for property $(\phi|\phi,s)$ is one, and by a similar argument to that in the previous paragraph for property (ϕ,f), it is plausible that $\alpha_\phi^\Theta = \alpha_{(\phi|\phi,s)}^\Theta$.

Referring to Figure 4.11, the corrections to the linear scaling form seem to be present in the plot of $\left\{\left(\sqrt{1-e^{\beta_i+\hat{\kappa}_\phi}}, \frac{\left\langle n_{\boldsymbol{\pi}_{z_i}(2,14)}\left(\mathscr{P}^\Theta(3_1|\phi,s)\right)\right\rangle}{\left\langle n_{\boldsymbol{\pi}_{z_i}(2,14)}\left(\mathscr{P}^\Theta(\phi)\right)\right\rangle}\right)\right\}_{i=1}^{14}$ for the values $\beta_1, ..., \beta_6$. Hence the estimates $\frac{\left\langle n_{\boldsymbol{\pi}_{z_i}(2,14)}\left(\mathscr{P}^\Theta(3_1|\phi,s)\right)\right\rangle}{\left\langle n_{\boldsymbol{\pi}_{z_i}(2,14)}\left(\mathscr{P}^\Theta(\phi)\right)\right\rangle}$ should not be used for the values $\beta_1, ..., \beta_6$ when trying to estimate the y-intercept for property $(3_1|\phi,s)$. Fitting a straight line to the data $\left\{\left(\sqrt{1-e^{\beta_i+\hat{\kappa}_\phi}}, \frac{\left\langle n_{\boldsymbol{\pi}_{z_i}(2,14)}\left(\mathscr{P}^\Theta(3_1|\phi,s)\right)\right\rangle}{\left\langle n_{\boldsymbol{\pi}_{z_i}(2,14)}\left(\mathscr{P}^\Theta(\phi)\right)\right\rangle}\right)\right\}_{i=7}^{14}$ via a Weighted Least-Squares Regression and estimating a 95% confidence interval for the y-intercept for property $(3_1|\phi,s)$ yields 0.95 ± 0.08. Since one is in this confidence interval, it is plausible that the y-intercept for property $(3_1|\phi,s)$ is one and by a similar argument to that in the paragraph estimating the y-intercept for property (ϕ,f), it is plausible that $\alpha_\phi^\Theta = \alpha_{3_1|\phi,s}^\Theta$.

The plot of the data $\left\{\left(\sqrt{1-e^{\beta_i+\hat{\kappa}_\phi}}, \frac{\left\langle n_{\boldsymbol{\pi}_{z_i}(2,14)}\left(\mathscr{P}^\Theta(4_1|\phi,s)\right)\right\rangle}{\left\langle n_{\boldsymbol{\pi}_{z_i}(2,14)}\left(\mathscr{P}^\Theta(\phi)\right)\right\rangle}\right)\right\}_{i=1}^{14}$ in Figure 4.11 indicates that, for the values $\beta_1, ..., \beta_{10}$, corrections to the linear scaling form appear to be present in each of the point estimates. Therefore the restricted data set given by $\left\{\left(\sqrt{1-e^{\beta_i+\hat{\kappa}_\phi}}, \frac{\left\langle n_{\boldsymbol{\pi}_{z_i}(2,14)}\left(\mathscr{P}^\Theta(4_1|\phi,s)\right)\right\rangle}{\left\langle n_{\boldsymbol{\pi}_{z_i}(2,14)}\left(\mathscr{P}^\Theta(\phi)\right)\right\rangle}\right)\right\}_{i=11}^{14}$ should be used to estimate the y-intercept for property $(4_1|\phi,s)$. By fitting a straight line to this restricted data set via a Weighted Least-Squares Regression, the following 95% confidence interval for the y-intercept for property $(4_1|\phi,s)$ was determined: 0.44 ± 0.57. Because of the size of the estimated 95% margin of error, the point estimate for the y-intercept is not very reliable. Consequently the value of the y-intercept could be one but it might not be as well.

4.7.4 Estimating $N^*_{\max}$

The purpose for including the quantity $N^*_{\max}$ in the model is to take into account the finite nature of the simulation, and specifically the fact that the observed proportion for a large polygon length N may not accurately represent the proportion for that N according to the true equilibrium distribution. For example, if the total number of polygons with property $* \in \Phi$ observed in Chain i of Replication r is denoted $\Psi_i^{(r)}(*)$, then

$$\Psi_i^{(r)}(*) := \sum_{t=0}^{t_0} \mathscr{M}_T(t)\psi_*(\omega_t^{(r)}(i)), \tag{4.165}$$

where, for $* \in \Phi$,

$$\psi_*(\omega) := \begin{cases} 1 & \text{if } \omega \text{ has property } *, \\ 0 & \text{otherwise.} \end{cases} \tag{4.166}$$

Further, if the total number of polygons with property $*$ observed in Chain i across all n_0 replications is denoted $\Psi_i(*)$, then

$$\Psi_i(*) := \sum_{r=1}^{n_0} \Psi_i^{(r)}(*). \tag{4.167}$$

Therefore, if the total number of polygons with property $*$ observed throughout the n_0 replications is denoted $\Psi(*)$, then

$$\Psi(*) := \sum_{i=1}^{M} \Psi_i(*). \tag{4.168}$$

The following table contains the values of $\Psi(*)$ for $* \in \{(\phi, f)$, $(\phi|\phi, s)$, $(3_1|\phi, s)$, $(4_1|\phi, s)$, $(5_2|\phi, s)$, $(6_1|\phi, s)$, $(6_2|\phi, s)$, $(6_3|\phi, s)$, $(7_2|\phi, s)$, $(7_6|\phi, s)$, $(8_{20}|\phi, s)\}$.

From Table 4.15, it is quite evident that the majority of the polygons generated during the simulation of the CMC Θ-BFACF algorithm are unsuccessful-strand-passage polygons; that the majority of the successful-strand-passage polygons generated during the simulation are unknotted after strand passage; and that there are relatively few observed successful-strand-passage Θ-SAPs that have a non-trivial knot-type after a strand passage about Θ. Hence in order to compute any estimate based on this data, the interval over which the data is most reliable needs to be determined. The technique discussed in Section 4.6 will be used to estimate $N^*_{\max}$ for the purposes of determining the most reliable data.

For each of the ten replications, suppose no data is thrown away. Let $\hat{N}_u^{(r)}$ be the largest unknotted polygon length observed in Replication r and let $\hat{N}_l^{(r)}$ be the smallest unknotted

Table 4.15: The total number of polygons sampled from the simulation of the CMC Θ-BFACF algorithm that have property $*$.

Property $*$	$\Psi(*)$	Property $*$	$\Psi(*)$
(ϕ, f)	9770500795	$(6_2\|\phi, s)$	55
$(\phi\|\phi, s)$	1300566055	$(6_3\|\phi, s)$	10
$(3_1\|\phi, s)$	16471677	$(7_2\|\phi, s)$	21
$(4_1\|\phi, s)$	443025	$(7_6\|\phi, s)$	1
$(5_2\|\phi, s)$	17872	$(8_{20}\|\phi, s)$	6
$(6_1\|\phi, s)$	483		

Table 4.16: The largest and smallest polygon lengths observed in Replication r.

Replication r	$\hat{N}_l^{(r)}$	$\hat{N}_u^{(r)}$	Replication r	$\hat{N}_l^{(r)}$	$\hat{N}_u^{(r)}$
1	14	6416	6	14	5628
2	14	5938	7	14	5584
3	14	5700	8	14	6642
4	14	5402	9	14	6960
5	14	6166	10	14	5826

polygon length observed in Replication r. Suppose the estimate for $N^*_{\max}$ determined using Replication r is denoted $\hat{N}^{(r)}_{\max}(*)$. Then, the estimate $\hat{N}_u^{(r)}$ in Table 4.16 is an upper bound for $\hat{N}^{(r)}_{\max}(*)$. The values of $\hat{N}_l^{(r)}$ and $\hat{N}_u^{(r)}$, for Replication r, $r \in \{1, ..., 10\}$, are presented in Table 4.16:

From the values of $\hat{N}_l^{(r)}$ and $\hat{N}_u^{(r)}$, for Replication r, $r \in \{1, ..., 10\}$, presented in Table 4.16, the values of $\hat{N}_l$ and $\hat{N}_u$ can be determined, where

$$\hat{N}_l = \max_r \hat{N}_l^{(r)} \tag{4.169}$$

and

$$\hat{N}_u = \min_r \hat{N}_u^{(r)}. \tag{4.170}$$

From the estimates presented in Table 4.16, $\hat{N}_l = 14$ and $\hat{N}_u = 5402$.

Because the same data is used in the analysis presented in Chapters 5 through 7, the reliability of the data will be determined using a function of the data that is common to

the analysis in all three chapters, that is the reliability of the data will be determined using the proportion of $(2n)$-edge Θ-SAPs with property $*$ generated in each of the replications. Then $\hat{g}_i^{(r)}(\phi, 2n)$ is the estimated proportion of $(2n)$-edge unknotted Θ-SAPs as sampled from Chain i during Replication r. If $*$ is one of the after-strand-passage properties $\{(\phi, f)$, (ϕ, s), $(\phi|\phi, s)$, $(3_1|\phi, s)$, $(4_1|\phi, s)\}$, let

$$\hat{g}_i^{(r)}(*, 2n) := \frac{\sum_{t=0}^{m} \psi_* \left(\omega_t^{(r)}(i)\right) \mathscr{I}_{2n} \left(\left|\omega_t^{(r)}(i)\right|\right)}{\sum_{t=0}^{m} \psi_\phi \left(\omega_t^{(r)}(i)\right) \mathscr{I}_{2n} \left(\left|\omega_t^{(r)}(i)\right|\right)}. \tag{4.171}$$

Then the quantity $\hat{g}^{(r)}(*, 2n)$ is the estimated proportion of $(2n)$-edge Θ-SAPs that have property $* \in \{(\phi, f)$, (ϕ, s), $(\phi|\phi, s)$, $(3_1|\phi, s)$, $(4_1|\phi, s)\}$ as sampled during Replication r.

For $* \in \{(\phi, f)$, (ϕ, s), $(\phi|\phi, s)$, $(3_1|\phi, s)$, $(4_1|\phi, s)\}$, the corresponding estimated standard error of $\hat{g}^{(r)}(*, 2n)$ is defined to be

$$\widehat{\mathrm{SE}}(\hat{g}^{(r)}(*, 2n)) := \sqrt{\frac{\widehat{\mathrm{var}}(\hat{g}^{(r)}(*, 2n))}{m'}}, \tag{4.172}$$

where $\widehat{\mathrm{var}}(\hat{g}^{(r)}(*, 2n))$ is given by Equation (A.30) in Section A.3 of Appendix A and m' is the number of essentially independent data points used to compute $\widehat{\mathrm{var}}(\hat{g}^{(r)}(*, 2n))$. Then for every $* \in \{(\phi, f)$, (ϕ, s), $(\phi|\phi, s)$, $(3_1|\phi, s)$, $(4_1|\phi, s)\}$, the corresponding estimated relative standard error of $\hat{g}^{(r)}(*, 2n)$ is defined to be

$$\hat{\delta}_{2n}^{(r)}(*) := \begin{cases} \dfrac{\widehat{\mathrm{SE}}(\hat{g}^{(r)}(*, 2n))}{\hat{g}^{(r)}(*, 2n)}, & \text{if } \hat{g}^{(r)}(*, 2n) > 0 \\ \infty, & \text{otherwise.} \end{cases} \tag{4.173}$$

Recall from Section 4.6 that $\hat{\delta}^{(r)} = \min_n \hat{\delta}_{2n}^{(r)}$; that $\hat{\eta}^{(r)}(*)$ is the first value of $2n$ for which $\hat{\delta}^{(r)}(*) = \hat{\delta}_{2n}^{(r)}(*)$; $\varepsilon_* := \min_r(\hat{\delta}^{(r)}(*) + c)$; and that $\hat{N}_{\max}^{(r)}(*)$ computed from Replication r is the smallest polygon length greater than $\hat{\eta}^{(r)}(*)$ for which $\hat{\delta}_{2n}^{(r)}(*) \geq \varepsilon_*$. For the purposes of this work, the most reliable data is data whose relative error is within 5% of the minimum estimated relative error. This corresponds to setting $c := 0.05$ in the definition of ε_*. The reason this cutoff was chosen results from the fact that the estimated proportions for all the properties $*$, save $* = \phi$, are ratio estimates and the goal is to minimize the effects of small fluctuations in the denominator as they could lead to large fluctuations in the resulting point estimates.

To see the necessity for including an $N_{\max}^*$, cf. Figure 4.13. Figure 4.13 is a plot of the estimated relative error associated with the estimated proportion of n-edge before-strand-passage polygons (from each of the ten replications) plotted as a function of polygon

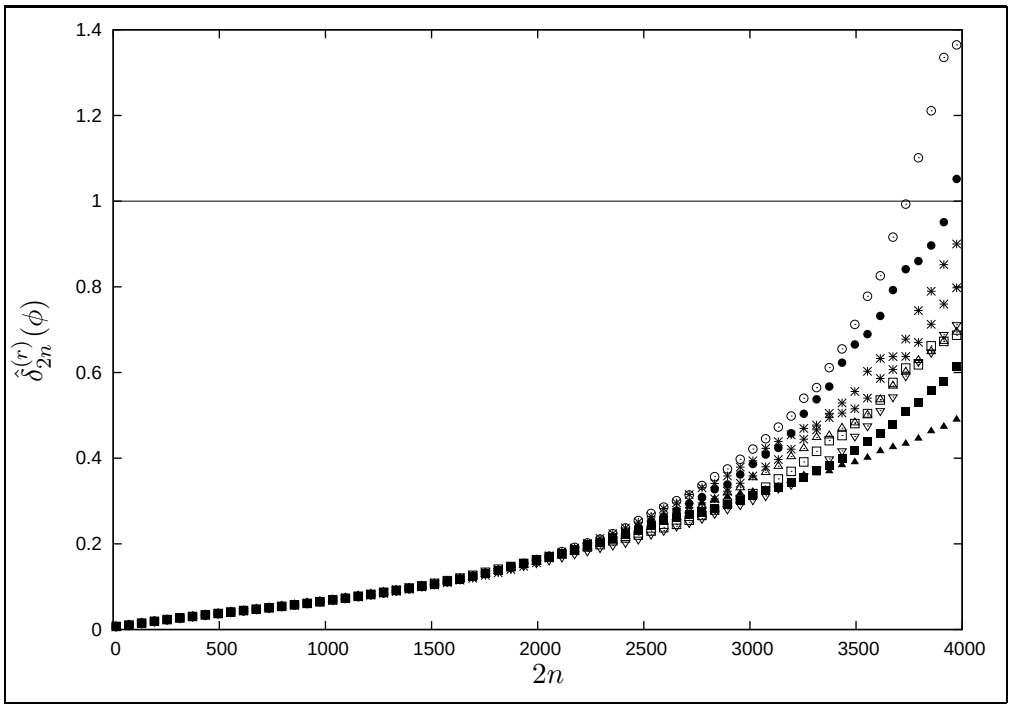

Figure 4.13: The estimated relative error associated with the estimated proportion of $(2n)$-edge before-strand-passage polygons generated in Replication r.

length $2n$. The horizontal line in the figure represents when the estimated relative error is one. This corresponds to the estimated standard error of the point estimate being equal to the estimated standard error of the point estimate. From Figure 4.13, if the maximum tolerated relative error is 1.0, then choosing 3700 as the estimate for $N_{\max}^{\phi}$ seems appropriate.

In order to determine how the estimates $\hat{\delta}_{2n}^{(r)}(\phi)$ (as defined by Equation (4.173)) are expected to behave as a function of n, assume that, for sufficiently large $n \geq N_{\min}/2$, there exist constants $A_{\phi}^{\Theta}, \mu_{\phi}, h_{\phi}^{\Theta}$, and α_{ϕ}^{Θ} such that $p_{2n}^{\Theta}(\phi) = A_{\phi}^{\Theta}\mu_{\phi}^{2n}(2n + h_{\phi}^{\Theta})^{\alpha_{\phi}^{\Theta}}$ and that, for

any positive integer q, $\pi_{2n}(\boldsymbol{\theta}_i)$ is defined by

$$\begin{aligned}
&\pi_{2n}(A_\phi^\Theta, \kappa_\phi, \alpha_\phi^\Theta, h_\phi^\Theta, q, z_i, N_{\min}) \\
&:= \frac{\left(\mathscr{I}_{[14,N_{\min})}(2n)\right) Q(q, z_i, N_{\min})}{Q(q, z_i, N_{\min}) + \sum\limits_{m \geq N_{\min}/2} A_\phi^\Theta (2m-6)(2m)^{q-1}(2m + h_\phi^\Theta)^{\alpha_\phi^\Theta} \left(e^{\kappa_\phi} z_i\right)^{2m}} \\
&+ \frac{\left(\mathscr{I}_{[N_{\min},\infty)}(2n)\right) \left[A_\phi^\Theta (2n-6)\,(2n)^{q-1}\,(2n + h_\phi^\Theta)^{\alpha_\phi^\Theta}\,\left(e^{\kappa_\phi} z_i\right)^{2n}\right]}{Q(q, z_i, N_{\min}) + \sum\limits_{m \geq N_{\min}/2} A_\phi^\Theta (2m-6)(2m)^{q-1}(2m + h_\phi^\Theta)^{\alpha_\phi^\Theta} \left(e^{\kappa_\phi} z_i\right)^{2m}}
\end{aligned} \tag{4.174}$$

with

$$Q(q, z, N_{\min}) := \sum_{14 \leq m < N_{\min}/2} (2m-6)\,(2m)^{q-1}\, z^{2m} p_{2m}^\Theta(\phi). \tag{4.175}$$

Then, as $n \to \infty$,

$$\breve{\pi}_{2n|N_{\min}}(q, z) \sim \pi_{2n}(A_\phi^\Theta, \kappa_\phi, \alpha_\phi^\Theta, h_\phi^\Theta, q, z, N_{\min}) \tag{4.176}$$

Now, for $q = 2$ and the a priori guess

$$\boldsymbol{\theta}_i = (1.0, 1.544125, -1.75, 0, 2, z_i, 14), \tag{4.177}$$

suppose

$$\pi_{2n}(\boldsymbol{\theta}_i) := \pi_{2n}(1.0, 1.544125, -1.75, 0, 2, z_i, 14), \tag{4.178}$$

$$\sigma^2_{\pi_{2n}}(\boldsymbol{\theta}_i) := \pi_{2n}(\boldsymbol{\theta}_i)\left(1 - \pi_{2n}(\boldsymbol{\theta}_i)\right)/T',$$

$$\bar{\pi}_{2n} := \frac{1}{M}\sum_{i=1}^{M} \pi_{2n}(\boldsymbol{\theta}_i), \tag{4.179}$$

and

$$\sigma^2\left[\bar{\pi}_{2n}\right] := \frac{1}{M}\sum_{i=1}^{M} \sigma^2_{\pi_{2n}}(\boldsymbol{\theta}_i). \tag{4.180}$$

Then the expected relative error associated with $\bar{\pi}_{2n}$ is $\dfrac{\sqrt{\sigma^2\left[\bar{\pi}_{2n}\right]}}{\bar{\pi}_{2n}}$.

Figure 4.14 is a plot of $\dfrac{\sqrt{\sigma^2\left[\bar{\pi}_{2n}\right]}}{\bar{\pi}_{2n}}$ versus $2n$ for the a priori guess

$$\boldsymbol{\theta}_i = (1.0, 1.544125, -1.75, 0, 2, z_i, 14). \tag{4.181}$$

Note from Figure 4.14 that the expected relative error associated with the proportion of observed polygons of length $2n$ is an increasing function of n. This feature needs to be taken into account when trying to determine an estimate for $N_{\max}^\phi$.

Because the relative error is expected to increase as a function of n, simply determining the estimate for $N_{\max}^\phi$ based on a fixed cutoff value is not a good measure for the reliability

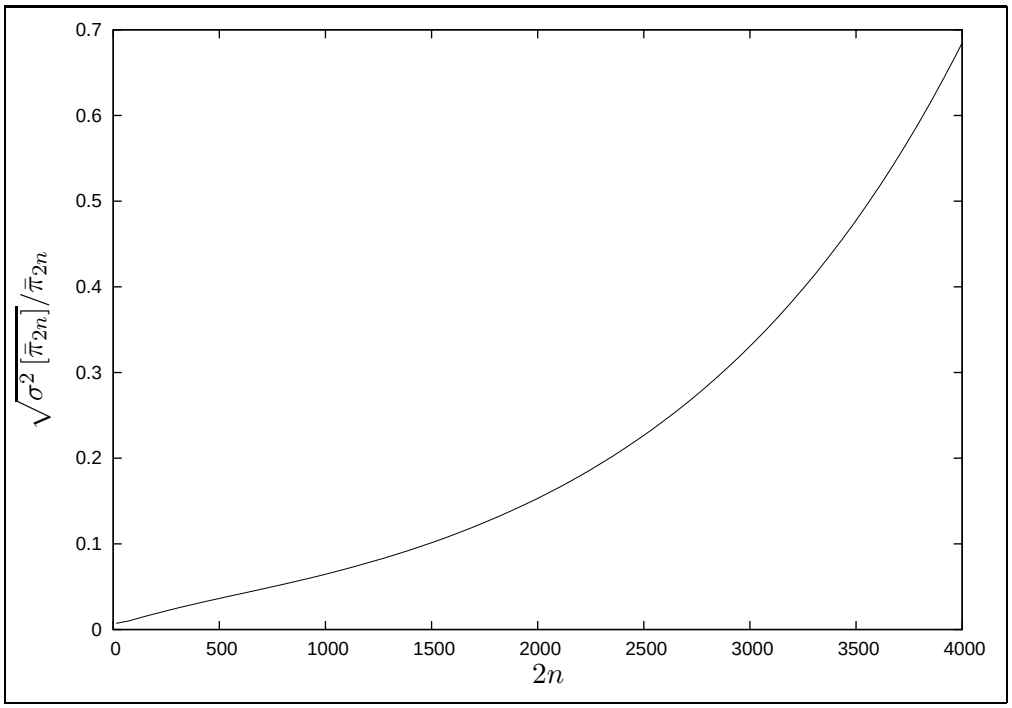

Figure 4.14: The expected relative errors for the proportion of $(2n)$-edge before-strand-passage polygons generated in Replication r. The expected values are computed based on assuming $\boldsymbol{\theta}_i = (1, 1.544125, -1.75, 0, 2, z_i, 14)$.

of the data. The estimated relative errors may still be well-approximating the trend of the expected relative errors beyond the fixed cutoff. This is why the method described in Section 4.6 for estimating $N^{\phi}_{\max}$ determines an estimate for $N^{\phi}_{\max}$ in terms of when the sequences of the estimated relative errors for each replication start diverging.

For each of the ten replications, the values of $\hat{\delta}^{(r)}_{2n}(*)$, for the properties (ϕ, f), $(\phi|\phi, s)$, $(3_1|\phi, s)$, and $(4_1|\phi, s)$, are respectively shown in Figures 4.15 through 4.18. For the purposes of creating a more meaningful figure, every tenth consecutive value for $\hat{\delta}^{(r)}_{2n}(*)$, that is the set of points $\left\{\left(\hat{N}^{(r)}_l + 20i, \hat{\delta}^{(r)}_{\hat{N}^{(r)}_l+20i}(*)\right)\right\}_{i=0}^{\left\lfloor(\hat{N}^{(r)}_u - \hat{N}^{(r)}_l)/20\right\rfloor}$, is plotted in Figures 4.15 through 4.18. The horizontal line in each of Figures 4.15 through 4.18 represents ε_*, that is where the estimated relative error is five percent of the smallest of the ten values $\hat{\delta}^{(r)}(*)$, $r \in \{1, 2, ..., 10\}$. Table 4.17 contains the values of ε_* for the same four properties. Table 4.18 summarizes the estimated values of $N^*_{\max}$ for the properties (ϕ, f), $(\phi|\phi, s)$, $(3_1|\phi, s)$, and $(4_1|\phi, s)$ for each of the ten replications.

Table 4.17: The maximum tolerated estimated relative error in the proportion of n-edge Θ-SAPs with property $*$.

Property	ε_*
(ϕ, f)	0.051
$(\phi\|\phi, s)$	0.070
$(3_1\|\phi, s)$	0.072
$(4_1\|\phi, s)$	0.074

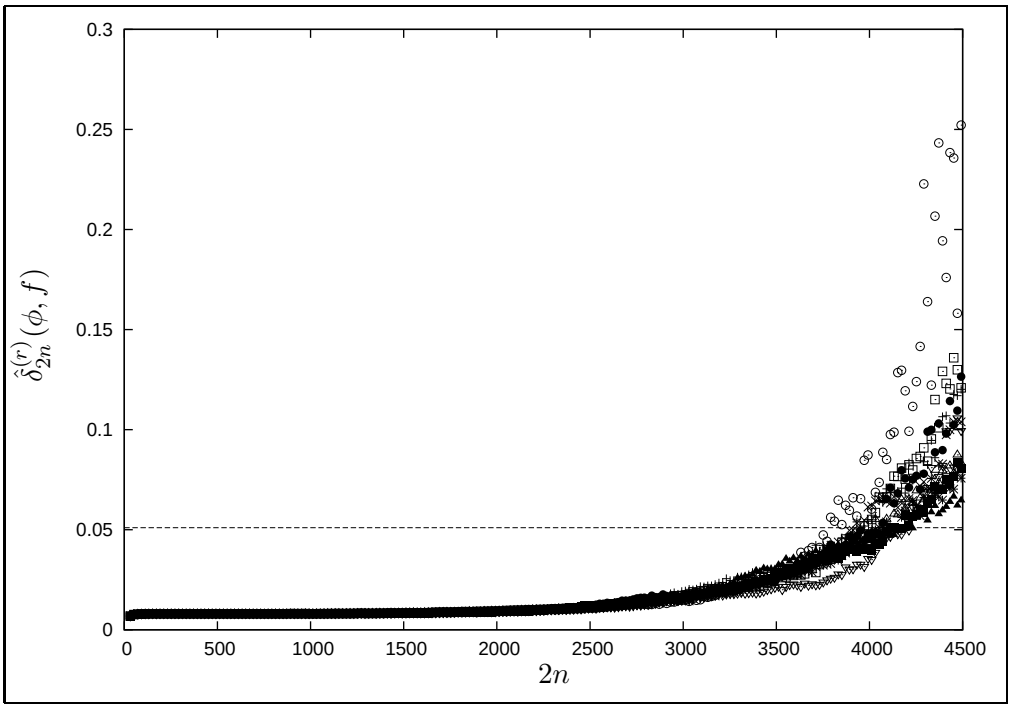

Figure 4.15: The estimated relative error associated with the estimated proportion of $(2n)$-edge failed-strand-passage polygons generated in Replication r. The horizontal line represents where the estimated relative error is five percent higher than the minimum (over all ten replications) estimated relative error.

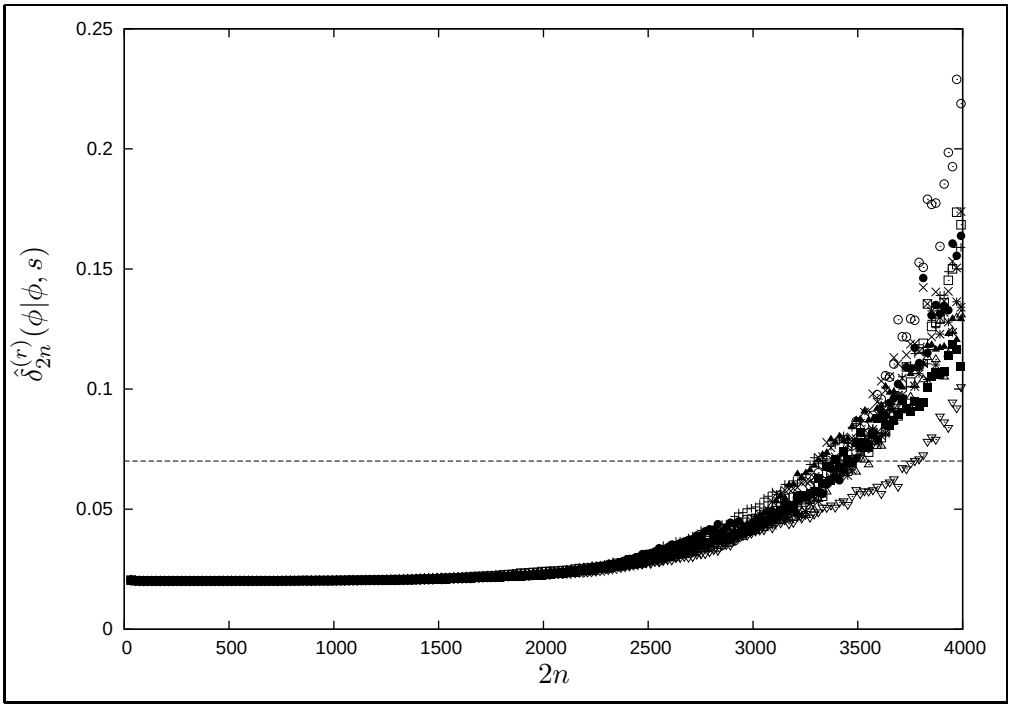

Figure 4.16: The estimated relative error associated with the estimated proportion of $(2n)$-edge Θ-SAPs that are unknotted given a successful strand passage and are generated in Replication r. The horizontal line represents where the estimated relative error is five percent higher than the minimum (over all ten replications) estimated relative error.

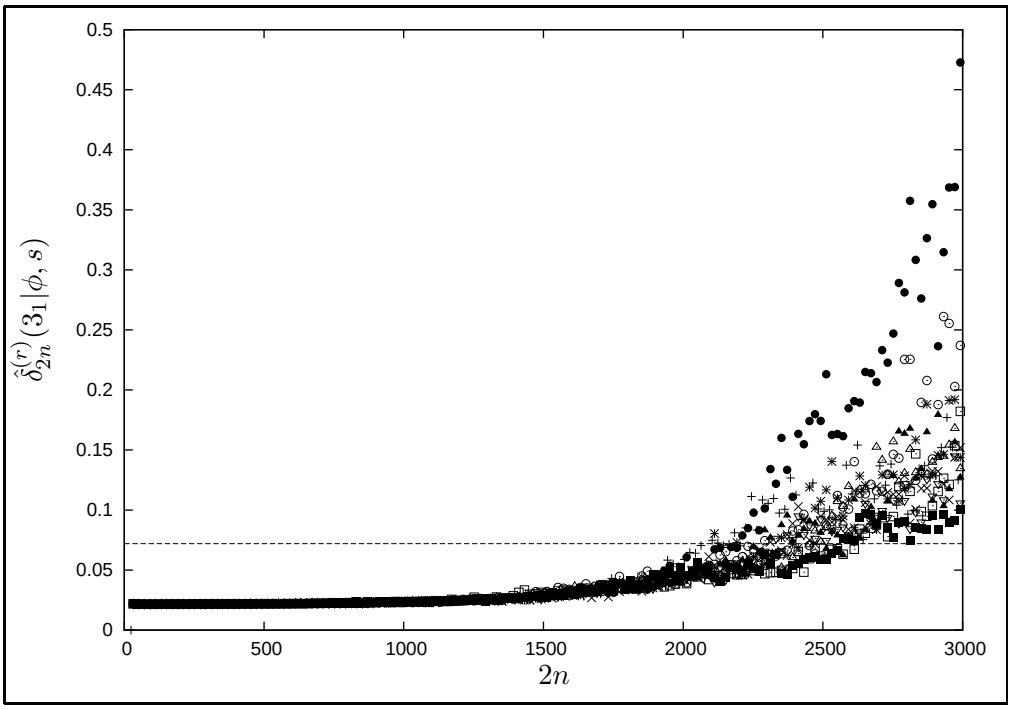

Figure 4.17: The estimated relative error associated with the estimated proportion of $(2n)$-edge Θ-SAPs that are a trefoil given a successful strand passage and are generated in Replication r. The horizontal line represents where the estimated relative error is five percent higher than the minimum (over all ten replications) estimated relative error.

Based on the estimates $\hat{N}_{\max}^{(r)}(\phi, f)$, $\hat{N}_{\max}^{(r)}(\phi|\phi, s)$, $\hat{N}_{\max}^{(r)}(3_1|\phi, s)$, and $\hat{N}_{\max}^{(r)}(4_1|\phi, s)$ presented in Table 4.18, $\hat{N}_{\max}(\phi, f) = 3700$, $\hat{N}_{\max}^{(r)}(\phi|\phi, s) = 3300$, $\hat{N}_{\max}^{(r)}(3_1|\phi, s) = 2000$ and $\hat{N}_{\max}^{(r)}(4_1|\phi, s) = 600$. Hence $\hat{N}_{\max}(\phi) = 3300$, $\hat{N}_{\max}(\phi, f) = 3300$, $\hat{N}_{\max}(\phi, s) = 3300$, and $\hat{N}_{\max}(\phi|\phi, s) = 3300$.

The estimates for $N_{\max}^*$ were also computed when the data collected during the first 5.0 billion and 11.0 billion Θ-BFACF moves in parallel are discarded. The values estimated for $N_{\max}^*$ in both of these scenarios are consistent with the values estimated for $N_{\max}^*$ when no data is burned. Therefore the estimates for $N_{\max}^*$ used in Chapter 5 are $\hat{N}_{\max}(\phi) = 3300$, $\hat{N}_{\max}(\phi, f) = 3300$, $\hat{N}_{\max}(\phi, s) = 3300$, $\hat{N}_{\max}(\phi|\phi, s) = 3300$, $\hat{N}_{\max}(3_1|\phi, s) = 2000$, and $\hat{N}_{\max}(4_1|\phi, s) = 600$.

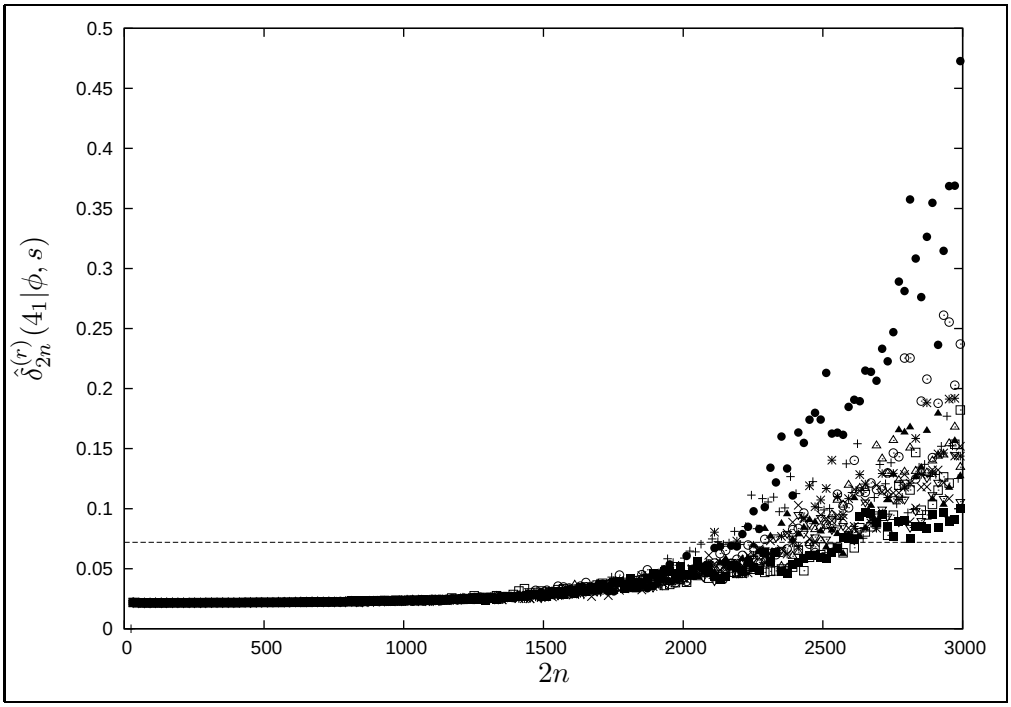

Figure 4.18: The estimated relative error associated with the estimated proportion of $(2n)$-edge Θ-SAPs that are a figure 8 given a successful strand passage and are generated in Replication r. The horizontal line represents where the estimated relative error is five percent higher than the minimum (over all ten replications) estimated relative error.

Table 4.18: The estimates for $N_{\max}^{*}$ for each of the 10 replications.

Replication r	$\hat{N}_{\max}^{(r)}(\phi, f)$	$\hat{N}_{\max}^{(r)}(\phi\|\phi, s)$	$\hat{N}_{\max}^{(r)}(3_1\|\phi, s)$	$\hat{N}_{\max}^{(r)}(4_1\|\phi, s)$
1	3900	3300	2000	700
2	3900	3300	2200	600
3	4100	3400	2100	700
4	3900	3400	2500	600
5	4100	3300	2500	700
6	3700	3300	2200	700
7	4000	3400	2100	600
8	4100	3400	2400	600
9	4100	3300	2200	600
10	4100	3700	2200	800

4.8 In Summary

This chapter provided a technique for estimating the time it takes a composite Markov chain to reach its stationary distribution and a technique for measuring the correlation that exists between the states of a composite Markov chain. The also chapter provides measures for determining the reliability and the consistency of the data that was generated from a composite Markov chain.

The above techniques and methods were illustrated with applications to the CMC Θ-BFACF data. Each replication in the data set consisted of 9.6×10^{10} time steps (8.0×10^{10} Θ-BFACF moves in parallel and 1.6×10^{10} attempted swaps) where every five Θ-BFACF moves in parallel are followed by an attempted swap. The realization in the r'th replication consisted of a sequence of $(t_0 + 1)$ 14-tuples of Θ-SAPs from $\left(\mathscr{P}^{\Theta}(\phi)\right)^{14}$ and this sequence was denoted

$$\boldsymbol{\omega}^{(r)} := \left(\left(\omega_t^{(r)}(1), \omega_t^{(r)}(2), ..., \omega_t^{(r)}(14) \right), t = 0, ..., 9.6 \times 10^{10} \right). \tag{4.182}$$

Data was collected after every 1000'th Θ-BFACF in parallel (but before the corresponding attempted swap) and the corresponding sample was denoted by

$$\hat{\boldsymbol{\omega}}^{(r)} := \left(\left(\hat{\omega}_j^{(r)}(1), \hat{\omega}_j^{(r)}(2), ..., \hat{\omega}_j^{(r)}(14) \right), j = 0, ..., l \right), \tag{4.183}$$

the sequence of 14-tuples of SAPs sampled from Replication r, where $l := \lfloor t_0/1200 \rfloor = 80,000,000$, and, for $t := 1200j$, the j'th term (for $1 \leq j \leq l$) of $\hat{\boldsymbol{\omega}}^{(r)}$ is given by

$$\left(\hat{\omega}_j^{(r)}(1), \hat{\omega}_j^{(r)}(2), ..., \hat{\omega}_j^{(r)}(14) \right) := \left(\omega_t^{(r)}(1), \omega_t^{(r)}(2), ..., \omega_t^{(r)}(14) \right). \tag{4.184}$$

Applying the technique to determine the time it took each replication to reach its stationary distribution yielded $\widehat{\tau}_{\text{exp}} = 5.0$ billion Θ-BFACF moves in parallel, that is after 5.0 billion Θ-BFACF moves in parallel, each replication appeared to have reached its stationary distribution. Applying the technique to determine the correlation that exists between the states generated in each replication yielded $\widehat{\tau}_{\text{int}} = 0.6$ billion Θ-BFACF moves in parallel. Hence states that are 1.2 billion Θ-BFACF moves in parallel apart are essentially independent and data that is subdivided into blocks of 1.2 million consecutive data points form essentially independent blocks of data. These estimates for τ_{exp} and τ_{int} will be used throughout the rest of this work. Consequently, before any data are burned, each

replication can be subdivided into 66 essentially independent blocks of data and hence, if the data from all ten replications are combined, there are 660 essentially independent blocks of data which can be used in any subsequent analysis. If 5.0 million data points are burned, then each replication consists of 62 essentially independent blocks of data, and hence, there are 620 essentially independent blocks of data (if the data from all ten replications are combined) available for any subsequent analysis.

The next portion of the preliminary analysis consisted of a verification of the accuracy and reliability of the CMC Θ-BFACF data. From a comparison of the average lengths of the unknotted Θ-SAPs generated in each of the fourteen chains to the average lengths of the unknotted SAPs generated in the fourteen chains characterized by the same fugacities used in the CMC Θ-BFACF simulation (as presented in [121]), it was concluded that the average lengths were in agreement and behaved as expected. Further, the average lengths of the property $*$ Θ-SAPs generated in each of the fourteen chains exhibited the behaviours expected as given by Approximations (4.101) and (4.102) thus supporting the data was generated from the correct distribution. For the final verification presented, recall that in Chapter 2, it was proved that, for all $* \in \Phi$, $\kappa_\phi^* = \kappa_\phi$ and it was conjectured that (assuming both Consequences 2.2.8 and 2.2.9 are true) $\alpha_\phi - 2 = \alpha_*^\Theta$. The final verification presented in this chapter was included as a method for checking the consistency of the data generated by using the data generated to verify that $\kappa_\phi^* = \kappa_\phi$ and to determine if the data supported the Consequence 2.2.8, that is $\alpha_\phi - 2 = \alpha_*^\Theta$. The estimate for $e^{\kappa_\phi^*}$ (4.6836) computed based on the CMC data is exactly the value estimated for e^{κ_ϕ} estimated by Orlandini *et al.* [125]. The estimate computed for $\alpha_\phi^\Theta \approx -1.78$ is completely consistent with Consequence 2.2.8 since Orlandini *et al.* [125] estimated $\alpha_\phi \approx 0.23$.

The final discussion in the chapter applied the technique for determining which data generated is reliable data. The analysis of the simulation data concluded that all property $*$ Θ-SAPs generated whose lengths are less than or equal to $\hat{N}_{\max}(*)$ can be considered reliable. The following estimates for $\hat{N}_{\max}(*)$ are obtained: $\hat{N}_{\max}(\phi) = 3300$, $\hat{N}_{\max}(\phi, f) = 3300$, $\hat{N}_{\max}(\phi, s) = 3300$, $\hat{N}_{\max}(\phi|\phi, s) = 3300$, $\hat{N}_{\max}(3_1|\phi, s) = 2000$, and $\hat{N}_{\max}(4_1|\phi, s) = 600$. These estimates for $\hat{N}_{\max}(*)$ will be used in Chapter 5. The estimates for $N_{\max}^*$ that are required in Chapters 6 and 7 are presented in those chapters respectively.

Chapter 5

A New Maximum Likelihood Estimation Technique for a CMC

The first section of the chapter provides a brief review of some notation, definitions, and results that will be required throughout the chapter with the goal being to obtain a point estimate and an associated $(1-\alpha)\cdot 100\%$ confidence interval for some parameter of interest. The next section provides a method for estimating how many time steps a simulation must be run (once in equilibrium) in order to obtain a particular $(1-\alpha)\cdot 100\%$ margin of error associated with a parameter of interest. The third section details a new technique developed by the author to compute maximum likelihood estimates (which is defined in Definition 5.1.2) for parameters of interest based on data generated by the CMC Θ-BFACF Algorithm. The following section outlines a method for determining the reliable data that is required in the statistical analysis presented at the ends of Chapters 5 and 6, and throughout the discussions in Chapter 7. The chapter concludes by applying the new maximum likelihood technique to the data generated and providing the estimates that result from the application.

5.1 $(1-\alpha)\cdot 100\%$ Confidence Intervals Based on Maximum Likelihood Estimates

The purpose of this section is two-fold. The section provides an outline for determining a point estimate and a $(1-\alpha)\cdot 100\%$ confidence interval based on an i.i.d. sample and the likelihood function (defined in Definition 5.1.2). The second purpose of the section is to introduce the notation and results that will be needed throughout the chapter. To this end, suppose that the random variables $X_1, X_2, ..., X_n$ have the same unknown distribution P from a *parametric family of distributions*, where each distribution in the parametric family

is completely determined by a finite k-dimensional real-valued *parameter* $\boldsymbol{\Xi} = (\Xi_1, .., \Xi_k) \in \mathbb{R}^k$. The set, denoted Ω, of all possible values of the parameter $\boldsymbol{\Xi}$ is called the *parameter space*. When a particular value from Ω is assigned to $\boldsymbol{\Xi}$, the notation $\boldsymbol{\Xi} = \boldsymbol{\theta}$ will be used.

In order to provide an example of a parametric family of distributions, suppose that W is a randomly chosen self-avoiding polygon from $\mathscr{P}^{\Theta}(\phi)$ that was chosen according to the probability mass function $\{\breve{\pi}_{\omega}(q,z), \omega \in \mathscr{P}^{\Theta}(\phi)\}$ where

$$\breve{\pi}_{\omega}(q,z) := \frac{|\omega|^{q-1}\left(|\omega|-6\right)z^{|\omega|}}{\sum\limits_{n\geq 7} p_{2n}^{\Theta}(\phi)(2n)^{q-1}(2n-6)z^{2n}}, \tag{5.1}$$

(as defined and discussed in Section 2.2.2), q is a given fixed positive integer, and $z < z_{\phi}$ is a fixed real value. Also, recall from Section 2.61 that the probability that W is a $(2n)$-edge SAP from $\mathscr{P}^{\Theta}(\phi)$ is given by

$$\breve{\pi}_{2n}(q,z) = \frac{(2n)^{q-1}(2n-6)p_{2n}^{\Theta}(\phi)z^{2n}}{\sum\limits_{m\geq 7} p_{2m}^{\Theta}(\phi)(2m)^{q-1}(2m-6)z^{2m}}, \tag{5.2}$$

which can be approximated by assuming that, for some fixed positive even integer $N_{\min} \geq 14$, for sufficiently large $n \geq N_{\min}/2$, there exist constants $A_{\phi}^{\Theta}, \mu_{\phi}, h_{\phi}^{\Theta}$, and α_{ϕ}^{Θ} such that

$$p_{2n}^{\Theta}(\phi) = A_{\phi}^{\Theta}\mu_{\phi}^{2n}(2n + h_{\phi}^{\Theta})^{\alpha_{\phi}^{\Theta}}. \tag{5.3}$$

The corresponding parametric family of discrete distributions for a fixed positive even integer $N_{\min}$ and fixed real values z, and h_{ϕ}^{Θ}, is given by the set of probability mass functions, $\wp(h_{\phi}^{\Theta}, z, N_{\min})$, where

$$\wp(h_{\phi}^{\Theta}, z, N_{\min}) := \left\{\boldsymbol{\pi}(A_{\phi}^{\Theta}, \kappa_{\phi}, \alpha_{\phi}^{\Theta}, Q | h_{\phi}^{\Theta}, z, N_{\min}) | (A_{\phi}^{\Theta}, \kappa_{\phi}, \alpha_{\phi}^{\Theta}, Q) \in \mathbb{R}^4\right\}, \tag{5.4}$$

$$\boldsymbol{\pi}(A_{\phi}^{\Theta}, \kappa_{\phi}, \alpha_{\phi}^{\Theta}, Q | h_{\phi}^{\Theta}, z, N_{\min}) := \left(\pi_{2m}(A_{\phi}^{\Theta}, \kappa_{\phi}, \alpha_{\phi}^{\Theta}, h_{\phi}^{\Theta}, z, N_{\min}, Q), 7 \leq m \in \mathbb{N}\right), \tag{5.5}$$

and

$$\begin{aligned}
&\pi_{2m}(A_{\phi}^{\Theta}, \kappa_{\phi}, \alpha_{\phi}^{\Theta}, h_{\phi}^{\Theta}, z, N_{\min}, Q) \\
&:= \frac{\left(\mathscr{I}_{[14, N_{\min})}(2m)\right) Q}{Q + \sum\limits_{n \geq N_{\min}/2} A_{\phi}^{\Theta}(2n-6)(2n)^{q-1}(2n + h_{\phi}^{\Theta})^{\alpha_{\phi}^{\Theta}}\left(e^{\kappa_{\phi}} z\right)^{2n}} \\
&+ \frac{\left(\mathscr{I}_{[N_{\min}, \infty)}(2m)\right)\left[A_{\phi}^{\Theta}(2m-6)\left(2m\right)^{q-1}\left(2m + h_{\phi}^{\Theta}\right)^{\alpha_{\phi}^{\Theta}}\left(e^{\kappa_{\phi}} z\right)^{2m}\right]}{Q + \sum\limits_{n \geq N_{\min}/2} A_{\phi}^{\Theta}(2n-6)(2n)^{q-1}(2n + h_{\phi}^{\Theta})^{\alpha_{\phi}^{\Theta}}\left(e^{\kappa_{\phi}} z\right)^{2n}}.
\end{aligned} \tag{5.6}$$

Unless otherwise stated, the remainder of the discussion in this section is based on [139], and, whenever relevant, related to elements in the parametric family $\wp(h_\phi^\Theta, z, N_{\min})$.

Another example of a parametric family of distributions is an exponential family of distributions, which is defined as follows.

Definition 5.1.1 (Schervish, p. 102-103) *A parametric family with parameter space Ω and density (probability mass function) $f_{\boldsymbol{X}|\boldsymbol{\Xi}}(\boldsymbol{x}|\boldsymbol{\theta})$ with respect to a measure ν on $(\mathscr{X}, \mathscr{B})$ is called an exponential family if*

$$f_{\boldsymbol{X}|\boldsymbol{\Xi}}(\boldsymbol{x}|\boldsymbol{\theta}) = c(\boldsymbol{\theta})h(\boldsymbol{x}) \exp\left\{\sum_{i=1}^{k} g_i(\boldsymbol{\theta})t_i(\boldsymbol{x})\right\}, \tag{5.7}$$

for some ν-measurable functions $g_1, g_2, ..., g_k, t_1, t_2, ..., t_k$ and some integer k.

The parametric family $\wp(h_\phi^\Theta, z, N_{\min})$, as defined by Equation (5.4), is an example of an exponential (parametric) family because, for a fixed positive even integer $N_{\min}$ and for fixed real values z and h_ϕ^Θ, the components of each element from $\wp(h_\phi^\Theta, z, N_{\min})$ can be rewritten in the form given by Equation (5.7), that is $\pi_{2m}(A_\phi^\Theta, \kappa_\phi, \alpha_\phi^\Theta, h_\phi^\Theta, z, N_{\min}, Q)$ can be written as

$$\pi_{2m}(A_\phi^\Theta, \kappa_\phi, \alpha_\phi^\Theta, h_\phi^\Theta, z, N_{\min}, Q) = c(\boldsymbol{\theta})h(2m) \exp\left\{\sum_{i=1}^{k} g_i(\boldsymbol{\theta})t_i(2m)\right\},$$

where $\boldsymbol{\theta} := (A_\phi^\Theta, \kappa_\phi, \alpha_\phi^\Theta, Q)$,

$$c(\boldsymbol{\theta}) := \exp\left(-\log\left[Q + \sum_{n \geq N_{\min}/2} A_\phi^\Theta (2n-6)(2n)^{q-1}(2n + h_\phi^\Theta)^{\alpha_\phi^\Theta} \left(e^{\kappa_\phi} z\right)^{2n}\right]\right), \tag{5.8}$$

$$h(2m) := \exp\left(\left(\mathscr{I}_{[N_{\min},\infty)}(2m)\right) \log\left[(2m-6)\,(2m)^{q-1}\, z^{2m}\right]\right), \tag{5.9}$$

and

$$\begin{aligned}\exp\left\{\sum_{i=1}^{k} g_i(\boldsymbol{\theta})t_i(2m)\right\} = \exp\Big(\left(\mathscr{I}_{[N_{\min},\infty)}(2m)\right) \log A_\phi^\Theta + \kappa_\phi \left(\mathscr{I}_{[N_{\min},\infty)}(2m)\right) 2m \\ + \log Q\left(\mathscr{I}_{[14,N_{\min})}(2m)\right) + \alpha\left(\mathscr{I}_{[N_{\min},\infty)}(2m)\right) \log(2m + h_\phi^\Theta)\Big).\end{aligned} \tag{5.10}$$

In addition to the definition of an exponential family of distributions, some more notation is required before the discussion can be continued. Let $X_1, ..., X_n$ be i.i.d. random variables defined on the sample space $\mathscr{X}$. Then the sample space of $\boldsymbol{X} := (X_1, X_2, ..., X_n)$

is $\mathscr{X}^n$. The notation $P_{\boldsymbol{\theta}}$ will be used to denote the element from an exponential family of distributions associated with $\boldsymbol{\Xi} = \boldsymbol{\theta}$, fixed, and $P_{\boldsymbol{\theta}}$ is distributed over the sample space $\mathscr{X}$. The notation $f_{X_i|\boldsymbol{\Xi}}(\cdot|\boldsymbol{\theta})$ will be used to represent the density function for $P_{\boldsymbol{\theta}}$ if X_i is continuous and will represent the probability mass function for $P_{\boldsymbol{\theta}}$ if X_i is discrete. $\mathrm{E}_{\boldsymbol{\theta}}(\cdot)$ will be used to denote the expected value taken with respect to the distribution $P_{\boldsymbol{\theta}}$, where $\boldsymbol{\Xi} = \boldsymbol{\theta}$ is fixed. With this notation established, the following is the definition of a maximum likelihood estimator (MLE) of the parameter $\boldsymbol{\Xi}$.

Definition 5.1.2 ([139], p. 307) *Let $\boldsymbol{X} := (X_1, X_2, ..., X_n)$ be a random vector where the X_i are i.i.d. random variables with density function (probability mass function) $f_{X_i|\boldsymbol{\Xi}}(\cdot|\boldsymbol{\theta})$. Suppose that $\boldsymbol{X} = \boldsymbol{x}$ is observed. Then the function $L(\boldsymbol{\theta}|\boldsymbol{X} = \boldsymbol{x}) := f_{\boldsymbol{X}|\boldsymbol{\Xi}}(\boldsymbol{x}|\boldsymbol{\theta})$, where*

$$f_{\boldsymbol{X}|\boldsymbol{\Xi}}(\boldsymbol{x}|\boldsymbol{\theta}) := \prod_{i=1}^{n} f_{X_1|\boldsymbol{\Xi}}(x_i|\boldsymbol{\theta}), \tag{5.11}$$

is considered a function of $\boldsymbol{\theta}$ for fixed $\boldsymbol{x}$ and is called the likelihood function. *Any random vector $\widehat{\boldsymbol{\Xi}}(\boldsymbol{X})$ such that*

$$\max_{\boldsymbol{\theta}\in\Omega} f_{\boldsymbol{X}|\boldsymbol{\Xi}}(\boldsymbol{X}|\boldsymbol{\theta}) = f_{\boldsymbol{X}|\boldsymbol{\Xi}}(\boldsymbol{X}|\widehat{\boldsymbol{\Xi}}(\boldsymbol{X})) \tag{5.12}$$

is called a maximum likelihood estimator (MLE) of $\boldsymbol{\Xi}$. *If no such vector $\widehat{\boldsymbol{\Xi}}(\boldsymbol{X})$ can be found, the maximum likelihood estimator is said to not exist. A* maximum likelihood estimate for $\boldsymbol{\Xi}$ *is any value $\hat{\boldsymbol{\theta}}$, after observing $\boldsymbol{X} = \boldsymbol{x}$, for which the likelihood function $L(\boldsymbol{\theta}|\boldsymbol{X} = \boldsymbol{x})$ attains a maximum, that is $\widehat{\boldsymbol{\Xi}}(\boldsymbol{x}) = \hat{\boldsymbol{\theta}}$.*

Let $\widehat{\boldsymbol{\Xi}}_n(\boldsymbol{X})$, assuming it exists, be the MLE of $\boldsymbol{\Xi}$ based on $\boldsymbol{X} := (X_1, X_2, ..., X_n)$. To form simultaneous $(1-\alpha)\cdot 100\%$ confidence intervals for the components of $\boldsymbol{\Xi}$, $\widehat{\boldsymbol{\Xi}}_n(\boldsymbol{X})$ must exist and the distribution of each of the components of $\widehat{\boldsymbol{\Xi}}_n(\boldsymbol{X})$ (under the assumed distribution $P_{\boldsymbol{\theta}}$, where $\boldsymbol{\Xi} = \boldsymbol{\theta}$ is fixed) must be known. The next theorem addresses both of these issues when the X_i are conditionally i.i.d. given $\boldsymbol{\Xi} = \boldsymbol{\theta}$ and a non-degenerate exponential family of distributions.

Theorem 5.1.1 ([139], p. 419) *Suppose that $\{X_i\}_{i=1}^{\infty}$ are conditionally i.i.d. given $\boldsymbol{\Xi} = \boldsymbol{\theta}$ with a non-degenerate exponential family distribution whose density with respect to a measure ν has the form of Equation (5.7). Suppose that the natural parameter space for $\boldsymbol{\theta}$ is Ω, an open subset of $\mathbb{R}^k$. Let $\widehat{\boldsymbol{\Xi}}_n(\boldsymbol{X})$, if it exists, be the MLE of $\boldsymbol{\Xi}$ based on $\boldsymbol{X} := (X_1, X_2, ..., X_n)$. Then*

1. $\lim_{n\to\infty} P_{\boldsymbol{\theta}}(\widehat{\boldsymbol{\Xi}}_n(\boldsymbol{X})$ *exists*$) = 1$, *and*

2. under $P_{\boldsymbol{\theta}}$, $\sqrt{n}\left(\widehat{\boldsymbol{\Xi}}_n(\boldsymbol{X}) - \boldsymbol{\theta}\right) \xrightarrow{D} N_k\left(\mathbf{0}, [\mathcal{I}_{\boldsymbol{X}}(\boldsymbol{\theta})]^{-1}\right)$, *where* $\mathcal{I}_{\boldsymbol{X}}(\boldsymbol{\theta})$ *is the Fisher Information Matrix.*

Before defining the Fisher Information matrix, the Fisher Information regularity conditions are required and hence are stated next.

Definition 5.1.3 ([139], p. 111) *Suppose that* $\boldsymbol{\Xi}$ *is* k*-dimensional and that* $f_{\boldsymbol{X}|\boldsymbol{\Xi}}(\boldsymbol{x}|\boldsymbol{\theta})$ *is the density of* $\boldsymbol{X}$ *with respect to some measure* ν*. Then the following three conditions are referred to as the Fisher Information regularity conditions:*

1. There exists some B *with* $\nu(B) = 0$ *such that for all* $\boldsymbol{\theta}$, $\dfrac{\partial}{\partial \boldsymbol{\theta}_i} \log\left(f_{\boldsymbol{X}|\boldsymbol{\Xi}}(\boldsymbol{x}|\boldsymbol{\theta})\right)$ *exists for* $\boldsymbol{x} \notin B$ *and each* i*.*

2. $\int_{\boldsymbol{X}|\boldsymbol{\Xi}} f_{\boldsymbol{X}|\boldsymbol{\Xi}}(\boldsymbol{x}|\boldsymbol{\theta}) d\nu(\boldsymbol{x})$ *can be differentiated under the integral sign with respect to each coordinate of* $\boldsymbol{\theta}$*.*

3. The set $C = \{\boldsymbol{x} : f_{\boldsymbol{X}|\boldsymbol{\Xi}}(\boldsymbol{x}|\boldsymbol{\theta}) > 0\}$ *is the same for all* $\boldsymbol{\theta}$*.*

With the Fisher Information regularity conditions specified, the Fisher Information Matrix can be defined.

Definition 5.1.4 ([139], p. 111) *Assuming that the Fisher Information regularity conditions hold, then the matrix,*

$$\mathcal{I}_{\boldsymbol{X}}(\boldsymbol{\theta}) = (I_{\boldsymbol{X},i,j}(\boldsymbol{\theta})) \tag{5.13}$$

where the elements $I_{X,i,j}(\boldsymbol{\theta})$ *are defined by*

$$I_{\boldsymbol{X},i,j}(\boldsymbol{\theta}) = \mathrm{Cov}_{\boldsymbol{\theta}}\left(\frac{\partial}{\partial \boldsymbol{\theta}_i} \log\left(f_{\boldsymbol{X}|\boldsymbol{\Xi}}(\boldsymbol{X}|\boldsymbol{\theta})\right), \frac{\partial}{\partial \boldsymbol{\theta}_j} \log\left(f_{\boldsymbol{X}|\boldsymbol{\Xi}}(\boldsymbol{X}|\boldsymbol{\theta})\right)\right), \tag{5.14}$$

is called the Fisher Information Matrix about $\boldsymbol{\Xi}$ *based on* X_1*. The random vector, whose coordinates are* $\dfrac{\partial}{\partial \boldsymbol{\theta}_i} \log\left(f_{\boldsymbol{X}|\boldsymbol{\Xi}}(\boldsymbol{X}|\boldsymbol{\theta})\right)$*, is called the score function.*

The next theorem states the conditions under which the elements of the Fisher Information Matrix via the expectation (with respect to $P_{\boldsymbol{\theta}}$) of the second partial derivatives of the logarithm of the likelihood function $f_{\boldsymbol{X}|\boldsymbol{\Xi}}(\boldsymbol{x}|\boldsymbol{\theta})$ can be computed.

Theorem 5.1.2 ([139], p. 112-113) *If*

1. the Fisher Information regularity conditions hold;

2. the second derivative of $f_{\boldsymbol{X}|\boldsymbol{\Xi}}(\boldsymbol{x}|\boldsymbol{\theta})$ *exists and is finite; and*

3. $\int f_{\boldsymbol{X}|\boldsymbol{\Xi}}(\boldsymbol{x}|\boldsymbol{\theta})d\nu(\boldsymbol{x})$ *can be differentiated TWICE under the integral sign with respect to each coordinate of* $\boldsymbol{\theta}$,

then

$$I_{\boldsymbol{X},i,j}(\boldsymbol{\theta}) = -\,\mathrm{E}_{\boldsymbol{\theta}}\left[\frac{\partial^2}{\partial\boldsymbol{\theta}_i\partial\boldsymbol{\theta}_j}\left(\log\left(f_{\boldsymbol{X}|\boldsymbol{\Xi}}(\boldsymbol{X}|\boldsymbol{\theta})\right)\right)\right]. \tag{5.15}$$

Theorem 5.1.2 provides a second method for calculating the Fisher Information Matrix when conditions (1)-(3) of the theorem hold. In the case of an exponential family of distributions with the natural parameterization, Equation (5.15) reduces to

$$I_{\boldsymbol{X},i,j}(\boldsymbol{\theta}) = -\frac{\partial^2}{\partial\boldsymbol{\theta}_i\partial\boldsymbol{\theta}_j}\left(\log c\left(\boldsymbol{\theta}\right)\right). \tag{5.16}$$

Because, for a fixed positive even integer $N_{\min}$ and for fixed real values z and h_ϕ^Θ, $\wp(h_\phi^\Theta, z, N_{\min})$ is an exponential parametric family of distributions, Theorems 5.1.1 and 5.1.2 applies to the distributions in $\wp(h_\phi^\Theta, z, N_{\min})$. Hence Part (1) of Theorem 5.1.1 implies that asymptotically $\widehat{\boldsymbol{\Xi}}_n(\boldsymbol{X})$ exists (with probability 1.0) and the components of $\widehat{\boldsymbol{\Xi}}_n(\boldsymbol{X})$, it exists, are asymptotically normally distributed. The conclusion of Theorem 5.1.2 yields that the components of the Fisher Information Matrix based on $\wp(h_\phi^\Theta, z, N_{\min})$ are simply the second partial derivatives of $\log[Q + \sum_{n\geq N_{\min}/2} A_\phi^\Theta(2n-6)(2n)^{q-1}(2n+h_\phi^\Theta)^{\alpha_\phi^\Theta}\left(e^{\kappa_\phi}z\right)^{2n}]^{-1}$ with respect to each of Q, A_ϕ^Θ, κ_ϕ, and α_ϕ^Θ.

But suppose $\{X_i\}_{i=1}^\infty$ are conditionally i.i.d. given $\boldsymbol{\Xi} = \boldsymbol{\theta}$ and their distribution is not in an exponential family of distributions but from some other parametric family of distributions. For example, if h_ϕ^Θ in Equation (5.6) is considered a parameter, not an a priori fixed constant, then $\wp(h_\phi^\Theta, z, N_{\min})$ is no longer an exponential family of distributions. The next theorem states when the MLEs for a non-exponential parametric family of distributions are asymptotically normal.

Theorem 5.1.3 ([139], P. 421) *Let* Ω *be a subset of* $\mathbb{R}^k$, *and suppose* $\{X_i\}_{i=1}^\infty$ *are conditionally i.i.d. given* $\boldsymbol{\Xi} = \boldsymbol{\theta}$, *each with a density* $f_{X_1|\boldsymbol{\Xi}}(\cdot|\boldsymbol{\theta})$. *Let* $\widehat{\boldsymbol{\Xi}}_n(\boldsymbol{X})$, *if it exists, be the MLE of* $\boldsymbol{\Xi}$ *based on* $\boldsymbol{X} := (X_1, X_2, ..., X_n)$. *Assume that:*

1. $\widehat{\boldsymbol{\Xi}}_n(\boldsymbol{X}) \xrightarrow{P} \boldsymbol{\theta}$, *under* $P_{\boldsymbol{\theta}}$ *for all* $\boldsymbol{\theta}$;

2. $f_{X_1|\boldsymbol{\Xi}}(x|\boldsymbol{\theta})$ *has continuous second partial derivatives with respect to* $\boldsymbol{\theta}$ *and that differentiation can be passed under the integral sign;*

3. there exists $H_r(x, y)$ *such that, for each* $\boldsymbol{\theta}_0 \in$ *interior*(Ω) *and each* k, j,

$$\sup_{||\boldsymbol{\theta}-\boldsymbol{\theta}_0||\leq r}\left|\frac{\partial^2}{\partial\theta_k\partial\theta_j}\log f_{X_1|\boldsymbol{\Xi}}(x|\boldsymbol{\theta}_0) - \frac{\partial^2}{\partial\theta_k\partial\theta_j}\log f_{\boldsymbol{X}_1|\boldsymbol{\Xi}}(x|\boldsymbol{\theta})\right| \leq H_r(x, \boldsymbol{\theta}_0), \tag{5.17}$$

with

$$\lim_{r \to 0} \mathrm{E}_{\boldsymbol{\theta}_0}(H_r(X_i, \boldsymbol{\theta}_0)) = 0; \tag{5.18}$$

and

4. the Fisher Information Matrix $\mathcal{I}_{\boldsymbol{X}}(\boldsymbol{\theta})$ is finite and non-singular.

Then, for each $\boldsymbol{\theta}_0 \in interior(\Omega)$, under $P_{\boldsymbol{\theta}_0}$,

$$\sqrt{n}\left(\widehat{\boldsymbol{\Xi}}_n(\boldsymbol{X}) - \boldsymbol{\theta}_0\right) \xrightarrow{D} N_k\left(\mathbf{0}, [\mathcal{I}_{\boldsymbol{X}}(\boldsymbol{\theta}_0)]^{-1}\right). \tag{5.19}$$

The upshot of Theorem 5.1.3 is that as long as:

1. the MLE $\widehat{\boldsymbol{\Xi}}_n(\boldsymbol{X})$ exists (Assumption (1) of the theorem) for a particular parametric family that has certain smoothness properties (Assumptions (2) and (3) of the theorem);
2. the second derivatives are bounded by a function satisfying $\lim_{r \to 0} \mathrm{E}_{\boldsymbol{\theta}_0}(H_r(X_i, \boldsymbol{\theta}_0)) = 0$ for each $\boldsymbol{\theta}_0 \in interior(\Omega)$; and
3. the Fisher Information Matrix $\mathcal{I}_{\boldsymbol{X}}(\boldsymbol{\theta})$ is finite and non-singular,

then the distribution of the components of $\widehat{\boldsymbol{\Xi}}_n(\boldsymbol{X})$ are asymptotically normal.

Suppose $\{X_i\}_{i=1}^{\infty}$ are conditionally i.i.d. given $\boldsymbol{\Xi} = \boldsymbol{\theta}$ and their distribution is from $\wp(h_\phi^\Theta, z, N_{\min})$ in which h_ϕ^Θ is now considered a parameter, that is from $\bigcup_{h_\phi^\Theta} \wp(h_\phi^\Theta, z, N_{\min})$. Then Theorem 5.1.3 implies that the MLEs for this parametric family of distributions are asymptotically normal because the four assumptions required for Theorem 5.1.3 to apply are expected to be true for $\wp(h_\phi^\Theta, z, N_{\min})$. Specifically:

1. Assumptions (1), (2), and (4) follow from the fact that $\wp(h_\phi^\Theta, z, N_{\min})$ is an exponential parametric family for fixed (but arbitrary) h_ϕ^Θ in Equation (5.6)

2. Schervish [139] shows that if the derivatives in Assumption (3) of Theorem 5.1.3 can be differentiated with respect $\boldsymbol{\theta}$ and the derivatives have a finite mean, then a function $H_r(X_i, \boldsymbol{\theta}_0)$ such that $\lim_{r \to 0} \mathrm{E}_{\boldsymbol{\theta}_0}(H_r(X_i, \boldsymbol{\theta}_0)) = 0$ for each $\boldsymbol{\theta}_0 \in interior(\Omega)$ exists. The derivatives required in Assumption (3) are provided in Section A.6 of Appendix A. Note that each of the derivatives in Section A.6 of Appendix A is differentiable at the estimated values of $\kappa_\phi, \alpha_\phi^\Theta, Q$, and h_ϕ^Θ. Also note that the author has numerically verified that each of these required derivatives has a finite mean when evaluated at the estimated values of $\kappa_\phi, \alpha_\phi^\Theta, Q$, and h_ϕ^Θ.

For a particular parametric family that has certain smoothness properties (which are either the Fisher Information regularity conditions if the parametric family is an exponen-

tial family or Assumptions (2) and (3) of Theorem 5.1.3), the information stored in the Fisher Information matrix is a measure of how much information a data set provides about a given parameter. The conclusion of both Theorem 5.1.1 and Theorem 5.1.3 indicates that the distribution of $\sqrt{n}\left(\widehat{\boldsymbol{\Xi}}_n(\boldsymbol{X}) - \boldsymbol{\theta}\right)$ converges to $N_k\left(\mathbf{0}, [\mathcal{I}_{\boldsymbol{X}}(\boldsymbol{\theta})]^{-1}\right)$ which allows $(1-\alpha)\cdot 100\%$ simultaneous confidence intervals to be determined for $\boldsymbol{\theta}$ using the following theorem.

Theorem 5.1.4 ([76], p. 192) *Let $\mathbf{X}_1, \mathbf{X}_2, ..., \mathbf{X}_n$ be a random sample from a $N_k(\boldsymbol{\mu}, \boldsymbol{\Sigma})$ population where $\boldsymbol{\Sigma}$ is positive definite. Then, simultaneously for any k-dimensional column vector $\boldsymbol{\xi}$, the interval*

$$\left(\boldsymbol{\xi}^t\overline{\boldsymbol{X}} - \sqrt{\frac{p(n-1)}{n(n-p)}F_{p,n-p}(\alpha)\boldsymbol{\xi}^t\boldsymbol{S}\boldsymbol{\xi}}, \boldsymbol{\xi}^t\overline{\boldsymbol{X}} + \sqrt{\frac{p(n-1)}{n(n-p)}F_{p,n-p}(\alpha)\boldsymbol{\xi}^t\boldsymbol{S}\boldsymbol{\xi}}\right) \tag{5.20}$$

will contain $\boldsymbol{\xi}^t\boldsymbol{\mu}$ with probability $1-\alpha$, where $\overline{\boldsymbol{X}}$ is the sample mean vector, $\boldsymbol{S}$ is the sample covariance matrix, and $F_{p,r}(\alpha)$ is the value of x for which the F-distribution, $F(x)$ with (p, r) degrees of freedom equals $1-\alpha$.

With the machinery necessary to determine $(1-\alpha)\cdot 100\%$ simultaneous confidence intervals for parameters of interest in hand, the discussion next turns to determining the maximum likelihood estimates for the parameters of interest from data generated from a Monte Carlo simulation. The technique developed in this thesis to determine maximum likelihood estimates based on a CMC Monte Carlo simulation is based on a method introduced by Berretti and Sokal [7] that uses the results of a Monte Carlo simulation to compute the maximum likelihood estimates for some parameters of interest. They also developed a technique to determine, a priori, error estimates for the parameters of interest and how to use these a priori error estimates in combination with an estimate for τ_{exp} to determine how long a simulation must be run to ensure a certain error margin for the parameter estimates. Before the new technique for determining maximum likelihood estimates based on CMC Monte Carlo data is presented, Berretti and Sokal's method for determining a priori error estimates and obtaining an estimate for τ_{exp} will be discussed next.

5.2 How Long is Long Enough?

Given an error tolerance $\delta > 0$ and starting in the equilibrium distribution, how long should the simulation be run in order to obtain a $(1-\alpha)\cdot 100\%$ confidence interval (whose half width is δ) for some parameter appearing in the probability mass function? The following is one method for determining this a priori estimate for the simulation length. This method is based on the method presented in [7] is demonstrated using the probability mass function $\boldsymbol{\pi}_z := \boldsymbol{\pi}_z(\kappa, \gamma, N_{\min}) := (\pi_{2m}(\kappa, \gamma | N_{\min}, z), N_{\min}/2 \leq m \in \mathbb{N})$, where z, κ, and γ are fixed real values, $N_{\min}$ is a fixed positive even integer, and

$$\pi_{2m}(\kappa, \gamma | N_{\min}, z) := \frac{(2m)^{\gamma-1} (e^{\kappa} z)^{2m}}{\sum\limits_{n \geq N_{\min}/2} (2n)^{\gamma-1} (e^{\kappa} z)^{2n}}. \tag{5.21}$$

Suppose that the SAPs $W_1, ..., W_T$ are i.i.d. with probability mass function as given by Equation (5.21) and respective lengths $N_1, ..., N_T$, where $N_i \geq N_{\min}$ for all $i \in \{1, .., T\}$. Then, for fixed $\boldsymbol{\Xi} = \boldsymbol{\theta} := (\kappa, \gamma)$, the likelihood of observing the random sequence $\boldsymbol{N}_T = \{N_1, ..., N_T\}$ is given by

$$f_{\boldsymbol{X}_T | \boldsymbol{\Xi}}(\boldsymbol{N}_T | \kappa, \gamma) = \prod_{1 \leq t \leq T} \frac{N_t^{\gamma-1} (e^{\kappa} z)^{N_t}}{\sum\limits_{n \geq N_{\min}/2} (2n)^{\gamma-1} (e^{\kappa} z)^{2n}}, \tag{5.22}$$

and the Fisher Information Matrix determined using the above likelihood function with $\boldsymbol{\theta} = (\kappa, \gamma)$ is

$$\mathcal{I}_{\boldsymbol{N}_T}(\kappa, \gamma) = -\operatorname{E} \begin{bmatrix} \frac{\partial^2 \log f_{\boldsymbol{X}_T | \boldsymbol{\Xi}}(\boldsymbol{N}_T | \kappa, \gamma)}{\partial \kappa^2} & \frac{\partial^2 \log f_{\boldsymbol{X}_T | \boldsymbol{\Xi}}(\boldsymbol{N}_T | \kappa, \gamma)}{\partial \gamma \partial \kappa} \\ \frac{\partial^2 \log f_{\boldsymbol{X}_T | \boldsymbol{\Xi}}(\boldsymbol{N}_T | \kappa, \gamma)}{\partial \gamma \partial \kappa} & \frac{\partial^2 \log f_{\boldsymbol{X}_T | \boldsymbol{\Xi}}(\boldsymbol{N}_T | \kappa, \gamma)}{\partial \gamma^2} \end{bmatrix} \tag{5.23}$$

$$= \begin{bmatrix} -\operatorname{var}_{\boldsymbol{\pi}_z}(N_1 | N_1 \geq N_{\min}) & -\operatorname{cov}_{\boldsymbol{\pi}_z}(N_1, \log N_1 | N_1 \geq N_{\min}) \\ -\operatorname{cov}_{\boldsymbol{\pi}_z}(N_1, \log N_1 | N_1 \geq N_{\min}) & -\operatorname{var}_{\boldsymbol{\pi}_z}(\log N_1 | N_1 \geq N_{\min}) \end{bmatrix}. \tag{5.24}$$

The inverse of the Fisher Information Matrix is

$$\mathcal{I}^{-1}_{\boldsymbol{N}_T}(\kappa, \gamma) = \frac{1}{\det[\mathcal{I}_{N_1}(\kappa, \gamma)]} \begin{bmatrix} -\operatorname{var}_{\boldsymbol{\pi}_z}(\log N_1 | N_1 \geq N_{\min}) & \operatorname{cov}_{\boldsymbol{\pi}_z}(N_1, \log N_1 | N_1 \geq N_{\min}) \\ \operatorname{cov}_{\boldsymbol{\pi}_z}(N_1, \log N_1 | N_1 \geq N_{\min}) & -\operatorname{var}_{\boldsymbol{\pi}_z}(N_1 | N_1 \geq N_{\min}) \end{bmatrix}. \tag{5.25}$$

Theorem 5.1.1 and Theorem 5.1.4 imply that, if the half widths of the $(1-\alpha)\cdot 100\%$ simultaneous confidence intervals for κ and γ are denoted δ_κ and δ_γ, respectively, and fixed, then

$$\delta_\kappa = \sqrt{\frac{2(T-1)}{T-2}F_{2,T-2}(\alpha)}\sqrt{\frac{-\operatorname{var}_{\boldsymbol{\pi}_z}(\log N_1 | N_1 \geq N_{\min})}{T\det\left[\mathcal{I}_{\boldsymbol{N}_T}(\kappa,\gamma)\right]}} \tag{5.26}$$

and

$$\delta_\gamma = \sqrt{\frac{2(T-1)}{T-2}F_{2,T-2}(\alpha)}\sqrt{\frac{-\operatorname{var}_{\boldsymbol{\pi}_z}(N_1 | N_1 \geq N_{\min})}{T\det\left[\mathcal{I}_{\boldsymbol{N}_T}(\kappa,\gamma)\right]}} \tag{5.27}$$

where $F_{p,t}(\alpha)$ is the value of x for which the F-distribution, $F(x)$, with (p,t) degrees of freedom equals $1-\alpha$. Since, in Equations 5.26 and 5.27, T represents the number of independent data points, a value of T, denoted $\widehat{T}$, that makes the following two inequalities true is required:

$$\sqrt{\frac{2(\widehat{T}-1)}{\widehat{T}\left(\widehat{T}-2\right)}F_{2,\widehat{T}-2}(\alpha)}\sqrt{\frac{-\operatorname{var}_{\boldsymbol{\pi}_z(\hat{\boldsymbol{\theta}},N_{\min})}(\log N_1 | N_1 \geq N_{\min})}{\det\left[\mathcal{I}_{\boldsymbol{N}_T}(\hat{\kappa},\hat{\gamma})\right]}} \leq \delta_\kappa \tag{5.28}$$

and

$$\sqrt{\frac{2(\widehat{T}-1)}{\widehat{T}\left(\widehat{T}-2\right)}F_{2,\widehat{T}-2}(\alpha)}\sqrt{\frac{-\operatorname{var}_{\boldsymbol{\pi}_z(\hat{\boldsymbol{\theta}},N_{\min})}(N_1 | N_1 \geq N_{\min}))}{\det\left[\mathcal{I}_{\boldsymbol{N}_T}(\hat{\kappa},\hat{\gamma})\right]}} \leq \delta_\gamma, \tag{5.29}$$

where $\hat{\boldsymbol{\theta}} := (\hat{\kappa},\hat{\gamma})$ is a fixed a priori guess for $\boldsymbol{\theta}$ and $\dfrac{-\operatorname{var}_{\boldsymbol{\pi}_z(\hat{\boldsymbol{\theta}},N_{\min})}(\log N_1 | N_1 \geq N_{\min})}{\det\left[\mathcal{I}_{\boldsymbol{N}_T}(\hat{\kappa},\hat{\gamma})\right]}$ and $\dfrac{-\operatorname{var}_{\boldsymbol{\pi}_z(\hat{\boldsymbol{\theta}},N_{\min})}(N_1 | N_1 \geq N_{\min}))}{\det\left[\mathcal{I}_{\boldsymbol{N}_T}(\hat{\kappa},\hat{\gamma})\right]}$ are computed using the a priori guess $\hat{\boldsymbol{\theta}}$. Then, given $\hat{\boldsymbol{\theta}}$, $\widehat{T}$ is the number of independent data points that need to be generated to ensure that the half widths of the $(1-\alpha)\cdot 100\%$ simultaneous confidence intervals for $\hat{\kappa}$ and $\hat{\gamma}$ are no wider than δ_κ and δ_γ.

If the data is generated from a MCMC experiment, the best that can be done is to generate $\widehat{T}$ essentially independent data points. In order to make the assumption that sampling starts from the equilibrium distribution, a technique for estimating τ_{exp}, such as the one discussed in Section 4.3.1, must be implemented. Then, given the estimate $\widehat{\tau}_{\text{exp}}$, as discussed in [142] and Section 4.7.1, after approximately $\widehat{\tau}_{\text{exp}}$ time steps, the amount of time between essentially independent data points is approximately $\dfrac{\widehat{\tau}_{\text{exp}}}{10}$, assuming

$$\tau_{\text{exp}} \approx 20\tau_{\text{int}}. \tag{5.30}$$

Consequently, in order to obtain a sample of $\widehat{T}$ essentially independent data points, a MCMC experiment of length

$$\widehat{\tau}_{\text{exp}} + \widehat{T}\cdot\frac{\widehat{\tau}_{\text{exp}}}{10} = \frac{\widehat{\tau}_{\text{exp}}}{10}\left(10+\widehat{T}\right) \tag{5.31}$$

needs to be implemented. Note that this technique was not used in this work to initially estimate the length of the simulation of the CMC Θ-BFACF algorithm. The technique is solely provided for the sake of the completeness of the overall method that this thesis represents.

The next section discusses how to implement maximum likelihood estimation based on $\widehat{T}$ essentially independent data points generated from a composite Markov chain simulation.

5.3 CMC Maximum Likelihood Estimation

In [7], a method (to be referred to as the Berretti-Sokal MC MLE Method in this work) was proposed for obtaining maximum likelihood estimates for κ (as defined by Theorem 1.3.1) and γ (where γ is the critical exponent in the asymptotic form for the number of SAWs of length n, that is $c_n \sim A_0 e^{\kappa n} n^{\gamma-1}$) from a Markov Chain Monte Carlo simulation consisting of several independent sample paths. Refer to Section A.1 of Appendix A for the details of the Berretti-Sokal MC MLE Method. A new modification of this method for the case that the Markov Chain data comes from a composite Markov chain sample path is presented next.

Though this work focuses on SAPs in $\mathbb{Z}^3$, the approach can be extended to other sample spaces where the asymptotic probability mass function falls in a parametric family whose elements, for a fixed positive even integer $N_{\min}$ and fixed real values h_ϕ^Θ and z, have the form $\left(\pi_{2m}(A_\phi^\Theta, \kappa_\phi, \alpha_\phi^\Theta, h_\phi^\Theta, z, N_{\min}, Q), m \geq 7\right)$ where

$$\begin{aligned}
&\pi_{2m}(A_\phi^\Theta, \kappa_\phi, \alpha_\phi^\Theta, h_\phi^\Theta, z, N_{\min}, Q) \\
&= \frac{\left(\mathscr{I}_{[14, N_{\min})}(2m)\right) Q}{Q + \sum\limits_{n \geq N_{\min}/2} A_\phi^\Theta (2n-6)(2n)^{q-1}(2n + h_\phi^\Theta)^{\alpha_\phi^\Theta} \left(e^{\kappa_\phi} z\right)^{2n}} \\
&+ \frac{\left(\mathscr{I}_{[N_{\min}, \infty)}(2m)\right) \left[A_\phi^\Theta (2m-6)\,(2m)^{q-1}\,(2m + h_\phi^\Theta)^{\alpha_\phi^\Theta}\,\left(e^{\kappa_\phi} z\right)^{2m}\right]}{Q + \sum\limits_{n \geq N_{\min}/2} A_\phi^\Theta (2n-6)(2n)^{q-1}(2n + h_\phi^\Theta)^{\alpha_\phi^\Theta} \left(e^{\kappa_\phi} z\right)^{2n}}.
\end{aligned} \tag{5.32}$$

The remainder of this section is dedicated to developing a maximum likelihood technique to estimate the parameters $A_\phi^\Theta, \kappa_\phi, \alpha_\phi^\Theta, h_\phi^\Theta$, and Q in $\pi_{2m}(A_\phi^\Theta, \kappa_\phi, \alpha_\phi^\Theta, h_\phi^\Theta, z, N_{\min}, Q)$ given above using a sample generated from a CMC. To this end, the remainder of the discussion first defines the log-likelihood function for the desired random sample. The derivatives with respect to each of the parameters are then computed . Finally values for the parameters

that simultaneously make each of the derivatives zero are determined. These values are the desired maximum likelihood estimates.

In order to define the log-likelihood function required for the CMC Maximum Likelihood Technique, the following definitions and notations are required. Let $\mathscr{S}$ be a given subset of the set of all SAPs in $\mathbb{Z}^3$ that are rooted at the origin and consider any fixed non-empty subset $\mathscr{S}^* \subseteq \mathscr{S}$. Then $\overline{\mathscr{S}^*} := \mathscr{S} - \mathscr{S}^*$. $\omega \in \mathscr{S}$ is said to have property $*$ if and only if $\omega \in \mathscr{S}^*$. Now define s_n to be the number of n-edge SAPs in $\mathscr{S}$; s_n^* to be the number of n-edge SAPs in $\mathscr{S}^*$; and $s_n^{\overline{*}}$ to be the number of n-edge SAPs in $\overline{\mathscr{S}^*}$. Note that

$$s_n = s_n^{\overline{*}} + s_n^*. \tag{5.33}$$

Finally assume that there exists $(\kappa_s, \alpha_s, h_s, A_s)$, $(\kappa_*, \alpha_*, h_*, A_*)$, $(\kappa_{\overline{*}}, \alpha_{\overline{*}}, h_{\overline{*}}, A_{\overline{*}}) \in \mathbb{R}^4$ and a positive even integer $N_{\min}^*$ such that

$$s_n = A_s(n + h_s)^{\alpha_s} e^{n\kappa_s}, \tag{5.34}$$

$$s_n^* = A_*(n + h_*)^{\alpha_*} e^{n\kappa_*}, \tag{5.35}$$

and

$$s_n^{\overline{*}} = A_{\overline{*}}(n + h_{\overline{*}})^{\alpha_{\overline{*}}} e^{n\kappa_{\overline{*}}} \tag{5.36}$$

for all $n \geq N_{\min}^*$.

Given a fixed real value β and a fixed polynomial function $w(n)$, let ω be a random element from $\mathscr{S}$ chosen according to the probability mass function

$$(\breve{\pi}_\omega(*, \beta, N_{\min}^*, N_{\max}^*), \omega \in \mathscr{S}), \tag{5.37}$$

where

$$\breve{\pi}_\omega(*, \beta, N_{\min}^*, N_{\max}^*) := \Pr(W = \omega) := \frac{w(|\omega|)e^{\beta|\omega|}}{\sum_{n=0}^{\infty} w(2n)s_{2n}e^{2\beta n}}. \tag{5.38}$$

Then given any even positive integers $N_{\min}^* < N_{\max}^*$, $\breve{\pi}_\omega(*, \beta, N_{\min}^*, N_{\max}^*)$ can be rewritten as

$$\begin{aligned}
&\breve{\pi}_\omega(*, \beta, N_{\min}^*, N_{\max}^*) \\
&:= I_{\langle 1 \rangle}(|\omega|) \left[\sum_{n < N_{\min}^*} \frac{w(n)s_n e^{\beta n}}{\breve{Q}(\beta)} \right] + I_{\langle 2 \rangle}(|\omega|)\psi_*(\omega) \frac{w(|\omega|)s_{|\omega|}^* e^{\beta|\omega|}}{\breve{Q}(\beta)} \\
&+ I_{\langle 2 \rangle}(|\omega|)(1 - \psi_*(\omega)) \frac{w(|\omega|)s_{|\omega|}^{\overline{*}} e^{\beta|\omega|}}{\breve{Q}(\beta)} + I_{\langle 3 \rangle}(|\omega|) \sum_{n > N_{\max}^*} \frac{w(n)\left[s_n^* + s_n^{\overline{*}}\right] e^{\beta n}}{\breve{Q}(\beta)},
\end{aligned} \tag{5.39}$$

where

$$\breve{Q}(\beta) := \sum_{n=0}^{\infty} w(2n) s_{2n} e^{2\beta n}, \tag{5.40}$$

$\psi_*(\omega)$ is defined by Equation (4.166), and for any even positive integer n,

$$I_{\langle 1 \rangle}(n) := \begin{cases} 1, & \text{if } 0 \leq n < N^*_{\min} \\ 0, & \text{otherwise} \end{cases}, \tag{5.41}$$

$$I_{\langle 2 \rangle}(n) := \begin{cases} 1, & \text{if } N^*_{\min} \leq n \leq N^*_{\max} \\ 0, & \text{otherwise} \end{cases}, \tag{5.42}$$

and

$$I_{\langle 3 \rangle}(n) := \begin{cases} 1, & \text{if } n > N^*_{\max} \\ 0, & \text{otherwise} \end{cases}. \tag{5.43}$$

Because Equations (5.34)-(5.36) hold only for $n \geq N^*_{\min}$, it makes sense that the asymptotic ($|\omega| \to \infty$) form of $\breve{\pi}_\omega(*, \beta, N^*_{\min}, N^*_{\max})$ should depend on $N^*_{\min}$, but why should it depend on $N^*_{\max}$? To see why, first note that the accuracy of the estimates for $A_*, A_{\overline{*}}, \kappa_s, \varepsilon_*, h_*, \alpha_{\overline{*}}, h_{\overline{*}}$ depends on the accuracy of the estimates for the statistical quantities $\langle \cdot \rangle_T$ in Equations (5.92)-(5.99). Based on the relative statistical error of the statistical quantities $\langle \cdot \rangle_T$ in Equations (5.92)-(5.99), there exists a value $N^*_{\max} \geq N^*_{\min}$ such that for all $n > N^*_{\max}$, the relative statistical error of the statistical quantities $\langle \cdot \rangle_T$ in Equations (5.92)-(5.99) becomes so large that the reliability of the statistical quantities $\langle \cdot \rangle_T$, and all functions based on these statistical quantities, becomes questionable at best. Consequently, for all $n > N^*_{\max}$, the estimates for A, κ_s, ε_*, $\alpha_{\overline{*}}$, h_*, $h_{\overline{*}}$, and $\tilde{Q}(\beta_i)$, for $1 \leq i \leq M$, based on the statistical quantities $\langle \cdot \rangle_T$ also become questionable. Therefore it makes sense that the asymptotic ($|\omega| \to \infty$) form of $\breve{\pi}_\omega(*, \beta, N^*_{\min}, N^*_{\max})$ should be defined in such a manner to take this into account.

Note that from Equations (5.34)-(5.36) the unknown parameters of interest are A_s, α_s, κ_s, h_s, A_*, $A_{\overline{*}}$, κ_*, $\kappa_{\overline{*}}$, α_*, $\alpha_{\overline{*}}$, h_*, and $h_{\overline{*}}$. However, for subsets of Θ-SAPs in $\mathscr{P}^{\Theta}(\phi)$, the relevant κ's are known to be equal. It is therefore assumed here that $\kappa_s = \kappa_* = \kappa_{\overline{*}}$ and for convenience the parameter set is transformed to

$$\boldsymbol{\theta} = (A_*, A_{\overline{*}}, \kappa_s, \varepsilon_*, h_*, \alpha_{\overline{*}}, h_{\overline{*}}) \in \mathbb{R}^7,$$

where

$$\varepsilon_* := \alpha_{\overline{*}} - \alpha_*. \tag{5.44}$$

Substituting Equations (5.34)-(5.36) into $\breve{\pi}_\omega(*, \beta, N^*_{\min}, N^*_{\max})$ and assuming that $\kappa_s = \kappa_* = \kappa_{\overline{*}}$ yields

$$\breve{\pi}_\omega(*, \beta, N^*_{\min}, N^*_{\max}) \sim \pi_\omega(\boldsymbol{\theta}|*, \beta, N^*_{\min}, N^*_{\max}), \tag{5.45}$$

where $\pi_\omega(\boldsymbol{\theta}|*, \beta, N^*_{\min}, N^*_{\max})$, for fixed even integers $N^*_{\min}$ and $N^*_{\max}$ and fixed

$$\boldsymbol{\theta} = (A_*, A_{\overline{*}}, \kappa_s, \varepsilon_*, h_*, \alpha_{\overline{*}}, h_{\overline{*}}) \in \mathbb{R}^7,$$

is given by

$$\begin{aligned}\pi_\omega(\boldsymbol{\theta}|*, \beta, N^*_{\min}, N^*_{\max}) = {} & I_{\langle 2\rangle}(|\omega|)\psi_*(\omega)\frac{A_* w(|\omega|)(|\omega| + h_*)^{\alpha_{\overline{*}} - \varepsilon_*} e^{(\kappa_s+\beta)|\omega|}}{Q(\beta)} \\ & + I_{\langle 2\rangle}(|\omega|)(1 - \psi_*(\omega))\frac{A_{\overline{*}} w(|\omega|)(|\omega| + h_{\overline{*}})^{\alpha_{\overline{*}}} e^{(\kappa_s+\beta)|\omega|}}{Q(\beta)} \\ & + I_{\langle 1\rangle}(|\omega|)\left[\sum_{n<N^*_{\min}} \frac{w(n)s_n e^{\beta n}}{Q(\beta)}\right] \\ & + I_{\langle 3\rangle}(|\omega|)\sum_{n>N^*_{\max}} \frac{w(n)\left[A_*(n + h_*)^{\alpha_{\overline{*}} - \varepsilon_*} + A_{\overline{*}}(n + h_{\overline{*}})^{\alpha_{\overline{*}}}\right] e^{(\kappa_s+\beta)n}}{Q(\beta)},\end{aligned} \tag{5.46}$$

$$Q(\beta) := Q_{\langle 1\rangle}(\beta) + Q_{\langle 2,3\rangle}(\beta), \tag{5.47}$$

$$\varepsilon_* := \alpha_{\overline{*}} - \alpha_*, \tag{5.48}$$

$$Q_{\langle 1\rangle}(\beta) := \tilde{Q}_{\langle 1\rangle}(\beta), \tag{5.49}$$

$$Q_{\langle 2,3\rangle}(\beta) := A_{\overline{*}} Q^{\overline{*}}_{\langle 2,3\rangle}(\beta) + A_* Q^*_{\langle 2,3\rangle}(\beta), \tag{5.50}$$

$$Q^*_{\langle 2,3\rangle}(\beta) := \sum_{n\geq N^*_{\min}} w(n)(n + h_*)^{\alpha_{\overline{*}} - \varepsilon_*} e^{(\kappa_s+\beta)n}, \tag{5.51}$$

and

$$Q^{\overline{*}}_{\langle 2,3\rangle}(\beta) := \sum_{n\geq N^*_{\min}} w(n)(n + h_{\overline{*}})^{\alpha_{\overline{*}}} e^{(\kappa_s+\beta)n}. \tag{5.52}$$

Now define

$$Q_{\langle 2\rangle}(\beta) := A_{\overline{*}} Q^{\overline{*}}_{\langle 2\rangle}(\beta) + A_* Q^*_{\langle 2\rangle}(\beta) \tag{5.53}$$

and

$$Q_{\langle 3\rangle}(\beta) := A_{\overline{*}} Q^{\overline{*}}_{\langle 3\rangle}(\beta) + A_* Q^*_{\langle 3\rangle}(\beta), \tag{5.54}$$

where

$$Q^*_{\langle 2\rangle}(\beta) := \sum_{N^*_{\min}\leq n\leq N^*_{\max}} w(n)(n + h_*)^{\alpha_{\overline{*}} - \varepsilon_*} e^{(\kappa_s+\beta)n}, \tag{5.55}$$

$$Q^{\overline{*}}_{\langle 2\rangle}(\beta) := \sum_{N^*_{\min} \le n \le N^*_{\max}} w(n)\,(n + h_{\overline{*}})^{\alpha_{\overline{*}}}\, e^{(\kappa_s+\beta)n}, \tag{5.56}$$

$$Q^{*}_{\langle 3\rangle}(\beta) := \sum_{n > N^*_{\max}} w(n)\,(n + h_{*})^{\alpha_{\overline{*}}-\varepsilon_*}\, e^{(\kappa_s+\beta)n}, \tag{5.57}$$

and

$$Q^{\overline{*}}_{\langle 3\rangle}(\beta) := \sum_{n > N^*_{\max}} w(n)\,(n + h_{\overline{*}})^{\alpha_{\overline{*}}}\, e^{(\kappa_s+\beta)n}. \tag{5.58}$$

Finally define $\breve{\pi}_{N,K}(*, \beta, N^*_{\min}, N^*_{\max})$ to be the probability that a randomly chosen polygon W with probability mass function given by Equation (5.39) has length $|W| = N$ and property $K := \psi_*(W)$. Then the probability that a randomly chosen M-tuple of polygons $(W_1, W_2, ..., W_M)$ in which W_i has probability mass function given by Equation (5.39) and has length $|W_i| = N_i$ and property $K_i := \psi_*(W_i)$ is given by

$$\breve{\boldsymbol{\pi}}_{\boldsymbol{N},\boldsymbol{K}}(*, \boldsymbol{\beta}, N^*_{\min}, N^*_{\max}) := \prod_{i=1}^{M} \breve{\pi}_{N_i,K_i}(*, \beta_i, N^*_{\min}, N^*_{\max}), \tag{5.59}$$

where $\boldsymbol{N} := (N_1, ..., N_M)$, $\boldsymbol{K} := (K_1, ..., K_M)$, and for $i \in \{1, ..., M\}$, N_i is an even positive integer and $K_i \in \{0, 1\}$. Then, for $\boldsymbol{N}_T = \{\boldsymbol{N}^{(t)}, t = 1, ..., T\}$ and $\boldsymbol{K}_T = \{\boldsymbol{K}^{(t)}, t = 1, ..., T\}$, independent sequences of random vectors with joint distribution $\breve{\boldsymbol{\pi}}_{\boldsymbol{N},\boldsymbol{K}}$ and for fixed $\boldsymbol{\theta} = (A_*, A_{\overline{*}}, \kappa_s, \varepsilon_*, h_*, \alpha_{\overline{*}}, h_{\overline{*}}) \in \mathbb{R}^7$, the likelihood of this random sample is given by

$$\breve{f}_{\boldsymbol{X}_T}(\boldsymbol{N}_T, \boldsymbol{K}_T) = \prod_{t=1}^{T} \breve{\boldsymbol{\pi}}_{\boldsymbol{N}^{(t)},\boldsymbol{K}^{(t)}}(*, \boldsymbol{\beta}, N^*_{\min}, N^*_{\max}), \tag{5.60}$$

and hence the log-likelihood of this random sample is

$$\log \breve{f}_{\boldsymbol{X}_T}(\boldsymbol{N}_T, \boldsymbol{K}_T) = \sum_{t=1}^{T} \sum_{i=1}^{M} \log \breve{\pi}_{N_i^{(t)},K_i^{(t)}}(*, \beta_i, N^*_{\min}, N^*_{\max}). \tag{5.61}$$

Substituting Equation (5.46) into the log-likelihood for the random sample $(\boldsymbol{N}_T, \boldsymbol{K}_T)$

given by Equation (5.61) yields

$$
\begin{aligned}
&\log f_{\boldsymbol{X}_T|\boldsymbol{\Xi}}(\boldsymbol{N}_T, \boldsymbol{K}_T|\boldsymbol{\theta}) \\
&:= \sum_{t=1}^{T}\sum_{i=1}^{M} \log \Bigg(\frac{A_* w(N_i^{(t)})(N_i^{(t)} + h_*)^{\alpha_{\overline{*}} - \varepsilon_*} e^{(\kappa_s + \beta_i) N_i^{(t)}}}{Q(\beta_i)} I_{\langle 2 \rangle}(N_i^{(t)}) K_i^{(t)} \\
&+ I_{\langle 2 \rangle}(N_i^{(t)}) \left[1 - K_i^{(t)})\right] \frac{A_{\overline{*}} w(N_i^{(t)})(N_i^{(t)} + h_{\overline{*}})^{\alpha_{\overline{*}}} e^{(\kappa_s + \beta_i) N_i^{(t)}}}{Q(\beta_i)} \\
&+ \frac{\sum\limits_{n < N^*_{\min}} w(n) s_n e^{\beta_i n}}{Q(\beta_i)} I_{\langle 1 \rangle}(N_i^{(t)}) \\
&+ \frac{\sum\limits_{n > N^*_{\max}} w(n) \left[A_*(n + h_*)^{\alpha_{\overline{*}} - \varepsilon_*} + A_{\overline{*}}(|\omega| + h_{\overline{*}})^{\alpha_{\overline{*}}}\right] e^{(\kappa_s + \beta_i) n}}{Q(\beta_i)} I_{\langle 3 \rangle}(N_i^{(t)}) \Bigg),
\end{aligned}
\tag{5.62}
$$

which can be rewritten as

$$
\begin{aligned}
&\log f_{\boldsymbol{X}_T|\boldsymbol{\Xi}}(\boldsymbol{N}_T, \boldsymbol{K}_T|\boldsymbol{\theta}) \\
&= [\log A_*] \sum_{t=1}^{T}\sum_{i=1}^{M} I_{\langle 2 \rangle}(N_i^{(t)}) K_i^{(t)} + [\log A_{\overline{*}}] \sum_{t=1}^{T}\sum_{i=1}^{M} I_{\langle 2 \rangle}(N_i^{(t)}) \left[1 - K_i^{(t)}\right] \\
&+ (\alpha_{\overline{*}} - \varepsilon_*) \sum_{t=1}^{T}\sum_{i=1}^{M} I_{\langle 2 \rangle}(N_i^{(t)}) K_i^{(t)} \log(N_i^{(t)} + h_*) - \sum_{t=1}^{T}\sum_{i=1}^{M} \log Q(\beta_i). \\
&+ \sum_{t=1}^{T}\sum_{i=1}^{M} I_{\langle 2 \rangle}(N_i^{(t)}) \left[\log w(N_i^{(t)}) + (\kappa_s + \beta_i) N_i^{(t)}\right] \\
&+ \sum_{t=1}^{T}\sum_{i=1}^{M} I_{\langle 2 \rangle}(N_i^{(t)}) \left[1 - K_i^{(t)})\right] \left[\alpha_{\overline{*}} \log(N_i^{(t)} + h_{\overline{*}})\right] \\
&+ \sum_{t=1}^{T}\sum_{i=1}^{M} \left[I_{\langle 1 \rangle}(N_i^{(t)}) \log Q_{\langle 1 \rangle}(\beta_i) + I_{\langle 3 \rangle}(N_i^{(t)}) \log Q_{\langle 3 \rangle}(\beta_i)\right].
\end{aligned}
\tag{5.63}
$$

Now expressing Equation (5.63) in terms of sample averages yields the log-likelihood function ℓ_T defined as

$$
\begin{aligned}
\ell_T := {} & T\left[\log A_*\right] \sum_{i=1}^{M} \left\langle I_{\langle 2\rangle}(N_i) K_i \right\rangle_T \\
& + \left(\alpha_{\overline{*}} - \varepsilon_*\right) T \sum_{i=1}^{M} \left\langle I_{\langle 2\rangle}(N_i) K_i \log(N_i + h_*) \right\rangle_T \\
& + T \sum_{i=1}^{M} \left[\left\langle I_{\langle 2\rangle}(N_i) \log w(N_i) \right\rangle_T + \left(\kappa_s + \beta_i\right) \left\langle I_{\langle 2\rangle}(N_i) N_i \right\rangle_T \right] \\
& + T\left[\log A_{\overline{*}}\right] \sum_{i=1}^{M} \left\langle I_{\langle 2\rangle}(N_i)\left[1 - K_i\right] \right\rangle_T \\
& + \alpha_{\overline{*}} T \sum_{i=1}^{M} \left\langle I_{\langle 2\rangle}(N_i)\left[1 - K_i\right] \log(N_i + h_{\overline{*}}) \right\rangle_T \\
& + T \sum_{i=1}^{M} \left[\left\langle I_{\langle 1\rangle}(N_i) \right\rangle_T \log Q_{\langle 1\rangle}(\beta_i) + \left\langle I_{\langle 3\rangle}(N_i) \right\rangle_T \log Q_{\langle 3\rangle}\left(\beta_i\right) \right] \\
& - T \sum_{i=1}^{M} \log Q(\beta_i),
\end{aligned} \tag{5.64}
$$

where

$$
\left\langle f(N_i, K_i) \right\rangle_T = \frac{\sum_{t=1}^{T} f(N_i^{(t)}, K_i^{(t)})}{T}. \tag{5.65}
$$

In practice $Q_{\langle 1\rangle}\left(\beta_i\right)$, for each $1 \leq i \leq M$, is unknown and hence it can be considered a parameter in the log-likelihood function ℓ_T. Therefore, for fixed values of $N^*_{\min}$ and $N^*_{\max}$ the log-likelihood function ℓ_T (as defined by Equation (5.64)) can be viewed as a function of the parameters A_*, $A_{\overline{*}}$, κ_s, ε_*, h_*, $\alpha_{\overline{*}}$, $h_{\overline{*}}$, $Q_{\langle 1\rangle}(\beta_1), ..., Q_{\langle 1\rangle}(\beta_M)$.

To simplify the Fisher Information Matrix, the log-likelihood function ℓ_T (as defined by Equation (5.64)) is transformed to be expressed in terms of A_*, $A_{\overline{*}}$, κ_s, ε_*, h_*, $\alpha_{\overline{*}}$, $h_{\overline{*}}$, and M new parameters $\tilde{Q}(\beta_i)$, for $1 \leq i \leq M$, where

$$
\tilde{Q}\left(\beta_i\right) := \frac{Q_{\langle 2,3\rangle}\left(\beta_i\right)}{Q_{\langle 1\rangle}\left(\beta_i\right) + Q_{\langle 2,3\rangle}\left(\beta_i\right)}, \text{ for } 1 \leq i \leq M. \tag{5.66}
$$

Under this transformation, for $1 \leq i \leq M$, $Q(\beta_i)$ and $Q_{\langle 1\rangle}(\beta_i)$ respectively can be expressed as

$$
Q(\beta_i) = \frac{Q_{\langle 2,3\rangle}\left(\beta_i\right)}{\tilde{Q}\left(\beta_i\right)} \tag{5.67}
$$

and

$$Q_{\langle 1\rangle}(\beta_i) = Q_{\langle 2,3\rangle}(\beta_i)\,\frac{\left[1-\tilde{Q}(\beta_i)\right]}{\tilde{Q}(\beta_i)}. \tag{5.68}$$

Also define the new variable A to be

$$A := \frac{A_*}{A_{\overline{*}}}. \tag{5.69}$$

Substituting Equations (5.67)-(5.69) into Equation (5.64) transforms the log-likelihood equation given by Equation (5.64) into the following log-likelihood equation:

$$\begin{aligned}
\widetilde{\ell_T} :=\ & T\sum_{i=1}^{M}\left[\left\langle I_{\langle 2\rangle}(N_i)\log w(N_i)\right\rangle_T + (\kappa_s+\beta_i)\left\langle I_{\langle 2\rangle}(N_i)N_i\right\rangle_T\right] \\
& + T\sum_{i=1}^{M}\left[(\alpha_{\overline{*}}-\varepsilon_*)\left\langle I_{\langle 2\rangle}(N_i)K_i\log(N_i+h_*)\right\rangle_T\right] \\
& + T\sum_{i=1}^{M}\alpha_{\overline{*}}\left\langle I_{\langle 2\rangle}(N_i)\left[1-K_i\right]\log(N_i+h_{\overline{*}})\right\rangle_T \\
& + T\sum_{i=1}^{M}\log A\left\langle I_{\langle 2\rangle}(N_i)K_i\right\rangle_T \\
& + T\sum_{i=1}^{M}\left\langle I_{\langle 1\rangle}(N_i)\right\rangle_T\log\left[1-\tilde{Q}(\beta_i)\right] \\
& + T\sum_{i=1}^{M}\left\langle I_{\langle 3\rangle}(N_i)\right\rangle_T\log\left[Q^{\overline{*}}_{\langle 3\rangle}(\beta_i) + AQ^{*}_{\langle 3\rangle}(\beta_i)\right] \\
& - T\sum_{i=1}^{M}\left\langle I_{\langle 2,3\rangle}(N_i)\right\rangle_T\left[\log\left[Q^{\overline{*}}_{\langle 2,3\rangle}(\beta_i) + AQ^{*}_{\langle 2,3\rangle}(\beta_i)\right] - \log\tilde{Q}(\beta_i)\right].
\end{aligned} \tag{5.70}$$

Since the realizations of $(\boldsymbol{N}_T, \boldsymbol{K}_T)$ studied here are generated by a Markov Chain Monte Carlo simulation, the sample averages that are available for the quantities required in the log-likelihood are not necessarily computed using independent data. Following the Berretti-Sokal Method (discussed in Section A.1 of Appendix A), to compensate for the lack of independence in the sample data, the number of essentially independent data points, T', as defined in Section 4.1.2, can be used in place of T in Equation (5.64), to

form the following modified log-likelihood function $\widetilde{\ell'_T}$ [7, 11]:

$$\begin{aligned}
\widetilde{\ell'_T} := T' \sum_{i=1}^{M} & \left[\left\langle I_{\langle 2 \rangle}(N_i) \log w(N_i) \right\rangle_T + (\kappa_s + \beta_i) \left\langle I_{\langle 2 \rangle}(N_i) N_i \right\rangle_T \right] \\
& + T' \sum_{i=1}^{M} \left[(\alpha_{\overline{*}} - \varepsilon_*) \left\langle I_{\langle 2 \rangle}(N_i) K_i \log(N_i + h_*) \right\rangle_T \right] \\
& + T' \sum_{i=1}^{M} \alpha_{\overline{*}} \left\langle I_{\langle 2 \rangle}(N_i) \left[1 - K_i \right] \log(N_i + h_{\overline{*}}) \right\rangle_T \\
& + T' \sum_{i=1}^{M} \log A \left\langle I_{\langle 2 \rangle}(N_i) K_i \right\rangle_T \\
& + T' \sum_{i=1}^{M} \left\langle I_{\langle 1 \rangle}(N_i) \right\rangle_T \log \left[1 - \tilde{Q}\left(\beta_i\right) \right] \\
& + T' \sum_{i=1}^{M} \left\langle I_{\langle 3 \rangle}(N_i) \right\rangle_T \log \left[Q^{\overline{*}}_{\langle 3 \rangle}\left(\beta_i\right) + A Q^{*}_{\langle 3 \rangle}\left(\beta_i\right) \right] \\
& - T' \sum_{i=1}^{M} \left\langle I_{\langle 2,3 \rangle}(N_i) \right\rangle_T \log \left[Q^{\overline{*}}_{\langle 2,3 \rangle}\left(\beta_i\right) + A Q^{*}_{\langle 2,3 \rangle}\left(\beta_i\right) \right] \\
& + T' \sum_{i=1}^{M} \left\langle I_{\langle 2,3 \rangle}(N_i) \right\rangle_T \log \tilde{Q}\left(\beta_i\right). \qquad (5.71)
\end{aligned}$$

Note that the sample averages in $\widetilde{\ell'_T}$ are still based on all T sample data points and are given by Equation (5.65).

Now that the log-likelihood function is defined, its derivatives are needed. To find these derivatives, some notation is needed. By defining

$$\pi_{\langle 1 \rangle}(n, \beta) := \frac{w(n) s_n e^{\beta n}}{Q_{\langle 1 \rangle}(\beta)}, \qquad (5.72)$$

$$\pi_{\langle i \rangle}(*, n, \beta) := \frac{w(n)(n + h_*)^{\alpha_{\overline{*}} - \varepsilon_*} e^{(\kappa_s + \beta) n}}{Q_{\langle i \rangle}(\beta)}, \text{if } i \in \{2, 3\}, \qquad (5.73)$$

$$\pi_{\langle i \rangle}(\overline{*}, n, \beta) := \frac{w(n)(n + h_{\overline{*}})^{\alpha_{\overline{*}}} e^{(\kappa_s + \beta) n}}{Q_{\langle i \rangle}(\beta)}, \text{if } i \in \{2, 3\}, \qquad (5.74)$$

$$\pi_{\langle 2,3 \rangle}(*, n, \beta) := \frac{w(n)(n + h_*)^{\alpha_{\overline{*}} - \varepsilon_*} e^{(\kappa_s + \beta) n}}{Q_{\langle 2,3 \rangle}(\beta)}, \qquad (5.75)$$

and

$$\pi_{\langle 2,3 \rangle}(\overline{*}, n, \beta) := \frac{w(n)(n + h_{\overline{*}})^{\alpha_{\overline{*}}} e^{(\kappa_s + \beta) n}}{Q_{\langle 2,3 \rangle}(\beta)}, \qquad (5.76)$$

the following expectations can be defined:

$$\mathrm{E}_{\pi_\beta}\left[f(N)\right] := \sum_{n \text{ even}} f(n) \pi_\beta(n, k | \boldsymbol{\theta}, N^*_{\min}, N^*_{\max}, *) \qquad (5.77)$$

$$\mathrm{E}_{\langle 1\rangle}\left[f(N)|\beta\right] := \sum_{n \text{ even}} \left[f(n) I_{\langle 1\rangle}(n)\right] \pi_{\langle 1\rangle}(n,\beta) \tag{5.78}$$

$$\mathrm{E}^{*}_{\langle i\rangle}\left[f(N)|\beta\right] := \sum_{n \text{ even}} \left[f(n) I_{\langle i\rangle}(n)\right] \pi_{\langle i\rangle}(*,n,\beta), \text{if } i \in \{2,3\}, \tag{5.79}$$

$$\mathrm{E}^{\overline{*}}_{\langle i\rangle}\left[f(N)|\beta\right] := \sum_{n \text{ even}} \left[f(n) I_{\langle i\rangle}(n)\right] \pi_{\langle i\rangle}(\overline{*},n,\beta), \text{if } i \in \{2,3\}, \tag{5.80}$$

$$\mathrm{E}^{*}_{\langle 2,3\rangle}\left[f(N)|\beta\right] := \sum_{n \text{ even}} \left[f(n) I_{\langle 2,3\rangle}(n)\right] \pi_{\langle 2,3\rangle}(*,n,\beta), \tag{5.81}$$

and

$$\mathrm{E}^{\overline{*}}_{\langle 2,3\rangle}\left[f(N)|\beta\right] := \sum_{n \text{ even}} \left[f(n) I_{\langle 2,3\rangle}(n)\right] \pi_{\langle 2,3\rangle}(\overline{*},n,\beta), \tag{5.82}$$

where, for $i,j \in \{1,2,3\}$,

$$I_{\langle i,j\rangle}(n) := \begin{cases} I_{\langle i\rangle}(n) + I_{\langle j\rangle}(n), & \text{if } i \neq j \\ I_{\langle i\rangle}(n), & \text{if } i = j. \end{cases} \tag{5.83}$$

Further, for $i \in \{2,3\}$, define the variances and covariances:

$$\mathrm{var}^{*}_{\langle i\rangle}\left[f(N)|\beta\right] := A\,\mathrm{E}^{*}_{\langle i\rangle}\left[\left[f(N)\right]^2|\beta\right] - \left(A\,\mathrm{E}^{*}_{\langle i\rangle}\left[f(N)|\beta\right]\right)^2, \tag{5.84}$$

$$\mathrm{var}^{\overline{*}}_{\langle i\rangle}\left[f(N)|\beta\right] := \mathrm{E}^{\overline{*}}_{\langle i\rangle}\left[\left[f(N)\right]^2|\beta\right] - \left(\mathrm{E}^{\overline{*}}_{\langle i\rangle}\left[f(N)|\beta\right]\right)^2, \tag{5.85}$$

$$\mathrm{var}^{*}_{\langle 2,3\rangle}\left[f(N)|\beta\right] := A\,\mathrm{E}^{*}_{\langle 2,3\rangle}\left[\left[f(N)\right]^2|\beta\right] - \left(A\,\mathrm{E}^{*}_{\langle 2,3\rangle}\left[f(N)|\beta\right]\right)^2, \tag{5.86}$$

$$\mathrm{var}^{\overline{*}}_{\langle 2,3\rangle}\left[f(N)|\beta\right] := \mathrm{E}^{\overline{*}}_{\langle 2,3\rangle}\left[\left[f(N)\right]^2|\beta\right] - \left(\mathrm{E}^{\overline{*}}_{\langle 2,3\rangle}\left[f(N)|\beta\right]\right)^2. \tag{5.87}$$

$$\mathrm{Cov}^{*}_{\langle i\rangle}\left[f(N),g(N)|\beta\right] := A\,\mathrm{E}^{*}_{\langle i\rangle}\left[f(N)g(N)|\beta\right] - A^2\,\mathrm{E}^{*}_{\langle i\rangle}\left[f(N)|\beta\right]\mathrm{E}^{*}_{\langle i\rangle}\left[g(N)|\beta\right], \tag{5.88}$$

$$\mathrm{Cov}^{\overline{*}}_{\langle i\rangle}\left[f(N),g(N)|\beta\right] := \mathrm{E}^{\overline{*}}_{\langle i\rangle}\left[f(N)g(N)|\beta\right] - \mathrm{E}^{\overline{*}}_{\langle i\rangle}\left[f(N)|\beta\right]\mathrm{E}^{\overline{*}}_{\langle i\rangle}\left[g(N)|\beta\right], \tag{5.89}$$

$$\mathrm{Cov}^{*}_{\langle 2,3\rangle}\left[f(N),g(N)|\beta\right] := A\,\mathrm{E}^{*}_{\langle 2,3\rangle}\left[f(N)g(N)|\beta\right] - A^2\,\mathrm{E}^{*}_{\langle 2,3\rangle}\left[f(N)|\beta\right]\mathrm{E}^{*}_{\langle 2,3\rangle}\left[g(N)|\beta\right], \tag{5.90}$$

and

$$\mathrm{Cov}^{\overline{*}}_{\langle 2,3\rangle}\left[f(N),g(N)|\beta\right] := \mathrm{E}^{\overline{*}}_{\langle 2,3\rangle}\left[f(N)g(N)|\beta\right] - \mathrm{E}^{\overline{*}}_{\langle 2,3\rangle}\left[f(N)|\beta\right]\mathrm{E}^{\overline{*}}_{\langle 2,3\rangle}\left[g(N)|\beta\right]. \tag{5.91}$$

Differentiating $\widetilde{\ell'_T}$ with respect to $A, \kappa_s, \varepsilon_*, \alpha_{\overline{*}}, h_*, h_{\overline{*}}$, and $\tilde{Q}(\beta_i)$, for $1 \leq i \leq M$, respectively, and defining $\tilde{\boldsymbol{Q}} := (\tilde{Q}(\beta_1), .., \tilde{Q}(\beta_M))$ and $\tilde{\boldsymbol{\theta}} := (A, \kappa_s, \varepsilon_*, \alpha_{\overline{*}}, h_*, h_{\overline{*}})$ leads to the following expressions:

$$a(\tilde{\boldsymbol{\theta}},\tilde{\boldsymbol{Q}}) := \frac{\partial\widetilde{\ell'_T}}{\partial A} = \frac{T'}{A}\sum_{i=1}^{M}\left\langle I_{\langle 2\rangle}(N_i)K_i\right\rangle_T + T'\sum_{i=1}^{M}\left\langle I_{\langle 3\rangle}(N_i)\right\rangle_T \frac{Q^*_{\langle 3\rangle}(\beta_i)}{AQ^*_{\langle 3\rangle}(\beta_i)+Q^{\overline{*}}_{\langle 3\rangle}(\beta_i)} - T'\sum_{i=1}^{M}\left\langle I_{\langle 2,3\rangle}(N_i)\right\rangle_T \frac{Q^*_{\langle 2,3\rangle}(\beta_i)}{AQ^*_{\langle 2,3\rangle}(\beta_i)+Q^{\overline{*}}_{\langle 2,3\rangle}(\beta_i)}; \tag{5.92}$$

$$g(\tilde{\boldsymbol{\theta}},\tilde{\boldsymbol{Q}}) := \frac{\partial\widetilde{\ell'_T}}{\partial \kappa_s} = T'\sum_{i=1}^{M}\left\langle I_{\langle 2\rangle}(N_i)N_i\right\rangle_T - T'\sum_{i=1}^{M}\left\langle I_{\langle 2,3\rangle}(N_i)\right\rangle_T\left[\mathrm{E}^{\overline{*}}_{\langle 2,3\rangle}\left[N_i|\beta_i\right] + A\,\mathrm{E}^{*}_{\langle 2,3\rangle}\left[N_i|\beta_i\right]\right] + T'\sum_{i=1}^{M}\left\langle I_{\langle 3\rangle}(N_i)\right\rangle_T\left[\mathrm{E}^{\overline{*}}_{\langle 3\rangle}\left[N_i|\beta_i\right] + A\,\mathrm{E}^{*}_{\langle 3\rangle}\left[N_i|\beta_i\right]\right]; \tag{5.93}$$

$$r(\tilde{\boldsymbol{\theta}},\tilde{\boldsymbol{Q}}) := \frac{\partial\widetilde{\ell'_T}}{\partial \varepsilon_*} = -T'\sum_{i=1}^{M}\left\langle I_{\langle 2\rangle}(N_i)K_i\log(N_i+h_*)\right\rangle_T - AT'\sum_{i=1}^{M}\left\langle I_{\langle 3\rangle}(N_i)\right\rangle_T \mathrm{E}^{*}_{\langle 3\rangle}\left[\log\left(N_i+h_*\right)|\beta_i\right] + AT'\sum_{i=1}^{M}\left\langle I_{\langle 2,3\rangle}(N_i)\right\rangle_T \mathrm{E}^{*}_{\langle 2,3\rangle}\left[\log\left(N_i+h_*\right)|\beta_i\right]; \tag{5.94}$$

$$f(\tilde{\boldsymbol{\theta}},\tilde{\boldsymbol{Q}}) := \frac{\partial\widetilde{\ell'_T}}{\partial \alpha_{\overline{*}}} = -r(\tilde{\boldsymbol{\theta}},\tilde{\boldsymbol{Q}}) + T'\sum_{i=1}^{M}\left\langle I_{\langle 2\rangle}(N_i)\left[1-\psi_*(K_i)\right]\log(N_i+h_{\overline{*}})\right\rangle_T \tag{5.95}$$

$$+ T'\sum_{i=1}^{M}\left\langle I_{\langle 3\rangle}(N_i)\right\rangle_T \mathrm{E}^{\overline{*}}_{\langle 3\rangle}\left[\log\left(N_i+h_{\overline{*}}\right)|\beta_i\right] - T'\sum_{i=1}^{M}\left\langle I_{\langle 2,3\rangle}(N_i)\right\rangle_T \mathrm{E}^{\overline{*}}_{\langle 2,3\rangle}\left[\log\left(N_i+h_{\overline{*}}\right)|\beta_i\right]; \tag{5.96}$$

$$\hbar_*(\tilde{\boldsymbol{\theta}},\tilde{\boldsymbol{Q}}) := \frac{\partial\widetilde{\ell'_T}}{\partial h_*} = \left(\alpha_{\overline{*}}-\varepsilon_*\right)T'\sum_{i=1}^{M}\left\langle\frac{I_{\langle 2\rangle}(N_i)K_i}{N_i+h_*}\right\rangle_T - \left(\alpha_{\overline{*}}-\varepsilon_*\right)AT'\sum_{i=1}^{M}\left\langle I_{\langle 2,3\rangle}(N_i)\right\rangle_T \mathrm{E}^{*}_{\langle 2,3\rangle}\left[\left(N_i+h_*\right)^{-1}|\beta_i\right] + \left(\alpha_{\overline{*}}-\varepsilon_*\right)AT'\sum_{i=1}^{M}\left\langle I_{\langle 3\rangle}(N_i)\right\rangle_T \mathrm{E}^{*}_{\langle 3\rangle}\left[\left(N_i+h_*\right)^{-1}|\beta_i\right]; \tag{5.97}$$

$$\begin{aligned}\hbar_{\overline{*}}(\tilde{\boldsymbol{\theta}},\tilde{\boldsymbol{Q}}) := \frac{\partial\widetilde{\ell'_T}}{\partial h_{\overline{*}}} &= \alpha_{\overline{*}}T'\sum_{i=1}^{M}\left\langle\frac{I_{\langle 2\rangle}(N_i)\left[1-K_i\right]}{N_i+h_{\overline{*}}}\right\rangle_T \\ &\quad - \alpha_{\overline{*}}T'\sum_{i=1}^{M}\left\langle I_{\langle 2,3\rangle}(N_i)\right\rangle_T \mathrm{E}^{\overline{*}}_{\langle 2,3\rangle}\left[(N_i+h_*)^{-1}\,|\beta_i\right] \\ &\quad + \alpha_{\overline{*}}T'\sum_{i=1}^{M}\left\langle I_{\langle 3\rangle}(N_i)\right\rangle_T \mathrm{E}^{\overline{*}}_{\langle 3\rangle}\left[(N_i+h_*)^{-1}\,|\beta_i\right]; \end{aligned} \tag{5.98}$$

and

$$\begin{aligned}\widetilde{q}_i(\tilde{\boldsymbol{\theta}},\tilde{\boldsymbol{Q}}) &:= \frac{\partial\widetilde{\ell'_T}}{\partial\tilde{Q}\left(\beta_i\right)} \\ &= T'\left[-\frac{\left\langle I_{\langle 1\rangle}(N_i)\right\rangle_T}{1-\tilde{Q}\left(\beta_i\right)}+\frac{\left\langle I_{\langle 2,3\rangle}(N_i)\right\rangle_T}{\tilde{Q}\left(\beta_i\right)}\right],\ \text{for } 1\le i\le M. \end{aligned} \tag{5.99}$$

In order to use these derivatives to determine estimates that maximize Equation (5.71), the following system of equations needs to be simultaneously solved.

$$\begin{cases} a(\tilde{\boldsymbol{\theta}},\tilde{\boldsymbol{Q}})=0 \\ g(\tilde{\boldsymbol{\theta}},\tilde{\boldsymbol{Q}})=0 \\ r(\tilde{\boldsymbol{\theta}},\tilde{\boldsymbol{Q}})=0 \\ f(\tilde{\boldsymbol{\theta}},\tilde{\boldsymbol{Q}})=0 \\ \hbar_*(\tilde{\boldsymbol{\theta}},\tilde{\boldsymbol{Q}})=0 \\ \hbar_{\overline{*}}(\tilde{\boldsymbol{\theta}},\tilde{\boldsymbol{Q}})=0 \\ \widetilde{q}_i(\tilde{\boldsymbol{\theta}},\tilde{\boldsymbol{Q}})=0,\ \text{for } 1\le i\le M. \end{cases} \tag{5.100}$$

Setting $\widetilde{q}_i(\tilde{\boldsymbol{\theta}},\tilde{\boldsymbol{Q}})=0$, for each $1\le i\le M$, and then solving for $\tilde{Q}\left(\beta_i\right)$ yields the following solutions for $\tilde{Q}\left(\beta_i\right)$:

$$\tilde{Q}\left(\beta_i\right)=\left\langle I_{\langle 2,3\rangle}(N_i)\right\rangle_T,\ \text{for } 1\le i\le M. \tag{5.101}$$

To find maximum likelihood estimates for $A,\kappa_\phi,\varepsilon,\alpha_{\overline{*}},h_*$, and $h_{\overline{*}}$, a solution to the non-linear system

$$\begin{cases} a(\tilde{\boldsymbol{\theta}},\tilde{\boldsymbol{Q}})=0 \\ g(\tilde{\boldsymbol{\theta}},\tilde{\boldsymbol{Q}})=0 \\ r(\tilde{\boldsymbol{\theta}},\tilde{\boldsymbol{Q}})=0 \\ f(\tilde{\boldsymbol{\theta}},\tilde{\boldsymbol{Q}})=0 \\ \hbar_*(\tilde{\boldsymbol{\theta}},\tilde{\boldsymbol{Q}})=0 \\ \hbar_{\overline{*}}(\tilde{\boldsymbol{\theta}},\tilde{\boldsymbol{Q}})=0 \end{cases} \tag{5.102}$$

needs to be determined using a numerical technique such as Newton-Raphson's Method [75]. (Newton-Raphson's Method is outlined in Section A.2 of Appendix A.)

The upshot of Theorem 5.1.2 from Section 5.1 is that the very derivatives required by Newton-Raphson's Method to simultaneously solve the System (5.102) for $A, \kappa_s, \varepsilon_*, \alpha_{\overline{*}}, h_*$, and $h_{\overline{*}}$, that is, the second partial derivatives of the modified log-likelihood equation (Equation (5.71)) with respect to $A, \kappa_s, \varepsilon_*, \alpha_{\overline{*}}, h_*$, and $h_{\overline{*}}$, are also the derivatives that are required to estimate the Fisher Information Matrix so that $(1-\alpha)\cdot 100\%$ confidence intervals can be determined using the maximum likelihood estimates for $A, \kappa_s, \varepsilon_*, \alpha_{\overline{*}}, h_*$, and $h_{\overline{*}}$. The second partial derivatives of Equation (5.71) with respect to $A, \kappa_s, \varepsilon_*, \alpha_{\overline{*}}, h_*$, and $h_{\overline{*}}$ have been included in Section A.6 of Appendix A.

Note that in addition to the derivatives with respect to $A, \kappa_s, \varepsilon_*, \alpha_{\overline{*}}, h_*$, and $h_{\overline{*}}$ given by Equations (A.51) to (A.85) (found in Section A.6 of Appendix A), the Fisher Information matrix also contains the derivatives of Equations (5.92) to (5.99) with respect to $\tilde{Q}(\beta_i)$, for $1 \leq i \leq M$. Hence in order to determine the standard error for the maximum likelihood estimates for $A, \kappa_s, \varepsilon_*, \alpha_{\overline{*}}, h_*$, and $h_{\overline{*}}$, via Theorem 5.1.1, the Fisher Information Matrix associated with the modified log-likelihood $\widetilde{\ell'_T}$ needs to be evaluated at the maximum likelihood estimates for $A, \kappa_s, \varepsilon_*, \alpha_{\overline{*}}, h_*$, $h_{\overline{*}}$, and $\tilde{\boldsymbol{Q}}$ and the inverse of this estimated Fisher Information Matrix needs to be computed.

One simplifying consequence of the transformation to $\tilde{Q}(\beta_i)$, for $1 \leq i \leq M$, is that, for $1 \leq i \leq M$,

$$\frac{\partial a}{\partial \tilde{Q}(\beta_i)} = \frac{\partial g}{\partial \tilde{Q}(\beta_i)} = \frac{\partial r}{\partial \tilde{Q}(\beta_i)} = \frac{\partial f}{\partial \tilde{Q}(\beta_i)} = \frac{\partial \hbar_*}{\partial \tilde{Q}(\beta_i)} = \frac{\partial \hbar_{\overline{*}}}{\partial \tilde{Q}(\beta_i)} = 0 \tag{5.103}$$

and that, for $1 \leq i, j \leq M$ such that $i \neq j$,

$$\frac{\partial \widetilde{q_i}}{\partial \tilde{Q}(\beta_j)} = 0. \tag{5.104}$$

Hence the only non-zero contributions to the Fisher Information Matrix resulting from derivatives of $\widetilde{q_i}(\tilde{\boldsymbol{\theta}}, \tilde{\boldsymbol{Q}})$ and derivatives with respect to $\tilde{Q}(\beta_i)$, for $1 \leq i \leq M$, are

$$\frac{\partial \widetilde{q_i}}{\partial \tilde{Q}(\beta_i)} = T' \left[-\frac{\left\langle I_{\langle 1 \rangle}(N_i) \right\rangle_T}{\left[1 - \tilde{Q}(\beta_i)\right]^2} - \frac{\left\langle I_{\langle 2,3 \rangle}(N_i) \right\rangle_T}{\left[\tilde{Q}(\beta_i)\right]^2} \right], \text{ for } 1 \leq i \leq M. \tag{5.105}$$

Furthermore, evaluating the derivatives given by Equation (5.105) at the maximum likelihood estimate for $\tilde{Q}(\beta_i)$, as given by Equation (5.101), reduces the contributions to the

Fisher Information matrix corresponding to the derivatives given by Equation (5.105) to

$$\left.\frac{\partial \widetilde{q}_i}{\partial \widetilde{Q}\left(\beta_i\right)}\right|_{\widetilde{Q}(\beta_i)=\left\langle I_{\langle 2,3\rangle}(N_i)\right\rangle_T} = T'\left[-\frac{1}{\left\langle I_{\langle 1\rangle}(N_i)\right\rangle_T \left\langle I_{\langle 2,3\rangle}(N_i)\right\rangle_T}\right], \text{ for } 1 \leq i \leq M. \quad (5.106)$$

Denoting the maximum likelihood estimates for $\tilde{\boldsymbol{\theta}}$ and $\tilde{\boldsymbol{Q}}$, for a particular value of $N^*_{\min}$ and $N^*_{\max}$, by $\widehat{\tilde{\boldsymbol{\theta}}}(N^*_{\min}, N^*_{\max})$ and $\widehat{\tilde{\boldsymbol{Q}}}(N^*_{\min}, N^*_{\max})$ respectively, the Fisher Information matrix, when evaluated at $\widehat{\tilde{\boldsymbol{\theta}}}(N^*_{\min}, N^*_{\max})$ and $\widehat{\tilde{\boldsymbol{Q}}}(N^*_{\min}, N^*_{\max})$ becomes

$$\begin{aligned}
&\mathcal{I}_{\boldsymbol{X}}(\widehat{\tilde{\boldsymbol{\theta}}}(N^*_{\min}, N^*_{\max}), \widehat{\tilde{\boldsymbol{Q}}}(N^*_{\min}, N^*_{\max})) \\
&= \begin{bmatrix}
\boldsymbol{J}(\widehat{\tilde{\boldsymbol{\theta}}}(N^*_{\min}, N^*_{\max}), \widehat{\tilde{\boldsymbol{Q}}}(N^*_{\min}, N^*_{\max})) & 0 & 0 & \cdots\ 0 \\
0 & -\dfrac{T'\left\langle I_{\langle 1\rangle}(N_1)\right\rangle_T^{-1}}{\left\langle I_{\langle 2,3\rangle}(N_1)\right\rangle_T} & 0 & \cdots\ 0 \\
0 & 0 & \ddots & \cdots\ 0 \\
0 & 0 & \cdots\ 0 & -\dfrac{T'\left\langle I_{\langle 1\rangle}(N_M)\right\rangle_T^{-1}}{\left\langle I_{\langle 2,3\rangle}(N_M)\right\rangle_T}
\end{bmatrix},
\end{aligned} \quad (5.107)$$

where

$$\boldsymbol{J}(\tilde{\boldsymbol{\theta}}, \tilde{\boldsymbol{Q}}) := \begin{bmatrix}
\frac{\partial a}{\partial A} & \frac{\partial a}{\partial \kappa_s} & \frac{\partial a}{\partial \varepsilon_*} & \frac{\partial a}{\partial \alpha_{\overline{*}}} & \frac{\partial a}{\partial h_*} & \frac{\partial a}{\partial h_{\overline{*}}} \\
\frac{\partial a}{\partial \kappa_s} & \frac{\partial g}{\partial \kappa_s} & \frac{\partial g}{\partial \varepsilon_*} & \frac{\partial g}{\partial \alpha_{\overline{*}}} & \frac{\partial g}{\partial h_*} & \frac{\partial g}{\partial h_{\overline{*}}} \\
\frac{\partial a}{\partial \varepsilon_*} & \frac{\partial g}{\partial \varepsilon_*} & \frac{\partial r}{\partial \varepsilon_*} & \frac{\partial r}{\partial \alpha_{\overline{*}}} & \frac{\partial r}{\partial h_*} & \frac{\partial r}{\partial h_{\overline{*}}} \\
\frac{\partial a}{\partial \alpha_{\overline{*}}} & \frac{\partial g}{\partial \alpha_{\overline{*}}} & \frac{\partial r}{\partial \alpha_{\overline{*}}} & \frac{\partial f}{\partial \alpha_{\overline{*}}} & \frac{\partial f}{\partial h_*} & \frac{\partial f}{\partial h_{\overline{*}}} \\
\frac{\partial a}{\partial h_*} & \frac{\partial g}{\partial h_*} & \frac{\partial r}{\partial h_*} & \frac{\partial f}{\partial h_*} & \frac{\partial \hbar_*}{\partial h_*} & \frac{\partial \hbar_*}{\partial h_{\overline{*}}} \\
\frac{\partial a}{\partial h_{\overline{*}}} & \frac{\partial g}{\partial h_{\overline{*}}} & \frac{\partial r}{\partial h_{\overline{*}}} & \frac{\partial f}{\partial h_{\overline{*}}} & \frac{\partial \hbar_*}{\partial h_{\overline{*}}} & \frac{\partial \hbar_{\overline{*}}}{\partial h_{\overline{*}}}
\end{bmatrix} \quad (5.108)$$

and $\boldsymbol{J}(\widehat{\tilde{\boldsymbol{\theta}}}(N^*_{\min}, N^*_{\max}), \widehat{\tilde{\boldsymbol{Q}}}(N^*_{\min}, N^*_{\max}))$ is the Jacobian required by Newton-Raphson's Method evaluated at the maximum likelihood estimates $\widehat{\tilde{\boldsymbol{\theta}}}(N^*_{\min}, N^*_{\max})$ and $\widehat{\tilde{\boldsymbol{Q}}}(N^*_{\min}, N^*_{\max})$.

Now for

$$\boldsymbol{S}(\widehat{\tilde{\boldsymbol{\theta}}}(N^*_{\min}, N^*_{\max}), \widehat{\tilde{\boldsymbol{Q}}}(N^*_{\min}, N^*_{\max})) := \left[\mathcal{I}_{\boldsymbol{X}}(\widehat{\tilde{\boldsymbol{\theta}}}(N^*_{\min}, N^*_{\max}), \widehat{\tilde{\boldsymbol{Q}}}(N^*_{\min}, N^*_{\max}))\right]^{-1}, \quad (5.109)$$

Theorem 5.1.4 yields the following simultaneous $(1-\alpha)\cdot 100\%$ confidence intervals for $A, \kappa_s, \varepsilon_*, \alpha_{\overline{*}}, h_*, h_{\overline{*}}$, and $\tilde{Q}\left(\beta_i\right)$, for $1 \leq i \leq M$:

$$\left[\hat{A} - \sqrt{\frac{p(t-1)}{t-p}F_{p,t-p}(\alpha)}\sqrt{\frac{\hat{s}_{11}}{t}}, \hat{A} + \sqrt{\frac{p(t-1)}{t-p}F_{p,t-p}(\alpha)}\sqrt{\frac{\hat{s}_{11}}{t}}\right] \quad (5.110)$$

$$\left[\hat{\kappa}_s - \sqrt{\frac{p(t-1)}{t-p}F_{p,t-p}(\alpha)}\sqrt{\frac{\hat{s}_{22}}{t}}, \hat{\kappa}_s + \sqrt{\frac{p(t-1)}{t-p}F_{p,t-p}(\alpha)}\sqrt{\frac{\hat{s}_{22}}{t}}\right] \tag{5.111}$$

$$\left[\hat{\varepsilon}_* - \sqrt{\frac{p(t-1)}{t-p}F_{p,t-p}(\alpha)}\sqrt{\frac{\hat{s}_{33}}{t}}, \hat{\varepsilon}_* + \sqrt{\frac{p(t-1)}{t-p}F_{p,t-p}(\alpha)}\sqrt{\frac{\hat{s}_{33}}{t}}\right] \tag{5.112}$$

$$\left[\hat{\alpha}_{\overline{*}} - \sqrt{\frac{p(t-1)}{t-p}F_{p,t-p}(\alpha)}\sqrt{\frac{\hat{s}_{44}}{t}}, \hat{\alpha}_{\overline{*}} + \sqrt{\frac{p(t-1)}{t-p}F_{p,t-p}(\alpha)}\sqrt{\frac{\hat{s}_{44}}{t}}\right] \tag{5.113}$$

$$\left[\hat{h}_* - \sqrt{\frac{p(t-1)}{t-p}F_{p,t-p}(\alpha)}\sqrt{\frac{\hat{s}_{55}}{t}}, \hat{h}_* + \sqrt{\frac{p(t-1)}{t-p}F_{p,t-p}(\alpha)}\sqrt{\frac{\hat{s}_{55}}{t}}\right] \tag{5.114}$$

$$\left[\hat{h}_{\overline{*}} - \sqrt{\frac{p(t-1)}{t-p}F_{p,t-p}(\alpha)}\sqrt{\frac{\hat{s}_{66}}{t}}, \hat{h}_{\overline{*}} + \sqrt{\frac{p(t-1)}{t-p}F_{p,t-p}(\alpha)}\sqrt{\frac{\hat{s}_{66}}{t}}\right] \tag{5.115}$$

and

$$\left[\widehat{\widetilde{Q}}\left(\beta_i\right) - \sqrt{\frac{p(t-1)}{t-p}F_{p,t-p}(\alpha)}\sqrt{\frac{\hat{s}_{(i+6,i+6)}}{t}}, \widehat{\widetilde{Q}}\left(\beta_i\right) + \sqrt{\frac{p(t-1)}{t-p}F_{p,t-p}(\alpha)}\sqrt{\frac{\hat{s}_{(i+6,i+6)}}{t}}\right] \tag{5.116}$$

where $p = M + 6$ is the number of parameters being estimated, t is the number of independent blocks used to compute the sample averages, $F_{m,n}(\alpha)$ is the value of x for which the F-distribution $F(x)$ with (m, n) degrees of freedom, equals $1 - \alpha$ and $\hat{s}_{ii}$ is the i'th diagonal component of $\boldsymbol{S}(\widehat{\widetilde{\boldsymbol{\theta}}}(N^*_{\min}, N^*_{\max}), \widehat{\widetilde{\boldsymbol{Q}}}(N^*_{\min}, N^*_{\max}))$ [76].

The next section provides a technique for estimating the values of $N^*_{\min}$ (for which the Equations (5.34)-(5.36) hold) and $N^*_{\max}$ in the probability mass function given by Equation (5.46).

5.4 How Big is Big Enough?

Given an observed set of polygon lengths, let N_L be the length of the smallest polygon observed and N_U be the length of the largest polygon observed. Then how can a value for $N^*_{\min}$, where $N_L \leq N^*_{\min} < N^*_{\max} \leq N_U$, be determined such that Equations (5.35) and (5.36) hold for all even integers $n_{\min}$ satisfying $n_{\min} \geq N^*_{\min}$?

For any even integer $n_{\min}$ such that $N_L \leq n_{\min} < N^*_{\max}$, denote the maximum likelihood estimates for A, κ_s, ε_*, $\alpha_{\overline{*}}$, h_*, $h_{\overline{*}}$, and $\tilde{Q}\left(\beta_i\right)$, for $1 \leq i \leq M$, obtained by solving the system of nonlinear equations (cf. the system given by Equation (5.100)) with $N^*_{\min} = n_{\min}$, respectively as $\hat{A}(n_{\min})$, $\hat{\kappa}_s(n_{\min})$, $\hat{\varepsilon}_*(n_{\min})$, $\hat{\alpha}_{\overline{*}}(n_{\min})$, $\hat{h}_*(n_{\min})$, $\hat{h}_{\overline{*}}(n_{\min})$, and $\widehat{\widetilde{Q}}\left(\beta_i\right)(n_{\min})$, for $1 \leq i \leq M$. Because the estimates $\hat{A}(n_{\min})$, $\hat{\kappa}_s(n_{\min})$, $\hat{\varepsilon}_*(n_{\min})$, $\hat{\alpha}_{\overline{*}}(n_{\min})$, $\hat{h}_*(n_{\min})$, $\hat{h}_{\overline{*}}(n_{\min})$, and $\widehat{\widetilde{Q}}\left(\beta_i\right)(n_{\min})$, for $1 \leq i \leq M$ are maximum likelihood estimates, they are

considered the best possible estimates for the unknown parameters in the distribution $\pi(\boldsymbol{n}, \boldsymbol{k}|*, \boldsymbol{\theta}, n_{\min}, N^*_{\max}, \boldsymbol{\beta})$. Of all the $n_{\min} \in [N_L, N^*_{\max})$, how is the value of $n_{\min}$ that best estimates $N^*_{\min}$ be determined, that is how is $N^*_{\min}$ estimated such that Equations (5.34)-(5.36) hold?

If Equations (5.34)-(5.36) hold, then the estimates $\hat{A}(n_{\min})$, $\hat{\kappa}_s(n_{\min})$, $\hat{\varepsilon}_*(n_{\min})$, $\hat{\alpha}_{\overline{*}}(n_{\min})$, $\hat{h}_*(n_{\min})$, and $\hat{h}_{\overline{*}}(n_{\min})$ should not change much for all $n_{\min} \geq N^*_{\min}$, that is for $n_{\min} \geq N^*_{\min}$ the estimates $\hat{A}(n_{\min})$, $\hat{\kappa}_s(n_{\min})$, $\hat{\varepsilon}_*(n_{\min})$, $\hat{\alpha}_{\overline{*}}(n_{\min})$, $\hat{h}_*(n_{\min})$, and $\hat{h}_{\overline{*}}(n_{\min})$ should not depend on the value of $n_{\min}$. Hence the best estimate for $N^*_{\min}$ is expected to be the value of $n_{\min}$ for which the estimated parameters first appear to be simultaneously constant in $n_{\min}$.

One method for identifying where the estimates first appear to be simultaneously constant in $n_{\min}$ is to locate the value of $n_{\min}$ for which the maximum likelihood estimates do not change much from $n_{\min}$ to $n_{\min} + 2$. In order to quantify the expression "do not change much from $n_{\min}$ to $n_{\min} + 2$", let

$$\boldsymbol{\lambda} := (\lambda_1, ..., \lambda_6) \tag{5.117}$$

$$:= (\hat{A}(n_{\min}), \hat{\kappa}_s(n_{\min}), \hat{\varepsilon}_*(n_{\min}), \hat{\alpha}_{\overline{*}}(n_{\min}), \hat{h}_*(n_{\min}), \hat{h}_{\overline{*}}(n_{\min})), \tag{5.118}$$

and define

$$m\left(\hat{\lambda}_i(n_{\min})\right) := \left|\hat{\lambda}_i(n_{\min}) - \hat{\lambda}_i(n_{\min} + 2)\right|, \tag{5.119}$$

where $\hat{\lambda}_i(n_{\min})$ is an estimate for λ_i based on $N^*_{\min} = n_{\min}$. Then define $\hat{N}_{\min}(*)(\lambda_i)$ to be the first value of $n_{\min}$ for which $m\left(\hat{\lambda}_i(n)\right) < \epsilon_{\lambda_i}$ for all $n \in [n_{\min}, \hat{N}_{\max}(*))$, where $\hat{N}_{\max}(*)$ is the estimate for $N^*_{\max}$, and some a priori fixed $\epsilon_{\lambda_i} > 0$. Then the estimate for $N^*_{\min}$ is defined as

$$\hat{N}_{\min}(*) := \max_i \left\{\hat{N}^*_{\min}(\lambda_i)\right\}. \tag{5.120}$$

The *flat region* for the point estimates is defined to be the set $\{n_{\min} \in \mathbb{N} : \hat{N}_{\min}(*) \leq n_{\min} < \hat{N}_{\max}(*)\}$. Once $N^*_{\min}$ has been estimated, the corresponding estimate $\hat{\lambda}_i(\hat{N}_{\min}(*))$ is considered to be the *best estimate for* λ_i.

Because the maximum likelihood estimates are a function of the estimates for $N^*_{\min}$ and $N^*_{\max}$, how do the estimates for A, κ_s, ε_*, $\alpha_{\overline{*}}$, h_*, $h_{\overline{*}}$, and $\tilde{Q}(\beta_i)$ depend on the estimates for $N^*_{\min}$ and $N^*_{\max}$. The next section provides a method for estimating how the estimates vary depending on the estimates for $N^*_{\min}$ and $N^*_{\max}$.

5.5 Systematic Error in MLEs

Since the maximum likelihood estimates depend on $N^*_{\min}$ and $N^*_{\max}$, a measure of the influence of $N^*_{\min}$ and $N^*_{\max}$ on the estimates for A, κ_s, ε_*, $\alpha_{\overline{*}}$, h_*, $h_{\overline{*}}$, and $\tilde{Q}(\beta_i)$ can be obtained from estimates for A, κ_s, ε_*, $\alpha_{\overline{*}}$, h_*, $h_{\overline{*}}$, and $\tilde{Q}(\beta_i)$ determined using various values of $N^*_{\min}$ and $N^*_{\max}$. This influence will provide one contribution to an estimate for the systematic error for the maximum likelihood estimates, that is the error that results from choosing estimates for A, κ_s, ε_*, $\alpha_{\overline{*}}$, h_*, $h_{\overline{*}}$, and $\tilde{Q}(\beta_i)$ based on a fixed value for $N^*_{\min}$ and $N^*_{\max}$.

Suppose λ is one of the parameters estimated using the maximum likelihood technique in Section 5.3 and that its estimate, $\hat{\lambda}(\hat{N}_{\min}(*), \hat{N}_{\max}(*))$, has been determined via the techniques discussed in Sections 4.6 and 5.4. For the estimates $\hat{N}_{\min}(*)$ and $\hat{N}_{\max}(*)$, let $\hat{\nu}_\lambda$ be the maximum deviation of the estimates $\hat{\lambda}(n_{\min}, \hat{N}_{\max}(*))$ from the best estimate $\hat{\lambda}(\hat{N}_{\min}(*), \hat{N}_{\max}(*))$, that is

$$\hat{\nu}_\lambda := \max_{\substack{n : N_L \le n_{\min} < N_U, \\ n_{\min} \text{ is even}}} \left| \hat{\lambda}(\hat{N}_{\min}(*), \hat{N}_{\max}(*)) - \hat{\lambda}(n_{\min}, \hat{N}_{\max}(*)) \right|, \tag{5.121}$$

where N_L is the minimum length of unknotted self-avoiding polygon observed in the data set and N_U is the first value of $n_{\min}$ greater than $\hat{N}_{\min}(*)$ such that $m\left(\hat{\lambda}_i(n_{\min})\right) > \epsilon_\lambda$, the value used in Section 5.4 to estimate $N^*_{\min}$. Then the estimated systematic error in the estimate for λ is denoted $\hat{\xi}(\lambda)$ and defined to be

$$\hat{\xi}(\lambda) := \max\left\{ \epsilon_\lambda, \hat{\nu}_\lambda, \left| \hat{\lambda}(\hat{N}_{\min}(*), \hat{N}_{\max}(*)) - \hat{\lambda}(\hat{N}_{\min}(*), \infty) \right| \right\}. \tag{5.122}$$

Note that $\hat{\xi}(\lambda)$ represents the error in the point estimate for λ that results from choosing too small an estimate for $N^*_{\max}$ and a different estimate for $N^*_{\min}$.

With methods for estimating $N^*_{\max}$, $N^*_{\min}$, and the systematic error in the maximum likelihood estimates in hand, the Maximum Likelihood Technique discussed in this chapter can be applied to the set of SAPs $\mathscr{P}^{\Theta}(\phi)$. The results of this application are presented next.

5.6 The Maximum Likelihood Estimates from the CMC-Implementation of the Θ-BFACF Algorithm

To apply the CMC Maximum Likelihood Technique developed in Section 5.3 to the CMC data (Θ-SAPs with property $*$ generated as discussed in Section 4.7 of Chapter 4), set s_n, s_n^*, and $s_n^{\overline{*}}$, as defined in Section 5.3, to $p_n^{\Theta}(\phi)$, $p_n^{\Theta}(*)$, and $p_n^{\Theta}(\phi) - p_n^{\Theta}(*)$ respectively. Then the maximum likelihood technique in Section 5.3 can be used to determine estimates for A, κ_s, ε_*, $\alpha_{\overline{*}}$, h_*, $h_{\overline{*}}$, and $\tilde{Q}(\beta_i)$, for $1 \leq i \leq M$, which depend on $N^*_{\min}$ and $N^*_{\max}$. The estimates for A, κ_*^{Θ}, ε_*, $\alpha_{\overline{*}}^{\Theta}$, h_*, $h_{\overline{*}}$, and $\tilde{Q}(\beta_i)$, for $1 \leq i \leq M$, obtained by applying the Maximum Likelihood Technique developed previously in this chapter to the CMC data will be referred to from-here-on-in as *CMC maximum likelihood estimates* or *CMC m.l.e.s* for short. Also, note that in the remainder of this chapter, unless otherwise stated, any reference to an estimate refers to a CMC m.l.e.. In order to determine the best CMC maximum likelihood estimates for A, κ_*^{Θ}, ε_*, $\alpha_{\overline{*}}^{\Theta}$, h_*, $h_{\overline{*}}$, and $\tilde{Q}(\beta_i)$, for $1 \leq i \leq M$, an estimate for $N^*_{\max}$ is first required, where $* \in \Phi_{\text{mle}}$ and

$$\Phi_{\text{mle}} := \{\phi, (\phi, f), (\phi, s), (\phi|\phi, s), (3_1|\phi, s), (4_1|\phi, s)\}. \tag{5.123}$$

Recall that the purpose for including the quantity $N^*_{\max}$ in the model is to take into account the finite nature of the simulation, and specifically the fact that, the observed proportion for a large polygon length N may not accurately represent the proportion for that N according to the true distribution. To estimate the value of $N^*_{\max}$ from the observed data, the estimates for $N^*_{\max}$ for each property $* \in \Phi_{\text{mle}}$ that were determined in Section 4.6 will be used in this maximum likelihood analysis. Hence the required estimated values for $N^*_{\max}$ are $\hat{N}_{\max}(\phi) = 3300$, $\hat{N}_{\max}(\phi, f) = 3300$, $\hat{N}_{\max}(\phi, s) = 3300$, $\hat{N}_{\max}(\phi|\phi, s) = 3300$, $\hat{N}_{\max}(3_1|\phi, s) = 2000$, and $\hat{N}_{\max}(4_1|\phi, s) = 600$.

From the estimate of τ_{int} in Chapter 4, each replication can be subdivided into 66 essentially independent blocks. Thus, if it is assumed that no data needs to be burned, the CMC Maximum Likelihood Technique could be implemented with $T\prime = 660$ essentially independent blocks of data. Although, in Chapter 4, it was determined that 5.0 million data points should be burned from each replication, the results presented in the following two sub-sections are based on no data being burned. The reason for presenting the results for the scenario in which no data is burned is that none of the CMC m.l.e.s differed statis-

tically when computed using either burn-time scenario and hence none of the conclusions based on the CMC m.l.e.s were affected by using all the data in the analysis. Thus the results presented in the remainder of this section are based on using all the data in the analysis.

Note that the smallest values of $n_{\min}$ for which CMC m.l.e.s were computed for each $* \in \Phi_{\text{mle}}$ are respectively 14, 14, 14, 14, 70, and 70. The reason CMC m.l.e.s were not computed for values of $n_{\min} < 70$ for the properties $(3_1|\phi, s)$ and $(4_1|\phi, s)$ is a consequence of the estimate $\hat{N}_{\min}(\phi|\phi, s) = 182$ and the belief that $N_{\min}(*)$ increases as property $*$ becomes more complex. Because of this estimate and belief, and the fact that finding starting states for Newton-Raphson's method (which is used to determine estimates for A, κ_*^{Θ}, ε_*, $\alpha_{\overline{*}}^{\Theta}$, h_*, and $h_{\overline{*}}$) becomes more and more difficult as $n_{\min}$ decreases, it was deemed unnecessary to compute CMC m.l.e.s for properties $(3_1|\phi, s)$ and $(4_1|\phi, s)$ when $n_{\min} < 70$.

Because the estimates for κ_*^{Θ}, ε_*, $\alpha_{\overline{*}}^{\Theta}$, h_*, and $h_{\overline{*}}$ can be used to explore the reliability of the programs that were written to implement the CMC Θ-BFACF algorithm and to implement the CMC Maximum Likelihood Technique and because the estimates for ε_* and $\alpha_{\overline{*}}^{\Theta}$ can be used to explore the validity of Conjectures 2.2.8 and 2.2.9, the CMC m.l.e.s presented for a range of values for $n_{\min}$ are those for the parameters κ_*^{Θ}, ε_*, $\alpha_{\overline{*}}^{\Theta}$, h_*, and $h_{\overline{*}}$. Only the best estimates for A and $\tilde{Q}(\beta_i)$, for $1 \leq i \leq M$, are presented.

5.6.1 The Reliability of the CMC M.L.E. Program

The first part of this discussion presents some of the CMC m.l.e.'s and uses these estimates to check the accuracy/consistency of the computer program that was written to implement the CMC Maximum Likelihood Technique. The first estimates discussed are those for κ_*^{Θ}, for properties $* \in \Phi_{\text{mle}}$.

Recall (from Section 2.2.1 of Chapter 2) the conclusions of Theorems 2.2.4 and 2.2.5, that is

$$\kappa_{\phi}^{\Theta} = \kappa_{(\phi,s)}^{\Theta} = \kappa_{(\phi,f)}^{\Theta} = \kappa_{\phi} = \kappa_{(K|\phi,s)}^{\Theta}, \tag{5.124}$$

where $K \in \mathscr{K}^{\Theta}(\phi)$, the set of knot-types possible after a strand-passage occurs in an unknotted successful-strand-passage Θ-SAP. In [125], Orlandini *et al.* estimate $\mu_{\phi} = e^{\kappa_{\phi}} \approx 4.6836$ which corresponds to $\kappa_{\phi} \approx 1.544067$.

Because $\mathscr{P}^{\Theta}(\phi, f)$, $\mathscr{P}^{\Theta}(\phi|\phi, s)$, $\mathscr{P}^{\Theta}(3_1|\phi, s)$, and $\mathscr{P}^{\Theta}(4_1|\phi, s)$ are mutually disjoint sets, CMC maximum likelihood estimates for κ_*^{Θ}, for each property $* \in \{(\phi, f), (\phi|\phi, s),$

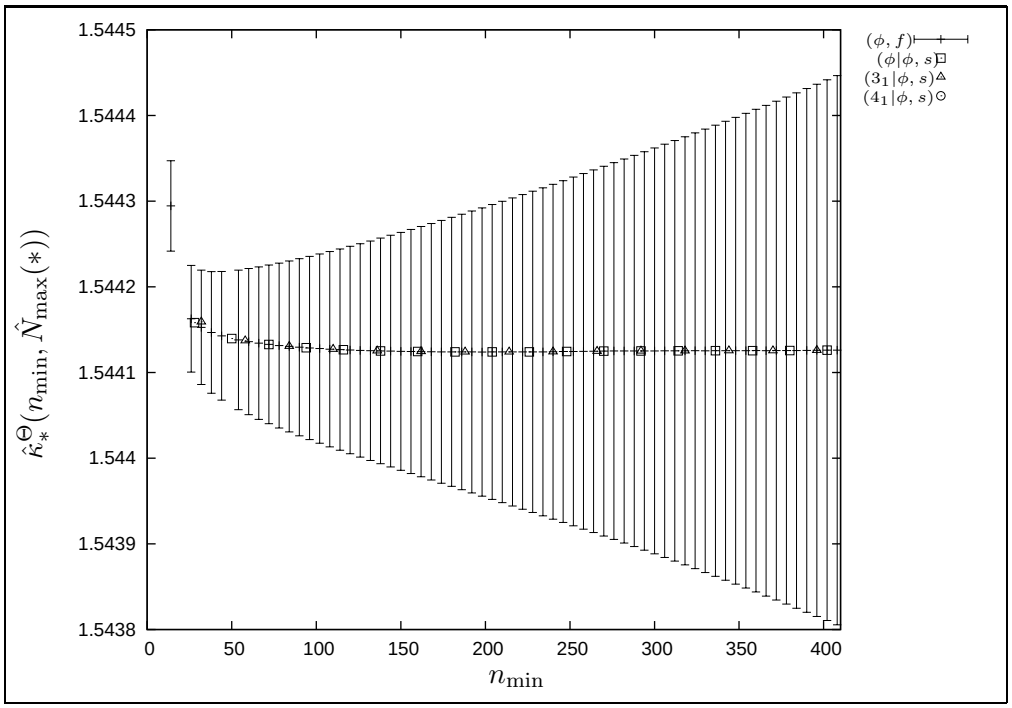

Figure 5.1: The CMC m.l.e.s for κ^{Θ}_{*} for each of the properties $* \in \{(\phi, f)\,[+],\ (\phi|\phi, s)\,[\boxdot],\ (3_1|\phi, s)\,[\triangle],\ (4_1|\phi, s)\,[\odot]\}$ plotted versus $n_{\min}$. The error bars plotted represent estimated 95% confidence intervals for $\kappa^{\Theta}_{(\phi,f)}$.

$(3_1|\phi, s)$, $(4_1|\phi, s)\}$, were computed as a function of $n_{\min}$ for $\hat{N}_{\max}(*)$ fixed. The resulting estimates denoted $\hat{\kappa}^{\Theta}_{*}(n_{\min}, \hat{N}_{\max}(*))$ are displayed as a function of $n_{\min}$ in Figure 5.1.

Figure 5.1 is a plot of the CMC maximum likelihood estimates for κ^{Θ}_{*}, as a function of $n_{\min}$. Note that the property-(ϕ, f) estimates are plotted using a $+$; the property-$(\phi|\phi, s)$ estimates are plotted using a $\boxdot$; the property-$(3_1|\phi, s)$ estimates are plotted using a $\triangle$; and the property-$(\phi|\phi, s)$ estimates are plotted using a $\odot$. The error bars represent the estimated 95% confidence intervals for κ^{Θ}_{*} as calculated for $* = (\phi, f)$ using Theorem 5.1.4. Referring to Figure 5.1, since the estimates for κ^{Θ}_{*} for each of the properties $* \in \{(\phi, f)$, $(\phi|\phi, s)$, $(3_1|\phi, s)$, $(4_1|\phi, s)\}$ plotted versus $n_{\min}$ are essentially indistinguishable from each other, regardless of the value of $n_{\min}$, the plotted estimates are consistent with Equation (5.124), that is

$$\kappa^{\Theta}_{(\phi,f)} = \kappa^{\Theta}_{(\phi|\phi,s)} = \kappa^{\Theta}_{(3_1|\phi,s)} = \kappa^{\Theta}_{(4_1|\phi,s)}. \tag{5.125}$$

Thus, this provides strong evidence for the validity of the programmed CMC m.l.e. algorithm.

The best estimate for κ_*^{Θ}, for each of the properties $* \in \Phi_{\text{mle}}$, was determined using the method outlined in Section 5.4. The best estimates for κ_*^{Θ} and the corresponding estimates for $N_{\min}^*$ are presented in Table 5.1.

Table 5.1: The best CMC m.l.e.s for κ_*^{Θ} based on $* \in \Phi_{\text{mle}}$. The values in parentheses are the estimated 95% margins of error.

	Parameter Estimated		
Property $*$	$N_{\min}^*$	$N_{\max}^*$	κ_*^{Θ} (95% ME)
ϕ	156	3300	1.544125 (0.000028)
(ϕ, f)	142	3300	1.544125 (0.000028)
(ϕ, s)	156	3300	1.544124 (0.000030)
$(\phi \vert \phi, s)$	182	3300	1.544124 (0.000033)
$(3_1 \vert \phi, s)$	408	2000	1.544135 (0.000094)
$(4_1 \vert \phi, s)$	296	1200	1.544125 (0.000049)

Because the final estimates for κ_*^{Θ} presented in Table 5.1 are all equal to four decimal places and are equal to four decimal places to Orlandini *et al.*'s estimate [125] for κ_ϕ (provided their estimate is rounded to four decimal places), it is concluded that the estimates for κ_*^{Θ}, based on each of the properties $* \in \Phi_{\text{mle}}$, support the fact that κ_ϕ is independent of property $* \in \Phi_{\text{mle}}$. Hence the CMC data generated from the CMC Θ-BFACF algorithm numerically support the conclusions of Theorems 2.2.4 and 2.2.5 of Section 2.2), that is,

$$\kappa_\phi^{\Theta} = \kappa_{(\phi,s)}^{\Theta} = \kappa_{(\phi,f)}^{\Theta} = \kappa_\phi = \kappa_{(K|\phi,s)}^{\Theta}. \tag{5.126}$$

Hence the program written to implement the CMC Θ-BFACF algorithm and the program written to perform the CMC Maximum Likelihood Technique can be concluded to implement the CMC Θ-BFACF algorithm and the CMC Maximum Likelihood Technique correctly.

Note that when $\hat{N}_{\max}(4_1|\phi, s) = 600$ is used to estimate A, κ_*^{Θ}, α_*^{Θ}, $\alpha_{\overline{*}}^{\Theta}$, h_*, and $h_{\overline{*}}$, no flat region could be found in any of the estimates. Because it was determined that $\hat{N}_{\min}(\phi|\phi, s) = 182$ and $\hat{N}_{\min}(3_1|\phi, s) = 408$, it is quite possible that $\hat{N}_{\min}(4_1|\phi, s) > \hat{N}_{\min}(3_1|\phi, s)$ and hence there might not be enough reliable data in the interval $\left[\hat{N}_{\min}(4_1|\phi, s), 600\right]$ to implement the CMC Maximum Likelihood Technique. In fact, if

$\hat{N}_{\min}(4_1|\phi,s) > N_{\max}(4_1|\phi,s)$, there would be no reliable data for which the asymptotic form of $p_n^{\Theta}(4_1|\phi,s)$ holds. Hence the CMC Maximum Likelihood Technique could not be used to estimate A, κ_*^{Θ}, ε_*, $\alpha_{\overline{*}}$, h_*, $h_{\overline{*}}$, and $\tilde{Q}(\beta_i)$, for $1 \leq i \leq M$. For comparison, $\hat{N}_{\max}(4_1|\phi,s) = 1200$ is used to determine estimates for κ_*^{Θ}, α_*^{Θ}, $\alpha_{\overline{*}}^{\Theta}$, h_*, and $h_{\overline{*}}$ for $* \in \{(4_1|\phi,s)\}$. Because of the unreliability (determined in determines of the relative error) of the estimates for $h_{(4_1|\phi,s)}$ over the interval $[30, 1200)$, the estimates presented for the property $* \in \{(4_1|\phi,s)\}$ are based on detecting a flat region in the estimates for κ_*^{Θ}, $\alpha_{\overline{*}}^{\Theta}$, and $h_{\overline{*}}$.

Because the largest amount of data available is for Θ-SAPs with property $* = \phi$, the best estimate of κ_ϕ is taken to be

$$\kappa_\phi = 1.544125 \pm 0.000028\,(\pm 0.00005)\,, \tag{5.127}$$

where the above is of the form

$$\text{parameter} = \text{point estimate} \pm 95\%\ \text{ME}\ (\pm\text{systematic error}), \tag{5.128}$$

the estimated 95% margin of error is calculated using Theorem 5.1.4, and the systematic error is determined using the technique discussed in Section 5.5.

Because the complement of the set of unsuccessful strand passage polygons (with respect to $\mathscr{P}^{\Theta}(\phi)$) is the set of successful strand passage polygons, $\alpha_{\overline{(\phi,f)}}^{\Theta} = \alpha_{(\phi,s)}^{\Theta}$; $\alpha_{\overline{(\phi,s)}}^{\Theta} = \alpha_{(\phi,f)}^{\Theta}$; $h_{\overline{(\phi,f)}} = h_{(\phi,s)}$; and $h_{\overline{(\phi,s)}} = h_{(\phi,f)}$. These four equalities can also be used to check the consistency of the program written to implement the CMC Θ-BFACF algorithm and the program written to perform the CMC Maximum Likelihood Technique.

Note that for the remainder of this chapter, for the purposes of creating more illustrative figures, only the point estimates computed for every tenth consecutive even value of $n_{\min}$ will be displayed. With this in mind, Figure 5.2 depicts the estimates for $\alpha_{\overline{(\phi,f)}}^{\Theta}$ and $\alpha_{(\phi,s)}^{\Theta}$ plotted as functions of $n_{\min}$ using a ($\times$) and ($\diamond$) respectively. Figure 5.3 depicts the estimates for $\alpha_{(\phi,f)}^{\Theta}$ and $\alpha_{\overline{(\phi,s)}}^{\Theta}$ plotted as functions of $n_{\min}$ using a ($\times$) and ($\diamond$) respectively. Figure 5.4 depicts the estimates for $h_{\overline{(\phi,f)}}$ and $h_{(\phi,s)}$ plotted as functions of $n_{\min}$ using a ($\times$) and ($\diamond$) respectively. Figure 5.5 depicts the estimates for $h_{(\phi,f)}$ and $h_{\overline{(\phi,s)}}$ plotted as functions of $n_{\min}$ using a ($\times$) and ($\diamond$) respectively. In each of Figures 5.2-5.5, the corresponding estimated 95% margins of error are not displayed so that each of the plotted point estimates can be clearly identified. With this in mind, on the scale of the plots,

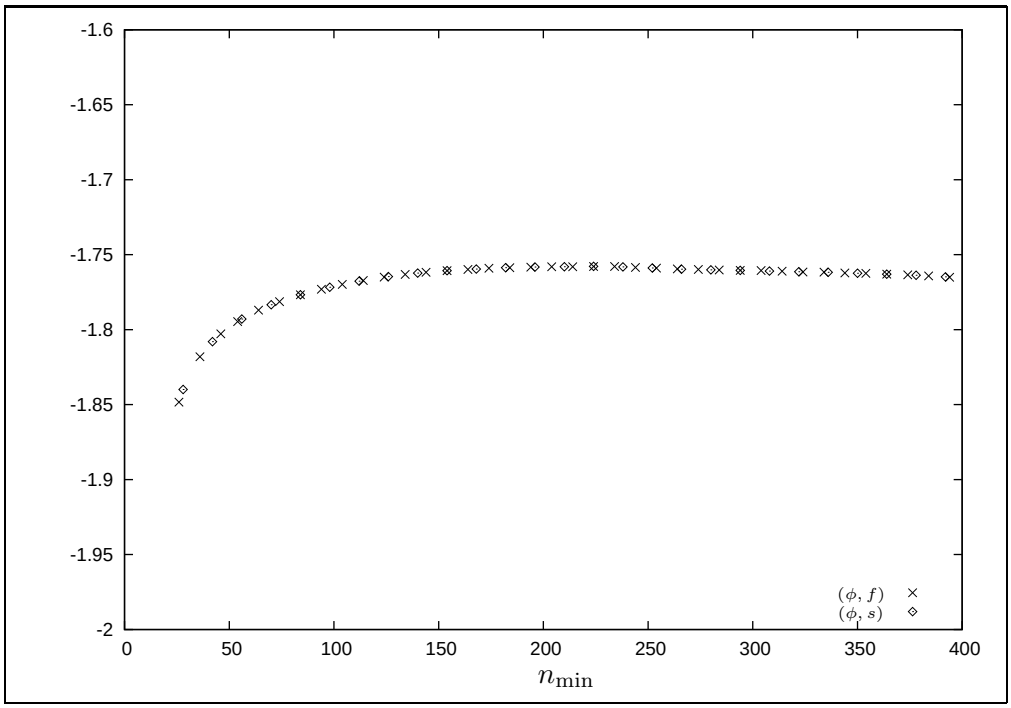

Figure 5.2: The CMC m.l.e.s for $\alpha^{\Theta}_{\overline{(\phi,f)}}\,[\times]$ and $\alpha^{\Theta}_{(\phi,s)}\,[\diamond]$ plotted versus $n_{\min}$.

the point estimates plotted in each of Figures 5.2-5.5 cannot be distinguished from each other. Hence the estimates displayed in Figures 5.2-5.5 numerically support, respectively, the relationships

$$\alpha^{\Theta}_{\overline{(\phi,f)}} = \alpha^{\Theta}_{(\phi,s)};\ \alpha^{\Theta}_{\overline{(\phi,s)}} = \alpha^{\Theta}_{(\phi,f)};\ h_{\overline{(\phi,f)}} = h_{(\phi,s)};\ \text{and}\ h_{\overline{(\phi,s)}} = h_{(\phi,f)}. \tag{5.129}$$

Because the data generated by the CMC Θ-BFACF algorithm, when analyzed using the CMC Maximum Likelihood Technique, numerically support the relations: $\alpha^{\Theta}_{\overline{(\phi,f)}} = \alpha^{\Theta}_{(\phi,s)}$; $\alpha^{\Theta}_{\overline{(\phi,s)}} = \alpha^{\Theta}_{(\phi,f)}$; $h_{\overline{(\phi,f)}} = h_{(\phi,s)}$; and $h_{\overline{(\phi,s)}} = h_{(\phi,f)}$; and the facts that $\kappa^{\Theta}_{\phi} = \kappa^{\Theta}_{(\phi,s)} = \kappa^{\Theta}_{(\phi,f)} = \kappa_{\phi} = \kappa^{\Theta}_{(K|\phi,s)}$, it is concluded that the program written to implement the CMC Θ-BFACF algorithm and the program written to implement the CMC Maximum Likelihood Technique perform their intended purpose correctly. Hence the discussion can now turn to the estimates for α^{Θ}_{*}, $\alpha^{\Theta}_{\overline{*}}$, h_{*}, and $h_{\overline{*}}$, respectively, based on each of the properties $* \in \Phi_{\text{mle}}$.

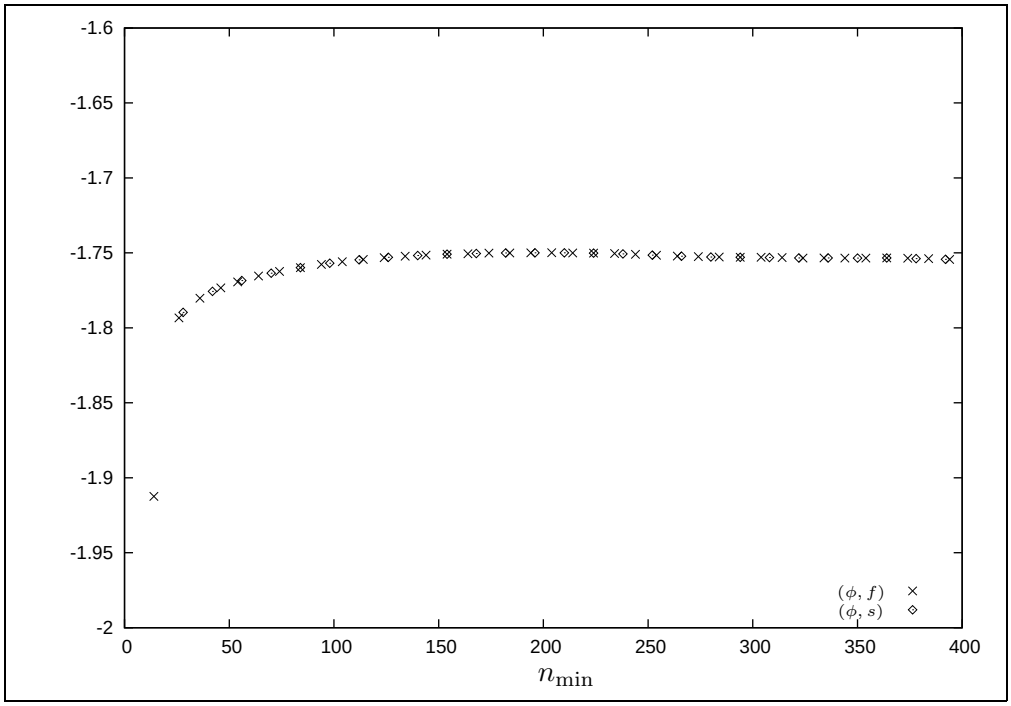

Figure 5.3: The estimates for $\alpha^{\Theta}_{\overline{(\phi,s)}}[\diamond]$ and $\alpha^{\Theta}_{(\phi,f)}[\times]$ plotted versus $n_{\min}$.

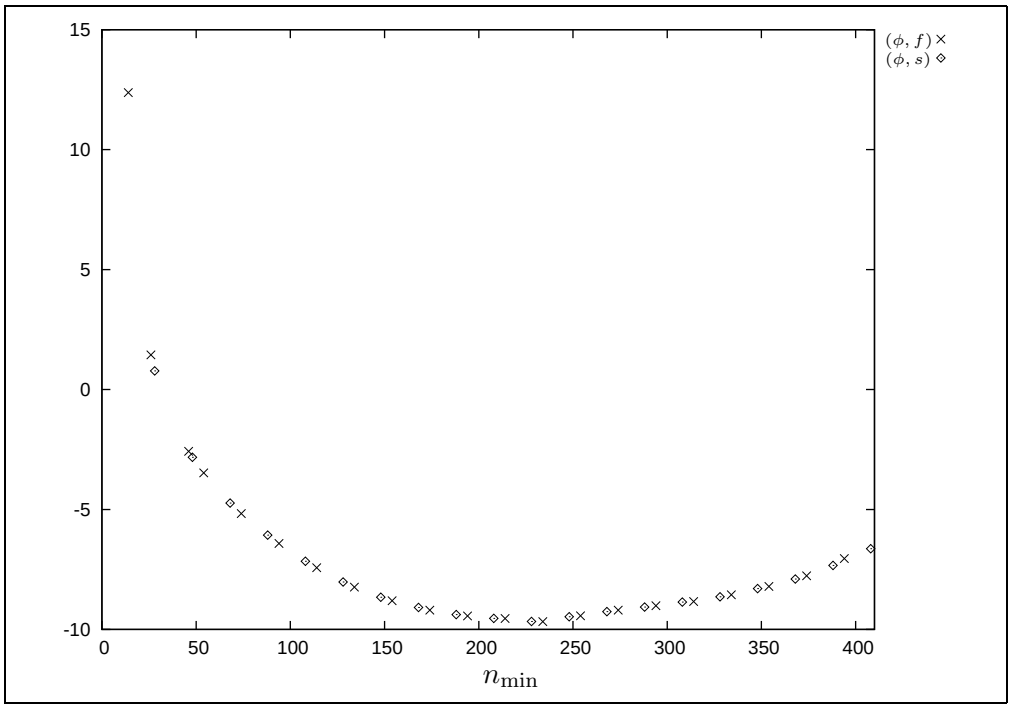

Figure 5.4: The CMC m.l.e.s for $h_{\overline{(\phi,f)}}[\times]$ and $h_{(\phi,s)}[\diamond]$ plotted versus $n_{\min}$.

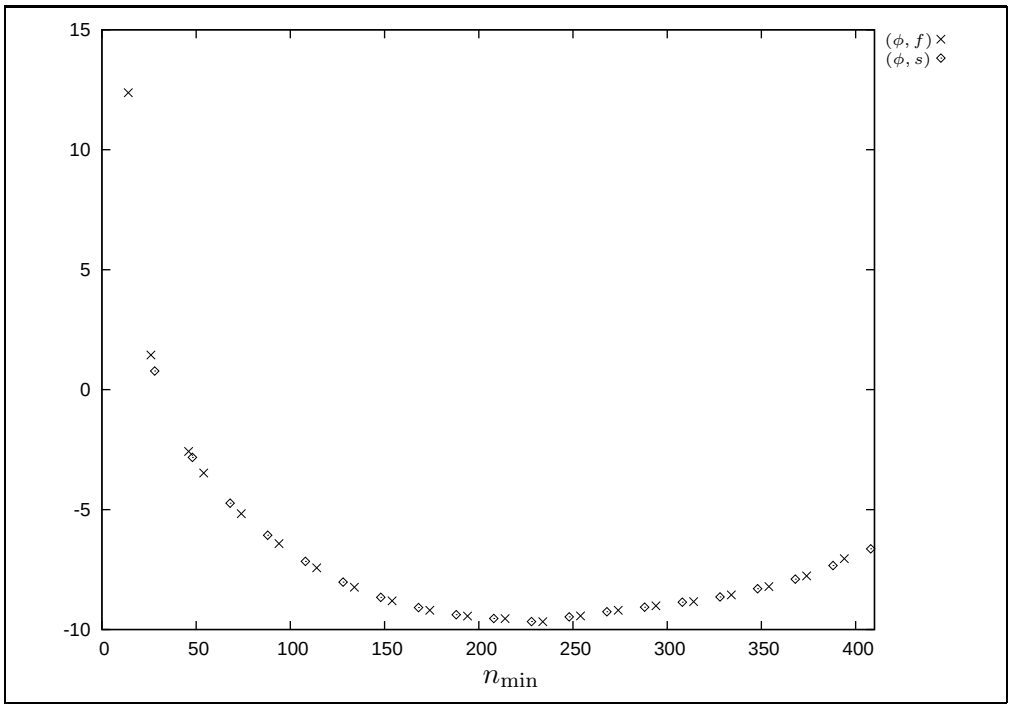

Figure 5.5: The CMC m.l.e.s for $h_{\overline{(\phi,s)}}\,[\diamond]$ and $h_{(\phi,f)}\,[\times]$ plotted versus $n_{\min}$.

5.6.2 The CMC M.L.E.'s for α_*^{Θ}, $\alpha_{\overline{*}}^{\Theta}$, h_*, and $h_{\overline{*}}$

The Maximum Likelihood technique presented in Section 5.3 was used to estimate κ_*^{Θ}, α_*^{Θ}, $\alpha_{\overline{*}}^{\Theta}$, A, h_*, $h_{\overline{*}}$, and $\tilde{Q}\left(\beta_i\right)$, for $1 \leq i \leq M$, for fixed $\hat{N}_{\max}^*$.

Recall that, for the purposes of creating more illustrative graphs, the CMC m.l.e. corresponding to every tenth consecutive even value of $n_{\min}$ is plotted in Figures 5.6 through 5.14. Also recall from the previous subsection that the best CMC maximum likelihood estimates for κ_*^{Θ} are presented in Table 5.1 and that these estimates support

$$\kappa_{\phi}^{\Theta} = \kappa_{(\phi,s)}^{\Theta} = \kappa_{(\phi,f)}^{\Theta} = \kappa_{\phi} = \kappa_{(K|\phi,s)}^{\Theta}. \tag{5.130}$$

Further recall that the best CMC maximum likelihood estimate for κ_{ϕ} is

$$\kappa_{\phi} = 1.544125 \pm 0.000028\,(\pm 0.00005)\,. \tag{5.131}$$

With κ_{ϕ} estimated, the next estimates to be presented are the CMC maximum likelihood estimates for the critical exponents α_*^{Θ} and $\alpha_{\overline{*}}^{\Theta}$.

Before discussing the CMC m.l.e.s for α_*^{Θ} and $\alpha_{\overline{*}}^{\Theta}$, recall that, for given values of $N_{\max}^*$ and $N_{\min}^*$, the CMC Maximum Likelihood technique presented in Section 5.3 computes

estimates for ε_* and $\alpha^{\Theta}_{\overline{*}}$. In order to obtain estimates for α^{Θ}_{*} recall from Equation (5.48) that

$$\varepsilon_* := \alpha^{\Theta}_{\overline{*}} - \alpha^{\Theta}_{*}. \tag{5.132}$$

Hence the estimates for $\alpha^{\Theta}_{\overline{*}}$ and ε_* (as functions of $n_{\min}$ and fixed $\hat{N}_{\max}(*)$) need to be presented before estimates for α^{Θ}_{*} can be determined.

Figure 5.6 contains the CMC m.l.e.s for $\alpha^{\Theta}_{\overline{*}}$ (as a function on $n_{\min}$ and fixed $\hat{N}_{\max}(*)$) for $* \in \{(\phi, f)\ [\times],\ (\phi|\phi, s)\ [\boxdot],\ (3_1|\phi, s)\ [\triangle],\ (4_1|\phi, s)\ [\odot]\}$. For the purposes of creating a more meaningful graph, note that the only error bars (which correspond to an estimated 95% confidence interval) plotted in Figure 5.6 are those corresponding to the estimates $\hat{\alpha}^{\Theta}_{\overline{(\phi,f)}}(n_{\min}, \hat{N}_{\max}(*))$. Referring to Figure 5.6, note that on the scale of the plot, for all plotted positive even values of $n_{\min} > 70$, the estimated 95% confidence interval for $\alpha^{\Theta}_{\overline{(\phi,f)}}$ contains the estimates $\hat{\alpha}^{\Theta}_{\overline{*}}(n_{\min}, \hat{N}_{\max}(*))$ for every property $* \in \{(\phi|\phi, s),\ (3_1|\phi, s),\ (4_1|\phi, s)\}$. Hence, the estimates presented in Figure 5.6 support, for any unknotting number one knot-type K,

$$\alpha^{\Theta}_{\overline{(\phi,f)}} = \alpha^{\Theta}_{\overline{(K|\phi,s)}}, \tag{5.133}$$

which is part of Conjecture 2.2.9. Furthermore, recall from Section 5.6.1 (cf. Figure 5.2) that the data numerically supports the relation

$$\alpha^{\Theta}_{(\phi,s)} = \alpha^{\Theta}_{\overline{(\phi,f)}}. \tag{5.134}$$

This, combined with Figure 5.6, results in the conclusion that the data supports the following equalities:

$$\alpha^{\Theta}_{(\phi,s)} = \alpha^{\Theta}_{\overline{(\phi,f)}} = \alpha^{\Theta}_{\overline{(K|\phi,s)}}. \tag{5.135}$$

The best CMC m.l.e.s for $\alpha^{\Theta}_{\overline{*}}$, for $* \in \Phi_{\text{mle}}$, are presented in Table 5.2.

In order to garner further numerical support for Conjecture 2.2.9, the discussion now turns to the estimates for ε_* (as a function of $n_{\min}$ and fixed $\hat{N}_{\max}(*)$). Figure 5.7 displays the estimated difference between $\alpha^{\Theta}_{\overline{*}}$ and α^{Θ}_{*}, that is it displays the CMC m.l.e.'s for ε_* (as a function of $n_{\min}$ and fixed $\hat{N}_{\max}(*)$). To test whether the estimated values of $\alpha^{\Theta}_{\overline{*}}$ and α^{Θ}_{*} numerically support Conjecture 2.2.9, the estimated differences for $\varepsilon_* = \alpha^{\Theta}_{\overline{*}} - \alpha^{\Theta}_{*}$, for each of the properties $* \in \{(\phi, s),\ (\phi, f),\ (\phi|\phi, s),\ (3_1|\phi, s),\ (4_1|\phi, s)\}$, are compared to zero. Without any error bars displayed in Figure 5.7, the estimates $\hat{\varepsilon}_*(n_{\min}, \hat{N}^*_{\max})$, for

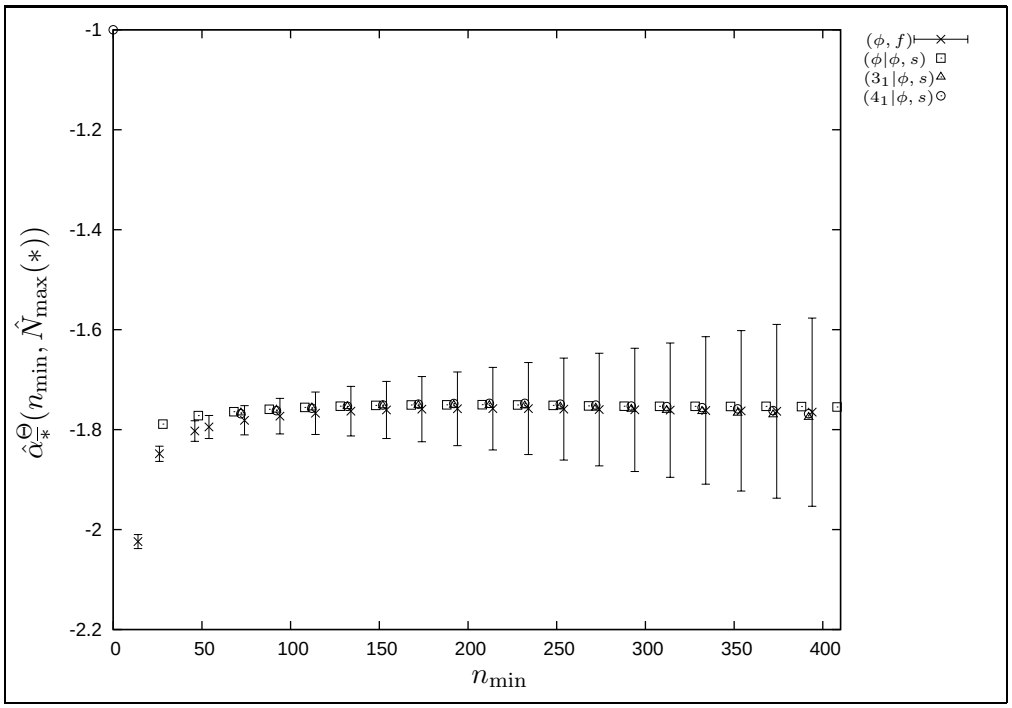

Figure 5.6: The CMC m.l.e.s for α^{Θ}_{*} for each of the properties $* \in \{(\phi, f)\,[\times],\ (\phi|\phi, s)\,[\boxdot],\ (3_1|\phi, s)\,[\triangle],\ (4_1|\phi, s)\,[\odot]\}$ plotted versus $n_{\min}$. The error bars represent estimated 95% confidence intervals for $\alpha^{\Theta}_{(\phi,f)}$.

each of the properties $* \in \{(\phi, f),\ (\phi|\phi, s),\ (3_1|\phi, s)\}$ (that is the points plotted with the symbols $(\times)$, $(\boxdot)$, and $(\triangle)$ respectively) seem to be approaching each other, and seem to be approaching zero. The estimates $\hat{\varepsilon}_{(4_1|\phi,s)}(n_{\min}, \hat{N}_{\max}(4_1|\phi, s))$ seem to be approaching one. To explore this further, plots with error bars (estimated 95% confidence intervals) are investigated next.

Figure 5.8 plots the estimated 95% confidence intervals for ε_*, for each of the properties $* \in \{(\phi, f),\ (\phi|\phi, s),\ (3_1|\phi, s)\}$. Because each of the plotted confidence intervals contains 0.0 for every plotted $n_{\min} \geq 100$, the hypothesis that $\varepsilon_* = 0.0$, for each $* \in \{(\phi, f),\ (\phi|\phi, s),\ (3_1|\phi, s)\}$, cannot be rejected, that is the hypothesis that $\alpha^{\Theta}_{*} = \alpha^{\Theta}_{*}$ for each $* \in \{(\phi, f),\ (\phi|\phi, s),\ (3_1|\phi, s)\}$ cannot be rejected.

Figure 5.9 plots the estimated 95% confidence intervals for $\varepsilon_{(4_1|\phi,s)}$ as a function of $n_{\min}$. Because zero is included in each of the plotted 95% confidence intervals for $\varepsilon_{(4_1|\phi,s)}$ regardless of the value of $n_{\min}$, the possibility exists that $\varepsilon_{(4_1|\phi,s)} = 0$ and hence that

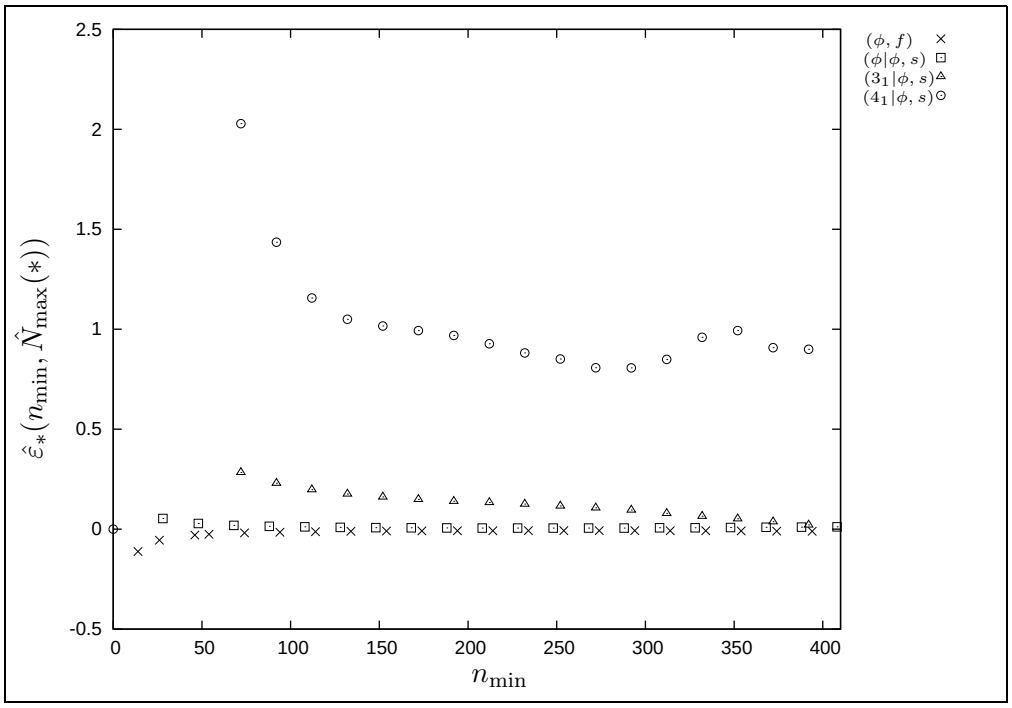

Figure 5.7: The CMC m.l.e.s for ε_* for each of the properties $* \in \{(\phi, f)\,[\times],\ (\phi|\phi, s)\,[\boxdot],\ (3_1|\phi, s)\,[\triangle],\ (4_1|\phi, s)\,[\odot]\}$ plotted versus $n_{\min}$.

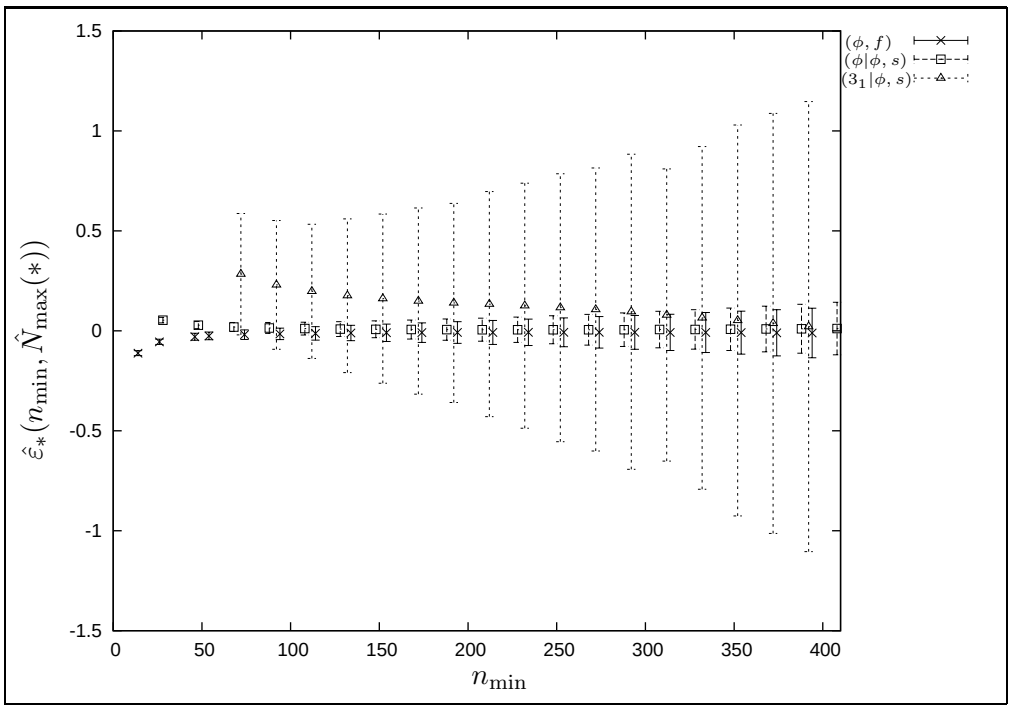

Figure 5.8: The CMC m.l.e.s for ε_* for each of the properties $* \in \{(\phi, f)\,[\times],\ (\phi|\phi, s)\,[\boxdot],\ (3_1|\phi, s)\,[\triangle]\}$ plotted versus $n_{\min}$. The error bars represent estimated 95% confidence intervals for ε_* for each of the properties $* \in \{(\phi, f),\ (\phi|\phi, s),\ (3_1|\phi, s)\}$.

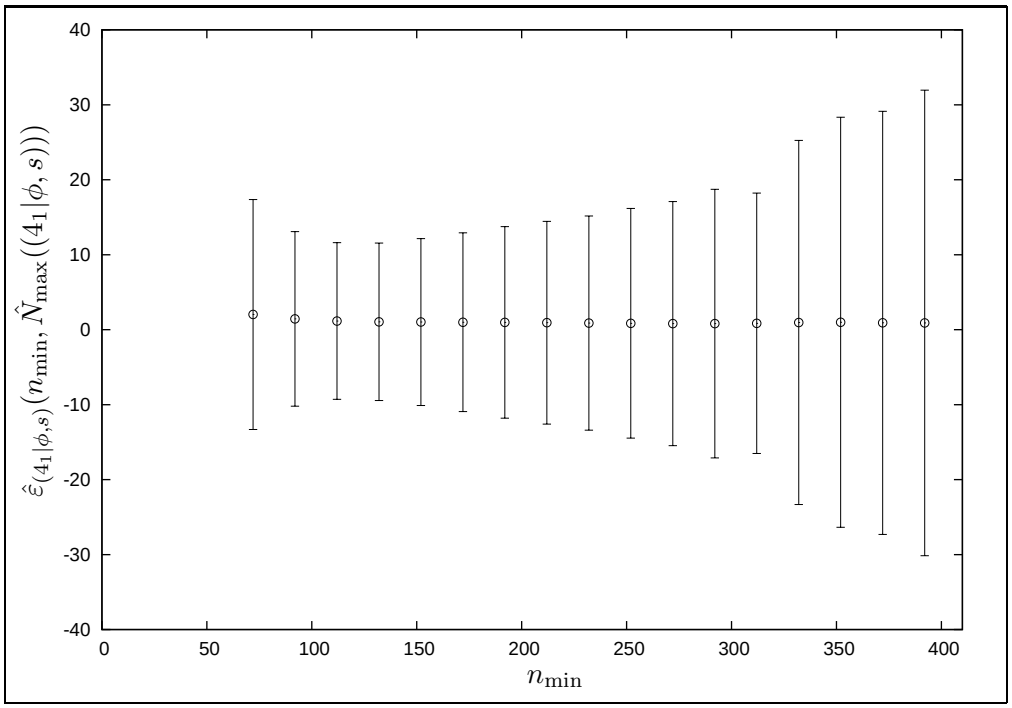

Figure 5.9: The CMC m.l.e.s for $\varepsilon_{(4_1|\phi,s)}$ plotted versus $n_{\min}$. The error bars represent estimated 95% confidence intervals for $\varepsilon_{(4_1|\phi,s)}$.

$\alpha^{\Theta}_{\overline{(4_1|\phi,s)}} = \alpha^{\Theta}_{(4_1|\phi,s)}$. Therefore the CMC m.l.e.s provide further support for Conjecture 2.2.9.

To be completely objective, based on the data plotted in Figure 5.9, the possibility exists that $\varepsilon_{(4_1|\phi,s)}$ is not zero. In particular, the estimates appear to be fluctuating around the value 1.0 for $n_{\min} \geq 130$. However, because the widths of the estimated 95% confidence intervals for $\varepsilon_{(4_1|\phi,s)}$ are so large (each is over 20 units in length) and the point estimates are approximately 1.0, it is concluded that more property-$(4_1|\phi,s)$ data needs to be generated to get a more accurate estimate for $\varepsilon_{(4_1|\phi,s)}$. With this in mind, note that the best existing CMC m.l.e.s for ε_*, for $* \in \Phi_{\text{mle}}$, are presented in Table 5.2.

For each $* \in \{(\phi,f),\ (\phi,s),\ (\phi|\phi,s),\ (3_1|\phi,s),\ (4_1|\phi,s)\}$, the CMC m.l.e.s for α^{Θ}_{*} and ε_* (as functions of $n_{\min}$ and fixed $\hat{N}_{\max}(*)$) can be combined using Equation (5.48) to obtain estimates for α^{Θ}_{*} (as functions of $n_{\min}$ and fixed $\hat{N}_{\max}(*)$) since

$$\alpha^{\Theta}_{*} = \alpha^{\Theta}_{*} - \varepsilon_*, \tag{5.136}$$

Figure 5.10 depicts the estimates for α^{Θ}_{*} (as functions of $n_{\min}$ and fixed $\hat{N}_{\max}(*)$), for each $* \in \Phi_{\text{mle}}$. For the purposes of creating a more meaningful graph, note that the only error bars (which correspond to an estimated 95% confidence interval) plotted in Figure 5.6 are

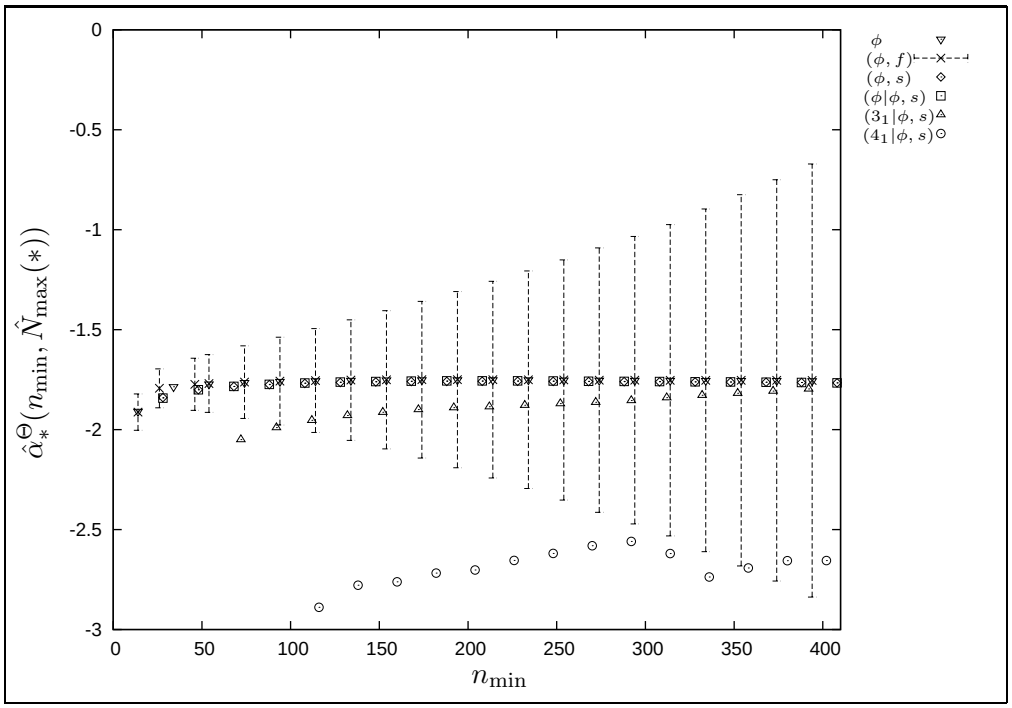

Figure 5.10: The CMC m.l.e.s for α^{Θ}_{*} for each of the properties $* \in \{\phi\,(\bigtriangledown),\ (\phi, f)\,[\times],\ (\phi, s)\,[\diamond],\ (\phi|\phi, s)\,[\boxdot],\ (3_1|\phi, s)\,[\bigtriangleup],\ (4_1|\phi, s)\,[\odot]\}$ plotted versus $n_{\min}$. The error bars represent estimated 95% confidence intervals for $\alpha^{\Theta}_{(\phi,f)}$.

those corresponding to the estimates $\hat{\alpha}^{\Theta}_{(\phi,f)}(n_{\min}, \hat{N}_{\max}(*))$.

From Figure 5.10, on the scale that the estimates are plotted, the estimates for α^{Θ}_{*}, for each $* \in \{\phi,\ (\phi, f),\ (\phi, s),\ (\phi|\phi, s)\}$ (the points plotted with the symbols $(\bigtriangledown)$, $(\times)$, $(\diamond)$, and $(\boxdot)$ respectively), appear to be the same value for all $n_{\min} \geq 140$. Further to this, as $n_{\min}$ increases, the estimates for $\alpha^{\Theta}_{(3_1|\phi,s)}$ (the points plotted with the symbol $(\bigtriangleup)$) are also approaching those estimates for α^{Θ}_{*} for $* \in \{\phi,\ (\phi, f),\ (\phi, s),\ (\phi|\phi, s)\}$. Hence the equalities

$$\alpha^{\Theta}_{\phi} = \alpha^{\Theta}_{(\phi,s)} = \alpha^{\Theta}_{(\phi,f)} = \alpha^{\Theta}_{(\phi|\phi,s)} = \alpha^{\Theta}_{(3_1|\phi,s)} \tag{5.137}$$

are supported numerically by the CMC m.l.e.s. The best CMC m.l.e.s for ε_{*}, for each $* \in \Phi_{\text{mle}}$, are presented in Table 5.2.

Table 5.2: The best CMC m.l.e.s for $\alpha_{\bar{*}}$, ϵ_* and α_* for each $* \in \Phi_{\text{mle}}$. The values in parentheses are the estimated 95% margins of error.

	Parameter Estimated				
Property $*$	$N^*_{\min}$	$N^*_{\max}$	$\alpha^{\Theta}_{\bar{*}}$ (95% ME)	ε_* (95% ME)	α^{Θ}_* (95% ME)
ϕ	156	3300	n/a	n/a	$-1.7521\,(0.0414)$
(ϕ, f)	142	3300	$-1.7619\,(0.0526)$	$-0.0104(0.0404)$	$-1.7516\,(0.0663)$
(ϕ, s)	156	3300	$-1.7508\,(0.0440)$	$0.0096(0.0440)$	$-1.7604\,(0.0623)$
$(\phi\|\phi, s)$	182	3300	$-1.7504\,(0.0529)$	$0.0061(0.0514)$	$-1.7565\,(0.0737)$
$(3_1\|\phi, s)$	408	2000	$-1.7800\,(0.2274)$	$0.0105(1.1918)$	$-1.7905\,(1.2117)$
$(4_1\|\phi, s)$	296	1200	$-1.7539\,(0.1819)$	$0.8352(18.6)$	$-2.8\,(18.7)$

Because the 95% confidence interval for $\alpha^{\Theta}_{(3_1|\phi,s)}$, as presented in Table 5.2, contains the 95% confidence intervals for $\alpha^{\Theta}_*, * \in \{\phi,\ (\phi, s),\ (\phi, f),\ (\phi|\phi, s)\}$, this provides further support for $\alpha^{\Theta}_{(3_1|\phi,s)} = \alpha^{\Theta}_*$, where $* \in \{\phi,\ (\phi, s),\ (\phi, f),\ (\phi|\phi, s)\}$. Similarly, because the 95% confidence interval for $\alpha^{\Theta}_{(4_1|\phi,s)}$, as presented in Table 5.2, contains the 95% confidence intervals for $\alpha^{\Theta}_*, * \in \{\phi,\ (\phi, s),\ (\phi, f),\ (\phi|\phi, s),\ (3_1|\phi, s)\}$, it is possible that $\alpha^{\Theta}_{(4_1|\phi,s)} = \alpha^{\Theta}_*$, where $* \in \{\phi,\ (\phi, s),\ (\phi, f),\ (\phi|\phi, s),\ (3_1|\phi, s)\}$. Hence the data supports that

$$\alpha^{\Theta}_{\phi} = \alpha^{\Theta}_{(\phi,s)} = \alpha^{\Theta}_{(\phi,f)} = \alpha^{\Theta}_{(\phi|\phi,s)} = \alpha^{\Theta}_{(3_1|\phi,s)} = \alpha^{\Theta}_{(4_1|\phi,s)} \tag{5.138}$$

which supports Conjecture 2.2.9, that is, for each $K \in \mathscr{K}^{\Theta}(\phi)$,

$$\alpha^{\Theta}_{\phi} = \alpha^{\Theta}_{(\phi,s)} = \alpha^{\Theta}_{(\phi,f)} = \alpha^{\Theta}_{(K|\phi,s)}. \tag{5.139}$$

Assuming that Conjecture 2.2.9 is true, because the largest amount of available data is for Θ-SAPs with property $* = \phi$, the best estimate of α^{Θ}_{ϕ} is taken to be

$$\alpha^{\Theta}_{\phi} = -1.7521 \pm 0.0414\,(\pm 0.02)\,, \tag{5.140}$$

where the above is of the form

$$\text{parameter} = \text{point estimate} \pm 95\%\ \text{ME}\ (\pm\text{systematic error}), \tag{5.141}$$

the estimated 95% margin of error is calculated using Theorem 5.1.4, and the systematic error was determined using the technique discussed in Section 5.5.

In order to determine if Conjecture 2.2.8 holds, that is whether $\alpha_\phi - 2 = \alpha_\phi^\Theta$ is supported numerically by the CMC Θ-BFACF data, recall that Orlandini *et al.* [125] estimated $\alpha_\phi \approx 0.23$. Using this value for α_ϕ, if Conjecture 2.2.8 is true, then $\alpha_\phi^\Theta = -1.77$. Since this value is contained in the estimated 95% confidence interval for α_ϕ^Θ given by Equation (5.140), Conjecture 2.2.8 is supported numerically.

The discussion now turns to the corrections to scaling terms h_* and $h_{\overline{*}}$. Recall from Section 1.3 that Orlandini *et al.* [125] proposed that $p_n(K)$ scales like

$$p_n(K) = A_K n^{\alpha_K - 3} \mu_K^n \left(1 + \frac{B_K}{n^{\Delta_K}} + \dots\right), \text{ for even } n, \tag{5.142}$$

where $\mu_K = e^{\kappa_K}$, α_K is the corresponding entropic critical exponent, and Δ_K is the exponent for the dominate correction due to scaling term. From the scaling form for $p_n(K)$ given by Equation (5.142), the first order correction term $\frac{B_K}{n^{\Delta_K}}$ is believed to be a function of the knot-type K because even though Δ_K is thought to be independent of knot-type [125], the coefficient B_K is believed to be dependent on knot-type. Because, in this work, it is similarly proposed that

$$p_n^\Theta(*) = A_*^\Theta n^{\alpha_*^\Theta} \mu_*^n \left(1 + \frac{B_*^\Theta}{n^{\Delta_*^\Theta}} + \dots\right), \text{ for even } n, \tag{5.143}$$

there is no reason to believe the first order correction term $\frac{B_*^\Theta}{n^{\Delta_*^\Theta}}$ is independent of the property $*$. If, for sufficiently large values of even n, $p_n^\Theta(*)$ can also be expressed as

$$p_n^\Theta(*) = A_*^\Theta \mu_*^n \left(n + h_*^\Theta\right)^{\alpha_*^\Theta} \tag{5.144}$$

$$= A_*^\Theta n^{\alpha_*^\Theta} \mu_*^n \left(1 + \frac{h_*^\Theta}{n}\right)^{\alpha_*^\Theta}, \tag{5.145}$$

then the first order term in the power series expansion of $\left(1 + \frac{h_*^\Theta}{n}\right)^{\alpha_*^\Theta}$ must be approximately $\frac{B_*^\Theta}{n^{\Delta_*^\Theta}}$. Hence there is no reason to expect h_* (and similarly $h_{\overline{*}}$) to be independent of the property $*$. The discussion turns to whether or not the estimates for h_* and $h_{\overline{*}}$ for $* \in \{\phi,\ (\phi, f),\ (\phi, s),\ (\phi|\phi, s),\ (3_1|\phi, s)\}$ support this hypothesis. Note that because there is the least amount of reliable data for property $(4_1|\phi, s)$ and in fact there is insufficient data to obtain a good estimate the critical exponent $\alpha_{(4_1|\phi,s)}^\Theta$, the estimates for $h_{(4_1|\phi,s)}$ and $h_{\overline{(4_1|\phi,s)},}$ are not used to investigate the dependence (or lack of dependence) of h_* (and similarly $h_{\overline{*}}$) on the property $*$.

Figures 5.11 and 5.12 display h_* and $h_{\overline{*}}$, the estimated first order corrections due to finite scaling defined by Equations (5.35) and (5.36) respectively, as a function of $n_{\min}$ as-

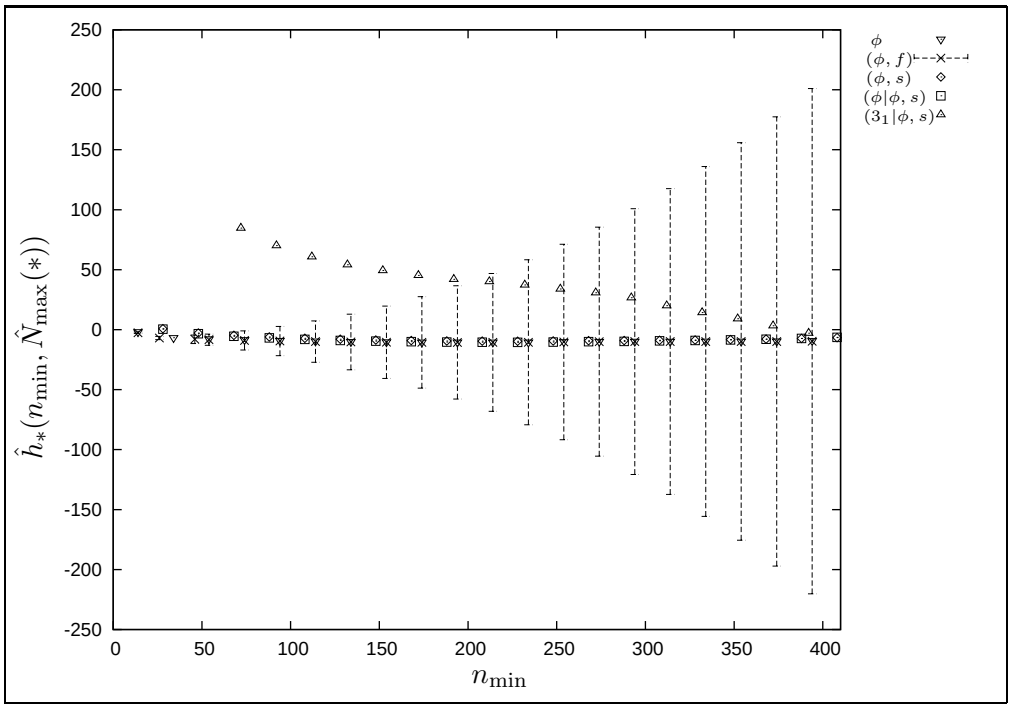

Figure 5.11: The CMC m.l.e.s for h_* for each of the properties $* \in \{\phi\,(\bigtriangledown), (\phi, f)\,[\times], (\phi, s)\,[\diamond], (\phi|\phi, s)\,[\boxdot], (3_1|\phi, s)\,[\bigtriangleup]\}$ plotted versus $n_{\min}$. The error bars represent estimated 95% confidence intervals for $h_{(\phi,f)}$.

sociated with properties $* \in \{\phi\ (\bigtriangledown)\,,\ (\phi, f)\ (\times)\,,\ (\phi, s)\ (\diamond)\,,\ (\phi|\phi, s)\ (\boxdot)\,,\ (3_1|\phi, s)\ (\bigtriangleup)\}$ and their corresponding complementary property $\overline{*}$. From Figures 5.11 and 5.12, note that as $n_{\min}$ increases, the estimates for h_* and $h_{\overline{*}}$ for the unknotted properties $\{\phi, (\phi, f), (\phi, s), (\phi|\phi, s)\}$ (that is the symbols $(\bigtriangledown)\,,\ (\times)\,,\ (\diamond)\,,$ and $(\boxdot)$ respectively) appear to be (at least on the scale of the figure) equal.

Table 5.3 displays the estimates for h_* and $h_{\overline{*}}$, for properties $* \in \Phi_{\text{mle}} \backslash \{(4_1|\phi, s)\}$ and $* \in \Phi_{\text{mle}} \backslash \{\phi, (4_1|\phi, s)\}$ respectively From the estimates for h_* and $h_{\overline{*}}$ in Table 5.3, it is interesting to note that there is considerable overlap of the 95% confidence intervals for h_* and $h_{\overline{*}}$ where $* \in \Phi_{\text{mle}}$. This suggests that the h_* and $h_{\overline{*}}$ may be independent of the property $* \in \Phi_{\text{mle}}$ until Figures 5.13 and 5.14 are considered. Figure 5.13 displays the same information as Figure 5.11 except Figure 5.13 does not include any error bars and it does not include the estimate for $h_{(3_1|\phi,s)}$. Figure 5.14 displays the same information as Figure 5.12 except Figure 5.14 does not include any error bars.

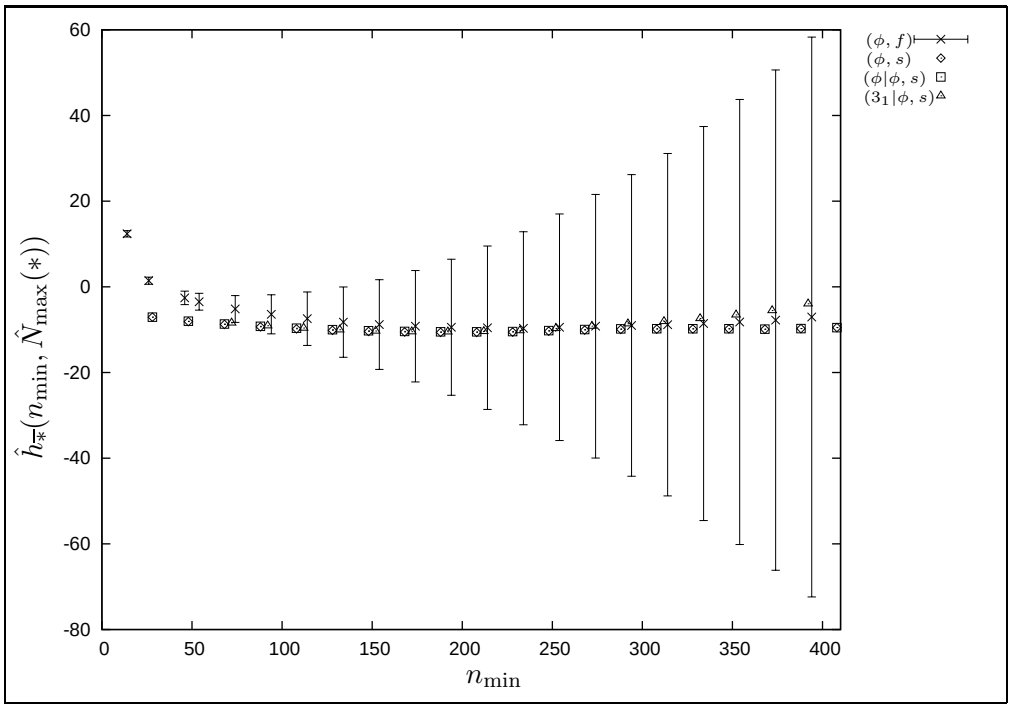

Figure 5.12: The CMC m.l.e.s for $h_{\overline{*}}$ for each of the properties $* \in \{(\phi, f)\,[\times], (\phi, s)\,[\diamond], (\phi|\phi, s)\,[\boxdot], (3_1|\phi, s)\,[\triangle]\}$ plotted versus $n_{\min}$. The error bars represent estimated 95% confidence intervals for $h_{\overline{(\phi,f)}}$.

Table 5.3: The best CMC m.l.e.s for h_* and $h_{\bar{*}}$ for each $* \in \Phi_{\text{mle}}$. The values in parentheses are the estimated 95% margins of error.

	Parameter Estimated			
Property $*$	$N^*_{\min}$	$N^*_{\max}$	h_* (95% ME)	$h_{\overline{*}}$ (95% ME)
ϕ	156	3300	$-10.3\,(5.9)$	n/a
(ϕ, f)	142	3300	$-10.3\,(5.4)$	$-8.5\,(9.1)$
(ϕ, s)	156	3300	$-8.7\,(10.7)$	$-10.5\,(6.4)$
$(\phi\|\phi, s)$	182	3300	$-10.3\,(14.2)$	$-10.5\,(8.7)$
$(3_1\|\phi, s)$	408	3300	$-6.8\,(506)$	$-2.5\,(59)$
$(4_1\|\phi, s)$	296	1200	$449\,(3158)$	$-9.8\,(13.1)$

Upon close examination of Figure 5.13, for every $n_{\min}$, the estimates plotted for $h_{(\phi,f)}$ are always strictly less than the estimates for h_* for each $* \in \{\phi, (\phi, s), (\phi|\phi, s)\}$. Because

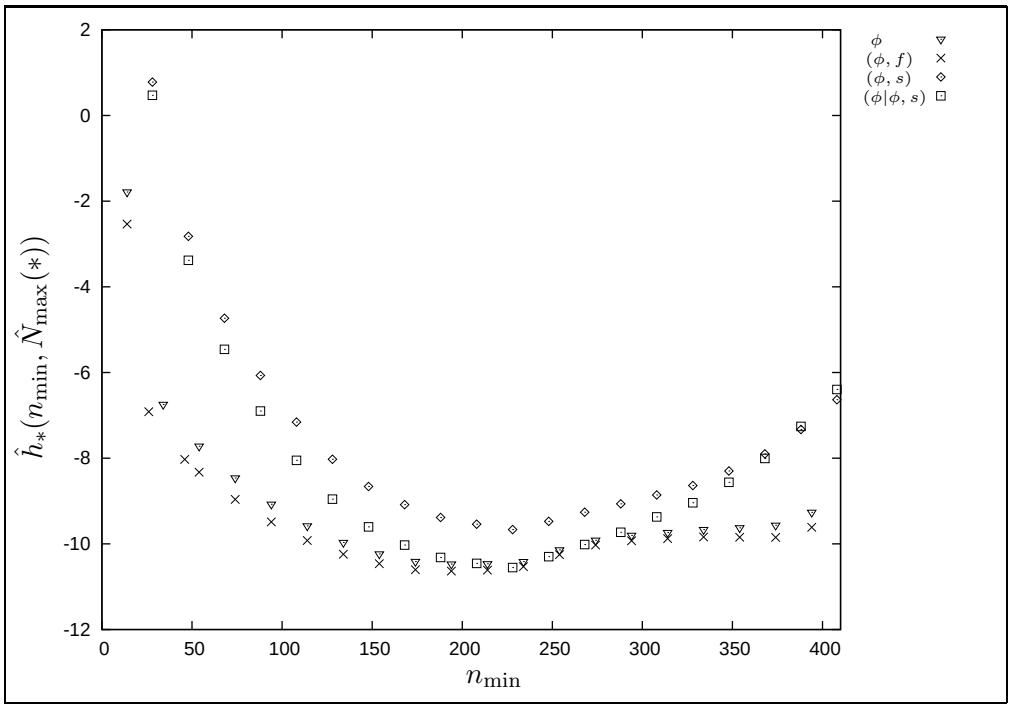

Figure 5.13: The CMC m.l.e.s for h_* for each of the properties $* \in \{\phi\,(\bigtriangledown), (\phi, f)\,[\times], (\phi, s)\,[\diamond], (\phi|\phi, s)\,[\boxdot]\}$ plotted versus $n_{\min}$.

for all $n_{\min}$,

$$\hat{h}_{(\phi,f)}(n_{\min}, \hat{N}_{\max}(\phi, f)) < \hat{h}_{(\phi|\phi,s)}(n_{\min}, \hat{N}_{\max}(\phi|\phi, s)) < \hat{h}_{(3_1|\phi,s)}(n_{\min}, \hat{N}_{\max}(3_1|\phi, s)), \tag{5.146}$$

h_* is seemingly dependent on the property $*$.

Upon close examination of Figure 5.14, for every $n_{\min}$, the estimates plotted for $h_{\overline{(\phi,f)}}$ are always strictly greater than the estimates for $h_{\overline{*}}$ for each $* \in \{(\phi, s),\ (\phi|\phi, s)\}$ and are always greater than the estimates for $h_{\overline{(3_1|\phi,s)}}$ for $n_{\min} \leq 260$. This suggests that $h_{\overline{(\phi,f)}}$ is larger than $h_{\overline{*}}$, for $* \in \{(\phi, s),\ (\phi|\phi, s),\ (3_1|\phi, s)\}$. Note that because the estimates for $h_{\overline{*}}$ for each $* \in \{(\phi, s),\ (\phi|\phi, s),\ (3_1|\phi, s)\}$ are all based on sets of polygons that contain $\mathscr{P}^{\Theta}(\phi, f)$, then the only major difference between how the estimates for $h_{\overline{(3_1|\phi,s)}}$ and the estimates for $h_{\overline{*}}$ for each $* \in \{(\phi, s),\ (\phi|\phi, s)\}$ are determined (beyond the actual property under study) is the value of $N_{\max}$. The drastic deviation of the estimates for $h_{\overline{(3_1|\phi,s)}}$ from the estimates for $h_{\overline{*}}$ for each $* \in \{(\phi, s),\ (\phi|\phi, s)\}$ and for all $n_{\min} \geq 250$ is thus likely a consequence of the different values of $N_{\max}$ used to compute the estimates. However, whether this behaviour is an actual property of the estimates for $h_{\overline{(3_1|\phi,s)}}$ or is a result of $\hat{N}_{\max}(3_1|\phi, s) = 2000 < 3300 = \hat{N}_{\max}(*)$, for $* \in \{(\phi, s),\ (\phi|\phi, s)\}$, is unknown. In order

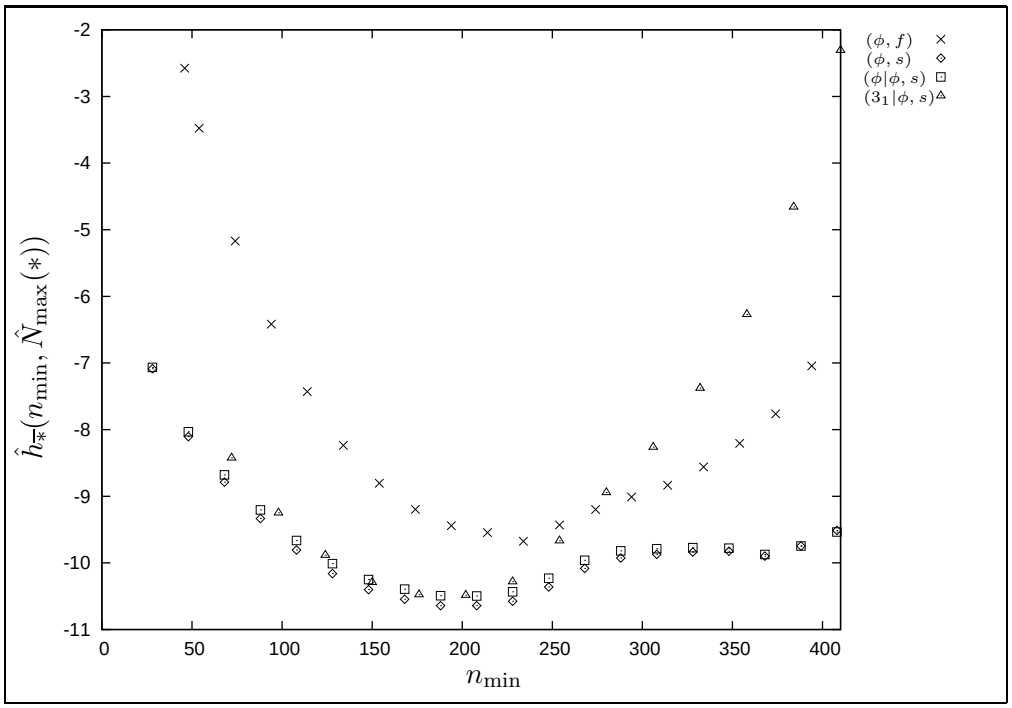

Figure 5.14: The CMC m.l.e.s for $h_{\overline{*}}$ for each of the properties $* \in \{(\phi, f)\,[\times],\ (\phi, s)\,[\diamond],\ (\phi|\phi, s)\,[\boxdot],\ (3_1|\phi, s)\,[\triangle]\}$ plotted versus $n_{\min}$.

to answer this question, further data is needed so that the estimate for $N_{\max}^{(3_1|\phi,s)}$ is at least 3300.

The displayed estimates for $h_{\overline{*}}$, $* \in \{(\phi, s),\ (\phi|\phi, s), (3_1|\phi, s)\}$, all exhibit the behaviour

$$\hat{h}_{\overline{(\phi,s)}}(n_{\min}, \hat{N}_{\max}(\phi, s)) < \hat{h}_{\overline{(\phi|\phi,s)}}(n_{\min}, \hat{N}_{\max}(\phi|\phi, s)) < \hat{h}_{\overline{(3_1|\phi,s)}}(n_{\min}, \hat{N}_{\max}(3_1|\phi, s)), \tag{5.147}$$

which also supports that $h_{\overline{*}}$ is dependent on the property $*$.

The conclusion here is that h_* and $h_{\overline{*}}$ are dependent on the property $*$.

5.7 In Summary

In this chapter, a new maximum likelihood technique is presented which computes maximum likelihood estimates from a realization of a composite Markov chain $((W_t(1), W_t(2), ..., W_t(M)), t = 0, ..., t_0)$ on state space $\mathscr{S}^M$ whose marginal equilibrium distribution for Chain i is characterized by the fugacity $z_i = e^{\beta_i}$ and is assumed to be

asymptotic (as $|\omega| \to \infty$) to

$$\begin{aligned}\pi_\omega(\boldsymbol{\theta}|*, \beta, N^*_{\min}, N^*_{\max}) \sim\ & I_{\langle 2\rangle}(|\omega|)\psi_* (\omega)\, \frac{A_* w(|\omega|)(|\omega| + h_*)^{\alpha_{\overline{*}} - \varepsilon_*} e^{(\kappa_s+\beta)|\omega|}}{Q(\beta)} \\ & + I_{\langle 2\rangle}(|\omega|)\,(1 - \psi_* (\omega))\, \frac{A_{\overline{*}} w(|\omega|)(|\omega| + h_{\overline{*}})^{\alpha_{\overline{*}}} e^{(\kappa_s+\beta)|\omega|}}{Q(\beta)} \\ & + I_{\langle 1\rangle}(|\omega|) \left[\sum_{n<N^*_{\min}} \frac{w(n) s_n e^{\beta n}}{Q(\beta)} \right] \\ & + I_{\langle 3\rangle}(|\omega|) \sum_{n>N^*_{\max}} \frac{w(n)\left[A_*(n + h_*)^{\alpha_{\overline{*}} - \varepsilon_*} + A_{\overline{*}}(n + h_{\overline{*}})^{\alpha_{\overline{*}}}\right] e^{(\kappa_s+\beta)n}}{Q(\beta)},\end{aligned} \tag{5.148}$$

where $\omega \in \mathscr{S}$ and $w(n) = (n-6)n^{q-1}$ for some fixed positive integer q. The details of this CMC Maximum Likelihood Technique can be found in Section 5.3.

Section 5.2 reviews Berretti and Sokal's technique [7] for determining how long a simulation must be run in order to attain a certain accuracy in the m.l.e.s from Markov chain data. Section 5.4 provides a method for estimating $N^*_{\min}$, the value for which the scaling form of $p^\Theta_n(*)$ holds for all $n \geq N^*_{\min}$, and consequently for determining the best CMC m.l.e.s. Section 5.5 then presents a technique for determining the error in using the best estimate as the estimate for the parameters of interest. Then in Section 5.6 the technique outlined in the chapter is used to analyze the data generated by the CMC Θ-BFACF algorithm.

Section 5.6 begins by using the data generated by the CMC Θ-BFACF algorithm to verify that the program written to implement the CMC Θ-BFACF algorithm and the program written to perform the CMC Maximum Likelihood Technique perform their functions correctly. In fact, by using the CMC m.l.e. estimates for A, κ^Θ_*, ε_*, $\alpha^\Theta_{\overline{*}}$, h_*, and $h_{\overline{*}}$, the expected relations: $\alpha^\Theta_{\overline{(\phi,f)}} = \alpha^\Theta_{(\phi,s)}$; $\alpha^\Theta_{\overline{(\phi,s)}} = \alpha^\Theta_{(\phi,f)}$; $h_{\overline{(\phi,f)}} = h_{(\phi,s)}$; and $h_{\overline{(\phi,s)}} = h_{(\phi,f)}$; and the facts that

$$\kappa^\Theta_\phi = \kappa^\Theta_{(\phi,s)} = \kappa^\Theta_{(\phi,f)} = \kappa_\phi = \kappa^\Theta_{(K|\phi,s)}, \tag{5.149}$$

were numerically estimates. Then the CMC m.l.e.s for $\alpha^\Theta_*, * \in \Phi_{\text{mle}}$, were presented and used to show that Conjectures 2.2.8 and 2.2.9 hold, that is that the critical exponents α^Θ_* are independent of the knot-type and that $\alpha^\Theta_\phi = \alpha_\phi - 2$. The section concludes with a discussion regarding the corrections due to scaling h_* and $h_{\overline{*}}$ and their dependence on property $*$. The conclusion from the current CMC estimates is that h_* and $h_{\overline{*}}$ both depend on the property $*$.

The best CMC m.l.e.s for κ_*^{Θ}, α_*^{Θ}, $\alpha_{\overline{*}}^{\Theta}$, h_*, $h_{\overline{*}}$, A, and $\tilde{Q}(\beta_i)$, for $1 \leq i \leq 14$, are summarized as follows. The best estimates for κ_ϕ, α_*^{Θ}, and $\alpha_{\overline{*}}^{\Theta}$ are

$$\begin{aligned} \kappa_\phi &= \kappa_\phi^{\Theta} = 1.544125 \pm 0.000028 \ \ (\pm 0.00005) \\ \alpha_*^{\Theta} &= \alpha_{\overline{*}}^{\Theta} = \alpha_\phi^{\Theta} = -1.7521 \pm 0.0414 \ \ (\pm 0.02)\,, \end{aligned} \tag{5.150}$$

where the above are of the form

$$\text{parameter} = \text{point estimate} \pm 95\% \text{ ME } (\pm\text{systematic error}), \tag{5.151}$$

the 95% margin of error is calculated using Theorem 5.1.4, and the systematic error was determined using the technique discussed in Section 5.5. The best estimates for h_* and $h_{\overline{*}}$ are given below in Table 5.4 which is a reproduction of Table 5.3.

Table 5.4: The best CMC m.l.e.s for h_* and $h_{\bar{*}}$ for each $* \in \Phi_{\text{mle}}$. The values in parentheses are the estimated 95% margins of error.

	Parameter Estimated			
Property $*$	$N^*_{\min}$	$N^*_{\max}$	h_* (95% ME)	$h_{\overline{*}}$ (95% ME)
ϕ	156	3300	$-10.3\,(5.9)$	No estimate
(ϕ, f)	142	3300	$-10.3\,(5.4)$	$-8.5\,(9.1)$
(ϕ, s)	156	3300	$-8.7\,(10.7)$	$-10.5\,(6.4)$
$(\phi\|\phi, s)$	182	3300	$-10.3\,(14.2)$	$-10.5\,(8.7)$
$(3_1\|\phi, s)$	408	3300	$-6.8\,(506)$	$-2.5\,(59)$
$(4_1\|\phi, s)$	296	1200	$449\,(3158)$	$-9.8\,(13.1)$

The best estimates for the amplitude ratios are given in Table 5.5.

Table 5.5: The best CMC m.l.e.s for the amplitude ratios. The values in parentheses are the estimated 95% margins of error.

	Parameter Estimated		
Property $*$	$N^*_{\min}$	$N^*_{\max}$	$\frac{A_*}{A_{\overline{*}}}$ (95% ME)
ϕ	156	3300	No estimate
(ϕ, f)	142	3300	5.8531 (1.6848)
(ϕ, s)	156	3300	0.1699 (0.0537)
$(\phi \vert \phi, s)$	182	3300	0.1611 (0.0514)
$(3_1 \vert \phi, s)$	408	2000	0.0032 (0.0290)
$(4_1 \vert \phi, s)$	296	1200	0.4930 (28.6)

The best estimates for $\tilde{Q}(\beta_i)$, for $1 \leq i \leq 14$, are provided in Tables 5.6 and 5.7.

Table 5.6: The best CMC m.l.e.s for $\tilde{Q}(\beta_i)$ for $* \in \{\phi, (\phi, f), (\phi, s)\}$. The values in parentheses are the estimated 95% margins of error.

	Property		
Chain i	ϕ	(ϕ, f)	(ϕ, s)
1	0.00102(0.34265)	0.00203(0.17169)	0.00102(0.14740)
2	0.00402(0.36336)	0.00700(0.15204)	0.00402(0.18564)
3	0.01565(0.24936)	0.02379(0.09006)	0.01565(0.13786)
4	0.05988(0.13460)	0.07960(0.04966)	0.05988(0.07372)
5	0.11615(0.09786)	0.14452(0.03688)	0.11615(0.05307)
6	0.16137(0.08350)	0.19426(0.03181)	0.16137(0.04504)
7	0.22365(0.07133)	0.26056(0.02747)	0.22365(0.03827)
8	0.30900(0.06103)	0.34847(0.02375)	0.30900(0.03256)
9	0.42508(0.05233)	0.46420(0.02058)	0.42508(0.02776)
10	0.54611(0.04638)	0.58139(0.01839)	0.54611(0.02450)
11	0.69648(0.04126)	0.72327(0.01649)	0.69648(0.02169)
12	0.78271(0.03901)	0.80311(0.01565)	0.78271(0.02046)
13	0.82811(0.03796)	0.84474(0.01526)	0.82811(0.01989)
14	0.87449(0.03698)	0.88700(0.01489)	0.87449(0.01936)

Table 5.7: The best CMC m.l.e.s for $\tilde{Q}(\beta_i)$ for $* \in \{(\phi|\phi,s),(3_1|\phi,s),(4_1|\phi,s)\}$. The values in parentheses are the estimated 95% margins of error.

	Property		
Chain i	$(\phi\|\phi,s)$	$(3_1\|\phi,s)$	$(4_1\|\phi,s)$
1	0.00028(0.08811)	0.00000(0.00033)	0.00001(0.00518)
2	0.00143(0.16144)	0.00000(0.00233)	0.00002(0.02082)
3	0.00718(0.22581)	0.00001(0.01483)	0.00023(0.08012)
4	0.03522(0.45092)	0.00033(0.09494)	0.00337(0.18600)
5	0.07729(0.66508)	0.00212(0.17413)	0.012721(0.18050)
6	0.11417(0.80783)	0.00535(0.17659)	0.024602(0.14644)
7	0.16817(0.98017)	0.01342(0.13359)	0.04738(0.10982)
8	0.24684(1.18735)	0.03347(0.08784)	0.090827(0.08024)
9	0.36057(1.43496)	0.08276(0.05621)	0.172893(0.05834)
10	0.48569(1.66538)	0.16924(0.03935)	0.287186(0.04530)
11	0.64886(1.92489)	0.34104(0.02772)	0.47145(0.03537)
12	0.74576(2.06361)	0.47918(0.02339)	0.59908(0.03138)
13	0.79772(2.13428)	0.56560(0.02153)	0.673037(0.02960)
14	0.85141(2.20493)	0.66472(0.01986)	0.753589(0.02798)

Chapter 6

Estimating the Probabilities Associated with Strand Passage

In this chapter, the fixed-n strand passage probabilities and the limiting strand passage probabilities associated with LSP Model that were introduced in Section 2.2.2 are estimated and used to explore the validity of Conjecture 2.2.3, that is to explore whether the limiting strand passage probabilities exist, whether their values are in the interval $(0,1)$, and, assuming the limiting probabilities exist, how the corresponding fixed-n probabilities (as $n \to \infty$) approach their limiting value. In order to investigate Conjecture 2.2.3, two methods (the *Fixed-n Method* and the *Grouped-n Method*) for estimating the limiting transition probabilities $\Pr^{\Theta}(\phi, s)$, $\Pr^{\Theta}(\phi, f)$, and $\Pr^{\Theta}(K|\phi, s)$ are presented and compared. The second method, which is concluded to be the better of the two methods, is then used to estimate $\Pr^{\Theta}(\phi, s)$, $\Pr^{\Theta}(\phi, f)$, and $\Pr^{\Theta}(K|\phi, s)$. These estimates are then used to investigate Conjecture 2.2.3.

Before the methods for estimating the fixed-n and the limiting strand passage probabilities can be presented, first recall from Section 2.2.2 that the fixed-n *probabilities associated with a strand passage about the structure* Θ *for* $K = \phi$ are respectively: the probability of a successful strand passage in a $(2n)$-edge Θ-SAP,

$$\Pr^{\Theta}_{2n}(\phi, s) := \frac{p^{\Theta}_{2n}(\phi, s)}{p^{\Theta}_{2n}(\phi)}; \tag{6.1}$$

the probability of an unsuccessful strand passage in a $(2n)$-edge Θ-SAP,

$$\Pr^{\Theta}_{2n}(\phi, f) := \frac{p^{\Theta}_{2n}(\phi, f)}{p^{\Theta}_{2n}(\phi)} = 1 - \Pr^{\Theta}_{2n}(\phi, s); \tag{6.2}$$

and, for each knot-type $K \in \mathscr{K}^{\Theta}(\phi)$, the probability of a $(2n)$-edge successful-strand-passage Θ-SAP having knot-type K after a strand passage,

$$\Pr^{\Theta}_{2n}(K|\phi, s) := \frac{p^{\Theta}_{2n}(K|\phi, s)}{p^{\Theta}_{2n}(\phi, s)}. \tag{6.3}$$

Also recall from Section 2.2.2 that the *limiting probabilities (if they exist) associated with a strand passage about the structure* Θ *for* $K = \phi$ are

$$\Pr^{\Theta}(\phi, s) := \lim_{n\to\infty} \Pr^{\Theta}_{2n}(\phi, s), \tag{6.4}$$

$$\Pr^{\Theta}(\phi, f) := \lim_{n\to\infty} \Pr^{\Theta}_{2n}(\phi, f) = 1 - \lim_{n\to\infty} \Pr^{\Theta}_{2n}(\phi, s), \tag{6.5}$$

and, for each knot-type $K \in \mathscr{K}^{\Theta}(\phi)$,

$$\Pr^{\Theta}(K|\phi, s) := \lim_{n\to\infty} \Pr^{\Theta}_{2n}(K|\phi, s). \tag{6.6}$$

The next section presents one method for estimating the limiting probabilities associated with the LSP Model is presented.

6.1 The Fixed-n Method Used to Estimate $\Pr^{\Theta}(*)$

If the conjectured forms for the fixed-n probabilities hold and the limiting probabilities $\Pr^{\Theta}(\phi, s)$, $\Pr^{\Theta}(\phi, f)$, and $\Pr^{\Theta}(K|\phi, s)$ exist, then, for sufficiently large n, plots of each of $\Pr^{\Theta}_{2n}(\phi, s), \Pr^{\Theta}_{2n}(\phi, f)$, and $\Pr^{\Theta}_{2n}(K|\phi, s)$ versus $2n$ will have the form

$$f(2n, a, b, \delta) = a + b(2n)^{-\delta} \tag{6.7}$$

where the constants a, b, and δ depend on the property $* \in \Phi$ and where the constant term a is the limiting strand passage probability $\Pr^{\Theta}(*)$, for $* \in \Phi$. Consequently one way to estimate $\Pr^{\Theta}(*)$, for $* \in \Phi$, is to estimate the constant a in Equation (6.7) by using each of the sequences of data $\{(2n, \Pr^{\Theta}_{2n}(*))\}, * \in \Phi$, for sufficiently many n's in the "Fixed-n Method for curve fitting" provided in Section A.5 of Appendix A. Thus estimating each of the limiting strand passage probabilities $\Pr^{\Theta}(*)$, $* \in \Phi$, via this approach, reduces to first computing $\Pr^{\Theta}_{n}(*)$.

Because computing $\Pr^{\Theta}_{2n}(*)$ appears to require the value of $p^{\Theta}_{2n}(*)$, a problem quickly arises. The values of $p^{\Theta}_{2n}(*)$ have not been enumerated for any value of n. However, this problem can be overcome, because the data generated from the CMC Θ-BFACF Algorithm discussed in Section 3.4 can be used to estimate the fixed-n probabilities $\Pr^{\Theta}_{2n}(*)$ without knowing $p^{\Theta}_{2n}(*)$. Then the "Fixed-n Method for curve fitting" can be used to fit an essentially independent sample of estimates for $\Pr^{\Theta}_{2n}(*)$ to Equation (6.7) to obtain estimates for a, b, and δ. Hence the "Fixed-n Method for estimating $\Pr^{\Theta}(*)$" requires estimating $\Pr^{\Theta}_{2n}(*)$ using CMC data.

6.2 Estimating $\Pr_{2n}^{\Theta}(*)$ Using CMC Θ-BFACF Data

Suppose $\boldsymbol{W} := \{(W_t(1), W_t(2), ..., W_t(14)), t = 0, ..., t_0\}$ is a CMC generated by the CMC Θ-BFACF Algorithm discussed in Section 3.4 and $\boldsymbol{\omega}^{(u)}$ is the u'th realization of $\boldsymbol{W}$, that is Replication u. The method for estimating $\Pr_{2n}^{\Theta}(*)$ will be presented for two different scenarios: via a single replication and via several replications. Before either of these two versions can be presented, some notation and definitions common to both versions must first be introduced.

Because ultimately the estimators for $\Pr_{2n}^{\Theta}(*)$ are ratio estimators, in order to determine $(1-\alpha)\cdot 100\%$ confidence intervals for $\Pr_{2n}^{\Theta}(*)$ using the theory in the Ratio Estimator Section (cf. Section A.3 of Appendix A), an i.i.d. sample of two-dimensional counters (X, Y) is required, where the count X is that required for the denominator and the count Y is needed for the numerator. One way to create this i.i.d. sample is to subdivide the t_0 time-steps as described in Section A.4. More specifically, define $X_{k,\cdot}$ and $Y_{k,\cdot}$ in Section A.4 as follows. For any $*_1, *_2 \in \Phi$, define

$$X_{k,\cdot}(*_1|2n, T) := \frac{1}{14}\sum_{i=1}^{14} Y_{k,i}(*_1|2n, T) \tag{6.8}$$

and

$$Y_{k,\cdot}(*_2|2n, T) := \frac{1}{14}\sum_{i=1}^{14} Y_{k,i}(*_2|2n, T), \tag{6.9}$$

where, for $* \in \Phi$.

$$Y_{k,i}(*|2n, T) := \sum_{t=0}^{t_0} \mathscr{M}_T(t)\mathscr{I}_{B(k)}(t)\, I_{2n}(|W_t(i)|)\ \psi_*(W_t(i)); \tag{6.10}$$

$$I_n(m) := \begin{cases} 1 & \text{if } m = n, \\ 0 & \text{otherwise;} \end{cases} \tag{6.11}$$

$B(k)$ is given by Equation (4.159); for each $\omega \in \mathscr{P}^{\Theta}(\phi)$ and $* \in \Phi$, $\psi_*(\omega)$ is given by Equation (4.166); and $\mathscr{M}_n(t)$ is given by Equation (4.42).

Then, for each natural number n, the sequence of two-tuples of counters

$$((X_{k,\cdot}(\phi|2n, T), Y_{k,\cdot}(\phi, s|2n, T)), k = 1, .., l) \tag{6.12}$$

and, for each $* \in \mathscr{K}^{\dagger}(\phi)$,

$$((X_{k,\cdot}(\phi, s|2n, T), Y_{k,\cdot}(*|2n, T)), k = 1, .., l), \tag{6.13}$$

can be used to form ratio estimators for $\Pr_{2n}^{\Theta}(*)$ (cf. Section A.3). Note that, for example, $Y_{k,\cdot}(\phi, s|2n, T)$ represents the number of $(2n)$-edge successful-strand-passage Θ-SAPs found across all fourteen chains in block k and $X_{k,\cdot}(\phi|2n, T)$ represents the number of $(2n)$-edge Θ-SAPs found across all fourteen chains in block k. Then the ratio $Y_{k,\cdot}(\phi, s|2n, T)/X_{k,\cdot}(\phi|2n, T)$ is the estimator for the probability of a successful strand passage in a $(2n)$-edge Θ-SAP in block k.

With these definitions and notations in hand, the two versions of the method for estimating $\Pr_{2n}^{\Theta}(*)$ are presented.

6.2.1 Scenario 1: Via a Single Replication

For a fixed natural number $n \geq 7$, in order to estimate $\Pr_{2n}^{\Theta}(*)$, an estimator (preferably unbiased) is required. To this end, let $\widehat{\Pr}_{2n}^{\Theta}(\phi, s)$ be the estimator (as defined by Equation (A.21) in Section A.4 of Appendix A) for $\Pr_{2n}^{\Theta}(\phi, s)$ using the sequence

$$((X_{k,\cdot}(\phi|2n, T), Y_{k,\cdot}(\phi, s|2n, T)), k = 1, .., l) \tag{6.14}$$

with $X_{k,\cdot}(\phi|2n, T)$ and $Y_{k,\cdot}(\phi, s|2n, T)$ defined respectively by Equations (6.8) and (6.9). Similarly, for each after-strand-passage property $* \in \mathscr{K}^{\dagger}(\phi)$, let $\widehat{\Pr}_{2n}^{\Theta}(*)$ be the estimator (as defined by Equation (A.21) in Section A.4 of Appendix A) for $\Pr_{2n}^{\Theta}(*)$ using the sequence

$$((X_{k,\cdot}(\phi, s|2n, T), Y_{k,\cdot}(*|2n, T)), k = 1, .., l) \tag{6.15}$$

with $X_{k,\cdot}(\phi, s|2n, T)$ and $Y_{k,\cdot}(*|2n, T)$ defined respectively by Equations (6.8) and (6.9). Also define

$$\widehat{\Pr}_{2n}^{\Theta}(\phi, f) = 1 - \widehat{\Pr}_{2n}^{\Theta}(\phi, s). \tag{6.16}$$

Theorem A.3.2 from Section A.3 of Appendix A implies that $\widehat{\Pr}_{2n}^{\Theta}(\phi, s)$, $\widehat{\Pr}_{2n}^{\Theta}(\phi, f)$, and $\widehat{\Pr}_{2n}^{\Theta}(*)$, for $* \in \mathscr{K}^{\dagger}(\phi)$, are respectively asymptotically (as $l \to \infty$) unbiased estimators for $\Pr_{2n}^{\Theta}(\phi, s)$, $\Pr_{2n}^{\Theta}(\phi, f)$, and $\Pr_{2n}^{\Theta}(*)$, $* \in \mathscr{K}^{\dagger}(\phi)$.

Now, for $*_1, *_2 \in \Phi$, let $x_{k,\cdot}^{(u)}(*_1|2n, T)$ and $y_{k,\cdot}^{(u)}(*_2|2n, T)$ respectively denote the realizations of $X_{k,\cdot}(*_1|2n, T)$ and $Y_{k,\cdot}(*_2|2n, T)$ based on sampling every T time-steps from $\boldsymbol{\omega}^{(u)}$. When $X_{k,\cdot}(*_1|2n, T)$ and $Y_{k,\cdot}(*_2|2n, T)$ in Sequences (6.14) and (6.15) are replaced by the realized sample from a single replication (say Replication u) with $t_0 = 9.6 \times 10^{10}$ time steps, $\tau_{\text{int}} = 0.72 \times 10^9$ time steps, $T = 1200$ time steps, and $l := 66$, the notation $\widehat{\text{pr}}_{2n}^{\Theta}((\phi, s), u)$,

$\widehat{\mathrm{pr}}_{2n}^{\Theta}((\phi,f),u)$, and $\widehat{\mathrm{pr}}_{2n}^{\Theta}(*,u)$, $*\in\mathscr{K}^{\dagger}(\phi)$, is used to denote the values corresponding to the estimators $\widehat{\mathrm{Pr}}_{2n}^{\Theta}(\phi,s)$, $\widehat{\mathrm{Pr}}_{2n}^{\Theta}(\phi,f)$, and $\widehat{\mathrm{Pr}}_{2n}^{\Theta}(*)$, $*\in\mathscr{K}^{\dagger}(\phi)$, respectively.

6.2.2 Scenario 2: Via Several Independent Replications

Suppose instead of using only one realization of $\boldsymbol{W}$, n_0 realizations of $\boldsymbol{W}$ are used in the analysis. Then, for each even $n\in\mathbb{N}$, with $n_0:=10$, $t_0=9.6\times10^{10}$ time steps, $\tau_{\mathrm{int}}=0.72\times10^{9}$ time steps, $T=1200$ time steps, and $l:=66$, for each natural number $n\geq7$, let $\widetilde{\mathrm{pr}}_{2n}^{\Theta}(\phi,s)$ be the point estimate for $\mathrm{Pr}_{2n}^{\Theta}(\phi,s)$ determined using the sequence

$$\left(\left(\left(x_{k,\cdot}^{(u)}(\phi|2n,T),y_{k,\cdot}^{(u)}(\phi,s|2n,T)\right),k=1,..,l\right),u=1,...,n_0\right) \tag{6.17}$$

in Equation (A.21) in Section A.4 of Appendix A; for each $*\in\mathscr{K}^{\dagger}(\phi)$, let $\widetilde{\mathrm{pr}}_{2n}^{\Theta}(*)$ be the point estimate for $\mathrm{Pr}_{2n}^{\Theta}(*)$ determined using the sequence

$$\left(\left(\left(x_{k,\cdot}^{(u)}(\phi,s|2n,T),y_{k,\cdot}^{(u)}(*|2n,T)\right),k=1,..,l\right),u=1,...,n_0\right) \tag{6.18}$$

in Equation (A.21) in Section A.4 of Appendix A; and let $\widetilde{\mathrm{pr}}_{2n}^{\Theta}(\phi,f):=1-\widetilde{\mathrm{pr}}_{2n}^{\Theta}(\phi,s)$ be the point estimate for $\mathrm{Pr}_{2n}^{\Theta}(\phi,f)$. Note that $\widetilde{\mathrm{pr}}_{2n}^{\Theta}(\phi,s)$, $\widetilde{\mathrm{pr}}_{2n}^{\Theta}(\phi,f)$, and $\widetilde{\mathrm{pr}}_{2n}^{\Theta}(*)$, $*\in\mathscr{K}^{\dagger}(\phi)$, are respectively the fixed-n point estimates for $\mathrm{Pr}_{2n}^{\Theta}(\phi,s)$, $\mathrm{Pr}_{2n}^{\Theta}(\phi,f)$, and $\mathrm{Pr}_{2n}^{\Theta}(*)$, $*\in\mathscr{K}^{\dagger}(\phi)$, based on n_0 independent replications. Note that if $n_0=1$ (that is there is only one replication), the two scenarios yield the same point estimates. Therefore in the following discussion of the two scenarios, it is assumed that $n_0>1$.

6.2.3 Discussion of the Two Scenarios

Figure 6.1 consists of the plots of the sequences of data: $\left(\left(2n,\widehat{\mathrm{pr}}_{2n}^{\Theta}((3_1|\phi,s),1)\right)\right)_{n=0}^{2000}$ (Line A: dashed line) and $\left(\left(2n,\widetilde{\mathrm{pr}}_{2n}^{\Theta}(3_1|\phi,s)\right)\right)_{n=0}^{2000}$ (Line B: solid line). The estimates $\widehat{\mathrm{pr}}_{2n}^{\Theta}((3_1|\phi,s),1)$ in the first sequence are determined from Replication 1 using "Scenario 1: Via a Single Replication", and the estimates $\widetilde{\mathrm{pr}}_{2n}^{\Theta}(3_1|\phi,s)$ in the second sequence are determined using "Scenario 2: Via Several Independent Replications" with all ten replications.

Because the data that was used to calculate the first sequence of estimates was generated using the CMC Θ-BFACF Algorithm, polygons generated, whose lengths are $2n$ and $2n+2$, respectively, are correlated. Hence the estimates $\widehat{\mathrm{pr}}_{2n}^{\Theta}((3_1|\phi,s),1)$ and $\widehat{\mathrm{pr}}_{2n+2}^{\Theta}((3_1|\phi,s),1)$ will also be correlated. In fact, recall from Section 3.1 that for polygons generated using

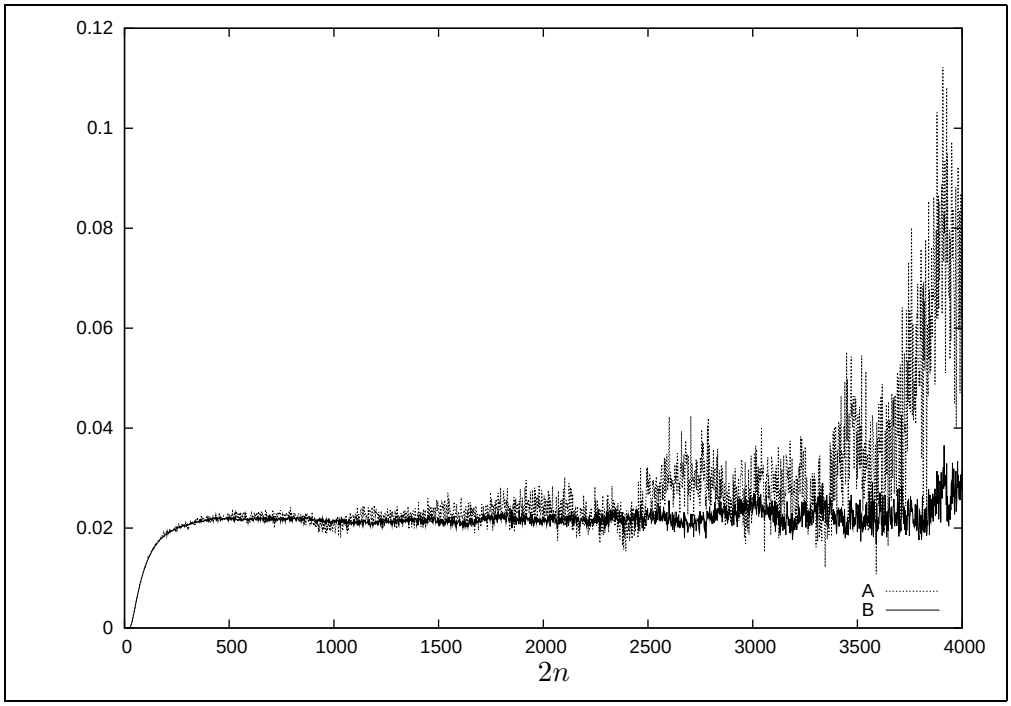

Figure 6.1: Line A: The estimated probabilities $\widehat{\mathrm{pr}}_{2n}^{\Theta}((3_1|\phi, s), 1)$. Line B: The estimated probabilities $\widetilde{\mathrm{pr}}_{2n}^{\Theta}(3_1|\phi, s)$. The estimates $\widehat{\mathrm{pr}}_{2n}^{\Theta}((3_1|\phi, s), 1)$ are determined using the data generated from Replication 1 and the estimates $\widetilde{\mathrm{pr}}_{2n}^{\Theta}(3_1|\phi, s)$ are determined using the data from all ten independent replications.

the BFACF Algorithm, as the polygon length increases, the time between two generated polygons being "essentially independent" also increases. Therefore the estimates $\widehat{\mathrm{pr}}_{2n}^{\Theta}((3_1|\phi,s),\cdot)$ and $\widehat{\mathrm{pr}}_{2n+2}^{\Theta}((3_1|\phi,s),\cdot)$, regardless of which replication is used, are expected to be more and more correlated as the polygon length $2n$ increases. The relationship between $\widehat{\mathrm{pr}}_{2n}^{\Theta}((3_1|\phi,s),\cdot)$ and $\widehat{\mathrm{pr}}_{2n+2l}^{\Theta}((3_1|\phi,s),\cdot)$ can be seen in Figure 6.1. Specifically, the dependence that exists between $\widehat{\mathrm{pr}}_{2n}^{\Theta}((3_1|\phi,s),\cdot)$ and $\widehat{\mathrm{pr}}_{2n+2}^{\Theta}((3_1|\phi,s),\cdot)$ manifests in Figure 6.1 as the oscillating trend that is present in the estimates $\widehat{\mathrm{pr}}_{2n}^{\Theta}((3_1|\phi,s),1)$ as $2n$ increases. This oscillating trend becomes more and more dramatic as $2n$ increases. Note that the estimates $\widehat{\mathrm{pr}}_{2n}^{\Theta}((\phi,s),\cdot)$ and $\widehat{\mathrm{pr}}_{2n+2}^{\Theta}((\phi,s),\cdot)$ (and likewise $\widehat{\mathrm{pr}}_{2n}^{\Theta}((K|\phi,s),\cdot)$ and $\widehat{\mathrm{pr}}_{2n+2}^{\Theta}((K|\phi,s),\cdot)$ for each unknotting number one knot-type K) are also expected to exhibit the same property. In order to reduce the impact of this oscillating trend on the estimates for $\mathrm{Pr}_{2n}(3_1|\phi,s)$, the estimates $\widetilde{\mathrm{pr}}_{2n}^{\Theta}(3_1|\phi,s)$ were computed using "Scenario 2: Via Several Independent Replications".

Regarding Figure 6.1, as the polygon length $2n$ increases, although for any given $2n$, the deviation $\left|\widetilde{\mathrm{pr}}_{2n}^{\Theta}(3_1|\phi,s)-\widetilde{\mathrm{pr}}_{2(n+1)}^{\Theta}(3_1|\phi,s)\right|$ is not as great as the deviation $\left|\widehat{\mathrm{pr}}_{2n}^{\Theta}((3_1|\phi,s),1)-\widehat{\mathrm{pr}}_{2n+2}^{\Theta}((3_1|\phi,s),1)\right|$, the estimates $\widetilde{\mathrm{pr}}_{2n}^{\Theta}(3_1|\phi,s)$ still exhibit a general oscillating trend as a function of $2n$. This suggests that, even after data from ten independent replications is combined to estimate $\mathrm{Pr}_{2n}^{\Theta}(\phi,s)$, some relationship still exists between $\widetilde{\mathrm{pr}}_{2n}^{\Theta}(3_1|\phi,s)$ and $\widetilde{\mathrm{pr}}_{2n+2l}^{\Theta}(3_1|\phi,s)$ for integer values of $l>0$ that are relatively small. Consequently it is concluded that ten replications are not sufficient to remove the correlation that exists between the estimates $\widetilde{\mathrm{pr}}_{2n}^{\Theta}(3_1|\phi,s)$ and $\widetilde{\mathrm{pr}}_{2(n+1)}^{\Theta}(3_1|\phi,s)$ for even relatively small values of n. The question then becomes, "How many replications are required so that the estimates $\widetilde{\mathrm{pr}}_{2n}^{\Theta}(3_1|\phi,s)$ and $\widetilde{\mathrm{pr}}_{2(n+1)}^{\Theta}(3_1|\phi,s)$ are essentially independent?".

To determine the number of replications that must be used to ensure that the point estimates $\widetilde{\mathrm{pr}}_{2n}^{\Theta}(3_1|\phi,s)$ and $\widetilde{\mathrm{pr}}_{2(n+1)}^{\Theta}(3_1|\phi,s)$ are essentially independent, consider the following. Starting from the equilibrium distribution, the goal is to obtain an estimate for the standard deviation which is within $\varepsilon>0$ of the population standard deviation. In this situation, using J replications only reduces the standard error associated with the point estimate by a factor of $\sqrt{J}$, and in order to reduce the estimated standard error associated with $\widehat{\mathrm{Pr}}_{n}^{\Theta}(3_1|\phi,s)$ by a factor of 10, 100 replications would be required. If the standard error based on a single replication is of the order 10^0, 100 replications would effectively reduce the estimated standard error by a factor of 10, that is an estimated stan-

dard error of the order 10^{-1} is expected. In the property-$(3_1|\phi, s)$ case, since the point estimate is of the order 10^{-2}, 100 replications would still produce a point estimate whose estimated standard error is approximately 10 times the point estimate. Hence continually increasing the number of replications to reduce the correlation between $\widetilde{\mathrm{pr}}^{\Theta}_{2n}(3_1|\phi, s)$ and $\widetilde{\mathrm{pr}}^{\Theta}_{2n+2}(3_1|\phi, s)$ is not an efficient method for estimating $\mathrm{Pr}^{\Theta}_{2n}(3_1|\phi, s)$. Because the estimates $\widetilde{\mathrm{pr}}^{\Theta}_{2n}(\phi, s)$, $\widetilde{\mathrm{pr}}^{\Theta}_{2n}(\phi, f)$, and $\widetilde{\mathrm{pr}}^{\Theta}_{2n}(K|\phi, s)$ (as a function of n) are expected to follow a similar trend to the estimates $\widetilde{\mathrm{pr}}^{\Theta}_{2n}(3_1|\phi, s)$ (as a function of n), continually increasing the number of replications is also not an efficient method for reducing the correlation between the point estimates $\widetilde{\mathrm{pr}}^{\Theta}_{2n}(\phi, s)$ and $\widetilde{\mathrm{pr}}^{\Theta}_{2n+2}(\phi, s)$, $\widetilde{\mathrm{pr}}^{\Theta}_{2n}(\phi, f)$ and $\widetilde{\mathrm{pr}}^{\Theta}_{2n+2}(\phi, f)$, and $\widetilde{\mathrm{pr}}^{\Theta}_{2n}(*)$ and $\widetilde{\mathrm{pr}}^{\Theta}_{2n+2}(*), * \in \mathscr{K}^{\dagger}(\phi)$. The method presented next, referred to as the Grouped-n Method for Estimating $\mathrm{Pr}^{\Theta}(*)$, is designed to minimize the effects of any correlation that exists between $\widetilde{\mathrm{pr}}^{\Theta}_{2n}(*)$ and $\widetilde{\mathrm{pr}}^{\Theta}_{2n+2}(*), * \in \mathscr{K}^{\dagger}(\phi) \cup \{(\phi, f), (\phi, s)\}$. The Grouped-$n$ Method for estimating $\mathrm{Pr}^{\Theta}(*)$ is discussed next.

6.3 The Grouped-n Method for Estimating $\mathrm{Pr}^{\Theta}(*)$

The Grouped-n Method for Estimating $\mathrm{Pr}^{\Theta}(*)$ allows all the generated data (not just the data in $H^{\Theta}_1(*)$, the essentially independent sample from the Fixed-n Method) to be used. To this end, for positive even values n_1 and n_2, such that $n_2 > n_1$, define the length $[n_1, n_2]$-grouped probabilities

$$\mathrm{Pr}^{\Theta}_{n_1,n_2}(\phi, s) := \frac{\sum_{n=n_1}^{n_2} \left[p_n^{\Theta}(\phi, s) \sum_{i=1}^{M} \frac{w(n) e^{\beta_i n}}{\breve{Q}(\beta_i)} \right]}{\sum_{n=n_1}^{n_2} \left[p_n^{\Theta}(\phi) \sum_{i=1}^{M} \frac{w(n) e^{\beta_i n}}{\breve{Q}(\beta_i)} \right]}, \tag{6.19}$$

$$\mathrm{Pr}^{\Theta}_{n_1,n_2}(\phi, f) := \frac{\sum_{n=n_1}^{n_2} \left[p_n^{\Theta}(\phi, f) \sum_{i=1}^{M} \frac{w(n) e^{\beta_i n}}{\breve{Q}(\beta_i)} \right]}{\sum_{n=n_1}^{n_2} \left[p_n^{\Theta}(\phi) \sum_{i=1}^{M} \frac{w(n) e^{\beta_i n}}{\breve{Q}(\beta_i)} \right]}, \tag{6.20}$$

and, for $* \in \mathscr{K}^{\dagger}(\phi)$,

$$\mathrm{Pr}^{\Theta}_{n_1,n_2}(*) := \frac{\sum_{n=n_1}^{n_2} \left[p_n^{\Theta}(*) \sum_{i=1}^{M} \frac{w(n) e^{\beta_i n}}{\breve{Q}(\beta_i)} \right]}{\sum_{n=n_1}^{n_2} \left[p_n^{\Theta}(\phi, s) \sum_{i=1}^{M} \frac{w(n) e^{\beta_i n}}{\breve{Q}(\beta_i)} \right]}, \tag{6.21}$$

where each sum is taken through even values of n. Then $\mathrm{Pr}^{\Theta}_{n_1,n_2}(\phi, s)$ is the probability of observing a successful-strand-passage Θ-SAP given that the Θ-SAP has length in $[n_1, n_2]$;

$\Pr^{\Theta}_{n_1,n_2}(\phi, f)$ is the probability of observing an unsuccessful-strand-passage Θ-SAP given that the Θ-SAP has length in $[n_1, n_2]$; and $\Pr^{\Theta}_{n_1,n_2}(*)$, for $* \in \mathscr{K}^{\dagger}(\phi)$, is the probability of observing a property-$*$ Θ-SAP given a successful-strand-passage Θ-SAP whose length is in $[n_1, n_2]$. An interesting question regarding the $[n_1, n_2]$-grouped probabilities $\Pr^{\Theta}_{n_1,n_2}(*)$, for $* \in \Phi \backslash \{\phi\}$ is "How does $\Pr^{\Theta}_{n_1,n_2}(*)$ behave as $n_1 \to \infty$?".

In order to determine the $n_1 \to \infty$ scaling form for $\Pr^{\Theta}_{n_1,n_2}(\phi, s)$, consider the following:

$$\Pr^{\Theta}_{n_1,n_2}(\phi, s) := \frac{\sum_{n=n_1}^{n_2} \left[p^{\Theta}_n(\phi, s) \sum_{i=1}^{M} \frac{w(n) e^{\beta_i n}}{\breve{Q}(\beta_i)} \right]}{\sum_{n=n_1}^{n_2} \left[p^{\Theta}_n(\phi) \sum_{i=1}^{M} \frac{w(n) e^{\beta_i n}}{\breve{Q}(\beta_i)} \right]} \tag{6.22}$$

$$= \frac{p^{\Theta}_{n_1}(\phi, s)}{p^{\Theta}_n(\phi)} \frac{\sum_{n=n_1}^{n_2} \left[\frac{p^{\Theta}_n(\phi, s)}{p^{\Theta}_{n_1}(\phi, s)} \sum_{i=1}^{M} \frac{w(n) e^{\beta_i n}}{\breve{Q}(\beta_i)} \right]}{\sum_{n=n_1}^{n_2} \left[\frac{p^{\Theta}_n(\phi)}{p^{\Theta}_{n_1}(\phi)} \sum_{i=1}^{M} \frac{w(n) e^{\beta_i n}}{\breve{Q}(\beta_i)} \right]}. \tag{6.23}$$

Substituting the believed scaling form for $p^{\Theta}_n(\phi, s)$ and $p^{\Theta}_n(\phi)$, as given by Equation (2.86), into the above equation yields the following scaling form as $n_1 \to \infty$:

$$\Pr^{\Theta}_{n_1,n_2}(\phi, s) \sim \frac{p^{\Theta}_{n_1}(\phi, s)}{p^{\Theta}_{n_1}(\phi)} \frac{\sum_{n=n_1}^{n_2} \left[\frac{n^{\alpha^{\Theta}_{(\phi,s)}+q} e^{\kappa_\phi n} \left(1 + \frac{B^{\Theta}_{(\phi,s)}}{n^{\Delta^{\Theta}_{(\phi,s)}}} \right)}{n_1^{\alpha^{\Theta}_{(\phi,s)}+q} e^{\kappa_\phi n_1} \left(1 + \frac{B^{\Theta}_{(\phi,s)}}{n_1^{\Delta^{\Theta}_{(\phi,s)}}} \right)} \sum_{i=1}^{M} \frac{w(n) e^{\beta_i n}}{\breve{Q}(\beta_i)} \right]}{\sum_{n=n_1}^{n_2} \left[\frac{n^{\alpha^{\Theta}_{\phi}+q} e^{\kappa_\phi n} \left(1 + \frac{B^{\Theta}_{\phi}}{n^{\Delta^{\Theta}_{\phi}}} + ... \right)}{n_1^{\alpha^{\Theta}_{\phi}+q} e^{\kappa_\phi n_1} \left(1 + \frac{B^{\Theta}_{\phi}}{n_1^{\Delta^{\Theta}_{\phi}}} + ... \right)} \sum_{i=1}^{M} \frac{w(n) e^{\beta_i n}}{\breve{Q}(\beta_i)} \right]}. \tag{6.24}$$

Assuming $\alpha^{\Theta}_{\phi} = \alpha^{\Theta}_{(\phi,s)}$ then the scaling form, as given by Equation (6.24), can be reduced as follows:

$$\Pr^{\Theta}_{n_1,n_2}(\phi, s) \sim \frac{p^{\Theta}_{n_1}(\phi, s)}{p^{\Theta}_{n_1}(\phi)} \frac{\left(1 + \frac{B^{\Theta}_{\phi}}{n_1^{\Delta^{\Theta}_{\phi}}} + ... \right)}{\left(1 + \frac{B^{\Theta}_{(\phi,s)}}{n_1^{\Delta^{\Theta}_{(\phi,s)}}} + ... \right)} \times$$
$$\frac{\sum_{n=n_1}^{n_2} \left[n^{\alpha^{\Theta}_{\phi}+q} e^{\kappa_\phi n} \left(1 + \frac{B^{\Theta}_{(\phi,s)}}{n^{\Delta^{\Theta}_{(\phi,s)}}} + ... \right) \sum_{i=1}^{M} \frac{w(n) e^{\beta_i n}}{\breve{Q}(\beta_i)} \right]}{\sum_{n=n_1}^{n_2} \left[n^{\alpha^{\Theta}_{\phi}+q} e^{\kappa_\phi n} \left(1 + \frac{B^{\Theta}_{\phi}}{n^{\Delta^{\Theta}_{\phi}}} + ... \right) \sum_{i=1}^{M} \frac{w(n) e^{\beta_i n}}{\breve{Q}(\beta_i)} \right]}. \tag{6.25}$$

To first order, the scaling form for $\Pr^{\Theta}_{n_1,n_2}(\phi,s)$, as $n_1 \to \infty$, is therefore

$$\Pr^{\Theta}_{n_1,n_2}(\phi,s) \sim \frac{p^{\Theta}_{n_1}(\phi,s)}{p^{\Theta}_{n_1}(\phi)} \frac{\left(1+\frac{B^{\Theta}_{\phi}}{n_1^{\Delta^{\Theta}_{\phi}}}\right)}{\left(1+\frac{B^{\Theta}_{(\phi,s)}}{n_1^{\Delta^{\Theta}_{(\phi,s)}}}\right)} \times \left[\frac{\sum_{n=n_1}^{n_2} \left[n^{\alpha^{\Theta}_{\phi}+q} e^{\kappa_{\phi} n} \sum_{i=1}^{M} \frac{w(n) e^{\beta_i n}}{\breve{Q}(\beta_i)} \right]}{\sum_{n=n_1}^{n_2} \left[n^{\alpha^{\Theta}_{\phi}+q} e^{\kappa_{\phi} n} \left(1+\frac{B^{\Theta}_{\phi}}{n^{\Delta^{\Theta}_{\phi}}}\right) \sum_{i=1}^{M} \frac{w(n) e^{\beta_i n}}{\breve{Q}(\beta_i)} \right]} + \frac{B^{\Theta}_{(\phi,s)} \sum_{n=n_1}^{n_2} \left[n^{\alpha^{\Theta}_{\phi}+q-\Delta^{\Theta}_{(\phi,s)}} e^{\kappa_{\phi} n} \sum_{i=1}^{M} \frac{w(n) e^{\beta_i n}}{\breve{Q}(\beta_i)} \right]}{\sum_{n=n_1}^{n_2} \left[n^{\alpha^{\Theta}_{\phi}+q} e^{\kappa_{\phi} n} \left(1+\frac{B^{\Theta}_{\phi}}{n^{\Delta^{\Theta}_{\phi}}}\right) \sum_{i=1}^{M} \frac{w(n) e^{\beta_i n}}{\breve{Q}(\beta_i)} \right]} \right], \tag{6.26}$$

which can be algebraically manipulated to be

$$\Pr^{\Theta}_{n_1,n_2}(\phi,s) \sim \frac{p^{\Theta}_{n_1}(\phi,s)}{p^{\Theta}_{n_1}(\phi)} \frac{\left(1+\frac{B^{\Theta}_{\phi}}{n_1^{\Delta^{\Theta}_{\phi}}}\right)}{\left(1+\frac{B^{\Theta}_{\phi,s}}{n_1^{\Delta^{\Theta}_{(\phi,s)}}}\right)} \times \left[\left[1+B^{\Theta}_{\phi} \frac{\sum_{n=n_1}^{n_2} \left[n^{\alpha^{\Theta}_{\phi}+q-\Delta^{\Theta}_{\phi}} e^{\kappa_{\phi} n} \sum_{i=1}^{M} \frac{w(n) e^{\beta_i n}}{\breve{Q}(\beta_i)} \right]}{\sum_{n=n_1}^{n_2} \left[n^{\alpha^{\Theta}_{\phi}+q} e^{\kappa_{\phi} n} \sum_{i=1}^{M} \frac{w(n) e^{\beta_i n}}{\breve{Q}(\beta_i)} \right]} \right]^{-1} + \left[\frac{\sum_{n=n_1}^{n_2} \left[n^{\alpha^{\Theta}_{\phi}+q} e^{\kappa_{\phi} n} \left(1+\frac{B^{\Theta}_{\phi}}{n^{\Delta^{\Theta}_{\phi}}}\right) \sum_{i=1}^{M} \frac{w(n) e^{\beta_i n}}{\breve{Q}(\beta_i)} \right]}{B^{\Theta}_{(\phi,s)} \sum_{n=n_1}^{n_2} \left[n^{\alpha^{\Theta}_{\phi}+q-\Delta^{\Theta}_{(\phi,s)}} e^{\kappa_{\phi} n} \sum_{i=1}^{M} \frac{w(n) e^{\beta_i n}}{\breve{Q}(\beta_i)} \right]} \right]^{-1} \right]. \tag{6.27}$$

By defining the new function

$$G_n := G_n(\kappa,\alpha,q,\breve{\boldsymbol{Q}},\boldsymbol{\beta}) := n^{\alpha+q} e^{\kappa n} \sum_{i=1}^{M} \frac{w(n) e^{\beta_i n}}{\breve{Q}(\beta_i)}, \tag{6.28}$$

Equation (6.27) can be expressed in terms of G_n, that is

$$\Pr^{\Theta}_{n_1,n_2}(\phi,s) \sim \frac{p^{\Theta}_{n_1}(\phi,s)}{p^{\Theta}_{n_1}(\phi)} \frac{\left(1+\frac{B^{\Theta}_{\phi}}{n_1^{\Delta^{\Theta}_{\phi}}}\right)}{\left(1+\frac{B^{\Theta}_{(\phi,s)}}{n_1^{\Delta^{\Theta}_{(\phi,s)}}}\right)} \times$$
$$\left[\left[1+B^{\Theta}_{\phi}\frac{\sum_{n=n_1}^{n_2} n^{-\Delta^{\Theta}_{\phi}}G_n}{\sum_{n=n_1}^{n_2} G_n}\right]^{-1} + \left[\frac{\sum_{n=n_1}^{n_2}\left[\left(1+B^{\Theta}_{\phi}n^{-\Delta^{\Theta}_{\phi}}\right)G_n\right]}{B^{\Theta}_{(\phi,s)}\sum_{n=n_1}^{n_2} n^{-\Delta^{\Theta}_{(\phi,s)}}G_n}\right]^{-1}\right]. \tag{6.29}$$
$$B^{\Theta}_{(\phi,s)}\sum_{n=n_1}^{n_2} n^{-\Delta^{\Theta}_{(\phi,s)}}G_n\left[1+B^{\Theta}_{\phi}\sum_{n=n_1}^{n_2} n^{-\Delta^{\Theta}_{\phi}}G_n\right]^{-1} \tag{6.30}$$

This scaling form can be manipulated to become

$$\Pr^{\Theta}_{n_1,n_2}(\phi,s)$$
$$\sim \frac{p^{\Theta}_{n_1}(\phi,s)}{p^{\Theta}_{n_1}(\phi)} \frac{\left(1+\frac{B^{\Theta}_{\phi}}{n_1^{\Delta^{\Theta}_{\phi}}}\right)}{\left(1+\frac{B^{\Theta}_{(\phi,s)}}{n_1^{\Delta^{\Theta}_{(\phi,s)}}}\right)} \left[\left[1+B^{\Theta}_{\phi}\frac{\sum_{n=n_1}^{n_2} n^{-\Delta^{\Theta}_{\phi}}G_n}{\sum_{n=n_1}^{n_2} G_n}\right]^{-1} + \right.$$
$$\left. \frac{B^{\Theta}_{(\phi,s)}\sum_{n=n_1}^{n_2} n^{-\Delta^{\Theta}_{(\phi,s)}}G_n}{\sum_{n=n_1}^{n_2} G_n}\left[1+\frac{B^{\Theta}_{\phi}\sum_{n=n_1}^{n_2} n^{-\Delta^{\Theta}_{\phi}}G_n}{\sum_{n=n_1}^{n_2} G_n}\right]^{-1}\right]. \tag{6.31}$$

Therefore

$$\Pr^{\Theta}_{n_1,n_2}(\phi,s)$$
$$\sim \Pr^{\Theta}_{n_1}(\phi,s)\frac{\left(1+\frac{B^{\Theta}_{\phi}}{n_1^{\Delta^{\Theta}_{\phi}}}\right)}{\left(1+\frac{B^{\Theta}_{(\phi,s)}}{n_1^{\Delta^{\Theta}_{(\phi,s)}}}\right)} \left[1+B^{\Theta}_{\phi}\frac{\sum_{n=n_1}^{n_2} n^{-\Delta^{\Theta}_{\phi}}G_n}{\sum_{n=n_1}^{n_2} G_n}\right]^{-1} \times$$
$$\left[1+\frac{B^{\Theta}_{(\phi,s)}\sum_{n=n_1}^{n_2} n^{-\Delta^{\Theta}_{(\phi,s)}}G_n}{\sum_{n=n_1}^{n_2} G_n}\right]. \tag{6.32}$$

Now substituting the scaling form for $\Pr^{\Theta}_{n_1}(\phi,s)$, given by Equation (2.109), into Equation (6.32), obtains, to first order,

$$\Pr^{\Theta}_{n_1,n_2}(\phi,s) \approx \frac{A^{\Theta}_{(\phi,s)}}{A^{\Theta}_{\phi}} + \frac{C^{\Theta}_{(\phi,s)}}{n_1^{\lambda^{\Theta}_{(\phi,s)}}}. \tag{6.33}$$

Through a similar argument, it can be shown that

$$\Pr^{\Theta}_{n_1,n_2}(\phi, s) \approx \frac{A^{\Theta}_{(\phi,f)}}{A^{\Theta}_{\phi}} + \frac{C^{\Theta}_{(\phi,f)}}{n_1^{\lambda^{\Theta}_{(\phi,f)}}}; \tag{6.34}$$

and, for $* \in \mathscr{K}^{\dagger}(\phi)$,

$$\Pr^{\Theta}_{n_1,n_2}(*) \approx \frac{A^{\Theta}_{*}}{A^{\Theta}_{(\phi,s)}} + \frac{C^{\Theta}_{*}}{n_1^{\lambda^{\Theta}_{(K|\phi,s)}}}. \tag{6.35}$$

Hence, to first order, $\Pr^{\Theta}_{n_1,n_2}(*)$ is expected to have the form

$$f(n) = a + bn^{-\delta}, \tag{6.36}$$

where a, b, and δ depend on property $*$.

Just as was the case for the "Fixed-n Method for Estimating $\Pr^{\Theta}(*)$", in order to estimate the limiting probabilities $\Pr^{\Theta}(\phi, s)$, $\Pr^{\Theta}(\phi, f)$, and $\Pr^{\Theta}(*)$, for $* \in \mathscr{K}^{\dagger}(\phi)$, an independent sample is required to estimate $\Pr^{\Theta}(\phi, s)$, $\Pr^{\Theta}(\phi, f)$, and $\Pr^{\Theta}(*)$, for $* \in \mathscr{K}^{\dagger}(\phi)$, by fitting the sample data to the scaling form

$$f(n) = a + bn^{-\delta}. \tag{6.37}$$

Therefore in order to estimate $\Pr^{\Theta}(\phi, s)$, $\Pr^{\Theta}(\phi, f)$, and $\Pr^{\Theta}(*)$, for $* \in \mathscr{K}^{\dagger}(\phi)$, estimates for $\Pr^{\Theta}_{n_1,n_2}(\phi, s)$, $\Pr^{\Theta}_{n_1,n_2}(\phi, f)$, and $\Pr^{\Theta}_{n_1,n_2}(*)$, for $* \in \mathscr{K}^{\dagger}(\phi)$, respectively are required.

Recall from Section 6.2 that, for $*_1, *_2 \in \Phi$, $X_{k,\cdot}(*_1|2n, T)$ and $Y_{k,\cdot}(*_2|2n, T)$ are the estimators that respectively represent the number of $(2n)$-edge property-$*_1$ and property-$*_2$ Θ-SAPs found across all fourteen chains in block k . Then using the estimators $X_{k,\cdot}(*_1|2n, T)$ and $Y_{k,\cdot}(*_2|2n, T)$, for fixed positive even integers n_1 and n_2, the point estimators $X^{*_1}_{k,\cdot}(n_1, n_2|T)$ and $Y^{*_2}_{k,\cdot}(n_1, n_2|T)$ defined by

$$X^{*_1}_{k}(n_1, n_2|T) := \sum_{n=n_1}^{n_2} X_k(*_1|n, T) \tag{6.38}$$

and

$$Y^{*_2}_{k}(n_1, n_2|T) := \sum_{n=n_1}^{n_2} Y_k(*_2|n, T) \tag{6.39}$$

respectively, where both sums are taken through even values of n, represent the number of property-$*_1$ and property-$*_2$ Θ-SAPs, whose lengths are in the interval $[n_1, n_2]$, found in all fourteen chains in block k. Now let $\widehat{\Pr}^{\Theta}_{n_1,n_2}(\phi, s)$ be the point estimator for $\Pr^{\Theta}_{n_1,n_2}(\phi, s)$ defined by Equation (A.21) (in Section A.4 of Appendix A) using the sequence

$$\left((X^{\phi}_k(n_1, n_2|T), Y^{(\phi,s)}_k(n_1, n_2|T)), k = 1, .., l\right); \tag{6.40}$$

let $\widehat{\Pr}^{\Theta}_{n_1,n_2}(\phi, f)$ be the point estimator for $\Pr^{\Theta}_{n_1,n_2}(\phi, f)$ defined by Equation (A.21) using the sequence

$$\left((X^{\phi}_k(n_1, n_2|T), Y^{(\phi,f)}_k(n_1, n_2|T)), k = 1, .., l\right); \tag{6.41}$$

and, for each after-strand-passage property $* \in \mathscr{K}^{\dagger}(\phi)$, let $\widehat{\Pr}^{\Theta}_{n_1,n_2}(*)$ be the point estimator for $\Pr^{\Theta}_{n_1,n_2}(*)$ defined by Equation (A.21) using the sequence

$$\left((X^{(\phi,s)}_k(n_1, n_2|T), Y^{*}_k(n_1, n_2|T)), k = 1, .., l\right). \tag{6.42}$$

Theorem A.3.2 from Section A.3 of Appendix A implies that $\widehat{\Pr}^{\Theta}_{n_1,n_2}(\phi, s)$, $\widehat{\Pr}^{\Theta}_{n_1,n_2}(\phi, f)$, and $\widehat{\Pr}^{\Theta}_{n_1,n_2}(*)$, for $* \in \mathscr{K}^{\dagger}(\phi)$, are respectively asymptotically (as $l \to \infty$) unbiased estimators for $\Pr^{\Theta}_{n_1,n_2}(\phi, s)$, $\Pr^{\Theta}_{n_1,n_2}(\phi, s)$, and $\Pr^{\Theta}_{n_1,n_2}(*)$.

Now, for $*_1, *_2 \in \Phi$, let $x^{(u)}_{k,\cdot}(*_1|n_1, n_2, T)$ and $y^{(u)}_{k,\cdot}(*_2|n_1, n_2, T)$ respectively denote the realizations of $X^{*_1}_{k,\cdot}(n_1, n_2|T)$ and $Y^{*_2}_{k,\cdot}(n_1, n_2|T)$ based on sampling every T time-steps from $\boldsymbol{\omega}^{(u)}$. Then the point estimators $\widehat{\Pr}^{\Theta}_{n_1,n_2}(\phi, s)$, $\widehat{\Pr}^{\Theta}_{n_1,n_2}(\phi, f)$, and $\widehat{\Pr}^{\Theta}_{n_1,n_2}(*)$, for $* \in \mathscr{K}^{\dagger}(\phi)$, defined with $t_0 = 9.6 \times 10^{10}$ time steps, $\tau_{\text{int}} = 0.72 \times 10^9$ time steps, $T = 1200$ time steps, and $l := 66$, are respectively used to compute the point estimate $\widehat{\text{pr}}^{\Theta}_{n_1,n_2}(\phi, s)$ for $\Pr^{\Theta}_{n_1,n_2}(\phi, s)$ using the sequence

$$\left(\left(\left(x^{(u)}_{k,\cdot}(\phi|n_1, n_2, T), y^{(u)}_{k,\cdot}(\phi, s|n_1, n_2, T)\right), k = 1, .., l\right), u = 1, ..., 10\right) \tag{6.43}$$

in Equation (A.21); the point estimate $\widehat{\text{pr}}^{\Theta}_{n_1,n_2}(\phi, f)$ for $\Pr^{\Theta}_{n_1,n_2}(\phi, f)$ using the sequence

$$\left(\left(\left(x^{(u)}_{k,\cdot}(\phi|n_1, n_2, T), y^{(u)}_{k,\cdot}(\phi, f|n_1, n_2, T)\right), k = 1, .., l\right), u = 1, ..., 10\right) \tag{6.44}$$

in Equation (A.21); and, for $* \in \mathscr{K}^{\dagger}(\phi)$, the point estimate $\widehat{\text{pr}}^{\Theta}_{n_1,n_2}(*)$ for $\Pr^{\Theta}_{n_1,n_2}(*)$ using the sequence

$$\left(\left(\left(x^{(u)}_{k,\cdot}(\phi, s|n_1, n_2, T), y^{(u)}_{k,\cdot}(*|n_1, n_2, T)\right), k = 1, .., l\right), u = 1, ..., 10\right) \tag{6.45}$$

in Equation (A.21).

In order to estimate $\Pr^{\Theta}(*)$, for $* \in \Phi \backslash \{\phi\}$, using the grouped-$n$ estimates $\widehat{\text{pr}}^{\Theta}_{n_1,n_2}(*)$, an independent sample of the values $\widehat{\text{pr}}^{\Theta}_{n_1,n_2}(*)$ is required. More specifically the value g_* needs to be estimated, where g_* is the number of consecutive even n's that must pass so that the point estimates $\widehat{\text{pr}}^{\Theta}_{n,n+2g_*-2}(*)$ and $\widehat{\text{pr}}^{\Theta}_{n+2g_*,n+4g_*-2}(*)$ are essentially independent. Let m_l be the smallest value of n for which $\widetilde{\text{pr}}^{\Theta}_{2n}(*)$ is non-zero. (Recall that $\widetilde{\text{pr}}^{\Theta}_{2n}(*)$ is a

fixed-n estimate for $\Pr_{2n}^{\Theta}(*)$.) Then the set

$$H_2^{\Theta}(*) := \bigcup_{i=1}^{t} \left\{ \left(2m_l + 2(i-1)g_*, \widehat{\mathrm{pr}}_{2m_l+2(i-1)g_*, 2m_l+2ig_*-2}^{\Theta}(*) \right) \right\}, \tag{6.46}$$

where t is the greatest integer that satisfies both $2m_l \leq 2m_l + 2g_*t \leq 2m_u$ and for all $j \leq 2m_l + 2g_*t - 2$, $\widetilde{\mathrm{pr}}_j^{\Theta}(*) \neq 0$, consists of t essentially independent data points. The data in $H_2^{\Theta}(*)$ can then be fit to the scaling form for $\Pr_{n_1,n_2}^{\Theta}(*)$.

Only one step in the Grouped-n Method remains to be clarified. How does one estimate the value of g_* required by the Grouped-n Method? Define $\mho_{*_t}^u$ as the set of estimates $\{u(*_t|2n)\}$ used in the numerators of the elements in $\left\{\widetilde{\mathrm{pr}}_{2n}^{\Theta}(*)\right\}$; $\mho_{*_b}^u$ as the set of estimates $\{u(*_b|2n)\}$ used in the denominator of the elements in $\left\{\widetilde{\mathrm{pr}}_{2n}^{\Theta}(*)\right\}$; and $\mho_*^P$ as the set of estimates $\left\{\dfrac{u(*_t|2n)}{u(*_b|2n)}\right\}$. For $k\left(P_*\right)$, the minimum number of n's that must pass before the point estimate $\widetilde{\mathrm{pr}}_{2n}^{\Theta}(*)$ and $\widetilde{\mathrm{pr}}_{2n+2k(P_*)}^{\Theta}(*)$ are essentially independent, and for $k\left(u_{*_\#}\right)$, for $\# \in \{t, b\}$, the minimum number of n's that must pass before the point estimate $u(*_\#|2n)$ and $u(*_\#|2n + 2k\left(u_{*_\#}\right))$ are essentially independent,

$$k\left(u_{*_t}\right) := \tau_{\mathrm{int}}(\mho_{*_t}^u), \tag{6.47}$$

$$k\left(u_{*_b}\right) := \tau_{\mathrm{int}}(\mho_{*_b}^u), \tag{6.48}$$

$$k\left(P_*\right) := \tau_{\mathrm{int}}(\mho_*^P) \tag{6.49}$$

and then

$$g_* := \max\left\{k\left(P_*\right), k\left(u_{*_t}\right), k\left(u_{*_b}\right)\right\}. \tag{6.50}$$

Define $\widehat{k}\left(u_{*_t}\right)$ to be the estimate for $k\left(u_{*_t}\right)$ that is obtained by calculating the first value of c such that for all $k \geq c$, the estimated correlation between $u(*_t|n)$ and $u(*_t|2n + 2k)$ is statistically insignificant at the 95% confidence level. Define $\widehat{k}\left(u_{*_b}\right)$ to be the estimate for $k\left(u_{*_b}\right)$ that is obtained by calculating the first value of c such that for all $k \geq c$, the estimated correlation between $u(*_b|n)$ and $u(*_b|2n + 2k)$ is statistically insignificant at the 95% confidence level. Define $\widehat{k}\left(P_*\right)$ to be the estimate for $k\left(P_*\right)$ that is the first value of c such that for all $k \geq c$, the correlation between $\widetilde{\mathrm{pr}}_{2n}^{\Theta}(*)$ and $\widetilde{\mathrm{pr}}_{2n+2k}^{\Theta}(*)$ is statistically insignificant at the 95% confidence level. Then let $\widehat{g}\left(*\right)$ be the estimator for $g\left(*\right)$ given by

$$\widehat{g}_* := \max\left\{\widehat{k}\left(P_*\right), \widehat{k}\left(u_{*_t}\right), \widehat{k}\left(u_{*_b}\right)\right\}. \tag{6.51}$$

After creating the set $H_2^{\Theta}(*)$ using $g_* = \widehat{g}_*$, weighted least-squares regression can be used to fit the data in $H_2^{\Theta}(*)$ to the scaling form for $\Pr_{n_1,n_2}^{\Theta}(*)$:

$$f(n) = a + bn^{-\delta}. \tag{6.52}$$

Then the estimate for a also estimates the desired limiting probability $\Pr^{\Theta}(*)$.

6.4 Comparison of the Fixed-n and Grouped-n Methods for Estimating $\Pr^{\Theta}(*)$

Recall from Section A.5 of Appendix A that k_* is the minimum positive even integer such that $\widetilde{\text{pr}}_{2n}^{\Theta}(*)$ and $\widetilde{\text{pr}}_{2n+k_*}^{\Theta}(*)$ are essentially independent. Then, the most obvious drawback of the "Fixed-n Method for Estimating $\Pr^{\Theta}(*)$" is that the larger the value of k_*, the fewer the number of points in $H_1^{\Theta}(*)$ and the more estimates $\widetilde{\text{pr}}_{2n}^{\Theta}(*)$ that are discarded, and finally, the more variability in the resulting fit to the scaling form for $\Pr_{2n}^{\Theta}(*)$. Another drawback of the "Fixed-n Method for Estimating $\Pr^{\Theta}(*)$" is that as n increases, the variance of $\widetilde{\text{pr}}_{2n}^{\Theta}(*)$ increases dramatically as well. Since the goal of this section is to estimate the limiting probabilities $\Pr^{\Theta}(\phi, s)$, $\Pr^{\Theta}(\phi, f)$, and $\Pr^{\Theta}(K|\phi, s)$, the estimates for $\Pr_{2n}^{\Theta}(*)$, for values of n as large as possible, are of interest, but these are the very estimates that have the largest variances. Consequently the very estimates that are most desirable in the fit to the scaling form for $\Pr_{2n}^{\Theta}(*)$ are the least accurate estimates. The most obvious drawback of the "Grouped-n Method for estimating $\Pr^{\Theta}(*)$" is that the larger the value of g_*, the fewer the number of points in $H_2^{\Theta}(*)$. However, at least the variability of the data in $H_2^{\Theta}(*)$ is less than the variability of the data in the set $H_1^{\Theta}(*)$ where $k_* = g_*$. For the purpose of illustrating these weaknesses of the two methods, refer to Figure 6.2 for a display of the sequences of estimates $\left\{\left(24 + 60i, \widetilde{\text{pr}}_{24+60i}^{\Theta}(3_1|\phi, s)\right)\right\}_{i=0}^{67}$ and $\left\{\left(24 + 140i, \widetilde{\text{pr}}_{24+140i,24+138(i+1)}^{\Theta}(3_1|\phi, s)\right)\right\}_{i=0}^{29}$ that are required by the Fixed-n and the Grouped-n Methods respectively.

Figure 6.2 displays the fixed-n estimates $\left\{\left(24 + 60i, \widetilde{\text{pr}}_{24+60i}^{\Theta}(3_1|\phi, s)\right)\right\}_{i=0}^{67}$ and the grouped-n estimates $\left\{\left(24 + 140i, \widetilde{\text{pr}}_{24+140i,24+138(i+1)}^{\Theta}(3_1|\phi, s)\right)\right\}_{i=0}^{29}$. The figure illustrates the fact that, over the same range of values, the grouped-n estimates do not vary as widely as the fixed-n estimates. As a result, the Grouped-n Method generates more reliable (i.e. less variable) point estimates for larger ranges of n than the Fixed-n Method. The

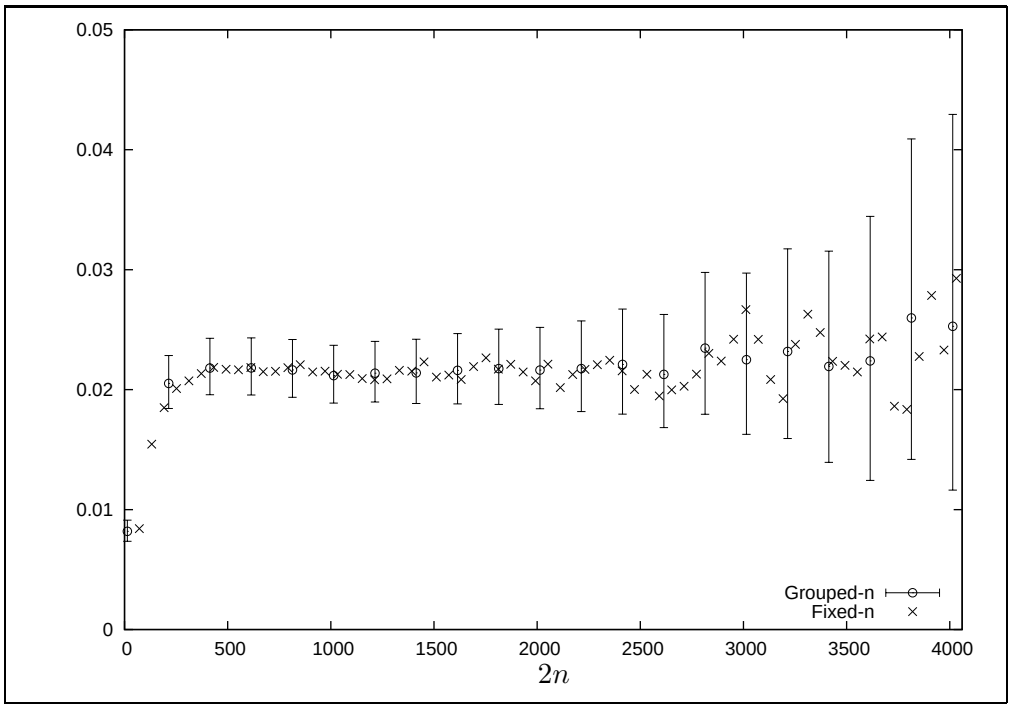

Figure 6.2: A comparison of the fixed-n estimates $\widetilde{\mathrm{pr}}^{\Theta}_{2n}((3_1|\phi, s))$ and the grouped-n estimates $\widehat{\mathrm{pr}}^{\Theta}_{n_1,n_2}(3_1|\phi, s)$, where the error bars are the estimated 95% margins of error for the grouped-n estimates.

error bars (estimated 95% confidence intervals) presented in Figure 6.2 for any particular grouped-n estimate (say calculated using the interval $[n_1, n_2]$) is consistently smaller than the estimated 95% confidence intervals for the fixed-n estimates computed for each even $n \in [n_1, n_2]$. The difference in lengths of the two intervals increases as n_1 increases. Hence it is concluded that, whenever possible, the Grouped-n Method for Estimating $\Pr^{\Theta}(*)$ should be used to estimate $\Pr^{\Theta}(*)$.

In the next section, the Grouped-n Method for Estimating $\Pr^{\Theta}(*)$ is used to estimate some of the limiting strand passage probabilities.

6.5 The Transition Knotting Probability Estimates

In order to estimate any of the limiting probabilities, the interval over which the data is believed to be reliable needs to be determined, that is estimates for $N^*_{\max}$ need to be determined. Because the probability of a successful strand passage appears in the denominators of the transition knotting probabilities $\Pr^{\Theta}(K|\phi, s)$, a logical choice for determining when the data is unreliable is when the estimates $\mathrm{pr}^{\Theta}_{2n}(\phi, s)$ become unreliable; any unreliability

in $\text{pr}_{2n}^{\Theta}(\phi, s)$ (due to it appearing in the denominator) gets magnified in the estimates for $\Pr_{n_1,n_2}^{\Theta}(K|\phi, s)$. Hence the procedure from Section 4.6 will be used to estimate $N_{\max}^{(\phi,s)}$ in which the $c = 0.003$ and

$$\hat{\delta}_{2n}^{(u)}(*) := \begin{cases} \dfrac{\widehat{\text{SE}}(\widehat{\text{pr}}_{2n}^{\Theta}((\phi, s), u))}{\widehat{\text{pr}}_{2n}^{\Theta}((\phi, s), u)}, & \text{if } \widehat{\text{pr}}_{2n}^{\Theta}((\phi, s), u) \neq 0 \\ \infty, & \text{otherwise,} \end{cases} \tag{6.53}$$

where

$$\widehat{\text{SE}}(\widehat{\text{pr}}_{2n}^{\Theta}((\phi, s), u)) := \sqrt{\frac{\widehat{\text{var}}(\widehat{\text{pr}}_{2n}^{\Theta}((\phi, s), u))}{m}}, \tag{6.54}$$

m is the number of essentially independent blocks of data used in the estimate $\widehat{\text{pr}}_{2n}^{\Theta}((\phi, s), u)$, and $\widehat{\text{var}}(\widehat{\text{pr}}_{2n}^{\Theta}((\phi, s), u))$ is given by Equation (A.30). The reason for choosing a cutoff value of 0.003 is that 0.003 corresponds to approximately fifteen percent of the estimate $\hat{\delta}^{(u)}(\phi, s)$.

Figure 6.3 illustrates the estimates $\hat{\delta}_{2n}^{(u)}(\phi, s) < \infty$ for the ten replications. The dashed line in Figure 6.3 is the line $y = \hat{\delta}(\phi, s) + 0.003$, where

$$\hat{\delta}(\phi, s) := \min_{u,n} \hat{\delta}_{2n}^{(u)}(\phi, s). \tag{6.55}$$

The values of $\hat{\delta}^{(u)}(\phi, s)$ and $\hat{N}_{\max}^{(u)}(\phi, s)$, for $u = 1, ..., 10$, are summarized in Table 6.1. From the estimates in Table 6.1, $\hat{N}_{\max}(\phi, s) = 1890$. Note that estimates for $N_{\max}^{(\phi,s)}$ were also computed when the data collected during the first 5.0 billion and 11.0 billion Θ-BFACF moves in parallel were discarded. The values estimated for $N_{\max}^{(\phi,s)}$ in both of these scenarios are consistent with the estimate $\hat{N}_{\max}(\phi, s) = 1890$ that was determined when no data was discarded. Therefore no data is burned when estimating the limiting strand passage probabilities and the data from polygons in each replication of sizes between 14 and $\hat{N}_{\max}(\phi, s) = 1890$ (including 14 and 1890) are used to determine the distance between n_l and n_m such that the estimates for $\widehat{\text{pr}}_{n_l}^{\Theta}(*, u)$ and $\widehat{\text{pr}}_{n_m}^{\Theta}(*, u)$ (for even n_l,$n_m \in [14, 1890]$) are essentially independent and to estimate the limiting strand passage probabilities $\Pr^{\Theta}(*)$.

For Replication u and for each property $* \in \{(\phi, s), (\phi|\phi, s), (3_1|\phi, s), (4_1|\phi, s), (5_2|\phi, s)\}$, half the length of the grouping interval $[n_1, n_2]$ must be estimated (recall from Section 6.3 that this quantity is denoted g_*). Using the method discussed in Section 6.3 to estimate g_*, the resulting estimates for g_* are presented in Table 6.2.

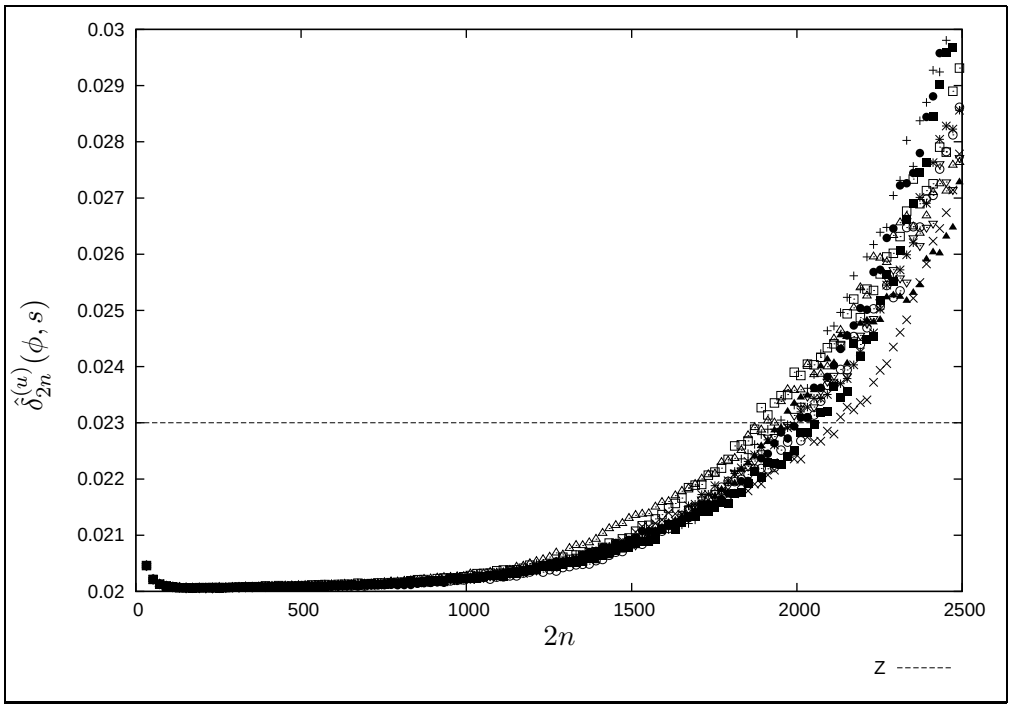

Figure 6.3: The relative standard error in the fixed-n estimates $\widehat{\mathrm{pr}}^{\Theta}_{2n}((3_1|\phi, s), u)$. Line Z represents the maximum tolerance in the estimated relative standard error.

Table 6.1: The estimates for $\delta^{(u)}(\phi, s)$ and $N_{\max}(\phi, s)$ from each of the 10 replications.

Replication u	$\hat{\delta}^{(u)}(\phi, s)$	$\hat{N}^{(u)}_{\max}(\phi, s)$
1	0.020060	1958
2	0.020059	2128
3	0.020060	1994
4	0.020061	1890
5	0.020054	2058
6	0.020057	2032
7	0.020058	1984
8	0.020059	1934
9	0.020059	1966
10	0.020059	1988

Table 6.2: The estimated values for g_* (half the estimated lengths of the grouping intervals for property $*$) so that an essentially independent sample can be formed using the data from Replication u . The estimates are based on the cutoff $\hat{N}_{\max}(*) = 1890$.

	Property $*$					
Replication u	ϕ	(ϕ, s)	$(\phi\|\phi, s)$	$(3_1\|\phi, s)$	$(4_1\|\phi, s)$	$(5_2\|\phi, s)$
1	40	50	50	70	80	90
2	40	50	50	70	80	80
3	40	50	50	70	80	70
4	40	50	50	70	80	90
5	40	50	50	70	80	60
6	40	50	50	70	80	80
7	40	50	50	70	80	80
8	40	50	50	70	80	60
9	40	50	50	70	80	60
10	40	50	50	70	80	80
$\hat{g}_*$	40	50	50	70	80	90

Table 6.3: The number of essentially independent grouped-n data points for property $*$ over the interval $[14, 1890]$.

Property $*$	(ϕ, s)	$(\phi\|\phi, s)$	$(3_1\|\phi, s)$	$(4_1\|\phi, s)$	$(5_2\|\phi, s)$
Number independent blocks	18	18	13	11	10

Using $\hat{N}_{\max}(\phi, s) = 1890$ as the maximum polygon length for which the data for each property $* \in \{(\phi, s), (\phi|\phi, s), (3_1|\phi, s), (4_1|\phi, s), (5_2|\phi, s)\}$ is reliable and the estimates $\hat{g}_*$ presented in Table 6.2, the number of essentially independent grouped-n data points formed based on groupings of length $2\hat{g}_*$ are presented in Table 6.3. Based on these groupings, essentially independent samples for $\Pr^{\Theta}_{n_1,n_2}(*)$, for each $* \in \{(\phi, s), (\phi|\phi, s), (3_1|\phi, s), (4_1|\phi, s), (5_2|\phi, s)\}$, are displayed in Figures 6.4-6.8 respectively and are presented in Tables B.6-B.10 (cf. Section B.1.2 of Appendix B) respectively. In order to estimate the limiting strand-passage probabilities using these essentially independent samples, recall from Equation (6.35) that it is expected that, to first order,

$$\Pr^{\Theta}_{n_1,n_2}(*) \approx \frac{A^{\Theta}_{*}}{A^{\Theta}_{(\phi,s)}} + \frac{C^{\Theta}_{*}}{n_1^{\lambda^{\Theta}_{*}}}, \tag{6.56}$$

where $* \in \{(\phi|\phi, s), (3_1|\phi, s), (4_1|\phi, s), (5_2|\phi, s)\}$; recall from Equation (6.33) that it is expected that, to first order,

$$\Pr^{\Theta}_{n_1,n_2}(\phi, s) \approx \frac{A^{\Theta}_{(\phi,s)}}{A^{\Theta}_{\phi}} + \frac{C^{\Theta}_{(\phi,s)}}{n_1^{\lambda^{\Theta}_{(\phi,s)}}}; \tag{6.57}$$

and recall that the constant terms in the scaling form for $\Pr^{\Theta}_{n_1,n_2}(*)$, for $* \in \{(\phi|\phi, s), (3_1|\phi, s), (4_1|\phi, s), (5_2|\phi, s)\}$, and $\Pr^{\Theta}_{n_1,n_2}(\phi, s)$ are the desired limiting probabilities $\Pr^{\Theta}(*)$ and $\Pr^{\Theta}(\phi, s)$.

To estimate the constant terms in these scaling forms, the grouped-n data displayed in Figures 6.4-6.8 can be fit to the form

$$f(n_1, n_2) = b + mn_1^{-\lambda} \tag{6.58}$$

using weighted non-linear least-squares regression. The following estimates are of the form:

$$\text{point estimate} \pm 95\% \text{ margin of error } (\pm \text{systematic error}). \tag{6.59}$$

The systematic error is determined to be the maximum of the largest difference between the grouped-n point estimates over the region $[14, 1890]$ and the estimated limiting probability.

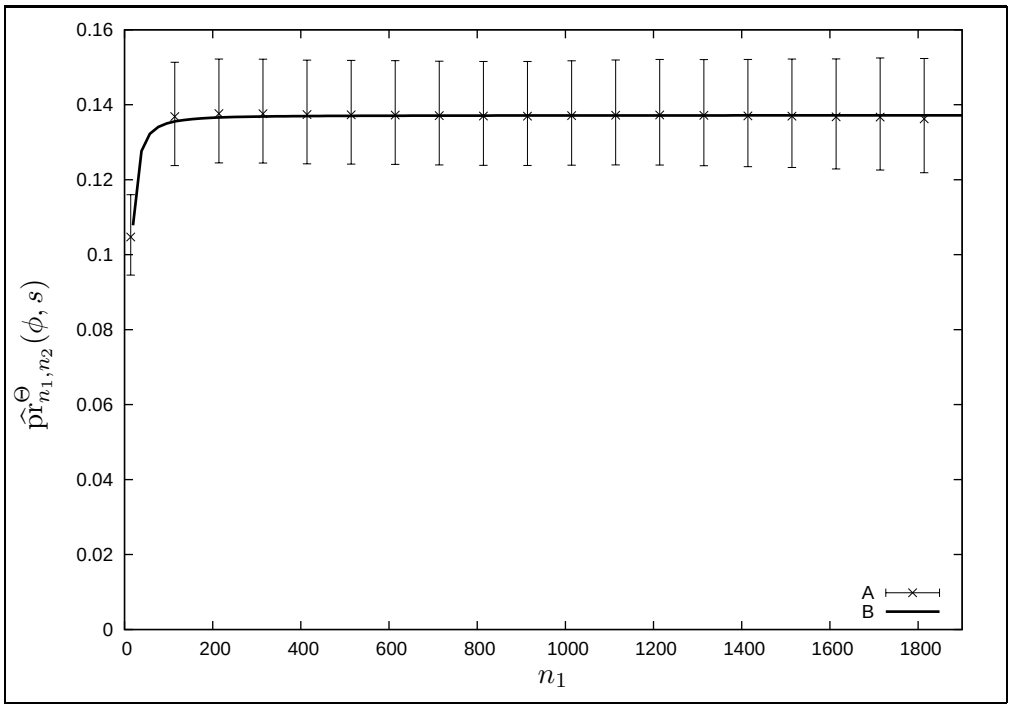

Figure 6.4: A: the grouped-n estimates for the probability of a successful strand passage. The error bars are the estimated 95% margins of error for the grouped-n estimates. B: the curve estimated from the grouped-n data in A.

Figure 6.4 displays the sequence of point estimates $((14+100(t-1), \widehat{\mathrm{pr}}^{\Theta}_{14+100(t-1),12+100t}(\phi,s)), t = 1, ..., 18)$ and the estimated scaling form for $\mathrm{Pr}^{\Theta}_{n_1,n_2}(\phi,s)$ versus n_1. The parameters in the scaling form for $\mathrm{Pr}^{\Theta}_{n_1,n_2}(\phi,s)$ are estimated to be:

$$\begin{aligned} \mathrm{Pr}^{\Theta}(\phi,s) = &\quad 0.13719 \quad \pm \quad 0.00019 \quad (\pm 0.03240) \\ m(\phi,s) = &\quad -3.52566 \quad \pm \quad 1.13622 \\ \lambda(\phi,s) = &\quad -1.62076 \quad \pm \quad 0.12146. \end{aligned}$$

The estimated scaling form for $\mathrm{Pr}^{\Theta}_{n_1,n_2}(\phi,s)$ fits the sequence of point estimates plotted in Figure 6.4 well, because, based on a χ^2- Test for Goodness of Fit, $\chi^2(14) = 9.1936$ and the corresponding p-value for the fit is 0.8185. Because the estimated scaling form for $\mathrm{Pr}^{\Theta}_{n_1,n_2}(\phi,s)$ is an increasing function in n_1 (as can be seen from Figure 6.4), the data numerically supports Conjecture 2.2.3, that is $\mathrm{Pr}^{\Theta}_{2n}(\phi,s)$ increases to the value $\mathrm{Pr}^{\Theta}(\phi,s)$ and that $\mathrm{Pr}^{\Theta}(\phi,s) \in (0,1)$.

Figure 6.5 displays the sequence of point estimates

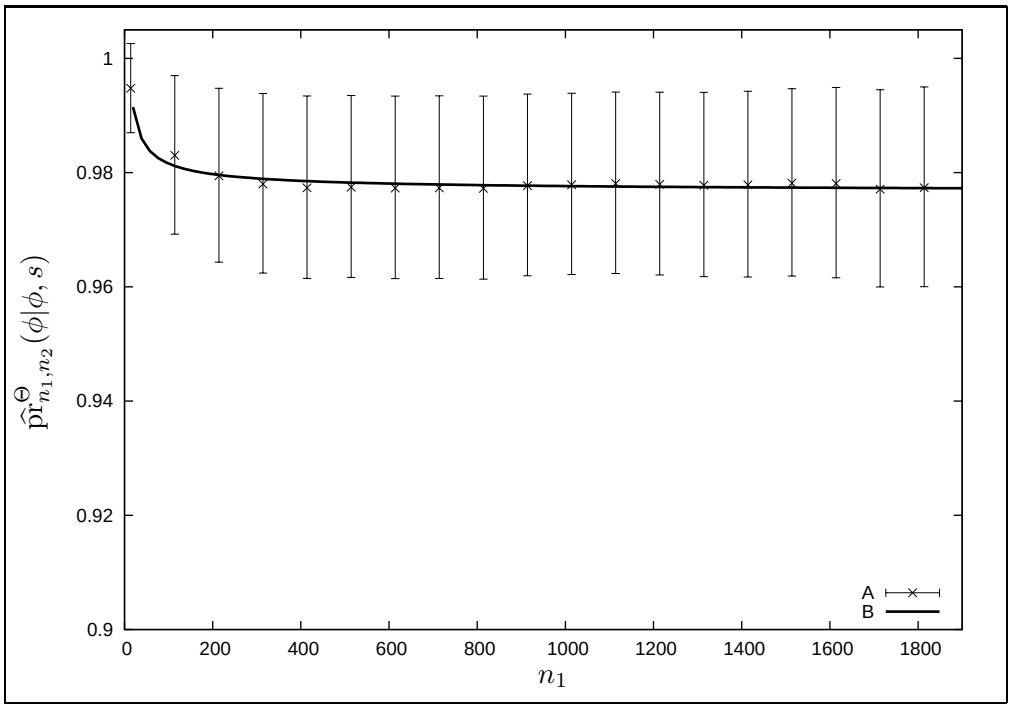

Figure 6.5: A: the grouped-n estimates for the probability of the unknot given a successful strand passage. The error bars are the estimated 95% margins of error for the grouped-n estimates. B: the curve estimated from the grouped-n data in A.

$((14+100(t-1), \widehat{\mathrm{pr}}^{\Theta}_{14+100(t-1),12+100t}(\phi|\phi,s)), t = 1, ..., 18)$ and the estimated scaling form for $\mathrm{Pr}^{\Theta}_{n_1,n_2}(\phi|\phi,s)$ versus n_1. The parameters in the scaling form for $\mathrm{Pr}^{\Theta}_{n_1,n_2}(\phi|\phi,s)$ are estimated to be:

$$\begin{aligned} \mathrm{Pr}^{\Theta}(\phi|\phi,s) = &\quad 0.97653 \quad \pm \quad 0.00133 \quad (\pm 0.01822) \\ m(\phi|\phi,s) = &\quad 0.10401 \quad \pm \quad 0.05589 \\ \lambda(\phi|\phi,s) = &-0.65717 \quad \pm \quad 0.21745. \end{aligned}$$

The estimated scaling form for $\mathrm{Pr}^{\Theta}_{n_1,n_2}(\phi|\phi,s)$ fits the sequence of point estimates plotted in Figure 6.5 well, because, based on a χ^2-Test for Goodness of Fit, $\chi^2(14) = 0.1631$ and the corresponding p-value for the fit is greater than 0.9999. Because the estimated scaling form for $\mathrm{Pr}^{\Theta}_{n_1,n_2}(\phi|\phi,s)$ is a decreasing function in n_1 (as can be seen from Figure 6.4), the data numerically supports Conjecture 2.2.3, that is $\mathrm{Pr}^{\Theta}_{2n}(\phi|\phi,s)$ decreases to the value $\mathrm{Pr}^{\Theta}(\phi|\phi,s)$ and that $\mathrm{Pr}^{\Theta}(\phi|\phi,s) \in (0,1)$.

Figure 6.6 displays the sequence of point estimates

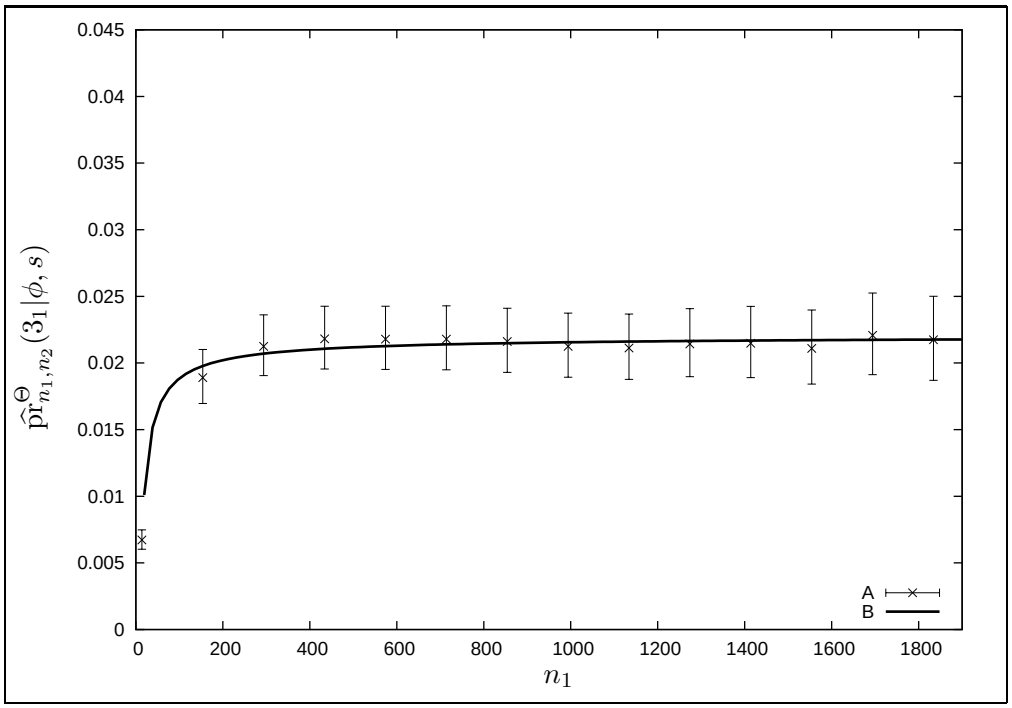

Figure 6.6: A: the grouped-n estimates for the probability of the trefoil given a successful strand passage. The error bars are the estimated 95% margins of error for the grouped-n estimates. B: the curve estimated from the grouped-n data in A.

$((14+140(t-1), \widehat{\mathrm{pr}}^{\Theta}_{14+140(t-1),12+140t}(3_1|\phi,s)), t = 1, ..., 13)$ and the estimated scaling form for $\mathrm{Pr}^{\Theta}_{n_1,n_2}(3_1|\phi,s)$ versus n_1. The parameters in the scaling form for $\mathrm{Pr}^{\Theta}_{n_1,n_2}(3_1|\phi,s)$ are estimated to be:

$$\begin{aligned} \mathrm{Pr}^{\Theta}(3_1|\phi,s) = &\quad 0.02208 \quad \pm \quad 0.00095 \quad (\pm 0.00672) \\ m(3_1|\phi,s) = &\quad -0.12450 \quad \pm \quad 0.09108 \\ \lambda(3_1|\phi,s) = &\quad -0.79237 \quad \pm \quad 0.29174. \end{aligned}$$

The estimated scaling form for $\mathrm{Pr}^{\Theta}_{n_1,n_2}(3_1|\phi,s)$ fits the estimates $\widehat{\mathrm{pr}}^{\Theta}_{n_1,n_2}(3_1|\phi,s)$ plotted in Figure 6.6 well, because, based on a χ^2-Test for Goodness of Fit, $\chi^2(9) = 2.1360$ and the corresponding p-value for the fit is 0.9891. Because the estimated scaling form for $\mathrm{Pr}^{\Theta}_{n_1,n_2}(3_1|\phi,s)$ is an increasing function in n_1 (as can be seen from Figure 6.4), the data numerically supports Conjecture 2.2.3, that is $\mathrm{Pr}^{\Theta}_{2n}(3_1|\phi,s)$ increases to the value $\mathrm{Pr}^{\Theta}(3_1|\phi,s)$ and that $\mathrm{Pr}^{\Theta}(3_1|\phi,s) \in (0,1)$.

Figure 6.7 plots the sequence of point estimates $((14+160(t-1), \widehat{\mathrm{pr}}^{\Theta}_{14+160(t-1),12+160t}(4_1|\phi,s)), t = 1, ..., 11)$ and the estimated scaling form for $\mathrm{Pr}^{\Theta}_{n_1,n_2}(4_1|\phi,s)$ versus n_1. The parameters in the scaling form for $\mathrm{Pr}^{\Theta}_{n_1,n_2}(4_1|\phi,s)$ are

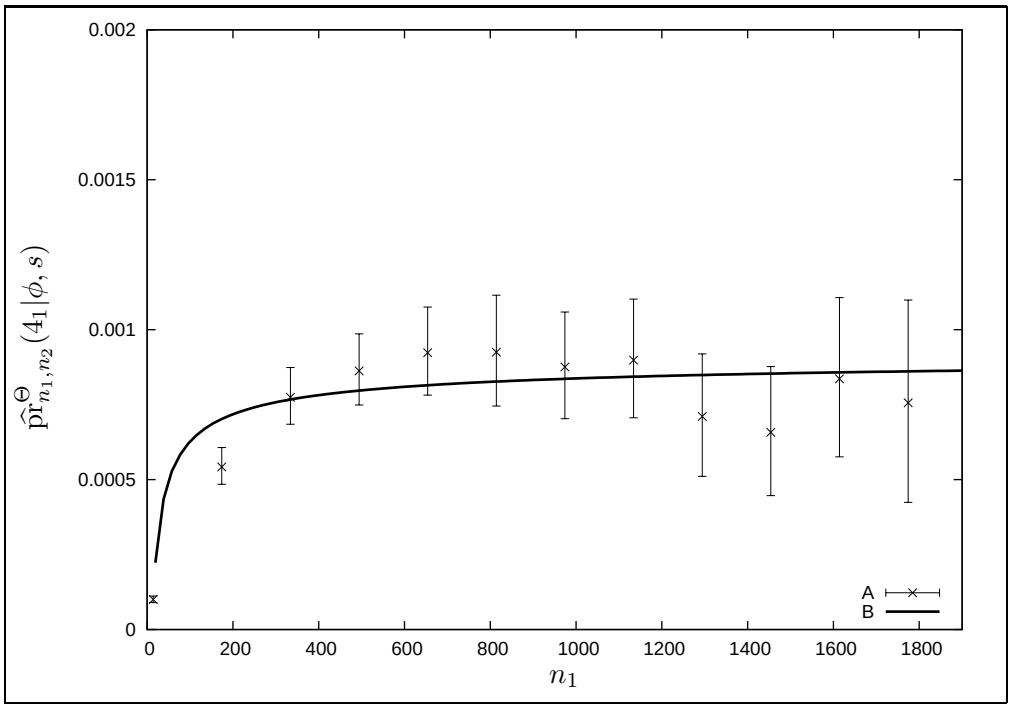

Figure 6.7: A: the grouped-n estimates for the probability of the figure 8 given a successful strand passage. The error bars are the estimated 95% margins of error for the grouped-n estimates. B: the curve estimated from the grouped-n data in A.

estimated to be:

$$\begin{aligned} \mathrm{Pr}^{\Theta}(4_1|\phi,s) = &\quad 0.00093 \quad \pm \quad 0.00048 \quad (\pm 0.00082) \\ m(4_1|\phi,s) = &\quad -0.00323 \quad \pm \quad 0.01021 \\ \lambda(4_1|\phi,s) = &\quad -0.51409 \quad \pm \quad 1.47002. \end{aligned}$$

The estimated scaling form for $\mathrm{Pr}^{\Theta}_{n_1,n_2}(4_1|\phi,s)$ fits the data in Figure 6.7 poorly, because, based on a χ^2-Test for Goodness of Fit, $\chi^2(7) = 36.1050$ and the corresponding p-value for the fit is less than 0.0001. Because of the variability in the point estimates and the poor fit, even though the estimated scaling form for $\mathrm{Pr}^{\Theta}_{n_1,n_2}(4_1|\phi,s)$ is an increasing function in n_1 (as can be seen from Figure 6.4), more property-$(4_1|\phi,s)$ data is required to determined whether or not the CMC Θ-data supports Conjecture 2.2.3, that is $\mathrm{Pr}^{\Theta}_{2n}(4_1|\phi,s)$ increases to the value $\mathrm{Pr}^{\Theta}(4_1|\phi,s)$ and that $\mathrm{Pr}^{\Theta}(4_1|\phi,s) \in (0,1)$.

Figure 6.8 displays the sequence of point estimates $((14+180(t-1), \widehat{\mathrm{pr}}^{\Theta}_{14+180(t-1),12+180t}(5_2|\phi,s)), t = 1, ..., 10)$ and the estimated scaling form for $\mathrm{Pr}^{\Theta}_{n_1,n_2}(5_2|\phi,s)$ versus n_1. The parameters in the scaling form for $\mathrm{Pr}^{\Theta}_{n_1,n_2}(5_2|\phi,s)$ were

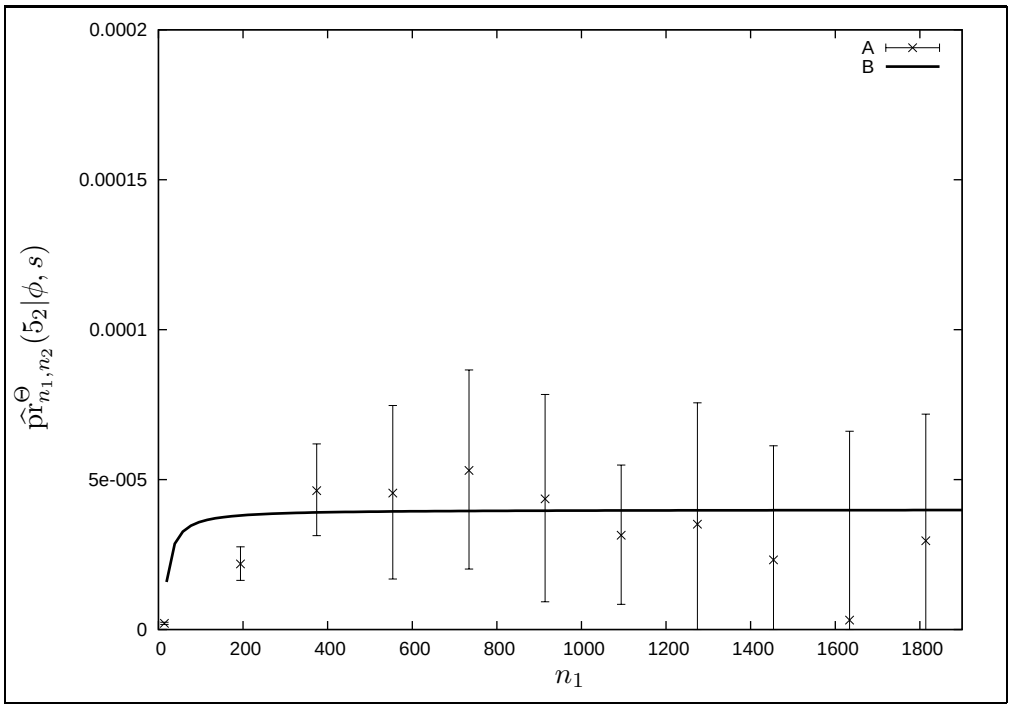

Figure 6.8: A: the grouped-n estimates for the probability of knot-type 5_2 given a successful strand passage. The error bars are the estimated 95% margins of error for the grouped-n estimates. B: the curve estimated from the grouped-n data in A.

estimated to be:

$$\begin{aligned} \Pr^{\Theta}(5_2|\phi,s) = &\quad 0.00004 \quad \pm \quad 0.00003 \quad (\pm 0.00004) \\ m(5_2|\phi,s) = &\quad -0.00060 \quad \pm \quad 0.00020 \\ \lambda(5_2|\phi,s) = &\quad -1.08720 \quad \pm \quad 2.14156. \end{aligned} \tag{6.60}$$

The estimated scaling form for $\Pr^{\Theta}_{n_1,n_2}(5_2|\phi,s)$ fits the data in Figure 6.8 poorly, very poorly, because, based on a χ^2-Test for Goodness of Fit, $\chi^2(6) = 483.0888$ and the corresponding p-value for the fit is less than 0.0001. Because of the variability in the point estimates and the poor fit, even though the estimated scaling form for $\Pr^{\Theta}_{n_1,n_2}(5_2|\phi,s)$ is an increasing function in n_1 (as can be seen from Figure 6.4), more property-$(5_2|\phi,s)$ data is required to determined whether or not the CMC Θ-data supports Conjecture 2.2.3, that is $\Pr^{\Theta}_{2n}(5_2|\phi,s)$ increases to the value $\Pr^{\Theta}(5_2|\phi,s)$ and that $\Pr^{\Theta}(5_2|\phi,s) \in (0,1)$.

The upshot of the estimated limiting strand passage probabilities is that:

1. the estimate for $\Pr^{\Theta}(\phi,s) = \quad 0.13719 \quad \pm \quad 0.00019 \quad (\pm 0.03240)$ supports Conjecture 2.2.3, that is the limiting strand passage probability $\Pr^{\Theta}(\phi,s)$ exists and $\Pr^{\Theta}(\phi,s) \in (0,1)$;

2. the estimates for $\Pr^{\Theta}(\phi|\phi,s) = 0.97653 \pm 0.00133 \ (\pm 0.01822)$ and $\Pr^{\Theta}(3_1|\phi,s) = 0.02208 \pm 0.00095 \pm 0.00672$ also support Conjecture 2.2.3, that is the limiting transition knotting probabilities $\Pr^{\Theta}(K|\phi,s)$, for every unknotting number one knot-type K, exist and $\Pr^{\Theta}(K|\phi,s) \in (0,1)$; and

3. though technically the estimates $\Pr^{\Theta}(4_1|\phi,s) = 0.00093 \pm 0.00048 \ (\pm 0.00082)$ and $\Pr^{\Theta}(5_2|\phi,s) = 0.00004 \pm 0.00003 \ (\pm 0.00004)$ support Conjecture 2.2.3, the estimates are not deemed to be reliable and therefore cannot be used as either confirmation or disproof of the conjecture.

As a consequence of 3. above, further data needs to be collected in order to compute better estimates for $\Pr^{\Theta}(4_1|\phi,s)$ and $\Pr^{\Theta}(5_2|\phi,s)$.

6.6 In Summary

In this chapter, two methods for estimating the limiting strand passage probabilities $\Pr^{\Theta}(*)$, for $* \in \Phi$, were presented. The first method presented was the Fixed-n Method and the second method presented was the Grouped-n Method. Both methods required determining a value for $N^*_{\max}$ so that the estimate values for $\Pr^{\Theta}(*)$ were based on the most reliable data available.

The advantage of the Fixed-n Method for Estimating $\Pr^{\Theta}(*)$ is that it only requires an independent set of estimated values for the fixed-n probabilities $\Pr^{\Theta}_n(*)$ in order to yield an estimate for $\Pr^{\Theta}(*)$. The major disadvantage of this method is that in order to determine the required independent set of fixed-n probability estimates, many of the estimated fixed-n probabilities have to be ignored due to the correlation that exists between the fixed-n probabilities for consecutive values of even n. The Grouped-n Method for Estimating $\Pr^{\Theta}(*)$ was designed so that all the fixed-n data could be used to determine the estimate for $\Pr^{\Theta}(*)$. Because a by-product of the Grouped-n Method for Estimating $\Pr^{\Theta}(*)$ is that the point estimates generated do not vary as much as the fixed-n probabilities over the same range of n values, the grouped-n estimates are considered more reliable. Hence it was concluded that whenever possible the Grouped-n Method for Estimating $\Pr^{\Theta}(*)$ should be used to estimate $\Pr^{\Theta}(*)$.

When the Grouped-n Method for Estimating $\Pr^{\Theta}(*)$ is used to estimate $\Pr^{\Theta}(*)$ for

$* \in \{(\phi, s),\ (\phi|\phi, s),\ (3_1|\phi, s),\ (4_1|\phi, s),\ (5_2|\phi, s)\}$, the following estimates result:

$$\Pr^{\Theta}(\phi, s) = \quad 0.13719 \quad \pm \quad 0.00019 \quad (\pm 0.03240)\,, \tag{6.61}$$

$$\Pr^{\Theta}(\phi|\phi, s) = \quad 0.97653 \quad \pm \quad 0.00133 \quad (\pm 0.01822)\,, \tag{6.62}$$

$$\Pr^{\Theta}(3_1|\phi, s) = \quad 0.02208 \quad \pm \quad 0.00095 \quad (\pm 0.00672)\,, \tag{6.63}$$

$$\Pr^{\Theta}(4_1|\phi, s) = \quad 0.00093 \quad \pm \quad 0.00048 \quad (\pm 0.00082)\,, \tag{6.64}$$

and

$$\Pr^{\Theta}(5_2|\phi, s) = \quad 0.00004 \quad \pm \quad 0.00003 \quad (\pm 0.00004)\,. \tag{6.65}$$

The data is concluded to numerical support Conjecture 2.2.3 which conjectures that the limiting strand passage probabilities $\Pr^{\Theta}(*)$ exist, that $\Pr^{\Theta}(*) \in (0, 1)$, and that $\Pr^{\Theta}_{2n}(\phi|\phi, s)$ decreases to $\Pr^{\Theta}(\phi|\phi, s)$ and that $\Pr^{\Theta}_{2n}(\phi, s)$ and $\Pr^{\Theta}_{2n}(K|\phi, s)$ for any non-trivial unknotting number one knot-type K increase to $\Pr^{\Theta}(\phi, s)$ and $\Pr^{\Theta}(K|\phi, s)$ respectively. But, because of the large 95% margins of error associated with the estimates for $\Pr^{\Theta}(4_1|\phi, s)$ and $\Pr^{\Theta}(5_2|\phi, s)$, the estimates for $\Pr^{\Theta}(4_1|\phi, s)$ and $\Pr^{\Theta}(5_2|\phi, s)$ are concluded to be unreliable. Thus more data needs to be generated in order to determine better estimates for $\Pr^{\Theta}(4_1|\phi, s)$ and $\Pr^{\Theta}(5_2|\phi, s)$. This is left for future work.

Chapter 7

The Size of a Θ-SAP

In this chapter, two measures of the "size" of a Θ-SAP in $\mathscr{P}^{\Theta}(\phi)$ are discussed. Both of these measures will be used to explore numerically the validity of Conjecture 2.2.8 which states that the set $\mathscr{P}^{\Theta}(\phi)$ is dominated by polygons that can be formed from one large uSAW, one small uSAW, and the structure Θ, (cf. Section 2.2.3).

Recall from Section 4.7.3 that one measure of the "size" of a self-avoiding polygon is the length of the SAP. Using this measure, the relationship between the expected lengths of the small and large uSAWs and the polygon length from which the uSAWs were taken, and the $(n \to \infty)$ scaling form of these expected lengths (that is Conjectures 2.2.10 and 2.2.11 respectively) are studied numerically in Section 7.1. Also in this section, questions regarding whether the exponent in the scaling forms for these expected lengths depends on the property $* \in \Phi$ and how the exponents compare to zero (that is Questions 2.2.2 and 2.2.3) are addressed. Also note that the numerical approach used in Section 7.1 has been adapted from a discussion in [125] regarding the size of a knot in a SAP in $\mathscr{P}(K)$.

The second measure of the "size" of a SAP in $\mathscr{P}^{\Theta}(\phi)$ is related to how much volume the uSAWs comprising Θ-SAPs occupy, that is the second measure is the radius of gyration (as defined by Equation (1.55)) of the uSAWs. In Section 7.2, this measure is used to investigate the validity of Conjecture 2.2.8 by comparing the radii of gyration of the two uSAWs to each other and to the radius of gyration of the SAP in $\mathscr{P}^{\Theta}(\phi)$ from which the two uSAWs were taken. Also in Section 7.2, for each property $* \in \Phi$, the possible relationships amongst the metric exponents $\nu_B^{\Theta}(*)$, $\nu_E^{\Theta}(*)$, $\nu_S^{\Theta}(*)$, $\nu_{\mathscr{B}}^{\Theta}(*)$, $\nu_{\mathscr{E}}^{\Theta}(*)$, $\nu_{\mathscr{S}}^{\Theta}(*)$, and ν (that is Conjectures 2.2.8-2.2.10 and Questions 2.2.11 and 2.2.12) are numerically investigated. Furthermore, the possible relationships between the amplitudes $A_{\mathscr{P}}^{\Theta}(*)$, $A_{\mathscr{E}}^{\Theta}(*)$, $A_{\mathscr{S}}^{\Theta}(*)$, $A_{\mathscr{B}}^{\Theta}(*)$, $A_E^{\Theta}(*)$, $A_S^{\Theta}(*)$, and $A_B^{\Theta}(*)$ (that is Questions 2.2.12 and 2.2.13) are also studied.

In order to numerically explore the conjectures and questions referenced in the previous two paragraphs, a sample of Θ-SAPs is required. To this end, let $\boldsymbol{W} := ((W_t(1), W_t(2),$

..., $W_t(14)), t = 0, ..., t_0)$ be a Markov chain formed by the CMC Θ-BFACF algorithm and let $\boldsymbol{\omega}^{(u)}$, where

$$\boldsymbol{\omega}^{(u)} := \left(\left(\omega_t^{(u)}(1), \omega_t^{(u)}(2), ..., \omega_t^{(u)}(14) \right), t = 0, ..., t_0 \right), \tag{7.1}$$

be the sequence of $(t_0 + 1)$ 14-tuples of Θ-SAPs from $\left(\mathscr{P}^{\Theta}(\phi)\right)^{14}$ realized in Replication u of the simulation of the CMC Θ-BFACF algorithm as described in Section 3.4.1. Then, the sample that is used in this chapter is one hundredth of the size of the sample used in the analysis in Chapters 4, 5, and 6. The reason the entire original sample is not used in this chapter is because calculating the radius of gyration requires the entire polygon configuration as opposed to only the polygon length and knot-type that were required for the analysis in Chapters 4, 5, and 6. Consequently a lot more physical storage space is required for this sample than for the sample used in Chapters 4, 5, and 6. At the time the simulation was implemented, the largest possible sample of polygon configurations (based on the physical storage space available at the time) was stored. This subsample of data consists of $l + 1$ ($l := \lfloor t_0/120000 \rfloor = 800,000$) 14-tuples of polygon configurations from Replication u and is denoted

$$\hat{\boldsymbol{\omega}}_R^{(u)} := \left(\left(\hat{\omega}_j^{(u)}(1), \hat{\omega}_j^{(u)}(2), ..., \hat{\omega}_j^{(u)}(14) \right), j = 0, ..., l \right), \tag{7.2}$$

where $\hat{\boldsymbol{\omega}}_R^{(u)}$ is the sequence of 14-tuples of SAPs sampled from Replication u such that the j'th term (for $1 \leq j \leq l$) of $\hat{\boldsymbol{\omega}}_R^{(u)}$ is given by

$$\left(\hat{\omega}_j^{(u)}(1), \hat{\omega}_j^{(u)}(2), ..., \hat{\omega}_j^{(u)}(14) \right) := \left(\omega_t^{(u)}(1), \omega_t^{(u)}(2), ..., \omega_t^{(u)}(14) \right), \tag{7.3}$$

for $t := 120,000j$. In fact, this is the subsample that results immediately from taking a sample following the attempted swap after every 100,000'th Θ-BFACF move in parallel.

Recall from Definition 2.2.3 of Section 2.2.3 that, for $\omega \in \mathscr{P}^{\Theta}(\phi)$, $w_+(\omega)$ is the uSAW on the right side of ω and $w_-(\omega)$ is the uSAW on the left side of ω. Also recall from Section 2.2.3 that, for $* \in \Phi$, the set of "big right-side $(2n)$-edge property-$*$ Θ-SAPs" is denoted $\mathscr{B}_{2n}^{+}(*)$; the set of "small right-side $(2n)$-edge property-$*$ Θ-SAPs" is denoted $\mathscr{S}_{2n}^{+}(*)$; the set of "big left-side $(2n)$-edge property-$*$ Θ-SAPs" is denoted $\mathscr{B}_{2n}^{-}(*)$; the set of "small left-side $(2n)$-edge property-$*$ Θ-SAPs" is denoted $\mathscr{S}_{2n}^{-}(*)$; and the set of "equal-sided $(2n)$-edge property-$*$ Θ-SAPs" is denoted $\mathscr{E}_{2n}(*)$. Also recall from Section

2.2.3 that, for $\omega \in \mathscr{E}^c(*)$,

$$s_{|\omega|}(\omega) := \begin{cases} |w_+(\omega)|, & \text{if } |w_+(\omega)| < |w_-(\omega)| \\ |w_-(\omega)|, & \text{otherwise,} \end{cases} \tag{7.4}$$

and

$$l_{|\omega|}(\omega) := \begin{cases} |w_+(\omega)|, & \text{if } |w_+(\omega)| > |w_-(\omega)| \\ |w_-(\omega)|, & \text{otherwise.} \end{cases} \tag{7.5}$$

In order to perform the analysis in this chapter, the following indicator function (as defined in Section 4.2.3) is required: for $A \subset \mathbb{R}$,

$$\mathscr{I}_A(x) := \begin{cases} 1, & \text{if } x \in A \\ 0, & \text{otherwise.} \end{cases} \tag{7.6}$$

Also note that for this entire chapter, the estimate for $N^*_{\max}$, for each $* \in \{\phi, (\phi, f), (\phi|\phi, s), (3_1|\phi, s)\}$, will be $\hat{N}_{\max}(*) = 1890$, as determined in Chapter 6. To explain this choice, recall that $\hat{N}_{\max}(*) = 1890$ was chosen in Chapter 6, because, for such a choice, the relative frequency data $\widehat{\text{pr}}^{\Theta}_{2n}((\phi, s), u)$ had a relative error bounded above by $\hat{\delta}_{\hat{\boldsymbol{\omega}}}(*) + 0.003 = 0.023$, where

$$\hat{\delta}_{\hat{\boldsymbol{\omega}}}(*) := \min_{n,u} \hat{\delta}^{(u)}_{2n}(*) \tag{7.7}$$

is the minimum relative error computed using the sample $\hat{\boldsymbol{\omega}}^{(u)}$, for $u \in \{1, 2, ..., 10\}$, and $\hat{\delta}^{(u)}_{2n}(*)$ is as defined by Equation (4.125). Using the same approach here, based on the subsample $\hat{\boldsymbol{\omega}}^{(u)}_R$, for $u \in \{1, 2, ..., 10\}$ and the relative error being bounded above by 0.023, results in $\hat{N}_{\max}(*) = 0$, for each $* \in \{\phi, (\phi, f), (\phi|\phi, s), (3_1|\phi, s)\}$. Hence the upper bound used to determine the $N^*_{\max}$ cut-off for the "reliable data" needs to be relaxed from the upper bound used in Chapter 6. In this chapter, since the analysis are based on 1/100'th of the data used in Chapter 6, the $N^*_{\max}$ cut-off for the "reliable data" is determined here using the upper bound $\hat{\delta}_{\hat{\boldsymbol{\omega}}_R}(*) + 0.003\sqrt{100}$ for the relative error in the relative frequencies calculated using the subsample $\hat{\boldsymbol{\omega}}^{(u)}_R$, for $u \in \{1, 2, ..., 10\}$. In this case, $\hat{N}_{\max}(*) = 1890$, for $* \in \{\phi, (\phi, f), (\phi|\phi, s)\}$, is appropriate. Using the same upper bound for property-$(3_1|\phi, s)$ yielded an estimate of 600 for $N^*_{\max}$ but because of the small amount of property-$(3_1|\phi, s)$ data and for the sake of convenience, $\hat{N}_{\max}(3_1|\phi, s) = 1890$.

In the next sections, the data set $\hat{\boldsymbol{\omega}}^{(u)}_R$ is used to address the conjectures and questions raised at the beginning of the chapter.

7.1 The Length of a uSAW

Given any $n \geq 7$, for each $* \in \Phi$, recall from Section 2.2.3 that $\mathrm{E}\left[S_{2n}(\mathscr{E}^c_{2n}(*))\right]$, defined by Equation (2.153), is the expected length of the small uSAW for a uniformly chosen $\omega \in \mathscr{E}^c_{2n}(*)$, and that $\mathrm{E}\left[L_{2n}(\mathscr{E}^c_{2n}(*))\right]$, defined by Equation (2.154), is the expected length of the large uSAW for a uniformly chosen $\omega \in \mathscr{E}^c_{2n}(*)$. In this section, estimates for $\mathrm{E}\left[S_{2n}(\mathscr{E}^c_{2n}(*))\right]$ and $\mathrm{E}\left[L_{2n}(\mathscr{E}^c_{2n}(*))\right]$, for a range of n and $* \in \{(\phi, f), (\phi|\phi, s), (3_1|\phi, s)\}$, are first calculated, are then used to check the consistency of the subsample $\hat{\boldsymbol{\omega}}^{(u)}_R$, for $u \in \{1, 2, ..., 10\}$ with the facts presented in Section 2.2.3, and are finally used to explore the validity of Conjecture 2.2.8 (that is, for sufficiently large n, $\mathscr{P}^{\Theta}_n(\phi)$ is dominated by SAPs with one large uSAW (length is $O(n)$) and one small uSAW) and Conjectures 2.2.10 and 2.2.11 (relationships involving $\mathrm{E}\left[S_{2n}(\mathscr{E}^c_{2n}(*))\right]$ and $\mathrm{E}\left[L_{2n}(\mathscr{E}^c_{2n}(*))\right]$ and their asymptotic (as $n \to \infty$) form). The estimates for $\mathrm{E}\left[S_{2n}(\mathscr{E}^c_{2n}(*))\right]$ and $\mathrm{E}\left[L_{2n}(\mathscr{E}^c_{2n}(*))\right]$ are also used to explore answers to Questions 2.2.2 and 2.2.3 (regarding the exponent of the scaling form for $\mathrm{E}\left[S_{2n}(\mathscr{E}^c_{2n}(*))\right]$). In order to begin these explorations, $\mathrm{E}\left[S_{2n}(\mathscr{E}^c_{2n}(*))\right]$ and $\mathrm{E}\left[L_{2n}(\mathscr{E}^c_{2n}(*))\right]$ need to be estimated.

For each $* \in \Phi$ and for the subset of $(2n)$-edge Θ-SAPs $\mathscr{E}^c_{2n}(*) \subseteq \mathscr{P}^{\Theta}(\phi)$, suppose W is a random property-$*$ Θ-SAP chosen from $\mathscr{E}^c_{2n}(*)$. Then define the random variables X and Y (as defined in Section A.4 of Appendix A) by

$$X(W, \mathscr{E}^c_{2n}(*)) := \xi_{\mathscr{E}^c_{2n}(*)}(W), \tag{7.8}$$

and

$$Y(W, \mathscr{E}^c_{2n}(*)) := \xi_{\mathscr{E}^c_{2n}(*)}(W)\mathfrak{s}\left(W\right), \tag{7.9}$$

where, for each $\omega \in \mathscr{P}^{\Theta}(\phi)$ and each subset of Θ-SAPs $\mathscr{V} \subseteq \mathscr{P}^{\Theta}(\phi)$,

$$\xi_{\mathscr{V}}(\omega) := \begin{cases} 1, & \text{if } \omega \in \mathscr{V} \\ 0, & \text{otherwise,} \end{cases} \tag{7.10}$$

and

$$\mathfrak{s}\left(\omega\right) := \begin{cases} 0, & \text{if } |w_+(\omega)| = |w_-(\omega)|, \\ s_{|\omega|}(\omega), & \text{otherwise.} \end{cases}$$

Further define $X_{k,i}$ and $Y_{k,i}$ (as used in Section A.4 of Appendix A) by

$$X_{k,i}(\mathscr{E}^c_{2n}(*)) := \sum_{t=0}^{t_0} \mathscr{M}_T(t)\mathscr{I}_{B(k)}\left(t\right) X(W_t(i), \mathscr{E}^c_{2n}(*)) \tag{7.11}$$

and

$$Y_{k,i}(\mathscr{E}_{2n}^{c}(*)) := \sum_{t=0}^{t_0} \mathscr{M}_T(t)\mathscr{I}_{B(k)}(t)\, Y(W_t(i), \mathscr{E}_{2n}^{c}(*))$$
$$:= N_{k,i}\left(\mathfrak{s}\left(\mathscr{E}_{2n}^{c}(*)\right)\right), \tag{7.12}$$

where $B(k)$ is defined by Equation (4.159); $\mathscr{M}_T(t)$ is defined by Equation (4.42); and, for $A \subseteq \mathbb{R}, \mathscr{I}_A(t)$is defined by Equation (7.6). Now redefine the random variables Y and $Y_{k,i}$ (as defined in Section A.4 of Appendix A) to be respectively

$$Y(W, \mathscr{E}_{2n}^{c}(*)) := \xi_{\mathscr{E}_{2n}^{c}(*)}(W)\mathfrak{b}(W), \tag{7.13}$$

and

$$Y_{k,i}(\mathscr{E}_{2n}^{c}(*)) := \sum_{t=0}^{t_0} \mathscr{M}_T(t)\mathscr{I}_{(2(k-1)\tau_{\text{int}}-1,2k\tau_{\text{int}}-1]}(t)\, Y(W_t(i), \mathscr{E}_{2n}^{c}(*))$$
$$:= N_{k,i}\left(\mathfrak{b}\left(\mathscr{E}_{2n}^{c}(*)\right)\right), \tag{7.14}$$

where, for each $\omega \in \mathscr{P}^{\Theta}(\phi)$,

$$\mathfrak{b}(\omega) := \begin{cases} 0, & \text{if } |w_+(\omega)| = |w_-(\omega)|, \\ l_{|\omega|}(\omega), & \text{otherwise,} \end{cases}$$

$B(k)$ is defined by Equation (4.159); $\mathscr{M}_T(t)$ is defined by Equation (4.42); and, for $A \subseteq \mathbb{R}, \mathscr{I}_A(t)$is defined by Equation (7.6). Note that $X_{k,i}(\mathscr{E}_{2n}^{c}(*))$ counts the number of property-$*$ $(2n)$-edge Θ-SAPs in block k of Chain i that contain a small uSAW and hence $X_{k,i}(\mathscr{E}_{2n}^{c}(*))$ also counts the number of property-$*$ $(2n)$-edge Θ-SAPs in block k of Chain i that contain a large uSAW.

Then let $\langle S_{2n}(\mathscr{E}^{c}(*))\rangle$ be the ratio estimator (as defined by Equation (A.21) in Section A.3 of Appendix A) for $\mathrm{E}[S_{2n}(\mathscr{E}^{c}(*))]$ formed using the sequence

$$((X_{k,i}(\mathscr{E}_{2n}^{c}(*)), N_{k,i}(\mathfrak{s}(\mathscr{E}_{2n}^{c}(*)))), k = 1, .., l), \tag{7.15}$$

and let $\langle L_{2n}(\mathscr{E}^{c}(*))\rangle$ be the ratio estimator (as defined by Equation (A.21) in Section A.3 of Appendix A) for $\mathrm{E}[L_{2n}(\mathscr{E}^{c}(*))]$ formed using the sequence

$$((X_{k,i}(\mathscr{E}_{2n}^{c}(*)), N_{k,i}(\mathfrak{b}(\mathscr{E}_{2n}^{c}(*)))), k = 1, .., l), \tag{7.16}$$

with $l := \lfloor t_0/(2\tau_{\text{int}})\rfloor$.

Based on the u'th realization $\boldsymbol{\omega}^{(u)}$ of $\boldsymbol{W}$, $u \in \{1, 2, ..., 10\}$, let $n_{k,i}^{(u)}\left(\mathfrak{s}\left(\mathscr{E}_{2n}^{c}(*)\right)\right)$ denote the u'th realization of $N_{k,i}\left(\mathfrak{s}\left(\mathscr{E}_{2n}^{c}(*)\right)\right)$; let $n_{k,i}^{(u)}\left(\mathfrak{b}\left(\mathscr{E}_{2n}^{c}(*)\right)\right)$ denote the u'th realization of $N_{k,i}\left(\mathfrak{b}\left(\mathscr{E}_{2n}^{c}(*)\right)\right)$; and let $x_{k,i}^{(u)}$ denote the u'th realization of $X_{k,i}\left(\mathscr{E}_{2n}^{c}(*)\right)$. Then, for each $* \in \Phi$ and for a fixed positive integer n, the estimators $\langle S_{2n}(\mathscr{E}^{c}(*))\rangle$ and $\langle L_{2n}(\mathscr{E}^{c}(*))\rangle$ defined with $t_0 = 9.6 \times 10^{10}$ time steps, $\tau_{\text{int}} = 0.72 \times 10^{9}$ time steps, $T = 120,000$ time steps, and $l := \lfloor t_0/(2\tau_{\text{int}})\rfloor = 66$ are used to calculate the point estimate $\langle s_{2n}(\mathscr{E}^{c}(*))\rangle$ for $\mathrm{E}\left[S_{2n}(\mathscr{E}^{c}(*))\right]$ by using the sequence

$$\left(\left(\left(x_{k,i}^{(u)}, n_{k,i}^{(u)}\left(\mathfrak{s}\left(\mathscr{E}_{2n}^{c}(*)\right)\right)\right), k = 1, .., l\right), u = 1, ..., 10\right) \tag{7.17}$$

in Equation (A.21) and the point estimate $\langle l_{2n}(\mathscr{E}^{c}(*))\rangle$ for $\mathrm{E}\left[L_{2n}(\mathscr{E}^{c}(*))\right]$ by using the sequence

$$\left(\left(\left(x_{k,i}^{(u)}, n_{k,i}^{(u)}\left(\mathfrak{b}\left(\mathscr{E}_{2n}^{c}(*)\right)\right)\right), k = 1, .., l\right), u = 1, ..., 10\right) \tag{7.18}$$

in Equation (A.21). The estimates $\langle s_{2n}(\mathscr{E}^{c}(*))\rangle$ and $\langle l_{2n}(\mathscr{E}^{c}(*))\rangle$ are used throughout the remainder of this section.

7.1.1 Checking the Consistency of the CMC Θ-BFACF Data

First, for all positive integers $n \in \{n_*^{\Theta}/2 + 1, n_*^{\Theta}/2 + 2, ..., 945\}$ and for each $* \in \{(\phi, f), (\phi|\phi, s), (3_1|\phi, s)\}$, the estimates $\langle s_{2n}(\mathscr{E}^{c}(*))\rangle$ and $\langle l_{2n}(\mathscr{E}^{c}(*))\rangle$ are used to check the consistency of the subsample $\hat{\boldsymbol{\omega}}_R^{(u)}$, for $u \in \{1, 2, ..., 10\}$, by verifying the following facts from Section 2.2.3:

Fact 1: Given an integer $n \geq n_*^{\Theta}/2 + 1$ and any property $* \in \Phi$,

$$\mathrm{E}\left[S_{2n}(\mathscr{E}_{2n}^{c}(*))\right] < n - 3 < \mathrm{E}\left[L_{2n}(\mathscr{E}_{2n}^{c}(*))\right]. \tag{7.19}$$

Fact 2: As $n \to \infty$, for each property $* \in \Phi$, $\mathrm{E}\left[L_{2n}(\mathscr{E}_{2n}^{c}(*))\right]$ is $O(n)$.

To explore whether the data support Fact 1, the estimates $\langle s_{2n}(\mathscr{E}^{c}(*))\rangle$ and $\langle l_{2n}(\mathscr{E}^{c}(*))\rangle$, for each $* \in \{(\phi, f)\,[\times],\ (\phi|\phi, s)\,[\boxdot],\ (3_1|\phi, s)\,[\triangle]\}$ and $n \in \{n_*^{\Theta}/2 + 1, n_*^{\Theta}/2 + 2, ..., 945\}$, are plotted in Figures 7.1 and 7.2. Note that for the purposes of creating a more illustrative plot, every tenth term in the corresponding sequence of estimates $(\langle l_{2n}(\mathscr{E}^{c}(*))\rangle, n \in \{n_*^{\Theta}/2 + 1, n_*^{\Theta}/2 + 2, ..., 945\})$ and $\left(\langle s_{2n}(\mathscr{E}^{c}(*))\rangle, n \in \{n_*^{\Theta}/2 + 1, n_*^{\Theta}/2 + 2, ..., 945\}\right)$ is plotted in Figures 7.1 and 7.2 and the dashed line in both figures represents the line $y = n - 3$.

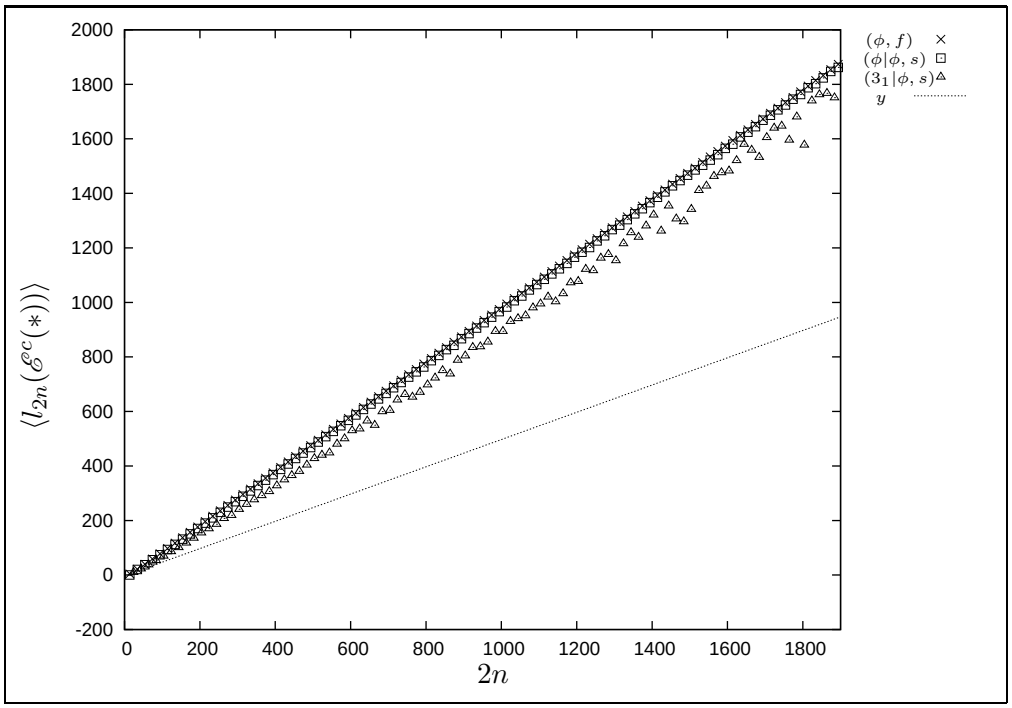

Figure 7.1: The estimates $\langle l_{2n}(\mathscr{E}^c(*))\rangle$, for $* \in \{(\phi, f)\,[\times],\ (\phi|\phi, s)\,[\boxdot],\ (3_1|\phi, s)\,[\triangle]\}$, plotted versus $2n$. The dashed line represents the line $y = n - 3$.

The estimates $\langle s_{2n}(\mathscr{E}^c(*))\rangle$ and $\langle l_{2n}(\mathscr{E}^c(*))\rangle$ plotted in Figures 7.1 and 7.2 are consistent with Fact 1, because, by comparing both figures, for each $* \in \{(\phi, f),\ (\phi|\phi, s),\ (3_1|\phi, s)\}$ and those values of n plotted,

$$\langle s_{2n}(\mathscr{E}^c(*))\rangle < n - 3 < \langle l_{2n}(\mathscr{E}^c(*))\rangle. \tag{7.20}$$

Note that the author has confirmed that the above inequality holds for each $* \in \{(\phi, f),\ (\phi|\phi, s),\ (3_1|\phi, s)\}$ and for every $n \in \{n_*^\Theta/2 + 1, n_*^\Theta/2 + 2, ..., 945\}$, thus numerically confirming Fact 1.

To determine, whether or not the data support Fact 2 above, if, as n increases, the estimates $\dfrac{\langle l_{2n}(\mathscr{E}^c(*))\rangle}{2n}$, for each $* \in \{(\phi, f)\,[\times],\ (\phi|\phi, s)\,[\boxdot],\ (3_1|\phi, s)\,[\triangle]\}$, become constant, then the data supports Fact 2. For each $* \in \{(\phi, f),\ (\phi|\phi, s),\ (3_1|\phi, s)\}$ and for every $n \in \{n_*^\Theta/2 + 1, n_*^\Theta/2 + 2, ..., 945\}$, the estimates $\dfrac{\langle l_{2n}(\mathscr{E}^c(*))\rangle}{2n}$ are plotted in Figure 7.3. In order to create a more illustrative figure, note that the estimate for $\dfrac{\langle l_{2n}(\mathscr{E}^c(*))\rangle}{2n}$ for every tenth value of n is displayed in the figure.

From Figure 7.3, it appears possible that, as $n \to \infty$,

$$\frac{\langle l_{2n}(\mathscr{E}^c\,(\phi, f))\rangle}{2n} \to 1,\ \frac{\langle l_{2n}(\mathscr{E}^c\,(\phi|\phi, s))\rangle}{2n} \to 1,\ \text{and}\ \frac{\langle l_{2n}(\mathscr{E}^c\,(3_1|\phi, s))\rangle}{2n} \to 1. \tag{7.21}$$

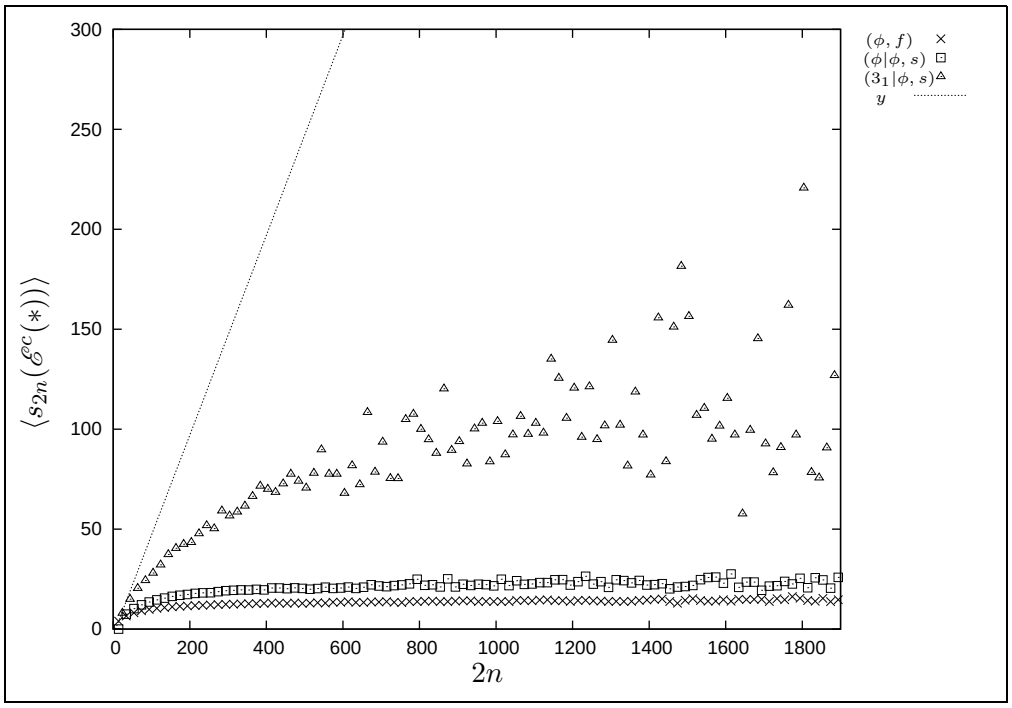

Figure 7.2: The estimates $\langle s_{2n}(\mathscr{E}^{cc}(*))\rangle$, for $* \in \{(\phi, f)\,[\times],\ (\phi|\phi, s)\,[\boxdot],\ (3_1|\phi, s)\,[\triangle]\}$, plotted versus $2n$. The dashed line represents the line $y = n - 3$.

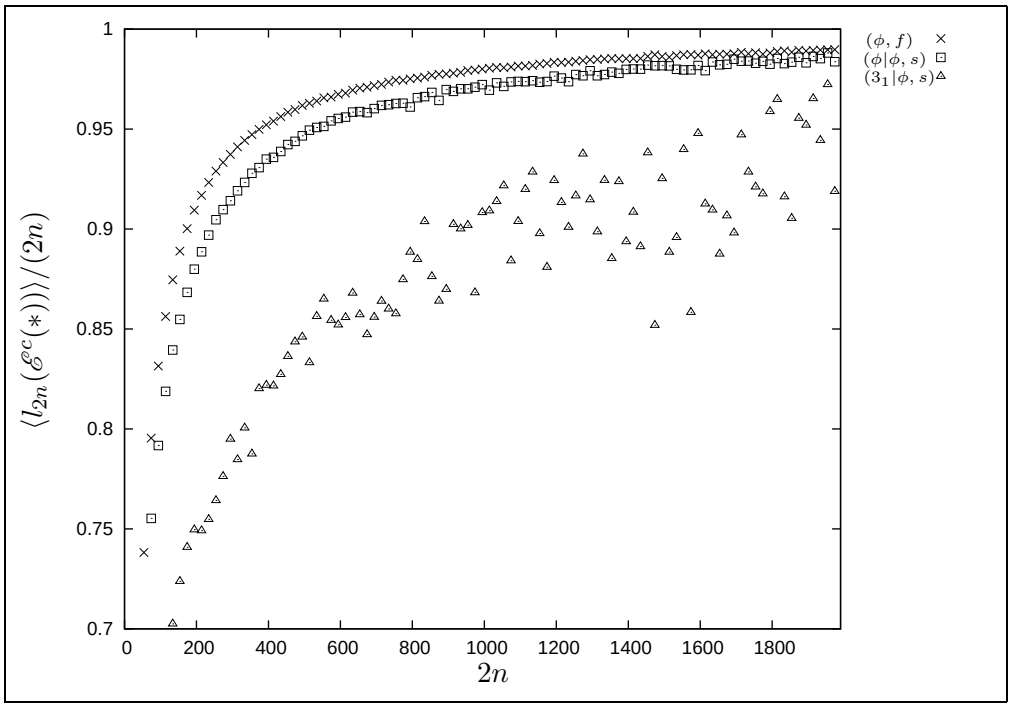

Figure 7.3: For each property $* \in \{(\phi, f)\,[\times],\ (\phi|\phi, s)\,[\boxdot],\ (3_1|\phi, s)\,[\triangle]\}$, the ratio of the estimated expected length of the large uSAW for a $(2n)$-edge SAP in $\mathscr{E}^{cc}(*)$, and $2n$.

To garner more conclusive numerical support for Fact 2, for $* \in \{(\phi, f),\ (\phi|\phi, s),\ (3_1|\phi, s)\}$, curves of the form

$$f(n) = m_l(*)n^{\zeta_l(*)} + b_l(*) \tag{7.22}$$

are fit to the data displayed in Figure 7.3 in order to estimate the exponents $\zeta_l(*)$, for $* \in \{(\phi, f),\ (\phi|\phi, s),\ (3_1|\phi, s)\}$. However, in order to estimate the exponents $\zeta_l(*)$, for each $* \in \{(\phi, f),\ (\phi|\phi, s),\ (3_1|\phi, s)\}$, using weighted non-linear regression and Equation (7.22), an essentially independent sample of estimates for $\mathrm{E}\left[L_{2n}(\mathscr{E}^c(*))\right]$ is required. Using the technique from Section 4.3.2, it was determined that $\langle l_{2n}(\mathscr{E}^c(*))\rangle$ and $\langle l_{2n+k}(\mathscr{E}^c(*))\rangle$, for each of the properties $* \in \{(\phi, f),\ (\phi|\phi, s),\ (3_1|\phi, s)\}$, are essentially independent if minimally $k = 180$.

For each $* \in \{(\phi, f)\,[\times],\ (\phi|\phi, s)\,[\boxdot],\ (3_1|\phi, s)\,[\triangle]\}$, one possible essentially independent sample of estimates for $\mathrm{E}\left[L_{2n}(\mathscr{E}^c(*))\right]$ over the interval of $n \in \{n_*^{\Theta}/2+1, n_*^{\Theta}/2+2, ..., 945\}$ is displayed in Figure 7.4. Because $\mathscr{P}^{\Theta}(\phi, f)$, $\mathscr{P}^{\Theta}(\phi|\phi, s)$, and $\mathscr{P}^{\Theta}(3_1|\phi, s)$ are mutually exclusive sets, the estimates displayed in Figure 7.4 best illustrate any relationships that exist or do not exist amongst the average lengths of the large uSAWs as a function of $2n$ for these subsets of $\mathscr{P}^{\Theta}(\phi)$. Note that the values (and the corresponding estimated 95% margins of error) plotted in Figure 7.4 can be found in Tables B.11, B.12, and B.13 (cf. Section B.2 of Appendix B).

Fitting a function of the form given by Equation (7.22) to each of the sequences of data plotted in Figure 7.4 yields the following estimates for the exponents $\zeta_l(*)$, for $* \in \{(\phi, f),\ (\phi|\phi, s),\ (3_1|\phi, s)\}$:

$$\zeta_l(\phi, f) = 1.0032(0.0046), \tag{7.23}$$

$$\zeta_l(\phi|\phi, s) = 1.0087(0.0140), \tag{7.24}$$

and

$$\zeta_l(3_1|\phi, s) = 1.0826(0.1666), \tag{7.25}$$

where the value in parentheses is the estimated 95% margin of error. Note that one is in each of the estimated 95% confidence intervals. Therefore, at the $\alpha = 0.05$ level of significance, it cannot be ruled out that $\zeta_l(\phi, f) = \zeta_l(\phi|\phi, s) = \zeta_l(3_1|\phi, s) = 1$. This supports Fact 2: $\mathrm{E}\left[L_{2n}(\mathscr{E}^c(\phi, f))\right]$, $\mathrm{E}\left[L_{2n}(\mathscr{E}^c(\phi|\phi, s))\right]$, and $\mathrm{E}\left[L_{2n}(\mathscr{E}^c(3_1|\phi, s))\right]$ are $O(n)$.

Having shown that the data supports Facts 1 and 2, the data is concluded to be consistent with Facts 1 and 2. As a result, the discussion turns to using the data to

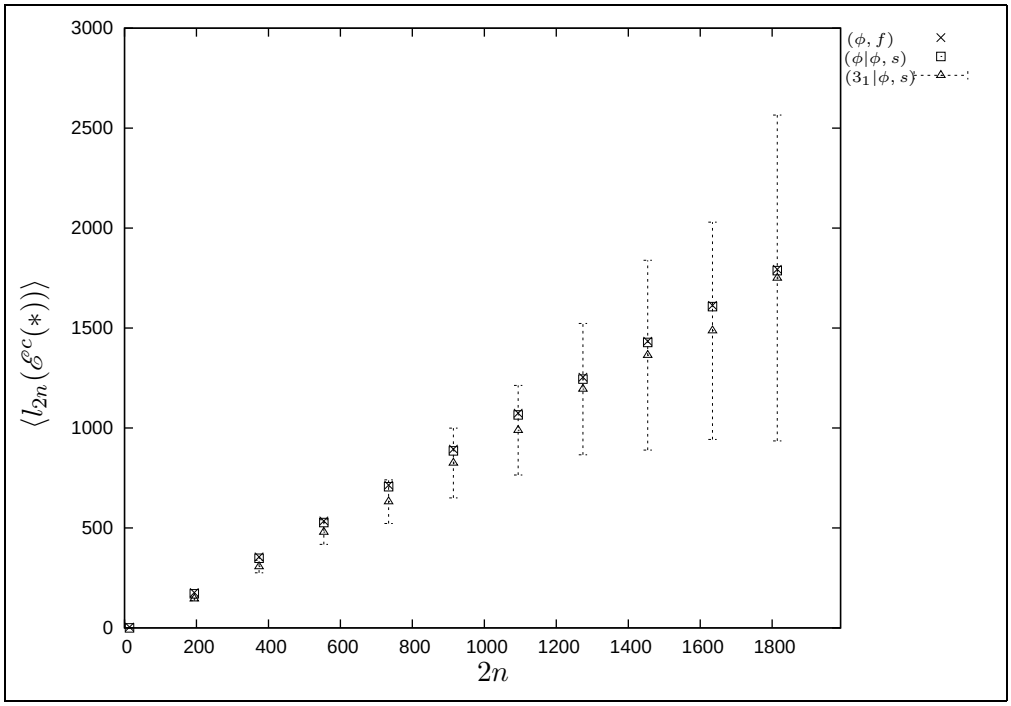

Figure 7.4: An essentially independent sample of the estimated expected lengths of the large uSAWs in $(2n)$-edge SAPs in $\mathscr{E}^c(*)$ for each $* \in \{(\phi, f)\,[\times],\ (\phi|\phi, s)\,[\boxdot],\ (3_1|\phi, s)\,[\triangle]\}$. The error bars represent the corresponding estimated 95% margins of error.

explore Conjectures 2.2.10 and 2.2.11 and Conjecture 2.2.8.

7.1.2 Testing the Validity of Conjectures 2.2.8, 2.2.10, and 2.2.11

The discussion in this chapter thus far has focused on testing the consistency of the data generated by the CMC Θ-BFACF algorithm using known facts. The remainder of the discussion in this section uses the sample of Θ-SAPs generated by the CMC Θ-BFACF algorithm to explore the validity of Conjectures 2.2.8, 2.2.10, and 2.2.11.

Exploring Conjecture 2.2.10

First, for each $* \in \{(\phi, f), (\phi|\phi, s), (3_1|\phi, s)\}$, the estimates $\langle s_{2n}(\mathscr{E}^c(*))\rangle$ and $\langle l_{2n}(\mathscr{E}^c(*))\rangle$ are used to explore the validity of Conjecture 2.2.10, that is to determine whether or not, for each natural number $n \geq 13 = n^{\Theta}_{(3_1|\phi,s)}/2+1$, $\langle s_{2n}(\mathscr{E}^c(*))\rangle$ and $\langle l_{2n}(\mathscr{E}^c(*))\rangle$ numerically support

$$\mathrm{E}\left[S_{2n}(\mathscr{E}^c(3_1|\phi, s))\right] \geq \mathrm{E}\left[S_{2n}(\mathscr{E}^c(\phi, f))\right] \tag{7.26}$$

and

$$\mathrm{E}\left[L_{2n}(\mathscr{E}^c(3_1|\phi, s))\right] \leq \mathrm{E}\left[L_{2n}(\mathscr{E}^c(\phi, f))\right]. \tag{7.27}$$

From Figure 7.1 (though on the scale of the plot as presented here, it is difficult to see), the author has verified that the following inequality holds for each plotted estimate.

$$\langle l_{2n}(\mathscr{E}^c\left(3_1|\phi, s\right))\rangle < \langle l_{2n}(\mathscr{E}^c\left(\phi|\phi, s\right))\rangle < \langle l_{2n}(\mathscr{E}^c\left(\phi, f\right))\rangle. \tag{7.28}$$

In fact, the author has verified that Inequality (7.28) holds for every integer $n \in \{13, 14, ..., 945\}$. Therefore the estimates $\langle l_{2n}(\mathscr{E}^c(*))\rangle$ for $\mathrm{E}\left[L_{2n}(\mathscr{E}^c(*))\right]$, for $* \in \{(\phi, f), (\phi|\phi, s), (3_1|\phi, s)\}$ and $n \in \{13, 14, ..., 945\}$, numerically support Conjecture 2.2.10.

Similarly, from Figure 7.2, it can be seen that for every point estimate plotted

$$\langle s_{2n}(\mathscr{E}^c\left(\phi, f\right))\rangle < \langle s_{2n}(\mathscr{E}^c\left(\phi|\phi, s\right))\rangle < \langle s_{2n}(\mathscr{E}^c\left(3_1|\phi, s\right))\rangle. \tag{7.29}$$

Further to this, the author has verified that Inequality (7.29) holds for every integer $n \in \{13, 14, ..., 945\}$. Hence the point estimates $\langle s_{2n}(\mathscr{E}^c(*))\rangle$ and $\langle l_{2n}(\mathscr{E}^c(*))\rangle$, for $* \in \{(\phi, f), (\phi|\phi, s), (3_1|\phi, s)\}$ and $n \in \{13, 14, ..., 945\}$, support Conjecture 2.2.10.

Exploring Conjecture 2.2.8

In order to determine whether or not the data numerically supports Conjecture 2.2.8 ($\mathscr{P}^{\Theta}(\phi)$ is dominated by SAPs with one large uSAW and one small uSAW), for each property $* \in \Phi$, the proportion of Θ-SAPs with equal-length uSAWs amongst the $(2n)$-edge property-$*$ Θ-SAPs is first estimated. To this end, consider $\mathscr{P}^{\Theta}_{2n}(\phi)$ for a fixed positive integer n. Note that for any $(2n)$-edge Θ-SAP in $\mathscr{P}^{\Theta}_{2n}(\phi)$, if $n-3$ is odd, then the Θ-SAP cannot have equal-length uSAWs. If it did, then the uSAW would have to have an odd number of edges which is impossible. Hence, for every $n \in \{8, 10, 12, ...\}$, the sets $\mathscr{P}^{\Theta}_{2n}(\phi)$ contain no Θ-SAPs formed by two equal-length uSAWs. Therefore consider, for each $n \in \{7, 9, 11, ...\}$, the sets $\mathscr{P}^{\Theta}_{2n}(\phi)$. Figure 7.5 plots, on a logarithmic (base 10) scale, the proportion of $(2n)$-edge property-$*$ ($* \in \{(\phi, f)\,[\times], (\phi|\phi, s)\,[\boxdot], (3_1|\phi, s)\,[\triangle]\}$) Θ-SAPs that contain equal-length uSAWs versus $2n$, where $n \in \{7, 9, 11, ..., 299\}$, that is, Figure 7.5 is a plot, on a logarithmic (base 10) scale, of the estimates

$$\left\langle \frac{|\mathscr{E}_{2n}(*)|}{\left|\mathscr{P}^{\Theta}_{2n}(*)\right|} \right\rangle := \frac{\sum_{u=1}^{10}\sum_{j=0}^{l} \xi_{\mathscr{E}_{2n}(*)}\left(\hat{\omega}_j^{(u)}(i)\right)}{\sum_{u=1}^{10}\sum_{j=0}^{l} \xi_{\mathscr{P}^{\Theta}_{2n}(*)}\left(\hat{\omega}_j^{(u)}(i)\right)}, \tag{7.30}$$

for $* \in \{(\phi, f), (\phi|\phi, s), (3_1|\phi, s)\}$ and the integer values $n \in \{7, 9, 11, ..., 299\}$. In order to create a more meaningful figure, the estimated proportions associated with every sixth consecutive value (starting with $n = 7$) in $\{7, 9, 11, ..., 299\}$ are plotted. For the same reason, because, for values of $n \in \{301, 304, ..., 945\}$, the associated estimated proportions are less than 10^{-5}, the plot is restricted to values of $n \leq 299$.

Note that for $* \in \{(\phi, f), (\phi|\phi, s)\}$, every Θ-SAP in $\mathscr{P}^{\Theta}_{14}(*)$ consists of two equal-length uSAWs and the structure Θ. Hence, in Figure 7.5, $\left\langle \frac{|\mathscr{E}_{14}(\phi,f)|}{\left|\mathscr{P}^{\Theta}_{14}(\phi,f)\right|} \right\rangle = \left\langle \frac{|\mathscr{E}_{14}(\phi|\phi,s)|}{\left|\mathscr{P}^{\Theta}_{14}(\phi|\phi,s)\right|} \right\rangle = 1$. Because the estimated proportions displayed in Figure 7.5 appear to be generally decreasing as polygon length $(2n)$ increases and because these proportions are less than 10^{-5} for all values of $n \in \{301, 303, .., 945\}$, the estimated proportions support the hypothesis that $\frac{|\mathscr{E}_{2n}(*)|}{\left|\mathscr{P}^{\Theta}_{2n}(*)\right|} \to 0$ as $n \to \infty$ (through odd values of $n \geq 7$) which in turn supports that, for every even integer $n \geq 8$ and for all sufficiently large odd values of n, $\mathscr{P}^{\Theta}_{2n}(*)$ is dominated by Θ-SAPs that contain one large and one small uSAW.

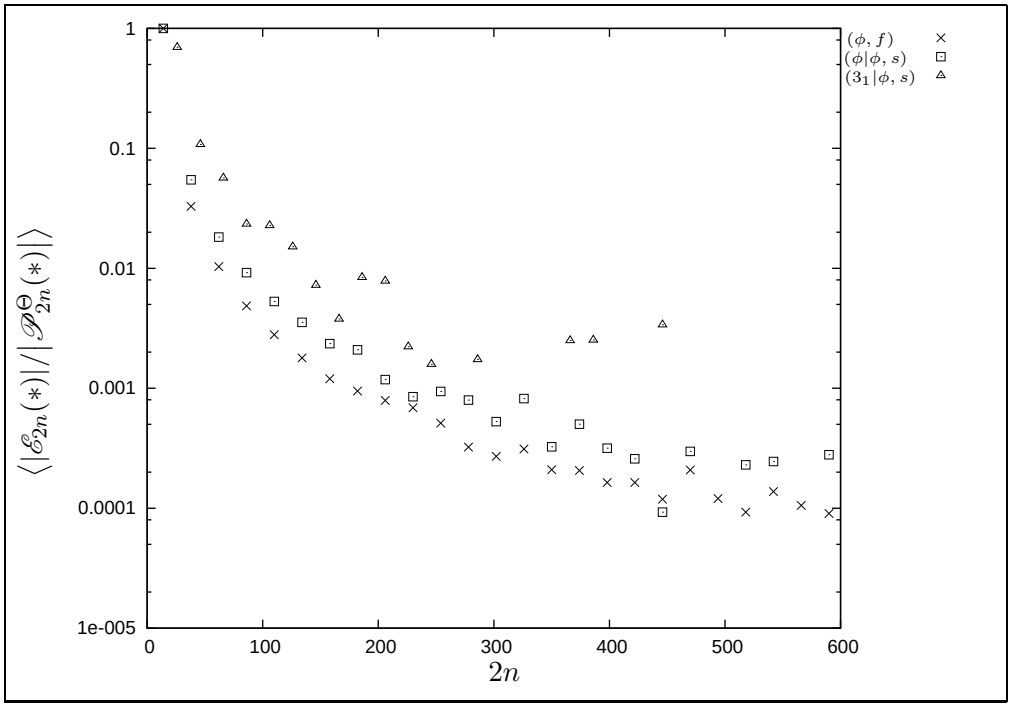

Figure 7.5: For $* \in \{(\phi, f)\,[\times],\ (\phi|\phi, s)\,[\boxdot],\ (3_1|\phi, s)\,[\triangle]\}$ and the odd values of $n \in \{n^{\Theta}_*/2, n^{\Theta}_*/2+1, ..., 299\}$, the estimates $\left\langle \frac{|\mathscr{E}_{2n}(*)|}{|\mathscr{P}^{\Theta}_{2n}(*)|} \right\rangle$ are plotted on a logarithmic (base 10) scale versus $2n$.

Exploring Conjecture 2.2.11

Recall that Conjecture 2.2.11 hypothesizes that $\mathrm{E}\left[S_{2n}(\mathscr{E}^{c}(*))\right]$ grows sub-linearly in $2n$ as $n \to \infty$. To explore how $\mathrm{E}\left[S_{2n}(\mathscr{E}^{c}(*))\right]$, for each $* \in \{(\phi, f),\ (\phi|\phi, s),\ (3_1|\phi, s)\}$, behaves as a function of polygon length $2n$, the ratios $\dfrac{\langle s_{2n}(\mathscr{E}^{c}(*))\rangle}{2n}$, for each $* \in \{(\phi, f),\ (\phi|\phi, s),\ (3_1|\phi, s)\}$ and for every $n \in \{n_*^{\Theta}/2+1, n_*^{\Theta}/2+2, ..., 945\}$, are used. If the expected length of the small uSAW in a randomly selected Θ-SAP from $\mathscr{E}_{2n}^{c}(*)$ grows linearly in $2n$, then it is expected that

$$\lim_{n\to\infty} \frac{\langle s_{2n}(\mathscr{E}^{c}(*))\rangle}{2n} = \upsilon_s^* > 0; \tag{7.31}$$

otherwise, if the expected length of the small uSAW in a randomly selected Θ-SAPs from $\mathscr{E}_{2n}^{c}(*)$ grows sub-linearly in $2n$, then it is expected that

$$\lim_{n\to\infty} \frac{\langle s_{2n}(\mathscr{E}^{c}(*))\rangle}{2n} = 0. \tag{7.32}$$

In Figure 7.6, it appears possible that, as $n \to \infty$,

$$\frac{\langle s_{2n}(\mathscr{E}^{c}(\phi, f))\rangle}{2n} \to 0,\ \frac{\langle s_{2n}(\mathscr{E}^{c}(\phi|\phi, s))\rangle}{2n} \to 0,\ \text{and}\ \frac{\langle s_{2n}(\mathscr{E}^{c}(3_1|\phi, s))\rangle}{2n} \to 0. \tag{7.33}$$

This supports the hypothesis that $\mathrm{E}\left[S_{2n}(\mathscr{E}^{c}(*))\right]$, for each $* \in \{(\phi, f),\ (\phi|\phi, s),\ (3_1|\phi, s)\}$, grows sub-linearly in $2n$, which, in turn, supports that the asymptotic ($n \to \infty$) form for $\mathrm{E}\left[S_{2n}(\mathscr{E}^{c}(*))\right]$ given by Conjecture 2.2.11 is plausible.

Additional support for the validity of Conjecture 2.2.11 can be obtained from the fact that

$$\mathrm{E}\left[S_{2n}(\mathscr{E}^{c}(*))\right] + \mathrm{E}\left[L_{2n}(\mathscr{E}^{c}(*))\right] + 6 = 2n. \tag{7.34}$$

Solving Equation (7.34) for $\mathrm{E}\left[S_{2n}(\mathscr{E}^{c}(*)\right]$ yields

$$\mathrm{E}\left[S_{2n}(\mathscr{E}^{c}(*))\right] = 2n - 6 - \mathrm{E}\left[L_{2n}(\mathscr{E}^{c}(*))\right]. \tag{7.35}$$

The fact that $\mathrm{E}\left[L_{2n}(\mathscr{E}^{c}(*))\right] = O(n)$ implies that, for n sufficiently large, there exist constant $m_l^{-}(*)$ and $m_l^{+}(*)$ and functions $f_*^{-}(n) = o(n)$ and $f_*^{+}(n) = o(n)$ such that

$$2m_l^{-}(*)n + f_*^{-}(2n) \leq \mathrm{E}\left[L_{2n}(\mathscr{E}^{c}(*))\right] \leq 2m_l^{-}(*)n + f_*^{+}(2n). \tag{7.36}$$

Combining Equation (7.35) with Inequality (7.36) yields that, for n sufficiently large,

$$2n - 6 - (2m_l^{+}(*)n + f_*^{+}(2n)) \leq \mathrm{E}\left[S_{2n}(\mathscr{E}^{c}(*))\right] \leq 2n - 6 - (2m_l^{-}(*)n + f_*^{-}(2n)). \tag{7.37}$$

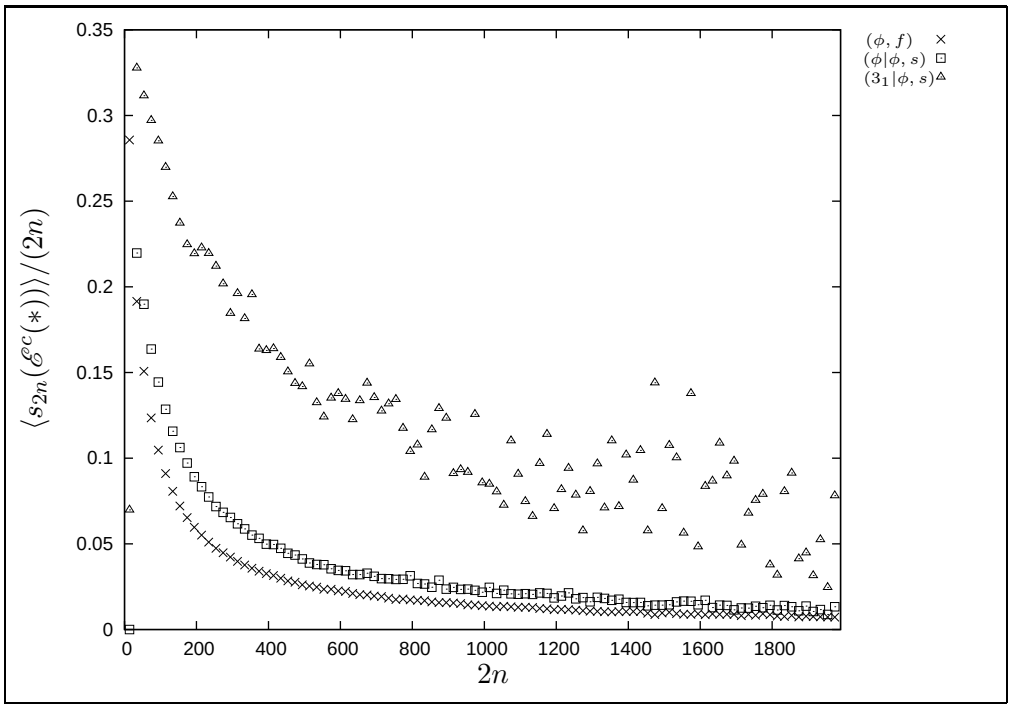

Figure 7.6: For each property $* \in \{(\phi, f)\,[\times], (\phi|\phi, s)\,[\boxdot], (3_1|\phi, s)\,[\triangle]\}$, the ratio of the estimated expected length of the small uSAW for a $(2n)$-edge SAP in $\mathscr{E}^c(*)$, and $2n$.

where $f_*^-(n) = o(n)$ and $f_*^+(n) = o(n)$. Dividing Inequality (7.37) by $2n$ yields, for n sufficiently large,

$$1 - m_l^+(*) - \frac{(6 + f_*^+(2n))}{2n} \leq \frac{\mathrm{E}\left[S_{2n}(\mathscr{E}^c(*))\right]}{2n} \leq 1 - m_l^-(*) - \frac{(6 + f_*^-(2n))}{2n}. \tag{7.38}$$

Hence if $m_l^+(*) = m_l^-(*) = 1$, then, as $n \to \infty$,

$$\frac{\mathrm{E}\left[S_{2n}(\mathscr{E}^c(*))\right]}{2n} \to 0 \tag{7.39}$$

and $\mathrm{E}\left[S_{2n}(\mathscr{E}^c(*))\right]$ grows sub-linearly in $2n$. If either $m_l^+(*) < 1$ or $m_l^-(*) < 1$, then, as $n \to \infty$, $\mathrm{E}\left[S_{2n}(\mathscr{E}^c(*)\right] = O(n)$.

In order to determine if, at least numerically, $m_l^+(*) = m_l^-(*) = 1$ is possible, functions of the form

$$f(n) = m_l(*)n^{\zeta_l(*)} + b_l(*) \tag{7.40}$$

are fit to the data displayed in Figure 7.3 using weighted, non-linear, least-squares regression. The following estimates for $m_l(*)$, for each $* \in \{(\phi, f), (\phi|\phi, s), (3_1|\phi, s)\}$, are obtained:

$$m_l(\phi, f) = 0.9744(0.0349), \tag{7.41}$$

$$m_l(\phi|\phi, s) = 0.9327(0.1024), \tag{7.42}$$

and

$$m_l(3_1|\phi, s) = 0.5144(0.6539), \tag{7.43}$$

where the value in parentheses is the estimated 95% margin of error. Note that the value one is in each of the estimated 95% confidence intervals. Therefore, at the $\alpha = 0.05$ level of significance, it cannot be ruled out that $m_l(\phi, f) = m_l(\phi|\phi, s) = m_l(3_1|\phi, s) = 1$. Hence, at least numerically, it is possible that $\mathrm{E}\left[S_{2n}(\mathscr{E}^c(*))\right]$ grows sub-linearly in $2n$.

To investigate further whether there is numerical support for Conjecture 2.2.11, curves of the form

$$f(n) = m_*^s n^{\zeta_s(*)} + b_*^s \tag{7.44}$$

are fit to the data displayed in Figure 7.6 in order to estimate the exponents $\zeta_s(*)$, for $* \in \{(\phi, f),\ (\phi|\phi, s),\ (3_1|\phi, s)\}$. However, as before, in order to estimate the exponents $\zeta_s(*)$, for $* \in \{(\phi, f), (\phi|\phi, s), (3_1|\phi, s)\}$, using weighted, non-linear, least-squares regression and Equation (7.44), an essentially independent sample of estimates for $\mathrm{E}\left[S_{2n}(\mathscr{E}^c(*))\right]$, for $* \in \{(\phi, f),\ (\phi|\phi, s),\ (3_1|\phi, s)\}$, is required. Using the technique from Section 4.3.2, it has been determined that $\langle s_{2n}(\mathscr{E}^c(*))\rangle$ and $\langle s_{2n+k}(\mathscr{E}^c(*))\rangle$, for each of the properties $* \in \{(\phi, f), (\phi|\phi, s), (3_1|\phi, s)\}$, are essentially independent if minimally $k = 180$. For each $* \in \{(\phi, f),\ (\phi|\phi, s),\ (3_1|\phi, s)\}$, one such essentially independent sample of estimates for $\mathrm{E}\left[S_{2n}(\mathscr{E}^c(*))\right]$ over the interval of $n \in \{n_*^\Theta/2 + 1, n_*^\Theta/2 + 2, ..., 945\}$ is displayed in Figure 7.7. Note that the values (and the corresponding estimated 95% margins of error) plotted in Figure 7.7 can be found in Tables B.11, B.12, and B.13 (cf. Section B.2 of Appendix B).

Using weighted, non-linear, least-squares regression, fitting a function of the form given by Equation (7.44) to each of the sequences of data in Figure 7.7, respectively, yields the following estimates for the exponents $\zeta_s(*)$, for $* \in \{(\phi, f),\ (\phi|\phi, s),\ (3_1|\phi, s)\}$:

$$\zeta_s(\phi, f) = 0.03(0.39), \tag{7.45}$$

$$\zeta_s(\phi|\phi, s) = 0.03(0.48), \tag{7.46}$$

and

$$\zeta_s(3_1|\phi, s) = 0.088(0.97), \tag{7.47}$$

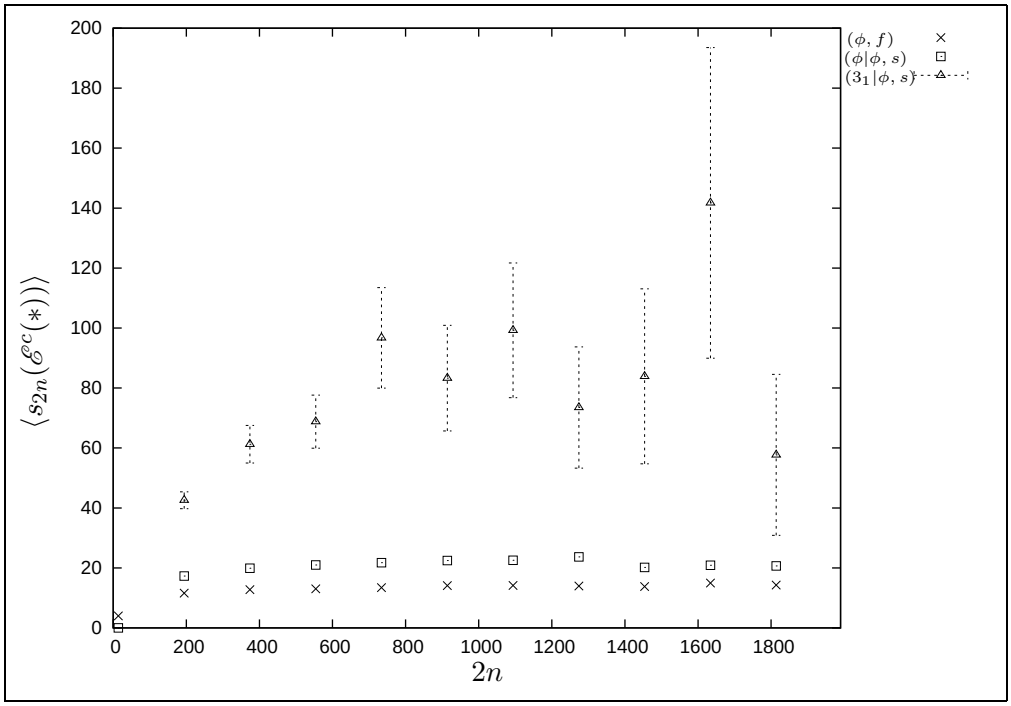

Figure 7.7: An essentially independent sample of the estimated expected lengths of the small uSAWs in $(2n)$-edge SAPs in $\mathscr{E}^c(*)$ for each $* \in \{(\phi, f)\,[\times],\ (\phi|\phi, s)\,[\boxdot],\ (3_1|\phi, s)\,[\triangle]\}$. The error bars represent the corresponding estimated 95% margins of error.

where the value in parentheses is the estimated 95% margin of error. Note that zero is in each of the estimated 95% confidence intervals. Therefore, at the $\alpha = 0.05$ level of significance, it cannot be ruled out that $\zeta_s(\phi, f) = \zeta_s(\phi|\phi, s) = \zeta_s(3_1|\phi, s) = 0$, that is, on average, it is possible that the small uSAWs created from $(2n)$-edge polygons in $\mathscr{E}^c(\phi)$ that have the property $* \in \{(\phi, f),\ (\phi|\phi, s),\ (3_1|\phi, s)\}$ are constant in the length of the polygon from which they were formed. This suggests that, on average, it is possible that the length of the small uSAW in a $(2n)$-edge polygon in $\mathscr{E}^c(\phi)$ is $O(1)$, which supports that $\mathrm{E}\left[S_{2n}(\mathscr{E}^c(*))\right] \sim (2n)^0$. Hence the numerical evidence supports Conjecture 2.2.11.

The numerical evidence also supports the following answer to Question 2.2.2 and 2.2.3: for each $* \in \Phi$, the exponents $\zeta_s(*) = 0$ and hence are independent of the property $*$. Due to the large 95% margins of error in the estimates for $\zeta_s(*)$ given by Equations (7.45)-(7.47), more data must be collected before the numerics can more conclusively support Conjecture 2.2.11 and that $\mathrm{E}\left[S_{2n}(\mathscr{E}^c(*))\right] = O(1)$.

An important issue to note is that due to the limited amount of property-$(3_1|\phi, s)$ data available and the lack of properties-$(K|\phi, s)$ (where $K \in \mathscr{K}^{\Theta}(\phi)$ and K is not the unknot or the trefoil) data available, the exploration of Conjecture 2.2.8, Conjectures 2.2.10 and 2.2.11 , and Questions 2.2.2 and 2.2.3 with respect to properties $(K|\phi, s)$, where K is a non-trivial knot-type in $\mathscr{K}^{\Theta}(\phi)$, is by no means finished. In fact these explorations are left as future work.

The discussion now turns to the final work presented in this thesis, that is the discussion turns to "How much volume in space do the uSAWs in $\mathscr{K}^{\Theta}(\phi)$ occupy?".

7.2 The Radius of Gyration of a uSAW

Recall from Section 2.2.3 of Chapter 2 that, for each $* \in \Phi$ and for each fixed positive integer $n \geq n_*^{\Theta}/2$ (where n_*^{Θ} is the length of a smallest Θ-SAP that has property $* \in \Phi$), the expected mean-square radius of gyration for a randomly selected $(2n)$-edge property-$*$ element from the finite non-empty subset $\mathscr{U}_{2n}(*) \subseteq \mathscr{P}^{\Theta}(\phi)$ is denoted $r^2\left(\mathscr{U}_{2n}(*)\right)$, and, for the function $f : \mathbb{Z}^3 \to \mathbb{Z}^3$, the f-transformed mean-square radius of gyration is denoted $r^2(f(\mathscr{U}_{2n}(*)))$. From Section 2.2.3, also recall that $\mathscr{E}_{2n}^c(*)$ is the set of property-$*$ $(2n)$-edge Θ-SAPs that contain one uSAW which is larger than the other uSAW, and that $\mathscr{E}_{2n}(*)$ is the set of property-$*$ $(2n)$-edge Θ-SAPs that contain equal-length uSAWs. Finally, from

Section 2.2.3, recall the small uSAW function $\mathfrak{w}_s$ (defined by Equation (2.168)), the large uSAW function $\mathfrak{w}_l$ (defined by Equation (2.169)), and the equal-length uSAW function $\mathfrak{w}_e$ (defined by Equation (2.170)).

In this section, for a range of n and each $* \in \{(\phi, f), (\phi|\phi, s), (3_1|\phi, s)\}$, estimates for $r^2\left(\mathfrak{w}_s\left(\mathscr{E}^c_{2n}(*)\right)\right)$, $r^2\left(\mathfrak{w}_e\left(\mathscr{E}_{2n}(*)\right)\right)$, and $r^2\left(\mathfrak{w}_l\left(\mathscr{E}^c_{2n}(*)\right)\right)$, and, for each set $\mathscr{U}_{2n}(*) \in \{\mathscr{P}^{\Theta}_{2n}(*)$, $\mathscr{E}_{2n}(*)$, $\mathscr{E}2^c_n(*)\}$, estimates for $r^2\left(\mathscr{U}_{2n}(*)\right)$ are calculated. These estimates are then used to explore how the expected mean-square radii of gyration depend on the subsets of $\mathscr{P}^{\Theta}(\phi)$, the property $* \in \Phi$, and the functions $\mathfrak{w}_s$, $\mathfrak{w}_e$, and $\mathfrak{w}_l$, (that is Questions 2.2.4-2.2.5). The estimates for $r^2\left(\mathfrak{w}_s\left(\mathscr{E}^c_n(*)\right)\right)$ and $r^2\left(\mathfrak{w}_l\left(\mathscr{E}^c_n(*)\right)\right)$ are also used to test the validity of Conjecture 2.2.8 where the radius of gyration is used to measure the size of a uSAW. Then, for each property $* \in \{(\phi, f)$, $(\phi|\phi, s)$, $(3_1|\phi, s)\}$, the possible relationships (that is Questions 2.2.8-2.2.12) amongst the metric exponents $\nu^{\Theta}_{\mathfrak{w}_l(\mathscr{E}^c)}(*)$, $\nu^{\Theta}_{\mathfrak{w}_e(\mathscr{E})}(*)$, and $\nu^{\Theta}_{\mathfrak{w}_s(\mathscr{E}^c)}(*)$ and $\nu^{\Theta}_{\mathscr{P}}(*)$, $\nu^{\Theta}_{\mathscr{E}}(*)$, and $\nu^{\Theta}_{\mathscr{E}^c}(*)$ (as defined in Conjectures 2.2.12 and 2.2.13 of Section 2.2.3) and ν (as defined in Section 1.5) and the possible relationships (that is Question 2.2.13) between the amplitudes $A^{\Theta}_{\mathfrak{w}_l(\mathscr{E}^c)}(*)$, $A^{\Theta}_{\mathfrak{w}_e(\mathscr{E})}(*)$, $A^{\Theta}_{\mathfrak{w}_s(\mathscr{E}^c)}(*)$, $A^{\Theta}_{\mathscr{P}}(*)$, $A^{\Theta}_{\mathscr{E}}(*)$, and $A^{\Theta}_{\mathscr{E}^c}(*)$ (as defined in Conjectures 2.2.12 and 2.2.13 of Section 2.2.3) are also explored.

Because the rest of the discussion in this section requires, for $* \in \{(\phi, f)$, $(\phi|\phi, s)$, $(3_1|\phi, s)\}$, knowing the values $r^2\left(\mathscr{P}^{\Theta}_{2n}(*)\right)$, $r^2\left(\mathscr{E}_{2n}(*)\right)$, $r^2\left(\mathscr{E}^c_{2n}(*)\right)$, $r^2\left(\mathfrak{w}_e(\mathscr{E}_{2n}(*))\right)$, $r^2\left(\mathfrak{w}_l\left(\mathscr{E}^c_{2n}(*)\right)\right)$, and $r^2\left(\mathfrak{w}_e\left(\mathscr{E}^c_{2n}(*)\right)\right)$, estimates for these mean-square radii of gyration need to be determined.

7.2.1 Estimating the Mean-square Radius of Gyration

Recall that $\boldsymbol{W} := \left(\left(W_t(1), W_t(2), ..., W_t(14)\right), t = 0, ..., t_0\right)$ is a Markov chain formed by the CMC Θ-BFACF algorithm and that $\boldsymbol{\omega}^{(u)}$, where

$$\boldsymbol{\omega}^{(u)} := \left(\left(\omega^{(u)}_t(1), \omega^{(u)}_t(2), ..., \omega^{(u)}_t(14)\right), t = 0, ..., t_0\right), \tag{7.48}$$

is the sequence of $(t_0 + 1)$ 14-tuples of Θ-SAPs from $\left(\mathscr{P}^{\Theta}(\phi)\right)^{14}$ realized in Replication u of the simulation of the CMC Θ-BFACF algorithm as described in Section 3.4.1.

For each $* \in \Phi$ and for the subset of $(2n)$-edge Θ-SAPs $\mathscr{U}_{2n}(*) \subseteq \mathscr{P}^{\Theta}(\phi)$, suppose W is a random property-$*$ Θ-SAP chosen from $\mathscr{U}_{2n}(*)$. Then define the random variables X and Y (as used in Section A.4 of Appendix A) by

$$X(W, \mathscr{U}_{2n}(*)) := \xi_{\mathscr{U}_{2n}(*)}(W), \tag{7.49}$$

and

$$Y(W, \mathscr{U}_{2n}(*)) := \xi_{\mathscr{U}_{2n}(*)}(W) r^2(W), \tag{7.50}$$

respectively, where, for $\omega \in \mathscr{P}^{\Theta}(\phi)$ and each subset $\mathscr{V} \subseteq \mathscr{P}^{\Theta}(\phi)$, $\xi_{\mathscr{V}}(\omega)$ is given by Equation (7.10). Then define $X_{k,i}$ and $Y_{k,i}$ (as used in Section A.4 of Appendix A) by

$$X_{k,i}(\mathscr{U}_{2n}(*)) := \sum_{t=0}^{t_0} \mathscr{M}_T(t) \mathscr{I}_{B(k)}(t) X(W_t(i), \mathscr{U}_{2n}(*)) \tag{7.51}$$

and

$$\begin{aligned} Y_{k,i}(\mathscr{U}_{2n}(*)) &:= \sum_{t=0}^{t_0} \mathscr{M}_T(t) \mathscr{I}_{B(k)}(t) Y(W_t(i), \mathscr{U}_{2n}(*)) \\ &:= R^2_{k,i}(\mathscr{U}_{2n}(*)), \end{aligned} \tag{7.52}$$

where $B(k)$ is defined by Equation (4.159); $\mathscr{M}_T(t)$ is defined by Equation (4.42); and, for $A \subseteq \mathbb{R}, \mathscr{I}_A(t)$is defined by Equation (7.6). Now, for the mapping $f : \mathbb{Z}^3 \to \mathbb{Z}^3$, redefine the random variables Y and $Y_{k,i}$ (as used in Section A.4 of Appendix A) by

$$Y(f(W), \mathscr{U}_{2n}(*)) := \xi_{\mathscr{U}_{2n}(*)}(W) r^2(f(W)) \tag{7.53}$$

and

$$\begin{aligned} Y_{k,i}(f(\mathscr{U}_{2n}(*))) &:= \sum_{t=0}^{t_0} \mathscr{M}_T(t) \mathscr{I}_{B(k)}(t) Y(f(W_t(i)), \mathscr{U}_{2n}(*)) \\ &:= R^2_{k,i}(f(\mathscr{U}_{2n}(*))), \end{aligned} \tag{7.54}$$

where $B(k)$ is defined by Equation (4.159); $\mathscr{M}_T(t)$ is defined by Equation (4.42); and, for $A \subseteq \mathbb{R}, \mathscr{I}_A(t)$is defined by Equation (7.6). Then let $\left\langle R^2(\mathscr{U}_{2n}(*)) \right\rangle$ be the ratio estimator (as defined by Equation (A.21) in Section A.3 of Appendix A) for $r^2(\mathscr{U}_{2n}(*))$ formed using the sequence

$$\left((X_{k,i}(\mathscr{U}_{2n}(*)), R^2_{k,i}(\mathscr{U}_{2n}(*))), k = 1, .., l \right) \tag{7.55}$$

and let $\left\langle R^2(f(\mathscr{U}_{2n}(*))) \right\rangle$ be the ratio estimator (as defined by Equation (A.21) in Section A.3 of Appendix A) for $r^2(f(\mathscr{U}_{2n}(*)))$ formed using the sequence

$$\left((X_{k,i}(\mathscr{U}_{2n}(*)), R^2_{k,i}(f(\mathscr{U}_{2n}(*)))), k = 1, .., l \right), \tag{7.56}$$

with $B(k)$ is defined by Equation (4.159).

Based on the u'th realization $\boldsymbol{\omega}^{(u)}$ of $\boldsymbol{W}$, $u \in \{1, 2, ..., 10\}$, let $r^{(u)}_{k,i}(\mathscr{U}_{2n}(*))$ denote the u'th realization of $R^2_{k,i}(\mathscr{U}_{2n}(*))$; let $r^{(u)}_{k,i}(f(\mathscr{U}_{2n}(*)))$ denote the u'th realization of

$R^2_{k,i}\left(f\left(\mathscr{U}_{2n}(*)\right)\right)$; and let $x^{(u)}_{k,i}$ denote the u'th realization of $X_{k,i}\left(\mathscr{U}_{2n}(*)\right)$. Then, for each $* \in \Phi$ and for a fixed positive integer n, the estimators $\left\langle R^2\left(\mathscr{P}^{\Theta}_{2n}(*)\right)\right\rangle$, $\left\langle R^2\left(\mathscr{E}^{c}_{2n}(*)\right)\right\rangle$, $\left\langle R^2\left(\mathscr{E}_{2n}(*)\right)\right\rangle$, $\left\langle R^2\left(\mathfrak{w}_s(\mathscr{E}^{c}_{2n}(*))\right)\right\rangle$, $\left\langle R^2\left(\mathfrak{w}_l(\mathscr{E}^{c}_{2n}(*))\right)\right\rangle$, and $\left\langle R^2\left(\mathfrak{w}_e(\mathscr{E}_{2n}(*))\right)\right\rangle$ defined with $t_0 = 9.6\times 10^{10}$ time steps, $\tau_{\text{int}} = 0.72\times 10^{9}$ time steps, $T = 120,000$ time steps, and $l := 66$ are respectively used to calculate: the point estimate $\left\langle r^2\left(\mathscr{P}^{\Theta}_{2n}(*)\right)\right\rangle$ for $r^2\left(\mathscr{P}^{\Theta}_{2n}(*)\right)$ by using the sequence

$$\left(\left(\left(x^{(u)}_{k,i}, r^{(u)}_{k,i}\left(\mathscr{P}^{\Theta}_{2n}(*)\right)\right), k = 1, .., l\right), u = 1, ..., 10\right) \tag{7.57}$$

in Equation (A.21); the point estimate $\left\langle r^2\left(\mathscr{E}^{c}_{2n}(*)\right)\right\rangle$ for $r^2\left(\mathscr{E}^{c}_{2n}(*)\right)$ by using the sequence

$$\left(\left(\left(x^{(u)}_{k,i}, r^{(u)}_{k,i}\left(\mathscr{E}^{c}_{2n}(*)\right)\right), k = 1, .., l\right), u = 1, ..., 10\right) \tag{7.58}$$

in Equation (A.21); the point estimate $\left\langle r^2\left(\mathscr{E}_{2n}(*)\right)\right\rangle$ for $r^2\left(\mathscr{E}_{2n}(*)\right)$ by using the sequence

$$\left(\left(\left(x^{(u)}_{k,i}, r^{(u)}_{k,i}\left(\mathscr{E}_{2n}(*)\right)\right), k = 1, .., l\right), u = 1, ..., 10\right) \tag{7.59}$$

in Equation (A.21); the point estimate $\left\langle r^2\left(\mathfrak{w}_s(\mathscr{E}^{c}_{2n}(*))\right)\right\rangle$ for $r^2\left(\mathfrak{w}_s(\mathscr{E}^{c}_{2n}(*))\right)$ by using the sequence

$$\left(\left(\left(x^{(u)}_{k,i}, r^{(u)}_{k,i}\left(\mathfrak{w}_s(\mathscr{E}^{c}_{2n}(*))\right)\right), k = 1, .., l\right), u = 1, ..., 10\right) \tag{7.60}$$

in Equation (A.21); the point estimate $\left\langle r^2_{2n}\left(\mathfrak{w}_l(\mathscr{E}^{c}(*))\right)\right\rangle$ for $r^2\left(\mathfrak{w}_l(\mathscr{E}^{c}(*))\right)$ by using the sequence

$$\left(\left(\left(x^{(u)}_{k,i}, r^{(u)}_{k,i}\left(\mathfrak{w}_l(\mathscr{E}^{c}_{2n}(*))\right)\right), k = 1, .., l\right), u = 1, ..., 10\right) \tag{7.61}$$

in Equation (A.21); and the point estimate $\left\langle r^2\left(\mathfrak{w}_e(\mathscr{E}_{2n}(*))\right)\right\rangle$ for $r^2\left(\mathfrak{w}_e(\mathscr{E}_{2n}(*))\right)$ by using the sequence

$$\left(\left(\left(x^{(u)}_{k,i}, r^{(u)}_{k,i}\left(\mathfrak{w}_e(\mathscr{E}_{2n}(*))\right)\right), k = 1, .., l\right), u = 1, ..., 10\right) \tag{7.62}$$

in Equation (A.21).

For each $* \in \{\phi,\ (\phi, f),\ (\phi|\phi, s),\ (3_1|\phi, s)\}$ and $n \in \{7, 8, ..., 945\}$, the point estimates $\left\langle r^2\left(\mathscr{P}^{\Theta}_{2n}(*)\right)\right\rangle$, $\left\langle r^2\left(\mathscr{E}^{c}_{2n}(*)\right)\right\rangle$, $\left\langle r^2\left(\mathscr{E}_{2n}(*)\right)\right\rangle$, $\left\langle r^2\left(\mathfrak{w}_s(\mathscr{E}^{c}_{2n}(*))\right)\right\rangle$, $\left\langle r^2\left(\mathfrak{w}_l(\mathscr{E}^{c}_{2n}(*))\right)\right\rangle$, and $\left\langle r^2\left(\mathfrak{w}_e(\mathscr{E}_{2n}(*))\right)\right\rangle$ are used throughout the discussion in the remainder of this section.

7.2.2 Properties of the Expected Mean-square Radius of Gyration

The discussion in this section investigates the set dependence (that is Questions (2.2.4) and (2.2.5)) and the property dependence (that is Questions (2.2.6) and (2.2.7)) of the expected mean-square radius of gyration using the epoint estimates $\left\langle r^2\left(\mathscr{P}^{\Theta}_{2n}(*)\right)\right\rangle$, $\left\langle r^2\left(\mathscr{E}^{c}_{2n}(*)\right)\right\rangle$, $\left\langle r^2\left(\mathscr{E}_{2n}(*)\right)\right\rangle$, $\left\langle r^2\left(\mathfrak{w}_s(\mathscr{E}^{c}_{2n}(*))\right)\right\rangle$, $\left\langle r^2\left(\mathfrak{w}_l(\mathscr{E}^{c}_{2n}(*))\right)\right\rangle$, and $\left\langle r^2\left(\mathfrak{w}_e(\mathscr{E}_{2n}(*))\right)\right\rangle$.

Exploring Question 2.2.4

For each $* \in \Phi$, Question 2.2.4 hypothesizes that, as $n \to \infty$, the expected mean-square radii of gyration of the sets $\mathscr{P}_{2n}^{\Theta}(*)$, $\mathscr{E}_{2n}(*)$, and $\mathscr{E}_{2n}^{c}(*)$ satisfy

$$\frac{r^2\left(\mathscr{E}_{2n}^{c}(*)\right)}{r^2\left(\mathscr{P}_{2n}^{\Theta}(*)\right)} \to 1. \tag{7.63}$$

and, through odd values of n,

$$\frac{r^2\left(\mathscr{E}_{2n}(*)\right)}{r^2\left(\mathscr{P}_{2n}^{\Theta}(*)\right)} \to 1 \tag{7.64}$$

To numerically investigate whether or not the ratios $\frac{r^2\left(\mathscr{E}_{2n}(*)\right)}{r^2\left(\mathscr{P}_{2n}^{\Theta}(*)\right)}$ and $\frac{r^2\left(\mathscr{E}_{2n}^{c}(*)\right)}{r^2\left(\mathscr{P}_{2n}^{\Theta}(*)\right)}$ tend to one as n increases, first note that because $\mathscr{E}_{14}^{c}(\phi, f) = \mathscr{E}_{14}^{c}(\phi|\phi, s) = \{\}$, $\frac{r^2\left(\mathscr{E}_{14}^{c}(\phi, f)\right)}{r^2\left(\mathscr{P}_{14}^{\Theta}(\phi, f)\right)}$ and $\frac{r^2\left(\mathscr{E}_{14}^{c}(\phi|\phi, s)\right)}{r^2\left(\mathscr{P}_{14}^{\Theta}(\phi|\phi, s)\right)}$ are not defined. Hence Figures 7.8 and 7.9 do not display a point estimate for either $\frac{r^2\left(\mathscr{E}_{14}^{c}(\phi, f)\right)}{r^2\left(\mathscr{P}_{14}^{\Theta}(\phi, f)\right)}$ and $\frac{r^2\left(\mathscr{E}_{14}^{c}(\phi|\phi, s)\right)}{r^2\left(\mathscr{P}_{14}^{\Theta}(\phi|\phi, s)\right)}$. Note that in order to construct more informative plots, the estimates for the expected mean-square radii of gyration corresponding to every tenth consecutive odd integer and the horizontal line $y = 1.0$ are plotted in Figures 7.8-7.10. Also note that Figures 7.8-7.10 are plotted over the range of n's for which samples from $\mathscr{E}_{2n}$ are available. With these two notes in mind, for odd values of $n \geq 9$, point estimates for $\frac{r^2\left(\mathscr{E}_{2n}(\phi, f)\right)}{r^2\left(\mathscr{P}_{2n}^{\Theta}(\phi, f)\right)}$ and $\frac{r^2\left(\mathscr{E}_{2n}^{c}(\phi, f)\right)}{r^2\left(\mathscr{P}_{2n}^{\Theta}(\phi, f)\right)}$ are plotted in Figure 7.8; for odd values of $n \geq 9$, point estimates for $\frac{r^2\left(\mathscr{E}_{2n}(\phi|\phi, s)\right)}{r^2\left(\mathscr{P}_{2n}^{\Theta}(\phi|\phi, s)\right)}$ and $\frac{r^2\left(\mathscr{E}_{2n}^{c}(\phi|\phi, s)\right)}{r^2\left(\mathscr{P}_{2n}^{\Theta}(\phi|\phi, s)\right)}$ are plotted in Figure 7.9; and for odd values of $n \geq 13$, point estimates for $\frac{r^2\left(\mathscr{E}_{2n}(3_1|\phi, s)\right)}{r^2\left(\mathscr{P}_{2n}^{\Theta}(3_1|\phi, s)\right)}$ and $\frac{r^2\left(\mathscr{E}_{2n}^{c}(3_1|\phi, s)\right)}{r^2\left(\mathscr{P}_{2n}^{\Theta}(3_1|\phi, s)\right)}$ are plotted in Figure 7.10. The error bars plotted in each of Figures 7.8-7.10 are the estimated 95% margins of error.

For those estimated 95% confidence intervals for $\frac{r^2\left(\mathscr{E}_{2n}^{c}(\phi, f)\right)}{r^2\left(\mathscr{P}_{2n}^{\Theta}(\phi, f)\right)}$ plotted in Figure 7.8, note that each plotted interval contains the value one. This observation similarly holds for Figures 7.9 and 7.10. The author has verified that, for each $* \in \{(\phi, f), (\phi|\phi, s), (3_1|\phi, s)\}$ fixed, and for each $n \in \{n_*^{\Theta}/2 + 1, n_*^{\Theta}/2 + 2, ..., 945\}$, the estimated 95% confidence intervals for $\frac{r^2\left(\mathscr{E}_{2n}^{c}(*)\right)}{r^2\left(\mathscr{P}_{2n}^{\Theta}(*)\right)}$ contain the value one. Because sample data is not currently available to obtain point estimates (and the associated estimated 95% margins of error) for $\frac{r^2\left(\mathscr{E}_{4n+2}(*)\right)}{r^2\left(\mathscr{P}_{4n+2}^{\Theta}(*)\right)}$ for sufficiently large integer values of n, and due to the large estimated 95% margins of error for $\frac{r^2\left(\mathscr{E}_{4n+2}(*)\right)}{r^2\left(\mathscr{P}_{4n+2}^{\Theta}(*)\right)}$, for each $* \in \{(\phi, f), (\phi|\phi, s), (3_1|\phi, s)\}$, for those

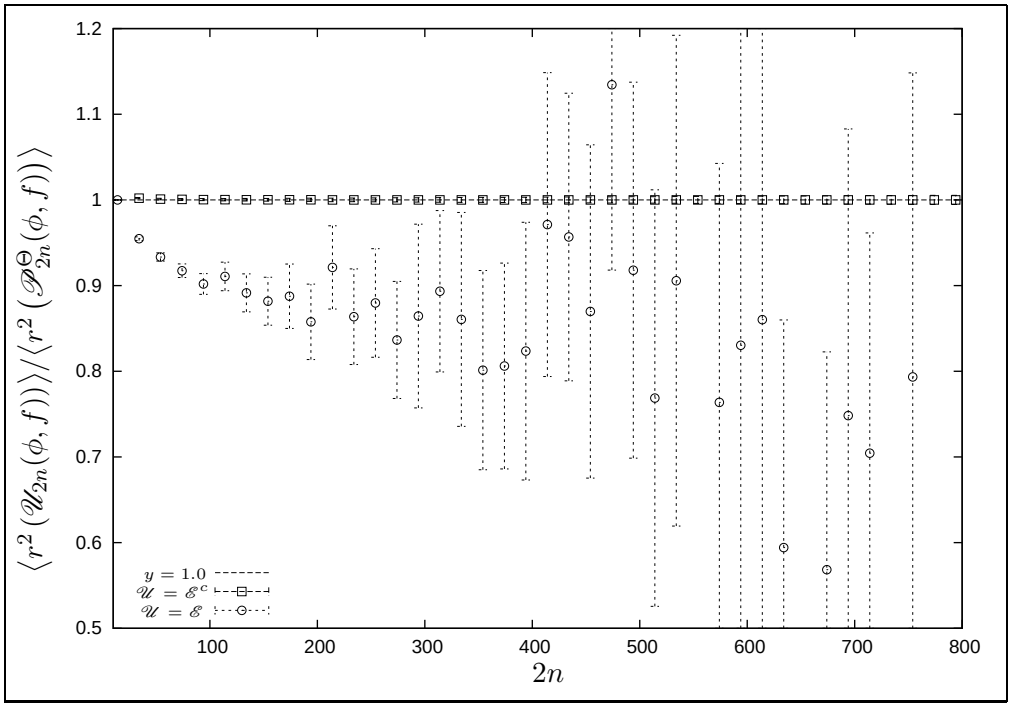

Figure 7.8: The estimates $\dfrac{\left\langle r^2\left(\mathscr{E}_{2n}(\phi,f)\right)\right\rangle}{\left\langle r^2\left(\mathscr{P}^{\Theta}_{2n}(\phi,f)\right)\right\rangle}$ [$\odot$] and $\dfrac{\left\langle r^2\left(\mathscr{E}^c_{2n}(\phi,f)\right)\right\rangle}{\left\langle r^2\left(\mathscr{P}^{\Theta}_{2n}(\phi,f)\right)\right\rangle}$ [$\boxdot$] plotted versus $2n$, for odd values of n. The error bars represent the estimated 95% margins of error.

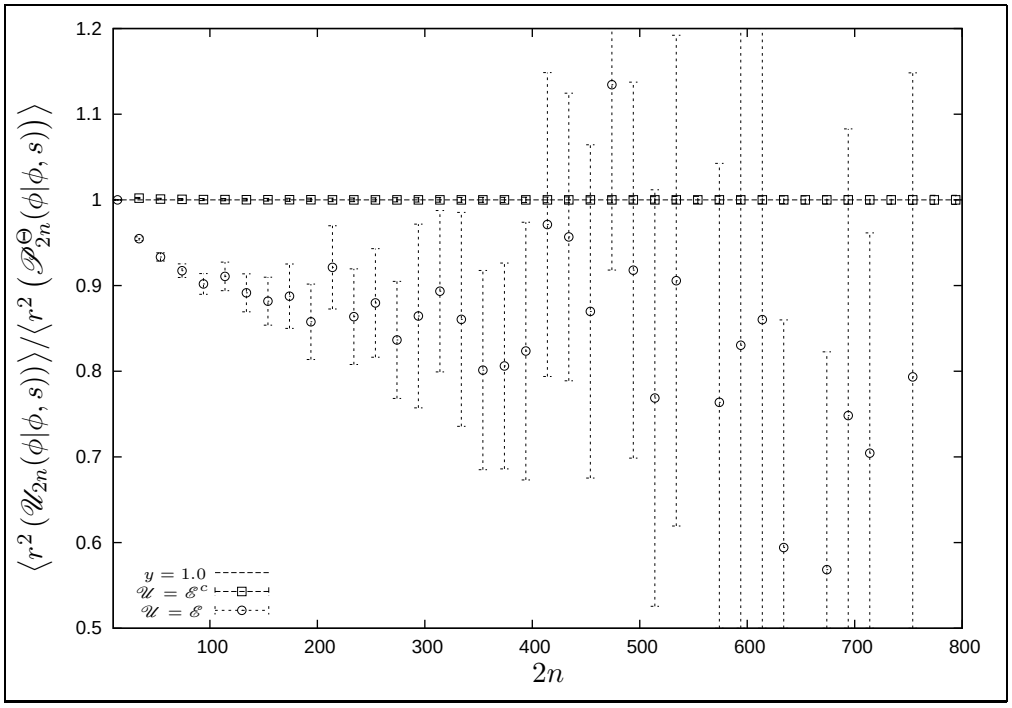

Figure 7.9: The estimates $\dfrac{\left\langle r^2\left(\mathscr{E}_{2n}(\phi|\phi,s)\right)\right\rangle}{\left\langle r^2\left(\mathscr{P}^{\Theta}_{2n}(\phi|\phi,s)\right)\right\rangle}$ [$\odot$] and $\dfrac{\left\langle r^2\left(\mathscr{E}^c_{2n}(\phi|\phi,s)\right)\right\rangle}{\left\langle r^2\left(\mathscr{P}^{\Theta}_{2n}(\phi|\phi,s)\right)\right\rangle}$ [$\boxdot$] plotted versus $2n$, for odd values of n. The error bars represent the estimated 95% margins of error.

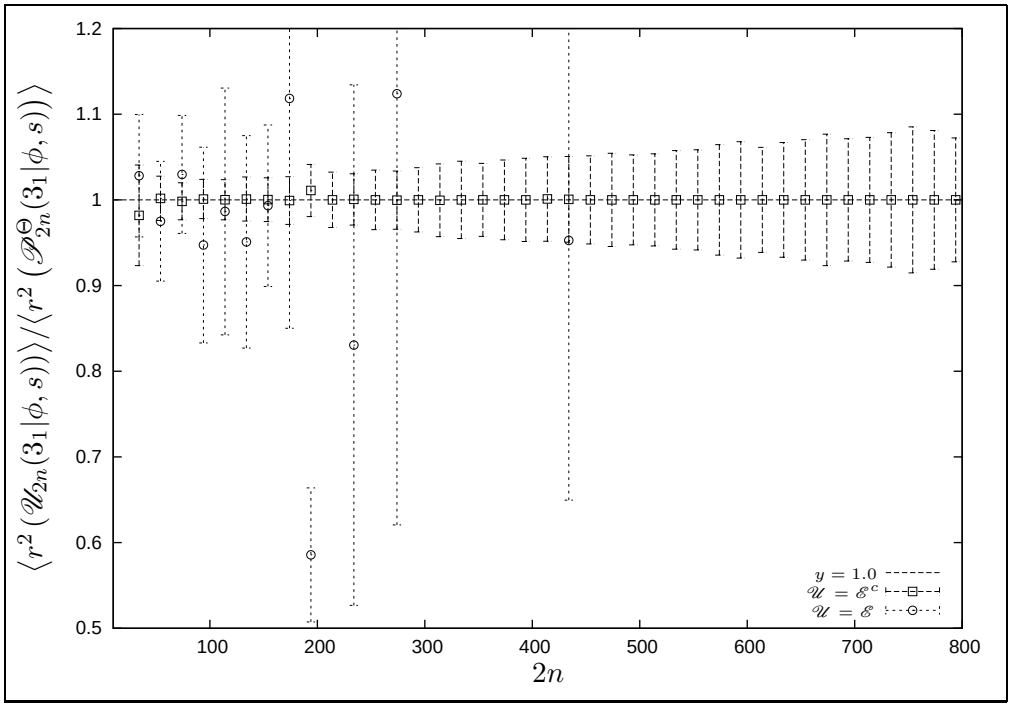

Figure 7.10: The estimates $\dfrac{\left\langle r^2\left(\mathscr{E}_{2n}(3_1|\phi,s)\right)\right\rangle}{\left\langle r^2\left(\mathscr{P}^{\Theta}_{2n}(3_1|\phi,s)\right)\right\rangle}$ [$\odot$] and $\dfrac{\left\langle r^2\left(\mathscr{E}^c_{2n}(3_1|\phi,s)\right)\right\rangle}{\left\langle r^2\left(\mathscr{P}^{\Theta}_{2n}(3_1|\phi,s)\right)\right\rangle}$ [$\boxdot$] plotted versus $2n$, for odd values of n. The error bars represent the estimated 95% margins of error.

values of n in which a sample from $\mathscr{E}_{2n}(*)$ is available, there is insufficient data to make any conclusion regarding the $n \to \infty$ behaviour of $\dfrac{r^2\left(\mathscr{E}_{4n+2}(*)\right)}{r^2\left(\mathscr{P}^{\Theta}_{4n+2}(*)\right)}$. Hence the conjecture that can be made based on the numerics in this discussion is:

Conjecture 7.2.1 *For each* $* \in \Phi$,

$$\lim_{n\to\infty} \frac{r^2\left(\mathscr{E}^c_{2n}(*)\right)}{r^2\left(\mathscr{P}^{\Theta}_{2n}(*)\right)} = 1. \tag{7.65}$$

Exploring Question 2.2.5

For each property $* \in \Phi$, Question 2.2.5 poses a possible relationship between the expected radii of gyration of the large, equal-length, and small uSAWs (as a function of polygon length) for randomly selected, property-$*$, $(2n)$-edge Θ-SAPs. In order to explore the hypothesized relationship that, for a given $* \in \Phi$ and for all integers $n \geq n^{\Theta}_*/2$ such that $\mathscr{E}_{2n}(*) \neq \{\}$,

$$r^2\left(\mathfrak{w}_s\left(\mathscr{E}^c_{2n}(*)\right)\right) < r^2\left(\mathfrak{w}_e(\mathscr{E}_{2n}(*))\right) < r^2\left(\mathfrak{w}_l\left(\mathscr{E}^c_{2n}(*)\right)\right), \tag{7.66}$$

the point estimates for $r^2\left(\mathfrak{w}_s\left(\mathscr{E}^c_{2n}(\phi,f)\right)\right)$, $r^2\left(\mathfrak{w}_e(\mathscr{E}_{2n}(\phi,f))\right)$, and $r^2\left(\mathfrak{w}_l\left(\mathscr{E}^c_{2n}(\phi,f)\right)\right)$ are plotted in Figure 7.11 using [$\times$], [$\boxdot$], and [$\odot$] respectively; the point estimates for $r^2\left(\mathfrak{w}_s\left(\mathscr{E}^c_{2n}(\phi|\phi,s)\right)\right)$, $r^2\left(\mathfrak{w}_e(\mathscr{E}_{2n}(\phi|\phi,s))\right)$, and $r^2\left(\mathfrak{w}_l\left(\mathscr{E}^c_{2n}(\phi|\phi,s)\right)\right)$ are plotted in Figure 7.12 using [$\times$], [$\boxdot$], and [$\odot$] respectively; and the point estimates for $r^2\left(\mathfrak{w}_s\left(\mathscr{E}^c_{2n}(3_1|\phi,s)\right)\right)$, $r^2\left(\mathfrak{w}_e(\mathscr{E}_{2n}(3_1|\phi,s))\right)$, and $r^2\left(\mathfrak{w}_l\left(\mathscr{E}^c_{2n}(3_1|\phi,s)\right)\right)$ are plotted in Figure 7.13 using [$\times$], [$\boxdot$], and [$\odot$] respectively. In order to create more meaningful figures, the point estimates for the expected mean-square radii of gyration corresponding to every tenth consecutive odd integer n are plotted in Figures 7.11-7.13. The error bars in each of these three figures represent the estimated 95% margins of error.

For those point estimates plotted in Figures 7.11 and 7.12 based on polygon lengths greater than 100 and for those point estimates plotted in Figure 7.13 based on polygon lengths greater than 200, it is observed that, for each $* \in \{(\phi,f),\ (\phi|\phi,s),\ (3_1|\phi,s)\}$, the point estimates satisfy

$$\left\langle r^2\left(\mathfrak{w}_s\left(\mathscr{E}^c_{2n}(*)\right)\right)\right\rangle < \left\langle r^2\left(\mathfrak{w}_e(\mathscr{E}_{2n}(*))\right)\right\rangle < \left\langle r^2\left(\mathfrak{w}_l\left(\mathscr{E}^c_{2n}(*)\right)\right)\right\rangle. \tag{7.67}$$

Note that the author has verified that, for each $* \in \{(\phi,f),\ (\phi|\phi,s),\ (3_1|\phi,s)\}$ and for each odd-valued $n \in \{n^{\Theta}_*/2, n^{\Theta}_*/2+1, ..., 945\}$ such that there was data to estimate

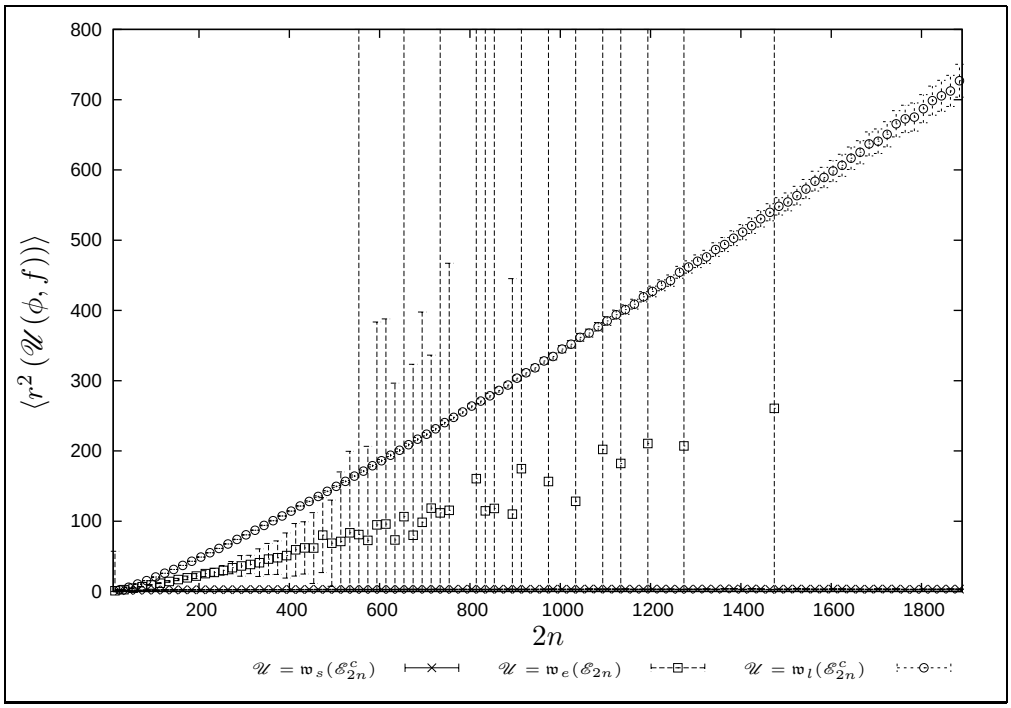

Figure 7.11: The estimates for $r^2(\mathfrak{w}_s(\mathscr{E}^c_{2n}(\phi, f)))$ [$\times$], $r^2(\mathfrak{w}_e(\mathscr{E}_{2n}(\phi, f)))$ [$\boxdot$], and $r^2(\mathfrak{w}_l(\mathscr{E}^c_{2n}(\phi, f)))$ [*odot*] plotted versus $2n$, for odd values of n. The error bars represent the estimated 95% margins of error.

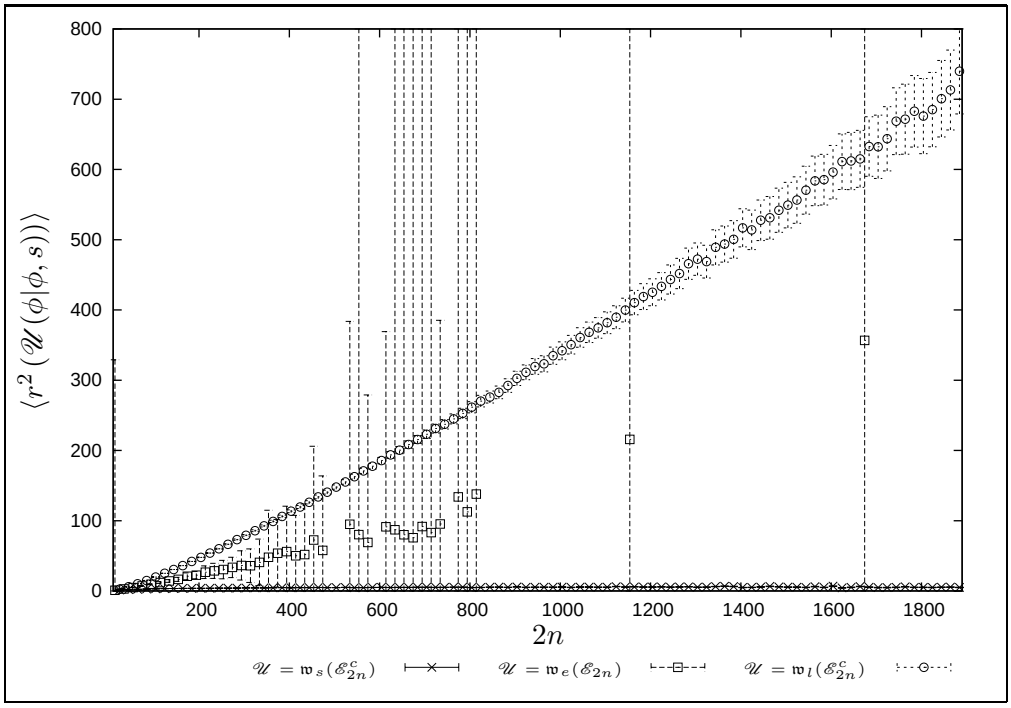

Figure 7.12: The estimates for $r^2\left(\mathfrak{w}_s\left(\mathscr{E}^c_{2n}(\phi|\phi, s)\right)\right)$ [$\times$], $r^2\left(\mathfrak{w}_e(\mathscr{E}_{2n}(\phi|\phi, s))\right)$ [$\boxdot$], and $r^2\left(\mathfrak{w}_l\left(\mathscr{E}^c_{2n}(\phi|\phi, s)\right)\right)$ [$\odot$] plotted versus $2n$, for odd values of n. The error bars represent the estimated 95% margins of error.

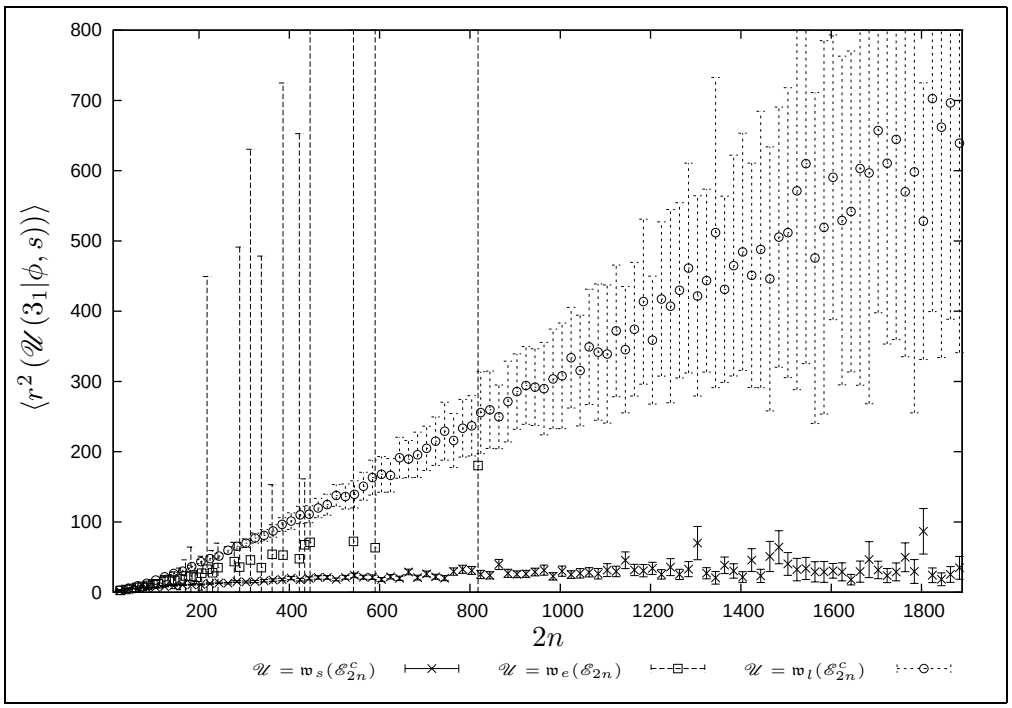

Figure 7.13: The estimates for $r^2\left(\mathfrak{w}_s\left(\mathscr{E}^c_{2n}(3_1|\phi,s)\right)\right)$ [$\times$], $r^2\left(\mathfrak{w}_e(\mathscr{E}_{2n}(3_1|\phi,s))\right)$ [$\boxdot$], and $r^2\left(\mathfrak{w}_l\left(\mathscr{E}^c_{2n}(3_1|\phi,s)\right)\right)$ [$\odot$] plotted versus $2n$, for odd values of n. The error bars represent the estimated 95% margins of error.

$r^2\left(\mathfrak{w}_e(\mathscr{E}_{2n}(*))\right)$,

$$\left\langle r^2\left(\mathfrak{w}_s\left(\mathscr{E}^c_{2n}(*)\right)\right)\right\rangle < \left\langle r^2\left(\mathfrak{w}_e(\mathscr{E}_{2n}(*))\right)\right\rangle < \left\langle r^2\left(\mathfrak{w}_l\left(\mathscr{E}^c_{2n}(*)\right)\right)\right\rangle, \tag{7.68}$$

which supports the relationship stated in Inequality (7.66). However, because the estimated 95% confidence intervals for $r^2\left(\mathfrak{w}_e(\mathscr{E}_{2n}(*))\right)$ displayed in Figures 7.11-7.13 include both the point estimates $r^2\left(\mathfrak{w}_s\left(\mathscr{E}^c_{2n}(*)\right)\right)$ and $r^2\left(\mathfrak{w}_l\left(\mathscr{E}^c_{2n}(*)\right)\right)$ and the intervals are extremely large, more data is required to fully explore the relationship between $r^2\left(\mathfrak{w}_e(\mathscr{E}_{2n}(*))\right)$ and both $r^2\left(\mathfrak{w}_s\left(\mathscr{E}^c_{2n}(*)\right)\right)$ and $r^2\left(\mathfrak{w}_l\left(\mathscr{E}^c_{2n}(*)\right)\right)$.

In order to explore the second relationship posed in Question 2.2.5, that is, for a given $* \in \Phi$ and for all integers $n > n^{\Theta}_*/2$,

$$r^2\left(\mathfrak{w}_s\left(\mathscr{P}^{\Theta}_{2n}(*)\right)\right) < r^2\left(\mathfrak{w}_l\left(\mathscr{P}^{\Theta}_{2n}(*)\right)\right), \tag{7.69}$$

note that the discussion thus far has only been for values of n for which $\mathscr{E}_{2n}(*) \neq \{\}$. For these values of n (that is odd values of n), it has already been observed that the corresponding point estimates support Inequality (7.69). The question becomes "Do $r^2\left(\mathfrak{w}_s\left(\mathscr{P}^{\Theta}_{2n}(*)\right)\right)$ and $r^2\left(\mathfrak{w}_l\left(\mathscr{P}^{\Theta}_{2n}(*)\right)\right)$ satisfy Inequality (7.69) for even values of n?". To answer explore this question for even values of n, the point estimates for $r^2\left(\mathfrak{w}_s\left(\mathscr{P}^{\Theta}_{2n}(\phi, f)\right)\right)$ and $r^2\left(\mathfrak{w}_l\left(\mathscr{P}^{\Theta}_{2n}(\phi, f)\right)\right)$ are plotted in Figure 7.14 using [$\times$] and [$\odot$] respectively; the point estimates for $r^2\left(\mathfrak{w}_s\left(\mathscr{P}^{\Theta}_{2n}(\phi|\phi, s)\right)\right)$ and $r^2\left(\mathfrak{w}_l\left(\mathscr{P}^{\Theta}_{2n}(\phi|\phi, s)\right)\right)$ are plotted in Figure 7.15; and the point estimates for $r^2\left(\mathfrak{w}_s\left(\mathscr{P}^{\Theta}_{2n}(3_1|\phi, s)\right)\right)$ and $r^2\left(\mathfrak{w}_l\left(\mathscr{P}^{\Theta}_{2n}(3_1|\phi, s)\right)\right)$ are plotted in Figure 7.16. As before, in order to create more meaningful figures, the estimates for the expected mean-square radii of gyration corresponding to every tenth consecutive even integer n are plotted in Figures 7.14-7.16. The error bars in each of these three figures represent the estimated 95% margins of error.

For those point estimates plotted in Figures 7.14 -7.16, for each $* \in \{(\phi, f),\ (\phi|\phi, s),\ (3_1|\phi, s)\}$, the estimates satisfy

$$\left\langle r^2\left(\mathfrak{w}_s\left(\mathscr{P}^{\Theta}_{2n}(*)\right)\right)\right\rangle < \left\langle r^2\left(\mathfrak{w}_l\left(\mathscr{P}^{\Theta}_{2n}(*)\right)\right)\right\rangle. \tag{7.70}$$

Furthermore, the author has verified that, for each $* \in \{(\phi, f),\ (\phi|\phi, s),\ (3_1|\phi, s)\}$ and for each even-valued $n \in \{n^{\Theta}_*/2, n^{\Theta}_*/2 + 1, ..., 945\}$,

$$\left\langle r^2\left(\mathfrak{w}_s\left(\mathscr{P}^{\Theta}_{2n}(*)\right)\right)\right\rangle < \left\langle r^2\left(\mathfrak{w}_l\left(\mathscr{P}^{\Theta}_{2n}(*)\right)\right)\right\rangle \tag{7.71}$$

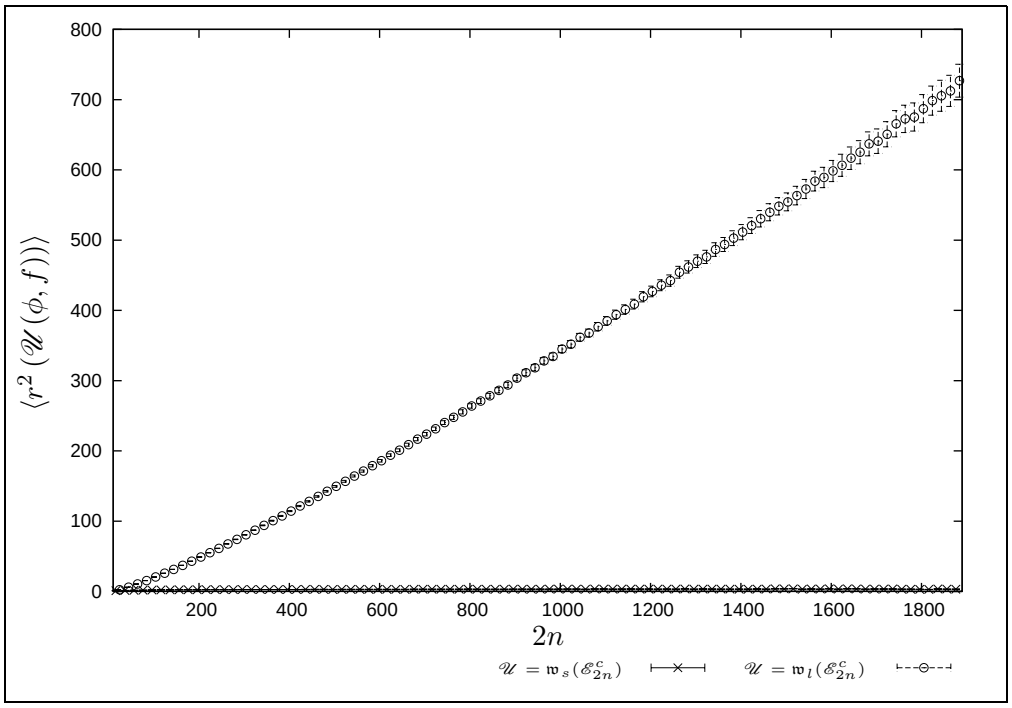

Figure 7.14: The estimates for $r^2\,(\mathfrak{w}_s\,(\mathscr{E}^c_{2n}(\phi,f)))$ [$\times$] and $r^2\,(\mathfrak{w}_l\,(\mathscr{E}^c_{2n}(\phi,f)))$ [$\odot$] plotted versus $2n$, for even values of n. The error bars represent the estimated 95% margins of error.

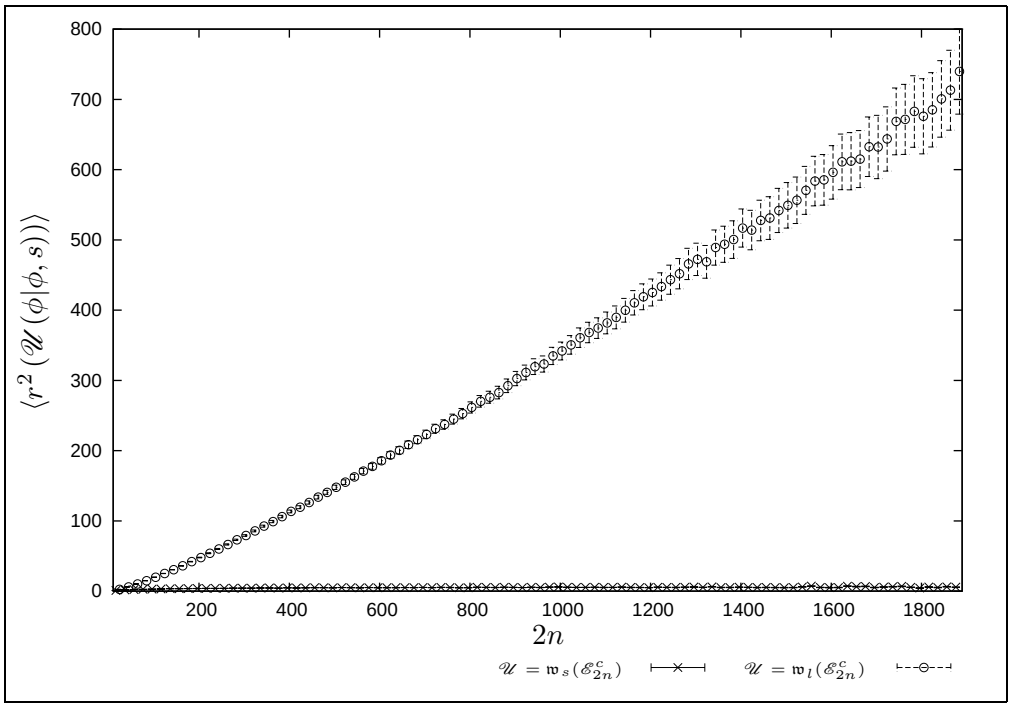

Figure 7.15: The estimates for $r^2\,(\mathfrak{w}_s\,(\mathscr{E}^c_{2n}(\phi|\phi,s)))$ [$\times$] and $r^2\,(\mathfrak{w}_l\,(\mathscr{E}^c_{2n}(\phi|\phi,s)))$ [$\odot$] plotted versus $2n$, for even values of n. The error bars represent the estimated 95% margins of error.

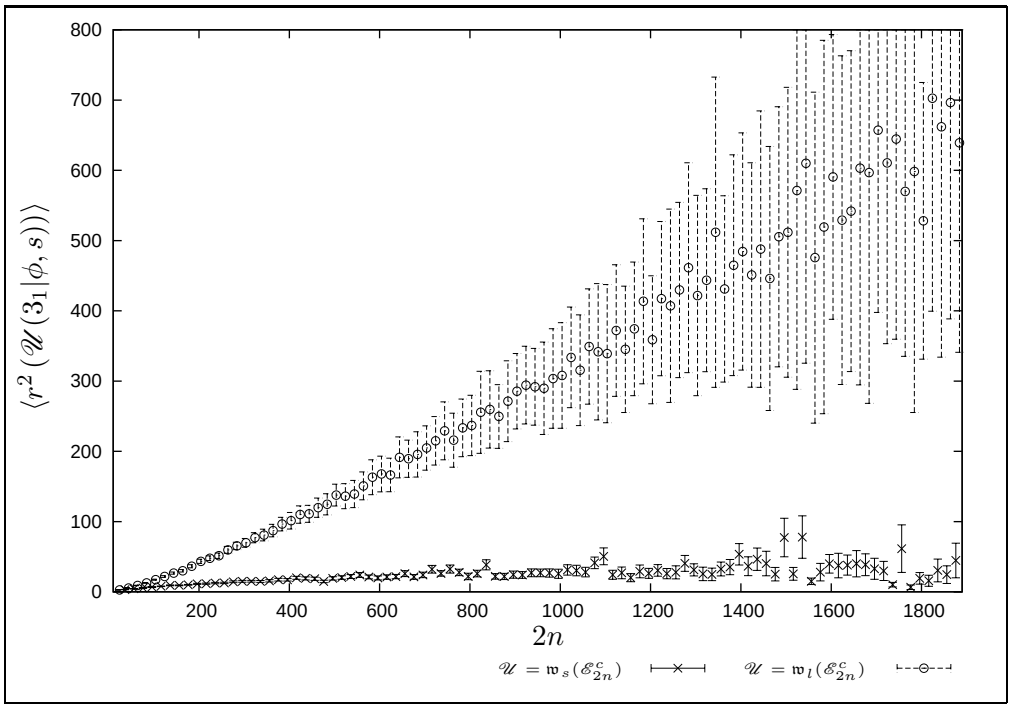

Figure 7.16: The estimates for $r^2\left(\mathfrak{w}_s\left(\mathscr{E}^c_{2n}(3_1|\phi,s)\right)\right)$ [$\times$] and $r^2\left(\mathfrak{w}_l\left(\mathscr{E}^c_{2n}(3_1|\phi,s)\right)\right)$ [$\odot$] plotted versus $2n$, for even values of n. The error bars represent the estimated 95% margins of error.

and that, for each $* \in \{(\phi,f),\ (\phi|\phi,s),\ (3_1|\phi,s)\}$ and for all $n \in \{40,41,...,945\}$, the estimated 95% confidence intervals for $\mathfrak{w}_s\left(\mathscr{E}^c_{2n}(*)\right)$ and $\mathfrak{w}_l\left(\mathscr{E}^c_{2n}(*)\right)$ do not intersect. Hence the data supports, for a given $* \in \Phi$ and for all integers $n > n^{\Theta}_*/2$,

$$r^2\left(\mathfrak{w}_s\left(\mathscr{P}^{\Theta}_{2n}(*)\right)\right) < r^2\left(\mathfrak{w}_l\left(\mathscr{P}^{\Theta}_{2n}(*)\right)\right). \tag{7.72}$$

Consequently the data supports both relationships posed in Question 2.2.5, that is the relationships given by Inequalities (7.66) and (7.69). However, due to the lack of data sampled from $\mathscr{E}^c(*)$, the following is conjectured.

Conjecture 7.2.2 *For each* $* \in \Phi$, *and for every integer* $n > n^{\Theta}_*/2$,

$$r^2\left(\mathfrak{w}_s\left(\mathscr{P}^{\Theta}_{2n}(*)\right)\right) < r^2\left(\mathfrak{w}_l\left(\mathscr{P}^{\Theta}_{2n}(*)\right)\right). \tag{7.73}$$

Note that more data needs to be generated before the relationship "For every odd integer $n \geq n^{\Theta}_*/2$,

$$r^2\left(\mathfrak{w}_s\left(\mathscr{E}^c_{2n}(*)\right)\right) < r^2\left(\mathfrak{w}_e(\mathscr{E}_{2n}(*))\right) < r^2\left(\mathfrak{w}_l\left(\mathscr{E}^c_{2n}(*)\right)\right)." \tag{7.74}$$

can be conjectured with any level of confidence.

Exploring Question 2.2.6

Question 2.2.6 hypothesizes that, for each $* \in \mathscr{K}^{\dagger}(\phi) \backslash \{(\phi|\phi, s)\}$ and each natural number $n \geq n_*^{\Theta}/2$, the expected mean-square radius of gyration of the small uSAW in a randomly chosen element from $\mathscr{E}_{2n}^{c}(*)$ is greater than the expected mean-square radii of gyration of the small uSAW in a randomly chosen element from either $\mathscr{E}_{2n}^{c}(\phi, f)$ and $\mathscr{E}_{2n}^{c}(\phi|\phi, s)$. The question also poses that the expected mean-square radius of gyration of the large uSAW in a randomly chosen element from $\mathscr{E}_{2n}^{c}(*)$ is smaller than the expected mean-square radii of gyration of the large uSAW in a randomly chosen element from either $\mathscr{E}_{2n}^{c}(\phi, f)$ and $\mathscr{E}_{2n}^{c}(\phi|\phi, s)$. In order to determine whether the data supports these hypothesized relationships, the point estimates $\left\langle r^2\left(\mathfrak{w}_s\left(\mathscr{E}_{2n}^{c}(3_1|\phi, s)\right)\right)\right\rangle$, $\left\langle r^2\left(\mathfrak{w}_s\left(\mathscr{E}_{2n}^{c}(\phi|\phi, s)\right)\right)\right\rangle$, and $\left\langle r^2\left(\mathfrak{w}_s\left(\mathscr{E}_{2n}^{c}(\phi, f)\right)\right)\right\rangle$ are plotted versus $2n$ in Figure 7.17 using [$\times$], [$\boxdot$], and [$\triangle$] respectively, and the point estimates $\left\langle r^2\left(\mathfrak{w}_l\left(\mathscr{E}_{2n}^{c}(3_1|\phi, s)\right)\right)\right\rangle$, $\left\langle r^2\left(\mathfrak{w}_l\left(\mathscr{E}_{2n}^{c}(\phi|\phi, s)\right)\right)\right\rangle$, and $\left\langle r^2\left(\mathfrak{w}_l\left(\mathscr{E}_{2n}^{c}(\phi, f)\right)\right)\right\rangle$ are plotted versus $2n$ in Figure 7.18 using [$\times$], [$\boxdot$], and [$\triangle$] respectively. As before, in order to create more meaningful figures, the point estimates for the expected mean-square radii of gyration corresponding to every tenth consecutive integer n are plotted in Figures 7.17 and 7.18.

From Figure 7.17, for those point estimates plotted,

$$\left\langle r^2\left(\mathfrak{w}_s\left(\mathscr{E}_{2n}^{c}(3_1|\phi, s)\right)\right)\right\rangle > \left\langle r^2\left(\mathfrak{w}_s\left(\mathscr{E}_{2n}^{c}(\phi, f)\right)\right)\right\rangle \tag{7.75}$$

and

$$\left\langle r^2\left(\mathfrak{w}_s\left(\mathscr{E}_{2n}^{c}(3_1|\phi, s)\right)\right)\right\rangle > \left\langle r^2\left(\mathfrak{w}_s\left(\mathscr{E}_{2n}^{c}(\phi|\phi, s)\right)\right)\right\rangle. \tag{7.76}$$

Furthermore, the point estimates plotted in Figure 7.17 also support the following inequality:

$$\left\langle r^2\left(\mathfrak{w}_s\left(\mathscr{E}_{2n}^{c}(\phi|\phi, s)\right)\right)\right\rangle > \left\langle r^2\left(\mathfrak{w}_s\left(\mathscr{E}_{2n}^{c}(\phi, f)\right)\right)\right\rangle. \tag{7.77}$$

The author has verified that the above three inequalities hold for every $n \in \{n_{(3_1|\phi,s)}^{\Theta}/2, n_{(3_1|\phi,s)}^{\Theta}/2 + 1, ..., 945\}$. Further note that the estimated 95% confidence intervals for $r^2\left(\mathfrak{w}_s\left(\mathscr{E}_{2n}^{c}(3_1|\phi, s)\right)\right)$, $r^2\left(\mathfrak{w}_s\left(\mathscr{E}_{2n}^{c}(\phi|\phi, s)\right)\right)$, and $r^2\left(\mathfrak{w}_s\left(\mathscr{E}_{2n}^{c}(\phi, f)\right)\right)$ displayed in Figure 7.17 do not intersect and that the author has verified that, for each $n \in \{n_{(3_1|\phi,s)}^{\Theta}/2, n_{(3_1|\phi,s)}^{\Theta}/2 + 1, ..., 945\}$, the estimated 95% confidence intervals for $r^2\left(\mathfrak{w}_s\left(\mathscr{E}_{2n}^{c}(3_1|\phi, s)\right)\right)$, $r^2\left(\mathfrak{w}_s\left(\mathscr{E}_{2n}^{c}(\phi|\phi, s)\right)\right)$, and $r^2\left(\mathfrak{w}_s\left(\mathscr{E}_{2n}^{c}(\phi, f)\right)\right)$ also do not intersect. Therefore, based on the numerical evidence displayed in Figure 7.17, the following is conjectured.

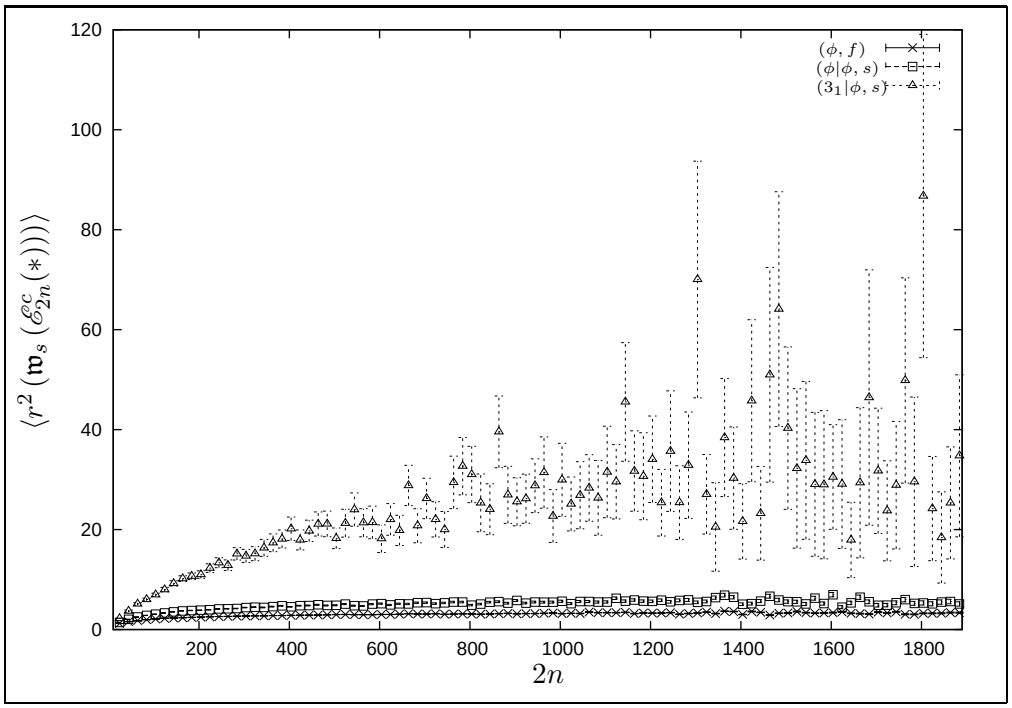

Figure 7.17: The estimates for $r^2\left(\mathfrak{w}_s\left(\mathscr{E}^c_{2n}(3_1|\phi,s)\right)\right)$ [$\triangle$], $r^2\left(\mathfrak{w}_s\left(\mathscr{E}^c_{2n}(\phi|\phi,s)\right)\right)$ [$\boxdot$], and $r^2\left(\mathfrak{w}_s\left(\mathscr{E}^c_{2n}(\phi,f)\right)\right)$ [$\times$] plotted versus $2n$.

Conjecture 7.2.3 *For each* $* \in \mathscr{K}^{\dagger}(\phi)\backslash\{(\phi|\phi,s)\}$ *and each natural number* $n \geq n^{\Theta}_{*}/2$,

$$r^2\left(\mathfrak{w}_s\left(\mathscr{E}^c_{2n}(*)\right)\right) > r^2\left(\mathfrak{w}_s\left(\mathscr{E}^c_{2n}(\phi|\phi,s)\right)\right) > r^2\left(\mathfrak{w}_s\left(\mathscr{E}^c_{2n}(\phi,f)\right)\right). \tag{7.78}$$

For those point estimates plotted in Figure 7.18, note that, for $n \in \{n^{\Theta}_{(3_1|\phi,s)}/2, n^{\Theta}_{(3_1|\phi,s)}/2+1, ..., 525\}$

$$\left\langle r^2\left(\mathfrak{w}_l\left(\mathscr{E}^c_{2n}(3_1|\phi,s)\right)\right)\right\rangle < \left\langle r^2\left(\mathfrak{w}_l\left(\mathscr{E}^c_{2n}(\phi,f)\right)\right)\right\rangle \tag{7.79}$$

and

$$\left\langle r^2\left(\mathfrak{w}_l\left(\mathscr{E}^c_{2n}(3_1|\phi,s)\right)\right)\right\rangle < \left\langle r^2\left(\mathfrak{w}_l\left(\mathscr{E}^c_{2n}(\phi|\phi,s)\right)\right)\right\rangle. \tag{7.80}$$

The author has verified that the two inequalities above hold for every $n \in \{n^{\Theta}_{(3_1|\phi,s)}/2, n^{\Theta}_{(3_1|\phi,s)}/2+1, ..., 525\}$. But, because, for all $n \geq 350$, $\left\langle r^2\left(\mathfrak{w}_l\left(\mathscr{E}^c_{2n}(\phi|\phi,s)\right)\right)\right\rangle$ and $\left\langle r^2\left(\mathfrak{w}_l\left(\mathscr{E}^c_{2n}(\phi,f)\right)\right)\right\rangle$ are within the estimated 95% confidence intervals for $r^2\left(\mathfrak{w}_l\left(\mathscr{E}^c_{2n}(3_1|\phi,s)\right)\right)$, the point estimates plotted in Figure 7.18 support no definitive relationship between $r^2\left(\mathfrak{w}_l\left(\mathscr{E}^c_{2n}(3_1|\phi,s)\right)\right)$ and $r^2\left(\mathfrak{w}_l\left(\mathscr{E}^c_{2n}(\phi|\phi,s)\right)\right)$ and $r^2\left(\mathfrak{w}_l\left(\mathscr{E}^c_{2n}(3_1|\phi,s)\right)\right)$ and $r^2\left(\mathfrak{w}_l\left(\mathscr{E}^c_{2n}(\phi,f)\right)\right)$. The upshot here is that more data is required in order to identify and explore any relationships amongst $r^2\left(\mathfrak{w}_l\left(\mathscr{E}^c_{2n}(*)\right)\right)$, $r^2\left(\mathfrak{w}_l\left(\mathscr{E}^c_{2n}(\phi,f)\right)\right)$, and $r^2\left(\mathfrak{w}_l\left(\mathscr{E}^c_{2n}(\phi|\phi,s)\right)\right)$.

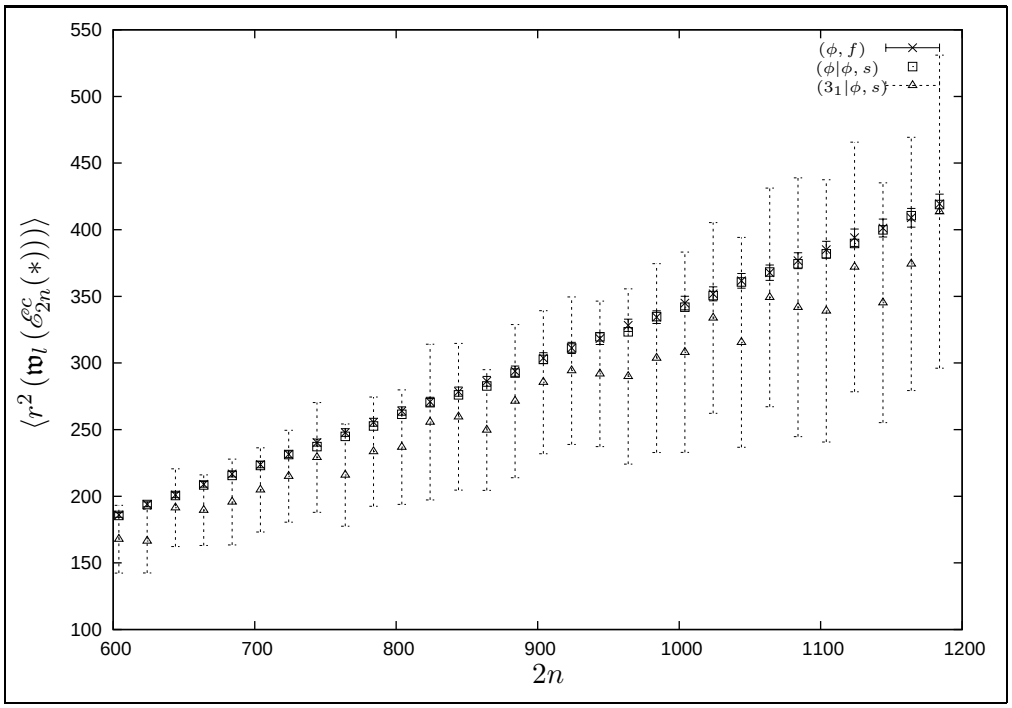

Figure 7.18: The estimates for $r^2\left(\mathfrak{w}_l\left(\mathscr{E}^c_{2n}(3_1|\phi,s)\right)\right)$ [$\triangle$], $r^2\left(\mathfrak{w}_l\left(\mathscr{E}^c_{2n}(\phi|\phi,s)\right)\right)$ [$\boxdot$], and $r^2\left(\mathfrak{w}_l\left(\mathscr{E}^c_{2n}(\phi,f)\right)\right)$ [$\times$] plotted versus $2n$.

Exploring Question 2.2.7

The final question posed in Section 2.2.3 of Chapter 2 regarding the expected mean-square radii of gyration of the large, equal-length, and small uSAWs for subsets of $\mathscr{P}^{\Theta}_{2n}(*)$ explores how these expected mean-square radii of gyration compare to the expected mean-square radius of gyration of a Θ-SAP from $\mathscr{P}^{\Theta}_{2n}(\phi)$ as n increases. To this end, Figure 7.19 displays the point estimates $\dfrac{\left\langle r^2\left(\mathfrak{w}_l\left(\mathscr{E}^c_{2n}(\phi,f)\right)\right)\right\rangle}{\left\langle r^2\left(\mathscr{P}^{\Theta}_{2n}(\phi)\right)\right\rangle}$, $\dfrac{\left\langle r^2\left(\mathfrak{w}_l\left(\mathscr{E}^c_{2n}(\phi|\phi,s)\right)\right)\right\rangle}{\left\langle r^2\left(\mathscr{P}^{\Theta}_{2n}(\phi)\right)\right\rangle}$, and $\dfrac{\left\langle r^2\left(\mathfrak{w}_l\left(\mathscr{E}^c_{2n}(3_1|\phi,s)\right)\right)\right\rangle}{\left\langle r^2\left(\mathscr{P}^{\Theta}_{2n}(\phi)\right)\right\rangle}$ versus $2n$ using [$\times$], [$\boxdot$], and [$\triangle$] respectively; Figure 7.20 displays the point estimates $\dfrac{\left\langle r^2\left(\mathfrak{w}_e\left(\mathscr{E}_{2n}(\phi,f)\right)\right)\right\rangle}{\left\langle r^2\left(\mathscr{P}^{\Theta}_{2n}(\phi)\right)\right\rangle}$, $\dfrac{\left\langle r^2\left(\mathfrak{w}_e\left(\mathscr{E}_{2n}(\phi|\phi,s)\right)\right)\right\rangle}{\left\langle r^2\left(\mathscr{P}^{\Theta}_{2n}(\phi)\right)\right\rangle}$, and $\dfrac{\left\langle r^2\left(\mathfrak{w}_e\left(\mathscr{E}_{2n}(3_1|\phi,s)\right)\right)\right\rangle}{\left\langle r^2\left(\mathscr{P}^{\Theta}_{2n}(\phi)\right)\right\rangle}$ versus $2n$ using [$\times$], [$\boxdot$], and [$\triangle$] respectively; and Figure 7.21 displays the point estimates $\dfrac{\left\langle r^2\left(\mathfrak{w}_s\left(\mathscr{E}^c_{2n}(\phi,f)\right)\right)\right\rangle}{\left\langle r^2\left(\mathscr{P}^{\Theta}_{2n}(\phi)\right)\right\rangle}$, $\dfrac{\left\langle r^2\left(\mathfrak{w}_s\left(\mathscr{E}^c_{2n}(\phi|\phi,s)\right)\right)\right\rangle}{\left\langle r^2\left(\mathscr{P}^{\Theta}_{2n}(\phi)\right)\right\rangle}$, and $\dfrac{\left\langle r^2\left(\mathfrak{w}_s\left(\mathscr{E}^c_{2n}(3_1|\phi,s)\right)\right)\right\rangle}{\left\langle r^2\left(\mathscr{P}^{\Theta}_{2n}(\phi)\right)\right\rangle}$ versus $2n$ using [$\times$], [$\boxdot$], and [$\triangle$] respectively. Note that, as before, in order to create less cluttered figures, the point estimates for the expected mean-square radii of gyration corresponding to every tenth consecutive integer n are plotted in Figures

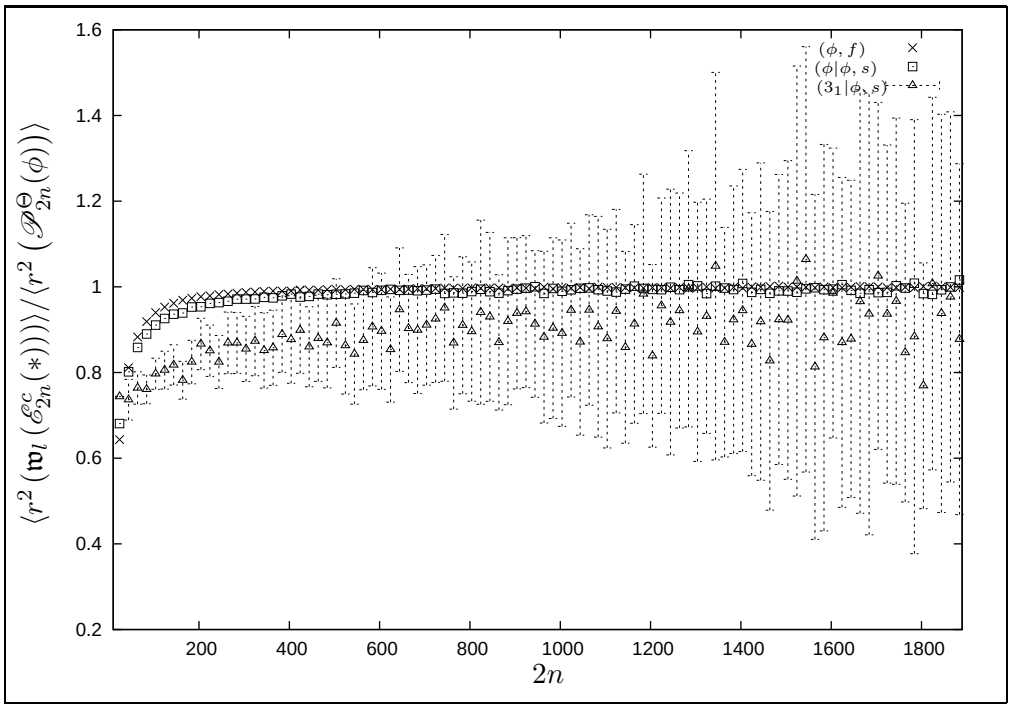

Figure 7.19: The estimates for $\dfrac{r^2\left(\mathfrak{w}_l\left(\mathscr{E}^c_{2n}(\phi, f)\right)\right)}{r^2\left(\mathscr{P}^\Theta_{2n}(\phi)\right)}$ [$\times$], $\dfrac{r^2\left(\mathfrak{w}_l\left(\mathscr{E}^c_{2n}(\phi|\phi, s)\right)\right)}{r^2\left(\mathscr{P}^\Theta_{2n}(\phi)\right)}$ [$\boxdot$], and $\dfrac{r^2\left(\mathfrak{w}_l\left(\mathscr{E}^c_{2n}(3_1|\phi, s)\right)\right)}{r^2\left(\mathscr{P}^\Theta_{2n}(\phi)\right)}$ [$\triangle$] plotted versus $2n$.

7.19-7.21.

Referring to Figure 7.19, as n increases, the point estimates $\dfrac{\left\langle r^2\left(\mathfrak{w}_l\left(\mathscr{E}^c_{2n}(\phi, f)\right)\right)\right\rangle}{\left\langle r^2\left(\mathscr{P}^\Theta_{2n}(\phi)\right)\right\rangle}$ and $\dfrac{\left\langle r^2\left(\mathfrak{w}_l\left(\mathscr{E}^c_{2n}(\phi|\phi, s)\right)\right)\right\rangle}{\left\langle r^2\left(\mathscr{P}^\Theta_{2n}(\phi)\right)\right\rangle}$ are both approaching one. Though the point estimates $\dfrac{\left\langle r^2\left(\mathfrak{w}_l\left(\mathscr{E}^c_{2n}(3_1|\phi, s)\right)\right)\right\rangle}{\left\langle r^2\left(\mathscr{P}^\Theta_{2n}(\phi)\right)\right\rangle}$ are not as convincingly approaching one, for all $n \geq 350$, the estimated 95% confidence intervals for $\dfrac{r^2\left(\mathfrak{w}_l\left(\mathscr{E}^c_{2n}(3_1|\phi, s)\right)\right)}{r^2\left(\mathscr{P}^\Theta_{2n}(\phi)\right)}$ do contain the value one. Thus, at the $\alpha = 0.05$ level of significance, the possibility that $\dfrac{r^2\left(\mathfrak{w}_l\left(\mathscr{E}^c_{2n}(3_1|\phi, s)\right)\right)}{r^2\left(\mathscr{P}^\Theta_{2n}(\phi)\right)} \to 1$ cannot be excluded. In order to make a stronger statement regarding the behaviour of $\dfrac{r^2\left(\mathfrak{w}_l\left(\mathscr{E}^c_{2n}(3_1|\phi, s)\right)\right)}{r^2\left(\mathscr{P}^\Theta_{2n}(\phi)\right)}$, as $n \to \infty$, more data is required.

The only statement that can be made based on Figure 7.20 is that there is not a large enough sample from $\mathscr{E}(\phi, f)$, $\mathscr{E}(\phi|\phi, s)$, and $\mathscr{E}(3_1|\phi, s)$ to conclude whether or not, for each of $* \in \{(\phi, f), (\phi|\phi, s), (3_1|\phi, s)\}$, the limit $\lim\limits_{n\to\infty} \dfrac{r^2\left(\mathfrak{w}_e\left(\mathscr{E}_{2n}(*)\right)\right)}{r^2\left(\mathscr{P}^\Theta_{2n}(\phi)\right)}$ exists, let alone, if it does exist, determine its limiting value.

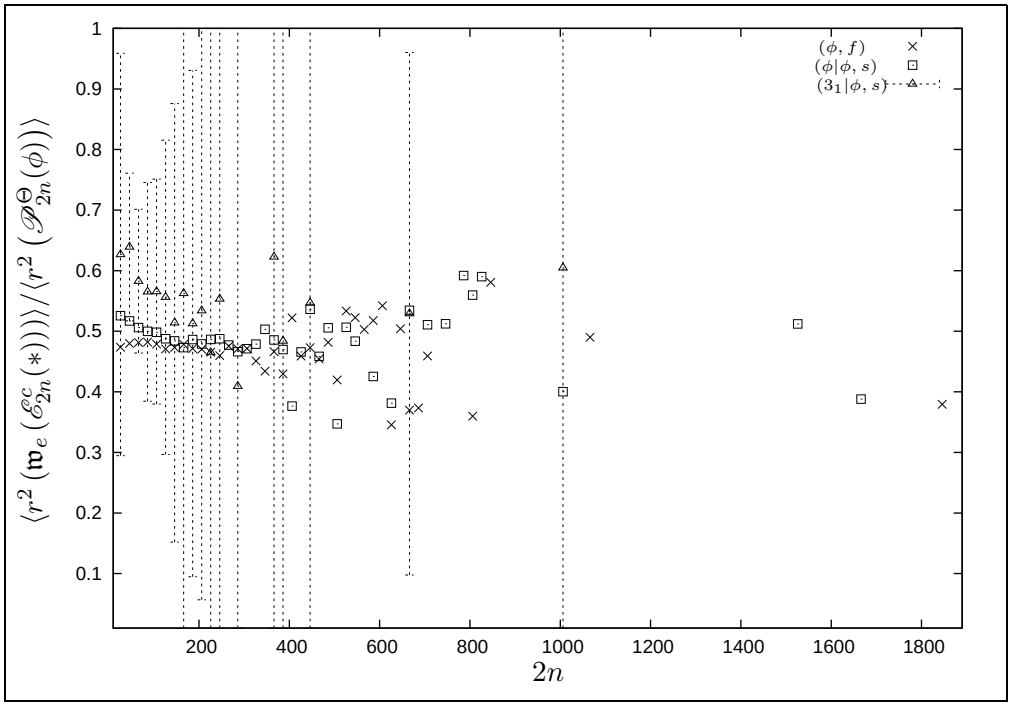

Figure 7.20: The estimates for $\dfrac{r^2\left(\mathfrak{w}_e\left(\mathscr{E}^c_{2n}(\phi, f)\right)\right)}{r^2\left(\mathscr{P}^\Theta_{2n}(\phi)\right)}$ [$\times$], $\dfrac{r^2\left(\mathfrak{w}_e\left(\mathscr{E}^c_{2n}(\phi|\phi, s)\right)\right)}{r^2\left(\mathscr{P}^\Theta_{2n}(\phi)\right)}$ [$\boxdot$], and $\dfrac{r^2\left(\mathfrak{w}_e\left(\mathscr{E}^c_{2n}(3_1|\phi, s)\right)\right)}{r^2\left(\mathscr{P}^\Theta_{2n}(\phi)\right)}$ [$\triangle$] plotted versus $2n$.

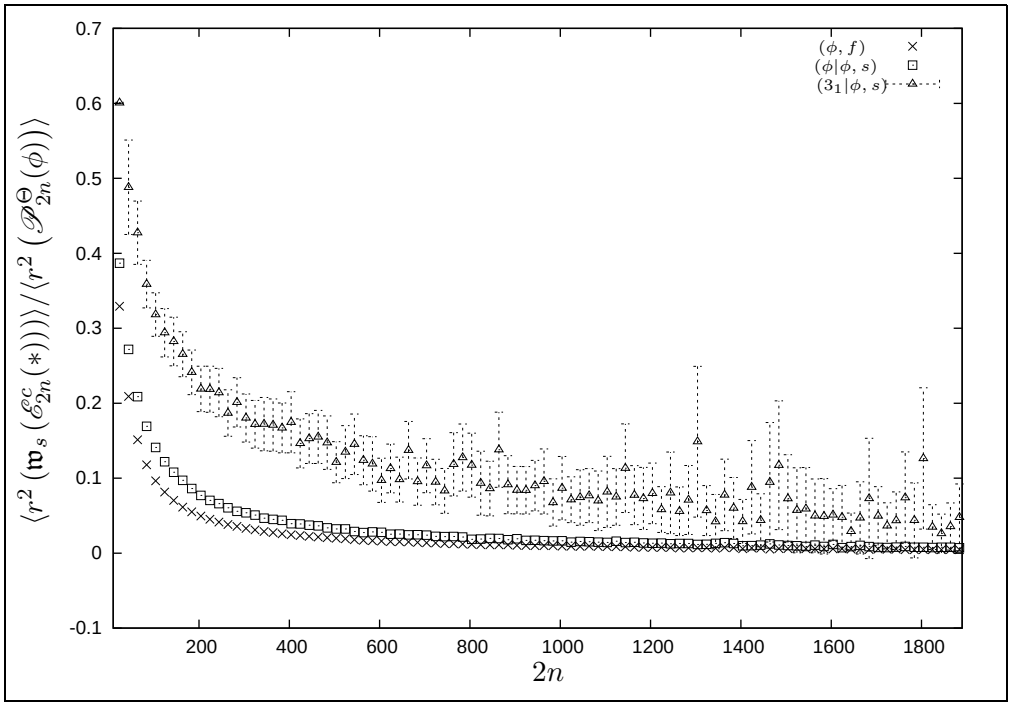

Figure 7.21: The estimates for $\dfrac{r^2\left(\mathfrak{w}_s\left(\mathscr{E}^c_{2n}(\phi, f)\right)\right)}{r^2\left(\mathscr{P}^\Theta_{2n}(\phi)\right)}$ [$\times$], $\dfrac{r^2\left(\mathfrak{w}_s\left(\mathscr{E}^c_{2n}(\phi|\phi, s)\right)\right)}{r^2\left(\mathscr{P}^\Theta_{2n}(\phi)\right)}$ [$\boxdot$], and $\dfrac{r^2\left(\mathfrak{w}_s\left(\mathscr{E}^c_{2n}(3_1|\phi, s)\right)\right)}{r^2\left(\mathscr{P}^\Theta_{2n}(\phi)\right)}$ [$\triangle$] plotted versus $2n$.

Referring to Figure 7.21, as n increases, the estimates $\frac{\left\langle r^2\left(\mathfrak{w}_s\left(\mathscr{E}^c_{2n}(\phi,f)\right)\right)\right\rangle}{\left\langle r^2\left(\mathscr{P}^{\Theta}_{2n}(\phi)\right)\right\rangle}$ and $\frac{\left\langle r^2\left(\mathfrak{w}_s\left(\mathscr{E}^c_{2n}(\phi|\phi,s)\right)\right)\right\rangle}{\left\langle r^2\left(\mathscr{P}^{\Theta}_{2n}(\phi)\right)\right\rangle}$ are both approaching zero. Because, for the range of n's plotted, the estimates $\frac{\left\langle r^2\left(\mathfrak{w}_s\left(\mathscr{E}^c_{2n}(3_1|\phi,s)\right)\right)\right\rangle}{\left\langle r^2\left(\mathscr{P}^{\Theta}_{2n}(\phi)\right)\right\rangle}$ are not as convincingly approaching zero, the numerically the possibility that $\frac{r^2\left(\mathfrak{w}_s\left(\mathscr{E}^c_{2n}(3_1|\phi,s)\right)\right)}{r^2\left(\mathscr{P}^{\Theta}_{2n}(\phi)\right)} \to 0$ cannot be excluded. In order to make a stronger statement regarding the behaviour of $\frac{r^2\left(\mathfrak{w}_s\left(\mathscr{E}^c_{2n}(3_1|\phi,s)\right)\right)}{r^2\left(\mathscr{P}^{\Theta}_{2n}(\phi)\right)}$, as $n \to \infty$, more data is required. However, without further data, the data displayed in Figures 7.19 and 7.21 suggest the following conjecture.

Conjecture 7.2.4 *For each* $* \in \Phi\backslash\{\phi,(\phi,s)\}$,

$$\lim_{n\to\infty} \frac{r^2\left(\mathfrak{w}_s\left(\mathscr{E}^c_{2n}(*)\right)\right)}{r^2\left(\mathscr{P}^{\Theta}_{2n}(\phi)\right)} = 0, \text{ and} \tag{7.81}$$

$$\lim_{n\to\infty} \frac{r^2\left(\mathfrak{w}_l\left(\mathscr{E}^c_{2n}(*)\right)\right)}{r^2\left(\mathscr{P}^{\Theta}_{2n}(\phi)\right)} = 1. \tag{7.82}$$

If the expected mean-square radius of gyration is to be used as a measure of the size of uSAWs in Θ-SAPs in $\mathscr{P}_{2n}(\phi)$, the numerical evidence presented throughout Section 7.2.2 supports Conjecture 2.2.8 as follows. The numerical evidence in throughout Section 7.2.2 suggests that $\mathscr{P}_{2n}(\phi)$ is dominated by Θ-SAPs with one large and one small uSAW such that the "size" (mean-square radius of gyration) of the large uSAW is $O\left(n^t\right)$ (where $t > 1$) and the "size" (mean-square radius of gyration) of the small uSAW is $O(n^s)$ (where $s < 1$).

7.2.3 Estimating the Metric Exponents and Amplitudes

In this section, the final questions posed in Section 2.2.3 of Chapter 2 regarding the metric exponents and amplitudes (as stated in Conjectures 2.2.12 and 2.2.13) are investigated. Questions 2.2.8-2.2.12 query possible relationships between the metric exponents, including their property dependence. Question 2.2.13 queries a possible relationship amongst the amplitudes, including their property dependence.

For convenience, for each $* \in \Phi$ and for every $n \geq n^{\Theta}_*/2$, define the set of sets

$$\Upsilon_{2n}(*) := \{\mathscr{P}^{\Theta}_{2n}(*), \mathscr{E}_{2n}(*), \mathscr{E}^c_{2n}(*), \mathfrak{w}_e(\mathscr{E}_{2n}(*)), \mathfrak{w}_l\left(\mathscr{E}^c_{2n}(*)\right), \mathfrak{w}_s\left(\mathscr{E}^c_{2n}(*)\right)\} \tag{7.83}$$

and the set of sets

$$\Upsilon := \{\mathscr{P}^{\Theta}, \mathscr{E}, \mathscr{E}^c, \mathfrak{w}_e(\mathscr{E}), \mathfrak{w}_l\left(\mathscr{E}^c\right), \mathfrak{w}_s\left(\mathscr{E}^c\right)\}. \tag{7.84}$$

Then, assuming that Conjectures 2.2.12 and 2.2.13 hold implies that, for sufficiently large values of $n \in \mathbb{N}$, there exist suitable constants and functions such that each of $r^2\left(\mathscr{P}^{\Theta}_{2n}(*)\right)$, $r^2\left(\mathscr{E}_{2n}(*)\right)$, $r^2\left(\mathscr{E}^c_{2n}(*)\right)$, $r^2\left(\mathfrak{w}_e(\mathscr{E}_{2n}(*))\right)$, $r^2\left(\mathfrak{w}_l\left(\mathscr{E}^c_{2n}(*)\right)\right)$, and $r^2\left(\mathfrak{w}_s\left(\mathscr{E}^c_{2n}(*)\right)\right)$ scale according to a function whose form is given by

$$\mathcal{R}_n(a^{\Theta}_{\bullet}(*), b^{\Theta}_{\bullet}(*), c^{\Theta}_{\bullet}(*), d^{\Theta}_{\bullet}(*), r^*_{\bullet}) = a^{\Theta}_{\bullet}(*) n^{2b^{\Theta}_{\bullet}(*)} \left(1 + c^{\Theta}_{\bullet}(*) n^{-d^{\Theta}_{\bullet}(*)} + r^*_{\bullet}(n))\right), \quad (7.85)$$

where $* \in \Phi$, $\bullet \in \Upsilon$, and $r^*_{\bullet}(n) = O(n^{-1})$. The constants represented by $a^{\Theta}_{\bullet}(*)$ and $b^{\Theta}_{\bullet}(*)$ in Equation (7.85) are, respectively, referred to as the amplitude and metric exponent.

In order to explore the final questions in Chapter 2, recall that the amplitude and metric exponent for the scaling form for: $r^2\left(\mathscr{P}^{\Theta}_{2n}(*)\right)$ are respectively denoted $A^{\Theta}_{\mathscr{P}}(*)$ and $\nu^{\Theta}_{\mathscr{P}}(*)$; $r^2\left(\mathscr{E}_{2n}(*)\right)$ are respectively denoted $A^{\Theta}_{\mathscr{E}}(*)$ and $\nu^{\Theta}_{\mathscr{E}}(*)$; $r^2\left(\mathscr{E}^c_{2n}(*)\right)$ are respectively denoted $A^{\Theta}_{\mathscr{E}^c}(*)$ and $\nu^{\Theta}_{\mathscr{E}^c}(*)$; $r^2\left(\mathfrak{w}_e(\mathscr{E}_{2n}(*))\right)$ are respectively denoted $A^{\Theta}_{\mathfrak{w}_e(\mathscr{E})}(*)$ and $\nu^{\Theta}_{\mathfrak{w}_e(\mathscr{E})}(*)$; $r^2\left(\mathfrak{w}_l\left(\mathscr{E}^c_{2n}(*)\right)\right)$ are respectively denoted $A^{\Theta}_{\mathfrak{w}_l(\mathscr{E}^c)}(*)$ and $\nu^{\Theta}_{\mathfrak{w}_l(\mathscr{E}^c)}(*)$; and $r^2\left(\mathfrak{w}_s\left(\mathscr{E}^c_{2n}(*)\right)\right)$ are respectively denoted $A^{\Theta}_{\mathfrak{w}_s(\mathscr{E}^c)}(*)$ and $\nu^{\Theta}_{\mathfrak{w}_s(\mathscr{E}^c)}(*)$. Then, given any $* \in \Phi$ and $n \geq n^{\Theta}_*/2$, when the expected mean-square radii of gyration of the elements in $\Upsilon_{2n}(*)$ are being discussed, the notation $r^2(\bullet)$, for $\bullet \in \Upsilon_{2n}(*)$ is used. The corresponding point estimate for $r^2(\bullet)$ is $\left\langle r^2(\bullet)\right\rangle$, where $\left\langle r^2(\bullet)\right\rangle$ is defined in Section 7.2.1. Also the notation $A^{\Theta}_{\bullet}(*)$ and $\nu^{\Theta}_{\bullet}(*)$, for each $* \in \Phi$ and $\bullet \in \Upsilon$, is used to represent the amplitude and metric exponent for an arbitrary set in Υ with property $*$. Because an estimate for $r^2(\bullet)$, for $\bullet \in \Upsilon_{2n}(*)$, is based on CMC data, estimates for $r^2(\bullet)$ for each $n \geq n^{\Theta}_*/2$ are correlated. In this situation, how can the parameters $A^{\Theta}_{\bullet}(*)$ and $\nu^{\Theta}_{\bullet}(*)$, for $\bullet \in \Upsilon$ and $* \in \Phi$, be estimated? This question is addressed next.

Given $\bullet \in \Upsilon$ and $* \in \Phi$, for the sake of comparison, two methods for estimating $\nu^{\Theta}_{\bullet}(*)$ are presented here. The first method presented is an implementation of the "Fixed-n Method for curve fitting" as discussed in Section A.5 of Appendix A. The results of this method will be used to explore Questions 2.2.8-2.2.13 The second method is referred to as the "Average-n Method for estimating $\nu^{\Theta}_{\bullet}(*)$" and is discussed in Section 7.2.3.

Estimating $A^{\Theta}_{\bullet}(*)$ and $\nu^{\Theta}_{\bullet}(*)$ using the "Fixed-n Method for curve fitting"

The method to be used in this section is an application of the "Fixed-n Method for curve fitting" as discussed in Section A.5 of Appendix B. To this end, first note that there exists a real value b such that, for all n sufficiently large, $\mathcal{R}_n(a, b, c, d, r)$ in Equation (7.85)

behaves like

$$\mathcal{R}_n(a,b,c,d,r) \sim \mathfrak{r}_n(a,b,h) := an^{2b} + b. \tag{7.86}$$

Now for each $* \in \{(\phi,f),\ (\phi|\phi,s),\ (3_1|\phi,s)\}$, $n \geq n_*^{\Theta}/2$, and each $\bullet \in \Upsilon_{2n}(*)$, the estimates $\left\langle r^2(\bullet)\right\rangle$, calculated as discussed in Section 7.2.1, based on a sub-sample taken after every 90'th n, passes the Test for Independence (as described in Algorithm 4.3.1). The resulting essentially independent samples are plotted versus $2n$ in Figures 7.23-7.29. It should be noted up front, that there is currently insufficient fixed-n data to estimate $A_{\bullet}^{\Theta}(*)$ and $\nu_{\bullet}^{\Theta}(*)$, for each $\bullet \in \{\mathscr{E}, \mathfrak{w}_e(\mathscr{E})\}$, regardless of the property $* \in \{(\phi,f),\ (\phi|\phi,s),\ (3_1|\phi,s)\}$. Hence no estimates for $A_{\bullet}^{\Theta}(*)$ and $\nu_{\bullet}^{\Theta}(*)$, for each $\bullet \in \{\mathscr{E}, \mathfrak{w}_e(\mathscr{E})\}$ and $* \in \{(\phi,f),(\phi|\phi,s),(3_1|\phi,s)\}$, are presented. Consequently the portion of Questions 2.2.8, 2.2.11, and 2.2.13 involving $\bullet \in \{\mathscr{E}, \mathfrak{w}_e(\mathscr{E})\}$ cannot be explored at this time and hence is left as future work. Based on the analysis in Section 7.2.2, the error in the estimates for property-$(3_1|\phi,s)$, are large and hence the reliability of any of the $(3_1|\phi,s)$-data is questionable at best. Estimates for $A_{\bullet}^{\Theta}(*)$ and $\nu_{\bullet}^{\Theta}(*)$ based on the $(3_1|\phi,s)$-data are presented but more $(3_1|\phi,s)$-data is really required. Hence investigating how the amplitude and metric exponents depend on the property-$(3_1|\phi,s)$ is also future work.

For $* \in \{(\phi,f),(\phi|\phi,s),(3_1|\phi,s)\}$, $k = 90$, $n \in \{12,\ 12+90,...,12+90t \leq 945\}$, $\bullet \in \Upsilon_{2n}(*)$, $f(2n, A_{\bullet}^{\Theta}(*), \nu_{\bullet}^{\Theta}(*), b_{\bullet}(*)) := \mathfrak{r}_{2n}(A_{\bullet}^{\Theta}(*), \nu_{\bullet}^{\Theta}(*), b_{\bullet}(*))$; $y_{2n} = \left\langle r^2(\bullet)\right\rangle$, the "Fixed-$n$ Method for curve fitting" of Section A.5 is used to estimate $A_{\bullet}^{\Theta}(*)$ and $\nu_{\bullet}^{\Theta}(*)$, for $* \in \{(\phi,f),\ (\phi|\phi,s),\ (3_1|\phi,s)\}$ and $\bullet \in \{\mathscr{P}^{\Theta}, \mathscr{E}^c, \mathfrak{w}_l(\mathscr{E}^c), \mathfrak{w}_s(\mathscr{E}^c)\}$. Figures 7.23-7.29 and the corresponding estimates for $A_{\bullet}^{\Theta}(*)$ and $\nu_{\bullet}^{\Theta}(*)$, for $* \in \{(\phi,f),\ (\phi|\phi,s),\ (3_1|\phi,s)\}$ and $\bullet \in \{\mathscr{P}^{\Theta}, \mathscr{E}^c, \mathfrak{w}_l(\mathscr{E}^c), \mathfrak{w}_s(\mathscr{E}^c)\}$, are presented in the following three subsections. Note that the essentially independent samples plotted in Figures 7.23-7.29 are provided in Tables B.14-B.17 (cf. Section B.3 of Appendix B).

Exploring Questions 2.2.8 and 2.2.9 Question 2.2.8 queries whether or not the metric exponents are independent of the sets $\mathscr{E}(*)$ and $\mathscr{E}^c(*)$, for each property $* \in \Phi$, and whether or not the metric exponents are all equal to $\nu_{\mathscr{P}}^{\Theta}(\phi)$. Because of insufficient data, the metric exponents associated with the sets $\mathscr{E}(*)$ could not be estimated. Hence the exploration here addresses whether the metric exponents associated with $\mathscr{E}^c(*)$, for each $* \in \Phi$, are property independent and furthermore, are equal to the metric exponent $\nu_{\mathscr{P}}^{\Theta}(\phi)$. Because $\mathscr{P}^{\Theta}(\phi,f)$, $\mathscr{P}^{\Theta}(\phi|\phi,s)$, and $\mathscr{P}^{\Theta}(3_1|\phi,s)$ are mutually exclusive sets, the sequences in $2n$ of

essentially independent estimates for $r^2\left(\mathscr{P}_{2n}^{\Theta}(\phi)\right)$ and $r^2\left(\mathscr{E}_{2n}^{c}(*)\right)$, for $* \in \{(\phi, f), (\phi|\phi, s), (3_1|\phi, s)\}$, best illustrate any relationship that may exist amongst the metric exponents for these subsets of $\mathscr{P}^{\Theta}(\phi)$.

Given $\bullet \in \Upsilon_{2n}(*)$, if the expected mean-square radius of gyration $r^2(\bullet)$ scales according to Equation (7.86) as a function of $2n$, then for sufficiently large values of n, the log-log plot of $r^2(\bullet)$ versus $2n$ should become more and more linear as n increases and the slope of this linear plot will correspond to $2\nu_{\bullet}^{\Theta}(*)$. If the metric exponent in the scaling form of $r^2(\bullet)$ is independent of the property $* \in \Phi$, then in the log-log plots for different choices of $\bullet \in \Upsilon_{2n}(*)$ (for sufficiently large values of n), the regression lines should appear parallel. From this point forward, any reference to sequences being parallel in a figure refers to the regression lines for the different sequences appearing in the figure being parallel.

Figure 7.22 is a log-log plot of the sequences $((2n, \langle r^2(\bullet)\rangle), n \in \{12, 13, , ..., 945\})$, for each $\bullet \in \{\mathscr{P}_{2n}^{\Theta}(\phi)\,[\odot],\ \mathscr{E}_{2n}^{c}(\phi, f)\,[\times],\ \mathscr{E}_{2n}^{c}(\phi|\phi, s)\,[\boxdot],\ \mathscr{E}_{2n}^{c}(3_1|\phi, s)\,[\triangle]\}$. Note that both the horizontal and vertical scales are logarithmic (base 10) scales and for the purposes of creating a more illustrative figure, every 50'th estimate from each sequence is plotted. Over the range of values for $2n$ plotted in Figure 7.22, it appears that the sequences are parallel and hence it is possible that the metric exponents corresponding to each of the sequences are equal.

To further explore this equality of the metric exponents, the values of the exponents are estimated using the "Fixed-n Method for curve fitting". The essentially independent sequences required by the "Fixed-n Method for curve fitting" are displayed in Figure 7.23 and are presented in Column 3 of Tables B.15, B.16, and B.17 in Section B.3 of Appendix B.

Recall that in Section 5.6.1 of Chapter 5, the smallest value estimated for $N_{\min}^{*}$ (for any $* \in \{\phi, (\phi, f), (\phi|\phi, s), (3_1|\phi, s)\}$) was 142. Because the conjectured form for the expected mean-square radius of gyration is based on the conjectured form for $p_{2n}^{\Theta}(*)$ which in turn only holds for values of $n \geq N_{\min}^{*}/2$, the conjectured forms for the expected mean-square radii of gyration are considered only to be valid for values of $2n$ above 142. Consequently the data points corresponding to $2n = 24$ (the first data point in each sequence) have been excluded from the data that is used in the fits.

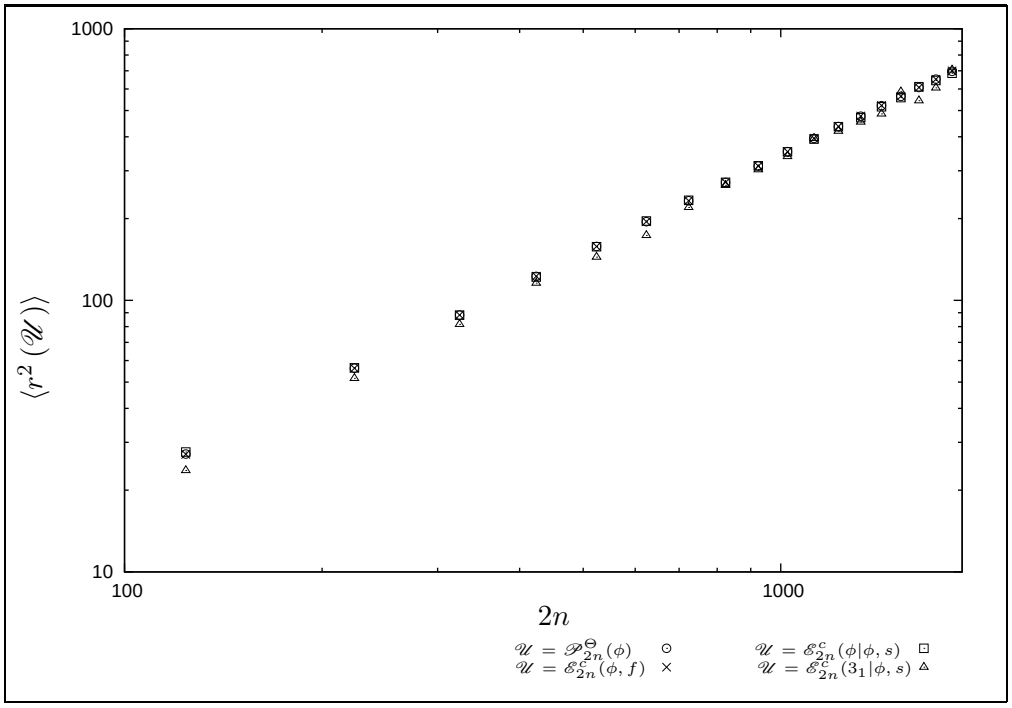

Figure 7.22: A log-log plot of the estimated mean-square radii of gyration of $(2n)$-edge SAPs from $\mathscr{P}^{\Theta}(\phi)$ [$\odot$], $\mathscr{E}^{c}(\phi, f)$ [$\times$], $\mathscr{E}^{c}(\phi|\phi, s)$ [$\boxdot$], and $\mathscr{E}^{c}(3_1|\phi, s)$ [$\triangle$].

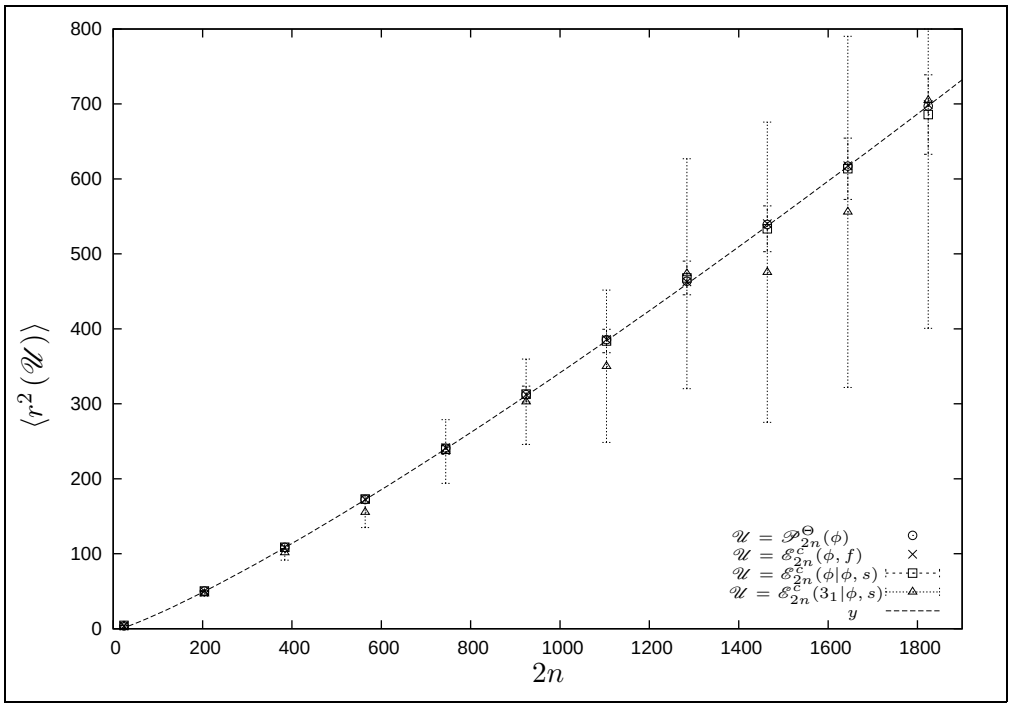

Figure 7.23: The estimated mean-square radius of gyration of $(2n)$-edge SAPs from $\mathscr{P}^{\Theta}(\phi)$ [$\odot$], $\mathscr{E}^{c}(\phi, f)$ [$\times$], $\mathscr{E}^{c}(\phi|\phi, s)$ [$\boxdot$], and $\mathscr{E}^{c}(3_1|\phi, s)$ [$\triangle$]. The line is the estimated regression curve $\hat{y}_{2n} = \hat{A}^{\Theta}_{\mathscr{P}}(\phi)(2n)^{2\hat{\nu}^{\Theta}_{\mathscr{P}}(\phi)} + \hat{b}_{\mathscr{P}}(\phi)$. The error bars are the estimated 95% margins of error.

Table 7.1: The estimates for $\nu_{\bullet}^{\Theta}(*)$, $A_{\bullet}^{\Theta}(*)$, and $b_{\bullet}(*)$ for the set $\bullet$ of property-$*$ SAPs in $\mathscr{P}^{\Theta}(\phi)$.

	Parameter Estimated		
$\bullet(*)$	$\nu_{\bullet}^{\Theta}(*)$	$A_{\bullet}^{\Theta}(*)$	$b_{\bullet}(*)$
$\mathscr{P}^{\Theta}(\phi)$	0.5907(0.0071)	0.0982(0.0164)	−2.8029(2.8576)
$\mathscr{E}^{c}(\phi, f)$	0.5854(0.0073)	0.1069(0.0121)	−4.5970(3.6207)
$\mathscr{E}^{c}(\phi\|\phi, s)$	0.5846(0.0166)	0.1072(0.0270)	−2.2051(6.8708)
$\mathscr{E}^{c}(3_1\|\phi, s)$	0.6189(0.1296)	0.0620(0.1220)	2.0377(48.7147)

Using the "Fixed-n Method for curve fitting" to fit the data plotted in Figure 7.23 to a curve of the form

$$y_{2n} = A_{\bullet}^{\Theta}(*)(2n)^{2\nu_{\bullet}^{\Theta}(*)} + b_{\bullet}(*), \tag{7.87}$$

for $2n \geq 142$, obtains the estimates for $\nu_{\bullet}^{\Theta}(*)$, $A_{\bullet}^{\Theta}(*)$, and $b_{\bullet}(*)$ presented in Table 7.1.

From the estimates $\nu_{\bullet}^{\Theta}(*)$ presented in Table 7.1, note that there is considerable overlap between the estimated 95% confidence intervals for each $\nu_{\bullet}^{\Theta}(*)$. Hence it is possible that the metric exponents $\nu_{\bullet}^{\Theta}(*)$ are all equal and thus independent of the property $*$. Because the most data available is from the set $\mathscr{P}^{\Theta}(\phi)$, the χ^2-Test for Goodness of Fit is used to determine how well the estimated regression curve

$$\hat{y}_{2n} = \hat{A}_{\mathscr{P}}^{\Theta}(\phi)(2n)^{2\hat{\nu}_{\mathscr{P}}^{\Theta}(\phi)} + \hat{b}_{\mathscr{P}}(\phi), \tag{7.88}$$

with $\hat{A}_{\mathscr{P}}^{\Theta}(\phi) = 0.0982$, $\hat{\nu}_{\mathscr{P}}^{\Theta}(\phi) = 0.5907$, and $\hat{b}_{\mathscr{P}}(\phi) = -2.8029$, fits the sequences of estimates $((2n, \langle r^2(\bullet)\rangle), n \in \{12 + 90, ..., 12 + 90t \leq 945\})$, for $\bullet \in \{\mathscr{E}_{2n}^{c}(\phi, f), \mathscr{E}_{2n}^{c}(\phi|\phi, s), \mathscr{E}_{2n}^{c}(3_1|\phi, s)\}$.

The estimated scaling form given by Equation (7.88) fits the sequence of estimates:

- $((2n, \langle r^2(\mathscr{E}_{2n}^{c}(\phi, f))\rangle), n \in \{12 + 90, ..., 12 + 90t \leq 945\})$ plotted in Figure 7.23 well, because, based on a χ^2-Test for Goodness of Fit, $\chi^2(6) = 0.1131$ and the corresponding p-value for the fit is greater than 0.9999;

- $((2n, \langle r^2(\mathscr{E}_{2n}^{c}(\phi|\phi, s))\rangle), n \in \{12 + 90, ..., 12 + 90t \leq 945\})$ plotted in Figure 7.23 well, because, based on a χ^2-Test for Goodness of Fit, $\chi^2(6) = 0.3943$ and the corresponding p-value for the fit is 0.9997; and

- $((2n, \langle r^2(\mathscr{E}^c_{2n}(3_1|\phi,s))\rangle), n \in \{12+90, ..., 12+90t \leq 945\})$ plotted in Figure 7.23 very poorly, because, based on a χ^2-Test for Goodness of Fit, $\chi^2(6) = 18.6052$ and the corresponding p-value for the fit is 0.0049.

However, regarding the final case above, observe from the plot of Equation (7.88) in Figure 7.23 that the plotted curve lies within all the plotted estimated 95% confidence intervals for $r^2(\mathscr{E}^c_{2n}(3_1|\phi,s))$. Considering this and the other numerical evidence presented in this section, the following is conjectured.

Conjecture 7.2.5 $\nu^{\Theta}_{\mathscr{E}^c}(*) = \nu^{\Theta}_{\mathscr{P}}(\phi)$, *for each property* $* \in \Phi$.

Question 2.2.9 queries whether or not the metric exponent $\nu^{\Theta}_{\mathscr{P}}(\phi)$ is equal to ν, the metric exponent associated with the set of all polygons $\mathscr{P}$ (cf. Equation (1.61)). Because the estimated 95% confidence interval for $\nu^{\Theta}_{\mathscr{P}}(\phi)$ presented in Table 7.1 includes the best estimated value for $\nu = 0.588$, the following is conjectured.

Conjecture 7.2.6 $\nu^{\Theta}_{\mathscr{P}}(\phi) = \nu$.

Exploring Question 2.2.10 Question 2.2.10 queries whether or not, for a fixed property $* \in \Phi$, $\nu^{\Theta}_{\mathfrak{w}_l(\mathscr{E}^c)}(*)$, the metric exponent of the expected mean-square radius of gyration for the large uSAWs in $\mathscr{E}^c(*)$, is the same as $\nu^{\Theta}_{\mathscr{E}^c}(*)$, the metric exponent for the expected mean-square radius of gyration for the polygons in $\mathscr{E}^c(*)$. Given $\bullet \in \Upsilon_{2n}(*)$, if the expected mean-square radius of gyration $r^2(\bullet)$ scales according to Equation (7.86) as a function of $2n$, then for sufficiently large values of n, the log-log plot of $r^2(\bullet)$ versus $2n$ should behave linearly as n increases and the slope of this linear plot corresponds to $2\nu^{\Theta}_{\bullet}(*)$. Figure 7.24 is a log-log plot of $\left(2n, \left\langle r^2\left(\mathscr{E}^c_{2n}(\phi,f)\right)\right\rangle\right),\ n \in \Lambda)$, $\left(\left(2n, \left\langle r^2\left(\mathfrak{w}_l\left(\mathscr{E}^c_{2n}(\phi,f)\right)\right)\right\rangle\right),\ n \in \Lambda\right)$, $\left(\left(2n, \left\langle r^2\left(\mathfrak{w}_e\left(\mathscr{E}_{2n}(\phi,f)\right)\right)\right\rangle\right),\ n \in \Lambda\right)$, and $\left(\left(2n, \left\langle r^2\left(\mathfrak{w}_s\left(\mathscr{E}^c_{2n}(\phi,f)\right)\right)\right\rangle\right),\ n \in \Lambda\right)$, where $\Lambda := \{12, 13, ..., 945\}$. Note that for the purposes of creating a more illustrative figure, every 30'th estimate from each sequence is plotted. Because the sequences associated with $\mathscr{E}^c(\phi,f)$, $\mathfrak{w}_l\left(\mathscr{E}^c(\phi,f)\right)$, and $\mathfrak{w}_e\left(\mathscr{E}(\phi,f)\right)$ in Figure 7.24 appear to be parallel, it is possible that $\nu^{\Theta}_{\mathfrak{w}_l(\mathscr{E}^c)}(\phi,f) = \nu^{\Theta}_{\mathscr{E}^c}(\phi,f) = \nu^{\Theta}_{\mathfrak{w}_e(\mathscr{E})}(\phi,f)$.

Figure 7.25 is a log-log plot of $\left(\left(2n, \left\langle r^2\left(\mathscr{E}^c_{2n}(\phi|\phi,s)\right)\right\rangle\right),\ n \in \Lambda\right)$, $\left(\left(2n, \left\langle r^2\left(\mathfrak{w}_l\left(\mathscr{E}^c_{2n}(\phi|\phi,s)\right)\right)\right\rangle\right),\ n \in \Lambda\right)$, $\left(\left(2n, \left\langle r^2\left(\mathfrak{w}_e\left(\mathscr{E}_{2n}(\phi|\phi,s)\right)\right)\right\rangle\right),\ n \in \Lambda\right)$, and

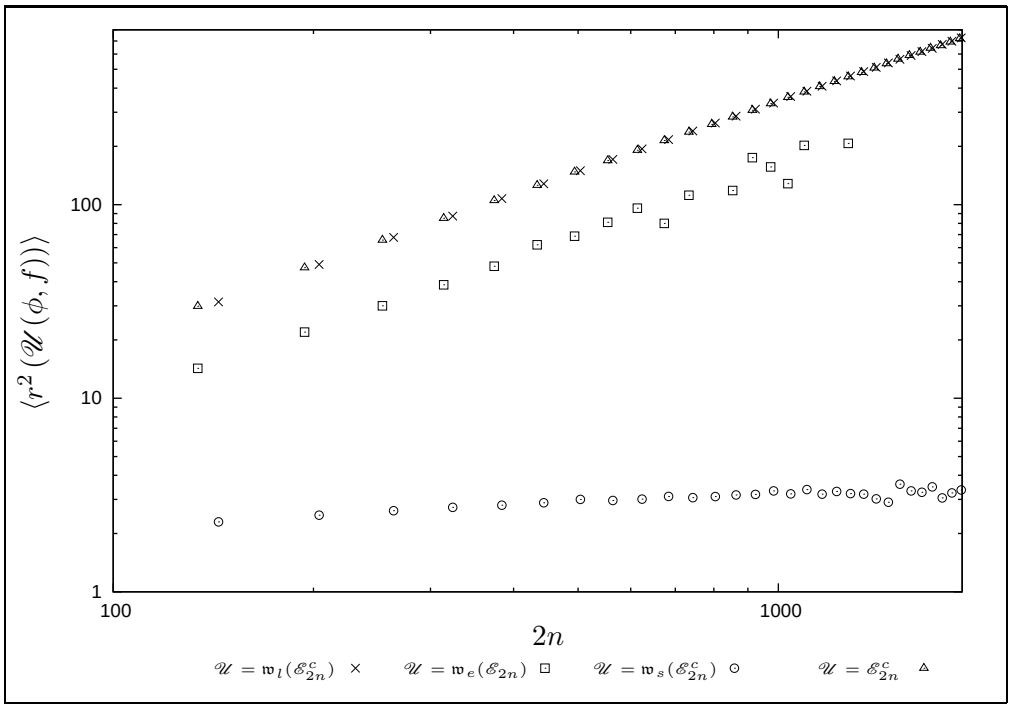

Figure 7.24: A log-log plot of the estimates for $r^2\left(\mathscr{E}^c_{2n}(\phi,f)\right)$ [△], $r^2\left(\mathfrak{w}_s\left(\mathscr{E}^c_{2n}(\phi,f)\right)\right)$ [⊙], $r^2\left(\mathfrak{w}_e\left(\mathscr{E}_{2n}(\phi,f)\right)\right)$ [⊡], and $r^2\left(\mathfrak{w}_l\left(\mathscr{E}^c_{2n}(\phi,f)\right)\right)$ [×] plotted versus $2n$.

$\left(\left(2n,\left\langle r^2\left(\mathfrak{w}_s\left(\mathscr{E}^c_{2n}(\phi|\phi,s)\right)\right)\right\rangle\right),\ n\in\Lambda\right)$, where $\Lambda:=\{12,13,...,945\}$. Note that, as before, for the purposes of creating a more illustrative figure, only every 30'th estimate from each sequence is plotted. In Figure 7.25, because the sequences associated with $\mathscr{E}^c(\phi|\phi,s)$, $\mathfrak{w}_l\left(\mathscr{E}^c(\phi|\phi,s)\right)$, and $\mathfrak{w}_e\left(\mathscr{E}(\phi|\phi,s)\right)$ appear parallel, it is possible that $\nu^{\Theta}_{\mathfrak{w}_l(\mathscr{E}^c)}(\phi|\phi,s)=\nu^{\Theta}_{\mathscr{E}^c}(\phi|\phi,s)=\nu^{\Theta}_{\mathfrak{w}_e(\mathscr{E})}(\phi|\phi,s)$.

Figure 7.26 is a log-log plot of $\left(\left(2n,\left\langle r^2\left(\mathscr{E}^c_{2n}(3_1|\phi,s)\right)\right\rangle\right),\ n\in\Lambda\right)$, $\left(\left(2n,\left\langle r^2\left(\mathfrak{w}_l\left(\mathscr{E}^c_{2n}(3_1|\phi,s)\right)\right)\right\rangle\right),\ n\in\Lambda\right)$, $\left(\left(2n,\left\langle r^2\left(\mathfrak{w}_e\left(\mathscr{E}_{2n}(3_1|\phi,s)\right)\right)\right\rangle\right),\ n\in\Lambda\right)$, and $\left(\left(2n,\left\langle r^2\left(\mathfrak{w}_s\left(\mathscr{E}^c_{2n}(3_1|\phi,s)\right)\right)\right\rangle\right),\ n\in\Lambda\right)$, where $\Lambda:=\{12,13,...,945\}$. Note that, once again, for the purposes of creating a more illustrative figure, every 30'th estimate from each sequence is plotted. In Figure 7.25, not enough data is available to draw any conclusion regarding the relationship between the metric exponent $\nu^{\Theta}_{\mathfrak{w}_e(\mathscr{E})}(3_1|\phi,s)$ and the exponents $\nu^{\Theta}_{\mathfrak{w}_l(\mathscr{E}^c)}(3_1|\phi,s)$ and $\nu^{\Theta}_{\mathscr{E}^c}(3_1|\phi,s)$. Because, however, the sequences associated with $\mathscr{E}^c(3_1|\phi,s)$ and $\mathfrak{w}_l\left(\mathscr{E}^c(3_1|\phi,s)\right)$ appear parallel, it is possible that $\nu^{\Theta}_{\mathfrak{w}_l(\mathscr{E}^c)}(3_1|\phi,s)=\nu^{\Theta}_{\mathscr{E}^c}(3_1|\phi,s)$.

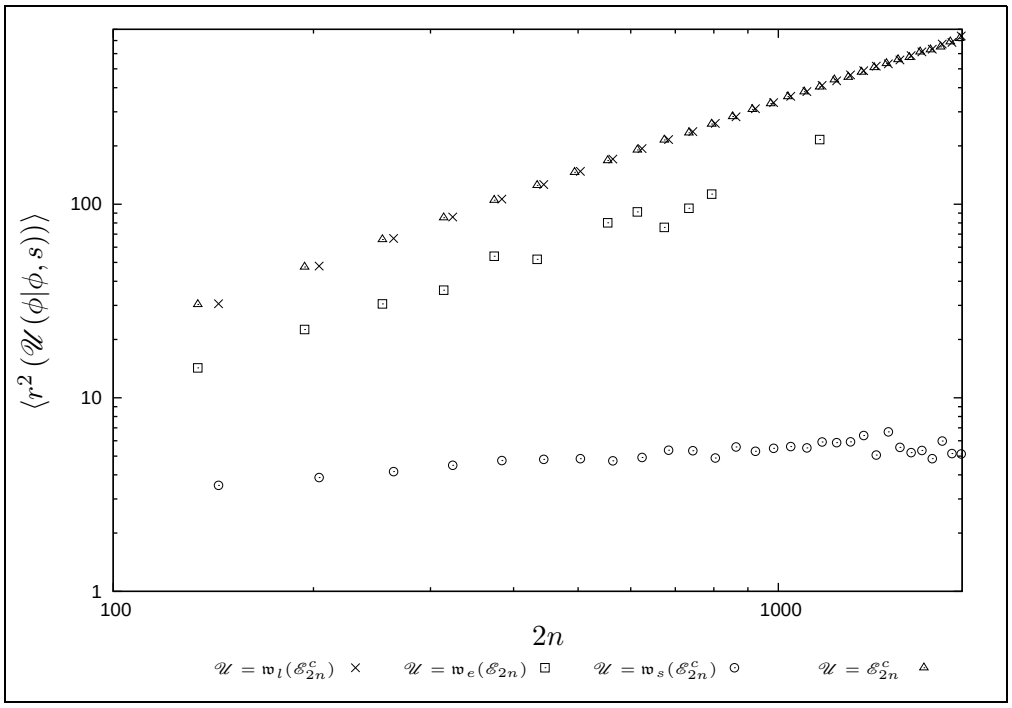

Figure 7.25: A log-log plot of the estimates for $r^2\,(\mathscr{E}^c_{2n}(\phi|\phi,s))$ [△], $r^2\,(\mathfrak{w}_s\,(\mathscr{E}^c_{2n}(\phi|\phi,s)))$ [⊙], $r^2\,(\mathfrak{w}_e\,(\mathscr{E}_{2n}(\phi|\phi,s)))$ [⊡], and $r^2\,(\mathfrak{w}_l\,(\mathscr{E}^c_{2n}(\phi|\phi,s)))$ [×] plotted versus $2n$.

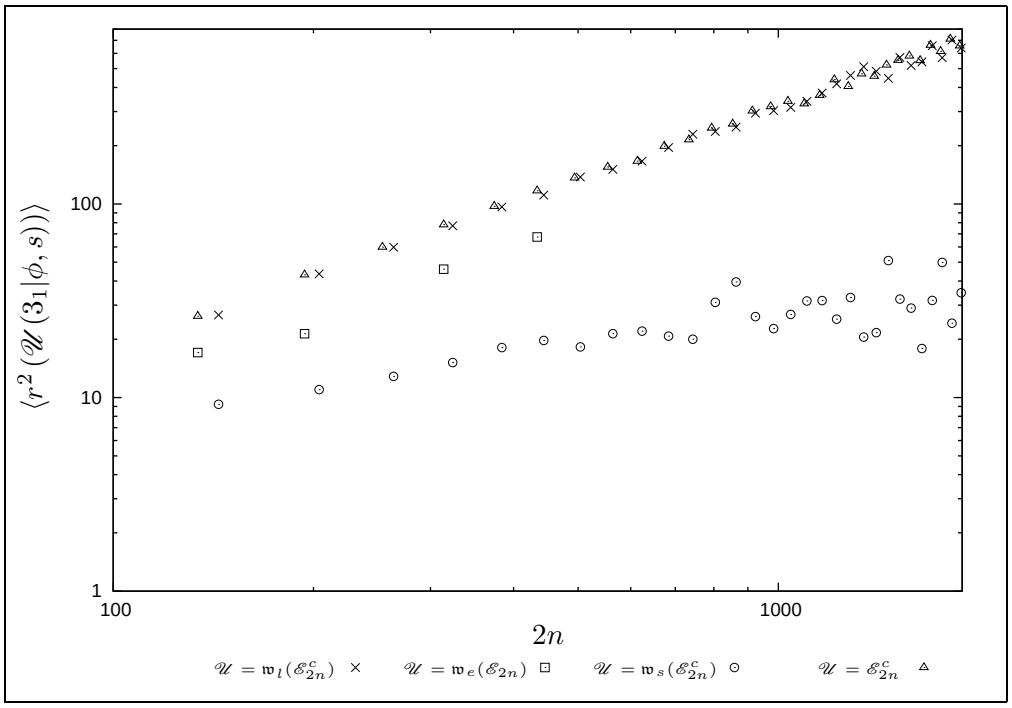

Figure 7.26: A log-log plot of the estimates for $r^2\,(\mathscr{E}^c_{2n}(3_1|\phi,s))$ [△], $r^2\,(\mathfrak{w}_s\,(\mathscr{E}^c_{2n}(3_1|\phi,s)))$ [⊙], $r^2\,(\mathfrak{w}_e\,(\mathscr{E}_{2n}(3_1|\phi,s)))$ [⊡], and $r^2\,(\mathfrak{w}_l\,(\mathscr{E}^c_{2n}(3_1|\phi,s)))$ [×] plotted versus $2n$.

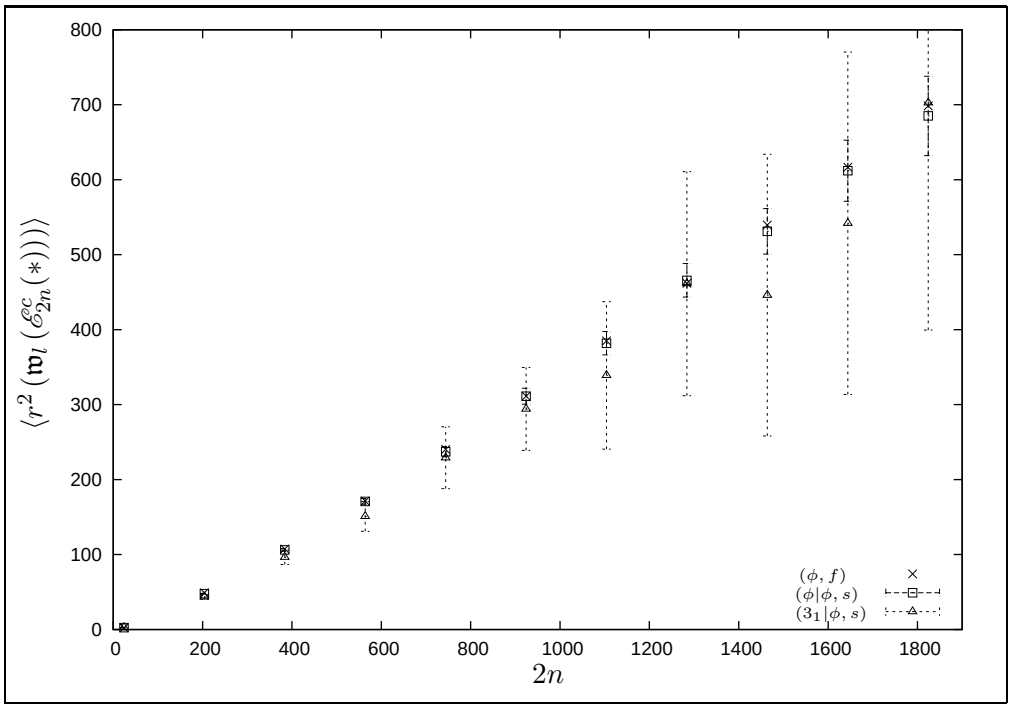

Figure 7.27: The estimated mean-square radius of gyration of the large uSAWs in $(2n)$-edge SAPs from $\mathscr{E}^c(\phi, f)$ [$\times$], $\mathscr{E}^c(\phi|\phi, s)$ [$\boxdot$], and $\mathscr{E}^c(3_1|\phi, s)$ [$\triangle$]. The error bars are the estimated 95% margins of error.

In order to further explore whether the exponents $\nu^{\Theta}_{\mathfrak{w}_l(\mathscr{E}^c)}(*)$ and $\nu^{\Theta}_{\mathscr{E}^c}(*)$ are equal, estimates for the exponents $\nu^{\Theta}_{\mathfrak{w}_l(\mathscr{E}^c)}(*)$ for $* \in \{(\phi, f),\ (\phi|\phi, s),\ (3_1|\phi, s)\}$, are required in addition to the estimates for $\nu^{\Theta}_{\mathscr{E}^c}(*)$ presented in Table 7.1. In order to use the "Fixed-n Method for curve fitting" to determine these additional estimates, sequences of essentially independent estimates for $r^2\left(\mathfrak{w}_l\left(\mathscr{E}^c_{2n}(*)\right)\right)$, for $* \in \{(\phi, f),\ (\phi|\phi, s),\ (3_1|\phi, s)\}$, are required. These required sequences are plotted in Figure 7.27 and also can be found in Column 4 of Tables B.15, B.16, and B.17 (cf. Section B.3 of Appendix B).

The estimates resulting from applying the "Fixed-n Method for curve fitting" to the data plotted in Figure 7.27 to a curve of the form

$$y_{2n} = A^{\Theta}_{\mathfrak{w}_l(\mathscr{E}^c)}(*)(2n)^{2\nu^{\Theta}_{\mathfrak{w}_l(\mathscr{E}^c)}(*)} + b_{\mathfrak{w}_l(\mathscr{E}^c)}(*) \tag{7.89}$$

yields the estimates for $\nu^{\Theta}_{\mathfrak{w}_l(\mathscr{E}^c)}(*)$, $A^{\Theta}_{\mathfrak{w}_l(\mathscr{E}^c)}(*)$, and $b_{\mathfrak{w}_l(\mathscr{E}^c)}(*)$ provided in Table 7.2.

If the metric exponents in the scaling form of $r^2(\bullet)$ are independent of the property $* \in \Phi$, then, for sufficiently large values of n, the log-log plots of the data sequences should appear parallel. Figure 7.28 is a log-log plot of the sequences of esti-

Table 7.2: The estimates for $\nu^{\Theta}_{\mathfrak{w}_l(\mathscr{E}^c)}(*)$, $A^{\Theta}_{\mathfrak{w}_l(\mathscr{E}^c)}(*)$, and $b_{\mathfrak{w}_l(\mathscr{E}^c)}(*)$ for the large uSAWs in polygons in $\mathscr{E}^c(*)$.

	Parameter Estimated		
Property $*$	$\nu^{\Theta}_{\mathfrak{w}_l(\mathscr{E}^c)}(*)$	$A^{\Theta}_{\mathfrak{w}_l(\mathscr{E}^c)}(*)$	$b_{\mathfrak{w}_l(\mathscr{E}^c)}(*)$
(ϕ, f)	0.5847(0.0075)	0.1080(0.0126)	−5.9280(3.7271)
$(\phi\|\phi, s)$	0.5851(0.0166)	0.1059(0.0267)	−4.0901(6.8560)
$(3_1\|\phi, s)$	0.6419(0.1673)	0.0428(0.1086)	5.1553(58.2663)

mates $((2n, \langle r^2(\bullet)\rangle), n \in \{12, 13, , ..., 945\})$, for each $\bullet \in \{\mathfrak{w}_l(\mathscr{E}^c_{2n}(\phi, f)), \mathfrak{w}_l(\mathscr{E}^c_{2n}(\phi|\phi, s)), \mathfrak{w}_l(\mathscr{E}^c_{2n}(3_1|\phi, s))\}$; note that both the horizontal and vertical scales are logarithmic (base 10) scales and for the purposes of creating a more illustrative figure, every 50'th estimate from each sequence is plotted. For the values of $2n$ plotted in Figure 7.28, it appears that, for sufficiently large values of $2n$, the sequences plotted are parallel and hence it is possible that the metric exponents corresponding to each of the sequences are equal.

For each of the properties $* \in \{(\phi, f), (\phi|\phi, s), (3_1|\phi, s)\}$, from the estimates $\nu^{\Theta}_{\mathfrak{w}_l(\mathscr{E}^c)}(*)$ presented in Table 7.2, note that there is considerable overlap between the estimated 95% confidence intervals for the three corresponding metric exponents. Hence it is possible that the metric exponent $\nu^{\Theta}_{\mathfrak{w}_l(\mathscr{E}^c)}(*)$ for the large uSAW is independent of the property $*$. Furthermore, because each point estimate for $\nu^{\Theta}_{\mathfrak{w}_l(\mathscr{E}^c)}(*)$ presented in Table 7.2 lies within the estimated 95% confidence interval for the metric exponent in Table 7.1 with the same property, and vice versa, the metric exponent associated with the expected mean-square radius of gyration of the large uSAWs in SAPs in $\mathscr{E}^c(*)$ is quite possibly equal to the metric exponent associated with the expected mean-square radius of gyration of SAPs in $\mathscr{E}^c(*)$. The χ^2-Test for Goodness of Fit is used to determine, for each $* \in \{(\phi, f), (\phi|\phi, s), (3_1|\phi, s)\}$, how well the estimated regression curve

$$\hat{y}_{2n} = \hat{A}^{\Theta}_{\mathscr{E}^c}(*)(2n)^{2\hat{\nu}^{\Theta}_{\mathscr{E}^c}(*)} + \hat{b}_{\mathscr{E}^c}(*), \tag{7.90}$$

with $\hat{A}^{\Theta}_{\mathscr{E}^c}(*)$, $\hat{\nu}^{\Theta}_{\mathscr{E}^c}(*)$, and $\hat{b}_{\mathscr{E}^c}(*)$ as given in Table 7.1, fits the sequences of estimates $((2n, \langle \mathfrak{w}_l(r^2(\bullet))\rangle), n \in \{12 + 90, ..., 12 + 90t \leq 945\})$, for $\bullet \in \{\mathscr{E}^c_{2n}(\phi, f), \mathscr{E}^c_{2n}(\phi|\phi, s), \mathscr{E}^c_{2n}(3_1|\phi, s)\}$.

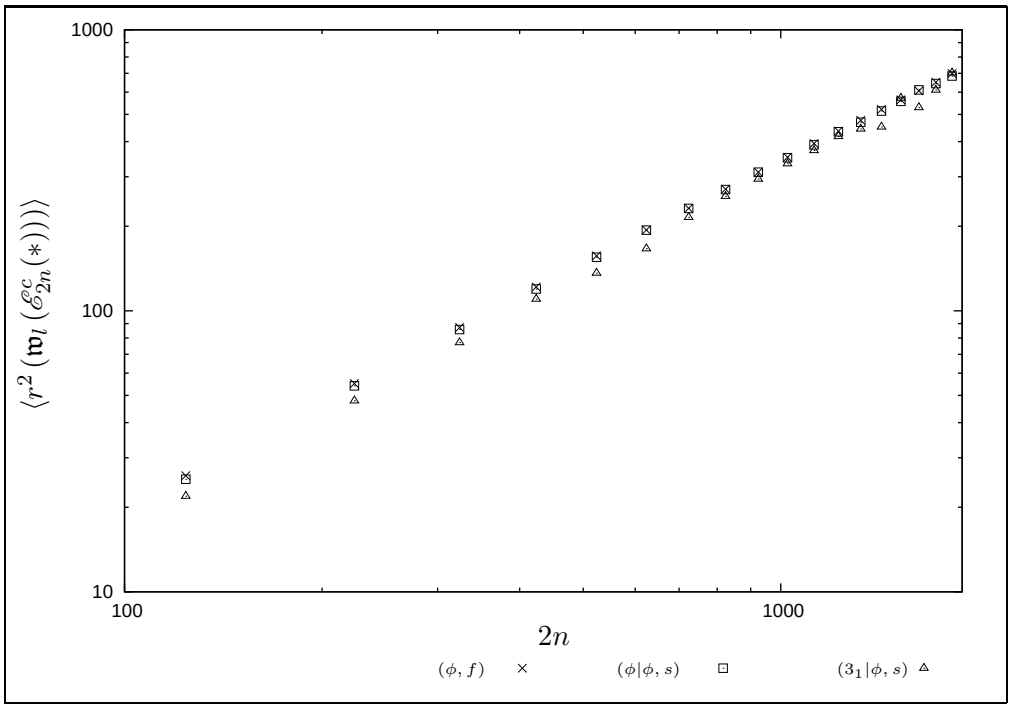

Figure 7.28: A log-log plot for the estimated mean-square radius of gyration of the large uSAWs in $(2n)$-edge SAPs from $\mathscr{E}^c(\phi, f)$ [×], $\mathscr{E}^c(\phi|\phi, s)$ [⊡], and $\mathscr{E}^c(3_1|\phi, s)$ [△]. The error bars are the estimated 95% margins of error.

The estimated scaling form given by Equation (7.90) with $* = (\phi, f)$ fits the sequence of estimates $((2n, \langle \mathfrak{w}_l\left(r^2(\mathscr{E}^c_{2n}(\phi, f))\right)\rangle), n \in \{12 + 90, ..., 12 + 90t \leq 945\})$ plotted in Figure 7.27 extremely well, because, based on a χ^2-Test for Goodness of Fit, $\chi^2(6) = 0.0596$ and the corresponding p-value for the fit is greater than 0.9999. Similarly the form given by Equation (7.90) with $* = (\phi|\phi, s)$ fits the sequence of estimates: $((2n, \langle \mathfrak{w}_l\left(r^2(\mathscr{E}^c_{2n}(\phi|\phi, s))\right)\rangle), n \in \{12 + 90, ..., 12 + 90t \leq 945\})$ plotted in Figure 7.27 well, because, based on a χ^2-Test for Goodness of Fit, $\chi^2(6) = 0.8837$ and the corresponding p-value for the fit is 0.9896. Due to the large 95% error margins for the $(3_1|\phi, s)$-estimates presented in Table 7.1, it is not surprising that Equation (7.90) with $* = (3_1|\phi, s)$ does not fit the sequence of estimates $((2n, \langle \mathfrak{w}_l\left(r^2(\mathscr{E}^c_{2n}(3_1|\phi, s))\right)\rangle), n \in \{12+90, ..., 12+90t \leq 945\})$ at all. In fact, based on a χ^2-Test for Goodness of Fit, $\chi^2(6) = 19.0323$ and the corresponding p-value for the fit is 0.0041. However, based on the numerical evidence presented in this section, the following conjecture is made.

Conjecture 7.2.7 $\nu^{\Theta}_{\mathfrak{w}_l(\mathscr{E}^c)}(*) = \nu^{\Theta}_{\mathscr{E}^c}(*)$, *for each property* $* \in \Phi$.

Exploring Question 2.2.12 Question 2.2.12 queries whether or not, for a fixed property $* \in \Phi$, $\nu^{\Theta}_{\mathfrak{w}_s(\mathscr{E}^c)}(*)$, the metric exponent of the expected mean-square radius of gyration for the small uSAWs in $\mathscr{E}^c(*)$, is less than $\nu^{\Theta}_{\mathscr{E}^c}(*)$, the metric exponent for the expected mean-square radius of gyration for the polygons in $\mathscr{E}^c(*)$. In Figure 7.24, because the sequences associated with $\mathscr{E}^c(\phi, f)$ and $\mathfrak{w}_s(\mathscr{E}^c(\phi, f))$ do not appear parallel and the slope of the estimated regression line based on the $\mathscr{E}^c(\phi, f)$-data appears to be greater than the slope of the estimated regression line based on the $\mathfrak{w}_s(\mathscr{E}^c(\phi, f))$-data, this supports $\nu^{\Theta}_{\mathfrak{w}_s(\mathscr{E}^c)}(\phi, f) < \nu^{\Theta}_{\mathscr{E}^c}(\phi, f)$. In Figure 7.25, because the sequences associated with $\mathscr{E}^c(\phi|\phi, s)$ and $\mathfrak{w}_s(\mathscr{E}^c(\phi|\phi, s))$ do not appear parallel and the slope of the estimated regression line based on the $\mathscr{E}^c(\phi|\phi, s)$-data appears to be greater than the slope of the estimated regression line based on the $\mathfrak{w}_s(\mathscr{E}^c(\phi|\phi, s))$-data, this supports $\nu^{\Theta}_{\mathfrak{w}_s(\mathscr{E}^c)}(\phi|\phi, s) < \nu^{\Theta}_{\mathscr{E}^c}(\phi|\phi, s)$. Similarly, in Figure 7.26, the sequences associated with $\mathscr{E}^c(3_1|\phi, s)$ and $\mathfrak{w}_s(\mathscr{E}^c(3_1|\phi, s))$ do not appear parallel and the slope of the estimated regression line based on the $\mathscr{E}^c(3_1|\phi, s)$-data appears to be greater than the slope of the estimated regression line based on the $\mathfrak{w}_s(\mathscr{E}^c(3_1|\phi, s))$-data. Thus supporting $\nu^{\Theta}_{\mathfrak{w}_s(\mathscr{E}^c)}(3_1|\phi, s) < \nu^{\Theta}_{\mathscr{E}^c}(3_1|\phi, s)$.

In order to further explore this possible relationship between, for a fixed property $* \in \Phi$, $\nu^{\Theta}_{\mathfrak{w}_s(\mathscr{E}^c)}(*)$ and $\nu^{\Theta}_{\mathscr{E}^c}(*)$, estimates for the exponents $\nu^{\Theta}_{\mathfrak{w}_s(\mathscr{E}^c)}(*)$, for $* \in \{(\phi, f), (\phi|\phi, s), (3_1|\phi, s)\}$, are required in addition to the estimates for $\nu^{\Theta}_{\mathscr{E}^c}(*)$ presented in Table 7.1. In order to use the "Fixed-n Method for curve fitting" to determine these additional estimates, sequences of essentially independent estimates for $r^2\left(\mathfrak{w}_s\left(\mathscr{E}^c_{2n}(*)\right)\right)$, for $* \in \{(\phi, f), (\phi|\phi, s), (3_1|\phi, s)\}$, are required. These required sequences are plotted in Figure 7.29 and also can be found in Column 5 of Tables B.15, B.16, and B.17 in Section B.3 of Appendix B.

From Figure 7.29, note that the general trend of the estimated mean-square radii of gyration of the small uSAWs plotted as a function of polygon length $2n$ seem to follow a different trend than the estimated mean-square radii of gyration that are plotted in Figures 7.23 and 7.27 respectively. Assuming the relationship between the fixed $2n$ expected mean-square radius of gyration and polygon length $2n$ is a power law relation of the form given by, for each $* \in \Phi$,

$$y_{2n} = A^{\Theta}_{\mathfrak{w}_s(\mathscr{E}^c)}(*)(2n)^{2\nu^{\Theta}_{\mathfrak{w}_s(\mathscr{E}^c)}(*)} + b_{\mathfrak{w}_s(\mathscr{E}^c)}(*) \tag{7.91}$$

then from Figures 7.23 and 7.27, the point estimates plotted for each property seem to follow a trend where $2\nu^{\Theta}_{\bullet}(*) > 1$, but the estimates plotted in Figure 7.29 as a function of polygon length seem to follow a trend where $0 \leq 2\nu^{\Theta}_{\mathfrak{w}_s(\mathscr{E}^c)}(*) < 1$.

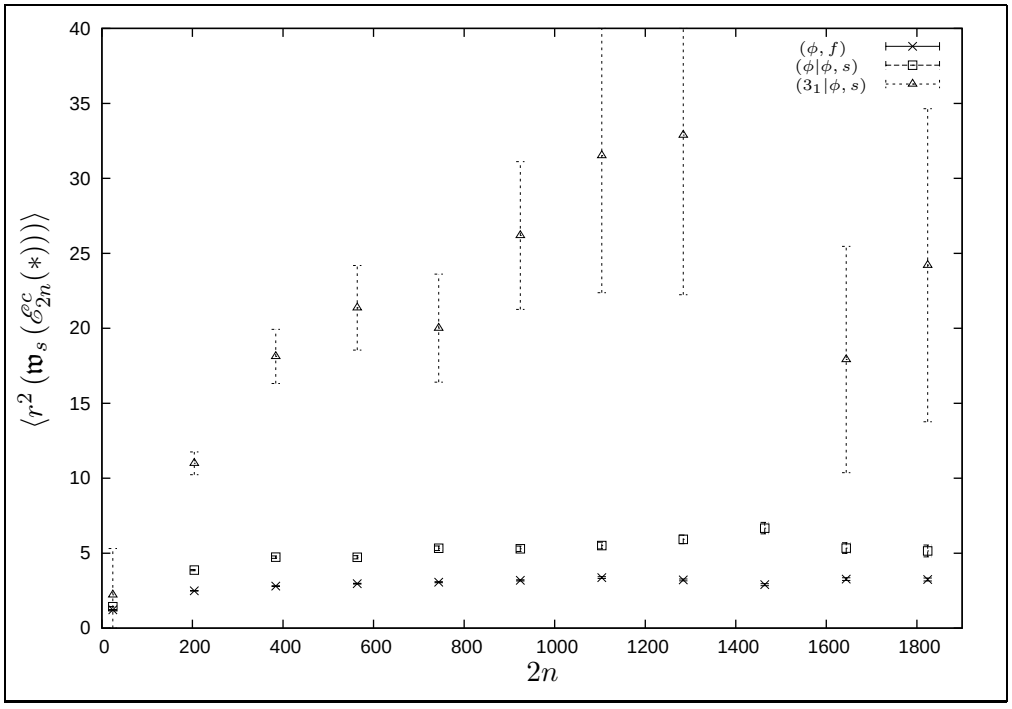

Figure 7.29: The estimated mean-square radius of gyration of the small uSAWs in $(2n)$-edge SAPs from $\mathscr{E}^c(\phi, f)$ [$\times$], $\mathscr{E}^c(\phi|\phi, s)$ [$\boxdot$], and $\mathscr{E}^c(3_1|\phi, s)$ [$\triangle$]. The error bars are the estimated 95% margins of error.

Table 7.3: The estimates for $\nu^{\Theta}_{\mathfrak{w}_s(\mathscr{E}^c)}(*)$, $A^{\Theta}_{\mathfrak{w}_s(\mathscr{E}^c)}(*)$, and $b_{\mathfrak{w}_s(\mathscr{E}^c)}(*)$ for the small uSAWs in polygons in $\mathscr{E}^c(*)$.

	Parameter Estimated		
Property $*$	$\nu^{\Theta}_{\mathfrak{w}_s(\mathscr{E}^c)}$	$A^{\Theta}_{\mathfrak{w}_s(\mathscr{E}^c)}$	$b_{\mathfrak{w}_s(\mathscr{E}^c)}$
ϕ	0.0179(0.0903)	13.2685(71.5134)	-13.4529(72.5984)
(ϕ, f)	0.0193(0.0915)	10.6506(54.6140)	-10.7057(55.5400)
$(\phi\|\phi, s)$	0.0360(0.1654)	10.1934(61.5720)	-11.2391(65.1067)
$(3_1\|\phi, s)$	0.1084(0.6717)	11.1331(155.9192)	-21.3703(235.5239)

Using the "Fixed-n Method for curve fitting" to fit the data plotted in Figure 7.29 to Equation (7.91) yields the estimates for $\nu^{\Theta}_{\mathfrak{w}_s(\mathscr{E}^c)}(*)$, $A^{\Theta}_{\mathfrak{w}_s(\mathscr{E}^c)}(*)$, and $b^{\Theta}_{\mathfrak{w}_s(\mathscr{E}^c)}(*)$ provided in Table 7.3. Because each point estimate for $\nu^{\Theta}_{\mathfrak{w}_s(\mathscr{E}^c)}(*)$ presented in Table 7.3 is not included in the estimated 95% confidence interval for the metric exponent in Table 7.1 with the same property, this supports the possibility that the metric exponent associated with the expected mean-square radius of gyration of the small uSAWs in SAPs in $\mathscr{E}^c(*)$ is smaller than the metric exponent associated with the expected mean-square radius of gyration of SAPs in $\mathscr{E}^c(*)$. Furthermore, from the parameter estimates provided in Table 7.3, the possibility that

$$\nu^{\Theta}_{\mathfrak{w}_s(\mathscr{E}^c)}(\phi, f) = \nu^{\Theta}_{\mathfrak{w}_s(\mathscr{E}^c)}(\phi|\phi, s) = \nu^{\Theta}_{\mathfrak{w}_s(\mathscr{E}^c)}(3_1|\phi, s) = 0 \tag{7.92}$$

cannot be ruled out but due to the large relative error in the estimates, this possibility is not strongly supported. Figure 7.30 is a log-log plot of the sequences $((2n, \langle r^2(\bullet)\rangle), n \in \{12, 13, ..., 945\})$, for each $\bullet \in \{\mathfrak{w}_s(\mathscr{E}^c_{2n}(\phi, f)), \mathfrak{w}_s(\mathscr{E}^c_{2n}(\phi|\phi, s)), \mathfrak{w}_s(\mathscr{E}^c_{2n}(3_1|\phi, s))\}$. The only conclusive statement that can be made, based on Figure 7.30, is that more data must be collected before the relationship between the exponents $\nu^{\Theta}_{\mathfrak{w}_s(\mathscr{E}^c)}(\phi, f)$, $\nu^{\Theta}_{\mathfrak{w}_s(\mathscr{E}^c)}(\phi|\phi, s)$, and $\nu^{\Theta}_{\mathfrak{w}_s(\mathscr{E}^c)}(3_1|\phi, s)$ can be specified. However, the numerical evidence presented here supports the following conjecture.

Conjecture 7.2.8 $0 \leq \nu^{\Theta}_{\mathfrak{w}_s(\mathscr{E}^c)}(*) < \frac{1}{2} < \nu^{\Theta}_{\mathscr{E}^c}(*)$, *for each property* $* \in \Phi$.

Exploring Question 2.2.13 Question 2.2.13 asks whether the amplitudes $A^{\Theta}_{\bullet}(*)$ are independent of $* \in \Phi$. From the estimates for $A^{\Theta}_{\bullet}(*)$ presented in Table 7.1, there is considerable overlap amongst all four estimated confidence intervals. Hence it is also possible that the amplitudes $A^{\Theta}_{\mathscr{E}^c}(*)$ and $A^{\Theta}_{\mathscr{P}}(\phi)$ are all equal and thus independent of the property $*$. Furthermore, comparing the estimates for the amplitudes $A^{\Theta}_{L}(*)$ presented in Table 7.1 to the amplitude estimates in Equation (1.65) leads to the conjecture that.

Conjecture 7.2.9 *For every property* $* \in \Phi$, $A^{\Theta}_{\mathscr{E}^c}(*) = A^{\Theta}_{\mathscr{P}}(\phi) = A_R(\phi)$, *where* $A_R(\phi)$ *is the amplitude in the scaling form for the radius of gyration for the set of polygons with knot-type* ϕ.

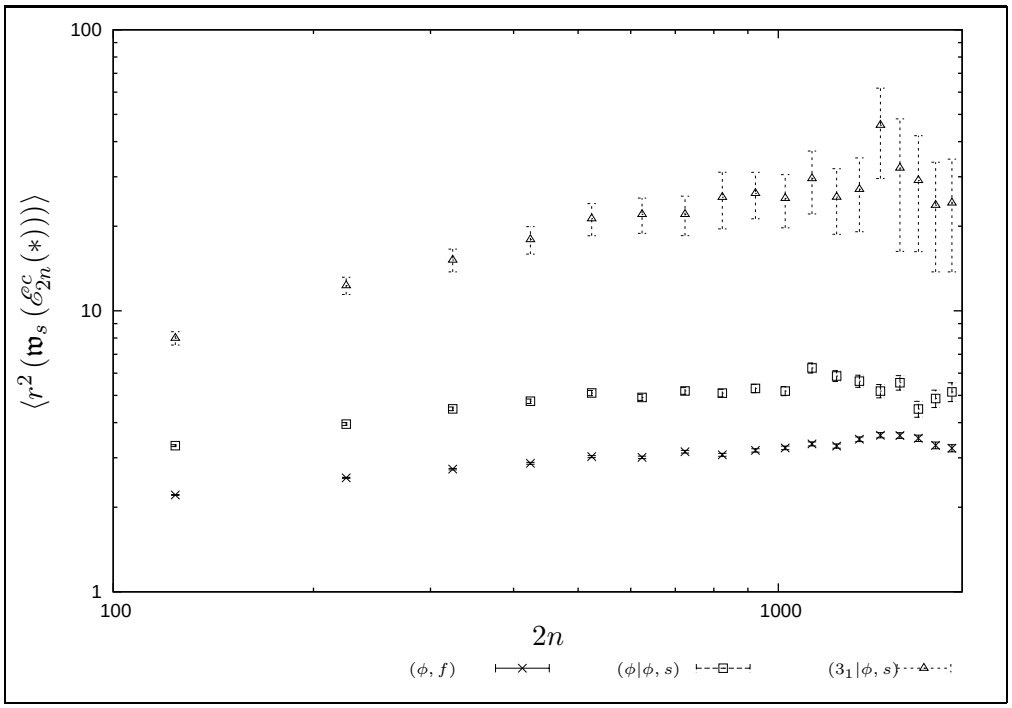

Figure 7.30: A log-log plot for the estimated mean-square radius of gyration of the small uSAWs in $(2n)$-edge SAPs from $\mathscr{E}^c(\phi, f)$ [$\times$], $\mathscr{E}^c(\phi|\phi, s)$ [$\boxdot$], and $\mathscr{E}^c(3_1|\phi, s)$ [$\triangle$]. The error bars are the estimated 95% margins of error.

For each of the properties $* \in \{(\phi, f), (\phi|\phi, s), (3_1|\phi, s)\}$, from the estimates $A^{\Theta}_{\mathfrak{w}_l(\mathscr{E}^c)}(*)$ presented in Table 7.2, note that there is considerable overlap in the estimated 95% confidence intervals for the three corresponding amplitudes. Hence it is possible that the amplitudes $A^{\Theta}_{\mathfrak{w}_l(\mathscr{E}^c)}(*)$ for the large uSAW is independent of the property $*$. Furthermore, because each point estimate for $A^{\Theta}_{\mathfrak{w}_l(\mathscr{E}^c)}(*)$ presented in Table 7.2 lies within the estimated 95% confidence interval for the amplitude with the same property in Table 7.1, and vice versa, this supports the possibility that the amplitude associated with the expected mean-square radius of gyration of the large uSAWs in SAPs in $\mathscr{E}^c(*)$ is equal to the amplitude associated with the expected mean-square radius of gyration of SAPs in $\mathscr{E}^c(*)$. This supports the following conjecture.

Conjecture 7.2.10 *For every property* $* \in \Phi$, $A^{\Theta}_{\mathfrak{w}_l(\mathscr{E}^c)}(*) = A^{\Theta}_{\mathscr{E}^c}(*)$.

The analysis, which lead to Conjectures 7.2.5-7.2.10, is really a preliminary analysis. In order to obtain better numerics that support these conjectures, more data must be collected and hence is left as future work.

A benefit of the "Fixed-n Method" is that it is straightforward and relatively simple to implement. The method estimates both the metric exponent and the amplitude in the assumed scaling form for the expected mean-square radius of gyration. The downside of this method is that the essentially independent sample ignores many of the generated estimates for $r^2\left(\mathscr{P}_{2n}^{\Theta}(\phi)\right)$, $r^2\left(\mathscr{E}_{2n}(*)\right)$, $r^2\left(\mathscr{E}_{2n}^{c}(*)\right)$, $r^2\left(\mathfrak{w}_e(\mathscr{E}_{2n}(*))\right)$, $r^2\left(\mathfrak{w}_l\left(\mathscr{E}_{2n}^{c}(*)\right)\right)$, and $r^2\left(\mathfrak{w}_s\left(\mathscr{E}_{2n}^{c}(*)\right)\right)$. The next method, "Average-n Method for estimating $\nu_{\bullet}^{\Theta}(*)$" uses estimates for $r^2\left(\mathscr{P}_{2n}^{\Theta}(\phi)\right)$, $r^2\left(\mathscr{E}_{2n}(*)\right)$, $r^2\left(\mathscr{E}_{2n}^{c}(*)\right)$, $r^2\left(\mathfrak{w}_e(\mathscr{E}_{2n}(*))\right)$, $r^2\left(\mathfrak{w}_l\left(\mathscr{E}_{2n}^{c}(*)\right)\right)$, and $r^2\left(\mathfrak{w}_s\left(\mathscr{E}_{2n}^{c}(*)\right)\right)$ generated for all $2n \geq N_{\min}^{*}$.

The Average-n Method for Estimating $\nu_{\bullet}^{\Theta}(*)$

Given a fixed positive integer q, a fixed even positive integer $N_{\min}$ and a conditional probability mass function $\boldsymbol{\pi}_z(q, N_{\min}) := \{\pi_{2n|N_{\min}}(q,z) : n \geq N_{\min}/2\}$ for the length of a randomly selected element from $\mathscr{U}(*) := \bigcup\limits_{n \geq N_{\min}/2} \mathscr{U}_{2n}(*)$ (with $\mathscr{U}_{2n}(*) \subseteq \mathscr{P}_{2n}^{\Theta}(\phi)$), recall from Section 2.2.3, that for some function $f : \mathbb{Z}^3 \to \mathbb{Z}^3$, the expected mean-square radii of gyration and the f-transformed expected mean-square radii of gyration for the length of a randomly selected element from $\mathscr{U}$ are respectively given by

$$r^2_{\boldsymbol{\pi}_z(N_{\min})}(\mathscr{U}(*)) := \sum_{n=N_{\min}/2}^{\infty} r^2(\mathscr{U}_{2n}(*))\pi_{2n|N_{\min}}(2,z) \tag{7.93}$$

and

$$r^2_{\boldsymbol{\pi}_z(N_{\min})}(f(\mathscr{U}(*))) := \sum_{n=N_{\min}/2}^{\infty} r^2(f(\mathscr{U}_{2n}(*)))\pi_{2n|N_{\min}}(2,z). \tag{7.94}$$

Further recall from Section 4.5.2 that, if $\pi_{2n|N_{\min}}(q,z)$ is defined by Equation (2.61), then, assuming that, for $N_{\min}$ sufficiently large, there exist constants $A_{\mathscr{U}}^{(1)}(*)$, $A_{\mathscr{U}}^{(2)}(*)$, $\nu_{\mathscr{U}}^{\Theta}(*)$, $\alpha_{\mathscr{U}}^{\Theta}(*)$, q, κ_ϕ, $B_{\mathscr{U}}^{(1)}(*)$, $B_{\mathscr{U}}^{(2)}(*)$, $\Delta_{\mathscr{U}}^{(1)}(*)$, and $\Delta_{\mathscr{U}}^{(2)}(*)$ and functions $g_{\mathscr{U}}^{*}$, and $h_{\mathscr{U}}^{*}$ (with $g_{\mathscr{U}}^{*}(n) = O(n^{-1})$ and $h_{\mathscr{U}}^{*}(n) = O(n^{-1})$) such that Conjectures 2.2.4, 2.2.12, and 2.2.13 hold,

$$\begin{aligned}
&r^2_{\boldsymbol{\pi}_z(N_{\min})}\left(\mathscr{U}(*)\right)\\
&\approx \left[A_1(a_1, \gamma_{1,1}, \gamma_{1,2}, \gamma_2)\right]\left(\mathrm{E}_{\boldsymbol{\pi}_z(2,N_{\min})}\left(\xi_{\mathscr{U}(*)}(\omega)\,|\omega|\right)\right)^{\gamma_{1,1}}\\
&+ B_1(\gamma_{1,1}, \gamma_{1,2}, \gamma_2, \gamma_{3,1}, \gamma_{3,2}, a_1, a_2, b_1, b_2, m_2, g),
\end{aligned} \tag{7.95}$$

where $a_1 = A_{\mathscr{U}}^{(1)}$, $a_2 = A_{\mathscr{U}}^{(2)}$, $\gamma_{1,1} = 2\nu_{\mathscr{U}}^{\Theta}(*)$, $\gamma_{1,2} = \alpha_{\mathscr{U}}^{\Theta}(*) + q$, $\gamma_2 = \kappa_\phi + \log(z)$, $\gamma_{3,1} = \Delta_{\mathscr{U}}^{(1)}(*)$, $\gamma_{3,2} = \Delta_{\mathscr{U}}^{(2)}(*)$, $b_1 = B_{\mathscr{U}}^{(1)}(*)$, $b_2 = B_{\mathscr{U}}^{(2)}(*)$, $m_1 = m_2 = N_{\min}$, $g =$

$g^*_{\mathscr{U}}$, $A_1(a_1, \gamma_{1,1}, \gamma_{1,2}, \gamma_2) = O(1)$ and $B_1(\gamma_{1,1}, \gamma_{1,2}, \gamma_2, \gamma_{3,1}, \gamma_{3,2}, a_1, a_2, b_1, b_2, m_2, g) = O(n^{-\gamma})$ with $\gamma = \min\{\gamma_{3,1}, \gamma_{3,2}\}$. Similarly, assuming that, for $N_{\min}$ sufficiently large, there exist constants $A^{(1)}_{f(\mathscr{U})}(*)$, $A^{(2)}_{f(\mathscr{U})}(*)$, $\nu^{\Theta}_{f(\mathscr{U})}(*)$, $\alpha^{\Theta}_{f(\mathscr{U})}(*)$, q, κ_ϕ, $B^{(1)}_{f(\mathscr{U})}(*)$, $B^{(2)}_{f(\mathscr{U})}(*)$, $\Delta^{(1)}_{f(\mathscr{U})}(*)$, and $\Delta^{(2)}_{f(\mathscr{U})}(*)$ and functions $g^*_{f(\mathscr{U})}$ and $h^*_{f(\mathscr{U})}$ (with $g^*_{f(\mathscr{U})}(n) = O(n^{-1})$ and $h^*_{f(\mathscr{U})}(n) = O(n^{-1})$) such that Conjectures 2.2.4, 2.2.12, and 2.2.13 hold, then

$$\begin{aligned} & r^2_{\boldsymbol{\pi}_z(N_{\min})}\left(f\left(\mathscr{U}(*)\right)\right) \\ & \approx \left[A_1(a_1, \gamma_{1,1}, \gamma_{1,2}, \gamma_2)\right]\left(\mathrm{E}_{\boldsymbol{\pi}_z(2,N_{\min})}\left(\xi_{\mathscr{U}(*)}(\omega)\left|f(\omega)\right|\right)\right)^{\gamma_{1,1}} \\ & + B_1(\gamma_{1,1}, \gamma_{1,2}, \gamma_2, \gamma_{3,1}, \gamma_{3,2}, a_1, a_2, b_1, b_2, m_2, g), \end{aligned} \tag{7.96}$$

where $a_1 = A^{(1)}_{f(\mathscr{U})}$, $a_2 = A^{(2)}_{f(\mathscr{U})}$, $\gamma_{1,1} = 2\nu^{\Theta}_{f(\mathscr{U})}(*)$, $\gamma_{1,2} = \alpha^{\Theta}_{f(\mathscr{U})}(*) + q$, $\gamma_2 = \kappa_\phi + \log(z)$, $\gamma_{3,1} = \Delta^{(1)}_{f(\mathscr{U})}(*)$, $\gamma_{3,2} = \Delta^{(2)}_{f(\mathscr{U})}(*)$, $b_1 = B^{(1)}_{f(\mathscr{U})}(*)$, $b_2 = B^{(2)}_{f(\mathscr{U})}(*)$, $m_1 = m_2 = N_{\min}$, $g = g^*_{f(\mathscr{U})}$, $A_1(a_1, \gamma_{1,1}, \gamma_{1,2}, \gamma_2) = O(1)$ and $B_1(\gamma_{1,1}, \gamma_{1,2}, \gamma_2, \gamma_{3,1}, \gamma_{3,2}, a_1, a_2, b_1, b_2, m_2, g) = O(n^{-\gamma})$ with $\gamma = \min\{\gamma_{3,1}, \gamma_{3,2}\}$. (Note that $\mathrm{E}_{\boldsymbol{\pi}_z(q,N_{\min})}(\xi_{\mathscr{U}(*)}(W)\,|W|)$ is the expected length of W and $\mathrm{E}_{\boldsymbol{\pi}_z(q,N_{\min})}(\xi_{\mathscr{U}(*)}(W)\,|f(W)|)$ is the expected length of $f(W)$, where W is a randomly selected polygon from $\mathscr{P}^{\Theta}(\phi)$ chosen according to $\boldsymbol{\pi}_z(q, N_{\min})$.)

For values of $\log(z)$ close to $-\kappa_\phi$, $r^2_{\boldsymbol{\pi}_z(N_{\min})}\left(\mathscr{U}(*)\right)$ should become linear in $\mathrm{E}_{\boldsymbol{\pi}_z(2,N_{\min})}(\xi_{\mathscr{U}(*)}(W)\,|W|)^{2\nu^{\Theta}_{\mathscr{U}}(*)}$ and $r^2_{\boldsymbol{\pi}_z(N_{\min})}\left(f\left(\mathscr{U}(*)\right)\right)$ should become linear in $\mathrm{E}_{\boldsymbol{\pi}_z(2,N_{\min})}(\xi_{\mathscr{U}(*)}(W)\,|f(W)|)^{2\nu^{\Theta}_{f(\mathscr{U})}(*)}$. Therefore if the values $r^2_{\boldsymbol{\pi}_z(N_{\min})}\left(\mathscr{U}(*)\right)$, $r^2_{\boldsymbol{\pi}_z(N_{\min})}\left(f\left(\mathscr{U}(*)\right)\right)$, $\mathrm{E}_{\boldsymbol{\pi}_z(2,N_{\min})}(\xi_{\mathscr{U}(*)}(W)\,|W|)$, and $\mathrm{E}_{\boldsymbol{\pi}_z(2,N_{\min})}(\xi_{\mathscr{U}(*)}(W)\,|f(W)|)$ are known, then the exponents $\nu^{\Theta}_{\mathscr{U}}(*)$ and $\nu^{\Theta}_{f(\mathscr{U})}(*)$ can be estimated by fitting these values (via a non-linear weighted least-squares fit) to an equation of the form

$$\mathfrak{r}(2n, a, b, \hbar) = a\,(2n)^{2b} + \hbar, \tag{7.97}$$

where b corresponds to the metric exponent of interest. In reality, $r^2_{\boldsymbol{\pi}_z(N_{\min})}\left(\mathscr{U}(*)\right)$, $r^2_{\boldsymbol{\pi}_z(N_{\min})}\left(f\left(\mathscr{U}(*)\right)\right)$, $\mathrm{E}_{\boldsymbol{\pi}_z(2,N_{\min})}(\xi_{\mathscr{U}(*)}(W)\,|W|)$, and $\mathrm{E}_{\boldsymbol{\pi}_z(2,N_{\min})}(\xi_{\mathscr{U}(*)}(W)\,|f(W)|)$ are unknown. This problem can be overcome by using the estimates for $r^2_{\boldsymbol{\pi}_z(N_{\min})}\left(\mathscr{U}(*)\right)$, $r^2_{\boldsymbol{\pi}_z(N_{\min})}\left(f\left(\mathscr{U}(*)\right)\right)$, $\mathrm{E}_{\boldsymbol{\pi}_z(2,N_{\min})}(\xi_{\mathscr{U}(*)}(W)\,|W|)$, and $\mathrm{E}_{\boldsymbol{\pi}_z(2,N_{\min})}(\xi_{\mathscr{U}(*)}(W)\,|f(W)|)$ calculated from the data generated in each chain of the CMC simulation.

Let $\boldsymbol{W} := \left(\left(W_t(1), W_t(2), ..., W_t(14)\right), t = 0, ..., t_0\right)$ be a Markov chain formed by the CMC Θ-BFACF algorithm and let $\boldsymbol{\omega}^{(u)}$, where

$$\boldsymbol{\omega}^{(u)} := \left(\left(\omega^{(u)}_t(1), \omega^{(u)}_t(2), ..., \omega^{(u)}_t(14)\right), t = 0, ..., t_0\right), \tag{7.98}$$

be the sequence of (t_0+1) 14-tuples of Θ-SAPs from $\left(\mathscr{P}^{\Theta}(\phi)\right)^{14}$ realized in Replication u of the simulation of the CMC Θ-BFACF algorithm as described in Section 3.4.1. For each $* \in \Phi$ and for $\mathscr{U}(*) \subseteq \mathscr{P}^{\Theta}(\phi)$, suppose W is a random polygon from $\mathscr{U}(*)$ chosen according to $\boldsymbol{\pi}_{z_i}(q, N_{\min})$. Then define, for the mapping $f : \mathbb{Z}^3 \to \mathbb{Z}^3$, the random variables X and Y (as defined in Section A.4 of Appendix A) by

$$X(L, W, \mathscr{U}(*)) := \mathscr{I}_{[L,\infty)}(|W|)\xi_{\mathscr{U}(*)}(W) \tag{7.99}$$

and

$$Y(L, W, \mathscr{U}(*)) := X(L, W, \mathscr{U}(*))\,|f(W)|\,, \tag{7.100}$$

respectively, where, for each $\omega \in \mathscr{P}^{\Theta}(\phi)$ and each subset of Θ-SAPs $\mathscr{V} \subseteq \mathscr{P}^{\Theta}(\phi)$, $\xi_{\mathscr{V}}(\omega)$ is given by Equation (4.156). Further define $X_{k,i}$ and $Y_{k,i}$ (as used in Section A.4 of Appendix A) by

$$\begin{aligned} X_{k,i} &:= X_{k,i}(L, W, \mathscr{U}(*)) \\ &:= \sum_{t=0}^{t_0} \mathscr{M}_T(t)\mathscr{I}_{B(k)}(t)\, X(N_{\min}, W_t(i), \mathscr{U}(*)). \end{aligned} \tag{7.101}$$

and

$$\begin{aligned} Y_{k,i} &:= Y_{k,i}(N_{\min}, W, \mathscr{U}(*)) \\ &:= \sum_{t=0}^{t_0} \mathscr{M}_T(t)\mathscr{I}_{B(k)}(t)\, Y(N_{\min}, W_t(i), \mathscr{U}(*)) \\ &:= N_{k,i}\left(f\left(\mathscr{U}(*)\right)\right), \end{aligned} \tag{7.102}$$

where $B(k)$ is given by Equation (4.159); $\mathscr{M}_T(t)$ is defined by Equation (4.42); and, for $A \subseteq \mathbb{R}$, $\mathscr{I}_A(t)$is defined by Equation (7.6). Now redefine Y and $Y_{k,i}$ respectively by

$$Y := Y(L, W, \mathscr{U}(*)) := \mathscr{I}_{[L,\infty)}(|W|)\xi_{\mathscr{U}(*)}(W)r^2(f(W)) \tag{7.103}$$

and

$$\begin{aligned} Y_{k,i} &:= Y_{k,i}(N_{\min}, W, \mathscr{U}(*)) \\ &:= \sum_{t=0}^{t_0} \mathscr{M}_T(t)\mathscr{I}_{B(k)}(t)\, Y(N_{\min}, W_t(i), \mathscr{U}(*)) \\ &:= R^{\pi}_{k,i}\left(f(\mathscr{U}(*))\right), \end{aligned} \tag{7.104}$$

where $B(k)$ is given by Equation (4.159); $\mathscr{M}_T(t)$ is defined by Equation (4.42); and, for $A \subseteq \mathbb{R}$, $\mathscr{I}_A(t)$is defined by Equation (7.6). Finally redefine Y and $Y_{k,i}$ respectively by

$$Y := Y(L, W, \mathscr{U}(*)) := \mathscr{I}_{[L,\infty)}(|W|)\xi_{\mathscr{U}(*)}(W)r^2(W) \tag{7.105}$$

and

$$\begin{aligned} Y_{k,i} &:= Y_{k,i}(N_{\min}, W, \mathscr{U}(*)) \\ &:= \sum_{t=0}^{t_0} \mathscr{M}_T(t)\mathscr{I}_{B(k)}(t)\, Y(N_{\min}, W_t(i), \mathscr{U}(*)) \\ &:= R^{\pi}_{k,i}(\mathscr{U}(*)), \end{aligned} \tag{7.106}$$

where $B(k)$ is given by Equation (4.159); $\mathscr{M}_T(t)$ is defined by Equation (4.42); and, for $A \subseteq \mathbb{R}$, $\mathscr{I}_A(t)$is defined by Equation (7.6).

For the remainder of this section define $\boldsymbol{\pi}_{z_i}(N_{\min}) := \boldsymbol{\pi}_{z_i}(2, N_{\min})$. Then let $\left\langle N_{\boldsymbol{\pi}_{z_i}(N_{\min})}(f(\mathscr{U}(*)))\right\rangle$ be the ratio estimator (as defined by Equation (A.21) in Section A.3 of Appendix A) for $\mathrm{E}_{\boldsymbol{\pi}_{z_i}(N_{\min})}(\xi_{\mathscr{U}(*)}(W)\,|f(W)|)$ formed using the sequence

$$((X_{k,i}, N_{k,i}(f(\mathscr{U}(*)))), k = 1, .., l), \tag{7.107}$$

and recall that $\left\langle N_{\boldsymbol{\pi}_{z_i}(N_{\min})}(\mathscr{U}(*))\right\rangle$ is the ratio estimator for $\mathrm{E}_{\boldsymbol{\pi}_{z_i}(2,N_{\min})}(\xi_{\mathscr{U}(*)}(W)\,|(W)|)$ defined in Section 4.7.3. Further let $\left\langle R^2_{\boldsymbol{\pi}_{z_i}(N_{\min})}(\mathscr{U}(*))\right\rangle$ be the ratio estimator (as defined by Equation (A.21) in Section A.3 of Appendix A) for $r^2_{\boldsymbol{\pi}_{z_i}(N_{\min})}(\mathscr{U}(*))$ formed using the sequence

$$\left((X_{k,i}, R^{\pi}_{k,i}(\mathscr{U}(*))), k = 1, .., l\right); \tag{7.108}$$

and let $\left\langle R^2_{\boldsymbol{\pi}_{z_i}(N_{\min})}(f(\mathscr{U}(*)))\right\rangle$ be the ratio estimator for $r^2_{\boldsymbol{\pi}_{z_i}(N_{\min})}(f(\mathscr{U}(*)))$ formed using the sequence

$$\left((X_{k,i}, R^{\pi}_{k,i}(f(\mathscr{U}(*)))), k = 1, .., l\right). \tag{7.109}$$

Based on the u'th realization $\boldsymbol{\omega}^{(u)}$ of $\boldsymbol{W}$, $u \in \{1, 2, ..., 10\}$, let $n^{(u)}_{k,i}(\mathscr{U}(*))$ denote the u'th realization of $N_{k,i}(\mathscr{U}(*))$; let $n^{(u)}_{k,i}(f(\mathscr{U}(*)))$ denote the u'th realization of $N_{k,i}(f(\mathscr{U}(*)))$; let $r^{\pi,(u)}_{k,i}(\mathscr{U}(*))$ denote the u'th realization of $R^{\pi}_{k,i}(\mathscr{U}(*))$; let $r^{\pi,(u)}_{k,i}(f(\mathscr{U}(*)))$ denote the u'th realization of $R^{\pi}_{k,i}(f(\mathscr{U}(*)))$; and let $x^{(u)}_{k,i}$ denote the u'th realization of $X_{k,i}$. Then, for each $* \in \Phi$ and for a fixed positive integer n, the estimators $\left\langle N_{\boldsymbol{\pi}_{z_i}(N_{\min})}(\mathscr{U}(*))\right\rangle$, $\left\langle N_{\boldsymbol{\pi}_{z_i}(N_{\min})}(f(\mathscr{U}(*)))\right\rangle$, $\left\langle R^2_{\boldsymbol{\pi}_{z_i}(N_{\min})}(\mathscr{U}(*))\right\rangle$, and $\left\langle R^2_{\boldsymbol{\pi}_{z_i}(N_{\min})}(f(\mathscr{U}(*)))\right\rangle$ defined with $t_0 = 9.6\times10^{10}$ time steps, $\tau_{\text{int}} = 0.72\times10^9$ time steps,

$T = 120,000$ time steps, and $l := \lfloor t_0/(2\tau_{\text{int}}) \rfloor = 66$ are respectively used to calculate: the point estimate $\left\langle n_{\boldsymbol{\pi}_{z_i}(N_{\min})}\left(\mathscr{U}(*)\right)\right\rangle$ for $\mathrm{E}_{\boldsymbol{\pi}_{z_i}(N_{\min})}(\xi_{\mathscr{U}(*)}(\omega)\,|\omega|)$ using the sequence

$$\left(\left(\left(x_{k,i}^{(u)}, n_{k,i}^{(u)}\left(\mathscr{U}(*)\right)\right), k = 1, .., l\right), u = 1, ..., 10\right) \tag{7.110}$$

in Equation (A.21); the point estimate $\left\langle n_{\boldsymbol{\pi}_{z_i}(N_{\min})}\left(f\left(\mathscr{U}(*)\right)\right)\right\rangle$ for $\mathrm{E}_{\boldsymbol{\pi}_{z_i}(N_{\min})}(\xi_{\mathscr{U}(*)}(\omega)\,|f(\omega)|)$ using the sequence

$$\left(\left(\left(x_{k,i}^{(u)}, n_{k,i}^{(u)}\left(f\left(\mathscr{U}(*)\right)\right)\right), k = 1, .., l\right), u = 1, ..., 10\right) \tag{7.111}$$

in Equation (A.21); the point estimate $\left\langle r^2_{\boldsymbol{\pi}_{z_i}(N_{\min})}\left(\mathscr{U}(*)\right)\right\rangle$ for $R^2_{\boldsymbol{\pi}_{z_i}(N_{\min})}\left(\mathscr{U}(*)\right)$ using the sequence

$$\left(\left(\left(x_{k,i}^{(u)}, r_{k,i}^{\pi,(u)}\left(\mathscr{U}(*)\right)\right), k = 1, .., l\right), u = 1, ..., 10\right) \tag{7.112}$$

and the point estimate $\left\langle r^2_{\boldsymbol{\pi}_{z_i}(N_{\min})}\left(f\left(\mathscr{U}(*)\right)\right)\right\rangle$ for $R^2_{\boldsymbol{\pi}_{z_i}(N_{\min})}\left(f\left(\mathscr{U}(*)\right)\right)$ using the sequence

$$\left(\left(\left(x_{k,i}^{(u)}, r_{k,i}^{\pi,(u)}\left(f\left(\mathscr{U}(*)\right)\right)\right), k = 1, .., l\right), u = 1, ..., 10\right) \tag{7.113}$$

in Equation (A.21).

Now by fitting Equation (7.97) using non-linear weighted least-squares regression to the sequences of data $\left(\left(\left\langle n_{\boldsymbol{\pi}_{z_i}(N_{\min})}\left(\mathscr{P}^{\Theta}(\phi)\right)\right\rangle, \left\langle r^2_{\boldsymbol{\pi}_{z_i}(N_{\min})}\left(\mathscr{U}(*)\right)\right\rangle\right), i \in \{1, 2, ..., 14\}\right)$ and $\left(\left(\left\langle n_{\boldsymbol{\pi}_{z_i}(N_{\min})}\left(\mathscr{P}^{\Theta}(\phi)\right)\right\rangle, \left\langle r^2_{\boldsymbol{\pi}_{z_i}(N_{\min})}\left(f\left(\mathscr{U}(*)\right)\right)\right\rangle\right), i \in \{1, 2, ..., 14\}\right)$ estimates for a, b, and h can be obtained, where $b = \nu^{\Theta}_{\bullet}(*)$.

Estimating $\nu^{\Theta}_{\bullet}(*)$ using the Average-n Method

In this section, $\nu^{\Theta}_{\mathscr{P}}(\phi)$, $\nu^{\Theta}_{\mathscr{E}^c}(\phi, f)$, $\nu^{\Theta}_{\mathscr{E}^c}(\phi|\phi, s)$, $\nu^{\Theta}_{\mathscr{E}^c}(3_1|\phi, s)$, $\nu^{\Theta}_{\mathfrak{w}_l(\mathscr{E}^c)}(\phi, f)$, $\nu^{\Theta}_{\mathfrak{w}_l(\mathscr{E}^c)}(\phi|\phi, s)$, $\nu^{\Theta}_{\mathfrak{w}_l(\mathscr{E}^c)}(3_1|\phi, s)$, $\nu^{\Theta}_{\mathfrak{w}_s(\mathscr{E}^c)}(\phi, f)$, $\nu^{\Theta}_{\mathfrak{w}_s(\mathscr{E}^c)}(\phi|\phi, s)$, and $\nu^{\Theta}_{\mathfrak{w}_s(\mathscr{E}^c)}(3_1|\phi, s)$ are estimated using the Average-n Method for the purposes of a comparison to the corresponding estimates computed using the Fixed-n Method. Then, for each $* \in \Phi$ and for a fixed positive even integer $N_{\min}$, the point estimates required to estimate these metric exponents are computed using the estimators $\left\langle N_{\boldsymbol{\pi}_{z_i}(N_{\min})}\left(\mathscr{P}^{\Theta}_{2n}(\phi)\right)\right\rangle$, $\left\langle R^2_{\boldsymbol{\pi}_{z_i}(N_{\min})}\left(\mathscr{P}^{\Theta}_{2n}(*)\right)\right\rangle$, $\left\langle R^2_{\boldsymbol{\pi}_{z_i}(N_{\min})}\left(\mathscr{E}^c_{2n}(*)\right)\right\rangle$, $\left\langle R^2_{\boldsymbol{\pi}_{z_i}(N_{\min})}\left(\mathscr{E}_{2n}(*)\right)\right\rangle$, $\left\langle R^2_{\boldsymbol{\pi}_{z_i}(N_{\min})}\left(\mathfrak{w}_s(\mathscr{E}^c_{2n}(*))\right)\right\rangle$, $\left\langle R^2_{\boldsymbol{\pi}_{z_i}(N_{\min})}\left(\mathfrak{w}_l(\mathscr{E}^c_{2n}(*))\right)\right\rangle$, and $\left\langle R^2_{\boldsymbol{\pi}_{z_i}(N_{\min})}\left(\mathfrak{w}_e(\mathscr{E}_{2n}(*))\right)\right\rangle$ defined with $t_0 = 9.6 \times 10^{10}$ time steps, $\tau_{\text{int}} = 0.72 \times 10^9$ time steps, $T = 120,000$ time steps, and $\lfloor t_0/(2\tau_{\text{int}}) \rfloor = 66$.

Recall from Section 4.5.2 that the sequences

$$\left(\left(\mathrm{E}_{\boldsymbol{\pi}_{z_i}(N_{\min})}(\xi_{\mathscr{P}^{\Theta}(\phi)}(\omega)\,|\omega|), R^2_{\boldsymbol{\pi}_{z_i}(N_{\min})}\left(\mathscr{U}(*)\right)\right), i \in \{1, 2, ..., 14\}\right)$$

and

$$\left(\left(\mathrm{E}_{\boldsymbol{\pi}_{z_i}(N_{\min})}(\xi_{\mathscr{P}^{\Theta}(\phi)}(\omega)\,|\omega|), R^2_{\boldsymbol{\pi}_{z_i}(N_{\min})}(f(\mathscr{U}(*)))\right), i \in \{1,2,...,14\}\right)$$

scale according to

$$R^2_{\boldsymbol{\pi}_{z_i}(N_{\min})}(\mathscr{U}(*)) \sim a_{\mathscr{U}}(*)\left(\mathrm{E}_{\boldsymbol{\pi}_{z_i}(N_{\min})}(\xi_{\mathscr{P}^{\Theta}(\phi)}(\omega)\,|\omega|)\right)^{2b_{\mathscr{U}}(*)} \tag{7.114}$$

and

$$R^2_{\boldsymbol{\pi}_{z_i}(N_{\min})}(f(\mathscr{U}(*))) \sim a_{f(\mathscr{U})}(*)\left(\mathrm{E}_{\boldsymbol{\pi}_{z_i}(N_{\min})}(\xi_{\mathscr{P}^{\Theta}(\phi)}(\omega)\,|\omega|)\right)^{2b_{f(\mathscr{U})}(*)}, \tag{7.115}$$

respectively for a suitable value of $N^*_{\min}$ sufficiently large. Also from the discussion in Section 4.5.2 that determined the above scaling form, recall that one of the assumptions made was that $N^*_{\min}$ needs to be sufficiently large so that $p^{\Theta}_{2n}(*)$ scales according to the form given by Conjecture 2.2.4. In Section 5.6, $N^{\phi}_{\min}$ was estimated to be 156; $N^{(\phi,f)}_{\min}$ was estimated to be 142; $N^{(\phi|\phi,s)}_{\min}$ was estimated to be 182; and $N^{(3_1|\phi,s)}_{\min}$ was estimated to be 408. Because the "Average-n Method for estimating $\nu^{\Theta}_{\bullet}(*)$" is based on $N_{\min}$ being sufficiently large that the approximate forms of both $\mathrm{E}_{\boldsymbol{\pi}_{z_i}(N_{\min})}(\xi_{\mathscr{P}^{\Theta}(\phi)}(W)\,|W|)$ (given by Approximation (4.95)) and $R^2_{\boldsymbol{\pi}_{z_i}(N_{\min})}(\mathscr{U}(*))$ or $R^2_{\boldsymbol{\pi}_{z_i}(N_{\min})}(f(\mathscr{U}(*)))$ (given by Approximation (4.118)) hold, the values of $N_{\min}$ to be used are $N^{\phi}_{\min} = N^{(\phi,f)}_{\min} = 156$, $N^{(\phi|\phi,s)}_{\min} = 182$, and $N^{(3_1|\phi,s)}_{\min} = 408$. But, because of the limited amount of data available for property-$(3_1|\phi,s)$, using 408 as the estimate for $N^{(3_1|\phi,s)}_{\min}$ results in having no data available to compute $\left\langle r^2_{\boldsymbol{\pi}_{z_i}(408)}\left(\mathscr{P}^{\Theta}(3_1|\phi,s)\right)\right\rangle$ for $i \in \{1,2,3,4,5\}$, and the estimated 95% confidence intervals based on the estimates $\left\langle r^2_{\boldsymbol{\pi}_{z_i}(408)}\left(\mathscr{P}^{\Theta}(3_1|\phi,s)\right)\right\rangle$ for $i \in \{6,7,...,14\}$ being so large that the point estimates $\left\langle r^2_{\boldsymbol{\pi}_{z_i}(408)}\left(\mathscr{P}^{\Theta}(3_1|\phi,s)\right)\right\rangle$ for $i \in \{6,7,...,14\}$ are considered unreliable. In an attempt to maximize the amount of data available for the property-$(3_1|\phi,s)$ analysis, $N^{(3_1|\phi,s)}_{\min}$=$N^{(\phi|\phi,s)}_{\min} = 182$ under the proviso that more property-$(3_1|\phi,s)$ data need to be collected in the future.

The point estimates and the corresponding estimated 95% confidence interval displayed in Figures 7.31-7.33 can be found in Tables B.18-B.41 (cf. Section B.3.2 of Appendix B).

The sequences of point estimates

$$\left(\left(\left\langle n_{\boldsymbol{\pi}_{z_i}(156)}\left(\mathscr{P}^{\Theta}(\phi)\right)\right\rangle, \left\langle r^2_{\boldsymbol{\pi}_{z_i}(156)}\left(\mathscr{P}^{\Theta}(\phi)\right)\right\rangle\right), i \in \{1,2,...,14\}\right) \quad (\odot),$$

$$\left(\left(\left\langle n_{\boldsymbol{\pi}_{z_i}(156)}\left(\mathscr{P}^{\Theta}(\phi)\right)\right\rangle, \left\langle r^2_{\boldsymbol{\pi}_{z_i}(156)}\left(\mathscr{E}^{c}(\phi,f)\right)\right\rangle\right), i \in \{1,2,...,14\}\right) \quad (\times),$$

$$\left(\left(\left\langle n_{\boldsymbol{\pi}_{z_i}(182)}\left(\mathscr{P}^{\Theta}(\phi)\right)\right\rangle, \left\langle r^2_{\boldsymbol{\pi}_{z_i}(182)}\left(\mathscr{E}^{c}(\phi|\phi,s)\right)\right\rangle\right), i \in \{1,2,...,14\}\right) \quad (\boxdot),$$

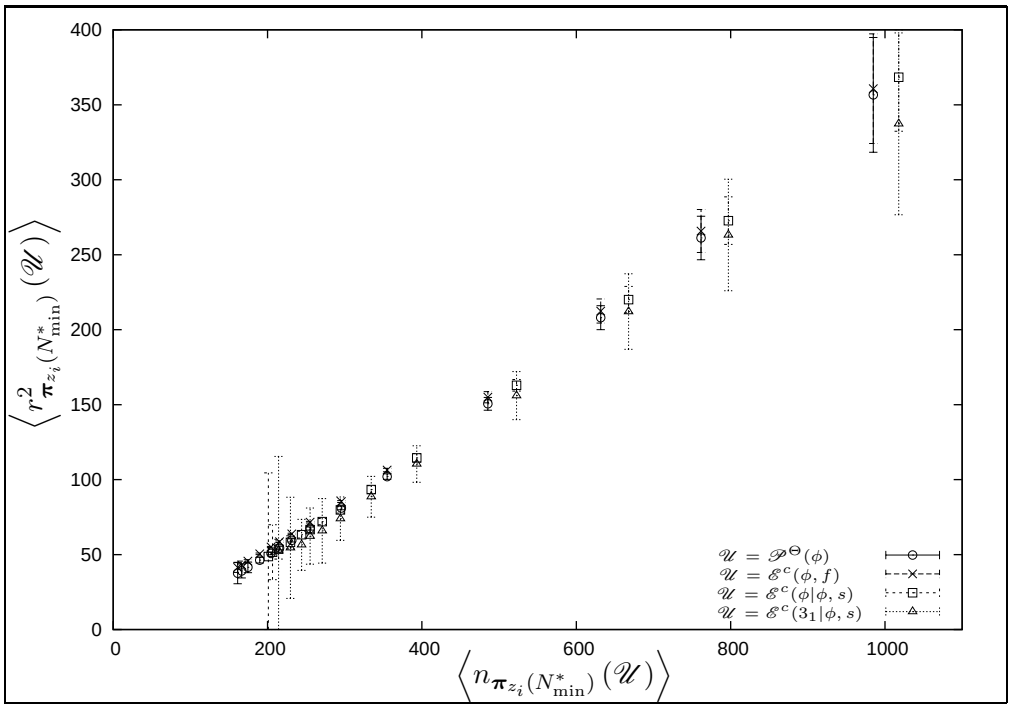

Figure 7.31: The point estimates $\langle n_{\boldsymbol{\pi}_{z_i}(156)}\left(\mathscr{P}^{\Theta}(\phi)\right)\rangle$, $\langle n_{\boldsymbol{\pi}_{z_i}(156)}\left(\mathscr{P}^{\Theta}(\phi)\right)\rangle$, $\langle n_{\boldsymbol{\pi}_{z_i}(182)}\left(\mathscr{P}^{\Theta}(\phi)\right)\rangle$, and $\langle n_{\boldsymbol{\pi}_{z_i}(156)}\left(\mathscr{P}^{\Theta}(\phi)\right)\rangle$ plotted respectively against $\langle r^2_{\boldsymbol{\pi}_{z_i}(156)}\left(\mathscr{P}^{\Theta}(\phi)\right)\rangle$ [$\odot$], $\langle r^2_{\boldsymbol{\pi}_{z_i}(156)}\left(\mathscr{E}^c(\phi, f)\right)\rangle$ [$\times$], $\langle r^2_{\boldsymbol{\pi}_{z_i}(182)}\left(\mathscr{E}^c(\phi|\phi, s)\right)\rangle$ [$\boxdot$], and $\langle r^2_{\boldsymbol{\pi}_{z_i}(182)}\left(\mathscr{E}^c(3_1|\phi, s)\right)\rangle$ [$\triangle$]. The error bars represent the corresponding estimated 95% margins of error.

and

$$\left(\left(\left\langle n_{\boldsymbol{\pi}_{z_i}(182)}\left(\mathscr{P}^{\Theta}(\phi)\right)\right\rangle, \left\langle r^2_{\boldsymbol{\pi}_{z_i}(182)}\left(\mathscr{E}^c(3_1|\phi, s)\right)\right\rangle\right), i \in \{3, 4, ..., 14\}\right) \quad (\triangle),$$

that are required to estimate $\nu^{\Theta}_{\mathscr{P}}(\phi)$, $\nu^{\Theta}_{\mathscr{E}^c}(\phi, f)$, $\nu^{\Theta}_{\mathscr{E}^c}(\phi|\phi, s)$, and $\nu^{\Theta}_{\mathscr{E}^c}(3_1|\phi, s)$ respectively using the Average-n Method, are illustrated in Figure 7.31. Note that there is no data available to compute the point estimates $\left\langle r^2_{\boldsymbol{\pi}_{z_i}(182)}\left(\mathscr{E}^c(3_1|\phi, s)\right)\right\rangle$, $i \in \{1, 2\}$.

Each of the data sequences plotted in Figure 7.31, when fitted via weighted non-linear least-squares regression to a curve of the form

$$y = a^{\Theta}_{\bullet}(*)x^{2\nu^{\Theta}_{\bullet}(*)} + d_{\bullet}(*), \tag{7.116}$$

yields the estimates for $\nu^{\Theta}_{\bullet}(*)$, $a^{\Theta}_{\bullet}(*)$, and $d_{\bullet}(*)$ presented in Table 7.4.

In order to facilitate the comparison between the estimates for $\nu^{\Theta}_{\bullet}(*)$ generated by the Fixed-n and Average-n Methods, the estimates for $\nu^{\Theta}_{\mathscr{P}}(\phi)$, $\nu^{\Theta}_{\mathscr{E}^c}(\phi, f)$, $\nu^{\Theta}_{\mathscr{E}^c}(\phi|\phi, s)$, and

Table 7.4: The estimates for $\nu_{\bullet}^{\Theta}(*)$, $a_{\bullet}^{\Theta}(*)$, and $d_{\bullet}(*)$ computed using the "Average-n Method". The values in parentheses are the estimated 95% margins of error.

	Parameter Estimated			
$\bullet(*)$	$N_{\min}^{*}$	$\nu_{\bullet}^{\Theta}(*)$	$a_{\bullet}^{\Theta}(*)$	$d_{\bullet}(*)$
$\mathscr{P}^{\Theta}(\phi)$	156	0.5905(0.0040)	0.0957(0.0055)	−4.5674(1.1018)
$\mathscr{E}^{c}(\phi, f)$	156	0.5944(0.0064)	0.1001(0.0093)	−1.0699(1.7770)
$\mathscr{E}^{c}(\phi\|\phi, s)$	182	0.5977(0.0094)	0.0917(0.0250)	−4.4469(2.6560)
$\mathscr{E}^{c}(3_1\|\phi, s)$	182	0.5679(0.0759)	0.1411(0.1525)	−15.5592(20.7470)

Table 7.5: A summary of the estimates for $\nu_{\bullet}^{\Theta}(*)$ computed using the "Fixed-n Method" and the "Average-n Method". The values in parentheses are the estimated 95% margins of error.

	Estimate of $\nu_{\bullet}^{\Theta}(*)$	
$\bullet(*)$	Average-n Method	Fixed-n Method
$\mathscr{P}^{\Theta}(\phi)$	0.5905(0.0040)	0.5907(0.0071)
$\mathscr{E}^{c}(\phi, f)$	0.5944(0.0064)	0.5854(0.0073)
$\mathscr{E}^{c}(\phi\|\phi, s)$	0.5977(0.0094)	0.5846(0.0166)
$\mathscr{E}^{c}(3_1\|\phi, s)$	0.5679(0.0759)	0.6189(0.1296)

$\nu_{\mathscr{E}^{c}}^{\Theta}(3_1|\phi, s)$ generated by both methods are summarized in Table 7.5. Note that for each $\bullet(*)$ in Table 7.5, there is considerable overlap between the estimated 95% confidence interval presented for $\nu_{\bullet}^{\Theta}(*)$. Hence the estimates generated via the two methods are comparable. It also should be noted that the 95% confidence intervals determined via the Average-n Method are slightly smaller than the corresponding interval estimated by the Fixed-n Method. Consequently the Average-n Method provides better estimates than the Fixed-n Method for $\nu_{\mathscr{P}}^{\Theta}(\phi)$, $\nu_{\mathscr{E}^{c}}^{\Theta}(\phi, f)$, $\nu_{\mathscr{E}^{c}}^{\Theta}(\phi|\phi, s)$, and $\nu_{\mathscr{E}^{c}}^{\Theta}(3_1|\phi, s)$.

The sequences of point estimates

$$\left(\left(\left\langle n_{\boldsymbol{\pi}_{z_i}(156)}\left(\mathscr{P}^{\Theta}(\phi)\right)\right\rangle, \left\langle r^{2}_{\boldsymbol{\pi}_{z_i}(156)}\left(\mathfrak{w}_l\left(\mathscr{E}^{c}(\phi, f)\right)\right)\right\rangle\right), i \in \{1, 2, ..., 14\}\right) \quad (\times),$$

$$\left(\left(\left\langle n_{\boldsymbol{\pi}_{z_i}(182)}\left(\mathscr{P}^{\Theta}(\phi)\right)\right\rangle, \left\langle r^{2}_{\boldsymbol{\pi}_{z_i}(182)}\left(\mathfrak{w}_l\left(\mathscr{E}^{c}(\phi|\phi, s)\right)\right)\right\rangle\right), i \in \{1, 2, ..., 14\}\right) \quad (\boxdot),$$

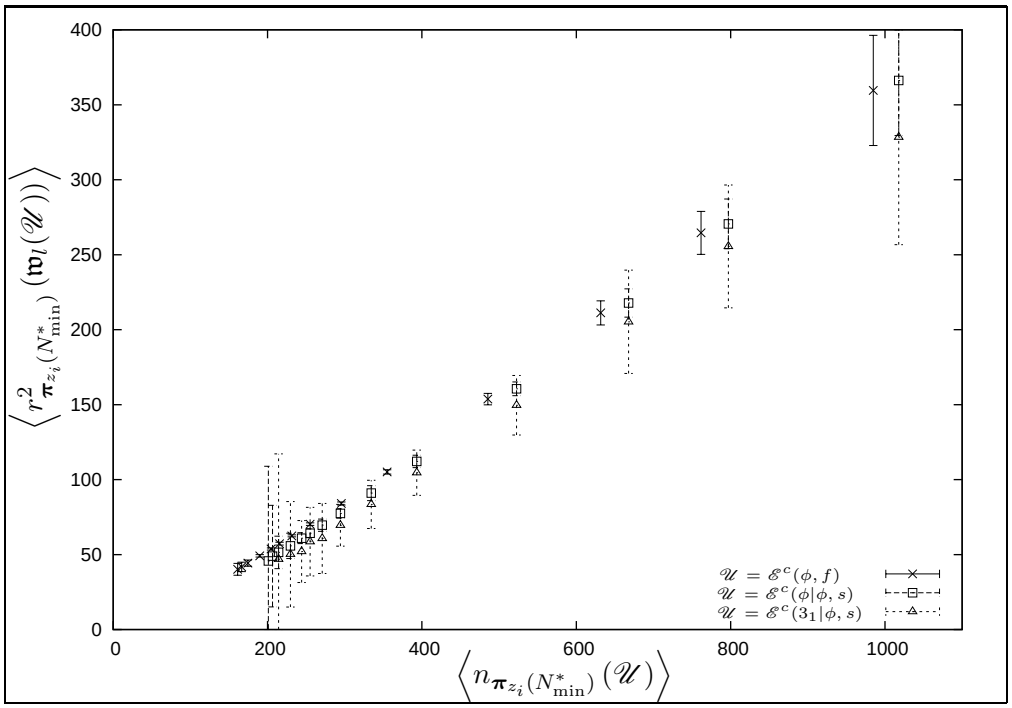

Figure 7.32: The point estimates $\langle n_{\boldsymbol{\pi}_{z_i}(156)}\left(\mathscr{P}^{\Theta}(\phi)\right)\rangle$, $\langle n_{\boldsymbol{\pi}_{z_i}(182)}\left(\mathscr{P}^{\Theta}(\phi)\right)\rangle$, and $\langle n_{\boldsymbol{\pi}_{z_i}(156)}\left(\mathscr{P}^{\Theta}(\phi)\right)\rangle$ plotted respectively against $\langle r^2_{\boldsymbol{\pi}_{z_i}(156)}(\mathfrak{w}_l(\mathscr{E}^c(\phi, f)))\rangle$ [×], $\langle r^2_{\boldsymbol{\pi}_{z_i}(182)}(\mathfrak{w}_l(\mathscr{E}^c(\phi|\phi, s)))\rangle$ [⊡], and $\langle r^2_{\boldsymbol{\pi}_{z_i}(182)}(\mathfrak{w}_l(\mathscr{E}^c(3_1|\phi, s)))\rangle$ [△]. The error bars represent the estimated 95% margins of error.

and

$$\left(\left(\left\langle n_{\boldsymbol{\pi}_{z_i}(182)}\left(\mathscr{P}^{\Theta}(\phi)\right)\right\rangle, \left\langle r^2_{\boldsymbol{\pi}_{z_i}(182)}(\mathfrak{w}_l(\mathscr{E}^c(3_1|\phi, s)))\right\rangle\right), i \in \{3, 4, ..., 14\}\right) \quad (\triangle),$$

that are required to respectively estimate $\nu^{\Theta}_{\mathfrak{w}_l(\mathscr{E}^c)}(\phi, f)$, $\nu^{\Theta}_{\mathfrak{w}_l(\mathscr{E}^c)}(\phi|\phi, s)$, and $\nu^{\Theta}_{\mathfrak{w}_l(\mathscr{E}^c)}(3_1|\phi, s)$ using the Average-n Method, are illustrated in Figure 7.32. Note that there is no data in the sample to compute the point estimates $\left\langle r^2_{\boldsymbol{\pi}_{z_i}(182)}(\mathfrak{w}_l(\mathscr{E}^c(3_1|\phi, s)))\right\rangle$, $i \in \{1, 2\}$.

Each of the data sequences plotted in Figure 7.32 is fit (via weighted non-linear least-squares regression) to a curve of the form

$$y = a^{\Theta}_{\bullet}(*)x^{2\nu^{\Theta}_{\bullet}(*)} + d_{\bullet}(*) \tag{7.117}$$

to obtain the estimates for $\nu^{\Theta}_{\mathfrak{w}_l(\mathscr{E}^c)}(*)$, $a^{\Theta}_{\mathfrak{w}_l(\mathscr{E}^c)}(*)$, and $d_{\mathfrak{w}_l(\mathscr{E}^c)}(*)$ presented in Table 7.6.

As before, in order to facilitate the comparison between the two estimates for $\nu^{\Theta}_{\mathfrak{w}_l(\mathscr{E}^c)}(*)$, the estimates for $\nu^{\Theta}_{\mathfrak{w}_l(\mathscr{E}^c)}(\phi, f)$, $\nu^{\Theta}_{\mathfrak{w}_l(\mathscr{E}^c)}(\phi|\phi, s)$, and $\nu^{\Theta}_{\mathfrak{w}_l(\mathscr{E}^c)}(3_1|\phi, s)$ generated by both methods are summarized in Table 7.7. Note that for each property $*$ presented in Table 7.5,

Table 7.6: The estimates for $\nu^{\Theta}_{\mathfrak{w}_l(\mathscr{E}^c)}(*)$, $a^{\Theta}_{\mathfrak{w}_l(\mathscr{E}^c)}(*)$, and $d_{\mathfrak{w}_l(\mathscr{E}^c)}(*)$ computed using the "Average-n Method". The error bars represent the estimated 95% margins of error.

	Parameter Estimated			
Property $*$	$N^*_{\min}$	$\nu^{\Theta}_{\mathfrak{w}_l(\mathscr{E}^c)}(*)$	$a^{\Theta}_{\mathfrak{w}_l(\mathscr{E}^c)}(*)$	$d_{\mathfrak{w}_l(\mathscr{E}^c)}(*)$
(ϕ, f)	156	0.5942(0.0064)	0.0959(0.0093)	-2.4548(1.7769)
$(\phi\|\phi, s)$	182	0.5998(0.0099)	0.0921(0.0131)	-6.929(2.795)
$(3_1\|\phi, s)$	182	0.5745(0.0772)	0.1265(0.1390)	-17.4646(20.3186)

Table 7.7: A summary of the estimates for $\nu^{\Theta}_{\mathfrak{w}_l(\mathscr{E}^c)}(*)$ computed using the "Fixed-n Method" and the "Average-n Method". The values in parentheses are the estimated 95% margins of error.

	Estimate of $\nu^{\Theta}_{\mathfrak{w}_l(\mathscr{E}^c)}(*)$	
Property $*$	Average-n Method	Fixed-n Method
(ϕ, f)	0.5942(0.0064)	0.5847(0.0075)
$(\phi\|\phi, s)$	0.5998(0.0099)	0.5851(0.0166)
$(3_1\|\phi, s)$	0.5745(0.0772)	0.6419(0.1673)

there is considerable overlap between the estimated 95% confidence interval presented for $\nu^{\Theta}_{\bullet}(*)$. Also note that the estimated 95% confidence intervals determined via the Average-n Method are slightly smaller than the corresponding interval estimated by the Fixed-n Method. Hence the estimates for each of $\nu^{\Theta}_{\mathfrak{w}_l(\mathscr{E}^c)}(\phi, f)$, $\nu^{\Theta}_{\mathfrak{w}_l(\mathscr{E}^c)}(\phi|\phi, s)$, and $\nu^{\Theta}_{\mathfrak{w}_l(\mathscr{E}^c)}(3_1|\phi, s)$ generated by both methods are also concluded to be comparable. Because the confidence intervals estimated by the Average-n Method are smaller than the corresponding confidence interval estimated by the Fixed-n Method, the Average-n Method is concluded to provide better estimates than the Fixed-n Method for $\nu^{\Theta}_{\mathfrak{w}_l(\mathscr{E}^c)}(\phi, f)$, $\nu^{\Theta}_{\mathfrak{w}_l(\mathscr{E}^c)}(\phi|\phi, s)$, and $\nu^{\Theta}_{\mathfrak{w}_l(\mathscr{E}^c)}(3_1|\phi, s)$.

The sequences of point estimates

$$\left(\left(\left\langle n_{\boldsymbol{\pi}_{z_i}(156)}\left(\mathscr{P}^{\Theta}(\phi)\right)\right\rangle, \left\langle r^2_{\boldsymbol{\pi}_{z_i}(156)}\left(\mathfrak{w}_s\left(\mathscr{E}^c(\phi, f)\right)\right)\right\rangle\right), i \in \{1, 2, ..., 14\}\right) \quad (\times),$$

$$\left(\left(\left\langle n_{\boldsymbol{\pi}_{z_i}(182)}\left(\mathscr{P}^{\Theta}(\phi)\right)\right\rangle, \left\langle r^2_{\boldsymbol{\pi}_{z_i}(182)}\left(\mathfrak{w}_s\left(\mathscr{E}^c(\phi|\phi, s)\right)\right)\right\rangle\right), i \in \{1, 2, ..., 14\}\right) \quad (\boxdot),$$

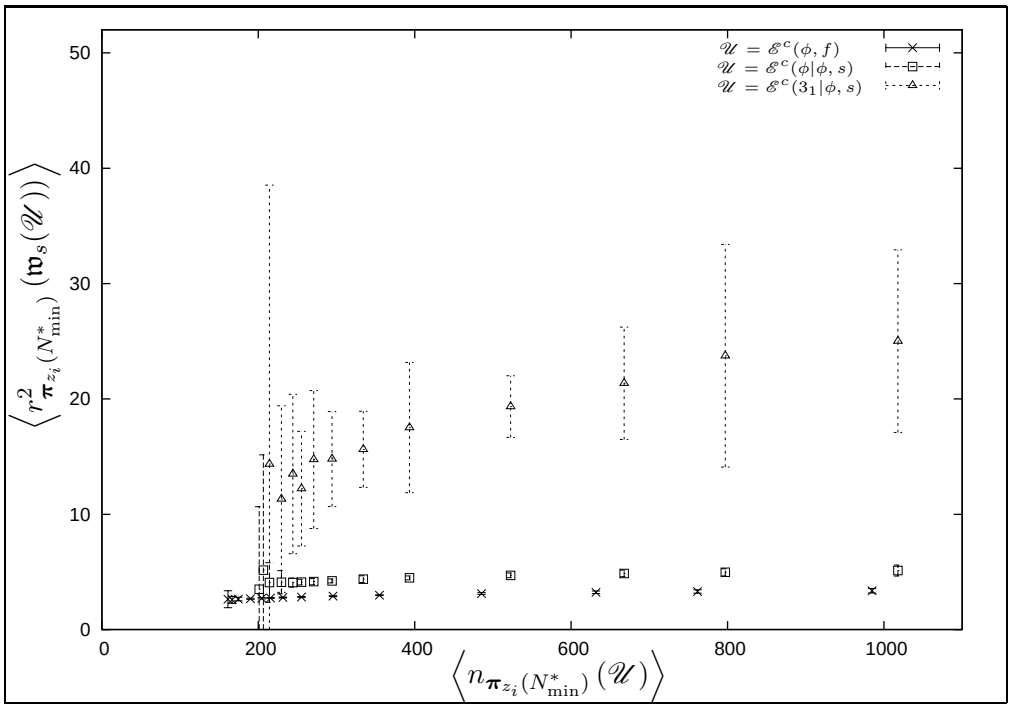

Figure 7.33: The point estimates $\langle n_{\boldsymbol{\pi}_{z_i}(156)}\left(\mathscr{P}^{\Theta}(\phi)\right)\rangle$, $\langle n_{\boldsymbol{\pi}_{z_i}(182)}\left(\mathscr{P}^{\Theta}(\phi)\right)\rangle$, and $\langle n_{\boldsymbol{\pi}_{z_i}(156)}\left(\mathscr{P}^{\Theta}(\phi)\right)\rangle$ plotted respectively against $\langle r^2_{\boldsymbol{\pi}_{z_i}(156)}(\mathfrak{w}_s(\mathscr{E}^c(\phi, f)))\rangle$ [$\times$], $\langle r^2_{\boldsymbol{\pi}_{z_i}(182)}(\mathfrak{w}_s(\mathscr{E}^c(\phi|\phi, s)))\rangle$ [$\boxdot$], and $\langle r^2_{\boldsymbol{\pi}_{z_i}(182)}(\mathfrak{w}_s(\mathscr{E}^c(3_1|\phi, s)))\rangle$ [$\triangle$]. The error bars represent the estimated 95% margins of error.

and

$$\left(\left(\left\langle n_{\boldsymbol{\pi}_{z_i}(182)}\left(\mathscr{P}^{\Theta}(\phi)\right)\right\rangle, \left\langle r^2_{\boldsymbol{\pi}_{z_i}(182)}(\mathfrak{w}_s(\mathscr{E}^c(3_1|\phi, s)))\right\rangle\right), i \in \{3, 4, ..., 14\}\right) \quad (\triangle),$$

that are respectively required to estimate $\nu^{\Theta}_{\mathfrak{w}_s(\mathscr{E}^c)}(\phi, f)$, $\nu^{\Theta}_{\mathfrak{w}_s(\mathscr{E}^c)}(\phi|\phi, s)$, and $\nu^{\Theta}_{\mathfrak{w}_s(\mathscr{E}^c)}(3_1|\phi, s)$ using the "Average-n Method", are illustrated in Figure 7.33. Once more, note that there is no data in the sample to compute the points estimates $\left\langle r^2_{\boldsymbol{\pi}_{z_i}(182)}(\mathfrak{w}_s(\mathscr{E}^c(3_1|\phi, s)))\right\rangle$, $i \in \{1, 2\}$.

Fitting each of the data sequences plotted in Figure 7.33 via weighted non-linear least-squares regression to a curve of the form

$$y = a^{\Theta}_{\bullet}(*)x^{2\nu^{\Theta}_{\bullet}(*)} + d_{\bullet}(*) \tag{7.118}$$

yields the estimates for $\nu^{\Theta}_{\mathfrak{w}_s(\mathscr{E}^c)}(*)$, $a^{\Theta}_{\mathfrak{w}_s(\mathscr{E}^c)}(*)$, and $d_{\mathfrak{w}_s(\mathscr{E}^c)}(*)$ given in Table 7.8.

As before, in order to facilitate the comparison between the two estimates for $\nu^{\Theta}_{\mathfrak{w}_s(\mathscr{E}^c)}(*)$, the estimates for $\nu^{\Theta}_{\mathfrak{w}_s(\mathscr{E}^c)}(\phi, f)$, $\nu^{\Theta}_{\mathfrak{w}_s(\mathscr{E}^c)}(\phi|\phi, s)$, and $\nu^{\Theta}_{\mathfrak{w}_s(\mathscr{E}^c)}(3_1|\phi, s)$ generated by both meth-

Table 7.8: The estimates for $\nu^{\Theta}_{\mathfrak{w}_s(\mathscr{E}^c)}(*)$, $a^{\Theta}_{\mathfrak{w}_s(\mathscr{E}^c)}(*)$, and $d_{\mathfrak{w}_s(\mathscr{E}^c)}(*)$ computed using the "Average-n Method". The error bars represent the estimated 95% margins of error.

	Parameter Estimated			
Property $*$	$N^*_{\min}$	$\nu^{\Theta}_{\mathfrak{w}_s(\mathscr{E}^c)}(*)$	$a^{\Theta}_{\mathfrak{w}_s(\mathscr{E}^c)}(*)$	$d_{\mathfrak{w}_s(\mathscr{E}^c)}(*)$
(ϕ, f)	156	0.0042(0.2900)	55(2784)	-54(2787)
$(\phi\|\phi, s)$	182	0.0041(0.5002)	93(11968)	-94(11981)
$(3_1\|\phi, s)$	182	0.0832(0.7537)	18.0(328)	-32(449)

Table 7.9: A summary of the estimates for $\nu^{\Theta}_{\mathfrak{w}_s(\mathscr{E}^c)}(*)$ computed using the "Fixed-n Method" and the "Average-n Method". The values in parentheses are the estimated 95% margins of error.

	Estimate of $\nu^{\Theta}_{\mathfrak{w}_s(\mathscr{E}^c)}(*)$	
Property $*$	Average-n Method	Fixed-n Method
(ϕ, f)	0.0042(0.2900)	0.0193(0.0915)
$(\phi\|\phi, s)$	0.0041(0.5002)	0.0360(0.1654)
$(3_1\|\phi, s)$	0.0832(0.7537)	0.1084(0.6717)

ods are summarized in Table 7.9. Note that for each property $*$ presented in Table 7.5, there is considerable overlap between the estimated 95% confidence interval presented for $\nu^{\Theta}_{\mathfrak{w}_s(\mathscr{E}^c)}(*)$. Hence the estimates for each of $\nu^{\Theta}_{\mathfrak{w}_l(\mathscr{E}^c)}(\phi, f)$, $\nu^{\Theta}_{\mathfrak{w}_l(\mathscr{E}^c)}(\phi|\phi, s)$, and $\nu^{\Theta}_{\mathfrak{w}_l(\mathscr{E}^c)}(3_1|\phi, s)$ generated by both methods are also concluded to be comparable. Note that the estimated 95% margins of error determined via both methods are much larger than the point estimate and that the margin of error determined by the Average-n Method is even larger than the corresponding margin of error estimated by the Fixed-n Method. Consequently neither method provides reliable estimates for $\nu^{\Theta}_{\mathfrak{w}_s(\mathscr{E}^c)}(\phi, f)$, $\nu^{\Theta}_{\mathfrak{w}_s(\mathscr{E}^c)}(\phi|\phi, s)$, and $\nu^{\Theta}_{\mathfrak{w}_s(\mathscr{E}^c)}(3_1|\phi, s)$.

The upshot based on this analysis is that the Average-n Method does not provide estimates for the metric exponent that are consistently much better (in terms of the size of the estimated 95% margin of error) than the Fixed-n Method and in some cases, actually provides estimates that are much more unreliable than the Fixed-n Method. Another downside of the Average-n Method is that, though it can be used to estimate $\nu^{\Theta}_{\bullet}(*)$, it

cannot be used to estimate the amplitude $A^{\Theta}_{\bullet}(*)$. A further drawback is that the sequence of points used to estimate the metric exponents is formed from estimates of two parameters whereas the sample of points required by the Fixed-n Method requires only one parameter estimate. If this second source of error is taken into account in the metric exponent's estimated error, then the estimates generated by the Average-n Method are actually less reliable than reported. Taking this extra source of error into account, since the Fixed-n Method can be used to estimate both $A^{\Theta}_{\bullet}(*)$ and $\nu^{\Theta}_{\bullet}(*)$, and it computes estimates that are as least as good as, if not better than, the Average-n Method estimates for $\nu^{\Theta}_{\bullet}(*)$, the conclusion is that whenever a sufficiently large, fixed-n sample of essentially independent points can be formed, the Fixed-n Method should be used .

7.3 In Summary

In this chapter, two measures of the "size" of a Θ-SAP in $\mathscr{P}^{\Theta}(\phi)$ were discussed. In Section 7.1 the lengths of the two uSAWs comprising each Θ-SAP are discussed as one measure of the size of a Θ-SAP. In Section 7.2, the mean-square radii of gyration of the two uSAWs comprising each Θ-SAP are discussed as the second measure of size of a Θ-SAP.

The discussion in Section 7.1 begins by verifying that the generated data supports the facts that, given an integer $n \geq n^{\Theta}_{*}/2 + 1$ and any property $* \in \Phi$,

$$\mathrm{E}\left[S_{2n}(\mathscr{E}^{c}(*))\right] < n - 3 < \mathrm{E}\left[L_{2n}(\mathscr{E}^{c}(*))\right], \tag{7.119}$$

and, as $n \to \infty$, for each property $* \in \Phi$ and for $W \in \mathscr{E}^{c}_{2n}(*)$ chosen uniformly at random, the expected length of the large uSAW in W is $O(n)$. Then the discussion demonstrated that the data supports Conjecture 2.2.10, that is for each natural number $n \geq 13 = n^{\Theta}_{(3_1|\phi,s)}/2 + 1$, the point estimates $\langle s_{2n}(\mathscr{E}^{c}(*))\rangle$ and $\langle l_{2n}(\mathscr{E}^{c}(*))\rangle$ satisfy the hypothesized relationships

$$\mathrm{E}\left[S_{2n}(\mathscr{E}^{c}(3_1|\phi,s))\right] \geq \mathrm{E}\left[S_{2n}(\mathscr{E}^{c}(\phi,f))\right] \tag{7.120}$$

and

$$\mathrm{E}\left[L_{2n}(\mathscr{E}^{c}(3_1|\phi,s))\right] \leq \mathrm{E}\left[L_{2n}(\mathscr{E}^{c}(\phi,f))\right]. \tag{7.121}$$

The section concludes with showing that for a fixed polygon length $2n$, the estimated proportion of $(2n)$-edge property-$*$ Θ-SAPs with equal-length uSAWs decreases to zero as

a function of $2n$. Thus the estimated proportions support Conjecture 2.2.8 (that is, for each property $* \in \Phi$, $\mathscr{P}^{\Theta}(*)$ is dominated by SAPs with one large uSAW and one small uSAW). The discussion then shows the numerical evidence supports Conjecture 2.2.11, that is, $\mathrm{E}\left[S_{2n}(\mathscr{E}^{c}(*))\right] \sim (n)^{\zeta_s(*)}$. It is also shown that it is possible that, on average, the length of the small uSAW in a $(2n)$-edge polygon in $\mathscr{E}^{c}(\phi)$ is $O(1)$, which supports that $\mathrm{E}\left[S_{2n}(\mathscr{E}^{c}(*))\right] \sim (n)^{0}$. The discussion then turns to the mean-square radius of gyration.

Section 7.2 begins by using the data to explore Question 2.2.4, that is, the discussion shows that it is possible that, for each $* \in \{(\phi, f), (\phi|\phi, s), (3_1|\phi, s)\}$,

$$\frac{r^2\left(\mathscr{E}^{c}_{2n}(*)\right)}{r^2\left(\mathscr{P}^{\Theta}_{2n}(*)\right)} \to 1, \tag{7.122}$$

and hence it is conjectured (refer to Conjecture 7.2.1), for each $* \in \Phi$,

$$\frac{r^2\left(\mathscr{E}^{c}_{2n}(*)\right)}{r^2\left(\mathscr{P}^{\Theta}_{2n}(*)\right)} \to 1. \tag{7.123}$$

Then the discussion numerically investigates a possible relationship between the expected radii of gyration of the large, equal-length, and small uSAWs (as a function of polygon length) for randomly selected, property-$*$, $(2n)$-edge Θ-SAPs (that is Question 2.2.5) and by conjecturing (refer to Conjecture 7.2.2) that for each $* \in \Phi$, and for every integer $n > n^{\Theta}_{*}/2$,

$$r^2\left(\mathfrak{w}_s\left(\mathscr{P}^{\Theta}_{2n}(*)\right)\right) < r^2\left(\mathfrak{w}_l\left(\mathscr{P}^{\Theta}_{2n}(*)\right)\right), \tag{7.124}$$

and concluding that more data needs to be generated before the relationship "For every odd integer $n \geq n^{\Theta}_{*}/2$,

$$r^2\left(\mathfrak{w}_s\left(\mathscr{E}^{c}_{2n}(*)\right)\right) < r^2\left(\mathfrak{w}_e(\mathscr{E}_{2n}(*))\right) < r^2\left(\mathfrak{w}_l\left(\mathscr{E}^{c}_{2n}(*)\right)\right)." \tag{7.125}$$

can be explored more thoroughly. The discussion then turns to showing that the data supports that, for each $* \in \mathscr{K}^{\dagger}(\phi)\backslash\{(\phi|\phi, s)\}$ and each natural number $n \geq n^{\Theta}_{*}/2$, the expected mean-square radius of gyration of the small uSAW in a randomly chosen element from $\mathscr{E}^{c}_{2n}(*)$ is greater than the expected mean-square radii of gyration of the small uSAW in a randomly chosen element from either $\mathscr{E}^{c}_{2n}(\phi, f)$ and $\mathscr{E}^{c}_{2n}(\phi|\phi, s)$ and that the expected mean-square radius of gyration of the large uSAW in a randomly chosen element from $\mathscr{E}^{c}_{2n}(*)$ is smaller than the expected mean-square radii of gyration of the large uSAW in a randomly chosen element from either $\mathscr{E}^{c}_{2n}(\phi, f)$ and $\mathscr{E}^{c}_{2n}(\phi|\phi, s)$ (that is Question 2.2.6). Hence it is conjectured that, for each $* \in \Phi\backslash\{\phi, (\phi, s)\}$,

$$\lim_{n\to\infty} \frac{r^2\left(\mathfrak{w}_s\left(\mathscr{E}^{c}_{2n}(*)\right)\right)}{r^2\left(\mathscr{P}^{\Theta}_{2n}(\phi)\right)} = 0, \text{ and} \tag{7.126}$$

$$\lim_{n\to\infty} \frac{r^2\left(\mathfrak{w}_l\left(\mathscr{E}^c_{2n}(*)\right)\right)}{r^2\left(\mathscr{P}^{\Theta}_{2n}(\phi)\right)} = 1, \tag{7.127}$$

cf. Conjecture 7.2.4. Furthermore, the numerical evidence presented throughout Section 7.2.2 suggests that $\mathscr{P}_{2n}(\phi)$ is dominated by Θ-SAPs with one large and one small uSAW such that the "size" (mean-square radius of gyration) of the large uSAW is $O\left(n^t\right)$ (where $t > 1$) and the "size" (mean-square radius of gyration) of the small uSAW is $O(n^s)$ (where $s < 1$).

The final part of Section 7.2 ends by presenting two methods for estimating the metric exponents $\nu^{\Theta}_{\bullet}(*)$ and a discussion of the possible properties of the exponents $\nu^{\Theta}_{\bullet}(*)$. The first method presented to estimate $\nu^{\Theta}_{\bullet}(*)$ is an implementation of the "Fixed-n Method for curve fitting" and a by-product of the method is that, in addition to estimating $\nu^{\Theta}_{\bullet}(*)$, the method estimates the amplitudes $A^{\Theta}_{\bullet}(*)$. The second method presented for estimating $\nu^{\Theta}_{\bullet}(*)$ is referred to as the "Average-n Method for estimating $\nu^{\Theta}_{\bullet}(*)$". $\nu^{\Theta}_{\bullet}(*)$ is estimated using both techniques. The estimates for the metric exponents and amplitudes determined using the "Fixed-n Method for curve fitting" were used to investigate whether the metric exponents are independent of the sets $\mathscr{E}(*)$ and $\mathscr{E}^c(*)$, for each property $* \in \Phi$, and that the metric exponents are all equal to $\nu^{\Theta}_{\mathscr{P}}(\phi)$ (that is Question 2.2.8). Because of insufficient data, the metric exponents associated with the sets $\mathscr{E}(*)$ could not be estimated. The estimates available for the metric exponents support the following conjectures: for each property $* \in \Phi$, $\nu^{\Theta}_{\mathscr{E}^c}(*) = \nu^{\Theta}_{\mathscr{P}}(\phi)$ (cf. Conjecture 7.2.5); $\nu^{\Theta}_{\mathscr{P}}(\phi) = \nu$ (cf. Conjecture 7.2.6); $\nu^{\Theta}_{\mathfrak{w}_l(\mathscr{E}^c)}(*) = \nu^{\Theta}_{\mathscr{E}^c}(*)$ (cf. Conjecture 7.2.7); and $0 \leq \nu^{\Theta}_{\mathfrak{w}_s(\mathscr{E}^c)}(*) < \frac{1}{2} < \nu^{\Theta}_{\mathscr{E}^c}(*)$ (cf. Conjecture 7.2.8). Based on the estimates for the amplitudes $A^{\Theta}_{\bullet}(*)$, the following conjectures are also made: for every property $* \in \Phi$, $A^{\Theta}_{\mathscr{E}^c}(*) = A^{\Theta}_{\mathscr{P}}(\phi) = A_R(\phi)$ (cf. Conjecture 7.2.9) and $A^{\Theta}_{\mathfrak{w}_l(\mathscr{E}^c)}(*) = A^{\Theta}_{\mathscr{E}^c}(*)$ (cf. Conjecture 7.2.10).

The final part of Section 7.2 ends by presenting the Average-n Method and then using the method to estimate the metric exponents. The resulting estimates were then compared to the corresponding estimates from the Fixed-n Method. The conclusion based on this comparison is that whenever a sufficiently large essentially independent sample (referred to as a good sample) of fixed-n estimates is available, the Fixed-n Method should be used to estimate the metric exponents.

Sections 7.1 and 7.2 both contain a word of caution regarding the amount of data available for exploring how the two measures of the size of a Θ-SAP depend on the property $* \in \Phi$ and how these two measures are impacted by Θ-SAPs in $\mathscr{E}$. The caution is that

more data needs to be collected before these dependencies of the two measures can be more conclusively determined. Hence the work presented in Chapter 7 is really the preliminary work of a future, more in-depth study.

Chapter 8

Conclusions and Future Work

This chapter first includes a synopsis of the results presented throughout this work and then provides some summary remarks regarding the work presented. The chapter ends with the presentation of some of the future work inspired by this dissertation.

8.1 Conclusions and Ending Remarks

Chapter 2 begins by reviewing the simplified SAP model that is used in this work to investigate Problems 1.1 and 1.2. This simplified model is the model for strand passage in a "pinched" ring polymer as introduced in [150]. The focus is on unknotted Θ-SAPs. For this set, in Section 2.2.1, the new result, that, for every $* \in \Phi$,

$$\kappa_\phi^* := \lim_{n\to\infty} \frac{\log p_n^\Theta(*)}{2n} = \kappa_\phi := \lim_{n\to\infty} \frac{\log p_n(\phi)}{2n} \tag{8.1}$$

is proved. Further to this, in Section 2.2.3, the new result that

$$\lim_{n\to\infty} \frac{\log w_B(2n)}{2n} = \lim_{n\to\infty} \frac{\log w_E(2n)}{2n} = \lim_{n\to\infty} \frac{\log w_S(2n)}{2n} = \kappa_\phi \tag{8.2}$$

is proved. The rest of the chapter presents heuristic arguments that lead to new conjectures and open questions (related to Problems 1.1 and 1.2) for unknotted Θ-SAPs. Specifically, the heuristic arguments presented here lead to new conjectures regarding the critical exponents α_*^Θ (as defined in Equation (2.84)), that is, for each $* \in \Phi$, it is conjectured that

$$\alpha_\phi - 2 = \alpha_\phi^\Theta = \alpha_*^\Theta. \tag{8.3}$$

The chapter also includes heuristic arguments leading to new conjectures regarding the scaling forms for the fixed-n strand passage probabilities and their limiting values as $n \to \infty$. Namely, it is conjectured for $* \in \{(\phi, s), (\phi, f)\}$ that

$$\Pr_{2n}^\Theta(*) = \frac{A_*^\Theta}{A_\phi^\Theta} + \left(B_*'^\Theta\right) n^{-\Delta_*'^\Theta} + g_1^*(n), \tag{8.4}$$

where

$$g_1^*(n) = O(\min\left\{n^{-1}, \max\left\{n^{-\Delta_\phi^\Theta}, n^{-\Delta_*^\Theta}\right\}\right\}), \tag{8.5}$$

and, for $* \in \mathscr{K}^\dagger(\phi)$ (the set of after-strand passage properties), that

$$\Pr_n^\Theta(*) = \frac{A_*^\Theta}{A_{(\phi,s)}^\Theta} + \left(B_*'^\Theta\right) n^{-\Delta_*'^\Theta} + g_2^*(n), \tag{8.6}$$

where

$$g_2^*(n) = O(\min\left\{n^{-1}, \max\left\{n^{-\Delta_{(\phi,s)}^\Theta}, n^{-\Delta_*^\Theta}\right\}\right\}). \tag{8.7}$$

The final conjectures and questions presented in Chapter 2 are regarding Problem 1.2, that is regarding the size of unknotted Θ-SAPs. The first conjecture related to this is that, for sufficiently large n, $\mathscr{P}_{2n}(\phi)$ consists primarily of Θ-SAPs formed from one large uSAW (length $O(n)$) and one small uSAW (length $O(1)$). The first question posed regarding the size of a Θ-SAP is, as $n \to \infty$, does

$$\mathrm{E}\left[L_{2n}(\mathscr{E}^c(*))\right] \sim n? \tag{8.8}$$

The next conjectures are that, for each $* \in \mathscr{K}^\dagger(\phi) \backslash \{(\phi|\phi, s)\}$ and every natural number $n \geq n_*^\Theta/2$,

$$\mathrm{E}\left[S_{2n}(\mathscr{E}^c(*))\right] > \mathrm{E}\left[S_{2n}(\mathscr{E}^c(\phi, f))\right], \tag{8.9}$$

$$\mathrm{E}\left[S_{2n}(\mathscr{E}^c(*))\right] > \mathrm{E}\left[S_{2n}(\mathscr{E}^c(\phi|\phi, s))\right], \tag{8.10}$$

$$\mathrm{E}\left[L_{2n}(\mathscr{E}^c(*))\right] < \mathrm{E}\left[L_{2n}(\mathscr{E}^c(\phi, f))\right], \tag{8.11}$$

and

$$\mathrm{E}\left[L_{2n}(\mathscr{E}^c(*))\right] < \mathrm{E}\left[L_{2n}(\mathscr{E}^c(\phi|\phi, s))\right]. \tag{8.12}$$

The final conjectures and questions in the chapter are related to the mean-square radii of gyration for subsets of $\mathscr{P}^\Theta(\phi)$. For $\mathcal{R}_{2n}(a, b, c, d, h)$ given by Equation (2.172) and $* \in \Phi$, the expected mean-square radius of gyration for Θ-SAPs in $\mathscr{U}_n(*) \subseteq \mathscr{P}_n^\Theta(\phi)$ is conjectured to scale (as $n \to \infty$) according to

$$r^2(\mathscr{U}_{2n}) \sim \mathcal{R}_{2n}\left(A_{\mathscr{U}}^\Theta(*), \nu_{\mathscr{U}}^\Theta(*), B_{\mathscr{U}}^\Theta(*), \Delta_{\mathscr{U}}^\Theta(*), h_{\mathscr{U}}^*\right), \tag{8.13}$$

and the expected f-transformed mean-square radius of gyration for Θ-SAPs in $\mathscr{U}_n(*) \subseteq \mathscr{P}_n^\Theta(\phi)$ is conjectured to scale (as $n \to \infty$) according to

$$r^2(f(\mathscr{U}_{2n})) \sim \mathcal{R}_{2n}\left(A_{f(\mathscr{U})}^\Theta(*), \nu_{f(\mathscr{U})}^\Theta(*), B_{f(\mathscr{U})}^\Theta(*), \Delta_{f(\mathscr{U})}^\Theta(*), h_{f(\mathscr{U})}^*\right). \tag{8.14}$$

Several questions are then asked regarding the expected mean-square radius of gyration and the corresponding metric exponent $\nu_{\bullet}^{\Theta}(*)$ and amplitude $A_{\bullet}^{\Theta}(*)$:

1. for each $* \in \Phi$ and for sufficiently large $n \geq n_*^{\Theta}/2$, does

$$r^2\left(\mathscr{E}_{2n}^{c}(*)\right) \sim r^2\left(\mathscr{P}_{2n}^{\Theta}(*)\right), \tag{8.15}$$

and, for n odd, does

$$r^2\left(\mathscr{E}_{2n}(*)\right) \sim r^2\left(\mathscr{P}_{2n}^{\Theta}(*)\right)? \tag{8.16}$$

2. for each $* \in \Phi$ and for every integer $n > n_*^{\Theta}/2$, is

$$r^2\left(\mathfrak{w}_s\left(\mathscr{P}_{2n}^{\Theta}(*)\right)\right) < r^2\left(\mathfrak{w}_l\left(\mathscr{P}_{2n}^{\Theta}(*)\right)\right), \tag{8.17}$$

and, n odd, is

$$r^2\left(\mathfrak{w}_s\left(\mathscr{E}_{2n}^{c}(*)\right)\right) < r^2\left(\mathfrak{w}_e(\mathscr{E}_{2n}(*))\right) < r^2\left(\mathfrak{w}_l\left(\mathscr{E}_{2n}^{c}(*)\right)\right)? \tag{8.18}$$

3. for each $* \in \mathscr{K}^{\dagger}(\phi)\backslash\{(\phi|\phi,s)\}$ and for every integer $n > n_*^{\Theta}/2$, is

$$r^2\left(\mathfrak{w}_s\left(\mathscr{E}_{2n}^{c}(*)\right)\right) > r^2\left(\mathfrak{w}_s\left(\mathscr{E}_{2n}^{c}(\phi,f)\right)\right), \tag{8.19}$$

$$r^2\left(\mathfrak{w}_s\left(\mathscr{E}_{2n}^{c}(*)\right)\right) > r^2\left(\mathfrak{w}_s\left(\mathscr{E}_{2n}^{c}(\phi|\phi,s)\right)\right), \tag{8.20}$$

$$r^2\left(\mathfrak{w}_l\left(\mathscr{E}_{2n}^{c}(*)\right)\right) < r^2\left(\mathfrak{w}_l\left(\mathscr{E}_{2n}^{c}(\phi,f)\right)\right), \tag{8.21}$$

and

$$r^2\left(\mathfrak{w}_l\left(\mathscr{E}_{2n}^{c}(*)\right)\right) < r^2\left(\mathfrak{w}_l\left(\mathscr{E}_{2n}^{c}(\phi|\phi,s)\right)\right)? \tag{8.22}$$

4. for each $* \in \Phi\backslash\{\phi,(\phi,s)\}$ and for every integer $n > n_*^{\Theta}/2$, do the following limits exist and, if they exist, what are their values:

$$\lim_{n\to\infty}\frac{r^2\left(\mathfrak{w}_s\left(\mathscr{E}_{2n}^{c}(*)\right)\right)}{r^2\left(\mathscr{P}_{2n}^{\Theta}(\phi)\right)}, \quad \lim_{n\to\infty}\frac{r^2\left(\mathfrak{w}_e\left(\mathscr{E}_{4n+2}(*)\right)\right)}{r^2\left(\mathscr{P}_{4n+2}^{\Theta}(\phi)\right)}, \text{ and } \lim_{n\to\infty}\frac{r^2\left(\mathfrak{w}_l\left(\mathscr{E}_{2n}^{c}(*)\right)\right)}{r^2\left(\mathscr{P}_{2n}^{\Theta}(\phi)\right)}? \tag{8.23}$$

Chapter 2 ends with several questions regarding the relationships between the metric exponents and the relationships between the amplitudes in the scaling forms for the expected mean-square radius of gyration and the expected f-transformed mean-square radius of gyration (assuming that the scaling forms hold).

Chapter 3 presents the details of the implementation of the CMC Θ-BFACF algorithm for collecting data to explore the conjectures and questions posed in Chapter 2. The

simulation consists of ten independent replications of fourteen chains characterized by the fugacities: $z_1 = 0.2030$, $z_2 = 0.2050$, $z_3 = 0.2070$, $z_4 = 0.2090$, $z_5 = 0.2100$, $z_6 = 0.2105$, $z_7 = 0.2110$, $z_8 = 0.2115$, $z_9 = 0.2120$, $z_{10} = 0.2124$, $z_{11} = 0.2128$, $z_{12} = 0.2130$, $z_{13} = 0.2131$, and $z_{14} = 0.2132$, and $q := 2$. Each replication consists of a total of 9.6×10^{10} time steps (8.0×10^{10} Θ-BFACF moves in parallel and 1.6×10^{10} attempted swaps) in which each five Θ-BFACF moves in parallel is followed by an attempted swap. The polygon lengths for the initial starting states of each chain and each replication can be found in Table 3.1. The realization given by the u'th replication consists of a sequence of $(t_0 + 1)$ 14-tuples of Θ-SAPs from $\left(\mathscr{P}^{\Theta}\right)^{14}$ denoted

$$\boldsymbol{\omega}^{(u)} := \left(\left(\omega_t^{(u)}(1), \omega_t^{(u)}(2), ..., \omega_t^{(u)}(14)\right), t = 0, ..., 9.6 \times 10^{10}\right). \tag{8.24}$$

Data is sampled after every 1000'th Θ-BFACF in parallel (but before the corresponding attempted swap) and the corresponding sequence of 14-tuples of SAPs sampled from Replication u is denoted by

$$\hat{\boldsymbol{\omega}}^{(u)} := \left(\left(\hat{\omega}_j^{(u)}(1), \hat{\omega}_j^{(u)}(2), ..., \hat{\omega}_j^{(u)}(14)\right), j = 0, ..., l\right), \tag{8.25}$$

where $l := \lfloor t_0/1200 \rfloor = 80,000,000$, and, for $t := 1200j$, the j'th term (for $1 \leq j \leq l$) of $\hat{\boldsymbol{\omega}}^{(u)}$ is given by

$$\left(\hat{\omega}_j^{(u)}(1), \hat{\omega}_j^{(u)}(2), ..., \hat{\omega}_j^{(u)}(14)\right) := \left(\omega_t^{(u)}(1), \omega_t^{(u)}(2), ..., \omega_t^{(u)}(14)\right). \tag{8.26}$$

Using the sample $(\hat{\boldsymbol{\omega}}^{(u)}, u = 1, ..., 10)$ (the CMC Θ-BFACF data), and the methods presented in Chapter 4, τ_{exp}, the time it takes each replication to reach its equilibrium distribution, and τ_{int}, half the time between essentially independent samples, are respectively estimated to be $\widehat{\tau}_{\text{exp}} = 5.0$ billion Θ-BFACF moves in parallel and $\widehat{\tau}_{\text{int}} = 0.6$ billion Θ-BFACF moves in parallel. Consequently it is concluded that: after 5.0 billion Θ-BFACF moves in parallel, each replication has reached its equilibrium distribution; states that are 1.2 billion Θ-BFACF moves in parallel apart are essentially independent; and data that is subdivided into blocks of 1.2 million consecutive data points form essentially independent blocks of data. Hence each replication can be subdivided into 66 essentially independent blocks of data. In Section 4.4, it is suggested that if the amount of data generated in the warm-up interval is less than 5% of the total sample size, then the data collected during the warm-up interval need not be discarded. For the CMC Θ-BFACF data, the number

of blocks in the warm-up interval corresponds to approximately 6% ($4/66 \approx 0.06$) of the total data generated. Since this is only slightly larger than the 5% cutoff value and none of the estimates computed using all the data differed statistically from the estimates computed from burning the first four blocks of data from each replication, no data is burned in the data analysis presented. The 660 essentially independent blocks of data (if the data from all ten replications is combined) are then used to show that the average lengths of the property-$*$ Θ-SAPs generated in each of the fourteen chains exhibit the behaviours predicted by Approximations (4.101) and (4.102). Hence it is concluded that the data is generated from the correct distribution.

Furthermore, in Chapter 4, the average lengths of the property-ϕ Θ-SAPs are fit to the form predicted by Approximation (4.101), thus producing an estimate for e^{κ_ϕ} to be 4.6836 and estimate for α_ϕ^Θ to be -1.78. This estimate for e^{κ_ϕ} is exactly the same as the estimate for e^{κ_ϕ} given by Orlandini *et al.* [125]. The estimate -1.78 for α_ϕ^Θ, when combined with Orlandini *et al.'s* [125] estimate $\alpha_\phi \approx 0.23$, supports the conjectured relationship $\alpha_\phi - 2 = \alpha_\phi^\Theta$.

The final discussion in Chapter 4 applies the proposed technique for determining the amount of "reliable" data. From the analysis of the simulation data it is concluded that all generated property-$*$ Θ-SAPs with lengths less than or equal to $\hat{N}_{\max}(*)$ are "reliable" for $\hat{N}_{\max}(*)$ given by: $\hat{N}_{\max}(\phi) = 3300$, $\hat{N}_{\max}(\phi, f) = 3300$, $\hat{N}_{\max}(\phi, s) = 3300$, $\hat{N}_{\max}(\phi|\phi, s) = 3300$, $\hat{N}_{\max}(3_1|\phi, s) = 2000$, and $\hat{N}_{\max}(4_1|\phi, s) = 600$. These estimates for $\hat{N}_{\max}(*)$ are used in Chapter 5. The estimates for $N^*_{\max}$ that are required in Chapters 6 and 7 are presented in those chapters respectively.

In Chapter 5, a new maximum likelihood technique is presented to compute the best maximum likelihood estimates from a realization of a composite Markov chain whose i'th equilibrium marginal distribution is characterized by the fugacity $z_i = e^{\beta_i}$ and is asymp-

totically given by

$$\begin{aligned}\pi_\omega(\boldsymbol{\theta}|*,\beta,N^*_{\min},N^*_{\max}) = I_{\langle 2\rangle}(|\omega|)\psi_*(\omega)\,\frac{A_* w(|\omega|)(|\omega|+h_*)^{\alpha^\Theta_{\overline{*}}-\varepsilon_*}e^{(\kappa_s+\beta)|\omega|}}{Q(\beta)}\\ + I_{\langle 2\rangle}(|\omega|)\left(1-\psi_*(\omega)\right)\frac{A_{\overline{*}} w(|\omega|)(|\omega|+h_{\overline{*}})^{\alpha^\Theta_{\overline{*}}}e^{(\kappa_s+\beta)|\omega|}}{Q(\beta)}\\ + I_{\langle 1\rangle}(|\omega|)\left[\sum_{n<N^*_{\min}}\frac{w(n)s_n e^{\beta n}}{Q(\beta)}\right]\\ + I_{\langle 3\rangle}(|\omega|)\sum_{n>N^*_{\max}}\frac{w(n)\left[A_*(n+h_*)^{\alpha^\Theta_{\overline{*}}-\varepsilon_*}+A_{\overline{*}}(n+h_{\overline{*}})^{\alpha^\Theta_{\overline{*}}}\right]e^{(\kappa_s+\beta)n}}{Q(\beta)}.\end{aligned} \tag{8.27}$$

The technique is then applied to the CMC Θ-BFACF data to obtain maximum likelihood estimates for κ^Θ_*, $\alpha^\Theta_* := \alpha^\Theta_{\overline{*}} - \varepsilon_*$, $\alpha^\Theta_{\overline{*}}$, h_*, $h_{\overline{*}}$, and $A_*/A_{\overline{*}}$.

The estimates for κ^Θ_*, α^Θ_*, $\alpha^\Theta_{\overline{*}}$, h_*, and $h_{\overline{*}}$ are shown to support the expected relations: $\alpha^\Theta_{\overline{(\phi,f)}} = \alpha^\Theta_{(\phi,s)}$; $\alpha^\Theta_{\overline{(\phi,s)}} = \alpha^\Theta_{(\phi,f)}$; $h_{\overline{(\phi,f)}} = h_{(\phi,s)}$; and $h_{\overline{(\phi,s)}} = h_{(\phi,f)}$; and the facts that

$$\kappa^\Theta_\phi = \kappa^\Theta_{(\phi,s)} = \kappa^\Theta_{(\phi,f)} = \kappa_\phi = \kappa^\Theta_{(K|\phi,s)}. \tag{8.28}$$

Then, based on the CMC m.l.e.s for α^Θ_*, the critical exponents α^Θ_* are concluded to be independent of the after strand passage knot-type and $\alpha^\Theta_\phi = \alpha_\phi - 2$. The section ends by concluding that the CMC m.l.e.s for h_* and $h_{\overline{*}}$ depend on the property $*$.

The best CMC m.l.e.s for κ^Θ_*, α^Θ_*, $\alpha^\Theta_{\overline{*}}$, h_*, $h_{\overline{*}}$, and A are as follows. Because the most data is available for property ϕ, and assuming $\alpha^\Theta_* = \alpha^\Theta_{\overline{*}}$, the best estimates for κ_ϕ, α^Θ_*, and $\alpha^\Theta_{\overline{*}}$ are

$$\begin{aligned}\kappa_\phi = \kappa^\Theta_\phi = &\quad 1.544125 \quad \pm \quad 0.000028 \quad (\pm 0.00005)\\ \alpha^\Theta_* = \alpha^\Theta_{\overline{*}} = \alpha^\Theta_\phi = &\quad -1.7521 \quad \pm \quad 0.0414 \quad (\pm 0.02)\,,\end{aligned} \tag{8.29}$$

where the above are in the form

$$\text{parameter} = \text{point estimate} \pm 95\%\ \text{ME}\ (\pm\,\text{systematic error}), \tag{8.30}$$

the estimated 95% margin of error is calculated using Theorem 5.1.4, and the systematic error is determined using the technique discussed in Section 5.5. The best estimates for h_* and $h_{\overline{*}}$ are given below in Table 8.1 which is a reproduction of Table 5.3.

Table 8.1: The estimates for h_* and $h_{\bar{*}}$ computed using all 10 replications combined.

	Parameter Estimated			
Property $*$	$N^*_{\min}$	$N^*_{\max}$	h_* (95% ME)	$h_{\bar{*}}$ (95% ME)
ϕ	156	3300	$-10.3\,(5.9)$	No estimate
(ϕ, f)	142	3300	$-10.3\,(5.4)$	$-8.5\,(9.1)$
(ϕ, s)	156	3300	$-8.7\,(10.7)$	$-10.5\,(6.4)$
$(\phi\|\phi, s)$	182	3300	$-10.3\,(14.2)$	$-10.5\,(8.7)$
$(3_1\|\phi, s)$	408	3300	$-6.8\,(506)$	$-2.5\,(59)$
$(4_1\|\phi, s)$	296	1200	$449\,(3158)$	$-9.8\,(13.1)$

The best estimates for the amplitude ratios are given below in Table 8.2 which is a reproduction of Table 5.5.

Table 8.2: The estimates for amplitude ratios computed using all 10 replications combined.

	Parameter Estimated		
Property $*$	$N^*_{\min}$	$N^*_{\max}$	$\frac{A_*}{A_{\bar{*}}}$ (95% ME)
ϕ	156	3300	No estimate
(ϕ, f)	142	3300	5.8531 (1.6848)
(ϕ, s)	156	3300	0.1699 (0.0537)
$(\phi\|\phi, s)$	182	3300	0.1611 (0.0514)
$(3_1\|\phi, s)$	408	2000	0.0032 (0.0290)
$(4_1\|\phi, s)$	296	1200	0.4930 (28.6)

In this chapter, two methods for estimating the limiting strand passage probabilities $\Pr^{\Theta}(*)$, for $* \in \Phi$, were presented. The first method presented is the Fixed-n Method for Estimating $\Pr^{\Theta}(*)$ and the second method presented is the Grouped-n Method for Estimating $\Pr^{\Theta}(*)$. Because the Grouped-n Method generates point estimates that are not as variable as the fixed-n probability estimates, the Grouped-n estimates are concluded

to be more reliable. Hence it is concluded that whenever possible the Grouped-n Method should be used. With $N^*_{\max}$ estimated by $\hat{N}_{\max}(*) = 1890$, applying the Grouped-n Method to the CMC Θ-BFACF data yields the following estimates for the limiting strand passage probabilities:

$$\Pr^{\Theta}(\phi, s) = \quad 0.13719 \quad \pm \quad 0.00019 \quad (\pm 0.03240)\,, \tag{8.31}$$

$$\Pr^{\Theta}(\phi|\phi, s) = \quad 0.97653 \quad \pm \quad 0.00133 \quad (\pm 0.01822)\,, \tag{8.32}$$

$$\Pr^{\Theta}(3_1|\phi, s) = \quad 0.02208 \quad \pm \quad 0.00095 \quad (\pm 0.00672)\,, \tag{8.33}$$

$$\Pr^{\Theta}(4_1|\phi, s) = \quad 0.00093 \quad \pm \quad 0.00048 \quad (\pm 0.00082)\,, \tag{8.34}$$

and

$$\Pr^{\Theta}(5_2|\phi, s) = \quad 0.00004 \quad \pm \quad 0.00003 \quad (\pm 0.00004)\,. \tag{8.35}$$

Because of the large error in the estimates for $\Pr^{\Theta}(4_1|\phi, s)$ and $\Pr^{\Theta}(5_2|\phi, s)$, the estimates are concluded to be unreliable and thus more data is required to determine better estimates for $\Pr^{\Theta}(4_1|\phi, s)$ and $\Pr^{\Theta}(5_2|\phi, s)$. Based on the estimates given by Equations (8.31)-(8.35), the limiting strand passage probabilities $\Pr^{\Theta}(*)$ are concluded to exist and $\Pr^{\Theta}(*) \in (0, 1)$.

Assuming that the LSP Model is an appropriate model to study Problem 1.1, the estimates given by Equations (8.31)-(8.35) estimate the transition probabilities for the $K = \phi$ case. More specifically, the point estimates indicate that the $(\phi \to \phi)$-transition probability is 0.97653; the $(\phi \to 3_1)$-transition probability is 0.02208; the $(\phi \to 4_1)$-transition probability is 0.00093; and the $(\phi \to 5_2)$-transition probability is 0.00004. These estimates suggest that once a ring polymer is unknotted, after any subsequent strand passage, the ring polymer will most likely remain unknotted.

The focus of Chapter 7 is to address Problem 1.2 using the CMC Θ-BFACF data $(\hat{\boldsymbol{\omega}}_R^{(u)}, u = 1, ..., 10)$, where $\hat{\boldsymbol{\omega}}_R^{(u)}$ is the sequence of 14-tuples of SAPs sampled from Replication u defined by

$$\hat{\boldsymbol{\omega}}_R^{(u)} := \left(\left(\hat{\omega}_j^{(u)}(1), \hat{\omega}_j^{(u)}(2), ..., \hat{\omega}_j^{(u)}(14) \right), j = 0, ..., l_R \right), \tag{8.36}$$

where $l_R := \lfloor t_0/120,000 \rfloor = 800,000$, and, for $t := 120,000j$, the j'th term (for $1 \le j \le l_R$) of $\hat{\boldsymbol{\omega}}_R^{(u)}$ is given by

$$\left(\hat{\omega}_j^{(u)}(1), \hat{\omega}_j^{(u)}(2), ..., \hat{\omega}_j^{(u)}(14) \right) := \left(\omega_t^{(u)}(1), \omega_t^{(u)}(2), ..., \omega_t^{(u)}(14) \right). \tag{8.37}$$

Note that for the remainder of this section, any reference to CMC Θ-BFACF data refers to $(\hat{\boldsymbol{\omega}}_R^{(u)}, u = 1, ..., 10)$ unless otherwise stated. Also note that, as property $*$ increases in complexity, the number of property-$*$ Θ-SAPs in the sample $(\hat{\boldsymbol{\omega}}_R^{(u)}, u = 1, ..., 10)$ decreases rapidly. Consequently the numerical evidence supporting the conjectures and questions discussed throughout Chapter 7 for more complex properties (such as $(3_1|\phi, s)$) is not strong and as a result, the discussions in Chapter 7 are to be considered preliminary discussions and more data needs to be generated to more conclusively address the conjectures and questions.

In Chapter 7, two measures of the "size" of a Θ-SAP in $\mathscr{P}^{\Theta}(\phi)$ are discussed. The lengths of the two uSAWs comprising each Θ-SAP are used as one measure of the "size" of a Θ-SAP and the mean-square radii of gyration of the two uSAWs comprising each Θ-SAP are used as the second measure of size of a Θ-SAP. The data supports the hypothesized relationships given by Inequalities (8.9)-(8.12), $* = (3_1|\phi, s)$ and for each natural number $n \geq 13 = n^{\Theta}_{(3_1|\phi,s)}/2+1$. The section ends by showing that for fixed polygon length $2n$ and property $*$, the estimated proportion of $(2n)$-edge property-$*$ Θ-SAPs with equal-length uSAWs decreases to zero as a function of $2n$, and hence, for each property $* \in \Phi$, $\mathscr{P}^{\Theta}(*)$ is dominated by SAPs with one large uSAW and one small uSAW. The numerical evidence supports that the relationship $\mathrm{E}\left[S_{2n}(\mathscr{E}^c(*))\right] \sim (n)^{\zeta_s(*)}$ is possible and that, on average, the length of the small uSAW in a $(2n)$-edge polygon in $\mathscr{E}^c(\phi)$ is $O(1)$, which supports that $\mathrm{E}\left[S_{2n}(\mathscr{E}^c(*))\right] \sim (n)^0$.

The second section in Chapter 7 focuses on the expected mean-square radius of gyration as the measure of the "size" of a Θ-SAP. The CMC Θ-BFACF data supports that, for each $* \in \Phi$,

$$\frac{r^2\left(\mathscr{E}^c_{2n}(*)\right)}{r^2\left(\mathscr{P}^{\Theta}_{2n}(*)\right)} \to 1; \tag{8.38}$$

that for each $* \in \Phi$, and for every integer $n > n^{\Theta}_*/2$, Equation (8.17) and Equations (8.19)-(8.22) holds

$$r^2\left(\mathfrak{w}_l\left(\mathscr{E}^c_{2n}(*)\right)\right) < r^2\left(\mathfrak{w}_l\left(\mathscr{E}^c_{2n}(\phi|\phi, s)\right)\right); \tag{8.39}$$

and that, for each $* \in \Phi\backslash\{\phi, (\phi, s)\}$,

$$\lim_{n\to\infty} \frac{r^2\left(\mathfrak{w}_s\left(\mathscr{E}^c_{2n}(*)\right)\right)}{r^2\left(\mathscr{P}^{\Theta}_{2n}(\phi)\right)} = 0, \text{ and} \tag{8.40}$$

$$\lim_{n\to\infty} \frac{r^2\left(\mathfrak{w}_l\left(\mathscr{E}^c_{2n}(*)\right)\right)}{r^2\left(\mathscr{P}^{\Theta}_{2n}(\phi)\right)} = 1. \tag{8.41}$$

The numerical evidence presented throughout Section 7.2.2 suggests that $\mathscr{P}_{2n}(\phi)$ is dominated by Θ-SAPs with one large and one small uSAW such that the "size" (mean-square radius of gyration) of the large uSAW is $O\left(n^{2t}\right)$ (where $t > 1/2$) and the "size" (mean-square radius of gyration) of the small uSAW is $O(n^{2s})$ (where $s < 1/2$). The estimates for the metric exponents and amplitudes determined using the "Fixed-n Method for curve fitting" are used to investigate whether the metric exponents are independent of the sets $\mathscr{E}(*)$ and $\mathscr{E}^c(*)$, for each property $* \in \Phi$, and that the metric exponents are all equal to $\nu^{\Theta}_{\mathscr{P}}(\phi)$. Because of insufficient data, the metric exponents associated with the sets $\mathscr{E}(*)$ could not be estimated. The estimates available for the metric exponents support the following conjectures: for each property $* \in \Phi$, $\nu^{\Theta}_{\mathscr{E}^c}(*) = \nu^{\Theta}_{\mathscr{P}}(\phi)$; $\nu^{\Theta}_{\mathscr{P}}(\phi) = \nu$; $\nu^{\Theta}_{\mathfrak{w}_l(\mathscr{E}^c)}(*) = \nu^{\Theta}_{\mathscr{E}^c}(*)$; and $0 \leq \nu^{\Theta}_{\mathfrak{w}_s(\mathscr{E}^c)}(*) < \frac{1}{2} < \nu^{\Theta}_{\mathscr{E}^c}(*)$. Based on the estimates for the amplitudes $A^{\Theta}_{\bullet}(*)$, the following conjectures are also made: for every property $* \in \Phi$, $A^{\Theta}_{\mathscr{E}^c}(*) = A^{\Theta}_{\mathscr{P}}(\phi) = A_R(\phi)$ and $A^{\Theta}_{\mathfrak{w}_l(\mathscr{E}^c)}(*) = A^{\Theta}_{\mathscr{E}^c}(*)$.

The final part of Section 7.2 ends by presenting the Average-n Method and then using the method to estimate the metric exponents. The resulting estimates were then compared to the corresponding estimates from Fixed-n Method. The conclusion based on this comparison is that whenever a sufficiently large essentially independent sample (referred to as a good sample) of fixed-n estimates is available, the "Fixed-n Method" should be used to estimate the metric exponents.

Again, both Sections 7.1 and 7.2 of Chapter 7 provide a cautionary warning regarding the amount of data available for exploring how both measures of the "size" of a Θ-SAP depend on the property $* \in \Phi$ and how both measures are impacted by Θ-SAPs in $\mathscr{E}$. The caution is that more data needs to be collected before these dependencies of the two measures can be more conclusively determined. Hence the work presented in Chapter 7 is preliminary to a future, more in-depth study, requiring more data.

8.2 Future Work

In this section, some of the future work that arises from the work in this thesis are outlined. The first future work discussed is work resulting directly from the analysis discussed in this thesis. Then some future work regarding the efficiency of the CMC Θ-BFACF algorithm is presented. The final future work discussed involves comparisons (if possible) of this

work to three separate works in the literature.

Some open questions that are not addressed in this thesis but are immediate extensions of the work in the thesis are:

1. For a fixed non-trivial knot-type K, how do the fixed-n probabilities $\Pr_{2n}^{\Theta}(K,s)$, $\Pr_{2n}^{\Theta}(K,f)$, and $\Pr_{2n}^{\Theta}(K'|K,s)$ depend on n?

2. For a fixed non-trivial knot-type K, do the limiting probabilities $\lim_{n\to\infty} \Pr_{2n}^{\Theta}(K,s)$, $\lim_{n\to\infty} \Pr_{2n}^{\Theta}(K,f)$, and $\lim_{n\to\infty} \Pr_{2n}^{\Theta}(K'|K,s)$ exist, and if they exist, to what are their limiting values?

3. For any fixed knot-type K, how do the fixed-n probabilities $\Pr_{2n}^{\Theta}(K,s)$, $\Pr_{2n}^{\Theta}(K,f)$, and $\Pr_{2n}^{\Theta}(K'|K,s)$ depend on the choice of structure Θ?

4. For any fixed knot-type K, how are the fixed-n probabilities $\Pr_{2n}^{\Theta}(K,s)$, $\Pr_{2n}^{\Theta}(K,f)$, and $\Pr_{2n}^{\Theta}(K'|K,s)$ affected by implementing an off-lattice strand-passage, such as the one described by Liu *et al.* in [96]? Is the probability of a successful strand passage increased?

5. For a fixed non-trivial knot-type K, do the connective constants κ_{K}^{Θ}, $\kappa_{(K,s)}^{\Theta}$, and $\kappa_{(K'|K,s)}^{\Theta}$ exist and, if they exist, what are their values and are they equal?

Investigating each of the above open questions requires collecting the data via a computer simulation of an algorithm such as the CMC Θ-BFACF algorithm.

From the simulation (ten replications in which each replication consisted of 96 billion time-steps) of the CMC Θ-BFACF algorithm in this work, enough data was sampled from $\mathscr{P}^{\Theta}(\phi|\phi,s)$ to estimate any of the property-$(\phi|\phi,s)$ parameters presented in the thesis. For each $* \in \mathscr{K}^{\dagger}(\phi)\setminus\{(\phi|\phi,s)\}$, the number of property-$*$ Θ-SAPs sampled was not sufficient to determine good estimates for any of the property-$*$ quantities presented in the thesis. Hence in order to obtain better numerical evidence regarding the questions and conjectures presented in Chapter 2 involving property $* \in \mathscr{K}^{\dagger}(\phi)\setminus\{(\phi|\phi,s)\}$, more property $* \in \mathscr{K}^{\dagger}(\phi)\setminus\{(\phi|\phi,s)\}$ Θ-SAPs need to be sampled. Creating this larger sample is left as future work.

With regard to generating more property-$*$ Θ-SAPs, recall from Section 6.5 that the estimated limiting probability of a successful strand passage in an unknotted Θ-SAP is

$\Pr^{\Theta}(\phi, s) = 0.13719 \pm 0.00019\,(\pm 0.03240)$, which suggests that a strand passage is possible in a sufficiently large unknotted Θ-SAP only about 14% of the time. Consequently the CMC Θ-BFACF algorithm is not a very efficient algorithm for generating successful-strand-passage Θ-SAPs or any subset of these (such as a sample of property $* \in \mathscr{K}^{\dagger}(\phi)$ Θ-SAPs). Thus developing an algorithm which samples more efficiently from $\mathscr{P}^{\Theta}(\phi, s)$ is required in order to study the conjectures and questions presented in Chapter 2 which depend on property $* \in \mathscr{K}^{\dagger}(\phi) \setminus \{(\phi|\phi, s)\}$; this is left as future work. Because the expected length of a property-$*$ Θ-SAP appears to be increasing as the complexity of the property $*$ increases, an algorithm which efficiently samples large polygons also needs to be developed in order to generate a larger sample of property $* \in \mathscr{K}^{\dagger}(\phi)$ Θ-SAPs.

A third efficiency issue of the CMC Θ-BFACF algorithm to be explored in the future is in regard to the time it takes to reach the equilibrium distribution. When proposing a distribution for the probability of swapping, the distribution will depend on the frequency at which one attempts to swap two distinct chains in a CMC. If a distribution is chosen such that only a few time steps pass between attempted swaps, the swap will be accepted with a high acceptance rate, but, because very little change occurs in the states of the two chains, the convergence to the desired equilibrium distribution will be slowed. Alternatively, if a large number of time steps passes between attempted swaps, the states in the two chains will be quite different; however, the acceptance rate of the swap will be low. The optimal rate (in terms of convergence to the equilibrium distribution) at which a swap should be attempted is somewhere between these two extremes. Developing criteria for determining the optimal swapping rate would be very beneficial.

The next three future works involve making comparisons of results from the LSP Model to results presented for other models, as in [61], [96] and [36]. Recall the strand passage model of Hua *et al.* [61] described in Section 1.6. Hua *et al.'s* model for a strand passage in an unknotted self-avoiding polygon differs from the Local Strand Passage Model in several ways. Firstly, in Hua *et al.'s* model, the segments of the polygon which form a strand passage crossing site may be quite far apart in the original polygon while in the LSP Model, such polygon segments are always "close together" that is they are always a fixed distance apart. Secondly, it might not be possible to implement the strand passage in Hua *et al.'s* model in $\mathbb{Z}^3$ whereas only those strand passages that can be implemented in $\mathbb{Z}^3$ are considered in the LSP Model. A third difference between the two models is that, for the

LSP Model, for those after-strand-passage polygons whose knot-type is chiral, only right handed knots are generated; however, for the Hua *et al.* [61] algorithm, both right-handed and left-handed knots are generated. Obtaining a better understanding of these model differences and whether or not the transition knotting probability estimates obtained from the two models can be compared is future work.

Also recall from Section 1.6, that in [96], Liu *et al.* study three types of juxtapositions: a hooked juxtaposition (cf. Figure 1.18 (a); a semi-hooked juxtaposition (cf. Figure 1.18 (b)); and free juxtapositions (cf. Figure 1.19). For one of these five juxtapositions, the bottom part of Θ resembles exactly one of the segments of the juxtaposition and the top part of Θ (with the appropriate adjacent edges) is just a translate of the other segment in the juxtaposition. Hence if the structure Θ is compared to the juxtapositions studied in [96], Θ can be viewed as another juxtaposition about which a strand passage in a SAP can be implemented and the LSP Model can be used to address those questions studied in [96]. This study is to be explored as future work.

In [36], an off-lattice simulation of a freely jointed isolateral 33-edge polygon is performed in which randomly selected strands (having lengths ranging from two to eight edges) of the polygon are allowed to pass through one another via a random rotation about the line formed through the first and last vertex of the strand. For this simulation, the knot-type of the after-strand-passage polygon will not necessarily be an unknotting number one knot-type. Given each pair of knot-types K_i and K_j, the frequency of the transitions from K_i to K_j via the strand passage was recorded and then the probability of this transition was estimated. Table 8.3 summarizes the limiting transition knotting probabilities estimated via the LSP Model of this thesis (Column 2) and the fixed-n transition knotting probability of the strand passage model of Flammini *et al.* [36] (Column 3). Note that currently for a number of reasons, the estimates presented in Table 8.3 cannot be compared directly. First note that for the LSP Model, for those after-strand-passage polygons whose knot-type is chiral, only right handed knots are generated; however, for the Flammini *et al.* [36] algorithm, both right-handed and left-handed knots are generated. Adjusting the estimates to take this key difference into account is left as future work. Also, the Flammini *et al.* estimates are based on a 33-edge, off-lattice polygon. It is unknown what edge length on the lattice is comparable to 33-edge polygons in the off-lattice regime. Furthermore, extending Flammini *et al.*'s work to include larger off-lattice polygons and from

Table 8.3: The limiting transition knotting probabilities estimated using a lattice model (The Local Strand Passage Model) and the fixed-n transition knotting probabilities estimated using an off-lattice model (Flammini et al [36]).

Transition	Strand Passage Model	Flammini *et al.*
$\phi \rightarrow \phi$	0.9765	0.9457
$\phi \rightarrow 3_1^+$	0.0221	0.0227
$\phi \rightarrow 4_1$	0.0009	0.0073
$\phi \rightarrow 5_2^+$	0.00004	0.0006

these larger polygons, estimating the limiting transition probabilities is of interest and left as future work.

Appendix A

Methods Used in the Thesis

For the sake of convenience and completeness, this appendix includes the methods and calculations that are referenced and/or used in the main body of this thesis that would have had to have been looked up or calculated.

A.1 Berretti-Sokal Markov Chain Maximum Likelihood Method

In [7] a method for obtaining maximum likelihood estimates for κ (as defined by Theorem 1.3.1) and γ (where γ is the exponent in Equation (A.3)) from a Markov Chain Monte Carlo simulation consisting of several independent sample paths was proposed. The following is a summary of their method. Suppose $w_1, ..., w_T$ are self-avoiding walks distributed according to the probability mass function

$$\Pr(w_i) = \frac{z^{|w_i|}}{\sum c_n z^n}. \tag{A.1}$$

Then

$$\Pr(w : |w| = N) = \frac{c_N z^N}{\sum c_n z^n} \tag{A.2}$$

can be approximated by assuming

$$c_n \sim A_0 \mu^n n^{\gamma-1}, \tag{A.3}$$

for some constant A_0 and $\mu := e^{\kappa}$, is exact for all $N \geq N_{\min}$ where $N_{\min}$ is some cutoff value. Therefore,

$$\begin{aligned} \pi_N(\mu, \gamma, N_{\min}|z) &:= \Pr(|w| = N : N \geq N_{\min}, z) \\ &= \frac{N^{\gamma-1} (\mu z)^N}{\sum\limits_{n \geq N_{\min}} n^{\gamma-1} (\mu z)^n}. \end{aligned} \tag{A.4}$$

In order to estimate μ and γ, suppose the SAWs $w_1, ..., w_T$ are independent with respective lengths $N_1, ..., N_T$, where $N_i \geq N_{\min}$ for all $i \in \{1, .., T\}$. Then the likelihood of observing the sequence $\boldsymbol{N}_T := (N_1, ..., N_T)$ is given by

$$\begin{aligned} f_{\boldsymbol{X}_T|\boldsymbol{\Xi}}(\boldsymbol{N}_T|\mu,\gamma) &= \prod_{t=1}^{T}\prod_{i=1}^{M} \pi_N(\mu,\gamma,N_{\min}|z) \\ &= \prod_{1\leq t\leq T}\prod_{i=1}^{M} \frac{N_t^{\gamma-1}\left(\mu z_i\right)^{N_t}}{\sum\limits_{n\geq N_{\min}} n^{\gamma-1}\left(\mu z_i\right)^n} \end{aligned} \tag{A.5}$$

and maximum likelihood estimates for μ and γ can be found by simultaneously solving the equations

$$\sum_{i=1}^{M} \langle N_i \rangle_T = \sum_{i=1}^{M} \frac{\sum\limits_{n\geq N_{\min}} n n^{\gamma-1}\left(\mu z_i\right)^n}{\sum\limits_{n\geq N_{\min}} n^{\gamma-1}\left(\mu z_i\right)^n} \tag{A.6}$$

and

$$\sum_{i=1}^{M} \langle \log N_i \rangle_T = \sum_{i=1}^{M} \frac{\sum\limits_{n\geq N_{\min}} (\log n)\, n^{\gamma-1}\left(\mu z_i\right)^n}{\sum\limits_{n\geq N_{\min}} n^{\gamma-1}\left(\mu z_i\right)^n}, \tag{A.7}$$

where

$$\langle f(N_i) \rangle_T = \frac{\sum_{t=1}^{T} f(N_i^{(t)})}{T}. \tag{A.8}$$

In practice, the sample of size T is not an independent sample. The solution that Sokal and Berretti advocate is, in the error analysis, to replace T with T_i, where T_i is the number of essentially independent data points that was generated associated with fugacity z_i. Then Equations (A.6) and (A.7) become

$$\sum_{i=1}^{M} T_i \cdot \langle N_i \rangle_T = \sum_{i=1}^{M} \frac{T_i \cdot \sum\limits_{n\geq N_{\min}} n n^{\gamma-1}\left(\mu z_i\right)^n}{\sum\limits_{n\geq N_{\min}} n^{\gamma-1}\left(\mu z_i\right)^n} \tag{A.9}$$

and

$$\sum_{i=1}^{M} T_i \cdot \langle \log N_i \rangle_T = \sum_{i=1}^{M} \frac{T_i \cdot \sum\limits_{n\geq N_{\min}} (\log n)\, n^{\gamma-1}\left(\mu z_i\right)^n}{\sum\limits_{n\geq N_{\min}} n^{\gamma-1}\left(\mu z_i\right)^n}. \tag{A.10}$$

Suppose $\hat{\kappa}$ and $\hat{\gamma}$ are the maximum likelihood estimates obtained using the fore-mentioned method. If the data from the Monte Carlo simulation consists of t independent observations, $n_1, n_2, ..., n_t$, of the size of SAWs where $n_i \geq N_{\min}, i = 1, ..., t$, then $\sqrt{t}(\hat{\kappa} -$

$\kappa, \hat{\gamma} - \gamma)$ is asymptotically bivariate normal [91] with mean $(0, 0)$ and covariance matrix $S = [\mathcal{I}_{\boldsymbol{N}_T}(\kappa, \gamma)]^{-1}$ where $\mathcal{I}_{\boldsymbol{N}_T}(\kappa, \gamma)$ is the Fisher information matrix given by

$$\begin{aligned}\mathcal{I}_{\boldsymbol{N}_T}(\kappa, \gamma) &= -E \begin{bmatrix} \frac{\partial^2 \log \pi(\kappa,\gamma,N_{\min}|N)}{\partial \kappa^2} & \frac{\partial^2 \log \pi(\kappa,\gamma,N_{\min}|N)}{\partial \gamma \partial \kappa} \\ \frac{\partial^2 \log \pi(\kappa,\gamma,N_{\min}|N)}{\partial \gamma \partial \kappa} & \frac{\partial^2 \log \pi(\kappa,\gamma,N_{\min}|N)}{\partial \gamma^2} \end{bmatrix} \\ &= \begin{bmatrix} \mathrm{var}(n) & -\mathrm{cov}(n, \log n) \\ -\mathrm{cov}(n, \log n) & \mathrm{var}(\log n) \end{bmatrix}. \end{aligned} \tag{A.11}$$

Approximating $\mathcal{I}_{\boldsymbol{N}_T}(\kappa, \gamma)$ using $\hat{\kappa}$ and $\hat{\gamma}$ and assuming normality, simultaneous $(1 - \alpha) \cdot 100\%$ confidence intervals for κ and γ can be obtained by

$$\left[\hat{\kappa}(\sigma) - \sqrt{\frac{p(t-1)}{t-p} F_{p,t-p}(\alpha)} \sqrt{\frac{\hat{s}_{11}}{t}}, \hat{\kappa}(\sigma) + \sqrt{\frac{p(t-1)}{t-p} F_{p,t-p}(\alpha)} \sqrt{\frac{\hat{s}_{11}}{t}}\right] \tag{A.12}$$

and

$$\left[\hat{\gamma} - \sqrt{\frac{p(t-1)}{t-p} F_{p,t-p}(\alpha)} \sqrt{\frac{\hat{s}_{22}}{t}}, \hat{\gamma} + \sqrt{\frac{p(t-1)}{t-p} F_{p,t-p}(\alpha)} \sqrt{\frac{\hat{s}_{22}}{t}}\right] \tag{A.13}$$

where p is the number of parameters being estimated, t is the number of essentially independent data points, $F_{p,t}(\alpha)$ is the value of x for which the F-distribution, $F(x)$, with (p, t) degrees of freedom such equals α and $\hat{s}_{11}$ and $\hat{s}_{22}$ are the diagonal components of $\hat{S} := [\mathcal{I}_{\boldsymbol{N}_T}(\hat{\kappa}, \hat{\gamma})]^{-1}$ [76].

To obtain confidence intervals one replaces t in Equations (A.12) and (A.13) with $\sum_{i=1}^{M} T_i$.

Equations (A.12) and (A.13) yield estimates for the statistical error of the maximum likelihood estimates given that Equation (A.3) is valid. Clearly the maximum likelihood estimates obtained depend on the value of $N_{\min}$ chosen. Thus we can get one measure of systematic error by obtaining estimates for various values of $N_{\min}$. Another possible source of systematic error is the fact that corrections to scaling have been ignored in Equation (A.3). In order to estimate the possible systematic error due to this, consider that, for $n \geq N_{\min}$,

$$c_n \sim A_0 \mu^n (n + h)^{\gamma - 1},$$

where the constant h is included to account for possible corrections to scaling. Then

$$\begin{aligned}\pi_N(\mu, \gamma, h, N_{\min}|z) &:= \Pr(|w| = N : N \geq N_{\min}, z) \\ &= \frac{(N + h)^{\gamma - 1} (\mu z)^N}{\sum\limits_{n \geq N_{\min}} (n + h)^{\gamma - 1} (\mu z)^n}. \end{aligned} \tag{A.14}$$

For a range of values h, one can use Equation (A.14) in the right hand sides of the coupled set of Equations (A.10) and solve for estimates for μ and γ. From this set of estimates one can estimate a systematic error due to disregarding any corrections due to scaling.

A.2 Newton-Raphson's Method

The following is based on a discussion of Newton-Raphson's Method in [75]. Suppose one wishes to solve simultaneously a system of n-nonlinear equations in n unknowns. Let $x_1, ..., x_n$ be n real-valued variables, $\boldsymbol{x} = (x_1, ..., x_n)$ be a row vector consisting of the n variables, $f_1(\boldsymbol{x}), ..., f_n(\boldsymbol{x})$ be n real-valued functions, and

$$\boldsymbol{f}(\boldsymbol{x}) = \begin{bmatrix} f_1(\boldsymbol{x}) \\ \vdots \\ f_n(\boldsymbol{x}) \end{bmatrix} \tag{A.15}$$

be the column vector consisting of the n real-valued functions $f_1(\boldsymbol{x}), ..., f_n(\boldsymbol{x})$. Then the problem of simultaneously solving a system of n-nonlinear equations in n unknowns, such as the system given by Equation (5.102), reduces to finding $\boldsymbol{s} = (s_1, ..., s_n)$ such that $f_i(\boldsymbol{s}) = 0$ for all i such that $1 \leq i \leq n$. In vector format, the problem can be expressed simply as finding $\boldsymbol{s} = (s_1, ..., s_n)$ such that $\boldsymbol{f}(\boldsymbol{s}) = \boldsymbol{0}$, where $\boldsymbol{0}$ is an $(n \times 1)$-column vector consisting of all zeroes. Then, if $\boldsymbol{s}_i$ is the $(i+1)$'st approximation of $\boldsymbol{s}$, then the next approximation of $\boldsymbol{s}$, denoted $\boldsymbol{s}_{i+1}$, is given by

$$\boldsymbol{s}_{i+1} = \boldsymbol{s}_i - [\boldsymbol{J}_i(\boldsymbol{s}_i)]^{-1} \boldsymbol{f}(\boldsymbol{s}_i), \tag{A.16}$$

where

$$\boldsymbol{J}_i(\boldsymbol{s}_i) := \begin{bmatrix} \dfrac{\partial f_1(\boldsymbol{s}_i)}{\partial x_1} & \cdots & \dfrac{\partial f_1(\boldsymbol{s}_i)}{\partial x_n} \\ \vdots & \ddots & \vdots \\ \dfrac{\partial f_n(\boldsymbol{s}_i)}{\partial x_1} & \cdots & \dfrac{\partial f_n(\boldsymbol{s}_i)}{\partial x_n} \end{bmatrix}. \tag{A.17}$$

Suppose a solution to $\boldsymbol{f}(\boldsymbol{x}) = \boldsymbol{0}$ exists. Given one starts the process at some initial guess $\boldsymbol{s}_0$, the process is iterated until for some natural value j, $|f_1(\boldsymbol{s}_j)|, ..., |f_n(\boldsymbol{s}_j)|$ are all simultaneously smaller than some $\varepsilon > 0$, the desired definition of zero.

A.3 Ratio Estimates and $(1-\alpha)\times 100\%$ Confidence Intervals

For the entirety of this section, suppose $\{(X_i, Y_i), i = 1, ..., n\}$ is a sequence of independent, identically-distributed (i.i.d.) random two-dimensional vectors with $\mu_Y := \mathrm{E}[Y_i]$, $\mu_X := \mathrm{E}[X_i] \neq 0, \sigma_Y^2 := \mathrm{E}[(Y_i - \mu_Y)^2] < \infty$, $\sigma_X^2 := \mathrm{E}[(X_i - \mu_X)^2] < \infty$, and $\sigma_{X,Y}^2 := \mathrm{E}[(X_i - \mu_X)(Y_i - \mu_Y)] < \infty$, for $i = 1, ..., n$. Now define $\theta := \frac{\mu_Y}{\mu_X}$ and

$$\overline{\theta}_n := \begin{cases} \frac{\overline{Y}_n}{\overline{X}_n}, & \text{if } \overline{X}_n \neq 0 \\ 0, & \text{otherwise,} \end{cases} \tag{A.18}$$

where

$$\overline{X}_n := \frac{1}{n}\sum_{i=1}^{n} X_i \text{ and } \overline{Y}_n := \frac{1}{n}\sum_{i=1}^{n} Y_i. \tag{A.19}$$

In [35], Fishman proves the following results regarding using $\overline{\theta}_n$ to estimate θ.

Theorem A.3.1 (Fishman, 1997) *1.* $\lim_{n\to\infty} nE[\overline{\theta}_n - \theta] = \theta\left[\frac{\sigma_X^2}{\mu_X^2} - \frac{\sigma_{X,Y}^2}{\mu_X\mu_Y}\right]$, *and*
2. $\lim_{n\to\infty} nE\left[\left(\overline{\theta}_n - \theta\right)^2\right] = \theta^2\left[\frac{\sigma_X^2}{\mu_X^2} - 2\frac{\sigma_{X,Y}^2}{\mu_X\mu_Y} + \frac{\sigma_Y^2}{\mu_Y^2}\right]$.

Theorem A.3.1 reveals that $\overline{\theta}$ is a biased estimator of θ and the dominant term of the bias is

$$\frac{\theta}{n}\left[\frac{\sigma_X^2}{\mu_X^2} - \frac{\sigma_{X,Y}^2}{\mu_X\mu_Y}\right]. \tag{A.20}$$

To reduce this bias, Fishman [35] recommends using the estimator

$$\widetilde{\theta}_n := \overline{\theta}_n\left[1 + \frac{1}{n}\left(\frac{\widehat{\sigma}_{X,Y}^2}{\overline{X}_n\overline{Y}_n} - \frac{\widehat{\sigma}_X^2}{\overline{X}_n^2}\right)\right], \tag{A.21}$$

where

$$\widehat{\sigma}_X^2 := \frac{1}{n-1}\sum_{i=1}^{n}\left(X_i - \overline{X}_n\right)^2, \tag{A.22}$$

$$\widehat{\sigma}_Y^2 := \frac{1}{n-1}\sum_{i=1}^{n}\left(Y_i - \overline{Y}_n\right)^2, \tag{A.23}$$

and

$$\widehat{\sigma}_{X,Y}^2 := \frac{1}{n-1}\sum_{i=1}^{n}\left(X_i - \overline{X}_n\right)\left(Y_i - \overline{Y}_n\right). \tag{A.24}$$

Fishman's recommendation is based on the following theorem from [156].

Theorem A.3.2 (Tin, 1965) *1.* $\lim_{n\to\infty} nE[\widetilde{\theta}_n - \theta] = 0$, *and*
2. $\lim_{n\to\infty} nE\left[\left(\widetilde{\theta}_n - \theta\right)^2\right] = \theta^2\left[\frac{\sigma_X^2}{\mu_X^2} - 2\frac{\sigma_{X,Y}^2}{\mu_X\mu_Y} + \frac{\sigma_Y^2}{\mu_Y^2}\right]$.

The upshot of Theorem A.3.2 is that for sufficiently large $n, \widetilde{\theta}_n$ can be considered essentially an unbiased estimator of θ and, when $\widetilde{\theta}_n$ is compared to $\overline{\theta}_n$ in terms of variance, there is no additional cost associated with using $\widetilde{\theta}_n$, that is even though $\widetilde{\theta}_n$ is less biased than $\overline{\theta}_n$ in estimating θ, $\widetilde{\theta}_n$ does not have a larger variance than $\overline{\theta}_n$. Therefore it is preferable to use $\widetilde{\theta}_n$ as an estimator of θ and, as a consequence, the ratio estimates presented in Section 6.5 of this work will use $\widetilde{\theta}_n$ to estimate θ.

Based on Part 2 of Theorem A.3.2, an estimator of the variance of $\widetilde{\theta}_n$, that is

$$\widehat{\text{var}}(\widetilde{\theta}_n) := \frac{\widetilde{\theta}_n^2}{n}\left[\frac{\widehat{\sigma}_X^2}{\overline{X}_n^2} + \frac{\widehat{\sigma}_Y^2}{\overline{Y}_n^2} - \frac{2\widehat{\sigma}_{X,Y}^2}{\overline{X}_n\overline{Y}_n}\right]. \tag{A.25}$$

To obtain a $(1-\alpha)\%$ confidence interval for θ, define

$$V_i := Y_i - \theta X_i, i = 1, \ldots, n, \tag{A.26}$$

and

$$\overline{V}_n = \overline{Y}_n - \theta\overline{X}_n. \tag{A.27}$$

Note that $E[\overline{V}_n] = 0$,

$$\text{var}\left(\overline{V}_n\right) := E[\left(\overline{V}_n - E[\overline{V}_n]\right)^2] \quad = \quad \left(\theta^2\sigma_X^2 - 2\theta\sigma_{X,Y}^2 + \sigma_Y^2\right)/n \ , \tag{A.28}$$

$$\text{var}\left(V_i\right) \quad = \quad n\text{var}\left(\overline{V}_n\right), \tag{A.29}$$

and

$$\widehat{\text{var}}\left(V\right) := \theta^2\widehat{\sigma}_X^2 - 2\theta\widehat{\sigma}_{X,Y}^2 + \widehat{\sigma}_Y^2. \tag{A.30}$$

Since $V_1, \ldots, V_n$ are i.i.d. random variables, the Central Limit Theorem yields the result that $\overline{V}_n/\sqrt{\text{var}\left(\overline{V}_n\right)}$ has an asymptotically normal distribution with mean zero and variance one (unit normal distribution). Fishman proves that $\overline{V}_n/\sqrt{\widehat{\text{var}}\left(V\right)/n}$ also has an asymptotic unit normal distribution and, for large values of n,

$$\Pr\left[\frac{|\overline{V}_n|}{\sqrt{\widehat{\text{var}}\left(V\right)/n}} \leq c(\alpha)\right] \approx 1 - \alpha, \tag{A.31}$$

where $c(\alpha)$ is the value for which

$$(2\pi)^{-1/2}\int_{-\infty}^{c(\alpha)} e^{-z^2/2}dz = 1-\alpha/2, \text{ for } 0<\alpha<1. \tag{A.32}$$

Because

$$\Pr\left[\frac{|\overline{V}_n|}{\sqrt{\widehat{\text{var}}\,(V)/n}} \le c(\alpha)\right] = \Pr\left[|\overline{Y}_n - \theta\overline{X}_n| \le c(\alpha)\sqrt{\frac{\theta^2\widehat{\sigma}_X^2 - 2\theta\widehat{\sigma}_{X,Y}^2 + \widehat{\sigma}_Y^2}{n}}\right],$$

$$(\overline{Y}_n - \theta\overline{X}_n)^2 \le \frac{c^2(\alpha)}{n}\left(\theta^2\widehat{\sigma}_X^2 - 2\theta\widehat{\sigma}_{X,Y}^2 + \widehat{\sigma}_Y^2\right).$$

Expanding the left hand side of the above inequality and then simplifying yields the following quadratic inequality in θ:

$$\left[\overline{X}_n^2 - \frac{c^2(\alpha)}{n}\widehat{\sigma}_X^2\right]\theta^2 - 2\theta\left[\overline{X}_n\overline{Y}_n - \frac{c^2(\alpha)}{n}\widehat{\sigma}_{X,Y}^2\right] + \left[\overline{Y}_n^2 - \frac{c^2(\alpha)}{n}\widehat{\sigma}_Y^2\right] \le 0. \tag{A.33}$$

Solving the previous quadratic inequality, provided real solutions to

$$\left[\overline{X}_n^2 - \frac{c^2(\alpha)}{n}\widehat{\sigma}_X^2\right]\theta^2 - 2\theta\left[\overline{X}_n\overline{Y}_n - \frac{c^2(\alpha)}{n}\widehat{\sigma}_{X,Y}^2\right] + \left[\overline{Y}_n^2 - \frac{c^2(\alpha)}{n}\widehat{\sigma}_Y^2\right] = 0 \tag{A.34}$$

exist, yields the interval $r_1 \le \theta \le r_2$ for θ, where

$$r_1 := \frac{\overline{X}_n\overline{Y}_n - \frac{c^2(\alpha)}{n}\widehat{\sigma}_{X,Y}^2 - \sqrt{\left[\overline{X}_n\overline{Y}_n - \frac{c^2(\alpha)}{n}\widehat{\sigma}_{X,Y}^2\right]^2 - \left[\overline{X}_n^2 - \frac{c^2(\alpha)}{n}\widehat{\sigma}_X^2\right]\left[\overline{Y}_n^2 - \frac{c^2(\alpha)}{n}\widehat{\sigma}_Y^2\right]}}{\overline{X}_n^2 - \frac{c^2(\alpha)}{n}\widehat{\sigma}_X^2} \tag{A.35}$$

and

$$r_2 := \frac{\overline{X}_n\overline{Y}_n - \frac{c^2(\alpha)}{n}\widehat{\sigma}_{X,Y}^2 + \sqrt{\left[\overline{X}_n\overline{Y}_n - \frac{c^2(\alpha)}{n}\widehat{\sigma}_{X,Y}^2\right]^2 - \left[\overline{X}_n^2 - \frac{c^2(\alpha)}{n}\widehat{\sigma}_X^2\right]\left[\overline{Y}_n^2 - \frac{c^2(\alpha)}{n}\widehat{\sigma}_Y^2\right]}}{\overline{X}_n^2 - \frac{c^2(\alpha)}{n}\widehat{\sigma}_X^2}. \tag{A.36}$$

Whenever $r_1, r_2 \in \mathbb{R}$, by the definitions of r_1 and r_2, $r_1 \le r_2$. Hence, whenever $r_1, r_2 \in \mathbb{R}$, the interval $r_1 \le \theta \le r_2$ is a $(1-\alpha)\cdot 100\%$ confidence interval for θ.

A.4 Ratio Estimation Using Composite Markov Chain Data

Let θ be a parameter of interest and let X and Y be real-valued random variables defined on a state space $\mathscr{S}$ such that $\theta = \frac{\mu_Y}{\mu_X}$, where $\mu_Y := \mathrm{E}[Y]$, $\mu_X := \mathrm{E}[X] \neq 0, \sigma_Y^2 := \mathrm{E}[(Y-\mu_Y)^2] < \infty$, $\sigma_X^2 := \mathrm{E}[(X-\mu_X)^2] < \infty$, and $\sigma_{X,Y}^2 := \mathrm{E}[(X-\mu_X)(Y-\mu_Y)] < \infty$. As discussed in Section A.3 of this appendix, a $(1-\alpha)\cdot 100\%$ confidence interval for θ can be obtained via Equations (A.35) and (A.36) using an i.i.d. sequence

$((X_i, Y_i), i = 1, ..., n)$ of random two-dimensional real-valued vectors defined on $\mathscr{S}$ satisfying $\mu_Y = \mathrm{E}[Y_i]$, $\mu_X = \mathrm{E}[X_i] \neq 0, \sigma_Y^2 = \mathrm{E}[(Y_i - \mu_Y)^2] < \infty$, $\sigma_X^2 = \mathrm{E}[(X_i - \mu_X)^2] < \infty$, and $\sigma_{X,Y}^2 = \mathrm{E}[(X_i - \mu_X)(Y_i - \mu_Y)] < \infty$, for $i = 1, ..., n$. In the situation where the data available is generated from a realization of a composite Markov chain, how is such an i.i.d. set formed?

To answer this question, recall from Section 4.2.3 that

$$\mathscr{M}_n(t) := \begin{cases} 1, & \text{if } t = 0 \,(\mathrm{mod}\, n) \\ 0, & \text{otherwise,} \end{cases} \tag{A.37}$$

and

$$\mathscr{I}_{(k,l]}(x) := \begin{cases} 1, & \text{if } x \in (k, l] \\ 0, & \text{otherwise} \end{cases} . \tag{A.38}$$

Suppose $\boldsymbol{W} := ((W_t(1), W_t(2), ..., W_t(M)), t = 0, ..., t_0)$ is a composite Markov chain with state space $\mathscr{S}^M$. Then one way to create an i.i.d. sample is to subdivide the t_0 time-steps into blocks each of whose length is $2\tau_{\mathrm{int}}$ time steps and then form a set of M two-dimensional real-valued vectors from a sub-sample taken every T time steps from each block. To clarify this, for a fixed block $k \in \{1, 2, ..., \lfloor t_0/(2\tau_{\mathrm{int}}) \rfloor\}$, the sequence of M two-dimensional vectors is denoted

$$((X_{k,i}, Y_{k,i}), i = 1, .., M), \tag{A.39}$$

where

$$\begin{aligned} X_{k,i} &:= X_{k,i}(\boldsymbol{W}|T) \\ &:= \sum_{t=0}^{t_0} \mathscr{M}_T(t) \mathscr{I}_{(2(k-1)\tau_{\mathrm{int}} - 1, 2k\tau_{\mathrm{int}} - 1]}(t)\, X(W_t(i)) \end{aligned} \tag{A.40}$$

and

$$\begin{aligned} Y_{k,i} &:= Y_{k,i}(\boldsymbol{W}|T) \\ &:= \sum_{t=0}^{t_0} \mathscr{M}_T(t) \mathscr{I}_{(2(k-1)\tau_{\mathrm{int}} - 1, 2k\tau_{\mathrm{int}} - 1]}(t)\, Y(W_t(i)). \end{aligned} \tag{A.41}$$

Now define the sequences of two-dimensional vectors

$$((X_{k,\cdot}, Y_{k,\cdot}), k = 1, .., \lfloor t_0/(2\tau_{\mathrm{int}}) \rfloor) \tag{A.42}$$

and

$$((X_{\cdot,i}, Y_{\cdot,i}), i = 1, .., M) \tag{A.43}$$

using

$$\begin{aligned} X_{k,\cdot} &:= X_{k,\cdot}(\boldsymbol{W}|T) \\ &:= M^{-1}\sum_{i=1}^{M} X_{k,i}(\boldsymbol{W}|T), \end{aligned} \tag{A.44}$$

$$\begin{aligned} Y_{k,\cdot} &:= Y_{k,\cdot}(\boldsymbol{W}|T) \\ &:= M^{-1}\sum_{i=1}^{M} Y_{k,i}(\boldsymbol{W}|T), \end{aligned} \tag{A.45}$$

$$\begin{aligned} X_{\cdot,i} &:= X_{\cdot,i}(\boldsymbol{W}|T) \\ &:= \frac{1}{\lfloor t_0/(2\tau_{\text{int}})\rfloor}\sum_{k=1}^{\lfloor t_0/(2\tau_{\text{int}})\rfloor} X_{k,i}(\boldsymbol{W}|T), \end{aligned} \tag{A.46}$$

and

$$\begin{aligned} Y_{\cdot,i} &:= Y_{\cdot,i}(\boldsymbol{W}|T) \\ &:= \frac{1}{\lfloor t_0/(2\tau_{\text{int}})\rfloor}\sum_{k=1}^{\lfloor t_0/(2\tau_{\text{int}})\rfloor} Y_{k,i}(\boldsymbol{W}|T). \end{aligned} \tag{A.47}$$

Now suppose that $\boldsymbol{w}^{(r)}$, $r \in \{1, 2, ..., n_0\}$ is the r'th realization of $\boldsymbol{W}$. Let $y_{k,i}^{(r)}$ denote the realization of $Y_{k,i}$ based on $\boldsymbol{\omega}^{(r)}$. Similarly, let $x_{k,i}^{(r)}$ denote the realization of $X_{k,i}$ based on $\boldsymbol{\omega}^{(r)}$. Then $y_{k,\cdot}^{(r)}$ and $x_{k,\cdot}^{(r)}$ are the realizations of $Y_{k,\cdot}$ and $X_{k,\cdot}$, respectively, based on $\boldsymbol{\omega}^{(r)}$ and $y_{\cdot,i}^{(r)}$ and $x_{\cdot,i}^{(r)}$ are the realizations of $Y_{\cdot,i}$ and $X_{\cdot,i}$, respectively, based on $\boldsymbol{\omega}^{(r)}$. Then a point estimates for θ, that is based on Chain i, uses the sequence

$$\left(\left((x_{k,i}^{(r)}, y_{k,i}^{(r)}), k = 1, .., \lfloor t_0/(2\tau_{\text{int}})\rfloor\right), r = 1, ..., n_0\right) \tag{A.48}$$

in Equation (A.21) and a point estimate for θ, that is based on the data in all the chains, uses the sequence

$$\left(\left((x_{k,\cdot}^{(r)}, y_{k,\cdot}^{(r)}), k = 1, .., \lfloor t_0/(2\tau_{\text{int}})\rfloor\right), r = 1, ..., n_0\right) \tag{A.49}$$

in Equation (A.21).

A.5 The Fixed-n Method for Curve Fitting

Let X and Y be two random variables defined on the state space $\mathscr{S}$ such that there exists a real-valued function f for which $Y = f(X, a_1, ..., a_l)$ and $a_1, ..., a_l$ are unknown parameters. Let $F := ((x_i, y_i), i = 1, ..., n)$ represent a sequence of observations of (X, Y) Then, in order to estimate the parameters $a_1, ..., a_l$, an independent sub-sample from F is required. To this end, the minimum value k such that the points (x_i, y_i) and (x_{i+k}, y_{i+k}) are essentially independent needs to be determined using the techniques from Section 4.3. Such a "k" is referred to as the *essentially independent frequency*. With k determined, the set

$$H_1 := \bigcup_{i=1}^{t} \left\{ \left(x_{1+(i-1)k}, y_{1+(i-1)k} \right) \right\}, \tag{A.50}$$

where t is the greatest integer that satisfies $1 + (t-1)k \leq n$, is an essentially independent set consisting of t two-dimensional data points. Using weighted least-squares regression, then fitting a curve of the form $f(x, a_1, ..., a_l)$ to the data in H_1 provides estimates for the parameters $a_1, ..., a_l$.

A.6 Second Partial Derivatives for the CMC Maximum Likelihood Estimation Technique

The required derivatives of $a(\widetilde{\boldsymbol{\theta}}, \widetilde{\boldsymbol{Q}})$ with respect to $A, \kappa_s, \varepsilon_*, \alpha_{\overline{*}}, h_*$, and $h_{\overline{*}}$ respectively are

$$\begin{aligned}
\frac{\partial a}{\partial A} := {} & T' \sum_{i=1}^{M} \left\langle I_{\langle 2,3 \rangle}(N_i) \right\rangle_T \left[\frac{Q^*_{\langle 2,3 \rangle}(\beta_i)}{Q^{\overline{*}}_{\langle 2,3 \rangle}(\beta_i) + A Q^*_{\langle 2,3 \rangle}(\beta_i)} \right]^2 \\
& - T' \sum_{i=1}^{M} \left\langle I_{\langle 3 \rangle}(N_i) \right\rangle_T \left[\frac{Q^*_{\langle 3 \rangle}(\beta_i)}{Q^{\overline{*}}_{\langle 3 \rangle}(\beta_i) + A Q^*_{\langle 3 \rangle}(\beta_i)} \right]^2 \\
& - \frac{T'}{A^2} \sum_{i=1}^{M} \left\langle I_{\langle 2 \rangle}(N_i) K_i \right\rangle_T,
\end{aligned} \tag{A.51}$$

$$\begin{aligned}\frac{\partial a}{\partial \kappa_s} := & T' \sum_{i=1}^{M} \left\langle I_{\langle 2,3\rangle}(N_i)\right\rangle_T \frac{Q^*_{\langle 2,3\rangle}(\beta_i)\, \mathrm{E}^{\overline{*}}_{\langle 2,3\rangle}[n|\beta_i]}{Q^{\overline{*}}_{\langle 2,3\rangle}(\beta_i) + AQ^*_{\langle 2,3\rangle}(\beta_i)} \\ & + AT' \sum_{i=1}^{M} \left\langle I_{\langle 2,3\rangle}(N_i)\right\rangle_T \frac{Q^*_{\langle 2,3\rangle}(\beta_i)\, \mathrm{E}^{*}_{\langle 2,3\rangle}[n|\beta_i]}{Q^{\overline{*}}_{\langle 2,3\rangle}(\beta_i) + AQ^*_{\langle 2,3\rangle}(\beta_i)} \\ & - T' \sum_{i=1}^{M} \left\langle I_{\langle 3\rangle}(N_i)\right\rangle_T \frac{Q^*_{\langle 3\rangle}(\beta_i)\, \mathrm{E}^{\overline{*}}_{\langle 3\rangle}[n|\beta_i]}{Q^{\overline{*}}_{\langle 3\rangle}(\beta_i) + AQ^*_{\langle 3\rangle}(\beta_i)} \\ & - AT' \sum_{i=1}^{M} \left\langle I_{\langle 3\rangle}(N_i)\right\rangle_T \frac{Q^*_{\langle 3\rangle}(\beta_i)\, \mathrm{E}^{*}_{\langle 3\rangle}[n|\beta_i]}{Q^{\overline{*}}_{\langle 3\rangle}(\beta_i) + AQ^*_{\langle 3\rangle}(\beta_i)} \\ & + T' \sum_{i=1}^{M} \left\langle I_{\langle 3\rangle}(N_i)\right\rangle_T \mathrm{E}^{*}_{\langle 3\rangle}[n|\beta_i] \\ & - T' \sum_{i=1}^{M} \left\langle I_{\langle 2,3\rangle}(N_i)\right\rangle_T \mathrm{E}^{*}_{\langle 2,3\rangle}[n|\beta_i], \end{aligned} \tag{A.52}$$

$$\begin{aligned}\frac{\partial a}{\partial \varepsilon_*} := & T' \sum_{i=1}^{M} \left\langle I_{\langle 2,3\rangle}(N_i)\right\rangle_T \mathrm{E}^{*}_{\langle 2,3\rangle}[\log(n+h_*)|\beta_i] \\ & - T' \sum_{i=1}^{M} \left\langle I_{\langle 3\rangle}(N_i)\right\rangle_T \mathrm{E}^{*}_{\langle 3\rangle}[\log(n+h_*)|\beta_i] \\ & + AT' \sum_{i=1}^{M} \left\langle I_{\langle 3\rangle}(N_i)\right\rangle_T \frac{Q^*_{\langle 3\rangle}(\beta_i)\, \mathrm{E}^{*}_{\langle 3\rangle}[\log(n+h_*)|\beta_i]}{Q^{\overline{*}}_{\langle 3\rangle}(\beta_i) + AQ^*_{\langle 3\rangle}(\beta_i)} \\ & - AT' \sum_{i=1}^{M} \left\langle I_{\langle 2,3\rangle}(N_i)\right\rangle_T \frac{Q^*_{\langle 2,3\rangle}(\beta_i)\, \mathrm{E}^{*}_{\langle 2,3\rangle}[\log(n+h_*)|\beta_i]}{Q^{\overline{*}}_{\langle 2,3\rangle}(\beta_i) + AQ^*_{\langle 2,3\rangle}(\beta_i)}, \end{aligned} \tag{A.53}$$

$$\begin{aligned}\frac{\partial a}{\partial \alpha_{\overline{*}}} := & T' \sum_{i=1}^{M} \left\langle I_{\langle 2,3\rangle}(N_i)\right\rangle_T \frac{Q^*_{\langle 2,3\rangle}(\beta_i)\, \mathrm{E}^{\overline{*}}_{\langle 2,3\rangle}[\log(n+h_{\overline{*}})|\beta_i]}{Q^{\overline{*}}_{\langle 2,3\rangle}(\beta_i) + AQ^*_{\langle 2,3\rangle}(\beta_i)} \\ & - T' \sum_{i=1}^{M} \left\langle I_{\langle 3\rangle}(N_i)\right\rangle_T \frac{Q^*_{\langle 3\rangle}(\beta_i)\, \mathrm{E}^{\overline{*}}_{\langle 3\rangle}[\log(n+h_{\overline{*}})|\beta_i]}{Q^{\overline{*}}_{\langle 3\rangle}(\beta_i) + AQ^*_{\langle 3\rangle}(\beta_i)} \\ & - \frac{\partial a}{\partial \varepsilon_*}, \end{aligned} \tag{A.54}$$

$$\begin{aligned}\frac{\partial a}{\partial h_*} := (\alpha_{\overline{*}} - \varepsilon_*)\, AT' \sum_{i=1}^{M} \left\langle I_{\langle 2,3\rangle}(N_i)\right\rangle_T \frac{Q^*_{\langle 2,3\rangle}(\beta_i)\, \mathrm{E}^*_{\langle 2,3\rangle}\left[(n+h_*)^{-1}\,|\beta_i\right]}{Q^{\overline{*}}_{\langle 2,3\rangle}(\beta_i) + AQ^*_{\langle 2,3\rangle}(\beta_i)} \\ - (\alpha_{\overline{*}} - \varepsilon_*)\, AT' \sum_{i=1}^{M} \left\langle I_{\langle 3\rangle}(N_i)\right\rangle_T \frac{Q^*_{\langle 3\rangle}(\beta_i)\, \mathrm{E}^*_{\langle 3\rangle}\left[(n+h_*)^{-1}\,|\beta_i\right]}{Q^{\overline{*}}_{\langle 3\rangle}(\beta_i) + AQ^*_{\langle 3\rangle}(\beta_i)} \\ + (\alpha_{\overline{*}} - \varepsilon_*)\, T' \sum_{i=1}^{M} \left\langle I_{\langle 3\rangle}(N_i)\right\rangle_T \mathrm{E}^*_{\langle 3\rangle}\left[(n+h_*)^{-1}|\beta_i\right] \\ - (\alpha_{\overline{*}} - \varepsilon_*)\, T' \sum_{i=1}^{M} \left\langle I_{\langle 2,3\rangle}(N_i)\right\rangle_T \mathrm{E}^*_{\langle 2,3\rangle}\left[(n+h_*)^{-1}|\beta_i\right], \end{aligned} \tag{A.55}$$

and

$$\begin{aligned}\frac{\partial a}{\partial h_{\overline{*}}} := \alpha_{\overline{*}} T' \sum_{i=1}^{M} \left\langle I_{\langle 2,3\rangle}(N_i)\right\rangle_T \frac{Q^*_{\langle 2,3\rangle}(\beta_i)\, \mathrm{E}^{\overline{*}}_{\langle 2,3\rangle}\left[(n+h_{\overline{*}})^{-1}\,|\beta_i\right]}{Q^{\overline{*}}_{\langle 2,3\rangle}(\beta_i) + AQ^*_{\langle 2,3\rangle}(\beta_i)} \\ - \alpha_{\overline{*}} T' \sum_{i=1}^{M} \left\langle I_{\langle 3\rangle}(N_i)\right\rangle_T \frac{Q^*_{\langle 3\rangle}(\beta_i)\, \mathrm{E}^{\overline{*}}_{\langle 3\rangle}\left[(n+h_{\overline{*}})^{-1}\,|\beta_i\right]}{Q^{\overline{*}}_{\langle 3\rangle}(\beta_i) + AQ^*_{\langle 3\rangle}(\beta_i)}. \end{aligned} \tag{A.56}$$

The required derivatives of $g(\widetilde{\boldsymbol{\theta}},\widetilde{\boldsymbol{Q}})$ with respect to $A, \kappa_s, \varepsilon_*, \alpha_{\overline{*}}, h_*$, and $h_{\overline{*}}$ respectively are

$$\frac{\partial g}{\partial A} := \frac{\partial a}{\partial \kappa_s}, \tag{A.57}$$

$$\begin{aligned}\frac{\partial g}{\partial \kappa_s} := T' \sum_{i=1}^{M} \left\langle I_{\langle 3\rangle}(N_i)\right\rangle_T \left[\mathrm{var}^*_{\langle 3\rangle}[n|\beta_i] + \mathrm{var}^{\overline{*}}_{\langle 3\rangle}[n|\beta_i]\right] \\ - 2AT' \sum_{i=1}^{M} \left\langle I_{\langle 3\rangle}(N_i)\right\rangle_T \mathrm{E}^*_{\langle 3\rangle}[n|\beta_i]\, \mathrm{E}^{\overline{*}}_{\langle 3\rangle}[n|\beta_i] \\ - T' \sum_{i=1}^{M} \left\langle I_{\langle 2,3\rangle}(N_i)\right\rangle_T \left[\mathrm{var}^*_{\langle 2,3\rangle}[n|\beta_i] + \mathrm{var}^{\overline{*}}_{\langle 2,3\rangle}[n|\beta_i]\right] \\ + 2AT' \sum_{i=1}^{M} \left\langle I_{\langle 2,3\rangle}(N_i)\right\rangle_T \mathrm{E}^*_{\langle 2,3\rangle}[n|\beta_i]\, \mathrm{E}^{\overline{*}}_{\langle 2,3\rangle}[n|\beta_i], \end{aligned} \tag{A.58}$$

$$\begin{aligned}\frac{\partial g}{\partial \varepsilon_*} := T' \sum_{i=1}^{M} \left\langle I_{\langle 2,3\rangle}(N_i)\right\rangle_T \mathrm{Cov}^*_{\langle 2,3\rangle}[n, \log(n+h_*)|\beta_i] \\ - AT' \sum_{i=1}^{M} \left\langle I_{\langle 2,3\rangle}(N_i)\right\rangle_T \mathrm{E}^*_{\langle 2,3\rangle}[\log(n+h_*)|\beta_i]\, \mathrm{E}^{\overline{*}}_{\langle 2,3\rangle}[n|\beta_i] \\ - T' \sum_{i=1}^{M} \left\langle I_{\langle 3\rangle}(N_i)\right\rangle_T \mathrm{Cov}^*_{\langle 3\rangle}[n, \log(n+h_*)|\beta_i] \\ + AT' \sum_{i=1}^{M} \left\langle I_{\langle 3\rangle}(N_i)\right\rangle_T \mathrm{E}^*_{\langle 3\rangle}[\log(n+h_*)|\beta_i]\, \mathrm{E}^{\overline{*}}_{\langle 3\rangle}[n|\beta_i], \end{aligned} \tag{A.59}$$

$$
\begin{aligned}
\frac{\partial g}{\partial \alpha_{\overline{*}}} := & -\frac{\partial g}{\partial \varepsilon_*} \\
& - T' \sum_{i=1}^{M} \left\langle I_{\langle 2,3\rangle}(N_i) \right\rangle_T \mathrm{Cov}^{\overline{*}}_{\langle 2,3\rangle} \left[n, \log(n + h_{\overline{*}}) | \beta_i \right] \\
& + AT' \sum_{i=1}^{M} \left\langle I_{\langle 2,3\rangle}(N_i) \right\rangle_T \mathrm{E}^{*}_{\langle 2,3\rangle} \left[n | \beta_i \right] \mathrm{E}^{\overline{*}}_{\langle 2,3\rangle} \left[\log(n + h_{\overline{*}}) | \beta_i \right] \\
& + T' \sum_{i=1}^{M} \left\langle I_{\langle 3\rangle}(N_i) \right\rangle_T \mathrm{Cov}^{\overline{*}}_{\langle 3\rangle} \left[n, \log(n + h_{\overline{*}}) | \beta_i \right] \\
& - AT' \sum_{i=1}^{M} \left\langle I_{\langle 3\rangle}(N_i) \right\rangle_T \mathrm{E}^{*}_{\langle 3\rangle} \left[n | \beta_i \right] \mathrm{E}^{\overline{*}}_{\langle 3\rangle} \left[\log(n + h_{\overline{*}}) | \beta_i \right], \qquad \text{(A.60)}
\end{aligned}
$$

$$
\begin{aligned}
\frac{\partial g}{\partial h_*} := & \left(\alpha_{\overline{*}} - \varepsilon_* \right) T' \sum_{i=1}^{M} \left\langle I_{\langle 3\rangle}(N_i) \right\rangle_T \mathrm{Cov}^{*}_{\langle 3\rangle} \left[n, (n + h_*)^{-1} | \beta_i \right] \\
& - \left(\alpha_{\overline{*}} - \varepsilon_* \right) AT' \sum_{i=1}^{M} \left\langle I_{\langle 3\rangle}(N_i) \right\rangle_T \mathrm{E}^{*}_{\langle 3\rangle} \left[(n + h_*)^{-1} | \beta_i \right] \mathrm{E}^{\overline{*}}_{\langle 3\rangle} \left[n | \beta_i \right] \\
& + \left(\alpha_{\overline{*}} - \varepsilon_* \right) AT' \sum_{i=1}^{M} \left\langle I_{\langle 2,3\rangle}(N_i) \right\rangle_T \mathrm{E}^{*}_{\langle 2,3\rangle} \left[(n + h_*)^{-1} | \beta_i \right] \mathrm{E}^{\overline{*}}_{\langle 2,3\rangle} \left[n | \beta_i \right] \\
& - \left(\alpha_{\overline{*}} - \varepsilon_* \right) T' \sum_{i=1}^{M} \left\langle I_{\langle 2,3\rangle}(N_i) \right\rangle_T \mathrm{Cov}^{*}_{\langle 2,3\rangle} \left[n, (n + h_*)^{-1} | \beta_i \right], \qquad \text{(A.61)}
\end{aligned}
$$

and

$$
\begin{aligned}
\frac{\partial g}{\partial h_{\overline{*}}} := & \alpha_{\overline{*}} AT' \sum_{i=1}^{M} \left\langle I_{\langle 2,3\rangle}(N_i) \right\rangle_T \mathrm{E}^{*}_{\langle 2,3\rangle} \left[n | \beta_i \right] \mathrm{E}^{\overline{*}}_{\langle 2,3\rangle} \left[(n + h_{\overline{*}})^{-1} | \beta_i \right] \\
& - \alpha_{\overline{*}} T' \sum_{i=1}^{M} \left\langle I_{\langle 2,3\rangle}(N_i) \right\rangle_T \mathrm{Cov}^{\overline{*}}_{\langle 2,3\rangle} \left[n, (n + h_{\overline{*}})^{-1} | \beta_i \right] \\
& - \alpha_{\overline{*}} AT' \sum_{i=1}^{M} \left\langle I_{\langle 3\rangle}(N_i) \right\rangle_T \mathrm{E}^{*}_{\langle 3\rangle} \left[n | \beta_i \right] \mathrm{E}^{\overline{*}}_{\langle 3\rangle} \left[(n + h_{\overline{*}})^{-1} | \beta_i \right] \\
& + \alpha_{\overline{*}} T' \sum_{i=1}^{M} \left\langle I_{\langle 3\rangle}(N_i) \right\rangle_T \mathrm{Cov}^{\overline{*}}_{\langle 3\rangle} \left[n, (n + h_{\overline{*}})^{-1} | \beta_i \right]. \qquad \text{(A.62)}
\end{aligned}
$$

The required derivatives of $r(\widetilde{\boldsymbol{\theta}}, \widetilde{\boldsymbol{Q}})$ with respect to $A, \kappa_s, \varepsilon_*, \alpha_{\overline{*}}, h_*$, and $h_{\overline{*}}$ respectively are

$$
\frac{\partial r}{\partial A} := \frac{\partial a}{\partial \varepsilon_*}, \qquad \text{(A.63)}
$$

$$
\frac{\partial r}{\partial \kappa_s} := \frac{\partial g}{\partial \varepsilon_*}, \qquad \text{(A.64)}
$$

$$\frac{\partial r}{\partial \varepsilon_*} := T' \sum_{i=1}^{M} \left\langle I_{\langle 3\rangle}(N_i) \right\rangle_T \operatorname{var}^*_{\langle 3\rangle} \left[\log\left(n + h_*\right) | \beta_i\right] - T' \sum_{i=1}^{M} \left\langle I_{\langle 2,3\rangle}(N_i) \right\rangle_T \operatorname{var}^*_{\langle 2,3\rangle} \left[\log\left(n + h_*\right) | \beta_i\right], \tag{A.65}$$

$$\begin{aligned}\frac{\partial r}{\partial \alpha_{\overline{*}}} := & -\frac{\partial r}{\partial \varepsilon_*} \\ & + AT' \sum_{i=1}^{M} \left\langle I_{\langle 3\rangle}(N_i) \right\rangle_T \mathrm{E}^*_{\langle 3\rangle} \left[\log\left(n + h_*\right) | \beta_i\right] \mathrm{E}^{\overline{*}}_{\langle 3\rangle} \left[\log(n + h_{\overline{*}}) | \beta_i\right] \\ & - AT' \sum_{i=1}^{M} \left\langle I_{\langle 2,3\rangle}(N_i) \right\rangle_T \mathrm{E}^*_{\langle 2,3\rangle} \left[\log\left(n + h_*\right) | \beta_i\right] \mathrm{E}^{\overline{*}}_{\langle 2,3\rangle} \left[\log(n + h_{\overline{*}}) | \beta_i\right],\end{aligned} \tag{A.66}$$

$$\begin{aligned}\frac{\partial r}{\partial h_*} := & -T' \sum_{i=1}^{M} \left\langle \frac{I_{\langle 2\rangle}(N_i) K_i}{N_i + h_*} \right\rangle_T \\ & - \left(\alpha_{\overline{*}} - \varepsilon_*\right) T' \sum_{i=1}^{M} \left\langle I_{\langle 3\rangle}(N_i) \right\rangle_T \operatorname{Cov}^*_{\langle 3\rangle} \left[\log\left(n + h_*\right), (n + h_*)^{-1} | \beta_i\right] \\ & - AT' \sum_{i=1}^{M} \left\langle I_{\langle 3\rangle}(N_i) \right\rangle_T \mathrm{E}^*_{\langle 3\rangle} \left[(n + h_*)^{-1} | \beta_i\right] \\ & + AT' \sum_{i=1}^{M} \left\langle I_{\langle 2,3\rangle}(N_i) \right\rangle_T \mathrm{E}^*_{\langle 2,3\rangle} \left[(n + h_*)^{-1} | \beta_i\right] \\ & + \left(\alpha_{\overline{*}} - \varepsilon_*\right) T' \sum_{i=1}^{M} \left\langle I_{\langle 2,3\rangle}(N_i) \right\rangle_T \operatorname{Cov}^*_{\langle 2,3\rangle} \left[\log\left(n + h_*\right), (n + h_*)^{-1} | \beta_i\right],\end{aligned} \tag{A.67}$$

and

$$\begin{aligned}\frac{\partial r}{\partial h_{\overline{*}}} := & \alpha_{\overline{*}} AT' \sum_{i=1}^{M} \left\langle I_{\langle 3\rangle}(N_i) \right\rangle_T \mathrm{E}^*_{\langle 3\rangle} \left[\log\left(n + h_*\right) | \beta_i\right] \mathrm{E}^{\overline{*}}_{\langle 3\rangle} \left[(n + h_{\overline{*}})^{-1} | \beta_i\right] \\ & - \alpha_{\overline{*}} AT' \sum_{i=1}^{M} \left\langle I_{\langle 2,3\rangle}(N_i) \right\rangle_T \mathrm{E}^*_{\langle 2,3\rangle} \left[\log\left(n + h_*\right) | \beta_i\right] \mathrm{E}^{\overline{*}}_{\langle 2,3\rangle} \left[(n + h_{\overline{*}})^{-1} | \beta_i\right].\end{aligned}$$

The required derivatives of $f(\widetilde{\boldsymbol{\theta}}, \widetilde{\boldsymbol{Q}})$ with respect to $A, \kappa_s, \varepsilon_*, \alpha_{\overline{*}}, h_*$, and $h_{\overline{*}}$ respectively are

$$\frac{\partial f}{\partial A} := \frac{\partial a}{\partial \alpha_{\overline{*}}}, \tag{A.68}$$

$$\frac{\partial f}{\partial \kappa_s} := \frac{\partial g}{\partial \alpha_{\overline{*}}}, \tag{A.69}$$

$$\frac{\partial f}{\partial \varepsilon_*} := \frac{\partial r}{\partial \alpha_{\overline{*}}}, \tag{A.70}$$

$$\begin{aligned}\frac{\partial f}{\partial \alpha_{\overline{*}}} := &-\frac{\partial r}{\partial \alpha_{\overline{*}}} + T' \sum_{i=1}^{M} \left\langle I_{\langle 3\rangle}(N_i)\right\rangle_T \operatorname{var}^{\overline{*}}_{\langle 3\rangle}\left[\log\left(n+h_{\overline{*}}\right)|\beta_i\right] \\ &- AT' \sum_{i=1}^{M} \left\langle I_{\langle 3\rangle}(N_i)\right\rangle_T \mathrm{E}^{*}_{\langle 3\rangle}\left[\log\left(n+h_{*}\right)|\beta_i\right] \mathrm{E}^{\overline{*}}_{\langle 3\rangle}\left[\log\left(n+h_{\overline{*}}\right)|\beta_i\right] \\ &- T' \sum_{i=1}^{M} \left\langle I_{\langle 2,3\rangle}(N_i)\right\rangle_T \operatorname{var}^{\overline{*}}_{\langle 2,3\rangle}\left[\log\left(n+h_{\overline{*}}\right)|\beta_i\right] \\ &+ AT' \sum_{i=1}^{M} \left\langle I_{\langle 2,3\rangle}(N_i)\right\rangle_T \mathrm{E}^{*}_{\langle 2,3\rangle}\left[\log\left(n+h_{*}\right)|\beta_i\right] \mathrm{E}^{\overline{*}}_{\langle 2,3\rangle}\left[\log\left(n+h_{\overline{*}}\right)|\beta_i\right], \end{aligned} \tag{A.71}$$

$$\begin{aligned}\frac{\partial f}{\partial h_{*}} := &-\frac{\partial r}{\partial h_{*}} \\ &- \left(\alpha_{\overline{*}} - \varepsilon_{*}\right) AT' \sum_{i=1}^{M} \left\langle I_{\langle 3\rangle}(N_i)\right\rangle_T \mathrm{E}^{*}_{\langle 3\rangle}\left[\left(n+h_{*}\right)^{-1}|\beta_i\right] \mathrm{E}^{\overline{*}}_{\langle 3\rangle}\left[\log\left(n+h_{\overline{*}}\right)|\beta_i\right] \\ &+ \left(\alpha_{\overline{*}} - \varepsilon_{*}\right) AT' \sum_{i=1}^{M} \left\langle I_{\langle 2,3\rangle}(N_i)\right\rangle_T \mathrm{E}^{*}_{\langle 2,3\rangle}\left[\left(n+h_{*}\right)^{-1}|\beta_i\right] \mathrm{E}^{\overline{*}}_{\langle 2,3\rangle}\left[\log\left(n+h_{\overline{*}}\right)|\beta_i\right], \end{aligned} \tag{A.72}$$

and

$$\begin{aligned}\frac{\partial f}{\partial h_{\overline{*}}} := &-\frac{\partial r}{\partial h_{\overline{*}}} \\ &+ T' \sum_{i=1}^{M} \left\langle \frac{I_{\langle 2\rangle}(N_i)\left[1-K_i\right]}{N_i + h_{\overline{*}}} \right\rangle_T \\ &+ T' \sum_{i=1}^{M} \left\langle I_{\langle 3\rangle}(N_i)\right\rangle_T \mathrm{E}^{\overline{*}}_{\langle 3\rangle}\left[\left(n+h_{\overline{*}}\right)^{-1}|\beta_i\right] \\ &+ \alpha_{\overline{*}} T' \sum_{i=1}^{M} \left\langle I_{\langle 3\rangle}(N_i)\right\rangle_T \operatorname{Cov}^{\overline{*}}_{\langle 3\rangle}\left[\log\left(n+h_{\overline{*}}\right), \left(n+h_{\overline{*}}\right)^{-1}|\beta_i\right] \\ &- T' \sum_{i=1}^{M} \left\langle I_{\langle 2,3\rangle}(N_i)\right\rangle_T \mathrm{E}^{\overline{*}}_{\langle 2,3\rangle}\left[\left(n+h_{\overline{*}}\right)^{-1}|\beta_i\right] \\ &- \alpha_{\overline{*}} T' \sum_{i=1}^{M} \left\langle I_{\langle 2,3\rangle}(N_i)\right\rangle_T \operatorname{Cov}^{\overline{*}}_{\langle 2,3\rangle}\left[\log\left(n+h_{\overline{*}}\right), \left(n+h_{\overline{*}}\right)^{-1}|\beta_i\right]. \end{aligned} \tag{A.73}$$

The required derivatives of $\hbar_{*}(\widetilde{\boldsymbol{\theta}},\widetilde{\boldsymbol{Q}})$ with respect to $A, \kappa_s, \varepsilon_{*}, \alpha_{\overline{*}}, h_{*}$, and $h_{\overline{*}}$ respectively are

$$\frac{\partial \hbar_{*}}{\partial A} := \frac{\partial a}{\partial h_{*}}, \tag{A.74}$$

$$\frac{\partial \hbar_{*}}{\partial \kappa_s} := \frac{\partial g}{\partial h_{*}}, \tag{A.75}$$

$$\frac{\partial \hbar_*}{\partial \varepsilon_*} := \frac{\partial r}{\partial h_*}, \tag{A.76}$$

$$\frac{\partial \hbar_*}{\partial \alpha_{\overline{*}}} := \frac{\partial f}{\partial h_*}, \tag{A.77}$$

$$\begin{aligned}
\frac{\partial \hbar_*}{\partial h_*} := & -\left(\alpha_{\overline{*}} - \varepsilon_*\right) T' \sum_{i=1}^{M} \left\langle \frac{I_{\langle 2\rangle}(N_i)\left[1 - K_i\right]}{\left[N_i + h_*\right]^2} \right\rangle_T \\
& + \left(\alpha_{\overline{*}} - \varepsilon_*\right)\left(\alpha_{\overline{*}} - \varepsilon_* - 1\right) AT' \sum_{i=1}^{M} \left\langle I_{\langle 3\rangle}(N_i)\right\rangle_T \mathrm{E}^*_{\langle 3\rangle}\left[(n+h_*)^{-2}\,|\beta_i\right] \\
& - \left(\alpha_{\overline{*}} - \varepsilon_*\right)^2 T' \sum_{i=1}^{M} \left\langle I_{\langle 3\rangle}(N_i)\right\rangle_T \left[A\,\mathrm{E}^*_{\langle 3\rangle}\left[(n+h_*)^{-1}|\beta_i\right]\right]^2 \\
& - \left(\alpha_{\overline{*}} - \varepsilon_*\right)\left(\alpha_{\overline{*}} - \varepsilon_* - 1\right) AT' \sum_{i=1}^{M} \left\langle I_{\langle 2,3\rangle}(N_i)\right\rangle_T \mathrm{E}^*_{\langle 2,3\rangle}\left[(n+h_*)^{-2}|\beta_i\right] \\
& + \left(\alpha_{\overline{*}} - \varepsilon_*\right)^2 T' \sum_{i=1}^{M} \left\langle I_{\langle 2,3\rangle}(N_i)\right\rangle_T \left[A\,\mathrm{E}^*_{\langle 2,3\rangle}\left[(n+h_*)^{-1}|\beta_i\right]\right]^2,
\end{aligned} \tag{A.78}$$

and

$$\begin{aligned}
\frac{\partial \hbar_*}{\partial h_{\overline{*}}} := & \,\alpha_{\overline{*}}\left(\alpha_{\overline{*}} - \varepsilon_*\right) AT' \sum_{i=1}^{M} \left\langle I_{\langle 2,3\rangle}(N_i)\right\rangle_T \mathrm{E}^*_{\langle 2,3\rangle}\left[(n+h_*)^{-1}\,|\beta_i\right] \mathrm{E}^{\overline{*}}_{\langle 2,3\rangle}\left[(n+h_{\overline{*}})^{-1}\,|\beta_i\right] \\
& - \alpha_{\overline{*}}\left(\alpha_{\overline{*}} - \varepsilon_*\right) AT' \sum_{i=1}^{M} \left\langle I_{\langle 3\rangle}(N_i)\right\rangle_T \mathrm{E}^*_{\langle 3\rangle}\left[(n+h_*)^{-1}\,|\beta_i\right] \mathrm{E}^{\overline{*}}_{\langle 3\rangle}\left[(n+h_{\overline{*}})^{-1}\,|\beta_i\right].
\end{aligned} \tag{A.79}$$

The required derivatives of $\hbar_{\overline{*}}(\widetilde{\boldsymbol{\theta}},\widetilde{\boldsymbol{Q}})$ with respect to $A, \kappa_s, \varepsilon_*, \alpha_{\overline{*}}, h_*$, and $h_{\overline{*}}$ respectively are

$$\frac{\partial \hbar_{\overline{*}}}{\partial A} := \frac{\partial a}{\partial h_{\overline{*}}}, \tag{A.80}$$

$$\frac{\partial \hbar_{\overline{*}}}{\partial \kappa_s} := \frac{\partial g}{\partial h_{\overline{*}}}, \tag{A.81}$$

$$\frac{\partial \hbar_{\overline{*}}}{\partial \varepsilon_*} := \frac{\partial r}{\partial h_{\overline{*}}}, \tag{A.82}$$

$$\frac{\partial \hbar_{\overline{*}}}{\partial \alpha_{\overline{*}}} := \frac{\partial f}{\partial h_{\overline{*}}}, \tag{A.83}$$

$$\frac{\partial \hbar_{\overline{*}}}{\partial h_*} := \frac{\partial \hbar_*}{\partial h_{\overline{*}}}, \tag{A.84}$$

and

$$\begin{aligned}\frac{\partial \hbar_{\overline{*}}}{\partial h_{\overline{*}}} := & -\alpha_{\overline{*}} T' \sum_{i=1}^{M} \left\langle \frac{I_{\langle 2\rangle}(N_i)\left[1-K_i\right]}{\left[N_i+h_{\overline{*}}\right]^2} \right\rangle_T \\ & + \alpha_{\overline{*}}\left(\alpha_{\overline{*}}-1\right) T' \sum_{i=1}^{M} \left\langle I_{\langle 3\rangle}(N_i)\right\rangle_T \mathrm{E}^{\overline{*}}_{\langle 3\rangle}\left[(n+h_{\overline{*}})^{-2}\,|\beta_i\right] \\ & - \left(\alpha_{\overline{*}}\right)^2 T' \sum_{i=1}^{M} \left\langle I_{\langle 3\rangle}(N_i)\right\rangle_T \left[\mathrm{E}^{\overline{*}}_{\langle 3\rangle}\left[(n+h_{\overline{*}})^{-1}|\beta_i\right]\right]^2 \\ & - \left(\alpha_{\overline{*}}\right)\left(\alpha_{\overline{*}}-1\right) T' \sum_{i=1}^{M} \left\langle I_{\langle 2,3\rangle}(N_i)\right\rangle_T \mathrm{E}^{\overline{*}}_{\langle 2,3\rangle}\left[(n+h_{\overline{*}})^{-2}|\beta_i\right] \\ & + \left(\alpha_{\overline{*}}\right)^2 T' \sum_{i=1}^{M} \left\langle I_{\langle 2,3\rangle}(N_i)\right\rangle_T \left[\mathrm{E}^{\overline{*}}_{\langle 2,3\rangle}\left[(n+h_{\overline{*}})^{-1}|\beta_i\right]\right]^2. \end{aligned} \tag{A.85}$$

Appendix B

Essentially Independent Data

In this appendix, tables of data that are generated using the methods discussed in Chapters 6 and 7 are provided.

B.1 Probability Estimates

B.1.1 Fixed-n Estimates

Tables B.1-B.5 contain essentially independent samples of the fixed-n probability estimates (from several replications) that were discussed in Chapter 6. The value t' in each of these tables is the number of non-zero blocks of data available to compute the point estimate and the estimated 95% margin of error. Tables B.1, B.2, B.3, B.4, and B.5 respectively display an essentially independent sample of the fixed-n point estimates $\widetilde{\mathrm{pr}}_{2n}^{\Theta}(\phi, s)$, $\widetilde{\mathrm{pr}}_{2n}^{\Theta}(\phi|\phi, s)$, $\widetilde{\mathrm{pr}}_{2n}^{\Theta}(3_1|\phi, s)$, $\widetilde{\mathrm{pr}}_{2n}^{\Theta}(4_1|\phi, s)$, and $\widetilde{\mathrm{pr}}_{2n}^{\Theta}(5_2|\phi, s)$ and their corresponding estimated 95% margins of error.

Note that the point estimates and the estimated 95% margins of error presented in Tables B.1-B.5 were computed using the point estimators $\widehat{\mathrm{Pr}}_{2n}^{\Theta}(\phi, s)$ and $\widehat{\mathrm{Pr}}_{2n}^{\Theta}(*)$, for $* \in \mathscr{K}^{\dagger}(\phi)$, defined with $t_0 = 9.6 \times 10^{10}$ time steps, $\tau_{\mathrm{int}} = 0.72 \times 10^{9}$ time steps, $T = 1200$ time steps, $l := 66$, and the data generated in each of the ten replications. Refer to Section 6.2.2 for a detailed discussion on how the estimates were precisely determined.

B.1.2 Grouped-n Estimates

Tables B.6-B.10 contain essentially independent samples of the grouped-n probability estimates that were used in the estimation of the limiting strand passage probabilities in Section 6.5 of Chapter 6. The value t' in each of these tables is the number of non-zero blocks of data available to compute the point estimate and the estimated 95% margin of error. Tables B.6, B.7, B.8, B.9, and B.10 respectively display the essentially independent

Table B.1: The fixed-n estimates for the probability of a successful strand passage. The values in parentheses are the estimated 95% margins of error.

$2n$	t'	$\widetilde{\mathrm{pr}}^{\Theta}_{2n}(\phi, s)$	$2n$	t'	$\widetilde{\mathrm{pr}}^{\Theta}_{2n}(\phi, s)$
112	660	0.135508(0.014146)	1012	660	0.137143(0.014548)
212	660	0.136592(0.015384)	1112	660	0.137149(0.015265)
312	660	0.136870(0.015151)	1212	660	0.137155(0.014460)
412	660	0.136986(0.014867)	1312	660	0.137159(0.014687)
512	660	0.137047(0.014545)	1412	660	0.137162(0.014825)
612	660	0.137083(0.014652)	1512	660	0.137165(0.015163)
712	660	0.137106(0.014547)	1612	660	0.137168(0.014663)
812	660	0.137122(0.014404)	1712	660	0.137170(0.015009)
912	660	0.137134(0.013833)	1812	660	0.137172(0.015263)

Table B.2: The fixed-n estimates for the probability of the unknot given a successful strand passage in a Θ-SAP. The values in parentheses are the estimated 95% margins of error.

$2n$	t'	$\widetilde{\mathrm{pr}}^{\Theta}_{2n}(\phi \vert \phi, s)$	$2n$	t'	$\widetilde{\mathrm{pr}}^{\Theta}_{2n}(\phi \vert \phi, s)$
112	660	0.986131(0.012633)	1012	660	0.978092(0.015912)
212	660	0.980421(0.014943)	1112	660	0.977809(0.016067)
312	660	0.978606(0.015604)	1212	660	0.978389(0.015949)
412	660	0.977429(0.016019)	1312	660	0.977526(0.016301)
512	660	0.977494(0.016004)	1412	660	0.978092(0.016110)
612	660	0.977285(0.016087)	1512	660	0.978297(0.016323)
712	660	0.977301(0.016076)	1612	660	0.978202(0.016572)
812	660	0.976972(0.016210)	1712	660	0.977031(0.017463)
912	660	0.977656(0.015996)	1812	660	0.977811(0.017279)

Table B.3: The fixed-n estimates for the probability of the trefoil given a successful strand passage in a Θ-SAP. The values in parentheses are the estimated 95% margins of error.

$2n$	t'	$\widetilde{\mathrm{pr}}^{\Theta}_{2n}(3_1\|\phi, s)$	$2n$	t'	$\widetilde{\mathrm{pr}}^{\Theta}_{2n}(3_1\|\phi, s)$
112	660	0.013693(0.001532)	1012	660	0.021166(0.002552)
212	660	0.019099(0.002136)	1112	660	0.021390(0.002608)
312	660	0.020735(0.002326)	1212	660	0.020823(0.002617)
412	660	0.021836(0.002458)	1312	660	0.021870(0.002792)
512	660	0.021678(0.002456)	1412	660	0.021292(0.002810)
612	660	0.021846(0.002494)	1512	660	0.021052(0.002874)
712	660	0.021780(0.002508)	1612	660	0.021049(0.003033)
812	660	0.022092(0.002591)	1712	660	0.022144(0.003367)
912	660	0.021471(0.002543)	1812	660	0.021706(0.003352)

Table B.4: The fixed-n estimates for the probability of the figure 8 given a successful strand passage in a Θ-SAP. The values in parentheses are the estimated 95% margins of error.

$2n$	t'	$\widetilde{\mathrm{pr}}^{\Theta}_{2n}(4_1\|\phi, s)$	$2n$	t'	$\widetilde{\mathrm{pr}}^{\Theta}_{2n}(4_1\|\phi, s)$
154	660	0.000609(0.000788)	1134	660	0.000533(0.000993)
294	660	0.000669(0.000890)	1274	660	0.000396(0.000946)
434	660	0.000691(0.000960)	1414	660	0.000308(0.000758)
574	660	0.000768(0.001105)	1554	660	0.000489(0.001136)
714	660	0.000668(0.001047)	1694	660	0.000389(0.000971)
854	660	0.000679(0.001104)	1834	660	0.000111(0.001731)
994	660	0.000646(0.001102)			

Table B.5: The fixed-n estimates for the probability of a knot-type 5_2 SAP resulting given a successful strand passage in a Θ-SAP. The values in parentheses are the estimated 95% margins of error.

$2n$	t'	$\widetilde{\mathrm{pr}}^{\Theta}_{2n}(5_2\|\phi,s)$
192	660	0.000015(0.000005)
372	660	0.000039(0.000020)
552	660	0.000048(0.000033)
732	660	0.000051(0.000044)
912	660	0.000045(0.000037)
1092	660	0.000042(0.000040)
1272	660	0.000041(0.000051)
1452	660	$n/a(n/a)$
1632	660	$n/a(n/a)$
1812	660	$n/a(n/a)$

samples of Grouped-n estimates $\widehat{\mathrm{pr}}^{\Theta}_{n_1,n_1+98}(\phi,s)$, $\widehat{\mathrm{pr}}^{\Theta}_{n_1,n_1+98}(\phi|\phi,s)$, $\widehat{\mathrm{pr}}^{\Theta}_{n_1,n_1+138}(3_1|\phi,s)$, $\widehat{\mathrm{pr}}^{\Theta}_{n_1,n_1+158}(4_1|\phi,s)$, and $\widehat{\mathrm{pr}}^{\Theta}_{n_1,n_1+178}(5_2|\phi,s)$ and their corresponding estimated 95% margins of error. The estimates in Tables B.6-B.10 are respectively plotted in Figures 6.4-6.8.

Note that the point estimates and the estimated 95% margins of error presented in Tables B.6-B.10 were computed using the point estimators $\widehat{\mathrm{Pr}}^{\Theta}_{n_1,n_2}(\phi,s)$, $\widehat{\mathrm{Pr}}^{\Theta}_{n_1,n_2}(\phi,f)$, and $\widehat{\mathrm{Pr}}^{\Theta}_{n_1,n_2}(*)$, for $* \in \mathscr{K}^{\dagger}(\phi)$, defined with $t_0 = 9.6 \times 10^{10}$ time steps, $\tau_{\mathrm{int}} = 0.72 \times 10^9$ time steps, $T = 1200$ time steps, and $l := 66$. Refer to Section 6.3 for a detailed discussion on how the estimates were precisely determined.

Table B.6: The grouped-n estimates for the probability of a successful strand passage. The values in parentheses are the estimated 95% margins of error.

n_1	t'	$\widehat{\mathrm{pr}}^{\Theta}_{n_1,n_1+98}(\phi,s)$	n_1	t'	$\widehat{\mathrm{pr}}^{\Theta}_{n_1,n_1+98}(\phi,s)$
14	660	0.104733(0.011275)	914	660	0.136967(0.014574)
114	660	0.136864(0.014458)	1014	660	0.137093(0.014630)
214	660	0.137656(0.014542)	1114	660	0.137226(0.014709)
314	660	0.137619(0.014546)	1214	660	0.137278(0.014804)
414	660	0.137399(0.014532)	1314	660	0.137168(0.014906)
514	660	0.137313(0.014530)	1414	660	0.137031(0.015050)
614	660	0.137254(0.014532)	1514	660	0.136969(0.015237)
714	660	0.137101(0.014531)	1614	660	0.136773(0.015467)
814	660	0.137004(0.014546)	1714	660	0.136728(0.015760)

Table B.7: The grouped-n estimates for the probability of the unknot given a successful strand passage in a Θ-SAP. The values in parentheses are the estimated 95% margins of error.

n_1	t'	$\widehat{\mathrm{pr}}^{\Theta}_{n_1,n_1+98}(\phi\|\phi,s)$	n_1	t'	$\widehat{\mathrm{pr}}^{\Theta}_{n_1,n_1+98}(\phi\|\phi,s)$
14	660	0.994759(0.007827)	914	660	0.977710(0.016029)
114	660	0.983008(0.013973)	1014	660	0.977888(0.015992)
214	660	0.979426(0.015336)	1114	660	0.978085(0.016017)
314	660	0.978001(0.015848)	1214	660	0.977949(0.016134)
414	660	0.977325(0.016089)	1314	660	0.977792(0.016257)
514	660	0.977441(0.016054)	1414	660	0.977847(0.016391)
614	660	0.977282(0.016116)	1514	660	0.978152(0.016534)
714	660	0.977320(0.016117)	1614	660	0.978096(0.016810)
814	660	0.977241(0.016164)	1714	660	0.977093(0.017416)

Table B.8: The grouped-n estimates for the probability of a trefoil given a successful strand passage in a Θ-SAP. The values in parentheses are the estimated 95% margins of error.

n_1	t'	$\widehat{\mathrm{pr}}^{\Theta}_{n_1,n_1+138}(3_1\|\phi,s)$	n_1	t'	$\widehat{\mathrm{pr}}^{\Theta}_{n_1,n_1+138}(3_1\|\phi,s)$
14	660	0.006725(0.000765)	994	660	0.021245(0.002532)
154	660	0.018904(0.002138)	1134	660	0.021129(0.002577)
294	660	0.021242(0.002405)	1274	660	0.021427(0.002683)
434	660	0.021816(0.002481)	1414	660	0.021476(0.002809)
574	660	0.021797(0.002496)	1554	659	0.021096(0.002914)
714	660	0.021797(0.002524)	1694	658	0.022077(0.003213)
854	660	0.021611(0.002533)			

Table B.9: The grouped-n estimates for the probability of a figure 8 given a successful strand passage in a Θ-SAP. The values in parentheses are the estimated 95% margins of error.

n_1	t'	$\widehat{\mathrm{pr}}^{\Theta}_{n_1,n_1+158}(4_1\|\phi,s)$	n_1	t'	$\widehat{\mathrm{pr}}^{\Theta}_{n_1,n_1+158}(4_1\|\phi,s)$
14	660	0.000100(0.000012)	974	454	0.000876(0.000183)
174	660	0.000542(0.000064)	1134	365	0.000899(0.000203)
334	660	0.000775(0.000099)	1294	271	0.000711(0.000208)
494	654	0.000862(0.000124)	1454	197	0.000657(0.000219)
654	629	0.000923(0.000152)	1614	153	0.000836(0.000271)
814	548	0.000925(0.000190)	1774	113	0.000756(0.000343)

Table B.10: The grouped-n estimates for the probability of observing knot-type 5_2 given a successful strand passage in a Θ-SAP. The values in parentheses are the estimated 95% margins of error.

n_1	t'	$\widehat{\mathrm{pr}}^{\Theta}_{n_1,n_1+178}(5_2\|\phi,s)$	n_1	t'	$\widehat{\mathrm{pr}}^{\Theta}_{n_1,n_1+178}(5_2\|\phi,s)$
14	373	0.000002(0.000002)	914	27	0.000044(0.000035)
194	320	0.000022(0.000006)	1094	21	0.000031(0.000023)
374	175	0.000046(0.000016)	1274	16	0.000035(0.000040)
554	111	0.000046(0.000029)	1454	8	0.000023(0.000038)
734	54	0.000053(0.000034)	1634	6	0.000003(0.000063)

B.2 Expected Length Estimates

Tables B.11-B.13 display the essentially independent samples of the estimated expected lengths (and their corresponding estimated 95% margins of error) of the large and the small uSAWs found in Θ-SAPs in $\mathscr{E}^c_{2n}(*)$ for each $* \in \{(\phi, f), (\phi|\phi, s), (3_1|\phi, s)\}$. These essentially independent samples are used throughout the analysis in Section 7.1 of Chapter 7. The essentially independent samples associated with the large uSAW in Θ-SAPs in $\mathscr{E}^c_{2n}(\phi, f)$, $\mathscr{E}^c_{2n}(\phi|\phi, s)$, and $\mathscr{E}^c_{2n}(3_1|\phi, s)$ are displayed in Column 3 of Tables B.11-B.13 respectively and are plotted in Figure 7.4. The essentially independent samples associated with the small uSAW in Θ-SAPs in $\mathscr{E}^c_{2n}(\phi, f)$, $\mathscr{E}^c_{2n}(\phi|\phi, s)$, and $\mathscr{E}^c_{2n}(3_1|\phi, s)$ are displayed in Column 4 of Tables B.11-B.13 respectively and are plotted in Figure 7.7. The value t' in each of these tables is the number of non-zero blocks of data available to compute the point estimate and the estimated 95% margin of error. Note that the point estimates and the estimated 95% margins of error presented in Tables B.11-B.13 were computed using the point estimators $\langle S_{2n}(\mathscr{E}^c(*))\rangle$ and $\langle L_{2n}(\mathscr{E}^c(*))\rangle$ defined in Section 7.1 with $t_0 = 9.6 \times 10^{10}$ time steps, $\tau_{\text{int}} = 0.72 \times 10^9$ time steps, $T = 120,000$ time steps, and $\lfloor t_0/(2\tau_{\text{int}})\rfloor = 66$.

Table B.11: For the set $\mathscr{P}^{\Theta}(\phi, f)$, an essentially independent sample for the estimated average length of the large (Column 3) and small (Column 4) uSAW in polygons in $\mathscr{E}^{ec}_{2n}(\phi, f)$. The values in parentheses are the estimated 95% margins of error.

$2n$	t'	$\langle l_{2n}\left(\mathscr{E}^{ec}(\phi, f)\right)\rangle$	$\langle s_{2n}\left(\mathscr{E}^{ec}(\phi, f)\right)\rangle$
18	660	8.00(0.00)	4.00(0.00)
198	660	180.22(5.71)	11.78(0.37)
378	660	359.09(11.26)	12.91(0.40)
558	660	538.62(16.71)	13.38(0.41)
738	660	718.15(22.12)	13.85(0.43)
918	660	898.32(27.56)	13.68(0.42)
1098	660	1077.55(33.20)	14.45(0.45)
1278	660	1257.65(38.64)	14.35(0.44)
1458	660	1438.14(43.36)	13.86(0.42)
1638	660	1616.88(49.45)	15.12(0.46)
1818	660	1798.30(53.82)	13.70(0.41)

Table B.12: For the set $\mathscr{P}^{\Theta}(\phi|\phi, s)$, an essentially independent sample for the estimated average length of the large (Column 3) and small (Column 4) uSAW in polygons in $\mathscr{E}^{c}_{2n}(\phi|\phi, s)$. The values in parentheses are the estimated 95% margins of error.

$2n$	t'	$\langle l_{2n}\left(\mathscr{E}^{c}(\phi|\phi, s)\right)\rangle$	$\langle s_{2n}\left(\mathscr{E}^{c}(\phi|\phi, s)\right)\rangle$
18	660	8.00(0.00)	4.00(0.00)
198	660	174.35(5.61)	17.65(0.56)
378	660	351.83(11.14)	20.17(0.64)
558	660	530.22(16.56)	21.78(0.68)
738	660	709.33(21.98)	22.67(0.70)
918	660	888.31(27.41)	23.69(0.73)
1098	660	1067.83(33.03)	24.17(0.75)
1278	660	1249.42(38.48)	22.58(0.74)
1458	660	1432.16(43.65)	19.84(0.79)
1638	660	1609.22(49.25)	22.78(0.70)
1818	649	1788.98(53.63)	23.02(0.69)

Table B.13: For the set $\mathscr{P}^{\Theta}(3_1|\phi,s)$, an essentially independent sample for the estimated average length of the large (Column 3) and small (Column 4) uSAW in polygons in $\mathscr{E}^{c}_{2n}(3_1|\phi,s)$. The values in parentheses are the estimated 95% margins of error.

$2n$	t'	$\langle l_{2n}\left(\mathscr{E}^{c}(3_1\|\phi,s)\right)\rangle$	$\langle s_{2n}\left(\mathscr{E}^{c}(3_1\|\phi,s)\right)\rangle$
24	2	0.00(0.00)	0.00(0.00)
204	660	154.58(10.67)	43.42(3.00)
384	355	306.43(30.49)	71.57(7.11)
564	209	480.44(63.28)	77.56(10.23)
744	108	662.68(119.07)	75.32(13.53)
924	101	835.33(156.76)	82.67(15.51)
1104	37	995.00(288.35)	103.00(29.85)
1284	37	1176.26(380.38)	101.74(32.90)
1464	20	1306.83(549.83)	151.17(63.01)
1644	24	1580.33(664.57)	57.67(24.25)
1824	23	1739.57(748.64)	78.43(33.76)

B.3 Expected Mean-Square Radius of Gyration Estimates

In this section, the point estimates and their estimated 95% margins of error that are required for the analysis presented in Section 7.2 are presented in the following two subsections. The first subsection presents the estimates used in the discussion in Sections 7.2.2 and 7.2.3 that are based on "fixed-n estimates". The second subsection presents the estimates used in the discussion of the "Average-n Method" in Section 7.2.3.

B.3.1 Fixed-n Estimates

Tables B.14-B.17 display the essentially independent samples of the estimated expected mean-square radii of gyration (and their corresponding estimated 95% margins of error) for Θ-SAPs in $\mathscr{P}_{2n}(*)$ for each $* \in \{\phi, (\phi,f), (\phi|\phi,s), (3_1|\phi,s)\}$ and the estimated expected mean-square radii of gyration (and their corresponding estimated 95% margins of error) for the large and the small uSAWs found in Θ-SAPs in $\mathscr{E}^{c}_{2n}(*)$ for each $* \in \{(\phi,f), (\phi|\phi,s), (3_1|\phi,s)\}$. These essentially independent samples are used throughout the analysis in Section 7.2 of Chapter 7. The essentially independent sample associated with Θ-SAPs

in $\mathscr{P}_{2n}(\phi)$ is presented in Table B.14 and is plotted in Figure 7.23. The essentially independent samples associated with Θ-SAPs in, and the large and small uSAWs in the Θ-SAPs in, $\mathscr{E}^{c}_{2n}(\phi, f)$ are respectively presented in Columns 3, 4, and 5 of Table B.15 and are respectively plotted in Figures 7.23, 7.27, and 7.29. The value t' in each of these tables is the number of non-zero blocks of data available to compute the point estimate and the estimated 95% margin of error.

Note that the point estimates and the estimated 95% margins of error presented in Tables B.14-B.17 were computed using the point estimators $\left\langle R^2\left(\mathscr{P}^{\Theta}_{2n}(*)\right)\right\rangle$, $\left\langle R^2\left(\mathscr{E}^{c}_{2n}(*)\right)\right\rangle$, $\left\langle R^2\left(\mathscr{E}_{2n}(*)\right)\right\rangle$, $\left\langle R^2\left(\mathfrak{w}_s(\mathscr{E}^{c}_{2n}(*))\right)\right\rangle$, $\left\langle R^2\left(\mathfrak{w}_l(\mathscr{E}^{c}_{2n}(*))\right)\right\rangle$, and $\left\langle R^2\left(\mathfrak{w}_e(\mathscr{E}_{2n}(*))\right)\right\rangle$ as defined in Section 7.2.1 with $t_0 = 9.6 \times 10^{10}$ time steps, $\tau_{\text{int}} = 0.72 \times 10^9$ time steps, $T = 120,000$ time steps, and $\lfloor t_0/(2\tau_{\text{int}})\rfloor = 66$.

Table B.14: An essentially independent sample of estimates for $r^2\left(\mathscr{P}_{2n}^{\Theta}(\phi)\right)$. t' is the number of non-empty essentially independent blocks of data that are used to compute the estimates. The values in parentheses are the estimated 95% margins of error.

$2n$	t'	$\left\langle r^2\left(\mathscr{P}_{2n}^{\Theta}(\phi)\right)\right\rangle$
24	660	3.70(0.00)
204	660	50.22(0.20)
384	660	108.49(0.69)
564	660	172.41(1.45)
744	660	240.99(2.53)
924	660	312.31(3.97)
1104	660	385.67(6.00)
1284	660	463.55(8.46)
1464	660	539.22(11.86)
1644	660	617.00(15.76)
1824	660	697.30(20.43)

B.3.2 The Average-n Estimates

The estimates in Column 2 of Table B.30 and Column 3 of Table B.33 are plotted versus the estimates in Column 2 of Table B.18 in Figure 7.31. The estimates in Column 3 of Tables B.34 and B.35 are plotted versus the estimates in Column 2 of Table B.19 also in Figure 7.31.

The estimates in Column 2 of Table B.39 are plotted versus the estimates in Column 2 of Table B.18 in Figure 7.32. The estimates in Column 2 of Tables B.40 and B.41 are plotted versus the estimates in Column 2 of Table B.19 also in Figure 7.32.

The estimates in Column 3 of Table B.39 are plotted versus the estimates in Column 2 of Table B.18 in Figure 7.33. The estimates in Column 3 of Tables B.40 and B.41 are plotted versus the estimates in Column 2 of Table B.19 also in Figure 7.33. The remainder of the estimates presented in Tables B.18-B.41 are included for the sake of completeness.

The point estimates and the estimated 95% margins of error presented in Tables B.18-

Table B.15: An essentially independent sample of estimates for $r^2\left(\mathscr{E}_{2n}^{c}(\phi,f)\right)$ (Column 3), $r^2\left(\mathfrak{w}_l\left(\mathscr{E}_{2n}^{c}(\phi,f)\right)\right)$ (Column 4), and $r^2\left(\mathfrak{w}_s\left(\mathscr{E}_{2n}^{c}(\phi,f)\right)\right)$ (Column 5). t' is the number of non-empty essentially independent blocks of data that are used to compute the estimates. The values in parentheses are the estimated 95% margins of error.

$2n$	t'	$\left\langle r^2\left(\mathscr{E}_{2n}^{c}(\phi,f)\right)\right\rangle$	$\left\langle r^2\left(\mathfrak{w}_l\left(\mathscr{E}_{2n}^{c}(\phi,f)\right)\right)\right\rangle$	$\left\langle r^2\left(\mathfrak{w}_s\left(\mathscr{E}_{2n}^{c}(\phi,f)\right)\right)\right\rangle$
24	660	3.64(0.00)	2.38(0.00)	1.22(0.00)
204	660	50.22(0.22)	49.06(0.21)	2.49(0.01)
384	660	108.48(0.74)	107.41(0.73)	2.80(0.02)
564	660	172.44(1.55)	171.40(1.55)	2.96(0.03)
744	660	241.29(2.69)	240.30(2.70)	3.06(0.03)
924	660	312.24(4.22)	311.28(4.25)	3.19(0.04)
1104	660	385.98(6.30)	385.01(6.44)	3.37(0.06)
1284	660	462.69(8.81)	461.88(9.06)	3.21(0.06)
1464	660	540.29(12.12)	539.70(12.72)	2.90(0.07)
1644	660	617.58(16.07)	616.67(16.86)	3.27(0.09)
1824	660	699.21(20.79)	698.55(21.88)	3.24(0.10)

Table B.16: An essentially independent sample of estimates for $\mathscr{E}^c_{2n}(\phi|\phi,s)$ (Column 3), $r^2\left(\mathfrak{w}_l\left(\mathscr{E}^c_{2n}(\phi|\phi,s)\right)\right)$ (Column 4), and $r^2\left(\mathfrak{w}_s\left(\mathscr{E}^c_{2n}(\phi|\phi,s)\right)\right)$ (Column 5). t' is the number of non-empty essentially independent blocks of data that are used to compute the estimates. The values in parentheses are the estimated 95% margins of error.

$2n$	t'	$\left\langle r^2\left(\mathscr{E}^c_{2n}(\phi\|\phi,s)\right)\right\rangle$	$\left\langle r^2\left(\mathfrak{w}_l\left(\mathscr{E}^c_{2n}(\phi\|\phi,s)\right)\right)\right\rangle$	$\left\langle r^2\left(\mathfrak{w}_s\left(\mathscr{E}^c_{2n}(\phi\|\phi,s)\right)\right)\right\rangle$
24	660	4.42(0.02)	2.52(0.01)	1.43(0.01)
204	660	50.27(0.54)	47.88(0.51)	3.87(0.04)
384	660	108.70(1.86)	106.19(1.81)	4.74(0.08)
564	660	173.03(3.92)	170.93(3.87)	4.72(0.11)
744	660	239.52(6.81)	237.25(6.74)	5.32(0.15)
924	660	313.01(10.67)	311.30(10.61)	5.29(0.18)
1104	660	383.91(15.62)	381.90(15.54)	5.51(0.22)
1284	660	467.90(22.43)	465.82(22.33)	5.92(0.28)
1464	660	533.54(30.54)	531.15(30.40)	6.67(0.38)
1644	660	613.58(40.94)	612.01(40.83)	5.34(0.36)
1824	646	685.84(52.99)	685.12(52.93)	5.15(0.40)

Table B.17: An essentially independent sample of estimates for $\mathscr{P}_{2n}^{\Theta}(3_1|\phi,s)$ (Column 3), $r^2\left(\mathfrak{w}_l\left(\mathscr{E}_{2n}^{c}(3_1|\phi,s)\right)\right)$ (Column 4), and $r^2\left(\mathfrak{w}_s\left(\mathscr{E}_{2n}^{c}(3_1|\phi,s)\right)\right)$ (Column 5). t' is the number of non-empty essentially independent blocks of data that are used to compute the estimates. The values in parentheses are the estimated 95% margins of error.

$2n$	t'	$\left\langle r^2\left(\mathscr{E}_{2n}^{c}(3_1\|\phi,s)\right)\right\rangle$	$\left\langle r^2\left(\mathfrak{w}_l\left(\mathscr{E}_{2n}^{c}(3_1\|\phi,s)\right)\right)\right\rangle$	$\left\langle r^2\left(\mathfrak{w}_s\left(\mathscr{E}_{2n}^{c}(3_1\|\phi,s)\right)\right)\right\rangle$
24	4	3.38(4.69)	2.75(3.82)	2.22(3.08)
204	660	46.73(3.23)	43.51(3.00)	11.00(0.76)
384	389	101.57(10.12)	96.45(9.61)	18.12(1.81)
564	223	155.48(20.51)	150.89(19.90)	21.37(2.82)
744	121	236.40(42.54)	229.13(41.23)	20.01(3.60)
924	111	302.77(56.93)	294.23(55.33)	26.19(4.93)
1104	48	350.11(101.60)	339.06(98.39)	31.52(9.15)
1284	39	473.59(153.38)	461.37(149.42)	32.89(10.65)
1464	24	475.55(200.34)	446.07(187.92)	50.97(21.47)
1644	24	556.05(234.25)	541.97(228.32)	17.92(7.55)
1824	23	704.73(303.97)	702.57(303.04)	24.20(10.44)

B.41 were computed using the point estimators $\left\langle N_{\boldsymbol{\pi}_{z_i}(N_{\min})}\left(\mathscr{U}(*)\right)\right\rangle$, $\left\langle N_{\boldsymbol{\pi}_{z_i}(N_{\min})}\left(f\left(\mathscr{U}(*)\right)\right)\right\rangle$, $\left\langle R^2_{\boldsymbol{\pi}_{z_i}(N_{\min})}\left(\mathscr{U}(*)\right)\right\rangle$, and $\left\langle R^2_{\boldsymbol{\pi}_{z_i}(N_{\min})}\left(f\left(\mathscr{U}(*)\right)\right)\right\rangle$ as defined in Section 7.2.3 with $t_0 = 9.6\times10^{10}$ time steps, $\tau_{\text{int}} = 0.72\times10^9$ time steps, $T = 120,000$ time steps, and $\lfloor t_0/(2\tau_{\text{int}})\rfloor = 66$.

Table B.18: The values in Columns 2-4 are the estimated average lengths of a Θ-SAP sampled from $\mathscr{P}^{\Theta}(\phi)$, $\mathscr{E}^{c}(\phi)$, and $\mathscr{E}(\phi)$ respectively according to $\boldsymbol{\pi}_{z_i}(156)$. The values in parentheses are the estimated 95% margins of error.

i	$\left\langle n_{\boldsymbol{\pi}_{z_i}(156)}\left(\mathscr{P}^{\Theta}(\phi)\right)\right\rangle$	$\left\langle n_{\boldsymbol{\pi}_{z_i}(156)}\left(\mathscr{E}^{c}(\phi)\right)\right\rangle$	$\left\langle n_{\boldsymbol{\pi}_{z_i}(156)}\left(\mathscr{E}(\phi)\right)\right\rangle$
1	161.20(29.91)	160.73(10.74)	161.27(9.67)
2	166.54(19.84)	166.37(6.68)	166.57(6.60)
3	174.41(14.90)	174.41(2.58)	174.41(2.80)
4	189.86(7.81)	189.87(1.78)	189.86(2.27)
5	204.44(3.59)	204.34(1.98)	204.48(3.35)
6	215.54(4.69)	215.70(2.78)	215.46(4.18)
7	231.44(4.11)	231.69(1.31)	231.27(3.44)
8	255.12(3.73)	255.17(2.68)	255.07(3.62)
9	295.55(4.20)	295.51(1.77)	295.59(5.78)
10	354.86(5.71)	354.89(2.64)	354.79(9.54)
11	485.43(10.75)	485.54(8.26)	485.06(24.45)
12	631.73(17.84)	631.80(14.94)	631.40(36.99)
13	761.64(30.16)	761.74(28.32)	761.05(56.59)
14	984.78(69.72)	985.60(69.53)	977.11(103.00)

Table B.19: The values in Columns 2-4 are the estimated average lengths of a Θ-SAP sampled from $\mathscr{P}^{\Theta}(\phi)$, $\mathscr{E}^{c}(\phi)$, and $\mathscr{E}(\phi)$ respectively according to $\boldsymbol{\pi}_{z_i}(182)$. The values in parentheses are the estimated 95% margins of error.

i	$\left\langle n_{\boldsymbol{\pi}_{z_i}(182)}\left(\mathscr{P}^{\Theta}(\phi)\right)\right\rangle$	$\left\langle n_{\boldsymbol{\pi}_{z_i}(182)}\left(\mathscr{E}^{c}(\phi)\right)\right\rangle$	$\left\langle n_{\boldsymbol{\pi}_{z_i}(182)}\left(\mathscr{E}(\phi)\right)\right\rangle$
1	201.07(66.57)	202.54(33.02)	200.61(50.91)
2	206.48(29.02)	206.45(27.62)	206.48(31.27)
3	214.25(13.18)	214.25(4.96)	214.25(5.78)
4	229.61(4.44)	229.69(2.11)	229.55(3.62)
5	244.10(2.97)	244.17(2.42)	244.03(5.08)
6	255.13(4.67)	255.12(2.35)	255.15(4.97)
7	270.85(2.65)	270.88(2.01)	270.79(6.72)
8	294.34(3.37)	294.24(2.08)	294.55(3.98)
9	334.31(4.06)	334.26(2.08)	334.47(8.19)
10	393.25(4.36)	393.23(3.19)	393.36(12.18)
11	522.68(9.73)	522.56(8.91)	523.56(22.89)
12	667.75(19.00)	667.85(18.10)	666.62(39.09)
13	797.14(29.77)	797.28(29.54)	795.25(56.09)
14	1017.83(67.74)	1018.30(68.63)	1008.16(87.41)

Table B.20: The values in Columns 2-4 are the estimated average lengths of a Θ-SAP sampled from $\mathscr{P}^{\Theta}(\phi, f)$, $\mathscr{E}^{c}(\phi, f)$, and $\mathscr{E}(\phi, f)$ respectively according to $\boldsymbol{\pi}_{z_i}(142)$. The values in parentheses are the estimated 95% margins of error.

i	$\left\langle n_{\boldsymbol{\pi}_{z_i}(142)}\left(\mathscr{P}^{\Theta}(\phi, f)\right)\right\rangle$	$\left\langle n_{\boldsymbol{\pi}_{z_i}(142)}\left(\mathscr{E}^{c}(\phi, f)\right)\right\rangle$	$\left\langle n_{\boldsymbol{\pi}_{z_i}(142)}\left(\mathscr{E}(\phi, f)\right)\right\rangle$
1	161.20(29.91)	160.73(10.74)	161.27(9.67)
2	166.54(19.84)	166.37(6.68)	166.57(6.60)
3	174.41(14.90)	174.41(2.58)	174.41(2.80)
4	189.86(7.81)	189.87(1.78)	189.86(2.27)
5	204.44(3.59)	204.34(1.98)	204.48(3.35)
6	215.54(4.69)	215.70(2.78)	215.46(4.18)
7	231.44(4.11)	231.69(1.31)	231.27(3.44)
8	255.12(3.73)	255.17(2.68)	255.07(3.62)
9	295.55(4.20)	295.51(1.77)	295.59(5.78)
10	354.86(5.71)	354.89(2.64)	354.79(9.54)
11	485.43(10.75)	485.54(8.26)	485.06(24.45)
12	631.73(17.84)	631.80(14.94)	631.40(36.99)
13	761.64(30.16)	761.74(28.32)	761.05(56.59)
14	984.78(69.72)	985.60(69.53)	977.11(103.00)

Table B.21: The values in Columns 2-4 are the estimated average lengths of a Θ-SAP sampled from $\mathscr{P}^{\Theta}(\phi, f)$, $\mathscr{E}^{c}(\phi, f)$, and $\mathscr{E}(\phi, f)$ respectively according to $\boldsymbol{\pi}_{z_i}(156)$. The values in parentheses are the estimated 95% margins of error.

i	$\left\langle n_{\boldsymbol{\pi}_{z_i}(156)}\left(\mathscr{P}^{\Theta}(\phi, f)\right)\right\rangle$	$\left\langle n_{\boldsymbol{\pi}_{z_i}(156)}\left(\mathscr{E}^{c}(\phi, f)\right)\right\rangle$	$\left\langle n_{\boldsymbol{\pi}_{z_i}(156)}\left(\mathscr{E}(\phi, f)\right)\right\rangle$
1	175.24(15.83)	174.93(13.12)	175.35(19.59)
2	180.35(12.07)	180.45(9.74)	180.31(14.17)
3	188.30(8.42)	188.20(3.25)	188.35(3.97)
4	203.77(2.95)	203.85(1.64)	203.70(3.12)
5	218.43(2.94)	218.48(1.59)	218.38(3.64)
6	229.38(3.76)	229.36(2.01)	229.41(4.34)
7	245.22(2.60)	245.24(1.52)	245.18(5.01)
8	268.82(3.19)	268.77(1.74)	268.92(3.78)
9	309.02(3.51)	309.00(1.79)	309.09(8.22)
10	368.27(4.04)	368.26(2.92)	368.27(11.13)
11	498.44(9.21)	498.34(8.47)	499.12(21.63)
12	644.18(18.45)	644.30(17.59)	642.87(37.31)
13	774.06(28.96)	774.20(28.70)	772.21(54.16)
14	995.57(66.67)	996.06(67.55)	985.55(86.37)

Table B.22: The values in Columns 2-4 are the estimated average lengths of a Θ-SAP sampled from $\mathscr{P}^{\Theta}(\phi|\phi,s)$, $\mathscr{E}^{c}(\phi|\phi,s)$, and $\mathscr{E}(\phi|\phi,s)$ respectively according to $\boldsymbol{\pi}_{z_i}(182)$. The values in parentheses are the estimated 95% margins of error.

i	$\left\langle n_{\boldsymbol{\pi}_{z_i}(182)}\left(\mathscr{P}^{\Theta}(\phi\|\phi,s)\right)\right\rangle$	$\left\langle n_{\boldsymbol{\pi}_{z_i}(182)}\left(\mathscr{E}^{c}(\phi\|\phi,s)\right)\right\rangle$	$\left\langle n_{\boldsymbol{\pi}_{z_i}(182)}\left(\mathscr{E}(\phi\|\phi,s)\right)\right\rangle$
1	199.09(232.10)	200.84(200.58)	198.36(236.05)
2	206.22(135.85)	207.30(65.29)	205.71(66.50)
3	214.64(44.29)	214.34(22.74)	214.70(16.51)
4	229.41(34.06)	229.59(17.12)	229.30(8.59)
5	244.28(14.12)	244.33(8.47)	244.23(8.43)
6	255.05(11.37)	255.19(7.41)	254.90(14.82)
7	270.93(15.40)	271.10(6.81)	270.70(19.25)
8	294.68(10.88)	294.57(6.49)	294.89(14.02)
9	333.82(17.57)	333.89(8.46)	333.65(23.10)
10	392.90(13.57)	392.75(8.54)	393.40(31.85)
11	521.40(13.09)	521.35(10.10)	521.72(37.27)
12	666.32(23.61)	666.49(20.88)	664.82(73.07)
13	793.34(33.97)	793.61(31.62)	790.92(154.39)
14	1016.90(69.42)	1017.51(67.60)	1007.24(254.56)

Table B.23: The values in Columns 2-4 are the estimated average lengths of a Θ-SAP sampled from $\mathscr{P}^{\Theta}(3_1|\phi,s)$, $\mathscr{E}^c(3_1|\phi,s)$, and $\mathscr{E}(3_1|\phi,s)$ respectively according to $\boldsymbol{\pi}_{z_i}(182)$. The values in parentheses are the estimated 95% margins of error.

i	$\left\langle n_{\boldsymbol{\pi}_{z_i}(182)}\left(\mathscr{P}^{\Theta}(3_1\|\phi,s)\right)\right\rangle$	$\left\langle n_{\boldsymbol{\pi}_{z_i}(182)}\left(\mathscr{E}^c(3_1\|\phi,s)\right)\right\rangle$	$\left\langle n_{\boldsymbol{\pi}_{z_i}(182)}\left(\mathscr{E}(3_1\|\phi,s)\right)\right\rangle$
1	n/a	n/a	n/a
2	n/a	n/a	n/a
3	218.25(305.08)	225.00(238.85)	215.57(249.10)
4	233.46(149.70)	232.43(123.92)	235.35(164.78)
5	244.72(89.23)	242.71(67.55)	249.32(179.43)
6	259.78(96.87)	260.25(74.27)	258.69(129.94)
7	273.26(92.56)	272.96(80.36)	273.12(191.04)
8	300.23(51.16)	300.19(53.83)	299.28(170.03)
9	341.00(63.28)	341.85(49.92)	336.17(419.62)
10	406.43(57.44)	406.86(42.78)	401.98(367.54)
11	531.89(57.81)	531.04(42.30)	539.93(448.04)
12	677.86(109.03)	678.64(73.85)	641.29(708.09)
13	807.43(115.51)	809.21(102.61)	785.47(998.48)
14	986.81(178.28)	988.67(137.99)	915.98(1248.10)

Table B.24: The values in Columns 2-4 are respectively the estimated average lengths of the large and small uSAW or the equal-length uSAWs in a Θ-SAP sampled from $\mathscr{P}^{\Theta}(\phi)$ according to $\boldsymbol{\pi}_{z_i}(156)$. The values in parentheses are the estimated 95% margins of error.

i	$\left\langle n_{\boldsymbol{\pi}_{z_i}(156)}\left(\mathfrak{w}_l\left(\mathscr{E}^c(\phi)\right)\right)\right\rangle$	$\left\langle n_{\boldsymbol{\pi}_{z_i}(156)}\left(\mathfrak{w}_s\left(\mathscr{E}^c(\phi)\right)\right)\right\rangle$	$\left\langle n_{\boldsymbol{\pi}_{z_i}(156)}\left(\mathfrak{w}_e\left(\mathscr{E}(\phi)\right)\right)\right\rangle$
1	143.24(26.90)	11.48(3.51)	6.05(0.49)
2	149.07(17.89)	11.30(1.91)	6.32(0.30)
3	156.98(13.51)	11.43(1.14)	6.68(0.13)
4	172.41(7.23)	11.46(0.56)	7.26(0.24)
5	186.73(3.47)	11.61(0.29)	7.70(0.14)
6	198.02(4.42)	11.68(0.30)	7.97(0.24)
7	213.88(3.87)	11.81(0.30)	8.29(0.22)
8	237.23(3.60)	11.94(0.24)	8.74(0.21)
9	277.37(4.04)	12.14(0.20)	9.21(0.35)
10	336.50(5.40)	12.39(0.22)	9.92(0.68)
11	466.77(10.27)	12.77(0.26)	10.75(1.01)
12	612.76(16.06)	13.04(0.29)	11.68(1.45)
13	742.55(28.93)	13.19(0.33)	12.34(1.49)
14	966.27(70.38)	13.33(0.50)	13.17(2.59)

Table B.25: The values in Columns 2-4 are respectively the estimated average lengths of the large and small uSAW or the equal-length uSAWs in a Θ-SAP sampled from $\mathscr{P}^{\Theta}(\phi)$ according to $\boldsymbol{\pi}_{z_i}(182)$. The values in parentheses are the estimated 95% margins of error.

i	$\left\langle n_{\boldsymbol{\pi}_{z_i}(182)}\left(\mathfrak{w}_l\left(\mathscr{E}^c(\phi)\right)\right)\right\rangle$	$\left\langle n_{\boldsymbol{\pi}_{z_i}(182)}\left(\mathfrak{w}_s\left(\mathscr{E}^c(\phi)\right)\right)\right\rangle$	$\left\langle n_{\boldsymbol{\pi}_{z_i}(182)}\left(\mathfrak{w}_e\left(\mathscr{E}(\phi)\right)\right)\right\rangle$
1	183.92(62.71)	12.62(8.99)	6.26(1.98)
2	187.88(27.27)	12.57(2.66)	6.53(1.05)
3	195.45(12.10)	12.81(0.96)	6.90(0.30)
4	210.89(4.12)	12.80(0.29)	7.60(0.24)
5	225.23(2.78)	12.93(0.29)	8.14(0.22)
6	236.11(4.35)	13.01(0.28)	8.43(0.26)
7	251.75(2.52)	13.13(0.19)	8.76(0.26)
8	274.97(3.17)	13.26(0.20)	9.34(0.25)
9	314.81(3.90)	13.45(0.21)	9.94(0.39)
10	373.53(4.29)	13.70(0.16)	10.75(0.54)
11	502.46(9.44)	14.10(0.27)	12.02(1.18)
12	647.47(18.17)	14.38(0.37)	12.95(1.44)
13	776.73(29.55)	14.55(0.43)	14.00(2.23)
14	997.61(68.96)	14.69(0.55)	14.56(2.76)

Table B.26: The values in Columns 2-4 are respectively the estimated average lengths of the large and small uSAW or the equal-length uSAWs in a Θ-SAP sampled from $\mathscr{P}^{\Theta}(\phi, f)$ according to $\boldsymbol{\pi}_{z_i}(142)$. The values in parentheses are the estimated 95% margins of error.

i	$\left\langle n_{\boldsymbol{\pi}_{z_i}(142)}\left(\mathfrak{w}_l\left(\mathscr{E}^c(\phi,f)\right)\right)\right\rangle$	$\left\langle n_{\boldsymbol{\pi}_{z_i}(142)}\left(\mathfrak{w}_s\left(\mathscr{E}^c(\phi,f)\right)\right)\right\rangle$	$\left\langle n_{\boldsymbol{\pi}_{z_i}(142)}\left(\mathfrak{w}_e\left(\mathscr{E}(\phi,f)\right)\right)\right\rangle$
1	143.24(26.90)	11.48(3.51)	6.05(0.49)
2	149.07(17.89)	11.30(1.91)	6.32(0.30)
3	156.98(13.51)	11.43(1.14)	6.68(0.13)
4	172.41(7.23)	11.46(0.56)	7.26(0.24)
5	186.73(3.47)	11.61(0.29)	7.70(0.14)
6	198.02(4.42)	11.68(0.30)	7.97(0.24)
7	213.88(3.87)	11.81(0.30)	8.29(0.22)
8	237.23(3.60)	11.94(0.24)	8.74(0.21)
9	277.37(4.04)	12.14(0.20)	9.21(0.35)
10	336.50(5.40)	12.39(0.22)	9.92(0.68)
11	466.77(10.27)	12.77(0.26)	10.75(1.01)
12	612.76(16.06)	13.04(0.29)	11.68(1.45)
13	742.55(28.93)	13.19(0.33)	12.34(1.49)
14	966.27(70.38)	13.33(0.50)	13.17(2.59)

Table B.27: The values in Columns 2-4 are respectively the estimated average lengths of the large and small uSAW or the equal-length uSAWs in a Θ-SAP sampled from $\mathscr{P}^{\Theta}(\phi, f)$ according to $\boldsymbol{\pi}_{z_i}(156)$. The values in parentheses are the estimated 95% margins of error.

i	$\left\langle n_{\boldsymbol{\pi}_{z_i}(156)}\left(\mathfrak{w}_l\left(\mathscr{E}^c(\phi,f)\right)\right)\right\rangle$	$\left\langle n_{\boldsymbol{\pi}_{z_i}(156)}\left(\mathfrak{w}_s\left(\mathscr{E}^c(\phi,f)\right)\right)\right\rangle$	$\left\langle n_{\boldsymbol{\pi}_{z_i}(156)}\left(\mathfrak{w}_e\left(\mathscr{E}(\phi,f)\right)\right)\right\rangle$
1	156.54(14.48)	12.40(3.15)	6.18(0.78)
2	162.32(11.44)	12.13(1.42)	6.52(0.55)
3	169.83(7.71)	12.38(0.71)	6.93(0.21)
4	185.33(2.69)	12.51(0.24)	7.61(0.17)
5	199.81(2.68)	12.67(0.25)	8.15(0.19)
6	210.63(3.47)	12.73(0.23)	8.45(0.25)
7	226.37(2.44)	12.87(0.18)	8.78(0.22)
8	249.74(3.01)	13.03(0.21)	9.36(0.27)
9	289.75(3.37)	13.25(0.20)	9.95(0.40)
10	348.74(3.96)	13.52(0.15)	10.77(0.55)
11	478.38(8.97)	13.96(0.25)	12.04(1.17)
12	624.03(17.67)	14.27(0.35)	12.96(1.44)
13	753.74(28.73)	14.46(0.41)	14.02(2.23)
14	975.43(67.85)	14.63(0.53)	14.60(2.84)

Table B.28: The values in Columns 2-4 are respectively the estimated average lengths of the large and small uSAW or the equal-length uSAWs in a Θ-SAP sampled from $\mathscr{P}^{\Theta}(\phi|\phi,s)$ according to $\boldsymbol{\pi}_{z_i}(182)$. The values in parentheses are the estimated 95% margins of error.

i	$\left\langle n_{\boldsymbol{\pi}_{z_i}(182)}\left(\mathfrak{w}_l\left(\mathscr{E}^c(*)\right)\right)\right\rangle$	$\left\langle n_{\boldsymbol{\pi}_{z_i}(182)}\left(\mathfrak{w}_s\left(\mathscr{E}^c(*)\right)\right)\right\rangle$	$\left\langle n_{\boldsymbol{\pi}_{z_i}(182)}\left(\mathfrak{w}_e\left(\mathscr{E}(*)\right)\right)\right\rangle$
1	178.31(213.96)	16.54(35.74)	8.81(12.26)
2	181.72(122.23)	19.58(21.46)	9.68(3.71)
3	190.23(40.52)	18.11(6.68)	10.86(1.06)
4	205.35(31.05)	18.24(3.53)	12.33(0.89)
5	220.13(13.06)	18.20(1.67)	13.40(1.07)
6	230.79(10.44)	18.39(1.08)	13.96(1.41)
7	246.61(14.14)	18.50(1.30)	14.86(1.89)
8	269.90(10.06)	18.67(0.76)	15.99(1.21)
9	308.71(16.47)	19.18(1.22)	17.47(2.39)
10	367.20(12.95)	19.55(0.74)	19.51(2.11)
11	495.14(12.47)	20.21(0.69)	23.41(5.88)
12	639.83(23.09)	20.67(0.94)	25.07(8.74)
13	766.67(34.05)	20.94(0.87)	27.28(8.08)
14	990.18(69.65)	21.33(1.30)	27.29(9.73)

Table B.29: The values in Columns 2-4 are respectively the estimated average lengths of the large and small uSAW or the equal-length uSAWs in a Θ-SAP sampled from $\mathscr{P}^{\Theta}(3_1|\phi,s)$ according to $\boldsymbol{\pi}_{z_i}(182)$. The values in parentheses are the estimated 95% margins of error.

i	$\left\langle n_{\boldsymbol{\pi}_{z_i}(182)}\left(\mathfrak{w}_l\left(\mathscr{E}^c(*)\right)\right)\right\rangle$	$\left\langle n_{\boldsymbol{\pi}_{z_i}(182)}\left(\mathfrak{w}_s\left(\mathscr{E}^c(*)\right)\right)\right\rangle$	$\left\langle n_{\boldsymbol{\pi}_{z_i}(182)}\left(\mathfrak{w}_e\left(\mathscr{E}(*)\right)\right)\right\rangle$
1	n/a	n/a	n/a
2	n/a	n/a	n/a
3	165.84(235.24)	53.17(83.67)	33.49(46.71)
4	180.31(117.02)	46.12(32.11)	33.16(27.93)
5	185.74(70.57)	50.98(23.31)	38.15(34.40)
6	205.84(78.20)	48.41(19.09)	38.41(26.77)
7	209.77(78.54)	57.18(22.88)	38.43(34.63)
8	238.05(42.83)	56.14(14.96)	56.58(45.62)
9	276.51(53.23)	59.34(13.01)	51.27(74.93)
10	335.14(46.43)	65.72(19.31)	52.48(61.04)
11	453.79(50.18)	71.25(9.28)	70.61(66.53)
12	595.29(96.42)	77.35(15.59)	64.20(90.15)
13	718.93(106.55)	84.28(26.95)	127.64(279.74)
14	894.79(167.52)	87.88(23.63)	91.47(162.77)

Table B.30: The values in Columns 2-4 are the estimated radii of gyration of a Θ-SAP sampled from $\mathscr{P}^{\Theta}(\phi)$, $\mathscr{E}^{c}(\phi)$, and $\mathscr{E}(\phi)$ respectively according to $\boldsymbol{\pi}_{z_i}(156)$. The values in parentheses are the estimated 95% margins of error.

i	$\left\langle r^2_{\boldsymbol{\pi}_{z_i}(156)}\left(\mathscr{P}^{\Theta}(\phi)\right)\right\rangle$	$\left\langle r^2_{\boldsymbol{\pi}_{z_i}(156)}\left(\mathscr{E}^{c}(\phi)\right)\right\rangle$	$\left\langle r^2_{\boldsymbol{\pi}_{z_i}(156)}\left(\mathscr{E}(\phi)\right)\right\rangle$
1	37.60(7.03)	37.63(3.24)	37.59(2.47)
2	39.11(4.67)	39.07(2.14)	39.11(1.57)
3	41.49(3.55)	41.34(1.00)	41.53(0.68)
4	46.28(1.92)	46.35(0.78)	46.26(0.58)
5	50.80(0.91)	50.76(0.53)	50.82(0.87)
6	54.36(1.19)	54.41(0.70)	54.34(1.07)
7	59.53(1.08)	59.63(0.43)	59.46(0.91)
8	67.36(1.01)	67.37(0.77)	67.36(0.97)
9	81.08(1.19)	81.07(0.62)	81.10(1.64)
10	102.02(1.83)	102.05(1.08)	101.97(2.92)
11	150.56(4.29)	150.62(3.56)	150.37(8.42)
12	208.00(7.96)	208.06(6.97)	207.71(14.91)
13	261.17(14.49)	261.24(14.03)	260.73(23.78)
14	356.64(38.28)	356.99(38.63)	353.29(49.83)

Table B.31: The values in Columns 2-4 are the estimated radii of gyration of a Θ-SAP sampled from $\mathscr{P}^{\Theta}(\phi)$, $\mathscr{E}^{c}(\phi)$, and $\mathscr{E}(\phi)$ respectively according to $\boldsymbol{\pi}_{z_i}(182)$. The values in parentheses are the estimated 95% margins of error.

i	$\left\langle r^2_{\boldsymbol{\pi}_{z_i}(182)}\left(\mathscr{P}^{\Theta}(\phi)\right)\right\rangle$	$\left\langle r^2_{\boldsymbol{\pi}_{z_i}(182)}\left(\mathscr{E}^{c}(\phi)\right)\right\rangle$	$\left\langle r^2_{\boldsymbol{\pi}_{z_i}(182)}\left(\mathscr{E}(\phi)\right)\right\rangle$
1	49.29(16.98)	49.38(10.16)	49.25(13.66)
2	50.97(7.26)	50.90(7.36)	51.00(7.78)
3	53.45(3.31)	53.43(1.57)	53.47(1.47)
4	58.29(1.20)	58.35(0.73)	58.24(1.01)
5	62.92(0.78)	62.95(0.63)	62.89(1.34)
6	66.59(1.23)	66.58(0.64)	66.60(1.33)
7	71.81(0.71)	71.82(0.56)	71.80(1.80)
8	79.75(0.93)	79.71(0.60)	79.82(1.10)
9	93.61(1.20)	93.59(0.70)	93.66(2.37)
10	114.74(1.54)	114.72(1.29)	114.83(3.70)
11	163.46(4.14)	163.42(3.90)	163.72(7.95)
12	220.94(8.67)	220.99(8.30)	220.34(15.69)
13	274.32(14.78)	274.41(14.78)	273.12(22.48)
14	369.12(36.57)	369.38(37.29)	363.85(37.50)

Table B.32: The values in Columns 2-4 are the estimated radii of gyration of a Θ-SAP sampled from $\mathscr{P}^{\Theta}(\phi, f)$, $\mathscr{E}^{c}(\phi, f)$, and $\mathscr{E}(\phi, f)$ respectively according to $\boldsymbol{\pi}_{z_i}(142)$. The values in parentheses are the estimated 95% margins of error.

i	$\left\langle r^2_{\boldsymbol{\pi}_{z_i}(142)}\left(\mathscr{P}^{\Theta}(\phi, f)\right)\right\rangle$	$\left\langle r^2_{\boldsymbol{\pi}_{z_i}(142)}\left(\mathscr{E}^{c}(\phi, f)\right)\right\rangle$	$\left\langle r^2_{\boldsymbol{\pi}_{z_i}(142)}\left(\mathscr{E}(\phi, f)\right)\right\rangle$
1	37.60(7.03)	37.63(3.24)	37.59(2.47)
2	39.11(4.67)	39.07(2.14)	39.11(1.57)
3	41.49(3.55)	41.34(1.00)	41.53(0.68)
4	46.28(1.92)	46.35(0.78)	46.26(0.58)
5	50.80(0.91)	50.76(0.53)	50.82(0.87)
6	54.36(1.19)	54.41(0.70)	54.34(1.07)
7	59.53(1.08)	59.63(0.43)	59.46(0.91)
8	67.36(1.01)	67.37(0.77)	67.36(0.97)
9	81.08(1.19)	81.07(0.62)	81.10(1.64)
10	102.02(1.83)	102.05(1.08)	101.97(2.92)
11	150.56(4.29)	150.62(3.56)	150.37(8.42)
12	208.00(7.96)	208.06(6.97)	207.71(14.91)
13	261.17(14.49)	261.24(14.03)	260.73(23.78)
14	356.64(38.28)	356.99(38.63)	353.29(49.83)

Table B.33: The values in Columns 2-4 are the estimated radii of gyration of a Θ-SAP sampled from $\mathscr{P}^{\Theta}(\phi, f)$, $\mathscr{E}^{c}(\phi, f)$, and $\mathscr{E}(\phi, f)$ respectively according to $\boldsymbol{\pi}_{z_i}(156)$. The values in parentheses are the estimated 95% margins of error.

i	$\left\langle r^2_{\boldsymbol{\pi}_{z_i}(156)}\left(\mathscr{P}^{\Theta}(\phi, f)\right)\right\rangle$	$\left\langle r^2_{\boldsymbol{\pi}_{z_i}(156)}\left(\mathscr{E}^{c}(\phi, f)\right)\right\rangle$	$\left\langle r^2_{\boldsymbol{\pi}_{z_i}(156)}\left(\mathscr{E}(\phi, f)\right)\right\rangle$
1	41.56(3.88)	41.46(3.36)	41.60(4.79)
2	43.15(2.96)	43.07(2.61)	43.18(3.46)
3	45.64(2.05)	45.65(0.88)	45.64(0.97)
4	50.44(0.78)	50.47(0.55)	50.41(0.83)
5	55.04(0.75)	55.05(0.41)	55.02(0.95)
6	58.59(0.97)	58.59(0.52)	58.60(1.14)
7	63.78(0.69)	63.79(0.43)	63.77(1.32)
8	71.63(0.86)	71.61(0.50)	71.66(1.02)
9	85.38(1.03)	85.38(0.60)	85.41(2.33)
10	106.40(1.42)	106.39(1.18)	106.45(3.36)
11	154.99(3.92)	154.96(3.71)	155.19(7.50)
12	212.38(8.39)	212.44(8.04)	211.73(15.01)
13	265.71(14.31)	265.80(14.30)	264.53(21.71)
14	360.49(35.89)	360.75(36.58)	355.11(37.02)

Table B.34: The values in Columns 2-4 are the estimated radii of gyration of a Θ-SAP sampled from $\mathscr{P}^{\Theta}(\phi|\phi,s)$, $\mathscr{E}^{c}(\phi|\phi,s)$, and $\mathscr{E}(\phi|\phi,s)$ respectively according to $\boldsymbol{\pi}_{z_i}(182)$. The values in parentheses are the estimated 95% margins of error.

i	$\left\langle r^2_{\boldsymbol{\pi}_{z_i}(182)}\left(\mathscr{P}^{\Theta}(\phi\|\phi,s)\right)\right\rangle$	$\left\langle r^2_{\boldsymbol{\pi}_{z_i}(182)}\left(\mathscr{E}^{c}(\phi\|\phi,s)\right)\right\rangle$	$\left\langle r^2_{\boldsymbol{\pi}_{z_i}(182)}\left(\mathscr{E}(\phi\|\phi,s)\right)\right\rangle$
1	48.49(58.06)	48.73(55.72)	48.22(58.99)
2	51.31(33.91)	51.59(18.31)	51.11(16.86)
3	53.74(11.16)	53.62(6.63)	53.81(4.23)
4	58.29(8.66)	58.17(4.37)	58.38(2.34)
5	63.17(3.70)	63.30(2.29)	63.05(2.24)
6	66.66(3.04)	66.65(2.07)	66.67(3.97)
7	71.90(4.17)	71.96(2.05)	71.82(5.18)
8	79.80(3.13)	79.77(2.17)	79.86(3.99)
9	93.39(4.97)	93.37(2.61)	93.46(6.56)
10	114.50(4.10)	114.50(2.81)	114.50(9.33)
11	162.81(4.68)	162.86(3.87)	162.60(12.16)
12	219.95(9.76)	220.01(8.81)	219.43(26.02)
13	272.61(16.24)	272.73(15.90)	271.52(54.36)
14	368.05(36.26)	368.36(35.98)	363.06(98.42)

Table B.35: The values in Columns 2-4 are the estimated radii of gyration of a Θ-SAP sampled from $\mathscr{P}^{\Theta}(3_1|\phi,s)$, $\mathscr{E}^{c}(3_1|\phi,s)$, and $\mathscr{E}(3_1|\phi,s)$ respectively according to $\boldsymbol{\pi}_{z_i}(182)$. The values in parentheses are the estimated 95% margins of error.

i	$\left\langle r^2_{\boldsymbol{\pi}_{z_i}(182)}\left(\mathscr{P}^{\Theta}(3_1\|\phi,s)\right)\right\rangle$	$\left\langle r^2_{\boldsymbol{\pi}_{z_i}(182)}\left(\mathscr{E}^{c}(3_1\|\phi,s)\right)\right\rangle$	$\left\langle r^2_{\boldsymbol{\pi}_{z_i}(182)}\left(\mathscr{E}(3_1\|\phi,s)\right)\right\rangle$
1	n/a	n/a	n/a
2	n/a	n/a	n/a
3	49.08(69.05)	52.58(62.87)	47.84(56.76)
4	54.70(36.85)	54.51(33.71)	54.36(39.28)
5	57.19(21.66)	56.48(17.06)	59.32(43.75)
6	62.17(23.54)	62.29(18.75)	61.79(31.36)
7	65.75(23.39)	65.84(21.54)	64.95(45.97)
8	73.91(13.25)	73.92(14.48)	73.47(42.16)
9	88.26(16.98)	88.56(13.64)	86.66(108.34)
10	110.07(15.81)	110.41(12.20)	107.95(98.96)
11	156.12(19.71)	156.02(16.03)	157.50(133.01)
12	211.75(35.61)	212.09(25.16)	195.19(221.17)
13	262.29(40.32)	263.16(37.23)	254.91(325.75)
14	336.86(71.85)	337.28(60.65)	315.20(432.99)

Table B.36: The values in Columns 2-4 are respectively the estimated average radii of gyration of the large and small uSAW or the equal-length uSAWs in a Θ-SAP sampled from $\mathscr{P}^{\Theta}(\phi)$ according to $\boldsymbol{\pi}_{z_i}(156)$. The values in parentheses are the estimated 95% margins of error.

i	$\left\langle r^2_{\boldsymbol{\pi}_{z_i}(156)}\left(\mathfrak{w}_l\left(\mathscr{E}^c(\phi)\right)\right)\right\rangle$	$\left\langle r^2_{\boldsymbol{\pi}_{z_i}(156)}\left(\mathfrak{w}_s\left(\mathscr{E}^c(\phi)\right)\right)\right\rangle$	$\left\langle r^2_{\boldsymbol{\pi}_{z_i}(156)}\left(\mathfrak{w}_e\left(\mathscr{E}(\phi)\right)\right)\right\rangle$
1	36.34(7.20)	2.38(0.83)	1.32(0.25)
2	37.86(4.73)	2.38(0.41)	1.37(0.17)
3	40.17(3.53)	2.40(0.26)	1.44(0.12)
4	45.16(1.99)	2.42(0.13)	1.55(0.08)
5	49.60(0.94)	2.46(0.07)	1.64(0.03)
6	53.25(1.18)	2.49(0.06)	1.69(0.05)
7	58.50(1.09)	2.52(0.06)	1.76(0.06)
8	66.23(1.05)	2.56(0.05)	1.86(0.05)
9	79.95(1.22)	2.62(0.04)	1.96(0.08)
10	100.94(1.77)	2.70(0.05)	2.13(0.16)
11	149.54(4.06)	2.82(0.07)	2.34(0.23)
12	207.00(7.25)	2.92(0.09)	2.57(0.37)
13	260.21(14.20)	2.97(0.11)	2.75(0.41)
14	355.97(38.89)	3.03(0.18)	2.97(0.70)

Table B.37: The values in Columns 2-4 are respectively the estimated average radii of gyration of the large and small uSAW or the equal-length uSAWs in a Θ-SAP sampled from $\mathscr{P}^{\Theta}(\phi)$ according to $\boldsymbol{\pi}_{z_i}(182)$. The values in parentheses are the estimated 95% margins of error.

i	$\left\langle r^2_{\boldsymbol{\pi}_{z_i}(182)}\left(\mathfrak{w}_l\left(\mathscr{E}^c(\phi)\right)\right)\right\rangle$	$\left\langle r^2_{\boldsymbol{\pi}_{z_i}(182)}\left(\mathfrak{w}_s\left(\mathscr{E}^c(\phi)\right)\right)\right\rangle$	$\left\langle r^2_{\boldsymbol{\pi}_{z_i}(182)}\left(\mathfrak{w}_e\left(\mathscr{E}(\phi)\right)\right)\right\rangle$
1	48.22(16.87)	2.70(2.28)	1.37(0.41)
2	49.59(7.66)	2.74(0.58)	1.42(0.23)
3	52.05(3.37)	2.77(0.23)	1.49(0.06)
4	57.03(1.23)	2.76(0.07)	1.63(0.05)
5	61.64(0.78)	2.80(0.07)	1.74(0.05)
6	65.27(1.22)	2.82(0.06)	1.80(0.05)
7	70.53(0.72)	2.86(0.04)	1.87(0.06)
8	78.42(0.93)	2.90(0.05)	2.00(0.06)
9	92.31(1.21)	2.96(0.05)	2.13(0.09)
10	113.45(1.55)	3.04(0.04)	2.33(0.13)
11	162.17(4.04)	3.17(0.08)	2.65(0.31)
12	219.77(8.32)	3.27(0.12)	2.89(0.41)
13	273.21(14.81)	3.33(0.15)	3.20(0.66)
14	368.20(37.46)	3.40(0.21)	3.33(0.77)

Table B.38: The values in Columns 2-4 are respectively the estimated average radii of gyration of the large and small uSAW or the equal-length uSAWs in a Θ-SAP sampled from $\mathscr{P}^{\Theta}(\phi, f)$ according to $\boldsymbol{\pi}_{z_i}(142)$. The values in parentheses are the estimated 95% margins of error.

i	$\left\langle r^2_{\boldsymbol{\pi}_{z_i}(142)}\left(\mathfrak{w}_l\left(\mathscr{E}^c(\phi,f)\right)\right)\right\rangle$	$\left\langle r^2_{\boldsymbol{\pi}_{z_i}(142)}\left(\mathfrak{w}_s\left(\mathscr{E}^c(\phi,f)\right)\right)\right\rangle$	$\left\langle r^2_{\boldsymbol{\pi}_{z_i}(142)}\left(\mathfrak{w}_e\left(\mathscr{E}(\phi,f)\right)\right)\right\rangle$
1	36.34(7.20)	2.38(0.83)	1.32(0.25)
2	37.86(4.73)	2.38(0.41)	1.37(0.17)
3	40.17(3.53)	2.40(0.26)	1.44(0.12)
4	45.16(1.99)	2.42(0.13)	1.55(0.08)
5	49.60(0.94)	2.46(0.07)	1.64(0.03)
6	53.25(1.18)	2.49(0.06)	1.69(0.05)
7	58.50(1.09)	2.52(0.06)	1.76(0.06)
8	66.23(1.05)	2.56(0.05)	1.86(0.05)
9	79.95(1.22)	2.62(0.04)	1.96(0.08)
10	100.94(1.77)	2.70(0.05)	2.13(0.16)
11	149.54(4.06)	2.82(0.07)	2.34(0.23)
12	207.00(7.25)	2.92(0.09)	2.57(0.37)
13	260.21(14.20)	2.97(0.11)	2.75(0.41)
14	355.97(38.89)	3.03(0.18)	2.97(0.70)

Table B.39: The values in Columns 2-4 are respectively the estimated average radii of gyration of the large and small uSAW or the equal-length uSAWs in a Θ-SAP sampled from $\mathscr{P}^{\Theta}(\phi, f)$ according to $\boldsymbol{\pi}_{z_i}(156)$. The values in parentheses are the estimated 95% margins of error.

i	$\left\langle r^2_{\boldsymbol{\pi}_{z_i}(156)}\left(\mathfrak{w}_l\left(\mathscr{E}^c(\phi,f)\right)\right)\right\rangle$	$\left\langle r^2_{\boldsymbol{\pi}_{z_i}(156)}\left(\mathfrak{w}_s\left(\mathscr{E}^c(\phi,f)\right)\right)\right\rangle$	$\left\langle r^2_{\boldsymbol{\pi}_{z_i}(156)}\left(\mathfrak{w}_e\left(\mathscr{E}(\phi,f)\right)\right)\right\rangle$
1	40.16(3.97)	2.64(0.73)	1.36(0.14)
2	41.80(3.12)	2.59(0.30)	1.42(0.10)
3	44.30(2.06)	2.65(0.16)	1.49(0.07)
4	49.13(0.79)	2.68(0.05)	1.63(0.04)
5	53.73(0.73)	2.72(0.06)	1.74(0.04)
6	57.27(0.94)	2.74(0.05)	1.80(0.05)
7	62.48(0.69)	2.78(0.04)	1.87(0.04)
8	70.31(0.87)	2.83(0.05)	2.00(0.06)
9	84.08(1.04)	2.90(0.05)	2.14(0.07)
10	105.11(1.42)	2.99(0.04)	2.34(0.12)
11	153.70(3.83)	3.13(0.08)	2.66(0.29)
12	211.22(8.06)	3.24(0.11)	2.89(0.39)
13	264.59(14.34)	3.31(0.14)	3.20(0.63)
14	359.56(36.74)	3.37(0.20)	3.34(0.78)

Table B.40: The values in Columns 2-4 are respectively the estimated average radii of gyration of the large and small uSAW or the equal-length uSAWs in a Θ-SAP sampled from $\mathscr{P}^{\Theta}(\phi|\phi,s)$ according to $\boldsymbol{\pi}_{z_i}(182)$. The values in parentheses are the estimated 95% margins of error.

i	$\left\langle r^2_{\boldsymbol{\pi}_{z_i}(182)}\left(\mathfrak{w}_l\left(\mathscr{E}^c(*)\right)\right)\right\rangle$	$\left\langle r^2_{\boldsymbol{\pi}_{z_i}(182)}\left(\mathfrak{w}_s\left(\mathscr{E}^c(*)\right)\right)\right\rangle$	$\left\langle r^2_{\boldsymbol{\pi}_{z_i}(182)}\left(\mathfrak{w}_e\left(\mathscr{E}(*)\right)\right)\right\rangle$
1	45.75(63.13)	3.50(7.16)	1.92(2.71)
2	48.99(33.86)	5.16(10.00)	2.06(0.80)
3	51.47(10.84)	4.08(1.72)	2.32(0.45)
4	55.82(8.46)	4.11(1.00)	2.63(0.41)
5	60.97(3.67)	4.08(0.39)	2.85(0.43)
6	64.28(2.97)	4.13(0.24)	2.97(0.49)
7	69.60(4.11)	4.16(0.28)	3.16(0.74)
8	77.43(3.14)	4.22(0.17)	3.43(0.67)
9	91.00(5.00)	4.38(0.29)	3.75(0.69)
10	112.15(4.15)	4.49(0.17)	4.27(0.80)
11	160.57(4.56)	4.71(0.20)	5.38(2.30)
12	217.77(9.42)	4.87(0.29)	5.74(2.82)
13	270.54(16.58)	4.97(0.31)	6.32(2.30)
14	366.18(36.75)	5.12(0.48)	6.32(2.49)

Table B.41: The values in Columns 2-4 are respectively the estimated average radii of gyration of the large and small uSAW or the equal-length uSAWs in a Θ-SAP sampled from $\mathscr{P}^{\Theta}(3_1|\phi,s)$ according to $\boldsymbol{\pi}_{z_i}(182)$. The values in parentheses are the estimated 95% margins of error.

i	$\left\langle r^2_{\boldsymbol{\pi}_{z_i}(182)}\left(\mathfrak{w}_l\left(\mathscr{E}^c(*)\right)\right)\right\rangle$	$\left\langle r^2_{\boldsymbol{\pi}_{z_i}(182)}\left(\mathfrak{w}_s\left(\mathscr{E}^c(*)\right)\right)\right\rangle$	$\left\langle r^2_{\boldsymbol{\pi}_{z_i}(182)}\left(\mathfrak{w}_e\left(\mathscr{E}(*)\right)\right)\right\rangle$
1	n/a	n/a	n/a
2	n/a	n/a	n/a
3	46.87(70.27)	14.35(24.19)	8.28(11.91)
4	50.20(35.15)	11.32(8.09)	8.00(6.87)
5	52.04(20.68)	13.50(6.91)	10.07(9.67)
6	58.60(22.86)	12.22(4.97)	9.96(7.59)
7	60.77(23.37)	14.75(5.98)	9.20(7.96)
8	69.56(13.89)	14.79(4.12)	14.55(11.68)
9	83.44(16.09)	15.63(3.30)	13.16(20.51)
10	104.60(15.08)	17.52(5.65)	14.54(17.83)
11	149.57(19.85)	19.34(2.68)	18.56(18.07)
12	205.26(34.42)	21.36(4.87)	16.73(24.45)
13	255.51(40.95)	23.74(9.65)	40.55(110.04)
14	328.40(71.72)	25.01(7.92)	25.58(47.56)

Bibliography

[1] J. Adams. *The Knot Book.* W. H. Freeman and Co. New York. (1994).

[2] J. W. Alexander. *Trans. American Mathematical Society*, 30:275 (1928).

[3] S. E. Alm and S. Janson. Random self-avoiding walks on one-dimensional lattices. *Commun. Statist.-Stochastic Models*, 6:169–212 (1990).

[4] T. W. Anderson. *The Statistical Analysis of Time Series.* Wiley. New York. (1971).

[5] P. Bickel and K. Doksum. *Mathematical Statistics: Basic Ideas and Selected Topics.* Holden-Day, Inc. San Franciso. (1977).

[6] A. Bates and A. Maxwell. *DNA Topology.* Oxford University Press. New York. (2005).

[7] A. Berretti and A. D. Sokal. New Monte Carlo method for the self-avoiding walk. *J. Stat. Phys.,* 40:483-531 (1985).

[8] G. Burde and H. Zieschang. *Knots.* de Gruyter. Berlin. (1985).

[9] B. Berg and D. Foester. Random paths and random surfaces on a digital computer. *Phys. Lett.*, 106B:323-326 (1981).

[10] S. Bigelow. Does the Jones Polynomial detect the unknot? *Journal of Knot Theory and its Ramifications*, 4:493-505 (2002).

[11] S. Caracciolo, A. Pelissetto, and A. D. Sokal. Monte Carlo Test of a hyperscaling relation for the two-dimensional self-avoiding walk. *J. Phys. A:Math. Gen.*, 23:4509-4517 (1990).

[12] K. L. Chung. *Markov Chains with Stationary Transition Probabilities.* Springer-Verlag. New York. (1967).

[13] N. Clisby, R. Liang, and G. Slade. Self-avoiding walk enumeration via the lace expansion. *J. Phys. A: Math. Theory*, 40:10973–11017 (2007).

[14] C.A. de Carvalho and S. Caracciolo. A new Monte Carlo approach to the critical properties of self-avoiding random walks. *J. Physique*, 44:323-331 (1983).

[15] C.A. de Carvalho, S. Caracciolo, and J. Fröhlich. Polymers and $g(|s|)$ theory in four dimensions. *Nucl. Phys. B*, 251:209-248 (1983).

[16] J.H. Conway and C.McA. Gordon. Knots and links in spatial graphs. *J. Graph Theory*, 7:445–453 (1983).

[17] P.Cromwell. *Knots and Links.* Cambridge University Press. Cambridge, UK. (2004).

[18] I. Darcy. A Strand Passage Metric for Topoisomerase Action, in *Knots '96: Proceedings of the Fifth MSJ International Research Institute of Mathematical Society of Japan* July 1996. Editor: Suzuki (World Scientific). 267-278 (1997).

[19] I. Darcy. Rational Tangle Distances on Knots and Links. *Mathematical Proceedings of the Cambridge Philosophical Society,* 128:497-510 (2000).

[20] T. Deguchi and K. Tsurusaki. Statistical study of random knotting using Vasiliev invariants. *Random Knotting and Linking.* Editors: Millet and Sumners (World Scientific). Singapore. (1994).

[21] T. Deguchi and K. Tsurusaki. A Statistical Study of Random Knotting Using the Vassiliev Invariants. *J. Knot Theory and Its Ramifications,* 3:321-353(1994).

[22] T. Deguchi and K. Tsurusaki. Universality of Random Knotting. *Phys. Rev. E.,* 55:6245-6248 (1997).

[23] T. Deguchi and K. Tsurusaki. Random knots and links and applications to polymer physics. *Lectures at Knots '96.* Editor: S. Suzuki. (World Scientific). Singapore. 95-122 (1997).

[24] M. Delbruck. *Mathematical Problems in the Biological Sciences.* American Mathematical Society. Providence, Rhode Island. (1962).

[25] W. R. Derrick. *Complex Analysis and Applications.* Wadsworth International Group. Belmont, California. (1984).

[26] Y. Diao. Minimal knotted polygons on the cubic lattice. *J. Knot Theory and its Ramifications*, 2:413-425 (1993).

[27] Y. Diao. The Number of Smallest Knots on the Cubic Lattice. *J. Stat. Phys.,* 74:1247-1254 (1993).

[28] Y. Diao, C. Ernst, X. Yu. Hamiltonian knot projections and lengths of thick knots. *Topology and its Applications*, 136:7-36 (2003).

[29] C. H. Dowker and M. B. Thistlethwaite. Classification of knot projections. *Topology Appl.*, 16: 19-31 (1983).

[30] L. E. Dubins, A. Orlitsky, J. A. Reads, and L. A. Shepp. Self-avoiding random loops. *IEEE Trans. Inform. Theory*, IT-34: 1509-1516 (1988).

[31] R. Dulbecco and M. Vogt. Evidence for a ring structure of polynoma virus DNA. *Proc. Natl. Acad. Sci.,* 50:236-243 (1963).

[32] M. E. Fisher. Discussion following "Statistics of long chains with repulsive interactions" by J. des Cloiseaux. *J. Phys. Soc. Japan*, 26: suppl.:42-45 (1969).

[33] M. E. Fisher and D. S. Gaunt. Ising model and self-avoiding walks on hypercubical lattices and "high-density" expansions. *Phys. Rev.*, 133:A224-A239 (1964).

[34] G. S. Fishman. *Principles of Discrete Event Simulation.* John Wiley & Sons, Toronto. (1978).

[35] G. S. Fishman. *Monte Carlo: Concepts, Algorithms, and Applications.* Springer-Verlag, New York. (1997).

[36] A. Flammini, A. Maritan, and A. Stasiak. Simulations of Action of DNA Topoisomerases to Investigate Boundaries and Shapes of Spaces of Knots. *Biophysical Journal,* 87: 2968-2975 (2004).

[37] P. Flory. The configuration of a real polymer chain. *J. Chem. Phys.,* 17:303-310

[38] P. Freyd, D. Yetter, J. Hoste, W. B. R. Lickorish, K. Millett, and A. Ocneanu. A new polynomial invariant of knots and links. *Bulletin American Mathematical Society*, 12:239-246 (1985).

[39] H. L. Frisch and E. Wasserman. Chemical Topology. *J. Am. Chem. Soc.*, 83:3789-3795 (1961).

[40] M. Garcia, E. Ilangko, and S. G. Whittington. The writhe of polygons on the face-centred cubic lattice. *J. Phys. A: Math. Gen.*, 32:4593-4600 (1999).

[41] A. Gelman. Inference and Monitoring Convergence. *Markov Chain Monte Carlo in Practice*. Editors: Gilks, Richardson, and Spiegelhalter. Chapman and Hall. London. 131-161 (1996).

[42] A. Gelman and D. Rubin. Inference from iterative simulation using multiple sequences (with discussion). *Statist. Science*, 7:457-511 (1992).

[43] C. J. Geyer. Practical Markov Chain Monte Carlo. *Statistical Science*, 7:473-511 (1992).

[44] C. J. Geyer. Markov chain Monte Carlo Maximum Likelihood. *Computing Science and Statistics: Proceedings of the 23rd Symposium on the Interface*. Editor: Keramidas (Interface Foundation). 156-163 (1991).

[45] G. R. Grimmett. A theorem about random fields. *Bull. London Math. Soc.*, 5:81-84 (1973).

[46] G. R. Grimmett and D. R. Stirzaker. *Probability and Random Process*. Oxford Science Publications. Clarendon Press. Oxford, New York. (1988).

[47] R. Guida and J. Zinn-Justin. Determination of critical exponents and equation of state by field theory method. *Nucl. Phys.,* B489:626 (1997); hep- th/9610223.

[48] E. Guitter and E. Orlandini. Monte Carlo results for projected self-avoiding polygons: a two-dimensional model for knotted polymers. *J. Phys. A: Math. Gen.*, 32:1359-1385 (1999).

[49] A. J. Guttmann. On the critical behavior of self-avoiding walks. *J. Phys. A: Math. Gen.*, 20:1839-1845 (1987).

[50] A. J. Guttmann and I. G. Enting. The size and number of rings on the square lattice. *J. Phys. A: Math. Gen.*, 21:L165-L172 (1988).

[51] A. J. Guttmann and J. Wang. The extension of the self-avoiding random walk series in two dimensions. *J. Phys. A: Math. Gen.*, 24:3107-3109 (1991).

[52] A. J. Guttmann and S. G. Whittington. Two-dimensional lattice embeddings of connected graphs of cyclomatic index two. *J. Phys. A: Math. Gen.*, 11:721-729 (1978).

[53] J. M. Hammersley. On the rate of convergence to the connective constant of the hypercubical lattice. *Quart. J. Math. Oxford* (2), 12:250-256 (1961).

[54] J. M. Hammersley and K. W. Morton. Poor man's Monte Carlo. *J. Roy. Stat. Soc. B*, 16:23-39 (1954).

[55] J. M. Hammersley. Percolation Processes II. The connective constant. *Proc. Cambridge Philos. Soc.,* 53:642–5 (1957).

[56] J. M. Hammersley. The number of polygons on a lattice. *Proc. Cambridge Philos. Soc.,* 57:516–23 (1961).

[57] J.M. Hammersley and D. J. A. Welsh. Further results on the rate of convergence to the connective constant of the hypercubical lattice. *Quart. J. Math. Oxford Ser. (2),* 53:642–645 (1962).

[58] Ulrich H. E. Hansmann. Parallel tempering algorithm for conformational studies of biological molecules. *Chemical Physical Letters*, 281:140-150 (1997).

[59] T. Hara and G. Slade. Self-avoiding walk in five or more dimensions. I. The critical behavior. *Commun. Math. Phys.*, 147:101-136 (1992).

[60] T. Hara and G. Slade. The lace expansion for self-avoiding walk in five or more dimensions. *Reviews in Math. Phys.*, 4:235-327 (1992).

[61] X. Hua, D. Nguyen, B. Raghavan, J. Arsuaga, and M. Vazquez. Random State Transitions of Knots: a first step towards modeling unknotting by type II topoisomerases. *Topology and its Applications*, 154:1381-1397 (2007).

[62] K. Hukushima and K. Nemoto. Exchange Monte Carlo method and application to spin glass simulations. *Journal of the Physical Society of Japan*, 42:281-300 (1996).

[63] E. W. James and C. E. Soteros. The statistics of collapsing square lattice trails with a fixed number of vertices of degree 4. *J. Phys. A: Math. Theor.*, 40: 14945-14962 (2007).

[64] E. J. Janse van Rensburg. Thoughts on Lattice Knot Statistics. *J. Math. Chem.,* DOI: 10.1007s/s10910-008-9364-9 (2007).

[65] E. J. Janse van Rensburg. The Probability of Knotting in Lattice Polygons. *Contemporary Mathematics*, 304:125-135 (2002).

[66] E. J. Janse van Rensburg and D. Gruner. *Private communication.*

[67] E. J. Janse van Rensburg and S. G. Whittington. The knot probability in lattice polygons. *J. Phys. A: Math. Gen.*, 23: 3573-3590 (1990).

[68] E. J. Janse van Rensburg and S. G. Whittington. The dimensions of knotted polygons. *J. Phys. A: Math. Gen.*, 24: 3935-3948 (1991).

[69] E. J. Janse van Rensburg and S. G. Whittington. The BFACF algorithm and knotted polygons. *J. Phys. A: Math. Gen.*, 24: 5553-5567 (1991).

[70] E. J. Janse van Rensburg, E. Orlandini, D. W. Sumners, M. C. Tesi, and S. G. Whittington. The writhe of a self-avoiding polygon. *J. Phys. A: Math. Gen.*, 26:L981-L986 (1993).

[71] E. J. Janse van Rensburg and S. D. Promislow. Minimal knots in the cubic lattice. *J. Knot Theory and its Ramifications*, 4:115-130 (1995).

[72] E. J. Janse van Rensburg, D. W. Sumners, and S. G. Whittington. The writhe of knots and links. *Ideal Knots*. Editors: Stasiak, Katritch, and Kauffman (World Scientific). (1999).

[73] I. Jensen. A parallel algorithm for the enumeration of self-avoiding polygons on the square lattice *J. Phys. A: Math. Gen.,* 36:5731–5745 (2003).

[74] I. Jensen and A. J. Guttmann. Self-avoiding polygons on the square lattice *J. Phys. A: Math. Gen.,* 32:4867–4876 (1999).

[75] L. W. Johnson and R. D. Reiss. *Numerical Analysis.* Addison-Wesley Publishing Company. Don Mills, Ontario. (1977).

[76] R. A. Johnson and D. W. Wichern. *Applied Multivariate Statistics.* Prentice Hall. New Jersey. (1982).

[77] V. F. R. Jones. A polynomial invariant for knots via von Neumann algebras. *Bulletin American Mathematical Society*, 12:103-111 (1985).

[78] S. Karlin and H. M. Taylor. *A First Course in Stochastic Processes.* Academic Press. New York. (1975).

[79] V. Katritch, J. Bednar, D. Michoud, R. Scharein, J. Dubochet, and A. Stasiak. Geometry and physics of knots. *Nature*, 384: 142-145 (1996).

[80] V. Katritch, W. K. Olson, A. Vologodskii, J. Dubochet, and A. Stasiak. Tightness of Random Knotting. *Phys. Rev. E*, 61:5545 (2000).

[81] L. H. Kauffman. State models and the Jones polynomial. *Topology*, 26:395-407 (1987).

[82] H. Kesten. On the number of self-avoiding walks. *J. Math. Phys.*, 4:960-969 (1963).

[83] H. Kim, G. T. Jin, C. B. Jeon, S. U. Chang, S. H. Moon, S. H. Park, and Y. S. Song. Lattice Edge Number of Figure-8 knot. Talk given at *The Fourth East Asian School of Knots and Related Topics*. January 21-24 (2008); available for download at http://faculty.ms.u-tokyo.ac.jp/˜topology/EAS4slides/HunKim.pdf.

[84] C. Kipnis and S. R. S. Varadhan. Central limit theorem for additive functionals of reversible Markov processes and applications to simple exclusions. *Comm. Math. Phys.*, 104:1-19 (1986).

[85] K. J. Koehler and K. Larntz. An empirical investigation of goodness-of-fit statistics for sparse multinomials. *Journal of the American Statistical Association*, 75: 336-344 (1980).

[86] M. A. Krasnow, A. Stasiak, S. J. Spengler, F. Dean, Th. Koller, and N. R. Cozzarelli. Determination of the absolute handedness of knots and catenanes of DNA. *Nature*, 304: 559-560 (1983).

[87] E. Kreyszig. *Introductory Mathematical Statistics*. John Wiley & Sons. Toronto. (1970).

[88] R. C. Lacher and D. W. Sumners. Data Structures and Algorithms for Computation of Topological Invariants of Entanglements: Link, Twist, and Writhe. *Computer Simulations of Polymers*. Editor: Roe. Prentice-Hall. Englewood Cliffs. 365-373 (1991).

[89] M. Lal. Monte Carlo computer simulations of chain molecules. I. *Molec. Phys.*, 17:57-64 (1969).

[90] J. C. Le Guillou and J. Zinn-Justin. Accurate critical exponents from field theory. *J. Phys. France*, 50: 1365-1370 (1989).

[91] E. L. Lehman. *Theory of Point Estimation.* Wiley. New York. (1983).

[92] C. Liang and K. Mislow. A left-right classification of topologically chiral knots. *J. Math. Chem.*, 15: 35-62 (1994).

[93] Z. Liu and H. S. Chan. Efficient chain moves for Monte Carlo simulation of a wormlike DNA model: Excluded volume, supercoils, site juxtapositions, knots, and comparisons with random-flight and lattice models. *J. Chem. Phys.,* 128: 145104: 1-31 (2008).

[94] L. F. Liu, R. E. Depew, and J. C. Wang. Knotted single-stranded DNA rings: a novel topological isomer of circular single-stranded DNA formed by treatment with *Escherichia coli* ω protein. *J. Mol. Biol.,* 106: 439-452. (1976).

[95] J. S. Liu. *Monte Carlo Strategies in Scientific Computing*. Springer. New York. (2001).

[96] Z. Liu, J. K. Mann, E. L. Zechiedrich and H. S. Chan. Topological Information Embodied in Local Juxtaposition Geometry Provides a Statistical Mechanical Basis for Unknotting by Type-2 DNA Topoisomerases. *J. Mol. Biol.*, 361: 268-285. (2006).

[97] B. Li, N. Madras, and A. D. Sokal. Critical Exponents, Hyperscaling and Universal Amplitude Ratios for Two- and Three-Dimensional Self-Avoiding Walks. *J. Stat. Phys.*, 80:661-754 (1995).

[98] C. Livingston. *Knot Theory*. The Mathematical Association of America. Washington, DC. (1993).

[99] D. MacDonald, S. Joseph, D. L. Hunter, L. L. Moseley, N. Jan, and A. J. Guttmann. Self-avoiding walks on the simple cubic lattice. *J. Phys. A: Math. Gen.*, 33:5973-5983 (2000).

[100] N. Madras. Umbrella sampling and simulated tempering. *Numerical methods for Polymeric Systems*. Editor: Whittington (IMA Volumes in Mathematics and its Applications). Springer-Verlag, New York. 19-32 (1998).

[101] N. Madras. *Lecture Notes on Monte Carlo Methods.* American Mathematical Society. Providence, RI. (2002).

[102] N. Madras, A. Orlitsky, and L. A. Shepp. Monte Carlo generation of self-avoiding walks with fixed endpoints and fixed length, *J. Stat. Phys.*, 58:159-183 (1990).

[103] N. Madras and G. Slade. *The Self-avoiding Walk*. Birkhäuser. Boston. (1992).

[104] N. Madras and A. D. Sokal. Nonergodicity of local, length-conserving Monte Carlo algorithms for the self-avoiding walk. *J. Stat. Phys.*, 47:573-595 (1987).

[105] N. Madras and A. D. Sokal. The pivot algorithm: a highly efficient Monte Carlo method for the self-avoiding walk. *J. Stat. Phys.*, 50:109-186, no. 1-2, (1988).

[106] J. K. Mann. *DNA Knotting: Occurrences, Consequences, & Resolution*. Ph.D. Thesis. The Florida State University. (2007).

[107] B. Marcone, E. Orlandini, A. L. Stella, and F. Zonta. What is the length of a knot in a polymer? *J. Phys. A: Math. Gen.*, 38:L15-L21 (2005).

[108] B. Marcone, E. Orlandini, A. L. Stella, and F. Zonta. Size of knots in ring polymers. *Phys. Rev. E,* 75:041105 (2007).

[109] G. Marsaglia and A. Zaman. A new class of random number generators. *The Annals of Applied Probability*, 1:462-480 (1991).

[110] B. Masand, U. Wilensky, J. P. Massar, and S. Redner. An extension of the two-dimensional self-avoiding walk series on the square lattice. *J. Phys. A: Math. Gen.*, 25:L365-L369 (1992).

[111] R. Metzler, A. Hanke, P. G. Dommersnes, Y. Kantor, and M. Kardar. Tightness of slip-linked polymer chains. *Phys. Rev. E*, 65:061103-1– 9 (2002).

[112] J. P. J. Michels and F. W. Wiegel. Probability of knots in a ring polymer. *Phys. Lett.*, 90A:381-384 (1982).

[113] J. P. J. Michels and F. W. Wiegel. On the topology of a polymer ring. *Proc. Roy. Soc. London Ser. A*, 403: 269–284, no. 1825 (1986).

[114] E. W. Montroll. Size Effects in Low Temperature Heat Capacities. *J. Chem. Phys.*, 18:183-186 (1950).

[115] J. Moussouris. Gibbs and Markov random systems with constraints. *J. Statist. Phys.*, 10:11-33 (1973).

[116] K. Murasugi *Knot Theory*. Birkhäuser. Boston. (1996).

[117] Nakamura, T., Four-genus and unknotting number of positive knots and links. *Osaka J. Math.*, 37: 441-451 (2000).

[118] B. Nienhuis. Exact critical points and critical exponents of O(n) models in two dimensions *Phys. Rev. Lett.,* 49:1062–1065 (1982).

[119] B. Nienhuis. Critical behavior of two-dimensional spin models and charge asymmetry in the Coulomb gas, *J. Stat. Phys.,* 34:731–761 (1984).

[120] E. Orlandini, E.J. Janse van Rensburg, M.C. Tesi, and S.G. Whittington. Random linking of lattice polygons. *J. Phys A: Math. Gen.*, 27 (1994), pp. 335–346.

[121] E. Orlandini, M. C. Tesi, E. J. Janse van Rensburg, and S. G. Whittington. Entropic exponents of lattice polygons with specified knot type. *J. Phys. A: Math. Gen.*, 29:L299-L303 (1996).

[122] E. Orlandini. Monte Carlo study of polymer systems by Multiple Markov Chain method. *Numerical methods for Polymeric Systems*. Editor: Whittington (IMA Volumes in Mathematics and its Applications). Springer-Verlag, New York. 33-57 (1998).

[123] E. Orlandini, M. C. Tesi, E. J. Janse van Rensburg, and S. G. Whittington. The shapes of self-avoiding polygons with torsion. *J. Phys. A: Math. Gen.*, 30:L693-L698 (1997).

[124] E. Orlandini, E. J. Janse van Rensburg, M. C. Tesi, and S. G. Whittington. Entropic exponents of knotted lattice polygons. *Topology and geometry in polymer science*. Editors: Whittington, Sumners and Lodge. (IMA Volumes in Mathematics and its Applications) Springer-Verlag, New York. 9-21 (1998).

[125] E. Orlandini, M. C. Tesi, E. J. Janse van Rensburg, and S. G. Whittington. Asymptotics of knotted lattice polygons. *J. Phys. A: Math. Gen.*, 31:5953-5967 (1998).

[126] E. Orlandini, M. C. Tesi, and S. G. Whittington. Entanglement complexity of semiflexible lattice polygons. *J. Phys. A: Math. Gen.*, 38:L795-L800 (2005).

[127] W. J. C. Orr. Statistical Treatment of Polymer Solutions at Finite Dilutions. *Trans Faraday Soc.*, 43:12-27 (1947).

[128] C. W. Patty. *Foundations of Topology*. PWS-Kent Publishing Company. Boston. (1992).

[129] N. Pippenger. Knots in random walks. *Discrete Appl. Math.*, 25:273-278, no. 3, (1989).

[130] A. A. Podtelezhnikov, N. R. Cozzarelli, and A. V. Vologodskii. Equilibrium distributions of topological states in circular DNA: Interplay of supercoiling and knotting. *Nature*, 96:12974-12979, no. 23, (1999).

[131] W. H. Press, S. A. Teukolsky, W. T. Vetterling, and B. P. Flannery. *Numerical Recipes in C: The Art of Scientific Computing, 2nd. Ed.* Cambridge University Press. Cambridge. Reprinted in 1997.

[132] M. B. Priestley. *Spectral Analysis and Time Series*. 2 vols. Academic. London. (1981).

[133] D. E. Pulleyblank, M. Shure, D. Tang, J. Vinograd, and H. P. Vosberg. Action of nicking-closing enzyme on supercoiled and nonsupercoiled closed circular DNA: formation of a Boltzmann distribution of topological isomers. *Proc. Natl Acad. Sci. USA*, 72: 4280–4284 (1975).

[134] S. R. Quake. Fast Monte Carlo algorithms for knotted polymers. *Phys. Rev. E*, 52: 1176-1180 (1995).

[135] K. Reidemeister. *Knotentheorie*. Springer. Berlin. (1932).

[136] D. Rolfsen. *Knots and Links.* Corrected Edition. Publish or Perish, Inc. Austin, Texas. (1990).

[137] V. V. Rybenkov, N. R. Cozzarelli, and A. V. Vologodskii. Probability of DNA knotting and the effective diameter of the DNA double helix. *Proc. Natl. Acad. Sci., USA*, 90: 5307-5311 (1993).

[138] V. V. Rybenkov, N. R. Cozzarelli, C. Ullsperger, and A. V. Vologodskii. Simplification of DNA topology below equilibrium values by type II topoisomerases. *Science*, 227: 690–693 (1997).

[139] M. J. Schervish. *Theory of Statistics*. Springer-Verlag, New York. (1997).

[140] S. Y. Shaw and J. C. Wang. Knotting of a DNA Chain During Ring Closure. *Science*, 260:533-536 (1993).

[141] M. K. Shimamura and T. Deguchi. Gyration radius of a circular polymer under a topological restraint with excluded volume. *Phys. Rev. E*, 64: 020801 (2001).

[142] A. D. Sokal. Monte Carlo Methods in Statistical Mechanics: Foundations and New Algorithms. Cours de Troisieme Cycle de la Physique en Suisse Romande 15, 22 et 29 juin 1989, Lausanne.

[143] A. D. Sokal and L. E. Thomas. Exponential convergence to equilibrium for a class of random walk models. *J. Stat. Phys.*, 54:797-828 (1989).

[144] C. E. Soteros. Knots in Graphs in Subsets of $\mathbb{Z}^3$. *IMA Volumes in Mathematics and its Applications*, 103:101-133 (1998).

[145] C. E. Soteros, D. W. Sumners, and S. G. Whittington. Entanglement complexity of graphs in $\mathbb{Z}^3$. *Math. Proc. Camb. Phil. Soc.*, 111:75-91 (1992).

[146] A. Stasiak, V. Katrich, J. Bednar, D. Michoud, and J. Dubochet. Electrophoretic mobility of DNA knots. *Nature*, 384:122 (1996).

[147] M. Sullivan, III. *Statistics: Informed Decisions Using Data*. 2nd Edition. Pearson Prentice Hall. Upper Saddle River, New Jersey. (2007).

[148] D. W. Sumners. Lifting the curtain: using topology to probe the hidden action of enzymes. *Notices Am. Math. Soc.*, 42:528-537 (1995).

[149] D. W. Sumners and S. G. Whittington. Knots in self-avoiding walks. *J. Phys. A: Math. Gen.*, 21:1689-1694 (1988).

[150] M. L. Szafron. *Monte Carlo Simulations of Strand Passage in Unknotted Self-Avoiding Polygons*. M.Sc. Thesis. University of Saskatchewan (2000).

[151] M.C. Tesi, E.J. Janse van Rensburg, E. Orlandini, and S.G. Whittington. Knot probability for lattice polygons in confined geometries, *J. Phys A: Math. Gen.*, 27:347–360 (1994).

[152] M. C. Tesi, E. J. Janse van Rensburg, E. Orlandini, and S. G. Whittington. Monte Carlo study of the interacting self-avoiding walk model. *J. Stat. Phys.*, 82:155-181 (1996).

[153] M.C. Tesi, E.J. Janse van Rensburg, E. Orlandini and S.G. Whittington, *Topological entanglement complexity of polymer chains in confined goemetries*, IMA Vol. in Math. and its Appl. Springer-Verlag. (1997).

[154] C. J. Thompson. *Mathematical Statistic Mechanics*. Princeton University Press. Princeton, New Jersey. (1972).

[155] C. J. Thompson. *Classical Equilibrium Statistic Mechanics*. Clarendon Press. Oxford. (1988).

[156] Tin, M. Comparison of Some Ratio Estimators. *J. Amer. Statist. Assoc.,* 60: 294-307 (1965).

[157] T. Tierney. Markov chains for exploring posterior distributions (with discussion). *Ann. Statist.*, 22:1701-1762 (1994).

[158] T. Tierney. Introduction to general state-space Markov chain theory. *Markov Chain Monte Carlo in Practice*. Editors: Gilks, Richardson, and Spiegelhalter. Chapman and Hall. London. (1996).

[159] J. Vinograd, J. Lebowitz, R. Radloff, R. Watson, and P. Laipis. Twisted circular form of polynoma viral DNA. *Proc. Natl. Acad. Sci.,* 53:1104-1111 (1965).

[160] A. Vologodskii. Circular DNA. *On-Line Biophysics Textbook*. Editor: Bloomfield, http://www.biophysics.org/btol/supramol.html#13 (1999).

[161] A. Vologodskii. Distributions of Topological States in Circular DNA. *Molecular Biology*, 35:240-250, no. 2, (2001)

[162] A. Vologodskii, N. Crisona, B. Laurie, P. Pieranski, V. Katritch, J. Dubochet, and A. Stasiak. Sedimentation and electrophoretic migration of DNA knots and catenanes *J. Mol. Biol.,* 278:1-3 (1998).

[163] A. V. Vologodskii, A. V. Lukashin, M. D. Frank-Kamenetskii, and V. V. Anshelevich. The knot problem in statistical mechanics of polymer chains. *Zh. Eksp. Teor. Fiz.*, 66:2153-2163 (1974).

[164] A. V. Vologodskii, W. Zhang, V. V. Rybenkov, A. A. Podtelezhnikov, D. Subramanian, J. D. Griffith, and N. R. Cozzarelli. Mechanism of topology simplification by type II DNA topoisomerases. *Proc. Natl Acad. Sci. USA*, 98: 3045–3049 (2001).

[165] S. A. Wasserman and N. R. Cozzarelli. Biochemical topology applications to DNA recombination and replication. *Science*, 232: 951-960 (1986).

[166] S. A. Wasserman and N. R. Cozzarelli. Supercoiled DNA-directed knotting by T4 topoisomerase. *J. Biol. Chem.,* 266: 20567-20573 (1991).

[167] J. D. Watson and F. H. C. Crick. A structure for deoxyribose nucleic acid. *Nature*, 171:737-738 (1953).

[168] R. Weil and J. Vinograd. The cyclic helix and cyclic coil forms of polynoma viral DNA. *Proc. Natl. Acad. Sci.,* 50:730-738 (1963).

[169] F. J. Wegner and E. K. Riedel. Logarithmic corrections to the molecular-field behavior of critical and tricritical systems. *Phys. Rev. B*, 7:248-256 (1973).

[170] S. G. Whittington, J. P. Valleau, and G. M. Torrie. How many figure eights are there? Some bounds. *J. Phys. A: Math. Gen.*, 10:L111-L112 (1977).

[171] S. G. Whittington. Statistical Mechanics of Polymer Solutions and Polymer Adsorption. *Advances in Chemical Physics*. Editors: Prigogine and Rice. Wiley. New York. (1983)

[172] R. J. Wilson. *Introduction to Graph Theory*. 4th Edition. Longman. Essex. (1996)

[173] A. Yao, H. Matsuda, H. Tsukahara, M. K. Shimamura, and T. Deguchi. On the dominance of trivial knots among SAPs on a cubic lattice. *J. Phys. A: Math. Gen.,* 34:7563–7577 (2001).

Index